

***Progress in
Inorganic Chemistry***

Volume 38

Advisory Board

JACQUELINE K. BARTON

CALIFORNIA INSTITUTE OF TECHNOLOGY, PASADENA,
CALIFORNIA

THEODORE L. BROWN

UNIVERSITY OF ILLINOIS, URBANA, ILLINOIS

JAMES P. COLLMAN

STANFORD UNIVERSITY, STANFORD, CALIFORNIA

F. ALBERT COTTON

TEXAS A&M UNIVERSITY, COLLEGE STATION, TEXAS

ALAN H. COWLEY

UNIVERSITY OF TEXAS, AUSTIN, TEXAS

RONALD J. GILLESPIE

McMASTER UNIVERSITY, HAMILTON, ONTARIO, CANADA

RICHARD H. HOLM

HARVARD UNIVERSITY, CAMBRIDGE, MASSACHUSETTS

KENNETH D. KARLIN

THE JOHNS HOPKINS UNIVERSITY, BALTIMORE, MARYLAND

TOBIN J. MARKS

NORTHWESTERN UNIVERSITY, EVANSTON, ILLINOIS

KARL WIEGHARDT

RUHR-UNIVERSITÄT, BOCHUM, FEDERAL REPUBLIC OF
GERMANY

GEOFFREY WILKINSON

IMPERIAL COLLEGE, LONDON, ENGLAND

Progress in Inorganic Chemistry:

**BIOINORGANIC
CHEMISTRY**

Edited by

STEPHEN J. LIPPARD

DEPARTMENT OF CHEMISTRY
MASSACHUSETTS INSTITUTE OF TECHNOLOGY
CAMBRIDGE, MASSACHUSETTS

VOLUME 38



AN INTERSCIENCE® PUBLICATION

JOHN WILEY & SONS

New York • Chichester • Brisbane • Toronto • Singapore

In recognition of the importance of preserving what has been written, it is a policy of John Wiley & Sons, Inc. to have books of enduring value published in the United States printed on acid-free paper, and we exert our best efforts to that end.

An Interscience® Publication

Copyright© 1990 by John Wiley & Sons, Inc.

All rights reserved. Published simultaneously in Canada.

Reproduction or translation of any part of this work beyond that permitted by Section 107 or 108 of the 1976 United States Copyright Act without the permission of the copyright owner is unlawful. Requests for permission or further information should be addressed to the Permissions Department, John Wiley & Sons, Inc.

Library of Congress Catalog Card Number: 59-13035

ISBN 0-471-50397-5

ISBN 0-471-52945-1 (pbk)

Printed in the United States of America

10 9 8 7 6 5 4 3 2

Preface

Work in bioinorganic chemistry has accelerated substantially since 1973, when Volume 18 of *Progress in Inorganic Chemistry* was published highlighting current research topics in the field. The Preface and Introduction to that volume are reprinted here as an historical benchmark by which to judge the enormous progress that has been made in the intervening 17 years. During this interval, the first International Conference on Bioinorganic Chemistry (ICBIC) was convened, and the fourth such conference was held last summer on the MIT campus. The present volume of *Progress in Inorganic Chemistry* was conceived in conjunction with ICBIC-4 as an opportunity to present authoritative reviews by many experts in bioinorganic chemistry who were gathering in Cambridge for the meeting. Accordingly, all of the plenary lecturers were invited to contribute a chapter, and most graciously agreed to do so. In addition, a number of other speakers at the conference were asked to review their areas of research expertise in order to provide additional scope of coverage for this volume.

The topics reviewed here touch on many aspects of current research in bioinorganic chemistry, exploring the amazing breadth of the field that ranges from solid state physics to cell biology and medicine. There are of course many subjects not covered, but from the eight chapters included the reader should be able to assess the full span of activities in what has become a forefront subject in both chemistry and biology. As witness to the latter claim one need only recall that the journal *CELL* recently displayed a zinc finger peptide on its cover, a debut that was hailed by many in the bioinorganic community as official recognition of the discipline by "big biology." Although zinc finger proteins are not specifically covered in this volume, they were the subject of an article by Jeremy Berg in Volume 37 of our series.

In order to produce this volume in a timely fashion, the publisher has agreed to a new, if somewhat risky, experiment. The chapters were set directly into pages, bypassing the usual reading of galley proofs. In addition, in an attempt to make the book more accessible to individual readers, as well as libraries, we are for the first time providing a paperback edition at a substantial reduction in cost. Both of these innovations were greatly facilitated with the assistance of our new in-house editor, Dr. Philip Manor, to whom I am very much indebted. In addition, I should like to thank Professor Kenneth D. Karlin, the organizer of ICBIC-4, for his help in planning this volume. Finally, the time has come to acknowledge publicly the talents of Jeannette Stiefel who, for many years, has served as the freelance copy-editor of the *Progress in Inorganic Chemistry* volumes; the uniform high quality of the chapters is in no small measure due to her efforts.

STEPHEN J. LIPPARD

Cambridge, Massachusetts
May 1990

Introduction

In the Introduction to Volume 18 of *Progress in Inorganic Chemistry*, subtitled "Current Research Topics in Bioinorganic Chemistry" and reprinted herein, three major avenues of research in the field were delineated. These subtopics, the direct study of metal ions in biological macromolecules, the use of simpler, model systems to gain insight into the properties of metalloprotein cores, and the application of inorganic reagents as probes of biological structure and function, all continue to be important facets of modern bioinorganic chemistry. They comprise a significant fraction of the research described in the present volume. A very significant area of growth in the discipline of bioinorganic chemistry, however, has been the application of metals in medicine. Included are the use of cisplatin in the highly successful treatment of genitourinary tumors, of technetium compounds as radiodiagnostic agents, of orally administered gold phosphine complexes for the management of rheumatoid arthritis, and of lithium to control manic-depressive behavior. In addition, much attention is now beginning to focus on the regulation of gene expression by metal ions, which bind to proteins causing them to fold in specific conformations for interaction with other macromolecules in the cell. Chapters illustrating these newer activities are also included in this volume.

Driving much of this research have been advances made in the fields of molecular and cell biology, including technical developments such as gel electrophoresis, DNA and RNA sequencing methodologies, site specific mutagenesis, cloning, and the ability to obtain monoclonal antibodies. Related instrumental developments from the physics and engineering communities have similarly spurred progress in bioinorganic research. Synchrotrons have afforded high intensity X-ray beams for absorption and diffraction measurements; the scanning tunneling microscope promises to yield high resolution images of single biomolecules; and new and more powerful computers and software developments have brought molecular mechanics, dynamics, and modelling calculations to the desktops of many practicing graduate and postdoctoral students. These technical improvements will be readily apparent to the reader in many of the review articles collected here.

This volume begins with a discussion of iron sulfur clusters, a familiar topic to bioinorganic chemists and one that has not lost its appeal. Although long known for their role in biological electron transfer, they have recently been shown also to possess catalytic activity through subsite specific chemistry, wherein one of the iron atoms in the cube catalyzes chemical transformation at its particular corner. To reproduce such dissymmetry in an

otherwise symmetric cluster has presented a challenge to the synthetic model builder that has been met by brilliant design and execution, which the reader is sure to appreciate. In the following two chapters are introduced the currently fashionable topic of nonheme iron and manganese bioinorganic chemistry, much of which involves aspects of dioxygen metabolism. The discovery of units such as the μ -oxobis(μ -carboxylato)diiron(III) center in the marine invertebrate O_2 -transport protein hemerythrin has spurred both the synthetic model builder and the protein biochemist to enter this arena. Some of the most exciting goals are to understand the diiron centers in methane monooxygenase, which uses CH_4 as its sole carbon and energy sources, and in ribonucleotide reductase, which activates dioxygen by a similar dinuclear iron center, and to elucidate the nature of the tetramanganese unit in photosystem II, which evolves O_2 from water.

Many enzymes catalyze the transformation of organic substrates by delivering a functional group held in or near the coordination sphere of a metal ion at their active sites. A thorough understanding of these reactions has been greatly facilitated by careful studies of well-designed model systems. The next review addresses this topic, with specific emphasis on phosphate chemistry. The regulation of cellular events by phosphatases and kinases, enzymes that remove or add phosphate groups to proteins, respectively, is central to many forefront areas of modern biology, including the study of oncogenes, development, and the cell cycle. Metal centers in proteins that do not function as group transfer agents frequently serve to facilitate electron transfer, the topic of the next chapter. It has now been demonstrated that electrons can be transferred over long distances (>10 Å) in proteins. How they do so, and how the rates of these reactions depend on their driving force, the distance between redox centers, and the intervening medium, are addressed in this review. An exciting development in this field has been the attachment of kinetically inert inorganic complexes to amino acid side chains on the surface of redox metalloproteins to probe the distance dependence of electron transfer to their naturally occurring metal cores.

The final three chapters all deal largely with metal-nucleic acid chemistry. This topic, only in its infancy in 1973 when Volume 18 of *Progress in Inorganic Chemistry* appeared, now accounts for a substantial fraction of the work done in bioinorganic chemistry. Metal regulated gene expression, exemplified by the mercury resistance phenomenon, offers a wonderful opportunity for the bioinorganic chemist to combine the power of inorganic synthesis and structure determination with that of cloning and protein structure determination. This relatively new subfield is replete with fascinating unstudied problems and systems, the understanding of which will undoubtedly benefit from a careful reading of this chapter. In the penultimate chapter are reviewed the powerful ways that metal complexes can be used as probes for DNA structure. By matching the shapes and

symmetries of metal complexes with their target sites on DNA emerges the possibility to outdo nature in recognizing and cleaving the genome at specific sequence-determined sites. This challenge has attracted many members of the organic as well as the inorganic chemical communities interested in the more general topic of molecular recognition. The practical consequences of success are enormous, and include the localization of gene defects responsible for diseases such as Huntington's chorea, cleavage of DNA into very long ($\sim 10^4$ nucleotide) segments required for mapping the human genome, and even chemotherapy by targeted destruction of viral genomes *in vivo*. Finally, the last chapter reviews an aspect of the still evolving platinum antitumor drug story that has not received attention elsewhere, one that could lead ultimately to the complete unravelling of the molecular mechanism of action of the drug. Although much is known about the binding of *cis*-[Pt(NH₃)₂Cl₂] to DNA and the resulting structural changes in the target, we are still deficient in understanding how cells process this damage such that cancer cells are selectively destroyed. Some new discoveries that promise to elucidate these mechanisms are set forth in the chapter.

As the reader of this volume will soon appreciate, the subject of bio-inorganic chemistry has matured to the point where activities previously labeled as "inorganic" or "biological" are now being carried out in the same laboratory. Collaborations between experts in these separate areas still occur, but increasingly entry level researchers want to do it all themselves. This development is most welcome and will continue to foster success in meeting the difficult challenges posed by the great unsolved problems of the field.

STEPHEN J. LIPPARD

Cambridge, Massachusetts
May 1990

Preface to *Progress in Inorganic Chemistry*, Volume 18

Work at the interface between the areas of inorganic and biological chemistry has greatly intensified in recent years. Organization of the subject material of this growing field of bioinorganic chemistry along topical lines is fairly straightforward, if not completely satisfying. Thus whole literatures have grown up around such problems as nitrogen fixation, heme proteins, vitamin B₁₂ chemistry, carboxypeptidase structure and biochemistry, metal ion transport through membranes, non-heme iron proteins, metal activation of ATP, and copper oxidases. In planning this special topics volume, some attempt was made to achieve a broader scope. For example, instead of a chapter on iron-sulfur redox proteins, it seemed desirable to have a discussion of the entire family of metallo-redox proteins. To the extent that the subject matter was amenable to such an approach, the chapters reflect this philosophy.

The choice of topics for this particular volume was dictated by two criteria. First, it was decided to sustain the long-standing policy of this series to provide critical, comprehensive, in-depth coverage of material. This decision necessitated a high selectivity since only a few such chapters could be accommodated in a single volume. The second criterion was to assure reasonably broad coverage by including subjects that represented the various kinds of available biological ligands, namely proteins and nucleic acids and their constituents, in addition to special-function ligands such as the heme or corrin ring. To the extent that we have been successful, this book should serve as a useful introduction and guide to scientists in all fields who are interested in obtaining an overview of the emerging discipline of bioinorganic chemistry. At the same time, the individual chapters should provide current information and critical discussion of the more specialized areas for both research workers and students. Parts of certain chapters have already been adopted in manuscript form for instructional purposes at the graduate student level.

I wish to thank the authors for their cooperation and efforts required to produce this volume. If there is sufficient positive response, future bioinorganic volumes will be scheduled in this series. As usual, comments of any kind are always welcome and will be given serious attention.

STEPHEN J. LIPPARD

New York, New York
February 1973

Introduction to *Progress in Inorganic Chemistry*, Volume 18

There are three major avenues of investigation in bioinorganic chemistry. The first involves direct study of the structure and function of "biometallic" molecules, an area traditionally that of the biochemist. Here one is interested in the role of metal ions in metalloenzymes, coenzymes, and proteins, as well as their function as cofactors in DNA and RNA biochemistry. In classic studies on carboxypeptidase, Vallee and co-workers recognized the importance of the zinc atom as a functional group unique among all others in the protein. By replacing the zinc with other metal ions, chemical and spectroscopic probes of the active site were made available. More recently, X-ray diffraction studies have yielded detailed structural information about several metallomacromolecules. The three-dimensional structure of a tRNA has just been made available through the efforts of Rich, Kim, and their associates. The critical role of magnesium ions in binding phosphate groups remote from each other in the sequence (not a new concept, incidentally) has begun to emerge, and correlates well with biochemical results from several laboratories. X-ray data serves not only to bridle the occasional untamed structural speculations derived from less direct approaches, but also provides the impetus and direction for attempts to elucidate the structure-function relationships that form our basic understanding of how biometallic molecules work. Delineation of the function of the metal ion as a structural keystone (as in the example just cited), specific reaction organizer, electron transfer agent, or substrate activator is the major objective of the direct approach, in which detailed studies are performed on specimens usually obtained directly from natural sources.

By contrast, the second major avenue involves an indirect approach, commonly the domain of the inorganic or organic chemist. Through the invention, synthesis, structure determination, physical study, and reactions of so-called "model" compounds, some insight into the workings of the natural system is sought. An additional objective might be to mimic in a simple system the catalytic function of a metalloenzyme for industrial or biomedical synthetic purposes. Current attempts to fix molecular nitrogen with homogeneous iron or molybdenum catalysts exemplify this aspect. Although few doubt that important chemistry might result from this approach, serious reservation has been expressed about the relevance of such work to the understanding of natural systems. Indeed, there are purists who believe that even to study biometallic molecule *in vitro* is to oversimplify. For instance, there are those who argue that to investigate solubilized

components of the membrane-bound cellular redox apparatus (e.g., cytochrome *c* oxidase) is a waste of effort. This attitude stems in part from an overreaction to claims of relevance by chemists interested in riding biological coattails for one reason or another. There is at least one instance where an organometallic molecule, of perfectly respectable interest for its own sake, was labeled a "model" for the nitrogenase enzyme even though it never could bind dinitrogen let alone catalyze its reduction. But unfortunate as statements of this kind may be, it is shortsighted not to recognize and cultivate the growing research activities on small molecule analogs of biometallic compounds.

For the skeptical, a detailed example might be offered. The copper blue proteins characterized chiefly by Malmström, Vänngård, and their co-workers are an important class of biological oxidases. The redox, optical, and epr spectroscopic properties of these proteins have been thoroughly studied, although their detailed structures are not yet available. Even if the structures were known, the interesting task of explaining the "unusual" spectroscopic features and high redox potentials of these proteins would remain. It is worth digressing a moment to discuss the concept of uniqueness that is used with increasing frequency in this context (Vallee and Williams have formalized one aspect and called it the "entatic nature of the active site"). Since Nature could not take advantage of the redox potentials available among the aquo ions of the transition metals (the ferric ion, e.g., would be a good biological oxidizing agent with a reduction potential of -0.77 V, but it hydrolyzes at pH 7 and is thus unavailable), substitute biometallic coordination compounds evolved. In the present example, the oxidizing power of the copper(II) ion has been substantially increased by the specialized ligand environment (as yet unknown) of the protein active site. Viewed in this context, it should not be surprising if the properties of the copper(II) centers appear unusual. The uniqueness should not then be taken as some mystical force available in proteins, as has sometimes been done. Rather, the properties of a biometallic molecule may be viewed as unusual in the sense that inorganic analogs with sufficiently complex ligand environments are simply not available. No one has taken the trouble to prepare them. It is therefore important that synthetic, structural, and physical studies be carried out to produce and characterize the appropriate relevant small molecules. In the case at point, copper coordination compounds that produce large positive reduction potentials will be deemed most relevant, and their study should contribute eventually to a fundamental understanding of how the proteins work.

Before turning to the third approach to bioinorganic chemistry, it is worth noting with approval that cooperation between inorganic and biological chemists has grown substantially in recent years. Not only are laboratories collaborating on specific problems, but there is an increasing tendency for biochemists to try their hand at preparing inorganic analogs, and for coordination chemists to establish a biological program. Surely such activities signify the emergence of a new discipline.

A third investigative avenue to this discipline involves the addition of metal ions or complexes as probes to biochemical structure and function. Here the word *addition* is emphasized as being different in kind from the *substitution* of one metal for another in a biometallic molecule. Particular examples might include spin-labels, fluorescent labels, and shift reagents, any of which might yield substantive information about the geometries and mechanistic workings of macromolecules. An especially appealing manifestation of this approach, suggested more than a decade ago by Michael Beer, is the design of heavy metal reagents to bind specifically and quantitatively to one or more (but not all) of the bases of a polynucleotide. The labeled polymer could then be sequenced by electron microscopy, the heavy metal ion serving to improve the contrast. Problems of this kind should have great appeal to inorganic as well as biochemists. At present there is not the vigorous activity in this area that it deserves.

The foregoing brief attempt to define and systematize the activities of bioinorganic chemists is of course highly subjective. Whether such a treatment will prove valid 10 years or even 10 months from now is not important. Of greater interest is that workers in the field have largely discarded parochial attitudes concerning the uniqueness of their approach to problems, and that both biological and inorganic chemists have shown a willingness to learn the techniques and literatures of the other's field. Continued activities of this kind will surely require future efforts to pull together the subject matter in the now firmly established but infant discipline of bioinorganic chemistry.

STEPHEN J. LIPPARD

New York, New York
February 1973

Contents

Subsite-Specific Structures and Reactions in Native and Synthetic (4Fe–4S) Cubane-Type Clusters.....	1
By RICHARD H. HOLM, STEFANO CIURLI, and JOHN A. WEIGEL <i>Department of Chemistry, Harvard University, Cambridge, Massachusetts</i>	
Indoleamine 2,3-Dioxygenase: Properties and Functions of a Superoxide Utilizing Enzyme.....	75
By OSAMU HAYAISHI, OSAMU TAKIKAWA, and RYOTARO YOSHIDA <i>Department of Cell Biology, Osaka Bioscience Institute, Osaka, Japan</i>	
Dinuclear Iron- and Manganese-Oxo Sites in Biology	97
By LAWRENCE QUE, JR., and ANNE E. TRUE <i>Department of Chemistry, University of Minnesota, Minneapolis, Minnesota</i>	
Metal Ion Promoted Reactions of Phosphate Derivatives	201
By PHILIP HENDRY and ALAN M. SARGESON <i>Research School of Chemistry, Australian National University, Canberra, Australia</i>	
Long-Range Electron Transfer in Donor(Spacer)Acceptor Molecules and Proteins	259
By BRUCE E. BOWLER, ADRIENNE L. RAPHAEL, and HARRY B. GRAY <i>Arthur Amos Noyes Laboratory, California Institute of Technology, Pasadena, California</i>	
Mercury(II)–Thiolate Chemistry and the Mechanism of the Heavy Metal Biosensor MerR.....	323
By JEFFREY G. WRIGHT, MICHAEL J. NATAN, FREDERICK M. MACDONNELL, DIANA M. RALSTON, and THOMAS V. O'HALLORAN <i>Department of Chemistry and Department of Biochemistry, Molecular Biology, and Cellular Biology, Northwestern University, Evanston, Illinois</i>	

Probing Nucleic Acids with Transition Metal Complexes.....	413
By ANNA MARIE PYLE and JACQUELINE K. BARTON <i>Department of Chemistry, Columbia University, New York</i>	
Biological Processing of DNA Modified by Platinum Compounds..	477
By SUZANNE L. BRUHN, JEFFREY H. TONEY, and STEPHEN J. LIPPARD <i>Department of Chemistry, Massachusetts Institute of Technology, Cambridge, Massachusetts</i>	
Subject Index.....	517
Cumulative Index, Volumes 1–38.....	525

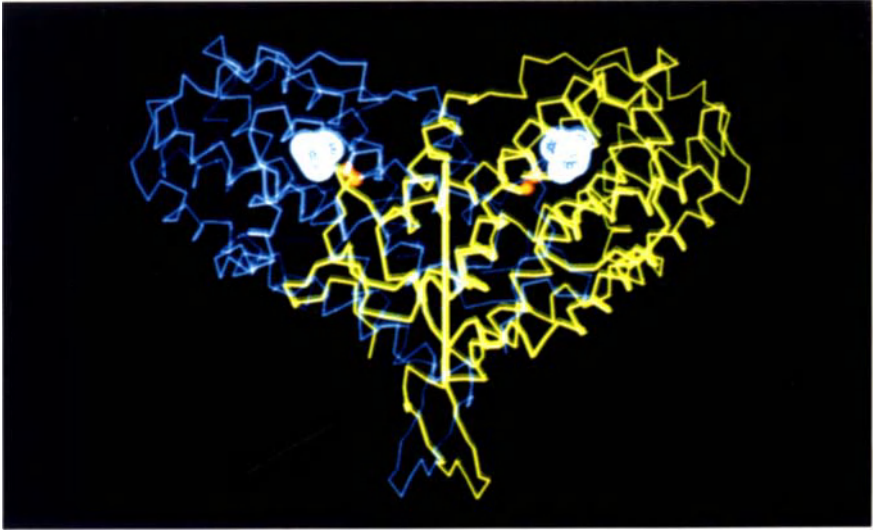


Figure 3 (a) (*Que and True*). Representation of the structure of the B2 subunit of the *E. coli* ribonucleotide reductase.

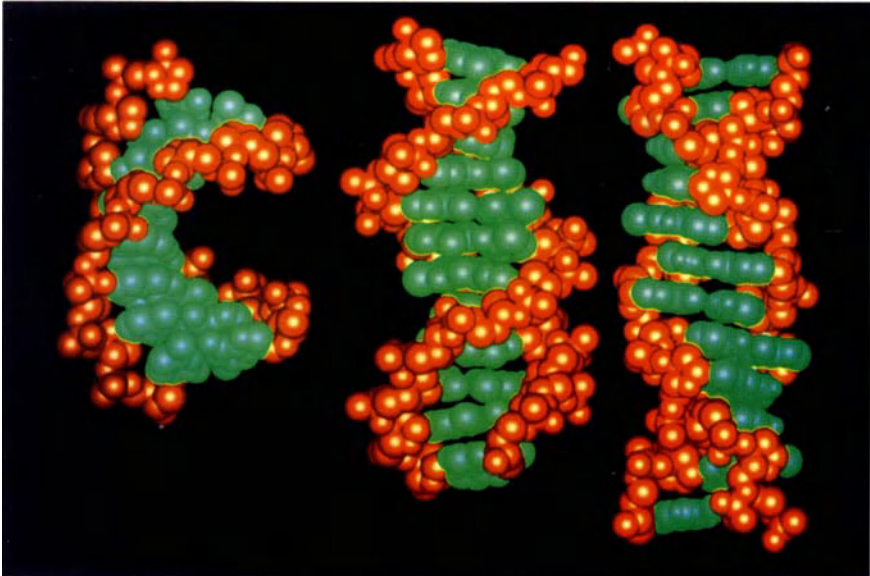


Figure 1 (*Pyle and Barton*). A- (left), B- (center), and Z- (right) DNA. Shown are space-filling models for the different double-stranded DNA helical conformations based upon crystallographic data for each form (1-3). The sugar-phosphate backbone is shown in red and the base pairs, in green. This and subsequent graphical representations were obtained using the program, Macromodel, for which we gratefully acknowledge W. C. Still.

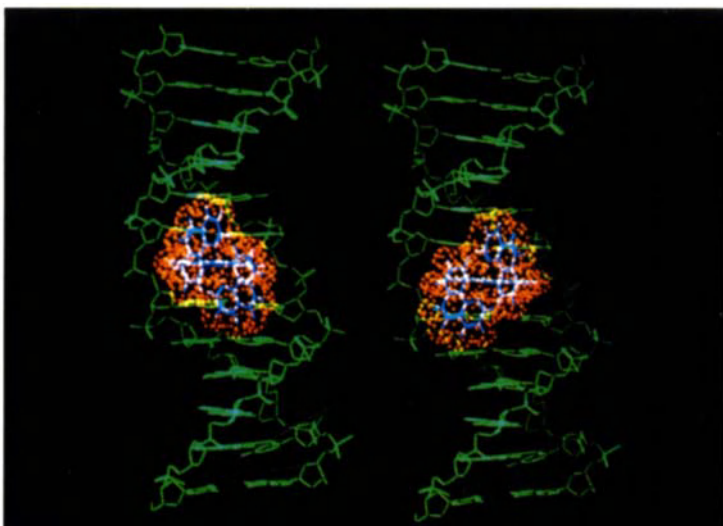


Figure 5 (b) (*Pyle and Barton*). Illustration of $[\text{Ru}(\text{phen})_3]^{2+}$ enantiomers bound by intercalation to B-DNA and the basis for the enantioselectivity (16). The Δ -enantiomer (right) fits easily into the right-handed helix, since the ancillary ligands are oriented along the right-handed groove. For the Λ -isomer (left), in contrast, steric interference is evident between the ancillary phenanthroline ligands and the phosphate backbone, since for this left-handed isomer the ancillary ligands are disposed contrary to the right-handed groove.

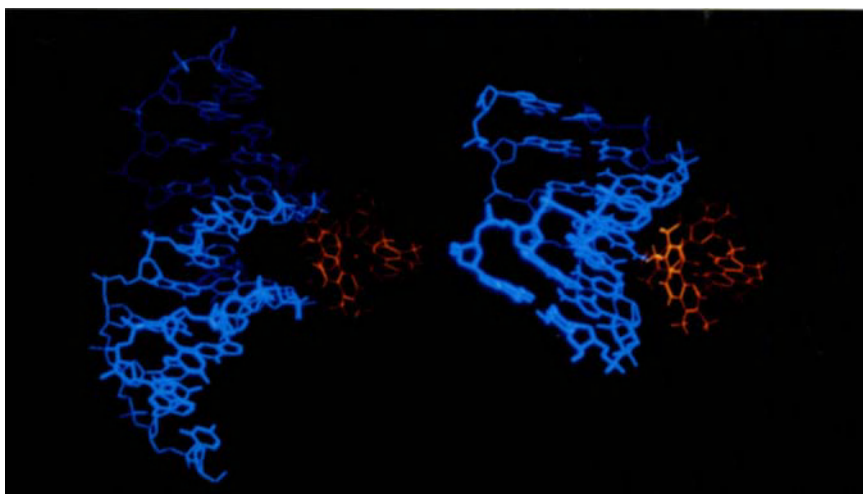


Figure 12 (*Pyle and Barton*). An illustration of the notion behind the design of $[\text{Ru}(\text{TMP})_3]^{2+}$, a probe for the A conformation, based upon shape selection. As is evident, the shape of the complex is well matched to bind against the shallow minor-groove surface of the A conformation (right) but is simply too large to fit snugly into the minor groove of B-DNA (left).

***Progress in
Inorganic Chemistry***

Volume 38

Subsite-Specific Structures and Reactions in Native and Synthetic [4Fe-4S] Cubane-Type Clusters

**RICHARD H. HOLM, STEFANO CIURLI, and
JOHN A. WEIGEL**

*Department of Chemistry
Harvard University
Cambridge, MA*

CONTENTS

I. INTRODUCTION	2
II. CLUSTER ENVIRONMENTS OBTAINED VIA TERMINAL LIGAND SUBSTITUTION	4
A. Mechanism of the Ligand Substitution Reaction	4
B. CysteinyI Peptide Environments	7
C. Macrocyclic Thiolate Environments	10
D. Cyclodextrin Thiolate Ligands	12
E. Aqueous Micellar Solutions	12
F. Inclusion in Non-Fe-S Proteins	14
G. Immobilization on Solid Supports	14
H. Statistical Ligand Substitution	15
III. SUBSITE-SPECIFIC PROPERTIES OF NATIVE CLUSTERS	16
A. Interconversion of [4Fe-4S] and [3Fe-4S] Clusters	17
1. Aconitase	19
2. <i>Desulfovibrio gigas</i> Ferredoxin II	22
B. Structures of [3Fe-4S] Clusters	23
C. Formation of Heterometal Clusters	26
D. Mechanism of Action of Aconitase	27
E. P-Clusters of Nitrogenase	30
F. Active Site of Sulfite Reductase	33
IV. SUBSITE-DIFFERENTIATED SYNTHETIC CLUSTERS	36
A. Synthesis	37
B. Structures	38
1. Solid State	38
2. Solution	41

Progress in Inorganic Chemistry: Bioinorganic Chemistry, Vol. 38, Edited by Stephen J. Lippard.

ISBN 0-471-50397-5 © 1990 John Wiley & Sons, Inc.

C. Substitution Reactions	44
D. Applications	48
1. Bridged Double-Cubane Clusters	48
2. Cluster Linkage to Iron Complexes	53
3. Relative Stabilities of Oxidation States	55
4. Modulation of Electron Distribution and Coupling	59
E. Prospectus	63
ABBREVIATIONS	64
ACKNOWLEDGMENTS	64
REFERENCES	64

I. INTRODUCTION

The past 20 years have witnessed impressive advances in the elucidation of the structures and reactivities of iron-sulfur clusters of both native and synthetic origin. Of the 10 types of structurally characterized Fe-S clusters (1-59) shown schematically in Fig. 1, those of types 1 (6-9), 3 (11-15), and 4 (42-46) are known to occur in proteins. In addition, cluster 2 is present in an unfolded form of the enzyme aconitase (60). The essential structural elements of the [2Fe-2S] site 1 of spinach ferredoxin (Fd) were deduced spectroscopically as early as 1966 (61, 62), and the [4Fe-4S] cubane-type core 4 was determined by crystallographic analysis of the *Chromatium* high-potential (HP) protein in 1972 (63) and in *Peptococcus aerogenes* Fd in 1972 (64). More recently, the voided-cubane structure 3 of the [3Fe-4S] core was proven by crystallography in *Azotobacter vinelandii* Fd I (11-14) and in *Desulfovibrio gigas* Fd II (15), nearly a decade after spectroscopic and chemical evidence indicated its existence.

The synthetic analogue approach towards modeling protein sites by low molecular weight compounds has been successful for sites 1 and 4. Thus, the clusters $[\text{Fe}_2\text{S}_2(\text{SR})_4]^{2-}$ and $[\text{Fe}_4\text{S}_4(\text{SR})_4]^{1-}$ are credible structural and electronic representations of their isoelectronic protein sites, where thiolate ligands simulate cysteinate binding in proteins. The synthesis, structures, and reactivities of these site analogues have been reviewed (1), and the reaction sequences leading to their formation have been determined (65), showing a systematic buildup of final cluster species from compounds of lower nuclearity.

While all Fe subsites in a protein-bound cluster are necessarily inequivalent, recent evidence has demonstrated that this inequivalence is amplified by the occurrence of significant structural and reactivity features at one subsite. These we refer to as subsite-specific properties. The purpose

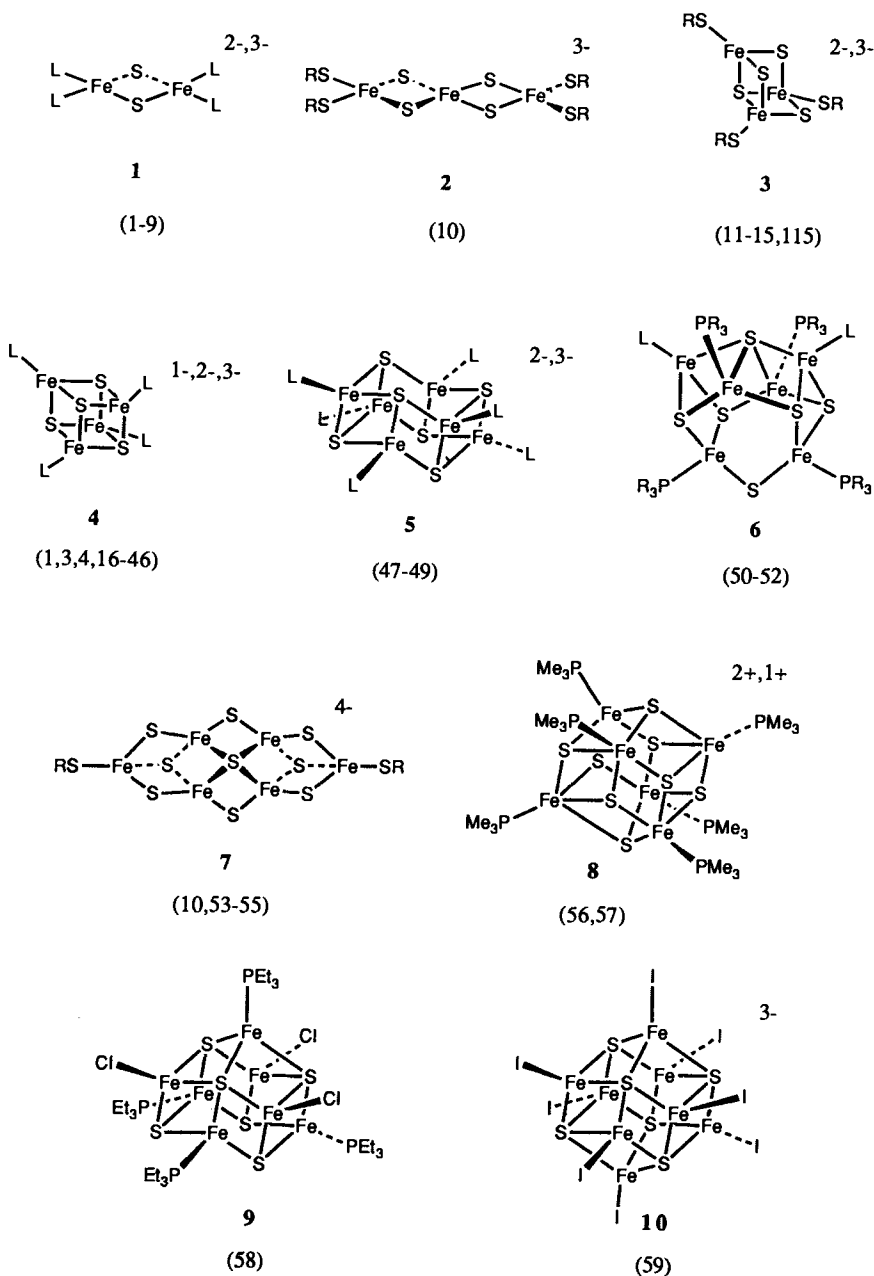


Figure 1. Schematic representation of the structures of Fe-S clusters **1-10** (organometallics excluded). Structure determinations of synthetic and native clusters are referenced (L = RS⁻, RO⁻, halide).

of this chapter is to examine such properties in biological systems and to discuss the development of site analogue clusters that can approach or simulate this subsite specificity. Considerations are restricted to the cubane-type [4Fe-4S] clusters and their derivatives.

II. CLUSTER ENVIRONMENTS OBTAINED VIA TERMINAL LIGAND SUBSTITUTION

The most important reactions of synthetic Fe-S clusters are electron transfer and ligand substitution. The latter reaction forms the basis of the core extrusion method (66), useful for identifying certain clusters present in proteins, and allows the introduction of diverse chemical environments around the Fe-S cluster. We begin our consideration of subsite properties by summarizing the environments thus far achieved synthetically in [4Fe-4S] clusters.

A. Mechanism of the Ligand Substitution Reaction

Thiolate ligand substitution reaction 1 occurs via stepwise, reversible equilibria ($n = 1-4$) and at fixed n has the characteristics of an acid-base reaction. Thus the reaction proceeds to the right when R'SH is a stronger acid than RSH, the conjugate acid of coordinated thiolate. Therefore, arylthiols are more effective than alkylthiols at promoting substitution. Substitution of the first ligand, and presumably others as well, is a bimolecular process, first order in both Fe-S cluster and added thiol (67), and reaction rates parallel thiol acidity. The probable mechanism for this process is shown in Fig. 2. The rate-limiting step is protonation of bound thiolate, followed by rapid separation of alkylthiol from the Fe atom, and coordination of arylthiolate. The same sequence of events (2) was shown to occur for reaction 2.



Reactions can be conveniently monitored by ^1H NMR spectroscopy or UV/vis spectrophotometry, and when conducted in nonaqueous solvents proceed without detectable core degradation. In aqueous solution at neutral and basic pH values, ligand substitution seems to be the first step in hydrolytic core degradation (68, 69). Therefore, when these reactions are carried out in an aprotic solvent, or in an aprotic-aqueous solvent mixture,

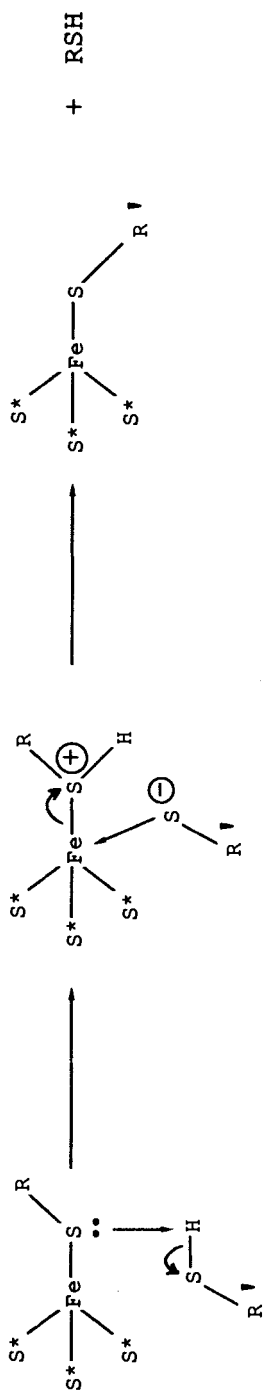


Figure 2. Mechanism of thiolate ligand substitution of $[\text{Fe}_4\text{S}_4(\text{SR})_4]^{2-}$ (67); S^* is core sulfide.

clusters may be obtained that are not necessarily accessible via direct methods (2, 16, 65, 70); that is, from an iron salt, a sulfide source, and thiolate. Ethanethiolate or *t*-butylthiolate are particularly good precursor ligands for a substitution reaction because the volatile thiol released after reaction may be removed *in vacuo*, thus driving the reaction to completion.

Reaction 3 is a general example of a ligand substitution reaction with an electrophile, EL (71, 72). Acids, acyl halides, and anhydrides have been shown to undergo Reaction 3, generating substitution products in solution. Reactions with the latter two



reagents are stepwise and irreversible. Isolation of the product upon reaction with a small excess of RCOX has led to characterization of the tetrahalide derivatives, $[\text{Fe}_n\text{S}_n\text{X}_4]^{2-}$ ($n = 2, 4$) (3, 71).

Clusters with the general formula $[\text{Fe}_4\text{S}_4\text{L}_4]^{2-}$ have been isolated with a wide variety of ligands. Alkylthiolates ranging in size from methyl (16) to adamantyl (73) have been reported, as has the "parent" cluster $[\text{Fe}_4\text{S}_4(\text{SH})_4]^{2-}$ (30). Arylthiolate ligands with sterically bulky side groups have facilitated isolation of the first high-potential Fe-S protein analogues containing the $[4\text{Fe}-4\text{S}]^{3+}$ core (34, 74). Clusters containing aryloxy ligands, $[\text{Fe}_4\text{S}_4(\text{OPh})_4]^{2-}$ and $[\text{Fe}_4\text{S}_4(\text{OC}_6\text{H}_4\text{-}i\text{p}\text{-Me})_4]^{2-}$, have been isolated and the former has been subjected to a structural analysis (21). Clusters fully ligated with methyl-L-serinate, methyl-L-tyrosinate, and methyl-L-prolinate have been claimed very recently (75), but have not yet been substantiated by a structure determination.

On the basis of structural and electronic similarities, the clusters $[\text{Fe}_4\text{S}_4(\text{SR})_4]^{2-}$ serve as close representations of protein sites with the iso-electronic $[4\text{Fe}-4\text{S}]^{2+.1+}$ core. Because the proteins function as electron carriers (where their function is known), the redox chemistry of synthetic clusters has been a matter of considerable interest. As seen in Fig. 3, the analogue electron-transfer series encompasses four core oxidation levels, three of which have been detected in proteins. Analogues corresponding to these three levels have been isolated and characterized in very considerable detail. The $[4\text{Fe}-4\text{S}]^{2+.1+}$ or $\text{Fd}_{\text{ox/red}}$ redox couple is one of the more pervasive in biology. Note that the native $[4\text{Fe}-4\text{S}]^{3+}$ state has been proven only in the HP proteins, which should be considered as a special class of ferredoxins. Synthetic cluster potentials, which are strongly dependent on the R substituent, have been found to be $\sim 0.2\text{--}0.6$ V more negative than the E'_0 values for $\text{Fd}_{\text{ox/red}}$ in aqueous solution (76, 77).

ELECTRON TRANSFER SERIES OF [4Fe-4S] CLUSTERS

	[4Fe-4S] ⁰	[4Fe-4S] ¹⁺	[4Fe-4S] ²⁺	[4Fe-4S] ³⁺
	4Fe(II)	3Fe(II) + Fe(III)	2Fe(II) + 2Fe(III)	Fe(II) + 3Fe(III)
proteins:	--	Fd _{red}	$\frac{-0.3 \text{ to}}{-0.5 \text{ V}}$ Fd _{ox} /HP _{red}	$\frac{+0.1 \text{ to}}{+0.3 \text{ V}}$ HP _{ox}
analogues:	[Fe ₄ S ₄ (SR) ₄] ⁴⁻	≡ *[Fe ₄ S ₄ (SR) ₄] ³⁻	≡ *[Fe ₄ S ₄ (SR) ₄] ²⁻	≡ *[Fe ₄ S ₄ (SR) ₄] ¹⁻

Fe = ferredoxin. HP = "high-potential" protein. *Isolated.

Figure 3. The electron-transfer series of [4Fe-4S] clusters as found with proteins and synthetic analogues. Approximate ranges of protein potentials E'_0 (vs. NHE) are given.

B. CysteinyI Peptide Environments

In order to assess the effects of peptide structure around the [4Fe-4S]^{2+,1+} core with respect to the observed positive potential shifts in proteins, several oligopeptides containing cysteinyl units have been synthesized and allowed to react with [Fe₄S₄(S-*t*-Bu)₄]²⁻, forming peptide complexes via ligand substitution.

In the initial work on peptide incorporation around [4Fe-4S] cores, peptides based on the sequence Cys-Gly-Gly-Cys were synthesized and allowed to react with [Fe₄S₄(S-*t*-Bu)₄]²⁻ in Me₂SO solutions (78). Reactions are summarized in Fig. 4. Those peptides containing more than one Cys residue are depicted as reacting with only one [4Fe-4S]²⁺ cluster, to form species 12-14. It was recognized that the peptides might bridge different clusters, however, a possibility difficult to distinguish by spectroscopic methods from single-cluster binding. Contact-shifted β-CH₂ cysteinyl resonances at 12-15 ppm fall within the range observed for Fd_{ox}. The redox potentials in 80% Me₂SO-H₂O solution (v/v) more closely resemble those of the proteins, but are still more negative by ~0.3 V. Similar complexes based on the peptide sequence Ac-Gly₂-(Cys-Gly)_{*n*}-Cys-Gly₂-NH₂ (*n* = 0-3) were synthesized independently (79). Significantly, the successive equilibrium constants for formation of [Fe₄S₄(Ac-Gly₂-Cys-Gly₂-NH₂)₄]²⁻ approached statistical values (see below).

It has been proposed that the reversible reducibility of the [4Fe-4S]²⁺ cluster in *P. aerogenes* Fd_{ox} vs. the nonreducibility of the isoelectronic cluster in *Chromatium* HP_{red} originates mainly in peptide-cluster hydrogen bonding (80). There are significantly more N-H...S hydrogen bonds in Fd_{ox}, shown schematically in Fig. 5, suggesting that it is better adapted to

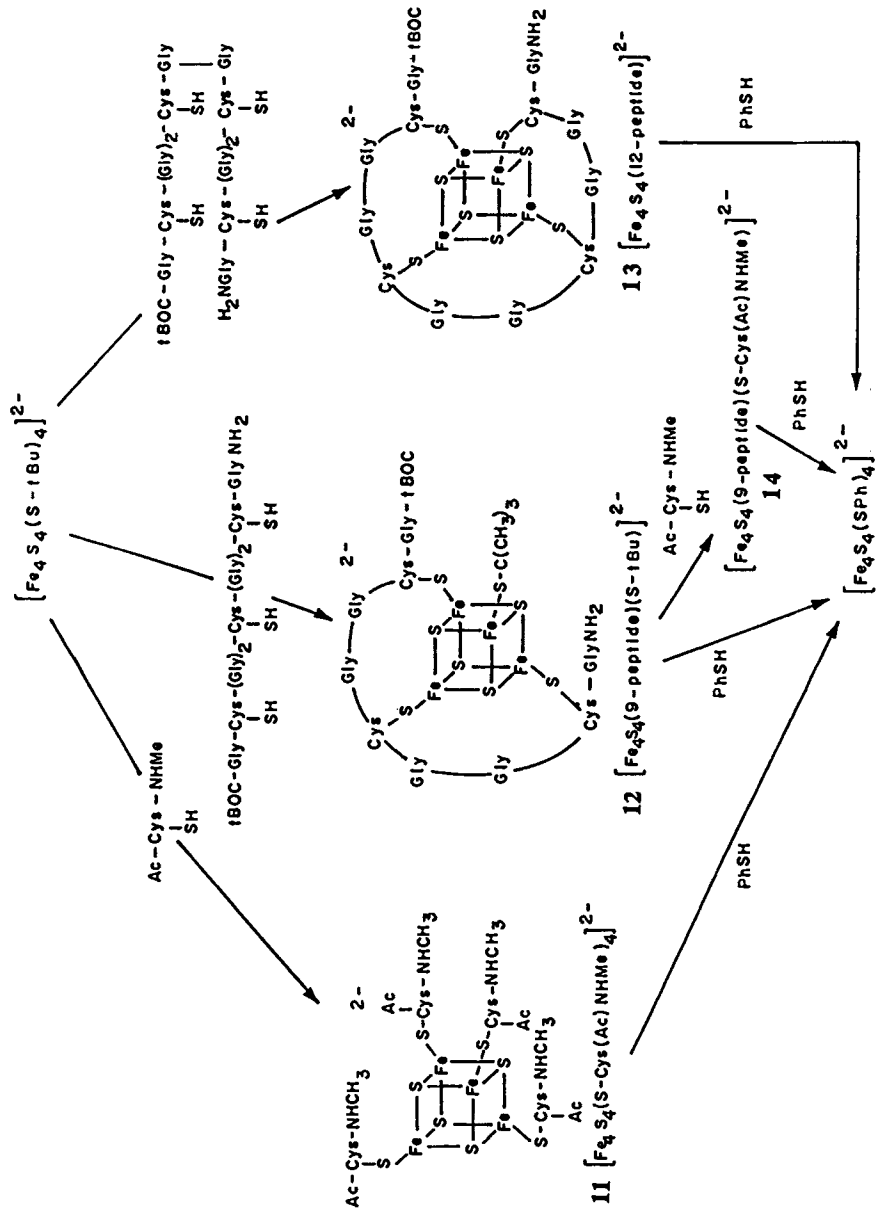


Figure 4. Depiction of ligand substitution reactions of $[\text{Fe}_4\text{S}_4(\text{S}-t\text{Bu})_4]^{2-}$ with cysteinyl peptides to yield peptide clusters **11-14** and their conversion to $[\text{Fe}_4\text{S}_4(\text{SPh})_4]^{2-}$ in Me_2SO solution (**78**).

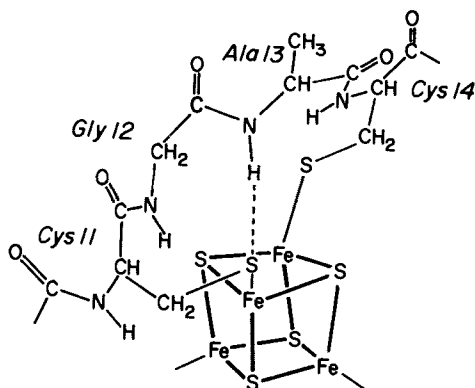


Figure 5. Structure of the peptide fragment Cys-Gly-Ala around the active site of *P. aerogenes* Fd, illustrated on the basis of the X-ray analysis of Adman et al. (80) and depicting the hydrogen bonding between N-H of Ala-13 and S of Cys-11 (adapted from Ref. 81).

stabilize the increased local negative charge of the cluster upon reduction, compared to the situation in the HP protein. The effect is one of producing a less negative reduction potential. As one test of this hypothesis, the compounds $[\text{Fe}_4\text{S}_4(\text{Z-Cys-Gly-Ala-OMe})_4]^{2-}$ (**15**), and $[\text{Fe}_4\text{S}_4(\text{Z-Cys-Gly-OMe})_4]^{2-}$ (**16**), ($\text{Z} = \text{PhCH}_2\text{OCO}$) were synthesized (81). Cluster **15** should favor $\text{N-H} \cdots \text{S}$ hydrogen bonding as in the protein, whereas **16** is not able to form an intramolecular hydrogen bond. Examination of the temperature dependence of the 2-,3- redox potential in dichloromethane and DMF solutions yielded the following results. A small positive shift of $E_{1/2}$ for **15** in dichloromethane occurred as the temperature was lowered. No temperature dependence was observed for **16**, nor for either compound in DMF. The results were interpreted in terms of $\text{N-H} \cdots \text{S}$ hydrogen-bond formation in **15**, which becomes more pronounced as the temperature is lowered owing to loss of conformational degrees of freedom in the peptide. The effect is observed only in a solvent of low dielectric constant, namely, dichloromethane, because DMF interferes by forming hydrogen bonds to the peptide. The redox potential becomes more positive in dichloromethane owing to the lowering of the electron density at the sulfur atom by the $\text{N-H} \cdots \text{S}$ interaction, and the attendant stabilization of the more reduced core oxidation level.

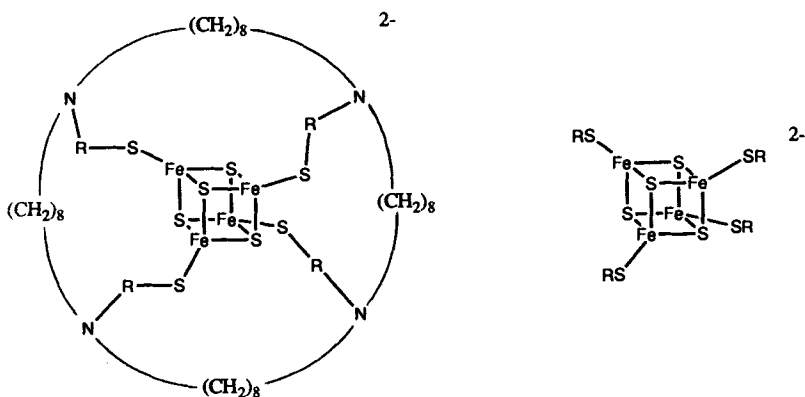
The same temperature-dependent redox potential behavior was found for $[\text{Fe}_4\text{S}_4(\text{Z-Cys-Gly-Ala-Cys-OMe})_2]^{2-}$ (**17**) in dichloromethane, but was not observed for $[\text{Fe}_4\text{S}_4(\text{Z-Cys-Ile-Ala-Cys-OMe})_2]^{2-}$ (**18**) (82). Evidently, the presence of a Cys-Gly residue is conducive to hydrogen-bond formation, whereas the sterically bulky Ile residue inhibits its formation.

The complex $[\text{Fe}_4\text{S}_4(\text{Z-Cys-Ile-Ala-Cys-OMe})_2]^{2-}$ was prepared and shows a quasireversible 2-,1- redox couple at +0.12 V (vs. SCE) in DMF (83). The hydrophobic nature of the peptide backbone is similar to that found in the HP protein (84), for which this cluster serves as a crude active site model.

Finally, the cluster $[\text{Fe}_4\text{S}_4(\text{Z-Cys-Gly-Cys-NH}_2)_2]^{2-}$ has been generated in solution and studied by NMR spectroscopy (85). Spectral evidence suggests binding of the tripeptide to one core. A similar conclusion for the tetrapeptide complexes **17** and **18** was drawn from circular dichroism (CD) spectra (82).

C. Macrocyclic Thiolate Environments

The factors governing the unique stability of the $[\text{4Fe-4S}]^{3+}$ core in HP proteins are of much interest but are not well understood. Current ideas include a relatively hydrophobic environment of low dielectric constant, possibly favoring the generation of a cluster with a lower overall charge from one with a higher charge. Moreover, a buried position in the protein structure which, with tight packing of hydrophobic residues around the electrophilic HP_{ox} core, would protect it from the attack of nucleophiles. As one means of increasing the hydrophobicity around Fe-S clusters in



19 R = *p*-C₆H₄C(O)-

20 R = *p*-CH₂C₆H₄C(O)-

21 R = CMe₂CH₂C(O)-

22 R = Ph

23 R = CH₂Ph

24 R = *t*-Bu

Figure 6. Depiction of macrocyclic Fe-S clusters **19-21** and their relatives **22-24** with non-cyclic ligands.

model compounds, thereby facilitating study of its effect on redox stability, cyclophane-type macrocycles were synthesized and ligated to the $[4\text{Fe-4S}]^{2+}$ core by substitution reactions (86, 87). The macrocycles contain four thiol functionalities per molecule and, when allowed to react with $[\text{Fe}_4\text{S}_4(\text{S-}t\text{-Bu})_4]^{2-}$ in DMF, afforded the complexes **19–21**, shown schematically in Fig. 6, as black powders. Although the $[4\text{Fe-4S}]^{2+}$ cores of **19–21** are depicted as complexes of a single tetradentate macrocyclic ligand, there is no compelling evidence supporting this description. The nonrigid nature of these ligands does not preclude bridging of $[4\text{Fe-4S}]$ clusters and formation of oligomers.

Comparison of the redox chemistry in Me_2SO of **19–21** with their non-macrocyclic counterparts **22–24** is provided in Table I. Cyclic voltammetric studies demonstrated that clusters **19** and **20** can be oxidized and reduced by one electron in chemically reversible processes. The potentials for the 2-,3- and 3-,4- steps of **19** and **20** are shifted to more positive values when compared with the corresponding clusters **22** and **23**. Cluster **21**, which

TABLE I
Redox Potentials of $[4\text{Fe-4S}]$ Clusters in Me_2SO

Cluster	$E_{1/2}$ (V) ^a		
	1-, 2-	2-, 3- ($E_{p,c} - E_{p,a}$) (mV)	3-, 4-
19	-0.36 (36)	-0.85 ^b (48)	-1.64 (50)
22		-0.92 ^b (74)	-1.70 (134)
20	-0.35 (70)	-1.12 ^b (20)	-1.86 (30)
23		-1.14 ^b (70)	
21	+0.25 (180)	-1.13 ^b (60)	
24	-0.11 (46)	-1.40 ^b (70)	
26		-0.54 ^c -0.90 ^d	
27		-0.51 ^c -0.89 ^d	
28		-1.06 ^c	

^aPotentials versus SCE

^bSolvent, Me_2SO .

^cSolvent, 10 mM phosphate buffer, pH 7.0.

^dSolvent, DMF.

^eSolvent, 5% aqueous DMF.

contains both hydrophobic and sterically bulky ligands, showed the greatest positive shift for the 1-,2- and 2-,3- cycles, 360 and 270 mV, respectively. These results suggest that a hydrophobic ligand environment does have a stabilizing effect on the oxidized core, possibly by providing steric shielding from attack by solvent at the cluster. Stability studies on exposure to dioxygen also indicated slower rates of decomposition of the macrocyclic clusters as compared to **22–24**.

D. Cyclodextrin Thiolate Ligands

Reaction of $[\text{Fe}_4\text{S}_4(\text{S}-t\text{-Bu})_4]^{2-}$ with the cyclodextrin dithiol **25** in DMF solution provided the cyclodextrin-modified cluster **26**. Clusters **27** and **28** were prepared from cyclodextrin monothiols. All clusters were obtained as water-soluble black powders (88, 89). The clusters are shown schematically in Fig. 7. The proposed structure of **26** is supported by light-scattering molecular weight measurements, indicating the absence of oligomeric compounds in solution. Apparently the thiol functionalities in **25** are held in sufficiently close proximity to facilitate binding to a single $[\text{4Fe-4S}]$ core. The reduction potentials of complexes **26** and **27**, given in Table I, undergo a positive shift of ~ 400 mV on changing the solvent from DMF to water (89), a result observed earlier in other systems (77). The complexes show enhanced stability towards hydrolytic degradation in aqueous solution, with half-lives at pH 7.0 of greater than 120 (**26**) and 70 (**27**) h, respectively. For comparison, the half-life of $[\text{Fe}_4\text{S}_4(\text{S}-\text{C}_6\text{H}_4\text{-}m\text{-SMe})_4]^{2-}$ in 5% aqueous DMF is only 5.6 h (89). This stability may be attributed to steric shielding of the cluster by the cyclodextrins, thus inhibiting hydrolysis. The 2-,3-reduction of **28** in 5% aqueous DMF occurs at -1.06 V, and represents a shift of $+240$ mV compared with $[\text{Fe}_4\text{S}_4(\text{S}-t\text{-Bu})_4]^{2-}$ in the same solvent. Part of this shift presumably arises from an alkyl substituent effect inasmuch as the $[\text{Fe}_4\text{S}_4(\text{S}-t\text{-Bu})_4]^{2-}$ and $[\text{Fe}_4\text{S}_4(\text{SEt})_4]^{2-}$ potentials differ by 90 mV in DMF (76). The remainder may be largely due to the electron-withdrawing nature of the hydroxyl groups in the cyclodextrin and differing extents of solvation.

E. Aqueous Micellar Solutions

In this approach, developed by Tanaka et al. (90, 91), $n\text{-Bu}_4\text{N}^+$ salts of the clusters $[\text{Fe}_4\text{S}_4(\text{SC}_6\text{H}_4\text{-}p\text{-R})_4]^{2-}$ with strongly hydrophobic substituents (e.g., $\text{R} = n\text{-C}_8\text{H}_{17}$) in Me_2SO or DMF solutions were added to buffered aqueous solutions containing micellar reagents such as Triton X-100 or dodecyltrimethylammonium chloride. The cluster resides in a partially aqueous environment in the hydrophobic interior of the micelle. Potentials are shifted ~ 400 mV in the positive direction when compared to the values

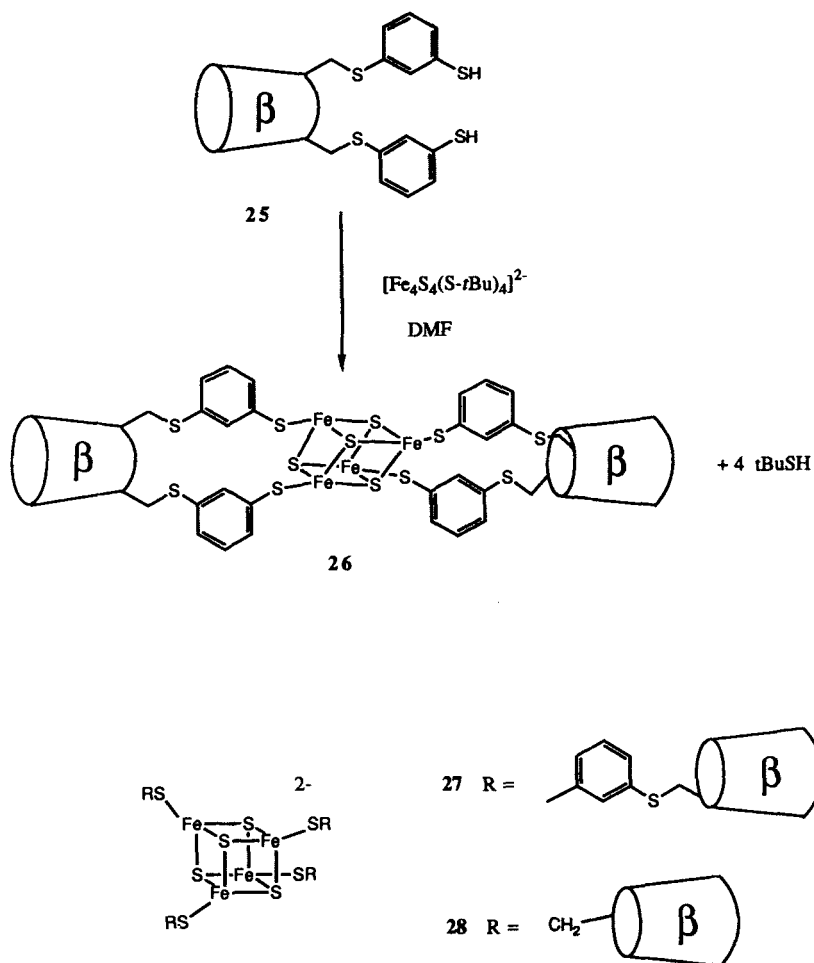
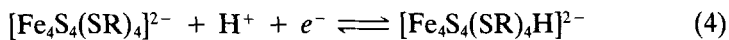


Figure 7. Schematic formulas of cyclodextrin dithiol ligand **25** and cyclodextrin thiolate clusters **26–28**.

in Me_2SO , again emphasizing the stabilization of the $[\text{4Fe-4S}]^{1+}$ state in a hydrogen-bonding medium. Up to pH 9, potentials exhibit a pH dependence consistent with the proton-linked reaction 4. In more alkaline



solutions, potentials are nearly independent of pH. For the clusters, the apparent $\text{p}K_a = 8.6\text{--}9.4$. Similar behavior has been observed for clusters

solubilized in a lecithin membrane, except that the potential becomes pH-independent above 10.5 (92). In these systems the site of protonation is not known (although thiolate is presumably the most basic site) nor has it been established that the clusters retain four thiolate–thiol ligands over the entire pH range of measurement. As shown by several further examples (93, 94), micellar solutions should find utility as a means of solubilizing and stabilizing clusters and examining reactivity in an aqueous medium.

F. Inclusion into Non-Fe–S Proteins

Artificial Fe–S proteins have been obtained via ligand exchange of the water-soluble cluster $[\text{Fe}_4\text{S}_4(\text{SCH}_2\text{CH}_2\text{CO}_2)_4]^{6-}$ (69) with bovine serum albumin (BSA) and bovine insulin (BI) (95). Upon reduction of disulfide linkages by thiolate buffer, the proteins BSA and BI contain thiol groups that can participate in ligand substitution in aqueous solution. The inclusion of $[\text{4Fe–4S}]^{2+}$ cores in these proteins was monitored by changes in the visible absorption and CD spectra.

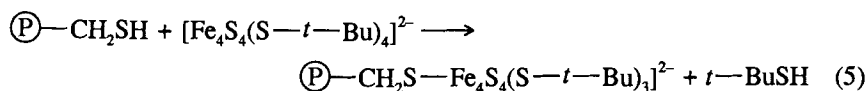
The proteins stabilize the Fe–S clusters towards aerial oxidation as monitored by following the loss of absorbance in the region 405–415 nm. Anodic shifts of the 2-,3- quasireversible reduction waves in water of +170 and +200 mV were detected for the BSA- and BI-bound clusters, as compared to the potential of $[\text{Fe}_4\text{S}_4(\text{SCH}_2\text{CH}_2\text{CO}_2)_4]^{6-}$. The potentials of the artificial proteins, –0.53 and –0.50 V for BSA and BI, respectively, are in the same range but ~70–100 mV more negative than those seen for conventional $\text{Fd}_{\text{ox/red}}$ couples in aqueous solution. These results suggest a roughly similar local protein environment for the synthetic and native systems.

A reaction system consisting of a Fe(II) salt, BSA, Na_2S , and 2-mercaptoethanol afforded a dark brown solution whose absorption spectrum (λ_{max} 420 nm) had the appearance of a $[\text{4Fe–4S}]^{2+}$ cluster (96). Formation of additional BSA-bound Fe–S species cannot be discounted, however. The albumin-cluster protein showed weak hydrogenase activity in the form of dihydrogen evolution in the presence of reduced methyl viologen (96). The protein was not further characterized.

G. Immobilization on Solid Supports

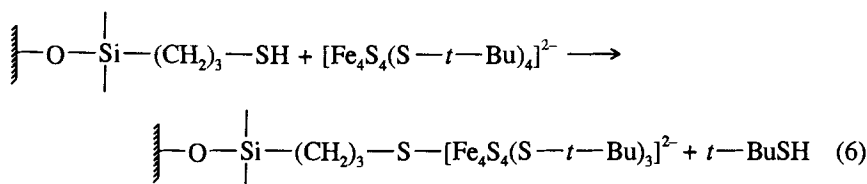
Synthetic Fe–S clusters have been immobilized on several types of solid supports. One impetus behind immobilization has been to mimic more closely the reactivity of native clusters by embedding them in a matrix that simulates steric shielding of the cluster by a peptide.

The [4Fe-4S]²⁺ core has been attached to suitably modified poly(styrene-divinylbenzene) supports (97, 98) via Reaction 5. Oxidation of one such



immobilized cluster by ferricyanide with hope of stabilizing the [3Fe-4S]¹⁺ core afforded no EPR signal assignable to such a species (98).

Iron-sulfur clusters have been attached to wide pore silica gel (99), to a modified tin electrode (100) in Reaction 6, and to a glassy carbon or

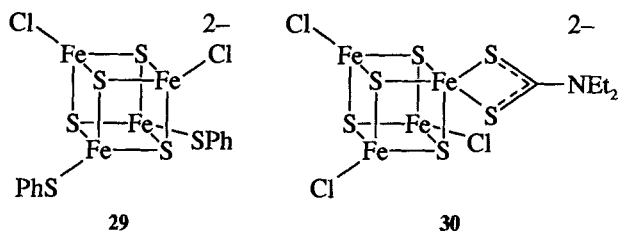


platinum electrode by incorporation in ion exchange polymers based on *N*-substituted polypyrroles (101). The first of these systems showed no catalytic activity for the hydrogenation of carbon monoxide, ethylene, propylene, 1,3-butadiene, or acetylene at 25–250 °C. The [Fe₄S₄(SPh)₄]²⁻³⁻ potential was shifted ~180 mV positive relative to the solution value when associated with the ion exchange polymer. The probable cause of this appreciable effect is differential stabilization of the reduced cluster by nearby cationic groups of the polymer. The potential of the [Fe(CN)₆]³⁻⁴⁻ couple is comparably shifted.

H. Statistical Ligand Substitution

None of the ligand environments discussed in the previous sections has afforded isolation of a subsite-differentiated [4Fe-4S] cluster. The complex [Fe₄S₄(9-peptide)(S-*t*-Bu)]²⁻ (**13**, Fig. 4) exhibits the correct ratio of peptide to *t*-butylthiolate by integration of the ¹H NMR resonances (78), and therefore meets our criterion for a subsite-differentiated compound. Cluster **13** was not isolated, however, and a structure determination was not performed.

The main barrier to isolation of a mixed-ligand cluster is its substitutional lability, which can lead to statistical disproportionation. Thus, site-differentiated clusters **29** and **30**, which have been trapped as sparingly soluble Ph₄P⁺ salts and structurally characterized in the solid state (102, 103),



disproportionate in solution to essentially statistical mixtures. Statistical ligand substitution in other cases has been substantiated by several lines of evidence. The stepwise addition of *p*-tolylthiol to a solution of $[\text{Fe}_4\text{S}_4(\text{S}-t\text{-Bu})_4]^{2-}$ has been followed by ^1H NMR spectroscopy (17). Successive additions of one equivalent of thiol produced spectra containing isotropically shifted resonances corresponding to all species in the series $[\text{Fe}_4\text{S}_4(\text{S}-t\text{-Bu})_{4-n}(\text{S}-p\text{-tol})_n]^{2-}$ ($n = 0-4$). By integration of the *p*-Me and *t*-Bu resonances, ratios of the equilibrium constants for formation of intermediate cluster species were determined and found to approach statistical values. Reaction of electrophiles with $[\text{Fe}_4\text{S}_4(\text{SR})_4]^{2-}$ shows statistical product formation, and mixtures of $[\text{Fe}_4\text{S}_4(\text{SR})_{4-n}\text{L}_n]^{2-}$ were observed by differential pulse polarography and ^1H NMR spectroscopy (72). Substitution of terminal thiolate ligands by Cl^- or OAc^- caused successive shifts in the 2-, 3- potentials by ~ 100 mV/equivalent, indicating a nearly linear dependence of potential on n . It is not surprising that the terminal ligands react independently, given that they are separated by 6–7 Å around a nearly dimensionally isotropic cluster core. Lastly, as we have already noted, the successive formation constants for the substitution of Ac-Gly₂-Cys-Gly₂-NH₂, terminating in the formation of the fully substituted cluster, approach statistical values (79).

The problem of performing site-specific chemistry at one iron site in a [4Fe–4S] cluster requires interrelating the reactivity of three of the iron atoms such that the fourth site can react independently. This relationship has been achieved by the synthesis of a semirigid tridentate thiolate ligand that readily binds several types of cubane clusters. The details of the synthesis and reactivity of site-differentiated clusters will be provided in Section IV. We next turn to the topic of subsite-specific properties observed in biological systems.

III. SUBSITE-SPECIFIC PROPERTIES OF NATIVE CLUSTERS

Because of protein structure, all subsites of any native [4Fe–4S] cluster are inequivalent. This inequivalence is most easily sensed by ^1H NMR

spectroscopy, commencing with the ground-breaking work of Phillips and co-workers (104) on the spectra of proteins containing [2Fe-2S] and [4Fe-4S] clusters. Thereafter, multiple α -CH and β -CH₂ resonances from cysteinyl residues in a wide variety of [4Fe-4S] proteins were detected (105-109). This method is sensitive to aspects of protein structure and environment extrinsic to the cluster, the differences of which are amplified by the isotropic (paramagnetic) contribution to the chemical shifts. Note that all native cluster states in the series of Fig. 3 are paramagnetic.

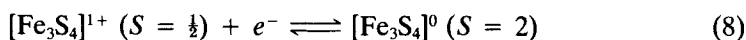
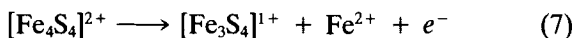
Odd- and even-electron clusters have ground states with $S \geq \frac{1}{2}$ and $S = 0$, respectively, and higher spin states that are thermally occupied. Protein effects propagated to the Fe subsites are presumably largely if not completely responsible for subsite inequivalence. This statement rests on structural determinations of [4Fe-4S]²⁺ analogue clusters, the core configurations of which without exception closely approach tetragonal (D_{2d}) symmetry. Thus there appears to be no intrinsic inequivalence in subsites. The situation for [4Fe-4S]¹⁺ analogue clusters is somewhat more complicated because they do not adopt a uniform core configuration (40). All these configurations, however, approach idealized symmetries in which all four subsites are equivalent. The nature of individual subsites is best investigated by ⁵⁷Fe Mössbauer spectroscopy (110-113). Most spectra have been interpreted in terms of two or four quadrupole doublets with the same or slightly different isomer shifts and distinctly different quadrupole splittings. We examine below, and restrict attention to, the leading examples of subsite-specific aspects of native [4Fe-4S] clusters. These aspects are evidenced in structural, reactivity, and/or Mössbauer spectroscopic properties. Broader descriptions of the proteins and enzymes in question may be found in the references cited.

A. Interconversion of [4Fe-4S] and [3Fe-4S] Clusters

One of the most significant discoveries in Fe-S biochemistry in the last decade has been that of [3Fe-4S] clusters. Beinert and Thomson (114) have summarized the early work leading to the recognition of these clusters. This work has culminated in the proof by protein crystallography of the voided-cubane structure **3** (Fig. 1) for clusters in *Azotobacter vinelandii* (Av) Fd I (which also contains one [4Fe-4S] cluster) (11, 13, 14), *Desulfovibrio gigas* (Dg) Fd II (12, 15), and aconitase from pig heart (115). In these clusters, Fe-Fe separations occur in the range 2.64-2.77 Å. As will be seen, aconitase and Dg Fd II assume particular significance in the context of site-specific properties.

The formal stoichiometry for the oxidative removal of an Fe atom from a [4Fe-4S]²⁺ cluster is represented by Reaction 7. It was initially thought

that EPR signals near $g \approx 2$ observed in Fd preparations carried out aerobically resulted from a "superoxidized" cluster state isoelectronic with HP_{ox} , which does have a signal in this region. Subsequent spectroscopic studies disproved any relationship between a [4Fe-4S] cluster and these EPR signals (114). Chemical analysis established the atom ratio 3Fe:4S (sulfide) (116-118). Also, reduction of the cluster produced in Reaction 7 demonstrated the existence of the reduced cluster in Reaction 8. Cluster ground spin states have been firmly established by magnetization measurements (119).



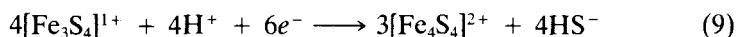
Trinuclear clusters have been detected in over 20 proteins as well as a number of enzymes, among them aconitase, beef heart succinate-ubiquinone oxidoreductase (120), *Escherichia coli* nitrate reductase (121), *E. coli* fumarate reductase (122), and succinate dehydrogenase (123). Selected instances of the occurrence of [3Fe-4S] clusters are listed in Table II. Because of the paramagnetic ground states of both oxidation levels, these clusters can be uniquely identified by a number of spectroscopic techniques. Among these, Mössbauer spectroscopy in applied magnetic fields (124, 128, 132, 141-143) and low temperature MCD spectroscopy (127, 138, 144-146) are decisive. While there are small spectroscopic differences among certain [3Fe-4S] centers, the similarities dominate and support the essential structure **3** for all. In a number of the earlier papers on protein

TABLE II
Cluster Conversion Reactions

Protein		References
	$[3\text{Fe}-4\text{S}] \rightleftharpoons [4\text{Fe}-4\text{S}]$	
Aconitase (beef heart)		116, 124-130
<i>Desulfovibrio gigas</i> Fd II		131-133
	$[3\text{Fe}-4\text{S}] \longrightarrow [4\text{Fe}-4\text{S}]$	
<i>Azotobacter vinelandii</i> Fd I		134
<i>Thermodesulfobacterium commune</i> Fd		135
	$[4\text{Fe}-4\text{S}] \longrightarrow [3\text{Fe}-4\text{S}]$	
<i>Bacillus stearothermophilus</i> Fd		136, 137
<i>Clostridium pasteurianum</i> Fd		138, 139
<i>Mycobacterium smegmatis</i> Fd		140
<i>Pseudomonas ovalis</i> Fd		140
<i>Thermus thermophilus</i> Fd		140

3-Fe sites, the clusters were written as [3Fe-3S] or [3Fe-*x*S]. There is now reason to believe that all such clusters are properly described as [3Fe-4S].

Summarized in Table II are examples of cluster conversion reactions. Those and others resulting in the formation of [3Fe-4S] from [4Fe-4S] were effected by aerial oxidation or by treating the proteins with a chemical oxidant, usually ferricyanide. In several instances of the conversion [3Fe-4S] \longrightarrow [4Fe-4S], dithionite, but no iron source, was added. Formation of the tetranuclear cluster must have utilized adventitious iron or proceeded by a "cannibalization" process with the formal stoichiometry of Reaction 9.



More pertinent in the present context are those proteins that support cluster *interconversion* reactions, whereby the initial cluster type is recovered. In this way it is possible to determine if the Fe atom added in the [3Fe-4S] \longrightarrow [4Fe-4S] conversion is removed in the reverse reaction. In defining a subsite in terms of its position in the protein structure, this type of process is subsite-specific if the same atom is added and removed, and the vacant subsite of the [3Fe-4S] cluster does not migrate during cluster conversion. An equivalent statement, under the same requirement for specificity, is that the [4Fe-4S] subsite voided in the formation of [3Fe-4S] is reoccupied upon reconstitution of the initial cluster. Observations relevant to this matter have been made mainly with two proteins, aconitase from beef heart and *Dg Fd II*, in the notable experiments of Beinert, Münck, and their co-workers.

1. Aconitase

The beef heart enzyme ($M_r \approx 80,000$) (117) is a component of the citric acid cycle. Its active form contains one [4Fe-4S] cluster. Although such a cluster is normally associated with electron transfer, the enzyme catalyzes the nonredox reaction of citrate-isocitrate interconversion via a dehydration-hydration pathway. The current state of understanding of cluster structures and reactions of beef heart aconitase has been thoroughly reviewed by Emptage (130). When isolated aerobically, aconitase is inactive and contains one [3Fe-4S] cluster. Upon incubation of the reduced protein with Fe(II), the fully active enzyme is generated. When a 3-Fe center is reduced to [3Fe-4S]⁰, Reaction 10 builds a 4-Fe cluster in a nonredox process. The Mössbauer spectra in Fig. 8 address the question of subsite specificity in this reaction of aconitase (124). If the externally supplied iron is ⁵⁶Fe²⁺, the resultant spectrum reveals the intrinsic (original) Fe atoms

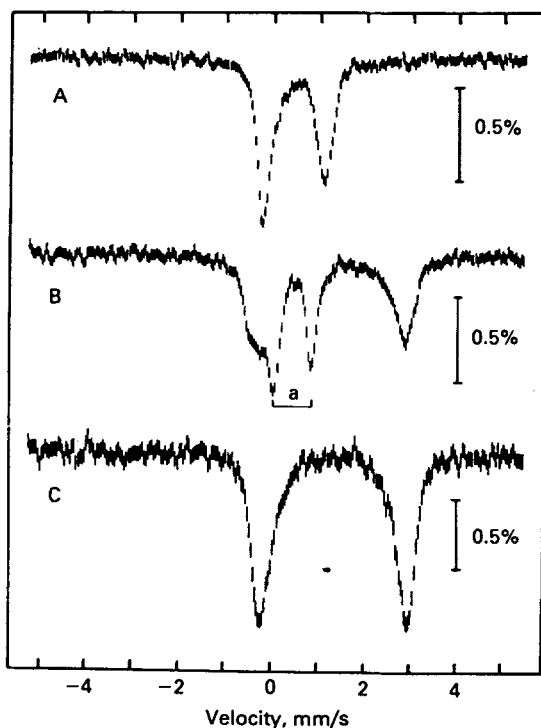


Figure 8. Mössbauer spectra of aconitase at 4.2 K with no applied magnetic field. (a) Dithionite-reduced enzyme activated with 99.9% enriched ^{56}Fe . (b) Dithionite-reduced enzyme activated with >90% enriched ^{57}Fe . (c) Apoaconitase incubated with dithionite and ^{57}Fe . Quadrupole doublet *a* arises from the unique subsite in the activated enzyme. (Reproduced with permission from Ref. 124.)

in the $[\text{4Fe-4S}]^{2+}$ cluster, whereas the spectrum of the $^{57}\text{Fe}^{2+}$ reaction product depicts the fate of extrinsic (added) iron. Reaction 10 is depicted schematically in Fig. 9, which includes isomer shifts* (δ) and quadrupole splittings (ΔE_Q) for reaction products of the two isotopes.



Spectrum A of Fig. 8 is that of ^{56}Fe -reconstituted aconitase and consists of the single quadrupole doublet 1. Spectrum B is that of ^{57}Fe -activated

*All isomer shifts are referenced to Fe metal at 4.2 K; to convert the reference to room temperature, add $0.12 \text{ mm} \cdot \text{s}^{-1}$.

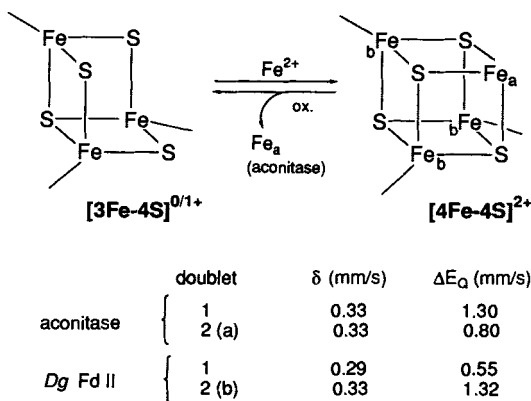
[3Fe-4S]/[4Fe-4S] CLUSTER INTERCONVERSION

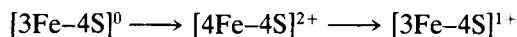
Figure 9. Schematic representation of cluster interconversion reactions of aconitase and Dg Fd II. Mössbauer spectroscopic parameters refer to $[4\text{Fe-4S}]^{2+}$ clusters (124, 132); ox = oxidant. With aconitase, subsite *a* is occupied by ^{57}Fe upon cluster conversion, whereas with Dg Fd II one or more of the subsites *b* are populated in this process.

enzyme, and spectrum C corresponds to the product of the reaction between $^{57}\text{Fe}^{2+}$ and apoenzyme in the presence of dithionite. The major doublet in B corresponds to that in C and is attributable to noncluster high-spin Fe(II) derived from the excess iron used in reconstitution. Doublet 2, or *a*, in spectrum B arises from ^{57}Fe in the cluster. Spectra in applied fields showed that the two cluster quadrupole doublets originate in a diamagnetic species. This result, together with the values of the spectral parameters, confirms the $[4\text{Fe-4S}]^{2+}$ cluster reaction product. Oxidation of the active enzyme removed virtually all ^{57}Fe , showing that the atom introduced in the first step of cluster conversion is removed in the reverse step. Thus, the aconitase cluster consists of two types of sites in a 1:3 ratio, with unique site *a* being differentiated, under the Mössbauer spectroscopic criterion, by a smaller quadrupole splitting.

Inactive aconitase can be activated by reduction without the addition of an iron source (125). In this case, an enzyme is obtained with $\sim 75\%$ of the activity attainable in the presence of added iron, an observation consistent with $[4\text{Fe-4S}]^{2+}$ cluster formation by means of the cannibalization Reaction 9.

Activation of aconitase with radioactive ^{59}Fe supports subsite-specific formation and conversion of the $[4\text{Fe-4S}]$ cluster (125). Continued exposure of the enzyme to activating conditions, however, wherein clusters

are assembled and disassembled, will ultimately lead to labeling of all subsites. The Mössbauer spectra of Fig. 8 demonstrate subsite-specific reactivity over one cycle,



of cluster interconversion.

2. *Desulfovibrio gigas* Fd II

The ferredoxin of *D. gigas* has been isolated in three different oligomeric forms (147, 148). One of these, *Dg* Fd II, is a tetramer with four identical subunits. Each subunit ($M_r \approx 6000$) contains a [3Fe-4S] cluster. This form of the protein may be converted to one containing a [4Fe-4S] center by means of Reaction 10 in the presence of sulfide (132). Sulfide was included because these experiments were done prior to establishment of the [3Fe-4S] cluster composition. Reconstitution of the apoprotein with an iron salt and sulfide afforded a product essentially indistinguishable from that resulting from cluster conversion (132). This form of the protein is monomeric and appears to function as an electron-transfer agent in the phosphoroclastic reaction (133), indicating a similar role to other ferredoxins with tetranuclear clusters.

The Mössbauer spectrum of the [4Fe-4S]²⁺ form of *Dg* Fd II consists of doublets 1 and 2 in a 1:3 intensity ratio (Fig. 9). When cluster conversion is carried out with 95% enriched ⁵⁷Fe, the spectrum of the product consists of the more intense doublet 2 (132). Thus, in this case the externally supplied Fe occupies one or more of the three subsites *b*, which are equivalent by Mössbauer spectroscopy. Analysis of the Mössbauer spectra of the [4Fe-4S]¹⁺ cluster produced by dithionite reduction yielded results consistent with this picture. It was also established that the different subsites do not equilibrate at 25 °C over a time sufficient for protein reconstitution and cluster conversion. Oxidation of the [4Fe-4S]²⁺ cluster with ferricyanide followed by examination of the product with EPR and Mössbauer spectroscopies proved transformation to the [3Fe-4S] form, thereby completing one cycle of cluster interconversion.

The [3Fe-4S]/[4Fe-4S] cluster interconversion of aconitase is clearly subsite-specific because one and the same site is involved in the two reactions. The similar interconversion of *Dg* Fd II may be equally subsite-specific, but this cannot be proven. In this case, the three subsites *b* of the [4Fe-4S]²⁺ cluster cannot actually be equivalent but are indistinguishable by the technique of resolution at hand, Mössbauer spectroscopy. What is

clear from the Mössbauer results is that the single site *a* is not occupied by ^{57}Fe upon formation of the tetranuclear cluster.

B. Structures of [3Fe-4S] Clusters

The initial interpretation of the 3-Fe site in *Av* Fd I from protein crystallography in terms of a cyclic $\text{Fe}_3(\mu_2\text{-S})_3$ unit (46, 149) has been corrected in favor of the voided cubane structure **3** (11, 13, 14). Currently, the most detailed structure available is that of the $[\text{3Fe-4S}]^{1+}$ cluster in *Dg* Fd II (12), which has been refined at 1.7-Å resolution and is set out in Fig. 10. The structures of this cluster in *Av* Fd I (1.9-Å resolution) (13, 14) and in pig heart aconitase (115) are quite similar.

The most prominent feature of the *Dg* Fd II cluster structure is its close adherence to the voided cubane configuration **3**. It might have been expected that, in the process of removing one Fe atom from a cubane-type structure, the product cluster might relax or readjust to a more open or flattened arrangement. With reference to Fig. 10, this flattening would increase the angles at Fe1 and S3 from those at these atoms in the parent

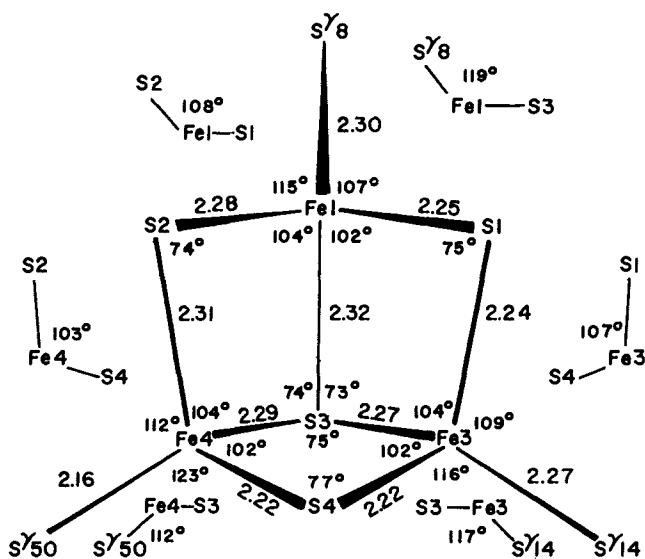


Figure 10. The structure of the $[\text{3Fe-4S}]^{1+}$ cluster of *Dg* Fd II, including cysteinyl sulfur atoms ($\text{S}\gamma$); selected interatomic distances (Å) and angles are given. (Reproduced with permission from Ref. 12.)

[4Fe-4S] cluster, among other effects. Kissinger et al. (12) have provided a comparison of Fe-S and Fe-Fe distances and Fe-S-Fe and S-Fe-S angles with those of the [4Fe-4S] clusters in *P. aerogenes* Fd_{ox} and *Chromatium vinosum* HP_{red}. The average values of corresponding parameters are similar and some may not be significantly different. In the more precisely determined structure of [Fe₄S₄(SCH₂Ph)₄]²⁻ (16), a rather typical analogue cluster in the [4Fe-4S]²⁺ oxidation state (1), the mean values of 12 Fe-S-Fe and 12 S-Fe-S angles are 73.8(2)° and 104.1(2)°, respectively. While the S1-Fe1-S2 angle of 108°, the largest S-Fe-S core angle in the protein structure, is presumably indicative of some cluster relaxation, the effect is not large. Mössbauer spectroscopic evidence shows that upon reduction of oxidized 3-Fe clusters, the added electron is delocalized over two Fe atoms and the remaining iron atom largely retains its Fe(III) character at temperatures below about 20 K (128, 132, 142). At least in the case of *Dg* Fd II (142), at higher temperatures the reduced cluster becomes fully delocalized. In that event the structural difference between oxidized and reduced cluster is expected to be small, with the result that cluster conversion reaction 10 need not surmount any large barrier associated with *core* structural reorganization.

A comparable picture emerges for pig heart aconitase from the work of Robbins and Stout (115), who have determined the crystal structures of the inactive and active forms. These forms are isomorphous. The seven Fe and S atoms common to the cores of the two clusters differ in position by only 0.11 Å on average, and the three common cysteinyl sulfur atoms differ by 0.25 Å.

Additional factors in a [3Fe-4S] → [4Fe-4S] cluster conversion are terminal ligation at the newly created iron site and whatever changes in protein structure are required to position the appropriate ligand at that site, should the ligand derive from an amino acid side chain. The conversion reaction is illustrated for *Dg* Fd II in Fig. 11, which also schematically represents the roles of the six cysteinyl residues of the total of 58 residues in the protein as established crystallographically (15). Three of these function as terminal ligands to the cluster and two are involved in a disulfide bridge. The remaining residue, Cys-11, was encountered in a modified form. Its side chain, whose shape and electron density suggest that it is methylated, is rotated away from the cluster. It is this residue, in its normal form or perhaps as *S*-methylcysteinyl, that is the likely candidate to bind to the metal atom completing the tetranuclear cluster. Rotation about the C_α-C_β bond of Cys-11, which would require some readjustment of the polypeptide chain in this area of the structure, brings the sulfur atom to a position near the binding site (15). If this rearrangement occurs in cluster conversion, the sequence run Cys-X-X-Cys-X-X-Cys of bound residues

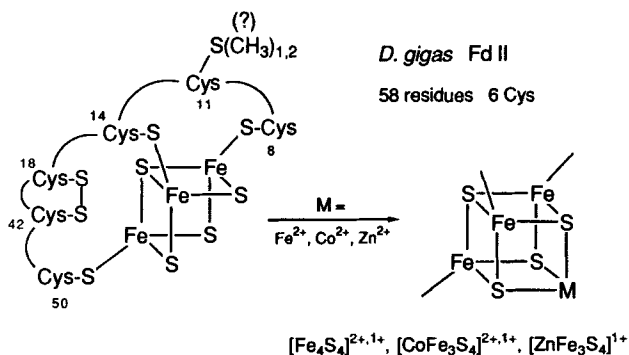


Figure 11. Schematic representations of the [3Fe-4S] cluster and the cysteinyl residues in *Dg* Fd II, the [3Fe-4S] → [4Fe-4S] cluster conversion, and the formation of heterometal clusters with Co(II) and Zn(II).

together with one remote residue (Cys-50) would resemble the binding arrangement in other [4Fe-4S] ferredoxins (44-46, 150).

Beef heart aconitase contains 11 or 12 cysteinyl residues. Other than one Cys-X-X-Cys run, the residues are isolated from each other (151). In the [4Fe-4S] → [3Fe-4S] conversion of the enzyme, no previously unreactive Cys residue becomes exposed or reactive to thiol reagents (129, 151). The failure to detect an increase in reactive -SH groups has several interpretations. These include the possibilities that a Cys residue does not coordinate to Fe_a, that the thiol reagents are unable to penetrate the protein structure to the cluster region, and that cluster conversion is more rapid than reaction of the liberated Cys residue with thiol reagents. The first interpretation appears to be correct inasmuch as recent electron nuclear double resonance (ENDOR) results indicate that water or hydroxide is the terminal ligand at the unique subsite *a* (152, 153). Furthermore, crystallographic work on the pig heart enzyme has proven that in the active form one subsite carries a terminal water or hydroxide ligand and is four coordinate (115). The remaining three subsites and those in the inactive form have terminal cysteinyl ligands. Because no polypeptide-based ligand need be detached, the very favorable circumstance of little required rearrangement of protein structure for cluster conversion in either direction is encountered. It is entirely probable that the essential cluster structural features of pig heart aconitase apply largely or completely to the beef heart enzyme. The pig heart enzyme has one aspartate and three histidyl residues in the vicinity of the Fe_a site, but they are not favorably positioned for ligation at that site.

The primary structure of *Av* Fd I consists of 106 residues, with all 9 Cys

units occurring in the first 49 residues (154). The [3Fe-4S] cluster is ligated by Cys-8, Cys-16, and Cys-49. Four other Cys residues bind the [4Fe-4S] cluster (13, 14). Of the two remaining free residues, Cys-11 is the better candidate to bind at the subsite created in cluster conversion because it is closer to the cluster. Its sulfur atom is 7.4 Å from the nearest Fe atom and 5.6 Å from the nearest sulfide atom of the [3Fe-4S] cluster. It would appear that substantial protein structural rearrangement is required to stabilize a [4Fe-4S] cluster with Cys-11 as a terminal ligand. The form of *A_v* Fd I with two [4Fe-4S] clusters has been prepared by anaerobic reconstitution of the apoprotein with an Fe(II) salt and sulfide (155). Its detailed structure is unknown. It is also possible to remove selectively the [4Fe-4S] cluster by oxidative destruction with ferricyanide. Spectroscopic properties of the resultant protein indicate that the structure of the [3Fe-4S] cluster is essentially unchanged from that in the native 7-Fe protein (156, 157).

C. Formation of Heterometal Clusters

It is now clear that, at least for aconitase and *Dg* Fd II, terminal ligation and protein structural features are particularly favorable for cluster inter-conversion reactions. Furthermore, conversion of [3Fe-4S] to a tetranuclear cluster need not necessarily involve iron as the added metal. Reasonable substitutes would be ions with an affinity for sulfur and a tetrahedral stereochemical preference. As depicted in Fig. 11, such reactions have been carried out with *Dg* Fd II using Co^{2+} (158) and Zn^{2+} (159). Typically, the protein in the [3Fe-4S]⁰ state is incubated with an excess of an M^{2+} salt and dithiothreitol and then repurified. Analytical and Mössbauer spectroscopic results support the MFe_3S_4 formulation, for which the most reasonable structure, given the preceding core conversion reactions, is that of a heterometal cubane with atom M occupying the previously vacant site. Electron spin resonance and Mössbauer spectroscopic properties are consistent with the $[\text{CoFe}_3\text{S}_4]^{2+}$ ($S = \frac{1}{2}$) and $[\text{ZnFe}_3\text{S}_4]^{1+}$ ($S = \frac{3}{2}$) oxidation states. The observation of ⁵⁷Fe line broadening of the ⁵⁹Co hyperfine signals shows that the EPR spectrum of the doublet state cluster originates in a species containing both Fe and Co. This cluster can be reduced with dithionite to $[\text{CoFe}_3\text{S}_4]^{1+}$ with integer spin. Oxidation of the Zn-containing cluster affords an EPR-silent species, presumably $[\text{ZnFe}_3\text{S}_4]^{2+}$.

Cobalt and zinc extended X-ray absorption fine structure (EXAFS) studies would prove quite effective in testing the proposed cubane stereochemistry. If correct, the $[\text{CoFe}_3\text{S}_4]$ and $[\text{ZnFe}_3\text{S}_4]$ clusters are members of an extensive set of cubane-type heterometal clusters $[\text{MFe}_3\text{S}_4]$ with, additionally, $\text{M} = \text{Mo}$ and W (160), V (161), and Re (162). The last four cluster types are of purely synthetic origin and utilize three terminal ligands

at the M site. In the absence of information to the contrary, the capture of heterometal ions by the [3Fe-4S]⁰ cluster of *Dg Fd II* can be considered a site-specific process in which the vacant site of the precursor cluster is occupied. The terminal ligand(s) at the heterometal site are unknown, but could well be the sulfur atom of unmodified Cys-11 (Fig. 11). Formation of heterometal species has not been reported for any other [3Fe-4S] protein.

D. Mechanism of Action of Aconitase

Through perspicacious use of Mössbauer and ENDOR spectroscopies and labeling of substrate and inhibitors with ¹⁷O ($I = \frac{5}{2}$), some of the leading structural aspects of the aconitase mechanism have been deduced (126, 128, 163-165). The relevant findings have been summarized by Emptage (130). Consequently, only a brief synopsis is presented here, with reference to the proposed mechanism of action set out schematically in Fig. 12. The enzyme converts citrate to isocitrate via the intermediate *cis*-aconitate by a dehydration-hydration pathway. In this scheme, X = H₂O/OH⁻ or a protein-based ligand, R = CH₂CO₂⁻, and B is a protein base, possibly a histidyl imidazole group or perhaps the carboxylate group of aspartate. The location of these residues near the cluster has previously been noted. The pH dependence of the kinetics for yeast aconitase is suggestive of the participation of a carboxylate group (166).

Among the first indications that the cluster in aconitase was involved in the mechanism of action were those from EPR spectroscopy. Addition of the competitive inhibitor *trans*-aconitate caused large changes in the $S = \frac{1}{2}$ EPR spectrum of the reduced form (126). Furthermore, incubation of the reduced enzyme with *trans*- or *cis*-aconitate in ¹⁷O-enriched water caused signal broadening. Citrate carboxyl groups enriched in ¹⁷O gave no broadening in ordinary water. The broadening is due to transferred hyperfine interactions from ¹⁷O derived from water, present as coordinated water and/or the hydroxyl group of citrate. The Mössbauer spectra in Fig. 13 reinforce these results. Spectrum *A* is that of the enzyme activated with ⁵⁷Fe and thus corresponds to Fe_a in Fig. 9. Addition of excess citrate affords spectrum *B*, which contains quadrupole doublets S₁ and S₂. Their larger upole splittings and isomer shifts are consistent with alteration of Fe_a to a condition of high-spin Fe(III) character with coordination numbers 5 or 6. Furthermore, for the reduced enzyme the parameters $\delta = 0.87 \text{ mm} \cdot \text{s}^{-1}$ and $\Delta E_Q = 2.20 \text{ mm} \cdot \text{s}^{-1}$ are typical of high-spin Fe(II). Activation of the enzyme with ⁵⁶Fe and addition of citrate gave spectrum *C*, which is that of the three Fe_b atoms. These Fe subsites are scarcely affected by

PROPOSED ACONITASE MECHANISM

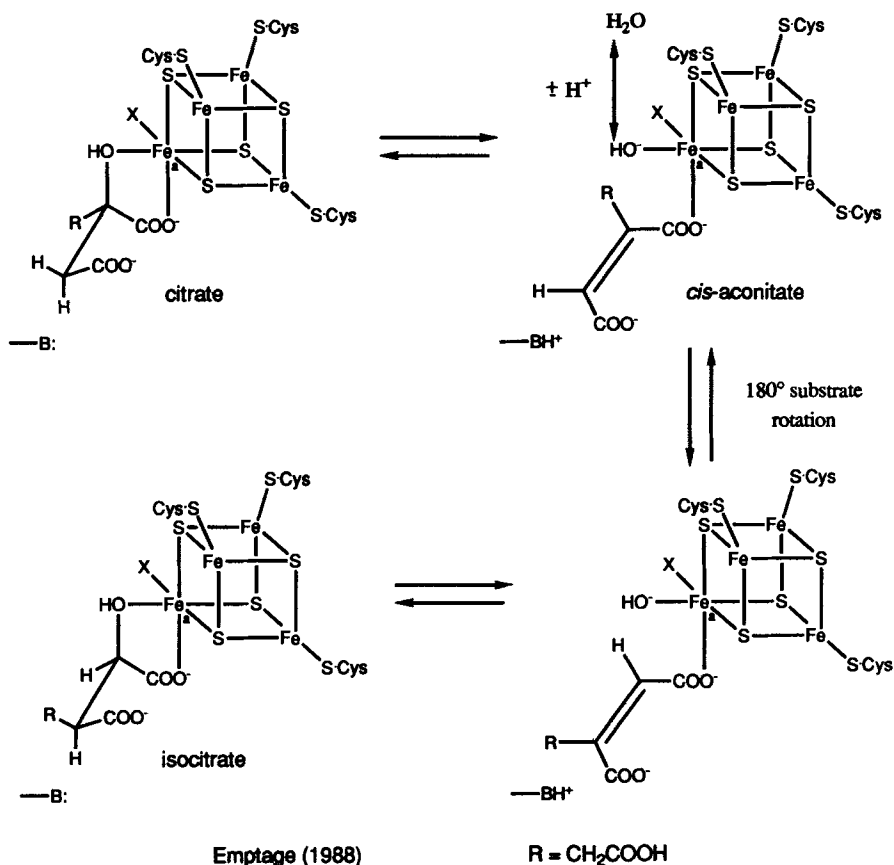
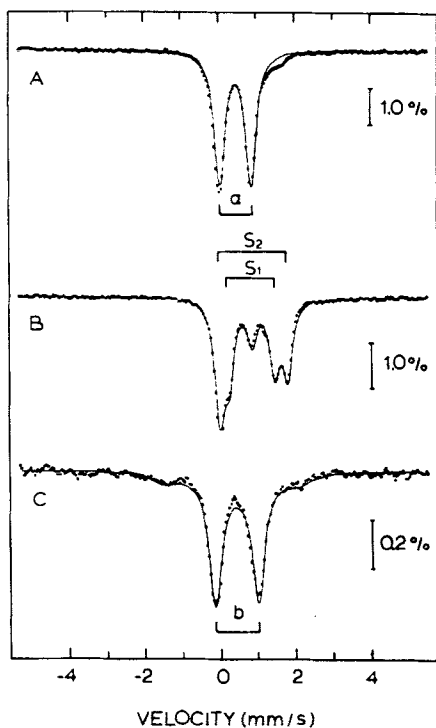


Figure 12. Proposed aconitase mechanism, with structural features deduced from spectroscopic results. (Reproduced with permission from Ref. 130.)

substrate binding, the only change being a small decrease ($0.15 \text{ mm} \cdot \text{s}^{-1}$) in the quadrupole splitting.

The foregoing results lead to the inescapable conclusion that substrate binding is a subsite-specific event. The species along the reaction pathway that are responsible for doublets S_1 and S_2 have not been unambiguously identified (128). The ¹⁷O and ¹³C ENDOR spectroscopic findings by Hoffman and co-workers (164, 165), however, using isotopically labeled substrate, intermediate, and inhibitors have been more informative in this



spectrum	doublet	δ (mm/s)	ΔE_Q (mm/s)
A	a	0.33	0.80
B	S ₁	0.72	1.26
	S ₂	0.77	1.83
C	b	0.33	1.15

Figure 13. Mössbauer spectra of activated aconitase at 4.2 K. (A) Enzyme activated with ^{57}Fe . (B) Enzyme in part A in the presence of excess citrate. (C) Enzyme activated with ^{56}Fe in the presence of excess citrate. Spectra A and B were recorded in zero applied magnetic field, and spectrum C was obtained in a parallel 60 mT applied field. (Reproduced with permission from Ref. 163.)

respect. These results are incorporated in the reaction scheme in Fig. 12. The five-membered chelate ring involving the hydroxyl and 2-carboxylate is commonly encountered in citrate binding to metals, including Fe(III) (167). In the next step, Fe_a is considered to activate substrate toward dehydration by means of hydroxide and base-assisted proton removal.

Reorientation of *cis*-aconitate such that the previously free carboxylate group becomes coordinated, followed by the stereospecific events of hydroxide delivery to the activated olefinic carbon atom and protonation at the other carbon atom, generates the isocitrate product.

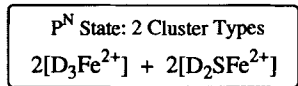
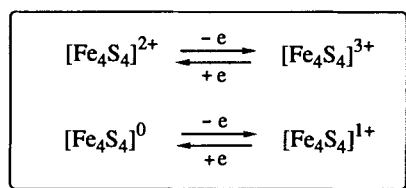
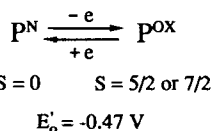
It is far from obvious why evolution has selected a [4Fe-4S] cluster instead of, for example, a single Fe atom to provide the substrate binding and activating factors responsible for the aconitase reaction. It is becoming increasingly likely that aconitase is not a special case, however. Maleic acid hydratase (168) and certain dehydratases (169-172) are activated by Fe addition or have been sufficiently well characterized to show that they are Fe-S enzymes. For example, one form of lactyl-CoA-dehydratase appears to contain Fe₃S₄ and Fe₄S₄ clusters (171) and dihydroxy acid dehydratase is thought to contain a Fe₂S₂ cluster (172). Similarly, glutamine phosphoribosylpyrophosphate amidotransferase contains one [4Fe-4S] cluster (173) and endonuclease III of *E. coli* has very recently been shown to contain a [4Fe-4S]²⁺ cluster that can be oxidized to [3Fe-4S]¹⁺ with ferricyanide (174). In these enzymes, the Fe-S clusters may be involved in catalysis, as with aconitase, or may serve a structural or regulatory purpose. In any event, it is now certain that, while electron storage and transfer may be the dominant biological function of Fe-S clusters, it is not their only function.

E. P-Clusters of Nitrogenase

Nitrogenase is an enzyme found both in free-living and symbiotic prokaryotic microorganisms and catalyzes the six-electron reduction of dinitrogen to ammonia. The enzyme complex consists of two proteins. The Fe protein ($M_r \approx 65,000$) is composed of two subunits (α_2) and one [4Fe-4S] cluster, and is the ultimate electron donor to the MoFe protein. The latter usually contains 24-32 Fe atoms and 1.5-2 Mo atoms per $\alpha_2\beta_2$ tetramer in an assembly of $M_r \approx 230,000$. Highly purified proteins have 30-32 Fe atoms and 2 Mo atoms per tetramer. The MoFe protein contains two identical dissociable cofactors that are Mo-Fe-S clusters of approximate composition MoFe₆₋₈S₈₋₁₀ and are the probable catalytic centers. The remaining Fe occurs as clusters that current evidence favors, but does not *prove* to be, [4Fe-4S] clusters. The present state of understanding of nitrogen fixation and of the metal clusters in the enzyme has been summarized in detail (175-178). Our concern here is with the Fe-S clusters of the MoFe protein, the so-called "P-clusters" from the original nomenclature of Zimmermann et al. (179). In the absence of strong evidence to the contrary, we consider these clusters to be of the [4Fe-4S] type.

Some of the salient properties of P-clusters are summarized in Fig. 14. As isolated, the FeMo protein contains the clusters in the P^N (native) state, which has a diamagnetic ground state. The clusters can be oxidized by one electron using controlled potential coulometry as by Watt et al. (180–182), who interpreted their results in terms of the presence of three P-clusters. Chemical oxidation using thioneine by Zimmermann et al. (179) was analyzed in terms of one-electron oxidations of four P-clusters. The two groups agree that a total of six electrons is removed from the P-clusters and cofactor clusters together upon full oxidation, and that the former are oxidized first. Reported potentials for this oxidation show hysteresis. The value of -0.47 V is taken from the electrochemical work of Watt and Wang (182), and is the E_1 value for the reduction of the protein after dye oxidation. The oxidized clusters are in the P^{OX} state, which was first shown to be paramagnetic by magnetic Mössbauer spectroscopy (179, 183) but is EPR silent. Examination of magnetic susceptibility changes upon oxidation from P^N to P^{OX} (184) and low temperature MCD spectroscopy of the P^{OX} state (185) indicate that clusters in this state have $S = \frac{5}{2}$ or $\frac{7}{2}$ ground states.

"P-CLUSTERS" OF NITROGENASE



subsite	δ	ΔE_Q
Fe^{2+}	0.55	3.03
S	0.51	1.33
D (a)	0.51	0.87
D (b)	0.52	0.68

Figure 14. Summary of some of leading properties of the P-clusters of nitrogenase. The redox potential (182) and Mössbauer parameters ($mm \cdot s^{-1}$) (186) are taken from literature sources. Redox couples possibly corresponding to the P^N/P^{OX} transition are indicated.

Consequently, the P^N/P^{OX} transition apparently involves one or the other of the two redox couples in Fig. 14.

The principal reason for considering P-clusters as subsite differentiated is found in the Mössbauer spectra of the P^N state. Parameters from the most recent Mössbauer study of the FeMo protein (from *Klebsiella pneumoniae*) in the P^N form are contained in Fig. 14 (186). In this enlightening experiment, a protein containing P-clusters but lacking the cofactor, produced by a mutant strain of the organism, has been used. This approach has permitted construction of an isotopic hybrid of the FeMo protein containing ^{57}Fe -enriched P-clusters and ^{56}Fe -enriched cofactor clusters. Highly resolved Mössbauer spectra not complicated by the need to remove contributions from the cofactor have thus been obtained. The spectrum of the P^N state is shown in Fig. 15, and contains three subsite quadrupole doublets, Fe^{2+} , D, and S. Spectral analysis has led to the conclusion that the Debye-Waller factors for the different cluster subsites do not have the same temperature dependence and that the intensity ratio of the Fe^{2+} , D, and S subsites is better described as 4:10:2 instead of 4:12:2, as in earlier work. It has been suggested that P-clusters occur in two slightly inequivalent pairs: $2 [\text{D}_3\text{Fe}^{2+}] + 2 [\text{D}_2\text{SFe}^{2+}]$. Parameters of the Fe^{2+} doublet are consistent with those of a tetrahedral Fe^{II}S_4 unit as in reduced rubredoxin, and may be considered to define the "unique" subsite. The remaining three subsites have nearly the same isomer shifts but rather different quadrupole splittings, none of which approach the large value of the Fe^{2+} subsite.

Definite problems, based on departures in behavior from normal $\text{Fe}_4\text{S}_4(\text{S}\cdot\text{Cys})_4$ native clusters, arise when attempting to formulate the structures of P-clusters. The $[\text{4Fe-4S}]^{2+,3+}$ couple normally operates at potentials far more positive (Fig. 3) than the P-cluster potential, and no instance of a ground state other than $S = \frac{1}{2}$ has been found for $[\text{4Fe-4S}]^{3+}$. The $[\text{4Fe-4S}]^0$ oxidation state has never been proven to exist in a protein. It has been electrochemically generated in synthetic systems as $[\text{Fe}_4\text{S}_4(\text{SR})_4]^{4-}$ but only at potentials so negative (76, 187-189) so as to cast serious doubt on its viability under physiological conditions unless, possibly, the core becomes protonated. Furthermore, the isomer shifts of the P^N state are most consistent with the all-ferrous ($[\text{4Fe-4S}]^0$) oxidation level. Values for the $[\text{4Fe-4S}]^{1+,2+}$ levels, especially the 2+ level, are substantially lower. Some evidence for the $[\text{4Fe-4S}]^0$ state might be adduced from occurrence of a transient species with an EPR spectrum like that of a $[\text{4Fe-4S}]^{1+}$ protein upon thioneine oxidation of the MoFe protein (190). It would appear that, in order to accommodate simultaneously the redox potential and some or all of the Mössbauer parameters, the terminal ligation must depart from the pattern of one cysteinate ligand per subsite, as found in the vast majority of Fe-S proteins.

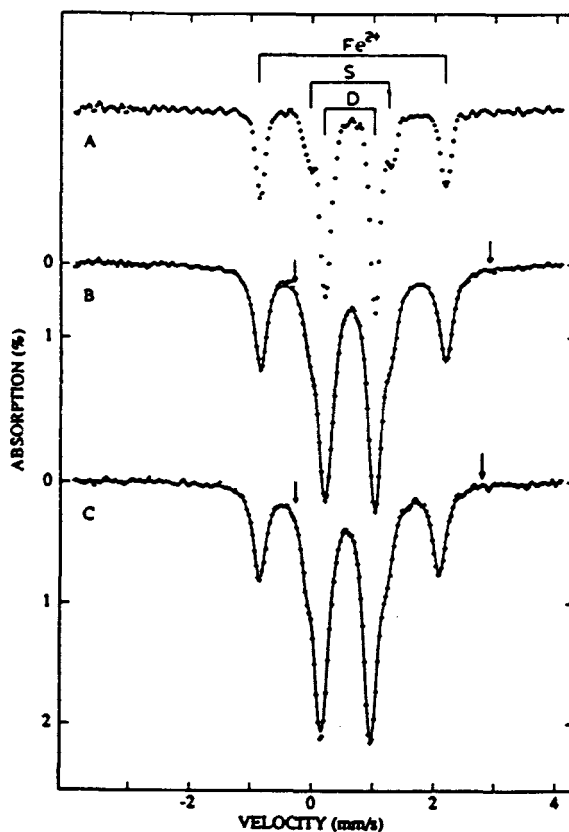


Figure 15. Mössbauer spectra of the P^N -clusters of nitrogenase in the isotopic hybrid containing ^{57}Fe -enriched P-clusters and ^{56}Fe -enriched cofactor in the absence of an applied magnetic field. Spectral components are indicated in part A; spectra B and C were recorded at 4.2 and 173 K, respectively. The solid lines are fits to the data; the fit of spectrum B uses the parameters in Fig. 14. (Reproduced with permission from Ref. 186.)

F. Active Site of Sulfite Reductase

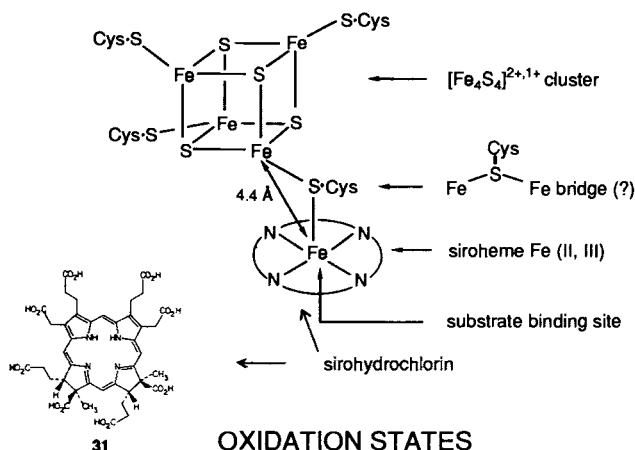
Assimilatory sulfite reductase catalyzes the six-electron reduction of sulfite to sulfide without release of intermediate reduction products. Owing to the now-classic investigations of Siegel and co-workers, *E. coli* sulfite reductase is the best understood of these enzymes. The enzyme is a complex hemoprotein ($M_r \approx 685,000$) with an $\alpha_8\beta_4$ subunit composition (191). The α subunit ($M_r \approx 59,000$) contains a NADPH binding site and a FAD or FMN prosthetic group, there being four of each group per holoenzyme.

The β subunit ($M_r \approx 54,600$) contains a special heme, siroheme (192, 193), of the isobacteriochlorin type, and one [4Fe-4S] cluster. The minimal electron-transfer sequence is $\text{NADPH} \longrightarrow \text{FAD} \longrightarrow \text{FMN} \longrightarrow \text{siroheme} \longrightarrow \text{sulfite}$. The minimal catalytic system is a β subunit, substrate, and a source of electrons (194).

The subsite-specific aspect of sulfite reductase derives from its structure, which has been determined by protein crystallography at 3.0-Å resolution on the native, or SiR^0 , state (195). The active site assembly, schematically illustrated in Fig. 16, consists of a [4Fe-4S] cluster bridged to siroheme, the macrocyclic ligand of which is sirohydrochlorin (31). The cluster and siroheme are weakly exchange coupled (196-198). Combinations of the cluster and siroheme oxidation states afford the three total oxidation levels of the assembly specified in Fig. 16. The EPR spectrum of the state SiR^0 is typical of Fe(III) isobacteriochlorins. One-electron reduction of SiR^0 produces SiR^{1-} , in which siroheme has been reduced to the Fe(II) level. Further reduction occurs at the cluster to afford the catalytic state SiR^{2-} , of which three substates classified by their EPR spectra are observed (199). These spectra depend on the presence or absence of an additional axial ligand and the identity of that ligand. The distinct EPR spectra of the substates arise from a $S = \frac{1}{2}$ [4Fe-4S] $^{1+}$ cluster, the exchange coupling of which is modified by different magnetic properties of the siroheme center.

The cluster and siroheme are juxtaposed such that the Fe...Fe separation is 4.4 Å and the distance from the siroheme Fe atom to the center of the cluster is 5.5 Å. A cysteinyl sulfur bridge is consistent with the X-ray results which, however, have not been obtained at a resolution sufficient to identify the bridge. Resonance Raman studies of the β subunit suggest that features at 352 and 393 cm^{-1} may involve a bridging thiolate (200), and are inconsistent with exogenous ligands as bridges or otherwise bound to the cluster. An imidazole or other bridge in which a nitrogen atom is coordinated has been eliminated by ENDOR spectroscopy (201). A plausible mode of operation of the active site involves reduction of siroheme Fe to the Fe(II) state, binding of substrate at the axial position opposite to the bridge, and electron flow from the cluster to siroheme to substrate with concomitant protonation of reduced forms of the latter. Electrons might pass through bridge orbitals, or directly to siroheme, inasmuch as the cluster and macrocycle are at or near van der Waals contact at the periphery of the sirohydrochlorin ring (195). Spectroscopic and other similarities, including the presence of siroheme, strongly indicate that other assimilatory sulfite reductases, such as that from *D. gigas* (202), contain the same or a closely related active site assembly. Although detailed information is much more limited, assimilatory nitrite reductases, which reduce nitrite to ammonia,

SULFITE REDUCTASE ACTIVE SITE



state	cluster	siroheme
oxidized (SiR^0)	$[\text{Fe}_4\text{S}_4]^{2+}$ ($S = 0$)	Fe(III), $S = 5/2$ (as isolated) $S = 1/2$ (SO_3^{2-} , CN^-)
$\downarrow e^-$		
semi-reduced (SiR^1)	$[\text{Fe}_4\text{S}_4]^{2+}$ ($S = 0$)	Fe(II), $S = 1$ or 2 $S = 0$ (CN^- , CO)
$\downarrow e^-$		
reduced (SiR^2) (catalytic)	$[\text{Fe}_4\text{S}_4]^{1+}$ ($S = 1/2$) $g = 2.53, 2.29, 2.07$ $g = 5.1, 2.6, 2; 4.9, 3.3, 2.1$ $g = 2.03, 1.93, 1.91$	Fe(II), $S = 0$ (CO , CN^- , S^2)

Figure 16. Summary of certain leading features of the active site of *E. coli* sulfite reductase (195), including a schematic representation of the active site with a (possible) cysteinyl sulfur bridge connecting cluster and siroheme, the structure of sirohydrochlorin (**31**), and the oxidation states of the enzyme with certain axial ligands that generate the indicated spin states of the siroheme.

may also accommodate a similar active site. For example, the enzyme from spinach contains a [4Fe-4S] cluster and siroheme (203, 204), but it has not been established if these units are structurally coupled. The subsite-specific bridged structure in *E. coli* sulfite reductase is, thus far, the only proven example of a [4Fe-4S] cluster bridged to another metal-containing protein-bound entity.

IV. SUBSITE-DIFFERENTIATED SYNTHETIC CLUSTERS

Despite the ready accessibility of clusters of the type $[\text{Fe}_4\text{S}_4\text{L}_4]^{2-}$ with L = alkyl- or arylthiolate, halide, or aryloxy, these species are not suitable for the examination of subsite-specific properties using the synthetic analogue approach. The reason for this situation, previously pointed out in Section II.H, is illustrated in Fig. 17. Ligand substitution reactions 1, 11 (an example of generalized Reaction 3), and 12 afford an essentially statistical product distribution (17, 71, 72, 79). Evidently, the Fe subsites are too weakly coupled electronically and the ligand positions are too far separated to cause significant deviations from statistical behavior. Thus, in Reaction 1, for example, with reactant $n = 1$ the product distribution is about 50% of $n = 1$ and 25% each of $n = 2$ and $n = 0$. Because of the substitutional lability of the products, there is no effective means of separating and maintaining a single product.

We note in passing that ligand substitution reactions have been studied only with $[4\text{Fe}-4\text{S}]^{2+}$ clusters carrying four monoanionic ligands, and that certain mixed-ligand cluster types of this and other oxidation levels might be stable under some conditions. Cluster **32** was prepared by the reaction of $[\text{Fe}(\text{thf})_6][\text{Fe}_4\text{S}_4\text{I}_4]$, Ph_3PS , and sulfur in toluene at 80°C and was recrystallized from dichloromethane (205). Evidently in low dielectric solvents the cluster is stable to disproportionation reactions, which necessarily would produce charged species. For similar reasons, one might expect the neutral

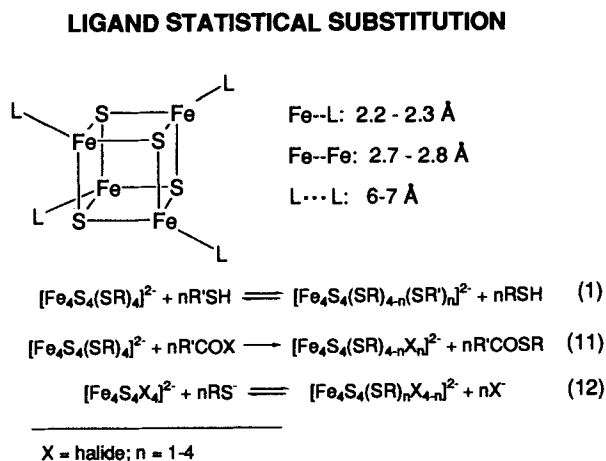
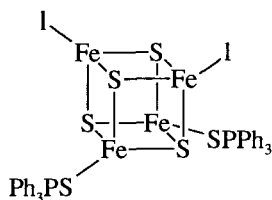


Figure 17. Three ligand substitution reactions that afford essentially statistical product mixtures, together with certain dimensions of $[\text{Fe}_4\text{S}_4\text{L}_4]^{2-}$ clusters.

clusters $\text{Fe}_4\text{S}_4\text{L}_3\text{L}'$ and $\text{Fe}_4\text{S}_4\text{LL}'_3$, where L is a monoanionic and L' an uncharged ligand, to be stable in low dielectric media. No such species have been isolated or generated in solution. Other than **32**, the structure

**32**

of which has been established by X-ray analysis (205), the only neutral [4Fe-4S] cluster that has been isolated (excluding cyclopentadienyl and nitrosyl derivatives) is $\text{Fe}_4\text{S}_4(\text{CO})_{12}$ (206). The reactivity of this compound is unexplored, perhaps because of its low solubility. It is the only isolated compound with the $[\text{4Fe-4S}]^0$ core.

In the following sections, we summarize the synthesis, structures, and pertinent reactivity aspects of $[\text{4Fe-4S}]^{2+}$ clusters that possess a 1:3 subsite differentiation.

A. Synthesis

A tridentate trithiolate ligand has been sought that would bind in a trigonally symmetric mode to a single cubane cluster, thereby effecting a 1:3 subsite differentiation with the unique subsite on the C_3 axis. Potential solutions to this problem of ligand design are conditioned in attractiveness by the difficulty of synthesis. Our approach, which originates with the considerations and experimentation of Stack (207), has as its basis the striking conformations of certain hexasubstituted benzenes shown in Fig. 18. These are two of a number of examples of this class of compounds prepared by MacNicol and co-workers (208-210). Both $\text{C}_6(\text{SPh})_6$ (209) and $\text{C}_6(\text{O-3,5-Me}_2\text{C}_6\text{H}_3)_6$ (210) possess the *bababa* conformation, in which the substituents are arranged below and above the central ring in serial order. One large substituent presumably buttresses its neighbors to positions on opposite sides of the ring. In the latter compound, the methyl group locations over the central ring in three substituents on the same side of the ring suggest positions for ligating atoms. Further analysis of these structures indicated that the corresponding trithiols would be dimensionally suitable for binding a cubane cluster. On that basis, the synthesis in Fig. 19 (33) was devised.

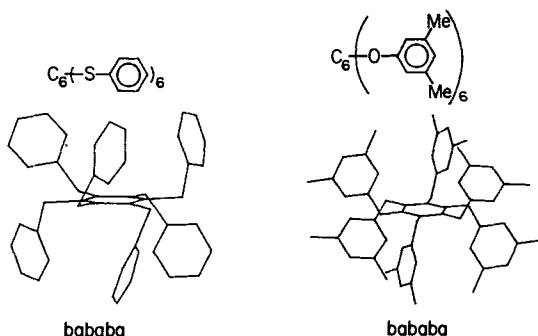
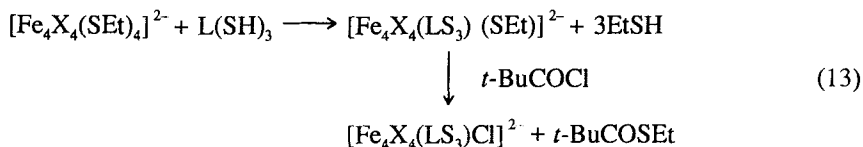


Figure 18. Structures of two hexasubstituted benzenes (209, 210) redrawn from atom coordinates and illustrating the *bababa* conformation.

Key steps in the synthesis are bromide displacement in 1,3,5-tribromo-2,4,6-trifluorobenzene by *p*-tolylthiocuprate to afford **33**, and its coupling with the sodium salt of monoprotected dithiol **34** to afford triprotected trithiol **35** in very good yield. Deprotection of **35** to trithiol ligand **36**, $L(SH)_3$, is essentially quantitative. The original synthesis has been improved to the indicated yields (211). The trithiol is quite air-sensitive and must be handled accordingly.

Entry to cluster complexes ($X = S, Se$) is afforded by reaction Scheme 13. Ligand substitution of the precursor cluster results in binding of the tridentate ligand with retention of one ethane-thiolate ligand. While these compounds as their Ph_4P^+ salts are microcrystalline, salts of the chloride clusters obtained by the reactions with pivaloyl chloride afford materials that gave diffraction-quality crystals. As will be seen, the chloride clusters $[Fe_4S_4(LS_3)Cl]^{2-}$ (**37**) and $[Fe_4Se_4(LS_3)Cl]^{2-}$ (**38**) are susceptible to substitution reactions affording a large variety of substituted clusters.



B. Structures

1. Solid State

The solid state structures of clusters **37** and **38** as their Ph_4P^+ salts (33, 211) are provided in Fig. 20. It is immediately apparent that the desired

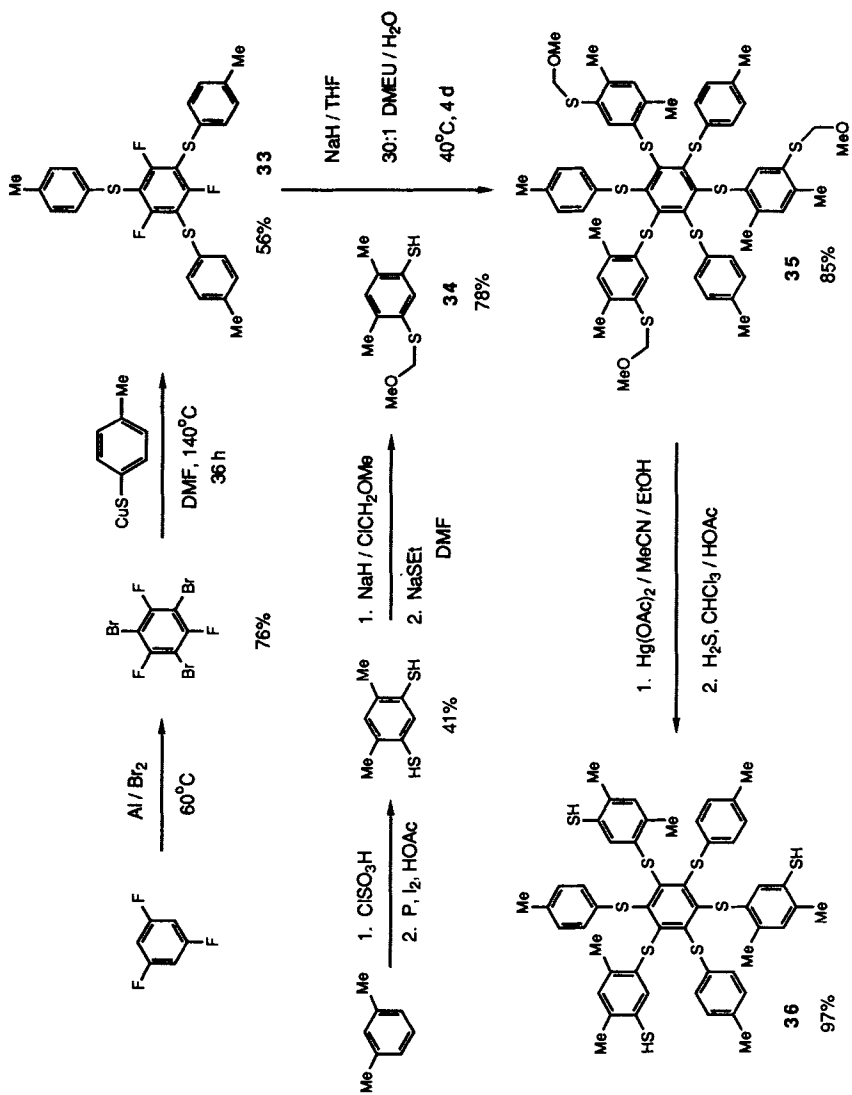


Figure 19. Synthesis of the tridentate ligand 1,3,5-tris((4,6-dimethyl-3-mercaptophenyl)thio)-2,4,6-tris(*p*-tolylthio)benzene [**36**]. (Adapted from Ref. 33.)

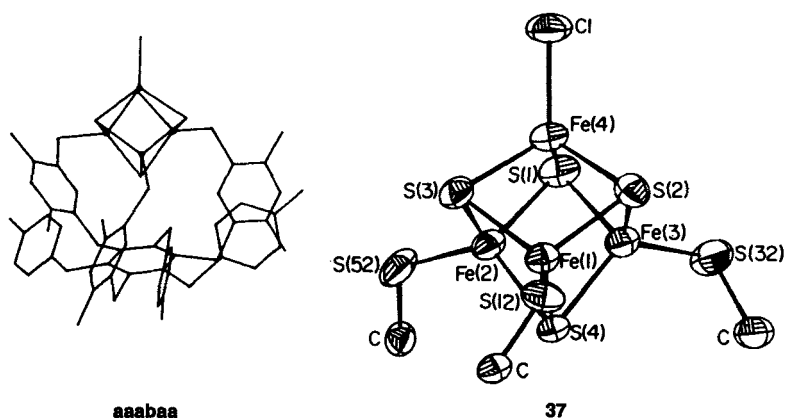
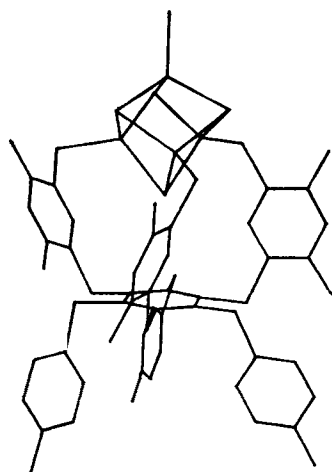
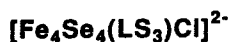


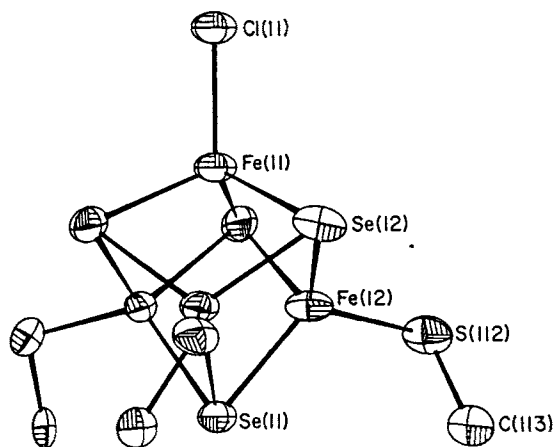
Figure 20. Structures of $[\text{Fe}_4\text{S}_4(\text{LS}_3)\text{Cl}]^{2-}$ (**37**) (33) and $[\text{Fe}_4\text{Se}_4(\text{LS}_3)\text{Cl}]^{2-}$ (**38**) (211), showing the ligand conformations and cluster portions. Only one of the three inequivalent anions in the structure of the Ph_4P^+ salt of **38** is shown.

structural result has been achieved. In **37**, the ligand conformation (*aaabaa*) is less symmetric than that in **38** (*ababab*), which has a trigonal arrangement. Both clusters have three coordinating "arms" on the same side of the central benzene ring, and in **37** only one of the "legs" is below this ring, whereas all three are in this position in **38**. Indeed, the structure of **38** is a case of the very infrequently encountered $P3$ space group. The asymmetric unit consists of three independent thirds of an anion, each with imposed C_3 symmetry. Two of the anions have the Δ absolute configuration and the other is Λ . The crystals are inversion twinned, however, and thus essentially racemic. The independent anions differ primarily in the elevation of the $[\text{4Fe-4Se}]^{2+}$ cores above the central benzene rings. Neither core exhibits the compressed tetragonal structure usually found for clusters with four identical terminal ligands. In **37**, the cluster structure is somewhat irregular whereas in **38** there are small but discernible trigonal distortions along the C_3 axes. These are the only cases of trigonal distortions of $[\text{4Fe-4S/Se}]^{2+}$ cores. Other than this distortion, core metric parameters are unexceptional.

Before proceeding further, the symbols and nomenclature of Fig. 21 are introduced. Note the cubane structural abbreviation for the cluster and the numbering scheme for the ligand arms and legs.



ababab



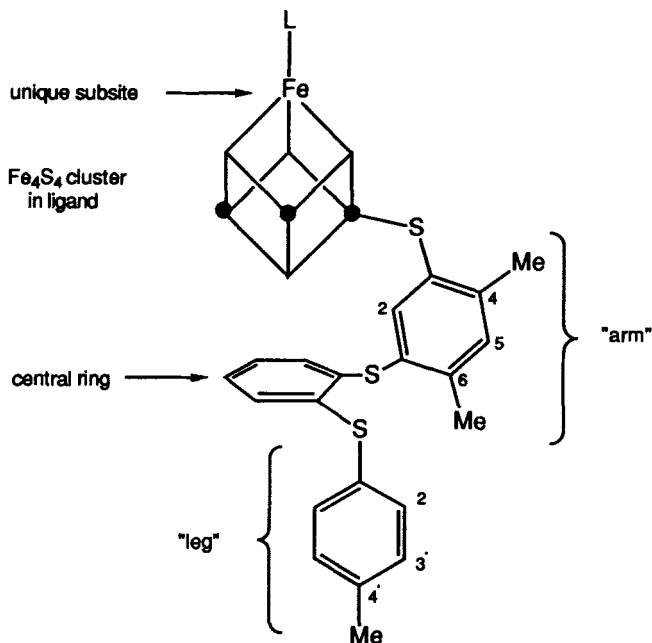
38

Figure 20. (Continued)

2. Solution

The ^1H NMR spectra in Fig. 22 demonstrate the occurrence of reaction Scheme 13. These spectra display three significant features that apply to all other spectra of LS_3 cluster complexes examined thus far. (a) One set of ligand resonances is observed. (b) Resonances are isotropically shifted. This behavior applies to all $[\text{4Fe-4S}]^{2+}$ clusters owing to the population of the excited states ($S > 0$) of the core spin ladder. Shifts are mainly or entirely contact in origin and have been treated elsewhere (212, 213). (c) Because of (b), shifts of the arm resonances 4-Me, 5-H, and 6-Me are extremely sensitive to changes in ligation at the unique subsite. Feature (a), which is also found well below ambient temperature, indicates that clusters in solution have effective trigonal symmetry. Because there are no exceptions to this feature in more than 30 clusters examined, we conclude that all possess a *trigonally symmetric conformation in solution*. This conformation must be very similar to those of cluster **38** in the solid state (Fig. 20). In the case of **37**, this result requires conformational modification of

SYMBOLS AND NOMENCLATURE



LS₃ = tridentate ligand (3-)

Figure 21. Symbols and nomenclature for the [4Fe-4S] cluster complexes derived from the tridentate ligand LS₃.

two of the legs upon passing into the solution phase. Feature (c) is exemplified by the downfield displacement of the 5-H resonance from 8.12 to 8.23 ppm upon replacement of EtS⁻ with Cl⁻. The contact interactions are detectably different over an eight-bond pathway! Sensitivity at this level has been indispensable in monitoring subsite-specific substitution reactions. Several additional examples of feature (c) follow.

Analysis of the ¹H NMR spectrum of **36** and related compounds, together with molecular dynamics calculations, has led to a description of the most probable conformations of the trithiol (211). In the overall *ababab* conformation, the molecule may be considered as a semirigid "cavitand" [in the sense of Cram (214)]. The cavity is defined by a floor which is the central benzene ring and walls which are the inward edges of the phenyl groups of the arms. The critical feature is the orienting effect of the 6-Me group, which disposes each arm such that the thiol group is directed inward,

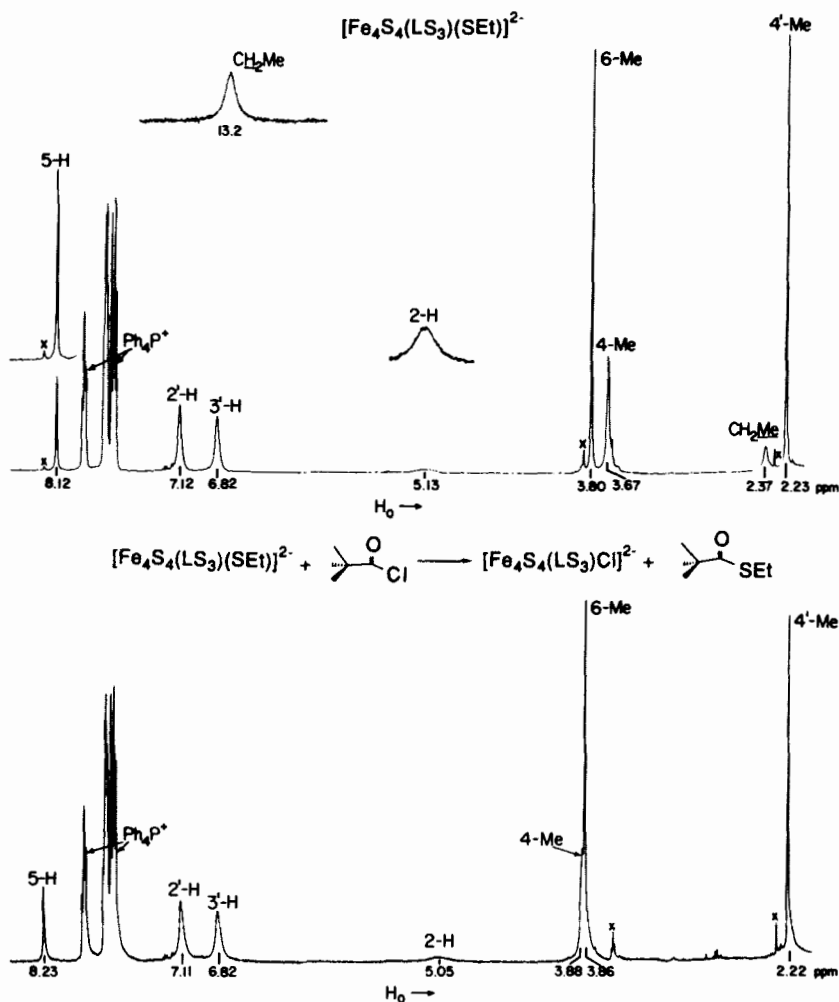
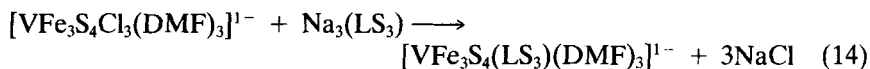


Figure 22. ^1H NMR spectra in CD_3CN solutions demonstrating reaction Scheme 13 ($X = \text{S}$). Upper: $[\text{Fe}_4\text{S}_4(\text{LS}_3)(\text{SEt})]^{2-}$, formed by ligand substitution. Lower: cluster **37**, formed by the indicated reaction using 1 equivalent of pivaloyl chloride. (Reproduced with permission from Ref. 33.)

toward or over the central ring. This orientation accounts for the strongly shielded 2-H resonance, which arises because 2-H is placed in the ring current shielding regime of the central ring. Conformations in which one or more arms are disposed such that the thiol groups point outward from the cavity are disfavored because of steric interactions within the cavity.

Thus trithiol **36** is preorganized to bind a cluster in a ligand substitution reaction such as that in Scheme 13. In stoichiometric reactions, *in situ* yields are essentially quantitative. When the substituent of the phenyl ring of an arm is 5-*t*-Bu, the reaction with $[\text{Fe}_4\text{S}_4(\text{SEt})_4]^{2-}$ is also quantitative. When these positions are unsubstituted, however, reaction with $[\text{Fe}_4\text{S}_4(\text{SEt})_4]^{2-}$ gives some soluble cluster but also appreciable quantities of an insoluble polymer (211). These observations support the view that trithiol **36** has a semirigid cavitand conformation, or range of conformations with the common feature of inwardly positioned thiol groups, that facilitates tridentate capture of a single cluster. The term "semirigid" follows from the dynamics calculations, and, experimentally, from the occurrence of the first reaction in Scheme 13 with $\text{X} = \text{Se}$ (211). On the basis of nuclear positions, the $[\text{4Fe-4Se}]^{2+}$ core has $\sim 10\%$ larger volume than $[\text{4Fe-4S}]^{2+}$. This difference is nearly 25% when volume is based on van der Waals radii (211). The cluster has also been shown to capture cubane-type $[\text{MoFe}_3\text{S}_4]^{3+}$ and $[\text{VFe}_3\text{S}_4]^{2+}$ clusters, as in reaction 14. The product cluster was isolated as its Me_4N^+ salt in almost quantitative yield (215). This result demonstrates that the ligand, even as the trianion, is preconfigured, or rapidly achieves the correct configuration during binding, to coordinate to a single cluster.



C. Substitution Reactions

If properly designed, cluster derivatives of LS_3 should undergo their first ligand substitution reaction at the unique subsite. Formation of **37** and **39** in Scheme 13 are subsite-specific reactions of this sort, and proceed to completion with 1 equivalent of pivaloyl chloride in acetonitrile. An additional equivalent of the reagent gave no reaction after 15 min and the reaction was not complete after 3 h (33). This result demonstrates the differential kinetic stability of the tridentate ligand to electrophilic attack.

A wide variety of substitution reactions specific to the unique subsite have been carried out in aprotic solvents such as acetonitrile, DMF, and Me_2SO at ambient temperature (33, 216–219). A number of these reactions are depicted in Figs. 23 and 24, and underscore the reactivity of chloride cluster **37** and the utility of the ligand design. The chloride–thiolate interchange **37**–**39** in Fig. 23 is quantitative in both directions with stoichiometric quantities of reagents (33). The first examples of $[\text{4Fe-4S}]$ double cubanes were obtained by reactions with dithiolates (**40**) and sulfide (**41**) (216). Reaction with cyanide is complete with one equivalent to yield **42**. Earlier,

SUBSITE-SPECIFIC REACTIONS

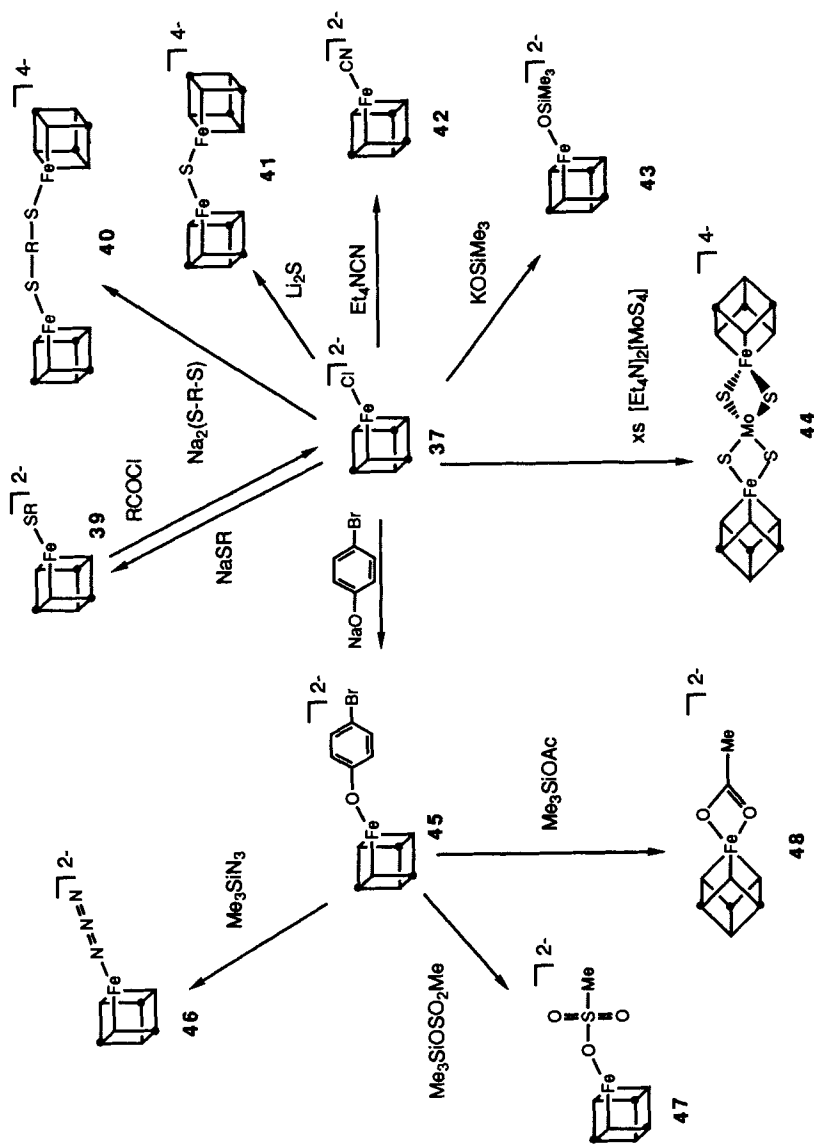


Figure 23. Ligand substitution reactions of $[Fe_2(L)_2]^{2-}$ (37) and $[Fe_2(LS_3)Cl]^{2-}$ (45) and $[Fe_2(LS_3)(OC_6H_4-p-Br)]^{2-}$ (46) to yield the clusters 39–45 and 46–48, respectively. Structures 46–48 are tentative.

SUBSITE-SPECIFIC REACTIONS

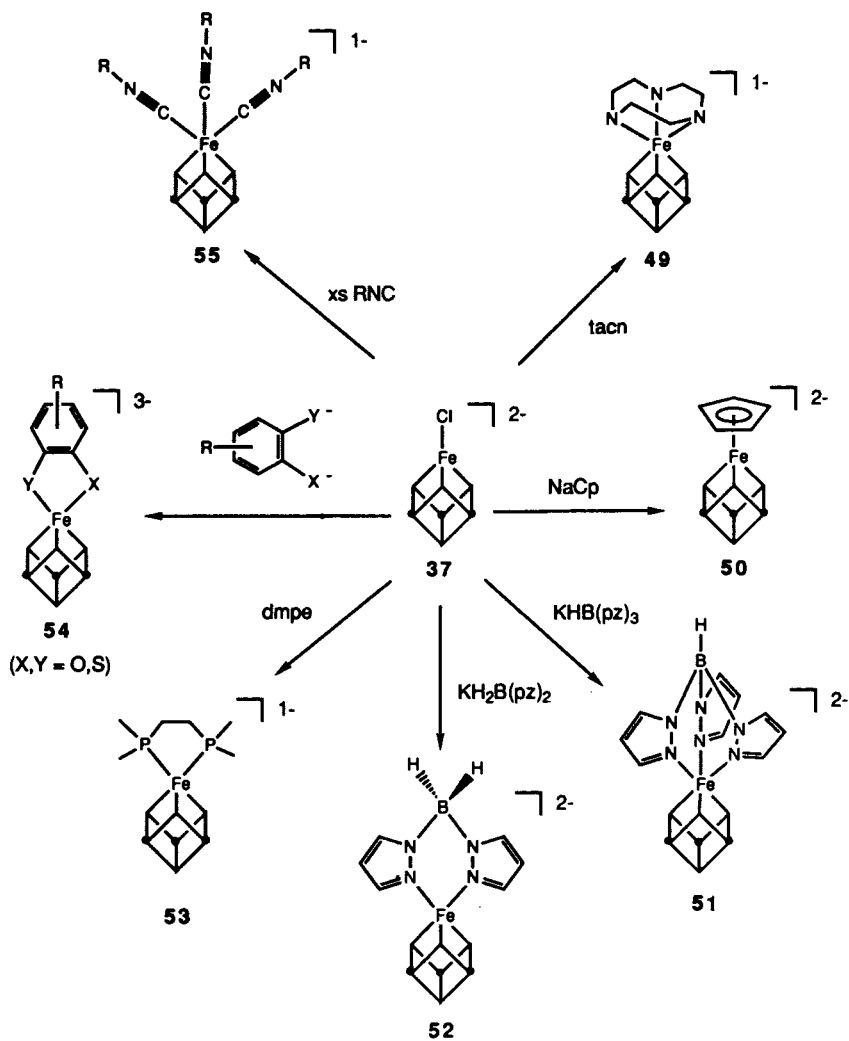


Figure 24. Ligand substitution reactions of $[\text{Fe}_4\text{S}_4(\text{LS}_3)\text{Cl}]^{2-}$ (37) to yield the clusters 49–55.

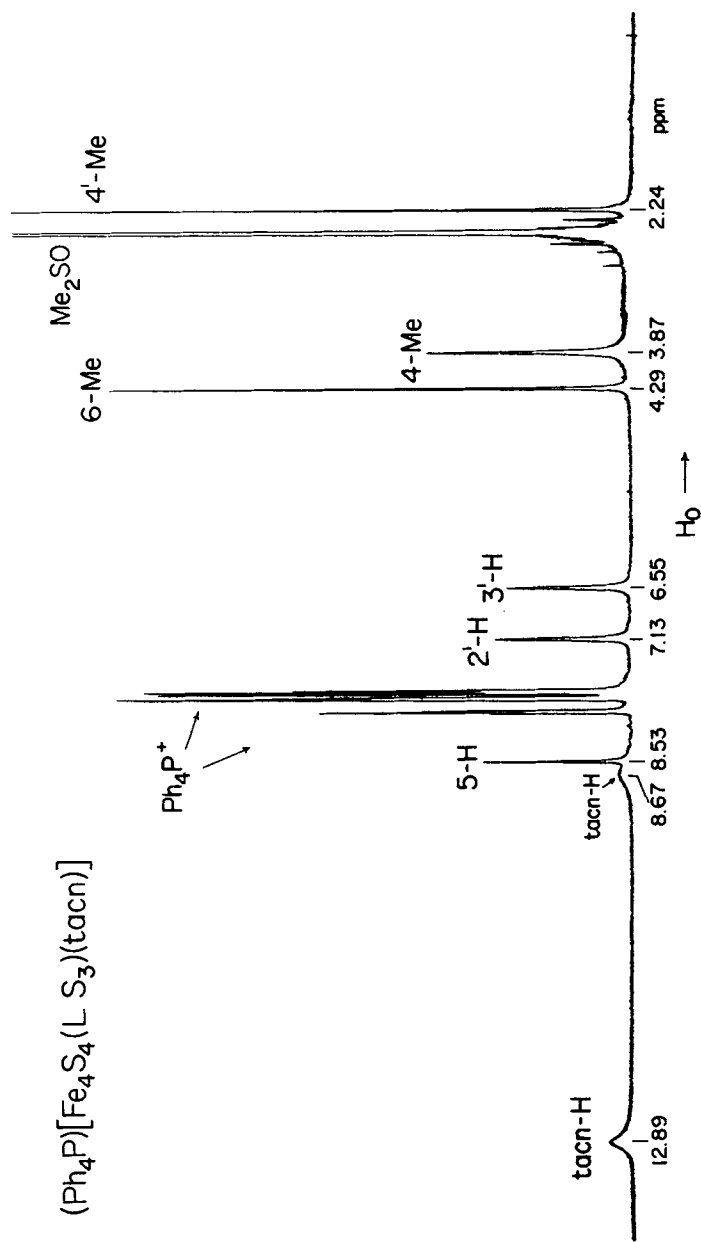


Figure 25. ^1H NMR spectrum of $[\text{Fe}_4\text{S}_4(\text{L,S}_3)(\text{tacn})]^-$ (**49**), formed by the reaction of **37** with 1 equivalent of tacn in Me_2SO solution.

cyanide had been placed at Fe subsites in a $[\text{MoFe}_3\text{S}_4]$ cluster by chloride displacement (220). A different type of bridged double cubane **44** is generated in an equilibrium reaction with $[\text{MoS}_4]^{2-}$. An apparently analogous cluster is formed with $[\text{VS}_4]^{3-}$. Displacement of chloride with *p*-bromophenolate gives **45**, which allows introduction of ligands that do not readily displace chloride. In this manner, clusters **46–48**, or possibly the cluster solvate, have been generated in high yield upon reaction with one equivalent of the appropriate trimethylsilyl reagent. The driving force of these reactions is, largely, the stability of the Si–O bond.

All reactions in Fig. 24 afford products in which the coordination number at the unique subsite is 5 or 6. Of product clusters **49–55**, **50** is the first organometallic derivative of a $[\text{4Fe–4S}]^{2+}$ cluster, and **49**, **51**, and **55** are the initial examples of six-coordinate subsites. Another example of a substituted cluster identified by ^1H NMR is provided by the spectrum in Fig. 25. Here 1 equivalent of tacn (1,4,7-triazacyclononane) reacts quantitatively with **37** to afford **49**, the 4-Me, 5-H, and 6-Me resonances of which are substantially shifted from their positions in the chloride cluster. The spectrum is indicative of trigonal symmetry. Certain of the clusters **40–55** are considered in subsequent sections.

D. Applications

With subsite-differentiated clusters in hand, we turn to their applications in examining subsite-specific properties of native $[\text{4Fe–4S}]$ clusters by the synthetic analogue approach. The potentially most important applications at this stage of development of subsite-specific cluster chemistry are listed below.

- Bridged double-cubane clusters
- Cluster linkage to Fe complexes
- Relative stabilities of oxidation states
- Modulation of electron distribution and coupling
- Cluster conversion $\text{Fe}_4\text{S}_4 \rightarrow \text{Fe}_3\text{S}_4$
- Heterometal clusters $\text{Fe}_3\text{S}_4 + \text{M} \rightarrow \text{MFe}_3\text{S}_4$
- Substrate binding and reactivity

Progress on the first four items is described in the following sections.

1. Bridged Double-Cubane Clusters

Interest in clusters of this type arises primarily from the possibility of examining interactions between component subclusters as dependent on their separation. In proteins magnetic interactions between $[\text{4Fe–4S}]^{1+}$ ($S = \frac{1}{2}$) clusters are often signaled by the appearance of additional features

in their rhombic $g = 1.94$ -type EPR spectra (221, 222). Clusters **40** and **41** provide the first opportunity to examine intramolecular cluster interactions modulated by the cluster spacers in **40**, with **41** containing the shortest bridge. The EPR spectra of fully reduced double cubanes are not well resolved but are roughly similar to those of proteins containing two [4Fe-4S]¹⁺ clusters separated by ~ 12 Å (216). The property of subcluster interactions that has been more profitably investigated is redox coupling in the successive reductions of the subclusters of **40** and **41**. These double-cubane clusters were isolated, but diffraction-quality crystals have not been obtained.* The ¹H NMR spectra fully support bridged structures inasmuch as the bridge resonances are indicative of twofold symmetry. In the case of **41**, the spectrum of which is shown in Fig. 26, the downfield shifts of 4-Me and 6-Me and, particularly, 5-H make very clear the presence of a structure not encountered previously.

Pertinent relationships for molecules containing two redox centers are given by the relationships 14–17 in Fig. 27. If, in the bridged double-cubane electron-transfer series 15, the subclusters behave as independent and identical centers, the separation in potentials and the comproportionation constant will have the statistical values of 36 mV and 4, respectively. Eisenstein and Wang (223) have derived the former value, in the context of the redox behavior of clostridial ferredoxins. Clusters **40a–40e** and **41** were prepared and examined by cyclic and differential pulse voltammetry (216); results are summarized in Table III. In order to interpret the peak potential separations ΔE_p for **40a–40e**, solution structures are required. The limiting transoid and cisoid conformations of subclusters are illustrated in Fig. 28 for cluster **40a**. In the interest of minimizing subcluster interactions, the transoid conformation is considered more probable than cisoid or any other arrangement that results in a shorter distance between subcluster centroids. The Ct···Ct distance is taken as a meaningful measure of subcluster separation. For cluster **41** there is only one conformation, assuming as in other cases free rotation about the bridge Fe–S bond. The Ct···Ct distance is based on an assumed Fe–S–Fe angle of 145°. The exact value is uncertain because the crystal structure of the compound is unknown. Angles of this type have been shown to be deformable by means of steric interactions across the bridge (224).

Electron-transfer coupling across bridges of variable length increases as the separation of subcluster centroids decreases. The order of coupling is **41** \gg **40e** > **40b** > **40a**, **40c**, and **40d**. The effect becomes detectable at < 11 Å and reaches a maximum at 7.5 Å, or less if the bridge angle is overestimated. With reference to Fig. 28, it is seen that subcluster sepa-

*The synthesis and structure of the sulfido-bridged double cubane [(Fe₄S₄Cl₃)₂S]⁴⁺ have been reported and the bridge Fe-S-Fe angle was shown to be 102° [P. R. Challen, S.-M. Koo, W. R. Dunham, and D. Coucouvanis, *J. Am. Chem. Soc.*, 112, 2455 (1990)].

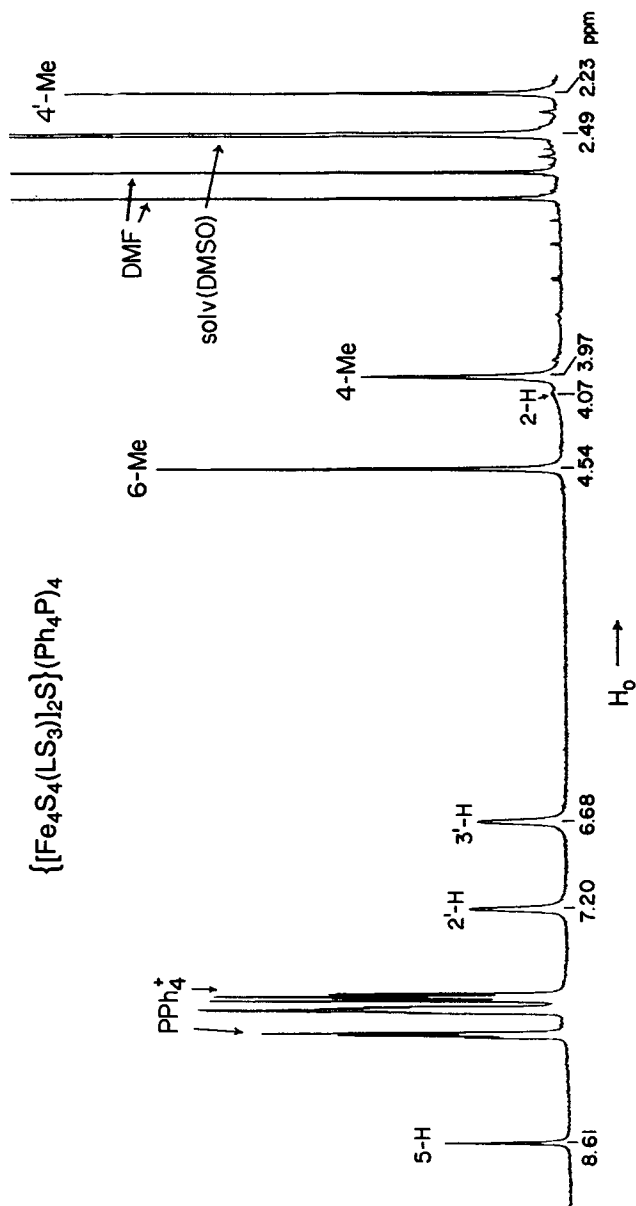


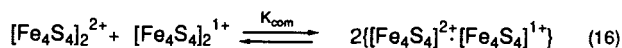
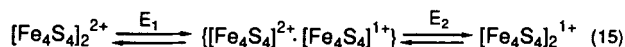
Figure 26. ¹H NMR spectrum of $\{[\text{Fe}_4\text{S}_4(\text{LS}_3)_2\text{S}]^+\}^-$ (41) in Me₂SO solution. The cluster was formed by the reaction of 37 and $\sim\frac{1}{2}$ equivalent of Li₂S. (Reproduced with permission from Ref. 216)

INTRAMOLECULAR REDOX CENTERS

two independent and identical centers:

$$E_1 - E_2 = \frac{2RT}{F} \ln 2 = 36 \text{ mV (298K)} \quad (14)$$

bridged double cubanes:



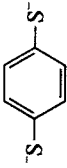
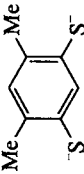
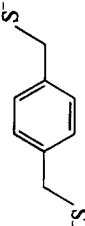
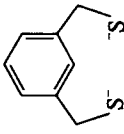

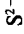
$$K_{\text{com}} = \frac{RT}{F} \exp(E_1 - E_2) = 4 \quad (298\text{K}) \quad (17)$$

Figure 27. Summary of information for two intramolecular redox centers, including the potential separation for two independent and identical centers (Eq. 14), the electron-transfer series 15 and comproportionation reaction 16 for double-cubane clusters, and the comproportionation constant (Eq. 17).

ration (under the foregoing assumption) is indistinguishable from that determined crystallographically for *P. aerogenes* ferredoxin (44). As found for this protein and other two-cluster proteins of comparable size, the synthetic double cubane shows no detectable coupling of its electron-transfer steps. The conjugated bridge offers no advantage over protein structure and the associated water molecules between the native subclusters. A plausible conclusion from these results is that in two-cluster proteins statistical or near-statistical potential differences imply a subcluster separation comparable to or larger than that in **40a**, provided cluster environments are similar. Based on the pseudo-twofold symmetry of *P. aerogenes* ferredoxin and sequence homology in the halves of the molecule, the two clusters are in very similar protein settings. Different environments around clusters would tend to uncouple potentials. Yet, no protein containing two [4Fe-4S] clusters is reported to have measurably different potentials. At the very least, a protein-bound sulfide-bridged double cubane should be recognizable by a potential separation comparable to the 220 mV of **41**, barring any bizarre protein effect to compensate for the intrinsic potential difference.

The cluster set **40** is merely one of a number with different bridging groups that can be conceived. An interesting question, but one difficult to explore experimentally because of the values of K_{com} for comproportionation reaction 16 (Fig. 27), is that of electron-transfer rates between sub-

TABLE III
Structural and Redox Properties of Bridged Double Cubanes^a

Cluster	Bridge	Distance, Å ^b			E _{pa} (V) ^d	ΔE _{pa} (mV)	K _{com}
		S...S	Fe...Fe	Ct...Ct ^c			
40a		6.35	8.75	11.4	-1.10	<30	~4
40b		5.50	7.87	10.6	-1.10, -1.14	~(40-60)	~7
40c		8.07	12.1	15.4	-1.11	<30	~4
40d		6.98	10.4	13.1	-1.10	<30	~4
40e		4.38	7.79	10.9	-1.13, -1.20	70	15
41		0	4.20	7.47	-1.28, -1.50	220	5.4 × 10 ³
<i>P. aerogenes</i> Fd ^e		6.43	8.87	11.5		<30 ^f	~4

^aSee Ref. 216.

^bCalculated for the transoid configuration using the indicated angles and distances (S* is a core atom). Clusters **40a-41**: for further details (cf. Ref. 216).

^cCt = centroid.

^dPotentials from differential pulse voltammetry in DMF solutions, vs. SCE.

^eDistances calculated from atom coordinates (44).

^fSee Ref. 223.

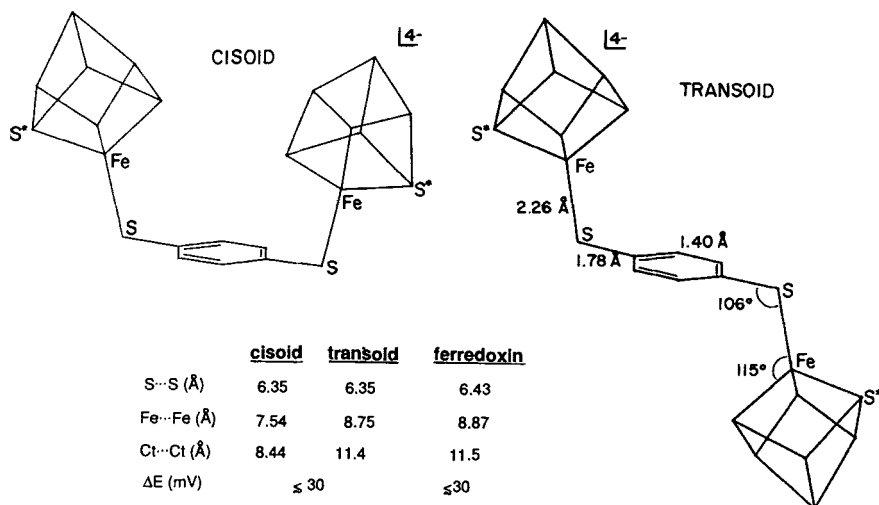


Figure 28. Depiction of the cisoid and transoid conformations of double-cubane cluster **40a**, including interatomic and centroid-centroid distances.

clusters as a function of the nature and length of the bridge. In the case of **41**, the reaction is much more favorable and is directed largely toward the half-reduced cluster. Unfortunately, this species has limited stability beyond the cyclic voltammetry time scale.

2. Cluster Linkage to Iron Complexes

The objective is to achieve a synthetic analogue of the sulfite reductase active site depicted in Fig. 16. Specific goals are detailed structural definition of the analogue, characterization of its magnetic interactions in different oxidation states, and determination of the mechanism of substrate reduction. From the protein crystal structure, the most desirable analogue would be one in which cluster and complex are bridged by a thiolate sulfur atom. Attempts by others to prepare such a species by the reaction of $[\text{Fe}_4\text{S}_4(\text{SPh})_4]^{2-}$ and $\text{Fe}(\text{OEP})\text{L}$ ($\text{L} = \text{ClO}_4^-$ or CF_3SO_3^-) gave $\text{Fe}(\text{OEP})(\text{SPh})$ or $\text{Fe}(\text{OEP})$, depending on the solvent (225). Attempts in this laboratory to prepare thiolate-bridged assemblies based on $[\text{Fe}_4\text{S}_4(\text{LS}_3)(\text{SMe})]^{2-}$ and several different $\text{Fe}(\text{II})$ complexes have thus far given inconclusive results; however, the first cluster-complex assemblies have been obtained with another type of bridge.

BRIDGED CLUSTER-Fe(COMPLEX) ASSEMBLIES

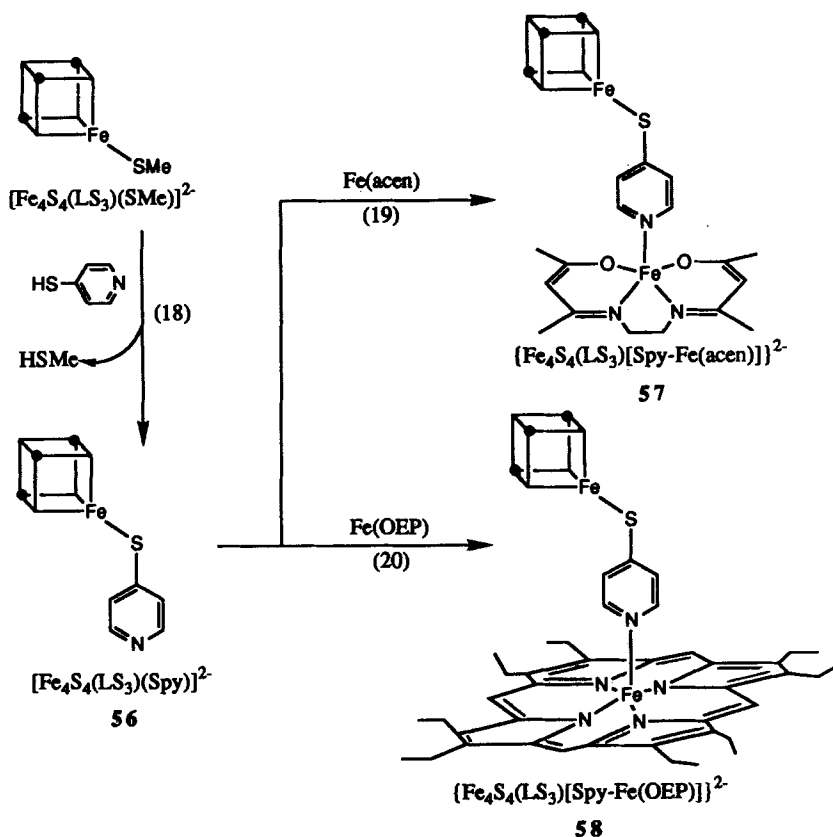


Figure 29. Preparation of functionalized cluster **56** by Reaction 18 and Fe(complex) assemblies **57** and **58** by Reactions 19 and 20.

One approach is set out in Fig. 29 (226). Subsite-derivatized cluster **56**, carrying a pyridine-4-thiolate ligand, reacts with the Fe(II) complexes Fe(acen) and Fe(OEP) to afford in equilibrium mixtures the bridged assemblies **57** and **58**, respectively, having an oxidation state corresponding to SiR^{1-} of the enzyme. Cluster **56** was isolated, and Reaction 19 was conducted in acetonitrile and Reaction 20 in thf. Products **57** and **58** have been identified by their ^1H NMR spectra, which show differences compared to the spectra of the uncombined cluster and complexes that are consistent

with bridge formation. The pyridyl resonances experience much larger isotropic shifts.

Species **57** and **58** comprise the first generation of bridged cluster-complex assemblies. Others with different features and more sophisticated design should be possible. For example, assemblies based on the pyridine-4-thiolate bridge do not allow cluster and porphyrin to achieve van der Waals contact. The pyridine-3-thiolate bridge, among others, does give rise to conformations in which such contact is possible. The desired Fe complex in the assembly is an Fe isobacteriochlorin, which would resemble siroheme, with its sirohydrochlorin ring **31**. Such complexes have been prepared (227). The isobacteriochlorin macrocycle appears to be more flexible in terms of ruffling and hole sizes (228), a possible advantage in bridge and substrate coordination. Indeed, it has recently been shown that sulfite reacts only with proteins containing the iron isobacteriochlorin ring system (229). Progress on cluster-complex assemblies is such that the specific goals noted above appear viable. Perhaps the most interesting of these is substrate reduction, in which electrons pass from cluster to complex to substrate. In this picture for the enzyme, the cluster appears between FMN and siroheme in the electron-transfer sequence given earlier. Appropriate site analogues may be useful in deciding whether electron transfer from cluster to macrocycle is significantly influenced by van der Waals contact of the two.

3. *Relative Stabilities of Oxidation States*

Extrinsic effects on the redox potentials of native [4Fe-4S] clusters arising from protein environment have been illustrated in Section II. As noted earlier, the $[4\text{Fe-4S}]^{2+.1+}$ potentials of analogue clusters can be altered significantly by variation of the four terminal ligands. Thus in the series $[\text{Fe}_4\text{S}_4\text{L}_4]^{2-.3-}$, $\text{L} = t\text{-BuS}^- (-1.42)$, $\text{PhS}^- (-1.04)$, $\text{Cl}^- (-0.79 \text{ V})$ (71, 76), the indicated potentials (V, vs. SCE, DMF, or acetonitrile) span a range of ~ 600 mV. This range is an intrinsic effect on cluster potentials inasmuch as it is caused by changes in covalently bound components of the cluster. With the availability of subsite-differentiated clusters, it becomes possible to explore the effects of ligand, coordination number, and charge variations at a single subsite on the relative stabilities of oxidation states. These are expressed by potentials for the three analogue redox couples in Fig. 3. Variation of unidentate, monoanionic ligands at the unique subsite usually produces only minor effects on $[\text{Fe}_4\text{S}_4]^{2+.1+}$ potentials inasmuch as only one subsite out of four is being altered. Attention is

restricted to clusters of type **54** (Fig. 24) where the coordination number at that site exceeds four.

In Fig. 30, the cyclic voltammograms of two clusters are compared in Me_2SO solutions. Cluster **59**, containing a conventional monodentate uninegative substituent at the singular site, reduces at $E_1 = -0.97$ V ($[\text{Fe}_4\text{S}_4]^{2+ \cdot 1+}$) and shows an irreversible oxidation. On the other hand,

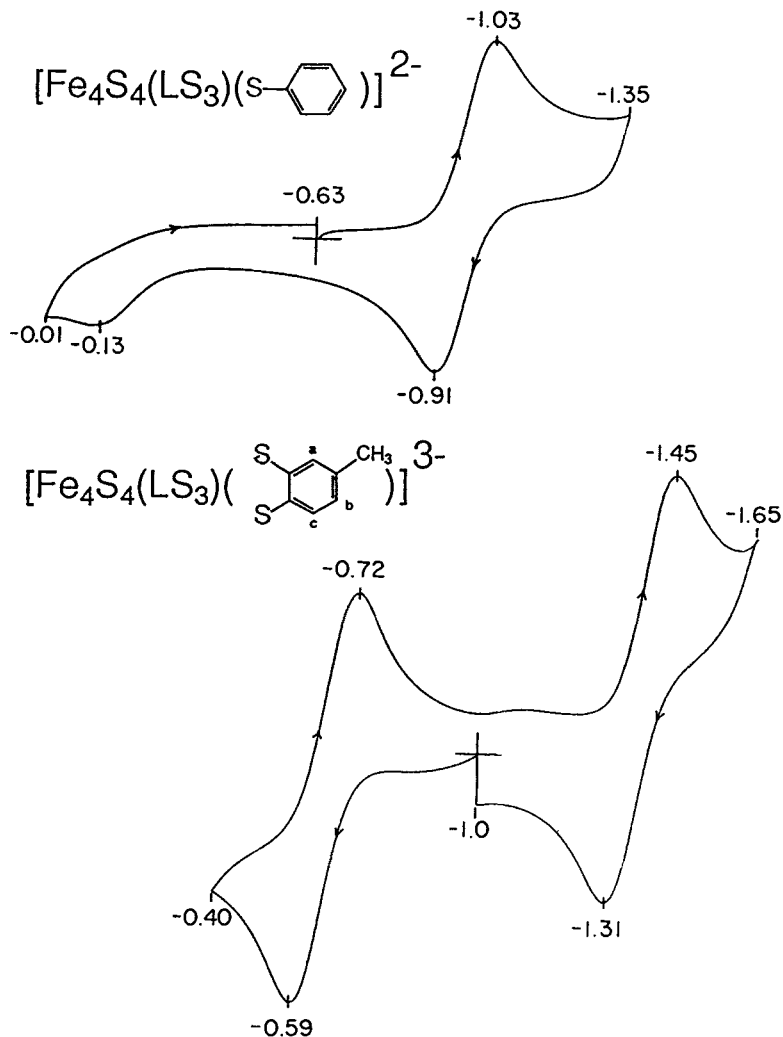
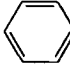
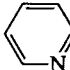
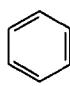
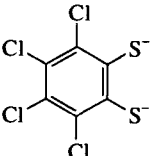
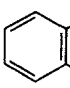
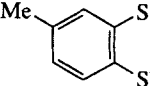


Figure 30. Cyclic voltammograms contrasting the redox behaviors of $[\text{Fe}_4\text{S}_4(\text{LS}_3)(\text{SPh})]^{2-}$ and $[\text{Fe}_4\text{S}_4(\text{LS}_3)(\text{tdt})]^{3-}$ in Me_2SO solution. Potentials are referenced to the SCE.

cluster **54d**, with toluene-3,4-dithiolate at that site, displays two reversible reactions. The $[\text{Fe}_4\text{S}_4]^{2+,1+}$ couple is found at $E_1 = -1.38$ V and the $[\text{Fe}_4\text{S}_4]^{3+,2+}$ couple at $E_1 = -0.66$ V. Chemically reversible oxidations of $[\text{Fe}_4\text{S}_4\text{L}_4]^{2-}$ clusters with L a uninegative ligand are most uncommon in the more polar aprotic solvents such as acetonitrile, DMF, and Me_2SO . Relative to benzenethiolate, the dithiolate ligand is expected to raise the electron density in the core, and increases by one unit the negative charge of the cluster. Both of these effects will shift potentials of the two couples to more negative values, increasing the ease of oxidation. The significant point is the magnitude of the effect. The oxidation is shifted by about 750 mV and the reduction by about 400 mV. The potentials in Table IV reveal similar but somewhat smaller shifts for related ligands. Note that the bidentate monoanionic ligand in **60** causes no significant change in behavior compared to **59**. The potential for the $[\text{VFe}_3\text{S}_4(\text{LS}_3)(\text{CN})_3]^{3-,4-}$ couple is more negative by 490 mV than is that for the isoelectronic couple $[\text{VFe}_3\text{S}_4-$

TABLE IV
Redox Potentials of Five-Coordinate [4Fe-4S] Clusters in Me_2SO

Cluster	L	$E_{1/2}$, (V) ^a	
		$[\text{Fe}_4\text{S}_4]^{3+,2+}$	$[\text{Fe}_4\text{S}_4]^{2+,1+}$
59		≥ -0.1 (irreversible)	-0.97
60		≥ 0.0 (irreversible)	-0.99
54a		-0.43	-1.26
54b		-0.48	-1.27
54c		-0.62	-1.38
54d		-0.66	-1.38

^aPotentials vs SCE at 297 K.

(LS₃)(Me₂SO)₃]^{0.1-} (215). In this case, the potential shift is comparable to that of **54b**, but cluster charge differs by three units instead of the one-unit difference between **54** and **59**.

Cluster charge differences do not necessarily produce large potential shifts or even shifts in the expected direction. As one example, the reduction of cluster **49** (Fig. 24), with a 1- charge, occurs at $E_1 = -1.13$ V in Me₂SO, a negative shift of 100 mV vs. **37** and 160 mV vs. **59**. The latter two clusters have a 2- charge. The positive shift expected for **49** on a charge basis alone is evidently overcompensated by electron donation to the core from the three nitrogen atoms of the tacn ligand.

The information in Table IV is part of our findings on the relative stabilities of oxidation states as effected by ligand changes at a single subsite. One particularly interesting possible behavior of native clusters is suggested by these data. Presumably, protein-directed attachment of two monoanionic ligands at one subsite would cause large negative potential shifts of the [4Fe-4S]^{3+.2+} couple. In synthetic clusters, chelate ligands are required to bind two negative atoms to the same subsite. Two cysteinate sulfur atoms might induce this effect. A shift of 400-600 mV would be sufficient to displace the potential from the region normally associated with the HP_{ox/red} couple. Because the potentials for this couple are the most positive of any known native [4Fe-4S]^{3+.2+} couple, there would appear to be no need to consider cluster modifications that would raise them further. We have already observed in Section II.C that bulky, hydrophobic ligands stabilize the 3+ state of synthetic clusters.

Potentials of the [4Fe-4S]^{1+.0} and [4Fe-4S]^{2+.1+} couples could be increased by one or more of these factors: (a) reduction of cluster net charge; (b) extensive hydrogen bonding to the cluster; (c) protonation of the reduced form of a couple. Other than the possibly anomalous examples of **49** and **55**, factor (a) has not yet been tested by substitution of a neutral ligand at the unique subsite. In early work, it was found that reduction of [Fe₄S₄(S-*p*-C₆H₄NMe₃)₄]²⁺ occurred at $E_1 = -0.79$ V (DMF), a positive shift of 240 mV compared to [Fe₄S₄(SPh)₄]²⁻ (76). Because of the inductive property of the Me₃N⁺ group, the effect is not simply that of a positive cluster charge. It is mildly suggestive, however, of a positive potential shift upon the introduction of one neutral π-donor ligand at a subsite of a [4Fe-4S]^{2+.1+} cluster. Factor (b) has been considered in Section II.B and is generally evident for clusters when redox potentials are compared in protic and aprotic solvents. Factor (c) is apparent in the results of Section II.E.

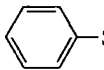
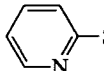
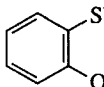
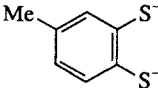
None of the preceding factors has yet been examined for the [4Fe-4S]^{1+.0} couple, which has not been established in proteins, and, for synthetic clusters, occurs at very negative potentials and is frequently irreversible. It is one of the two candidates for the P^N/P^{OX} couple of nitrogenase (Fig.

14). Conceivably, the $[4\text{Fe}-4\text{S}]^{3+,2+}$ potential could be shifted in the negative direction by effects of the type operative in the clusters in Table IV. In a study of the oxidation of the dithionite-reduced FeMo protein of *K. pneumoniae*, however, the first EPR-observable event is removal of electrons from P-clusters to afford a spectrum typical of the $[4\text{Fe}-4\text{S}]^{1+}$ ($S = \frac{1}{2}$) oxidation state (190). A protein conformational change most likely is responsible, for a spin change to a higher spin state of P^{OX} , which is EPR silent. While the full significance of this transient spectrum, which maximally accounts for only $0.16e^-$ /molecule under the particular experimental conditions employed, is not yet understood, its observation does favor the $[4\text{Fe}-4\text{S}]^{1+,0}$ couple for the $\text{P}^{\text{N}}/\text{P}^{\text{OX}}$ transition. If this interpretation is correct, the factors that raise the potential of this couple to near -0.5 V vs. NHE remain to be elucidated.

4. Modulation of Electron Distribution and Coupling

The Mössbauer spectral data in Table V, drawn from a larger data set for clusters with varying coordination number at the unique subsite (219), illustrate how the isomer shift and quadrupole splitting of that subsite can

TABLE V
Mössbauer Parameters of Five-Coordinate [4Fe-4S] Clusters^{a,b}

Cluster	L		δ^c (mm·s ⁻¹)	ΔE_Q (mm·s ⁻¹)
59		{ 1	0.34	1.40
		{ 2, 3	0.34	1.04
60		{ 1	0.52	1.70
		{ 2, 3	0.34, 0.34	1.26, 0.94
54a		{ 1	0.52	1.45
		{ 2, 3	0.33, 0.34	1.37, 1.03
54d	 "P-Clusters"	{ 1	0.52	1.97
		{ 2, 3	0.36, 0.37	1.29, 0.96
		{ Fe ²⁺	0.55	3.03
		{ D,S	0.51, 0.52	1.33, 0.68

^aUnique subsite bolded.

^bParameters are from fits of spectra at 4.2 K to three doublets, with that of subsite 1 constrained to 25% of the total intensity.

^cRelative to Fe metal at 4.2 K.

be affected by the binding of a bidentate ligand. In the case of reference cluster **59**, the isomer shifts are normal for a $[4\text{Fe}-4\text{S}]^{2+}$ cluster with terminal thiolate ligands, and the unique subsite is recognized only by a somewhat larger quadrupole splitting. Incorporation of a bidentate monoanionic ligand in cluster **60** causes a large increase in the isomer shift and a smaller increase in the quadrupole splitting. The $\text{Me}_2\text{NCS}_2^-$ ligand at the unique site gives the same isomer shift but a slightly larger quadrupole splitting ($1.85 \text{ mm}\cdot\text{s}^{-1}$). The two bidentate dianionic ligands afford the same isomer shift as in **60**. In this group of clusters, the isomer shift reaches a maximum of $\sim 2 \text{ mm}\cdot\text{s}^{-1}$ in **54d**. For a set of $[4\text{Fe}-4\text{S}]^{2+}$ clusters with one or two dithiocarbamate ligands, $\delta = 0.50\text{--}0.52 \text{ mm}\cdot\text{s}^{-1}$ and $\Delta E_{\text{O}} = 1.8\text{--}2.1 \text{ mm}\cdot\text{s}^{-1}$ (24).

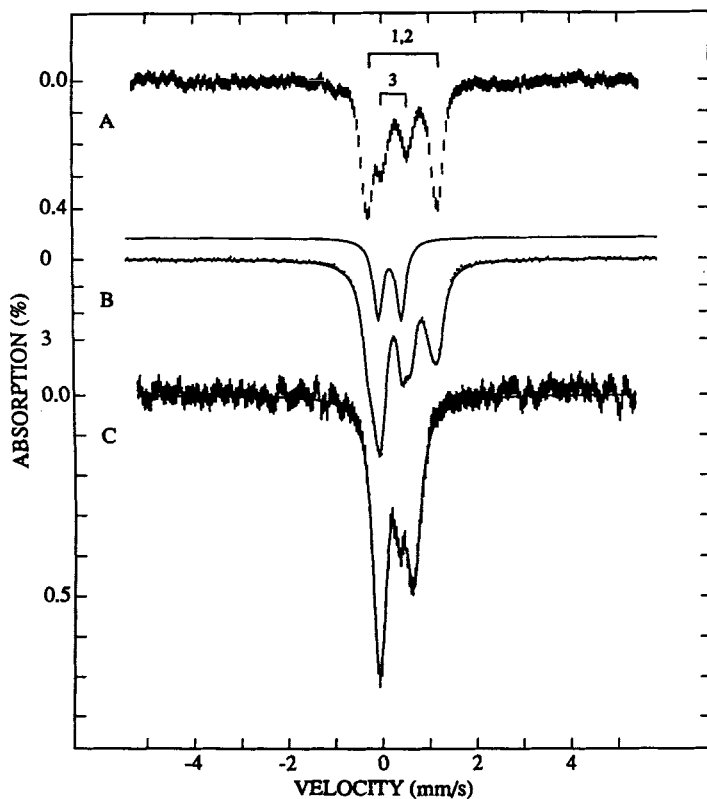
From the foregoing results, it is apparent that bidentate ligands can increase both δ and ΔE_{O} values appreciably compared to cluster **59** as a reference. Indeed, both terminal ligand interactions need not be strong to achieve this result. In $(\text{Et}_4\text{N})_2[\text{Fe}_4\text{S}_4(\text{SC}_6\text{H}_4\text{-2-OH})_4]$, the FeS_4O subsite ($\delta = 0.49 \text{ mm}\cdot\text{s}^{-1}$, $\Delta E_{\text{O}} = 1.82 \text{ mm}\cdot\text{s}^{-1}$) is formed by terminal ligand bonding with a Fe-S distance of 2.313 \AA , which is 0.035 \AA longer than the Fe-S distances at the three tetrahedral subsites. The Fe-O distance is 2.318 \AA , which is 0.45 \AA longer than the mean Fe-O distance in $[\text{Fe}_4\text{S}_4(\text{Oph})_4]^{2-}$ (21). Note that the Mössbauer parameters approach those of **54a** but, unlike that cluster, the hydroxyl group is not deprotonated. The largest isomer shift encountered thus far is $0.83 \text{ mm}\cdot\text{s}^{-1}$ in cluster **52**, which has a five-coordinate (FeS_3N_2) subsite; for this species $\Delta E_{\text{O}} = 2.38 \text{ mm}\cdot\text{s}^{-1}$. In the general case, ligand alterations at other subsites should afford (hypothetical) clusters with Mössbauer parameters comparable to those for the unique subsites in the preceding set.

Isomer shifts of P^{N} cluster subsites are consistent with the $[4\text{Fe}-4\text{S}]^0$ description, with the unique site having the parameters of a tetrahedral $\text{Fe}^{\text{II}}\text{S}_4$ unit as in reduced rubredoxin. If the other three subsites have terminal thiolate ligation, it is most unclear why their quadrupole splittings are so much lower. If the P^{N} clusters exist in the $[4\text{Fe}-4\text{S}]^{2+}$ state, it follows from the data at hand that there are ligation modes that could produce isomer shifts of $\sim 0.5 \text{ mm}\cdot\text{s}^{-1}$ at all subsites. But there is presently no demonstrated means of achieving this result with either oxidation state while effecting a quadrupole splitting of $3 \text{ mm}\cdot\text{s}^{-1}$. It is a reasonable conclusion that isomer shifts are far easier to simulate in analogue clusters than are quadrupole splittings, which can be highly sensitive to ligand type and the precise geometry at an Fe site.

In addition to producing biased electron distributions in the otherwise symmetrically delocalized $[4\text{Fe}-4\text{S}]^{2+}$ core, subsite-specific substitution can

alter spin coupling within the core. In the simplest view, the two Fe^{2+} and two Fe^{3+} ions in the core are antiferromagnetically coupled to yield an $S = 0$ ground state and a ladder of excited paramagnetic states. The tris(isocyanide) cluster **55** ($R = t\text{-Bu}$) is formed in an equilibrium reaction with **37** in Me_2SO , 10 equivalents of isocyanide affording essentially quantitative formation of the cluster (217). Methyl- and ethylisocyanide react in the same way to afford clusters with properties analogous to those of **55**. The ^1H NMR spectrum of the clusters indicate trigonal symmetry and relative signal intensities establish the composition. The isotropic shifts of **55** are 5–8 times larger than those of **37** or of **42**, which has one anionic π -acid ligand. This result indicates a ground state with $S > 0$, unprecedented behavior for the $[\text{4Fe-4S}]^{2+}$ state that was clarified by Mössbauer spectroscopy (217). Spectrum *b* in Fig. 31 is that of the Ph_4P^+ salt of cluster **55** and consists of several overlapping quadrupole doublets. It can be understood with reference to spectrum *a*, that of reduced *Dg Fd II* (132), which contains a $[\text{3Fe-4S}]^0$ cluster with $S = 2$. This spectrum consists of two doublets in 2:1 area ratio. Indistinguishable subsites 1 and 2 are a $\text{Fe}^{3+}/\text{Fe}^{2+}$ delocalized pair ($\text{Fe}^{2.5+}$) and subsite 3 is trapped-valence Fe^{3+} . This type of spectrum is an unambiguous signature of all protein $[\text{3Fe-4S}]^0$ clusters examined to date (124, 128, 132, 141, 142, 230, 231).

Spectrum *b* can be decomposed into four equally intense doublets with the parameters given in Fig. 31. Three of the four doublets (subsites 1–3) have parameters similar to *Dg Fd II*, whereas those of subsite 4 are typical of low-spin Fe^{2+} . This interpretation was confirmed by analysis of the magnetically perturbed spectrum of **55**. The spectral analysis convincingly demonstrates the following points. (a) The $[\text{4Fe-4S}]^{2+}$ core contains a unique Fe^{2+} subsite that is diamagnetic, leaving a *spin-isolated* $[\text{3Fe-4S}]^0$ cluster fragment. (b) The cluster fragment has an $S = 2$ ground state and effectively the same electron distribution as protein $[\text{3Fe-4S}]^0$ clusters. (c) Because the cluster fragment closely approaches or achieves its highest possible symmetry (trigonal), *the electronic ground state consisting of a delocalized pair of Fe atoms ($\text{Fe}^{2.5+}$) and localized Fe^{3+} is intrinsic to a $[\text{3Fe-4S}]^0$ cluster*, and is not induced by protein structure and environment. The key feature of cluster **55** is clearly the presence of three isocyanide ligands, which induce a low-spin Fe^{2+} condition at the unique subsite. This Fe atom functions magnetically as does Zn^{2+} in the artificial $[\text{ZnFe}_3\text{S}_4]^{1+}$ cluster of *Dg Fd II* (159). Above 100 K, doublets 1–3 decrease in intensity as a new doublet appears. At 260 K, spectrum *C* is observed. It consists of the low-spin Fe^{2+} doublet and the new doublet with an isomer shift the average of the shifts of sites 1–3. This result indicates that the cluster has become electronically delocalized, or “valence-detrapped” at higher tem-



Subsite	δ (mm/s)	ΔE_Q (mm/s)	type
1	0.34	1.21	Fe ^{2.5+}
2	0.35	1.49	Fe ^{2.5+}
3	0.22	0.59	Fe ³⁺
4	0.08	0.50	low-spin Fe ²⁺

Figure 31. Zero-field Mössbauer spectra of reduced *Dg* Fd II (a) (137) and cluster 55 (b, c) at 4.2 K (A, B) and 260 K (c). The doublets of Fd II subsite 4 (Fe³⁺) and delocalized pair subsites 2 and 3 (Fe^{2.5+}) are marked by brackets. The solid line in spectrum b is a least-squares fit to four sites of equal intensity. The doublet of low-spin Fe²⁺ is drawn separately above spectrum b. The solid line in spectrum c is a least-squares fit to two doublets with a 1:3 intensity ratio. (Reproduced with permission from Ref. 217.)

peratures. As observed earlier, reduced *Dg Fd II* behaves in the same way (142).

The structure at the unique subsite of **55** may resemble that of the $\text{Fe}(\text{CO})_3$ subsites in $\text{Fe}_4\text{S}_4(\text{CO})_{12}$ (232), in which case longer Fe-Fe and Fe-S distances will tend to separate this subsite from the others. Normally, the $[\text{4Fe-4S}]^{2+}$ core of protein and analogue clusters are characterized by close or exact tetragonal symmetry.

E. Prospectus

In 1972, when Sieker, Adman, and Jensen (64) demonstrated the existence of cubane-type [4Fe-4S] clusters in a protein and when Herskovitz et al. (233) reported the simple synthesis and the structure of a synthetic analogue, no one could have foreseen the pervasive occurrence of these structures in organisms at all levels of life. Today, a [4Fe-4S] cluster must be considered a prosthetic group of the fundamental importance of a heme or a flavin. During the last 15 years iron-sulfur biochemistry has passed from a state of near obscurity to scientific prosperity. One need only reflect upon the evolution of our understanding of aconitase, due to the superb contributions of Beinert, Hoffman, Münck, Stout, and their co-workers, to appreciate the sophistication in experimentation and thought that has developed in this field. The principal advantage of synthetic analogues is that it places in the hands of anyone accurate representations of protein clusters that submit to an examination of intrinsic properties by appropriate manipulation of terminal ligation and oxidation state.

Site-specific properties are merely the newest, but certainly not the last, features of these clusters that may be profitably pursued with analogue clusters. Our research to date has approached the first four of the seven potential applications in Section IV.D. Much more remains to be done. For example, cluster **55** and a number of others of the general $[\text{Fe}_4\text{S}_4(\text{LS}_3)\text{L}]^z$ type exhibit chemically reversible $[\text{4Fe-4S}]^{3+.2+}$ and $[\text{4Fe-4S}]^{2+.1+}$ redox steps in dichloromethane. This property potentially provides access to the $[\text{4Fe-4S}]^{1+.3+}$ states of site-derivatized clusters. In the context of [3Fe-4S] clusters, it provides a potential means to examine the 1- and 1+ oxidation states. Iron atom removal from **55** or another $[\text{Fe}_4\text{S}_4(\text{LS}_3)\text{L}]^z$ cluster would accomplish $[\text{4Fe-4S}] \rightarrow [\text{3Fe-4S}]$ cluster conversion, and open the way to what will surely be an extensive family of heterometal MFe_3S_4 clusters. Lastly, clusters with particularly labile ligands such as the methanesulfonate species **47** (Fig. 23) may be effective in binding and activating enzyme substrates such as citrate. In this event, it may be possible to isolate and examine individual states along a simulated enzymatic reaction pathway.

ABBREVIATIONS

acen	N,N'-(Acetylacetonato)ethylenediamine(2-)
<i>Av</i>	<i>Azotobacter vinelandii</i>
BI	bovine insulin
BSA	bovine serum albumin
<i>Dg</i>	<i>Desulfovibrio gigas</i>
DMF	N,N-dimethylformamide
Fd	ferredoxin
HP	high-potential protein
LS ₃	1,3,5-tris[(4,6-dimethyl-3-mercaptophenyl)thio]-2,4,6-tris(<i>p</i> -tolylthio)benzene(3-)
MCD	magnetic circular dichroism
NHE	normal hydrogen electrode
OEP	2,3,7,8,12,13,17,18-Octaethylporphinate(2-)
SCE	saturated calomel electrode
taen	1,4,7-triazacyclononane
tdt	toluene-3,4-dithiolate(2-)

ACKNOWLEDGMENTS

Our research in Fe-S chemistry is supported by NIH Grant GM 28856. We thank Professor H. Beinert and Professor B. M. Hoffman for information prior to publication, and Dr. T. D. P. Stack for useful discussions. We are particularly indebted to our enthusiastic and accomplished co-workers in this field. The names of many of them are found in the references.

REFERENCES

1. J. M. Berg and R. H. Holm, in *Iron-Sulfur Proteins*, Vol. 4, T. G. Spiro, Ed., Wiley-Interscience, New York, 1982, Chapter 1.
2. J. J. Mayerle, S. E. Denmark, B. V. DePamphilis, J. A. Ibers, and R. H. Holm, *J. Am. Chem. Soc.*, **97**, 1032 (1975).
3. M. A. Bobrik, K. O. Hodgson, and R. H. Holm, *Inorg. Chem.*, **16**, 1851 (1977).
4. W. Saak and S. Pohl, *Z. Naturforsch.*, **40b**, 1105 (1985).
5. A. Salifoglou, A. Simopoulos, A. Kostikas, W. R. Dunham, M. G. Kanatzidis, and D. Coucouvanis, *Inorg. Chem.*, **27**, 3394 (1988).
6. T. Tsukihara, K. Fukuyama, M. Nakamura, Y. Katsube, N. Tanaka, M. Kakudo, K. Wada, T. Hase, and H. Matsubara, *J. Biochem. (Tokyo)*, **90**, 1763 (1981).

7. T. Tsutsui, T. Tsukihara, K. Fukuyama, Y. Katsube, T. Hase, H. Matsubara, Y. Nishikawa, and N. Tanaka, *J. Biochem. (Tokyo)*, **94**, 299 (1983).
8. T. Tsukihara, K. Fukuyama, and Y. Katsube, in *Iron-Sulfur Protein Research*; H. Matsubara, Y. Katsube, and K. Wada, Eds., Japan Scientific Societies Press, Tokyo, 1986, pp. 59-68.
9. J. L. Sussman, J. H. Brown, and M. Shoham, in *Iron-Sulfur Protein Research*; H. Matsubara, Y. Katsube, and K. Wada, Eds., Japan Scientific Societies Press, Tokyo, 1986, pp. 69-82.
10. K. S. Hagen, A. D. Watson, and R. H. Holm, *J. Am. Chem. Soc.*, **105**, 3905 (1983).
11. G. H. Stout, S. Turley, L. C. Sieker, and L. H. Jensen, *Proc. Natl. Acad. Sci. USA*, **85**, 1020 (1988).
12. C. R. Kissinger, E. T. Adman, L. C. Sieker, and L. H. Jensen, *J. Am. Chem. Soc.*, **110**, 8721 (1988).
13. C. D. Stout, *J. Biol. Chem.*, **263**, 9256 (1988).
14. C. D. Stout, *J. Mol. Biol.*, **205**, 545 (1989).
15. C. R. Kissinger, E. T. Adman, L. C. Sieker, L. H. Jensen, and J. LeGall, *FEBS Lett.*, **244**, 447 (1989).
16. B. A. Averill, T. Herskovitz, R. H. Holm, and J. A. Ibers, *J. Am. Chem. Soc.*, **95**, 3523 (1973).
17. L. Que, Jr., M. A. Bobrik, J. A. Ibers, and R. H. Holm, *J. Am. Chem. Soc.*, **96**, 4168 (1974).
18. M. A. Bobrik, E. J. Laskowski, R. W. Johnson, W. O. Gillum, J. M. Berg, K. O. Hodgson, and R. H. Holm, *Inorg. Chem.*, **17**, 1402 (1978).
19. P. K. Mascharak, K. S. Hagen, J. T. Spence, and R. H. Holm, *Inorg. Chim. Acta*, **80**, 157 (1983).
20. G. Christou, C. D. Garner, M. G. B. Drew, and R. Cammack, *J. Chem. Soc. Dalton Trans.*, 1550 (1981).
21. W. E. Cleland, D. A. Holtman, M. Sabat, J. A. Ibers, G. C. DeFotis, and B. A. Averill, *J. Am. Chem. Soc.*, **105**, 6021 (1983).
22. R. E. Johnson, G. C. Papaefthymiou, R. B. Frankel, and R. H. Holm, *J. Am. Chem. Soc.*, **105**, 7280 (1983).
23. M. G. Kanatzidis, N. C. Baenziger, D. Coucouvanis, A. Simopoulos, and A. Kostikas, *J. Am. Chem. Soc.*, **106**, 4500 (1984).
24. M. G. Kanatzidis, D. Coucouvanis, A. Simopoulos, A. Kostikas, and V. Papaefthymiou, *J. Am. Chem. Soc.*, **107**, 4925 (1985).
25. A. Müller, N. Schladerbeck, and H. Bögge, *Chimia*, **39**, 24 (1985).
26. T. J. Ollerenshaw, C. D. Garner, B. Odell, and W. Clegg, *J. Chem. Soc. Dalton Trans.*, 2161 (1985).
27. N. Ueyama, T. Sugawara, M. Fuji, A. Nakamura, and N. Yasuoka, *Chem. Lett.*, 175 (1985).

28. W. Cen and H. Liu, *Jiegou Huaxue (J. Struct. Chem)*, **5**, 203 (1986).
29. J. Gloux, P. Gloux, H. Hendriks, and G. Rius, *J. Am. Chem. Soc.*, **109**, 3220 (1987).
30. A. Müller, N. Schladerbeck, and H. Bögge, *J. Chem. Soc. Chem. Commun.*, **35** (1987).
31. S. Pohl and W. Saak, *Z. Naturforsch.*, **43b**, 457 (1988).
32. S. Rutchik, S. Kim, and M. A. Walters, *Inorg. Chem.*, **27**, 1513 (1988).
33. T. D. P. Stack and R. H. Holm, *J. Am. Chem. Soc.*, **109**, 2546 (1987); **110**, 2484 (1988).
34. T. O'Sullivan and M. M. Millar, *J. Am. Chem. Soc.*, **107**, 4096 (1985).
35. E. J. Laskowski, R. B. Frankel, W. O. Gillum, G. C. Papaefthymiou, J. Renaud, J. A. Ibers, and R. H. Holm, *J. Am. Chem. Soc.*, **100**, 5322 (1985).
36. J. M. Berg, K. O. Hodgson, and R. H. Holm, *J. Am. Chem. Soc.*, **101**, 4586 (1979).
37. D. W. Stephan, G. C. Papaefthymiou, R. B. Frankel, and R. H. Holm, *Inorg. Chem.*, **22**, 1550 (1983).
38. K. S. Hagen, A. D. Watson, and R. H. Holm, *Inorg. Chem.*, **23**, 2984 (1984).
39. M. J. Carney, G. C. Papaefthymiou, M. A. Whitener, K. Spartalian, R. B. Frankel, and R. H. Holm, *Inorg. Chem.*, **27**, 346 (1988).
40. M. J. Carney, G. C. Papaefthymiou, K. Spartalian, R. B. Frankel, and R. H. Holm, *J. Am. Chem. Soc.*, **110**, 6084 (1988).
41. M. J. Carney, G. C. Papaefthymiou, R. B. Frankel, and R. H. Holm, *Inorg. Chem.*, **28**, 1497 (1989).
42. C. W. Carter, Jr., J. Kraut, S. T. Freer, R. A. Alden, L. C. Sieker, E. Adman, and L. H. Jensen, *Proc. Natl. Acad. Sci. USA*, **69**, 3526 (1972).
43. C. W. Carter, Jr., J. Kraut, S. T. Freer, and R. A. Alden, *J. Biol. Chem.*, **249**, 6339 (1974).
44. E. T. Adman, L. C. Sieker, and L. H. Jensen, *J. Biol. Chem.*, **248**, 3987 (1973).
45. K. Fukuyama, Y. Nagahara, T. Tsukihara, Y. Katsube, T. Hase, and H. Matsubara, *J. Mol. Biol.*, **199**, 183 (1988).
46. C. D. Stout, in *Iron-Sulfur Proteins*, T. G. Spiro, Ed., Wiley-Interscience, New York, 1982, Chapter 3.
47. M. G. Kanatzidis, W. R. Hagen, W. R. Dunham, R. K. Lester, and D. Coucouvanis, *J. Am. Chem. Soc.*, **107**, 953 (1985).
48. M. G. Kanatzidis, A. Salifoglou, and D. Coucouvanis, *Inorg. Chem.*, **25**, 2460 (1986).
49. W. Saak, G. Henkel and S. Pohl, *Angew. Chem. Int. Ed. Engl.*, **23**, 150 (1984).
50. B. S. Snyder, M. S. Reynolds, I. Noda, and R. H. Holm, *Inorg. Chem.*, **27**, 595 (1988).

51. B. S. Snyder and R. H. Holm, *Inorg. Chem.*, **27**, 2339 (1988).
52. M. S. Reynolds and R. H. Holm, *Inorg. Chem.*, **27**, 4494 (1988).
53. G. Christou, M. Sabat, J. A. Ibers, and R. H. Holm, *Inorg. Chem.*, **21**, 3518 (1982).
54. H. Strasdeit, B. Krebs, and G. Henkel, *Inorg. Chem.*, **23**, 1816 (1984).
55. H. Strasdeit, B. Krebs, and G. Henkel, *Z. Naturforsch.*, **42b**, 565 (1987).
56. A. Agresti, M. Bacci, F. Cecconi, C. A. Ghilardi, and S. Midollini, *Inorg. Chem.*, **24**, 689 (1985).
57. F. Cecconi, C. A. Ghilardi, S. Midollini, A. Orlandini, and P. Zanello, *J. Chem. Soc. Dalton Trans.*, 831 (1987).
58. I. Noda, B. S. Snyder, and R. H. Holm, *Inorg. Chem.*, **25**, 3851 (1986).
59. S. Pohl and W. Saak, *Angew. Chem. Int. Ed. Engl.*, **23**, 907 (1984).
60. M. C. Kennedy, T. A. Kent, M. Emptage, H. Merkle, H. Beinert, and E. Münck, *J. Biol. Chem.*, **259**, 14463 (1984).
61. H. Brintzinger, G. Palmer, and R. H. Sands, *Proc. Natl. Acad. Sci. USA*, **55**, 397 (1966).
62. J. F. Gibson, D. O. Hall, J. H. M. Thornley, and F. R. Whatley, *Proc. Natl. Acad. Sci. USA*, **56**, 987 (1966).
63. C. W. Carter, Jr., S. T. Freer, Ng. H. Xuong, R. A. Alden, and J. Kraut, *Cold Spring Harbor Symp. Quant. Biol.*, **36**, 381 (1972).
64. L. C. Sieker, E. Adman, and L. H. Jensen, *Nature (London)*, **235**, 40 (1972).
65. K. S. Hagen, J. G. Reynolds, and R. H. Holm, *J. Am. Chem. Soc.*, **103**, 4054 (1981).
66. W. O. Gillum, L. E. Mortenson, J.-S. Chen, and R. H. Holm, *J. Am. Chem. Soc.*, **99**, 584 (1977).
67. G. R. Dukes and R. H. Holm, *J. Am. Chem. Soc.*, **97**, 528 (1975).
68. T. C. Bruice, R. Maskiewicz, and R. Job, *Proc. Natl. Acad. Sci. USA*, **72**, 231 (1975).
69. R. C. Job and T. C. Bruice, *Proc. Natl. Acad. Sci. USA*, **72**, 2478 (1975).
70. G. Christou and C. D. Garner, *J. Chem. Soc. Dalton Trans.*, 1093 (1979).
71. G. B. Wong, M. A. Bobrik, and R. H. Holm, *Inorg. Chem.*, **17**, 578 (1978).
72. R. W. Johnson and R. H. Holm, *J. Am. Chem. Soc.*, **100**, 5338 (1978).
73. M. Nakamoto, K. Tanaka, and T. Tanaka, *J. Chem. Soc. Chem. Commun.*, 1422 (1988).
74. V. Papaefthymiou, M. M. Millar, and E. Münck, *Inorg. Chem.*, **25**, 3010 (1986).
75. D. J. Evans and G. J. Leigh, *J. Chem. Soc. Chem. Commun.*, 395 (1988).
76. B. V. DePamphilis, B. A. Averill, T. Herskovitz, L. Que, Jr., and R. H. Holm, *J. Am. Chem. Soc.*, **96**, 4159 (1974).
77. C. L. Hill, J. Renaud, R. H. Holm, and L. E. Mortenson, *J. Am. Chem. Soc.*, **99**, 2549 (1977).

78. L. Que, Jr., J. R. Anglin, M. A. Bobrik, A. Davison, and R. Holm, *J. Am. Chem. Soc.*, **96**, 6042 (1974).
79. R. J. Burt, B. Ridge, and H. N. Rydon, *J. Chem. Soc. Dalton Trans.*, 1228 (1980).
80. E. T. Adman, K. D. Watenpaugh, and L. H. Jensen, *Proc. Natl. Acad. Sci. USA*, **72**, 4854 (1975).
81. N. Ueyama, T. Terakawa, M. Nakata, and A. Nakamura, *J. Am. Chem. Soc.*, **105**, 7098 (1983).
82. M. Ueyama, A. Kajiwarra, T. Terakawa, S. Ueno, and A. Nakamura, *Inorg. Chem.*, **24**, 4700 (1985).
83. N. Ueyama, T. Terakawa, T. Sugawara, M. Fugi, and A. Nakamura, *Chem. Lett.*, 1287 (1984).
84. J. Peisach, N. Orme-Johnson, W. B. Mims, and W. H. Orme-Johnson, *J. Biol. Chem.*, **252**, 5643 (1977).
85. J. Neiman, A. J. Naaktgeboren, and J. Reedijk, *Inorg. Chim. Acta*, **93**, L9 (1984).
86. Y. Okuno, K. Uoto, Y. Sasaki, O. Yonemitsu, and T. Tomohiro, *J. Chem. Soc. Chem. Commun.*, 874 (1987).
87. Y. Okuno, K. Uoto, O. Yonemitsu, and T. Tomohiro, *J. Chem. Soc., Chem. Commun.*, 1018 (1987).
88. B. Siegel, *J. Inorg. Nucl. Chem.*, **41**, 609 (1979).
89. Y. Kuroda, Y. Sasaki, Y. Shiroywa, and I. Tabushi, *J. Am. Chem. Soc.*, **110**, 4049 (1988).
90. K. Tanaka, T. Tanaka, and I. Kawafume, *Inorg. Chem.*, **23**, 518 (1984).
91. K. Tanaka, M. Moriya, and T. Tanaka, *Inorg. Chem.*, **25**, 835 (1986).
92. K. Tanaka, M. Masanaga, and T. Tanaka, *J. Am. Chem. Soc.*, **108**, 5448 (1986).
93. I. Tabushi, Y. Kuroda, and Y. Sasaki, *Tetrahedron Lett.*, **27**, 1187 (1986).
94. I. Tabushi, Y. Kuroda, and Y. Sasaki, *J. Chem. Soc. Chem. Commun.*, 1622 (1987).
95. B. Odell and P. J. Geary, *J. Chem. Soc. Dalton Trans.*, 29 (1984).
96. I. Okura, S. Nakamura, and M. Kobayashi, *Bull. Chem. Soc. Jpn.*, **54**, 3794 (1981).
97. M. D. Monteil, J. B. Nguini Effa, J. Lieto, P. Verlaque, and D. Benlian, *Inorg. Chim. Acta*, **76**, L309 (1983).
98. J. P. Weterings and R. Prins, *Inorg. Chim. Acta*, **125**, L23 (1986).
99. R. G. Bowman and R. L. Burwell, Jr., *J. Am. Chem. Soc.*, **101**, 2877 (1977).
100. R. J. Burt, G. J. Leigh, and C. J. Pickett, *J. Chem. Soc. Chem. Commun.*, 940 (1976).
101. J.-C. Moutet and C. J. Pickett, *J. Chem. Soc. Chem. Commun.*, 188 (1989).
102. M. G. Kanatzidis, N. C. Baenziger, D. Coucouvanis, A. Simopoulos, and A. Kostikas, *J. Am. Chem. Soc.*, **106**, 4500 (1984).

103. M. G. Kanatzidis, D. Coucouvanis, A. Simopoulos, A. Kostikas, and V. Papaefthymiou, *J. Am. Chem. Soc.*, *107*, 4925 (1985).
104. W. D. Phillips and M. Poe, in *Iron-Sulfur Proteins*, Vol. II, W. Lovenberg, Ed., Academic Press, New York, 1973, Chapter 7.
105. E. L. Packer, W. V. Sweeney, J. C. Rabinowitz, H. Sternlicht, and E. N. Shaw, *J. Biol. Chem.*, *252*, 2245 (1977).
106. D. G. Nettlesheim, T. E. Meyer, B. A. Feinberg, and J. D. Otvos, *J. Biol. Chem.*, *258*, 8235 (1983).
107. R. Krishnamoorthi, J. L. Markley, M. A. Cusanovich, C. T. Przysiecki, and T. E. Meyer, *Biochemistry*, *25*, 60 (1986).
108. J. Meyer, J. Gaillard, and J.-M. Moulis, *Biochemistry*, *27*, 6150 (1988).
109. J. Gaillard, J.-M. Moulis, and J. Meyer, *Inorg. Chem.*, *26*, 320 (1987).
110. P. Middleton, D. P. E. Dickson, C. E. Johnson, and J. D. Rush, *Eur. J. Biochem.*, *88*, 135 (1978).
111. P. Middleton, D. P. E. Dickson, C. E. Johnson, and J. D. Rush, *Eur. J. Biochem.*, *104*, 289 (1980).
112. J.-M. Moulis, P. Auric, J. Gaillard, and J. Meyer, *J. Biol. Chem.*, *259*, 11396 (1984).
113. P. Auric, J. Gaillard, J. Meyer, and J.-M. Moulis, *Biochem. J.*, *242*, 525 (1987).
114. H. Beinert and A. J. Thomson, *Arch. Biochem. Biophys.*, *222*, 333 (1983).
115. A. H. Robbins and C. D. Stout, *Proc. Nat. Acad. Sci. USA*, *86*, 3639 (1989).
116. H. Beinert, M. H. Emptage, J.-L. Dreyer, R. A. Scott, J. E. Hahn, K. O. Hodgson, and A. J. Thomson, *Proc. Natl. Acad. Sci. USA*, *80*, 393 (1983).
117. L. Rydèn, L. G. Öfverstedt, H. Beinert, M. H. Emptage, and M. C. Kennedy, *J. Biol. Chem.*, *259*, 3141 (1984).
118. H. Beinert, *Anal. Biochem.*, *131*, 373 (1983).
119. E. P. Day, J. Peterson, J. J. Bonvoisin, I. Moura, and J. J. G. Moura, *J. Biol. Chem.*, *263*, 3684 (1988).
120. B. A. C. Ackrell, E. B. Kearney, W. B. Mims, J. Peisach, and H. Beinert, *J. Biol. Chem.*, *259*, 4015 (1984).
121. M. K. Johnson, D. E. Bennett, J. E. Morningstar, M. W. W. Adams, and L. E. Mortenson, *J. Biol. Chem.*, *260*, 5456 (1985).
122. J. E. Morningstar, M. K. Johnson, G. Cecchini, B. A. C. Ackrell, and E. B. Kearney, *J. Biol. Chem.*, *260*, 13631 (1985).
123. M. K. Johnson, J. E. Morningstar, D. E. Bennett, B. A. C. Ackrell, and E. B. Kearney, *J. Biol. Chem.*, *260*, 7368 (1985).
124. T. A. Kent, J.-L. Dreyer, M. C. Kennedy, B. H. Huynh, M. H. Emptage, H. Beinert, and E. Münck, *Proc. Natl. Acad. Sci. USA*, *79*, 1096 (1982).
125. M. C. Kennedy, M. H. Emptage, J.-L. Dreyer, and H. Beinert, *J. Biol. Chem.*, *258*, 11098 (1983).
126. M. H. Emptage, J.-L. Dreyer, M. C. Kennedy, and H. Beinert, *J. Biol. Chem.*, *258*, 11106 (1983).

127. M. K. Johnson, A. J. Thomson, A. J. M. Richards, J. Peterson, A. E. Robinson, R. R. Ramsey, and T. P. Singer, *J. Biol. Chem.*, **259**, 2274 (1984).
128. T. A. Kent, M. H. Emptage, H. Merkle, M. C. Kennedy, H. Beinert, and E. Münck, *J. Biol. Chem.*, **260**, 6871 (1985).
129. M. C. Kennedy and H. Beinert, *J. Biol. Chem.*, **263**, 8194 (1988).
130. M. H. Emptage, in *Metal Clusters in Proteins*, L. Que, Jr., Ed.; ACS Symposium Series 392; American Chemical Society, Washington, DC, 1988, Chapter 17.
131. T. A. Kent, I. Moura, J. J. G. Moura, B. H. Huynh, J. LeGall, A. V. Xavier, and E. Münck, *FEBS Lett.*, **138**, 55 (1982).
132. J. J. G. Moura, I. Moura, T. A. Kent, J. D. Lipscomb, B. H. Huynh, J. LeGall, A. V. Xavier, and E. Münck, *J. Biol. Chem.*, **257**, 6259 (1982).
133. J. J. G. Moura, J. LeGall, and A. V. Xavier, *Eur. J. Biochem.*, **141**, 319 (1984).
134. P. J. Stephens, T. V. Morgan, C. D. Stout, and B. K. Burgess, in *Frontiers in Bioinorganic Chemistry*, A. V. Xavier, Ed., VCH Publishers, Weinheim, 1985, pp. 637-646.
135. B. Guigliarelli, P. Bertrand, C. More, P. Papavassiliou, E. C. Hatchikian, and J. P. Gayda, *Biochim. Biophys. Acta*, **810**, 319 (1985).
136. S. H. Bell, D. P. E. Dickson, C. E. Robinson, R. Cammack, D. O. Hall, and K. K. Rao, *FEBS Lett.*, **142**, 143 (1982).
137. K. Nagayama, Y. Ozaki, Y. Kyogoku, T. Hase, and H. Matsubara, *J. Biochem. (Tokyo)*, **94**, 893 (1983).
138. A. J. Thomson, A. E. Robinson, M. K. Johnson, R. Cammack, K. K. Rao, and D. O. Hall, *Biochim. Biophys. Acta*, **637**, 423 (1981).
139. M. K. Johnson, T. G. Spiro, and L. E. Mortenson, *J. Biol. Chem.*, **257**, 2447 (1982).
140. K. Nagayama, T. Imai, D. Ohmori, and T. Oshima, *FEBS Lett.*, **169**, 79 (1984).
141. M. H. Emptage, T. A. Kent, B. H. Huynh, J. Rawlings, W. H. Orme-Johnson, and E. Münck, *J. Biol. Chem.*, **255**, 1793 (1980).
142. V. Papaefthymiou, J.-J. Girerd, I. Moura, J. J. G. Moura, and E. Münck, *J. Am. Chem. Soc.*, **109**, 4703 (1987).
143. R. Hille, T. Yoshida, G. E. Tarr, C. H. Williams, Jr., M. L. Ludwig, J. A. Fee, T. A. Kent, B. H. Huynh, and E. Münck, *J. Biol. Chem.*, **258**, 13008 (1983).
144. P. J. Stephens, T. V. Morgan, F. Devlin, J. E. Penner-Hahn, K. O. Hodgson, R. A. Scott, C. D. Stout, and B. K. Burgess, *Proc. Natl. Acad. Sci. USA*, **82**, 5661 (1985).
145. A. J. Thomson, A. E. Robinson, M. K. Johnson, J. J. G. Moura, I. Moura, A. V. Xavier, and J. LeGall, *Biochim. Biophys. Acta*, **670**, 93 (1981).
146. M. K. Johnson, D. E. Bennett, J. A. Fee, and W. V. Sweeney, *Biochim. Biophys. Acta*, **911**, 81 (1987).

147. M. Bruschi, E. C. Hatchikian, J. LeGall, J. J. G. Moura, and A. V. Xavier, *Biochim. Biophys. Acta*, **449**, 275 (1976).
148. R. Cammack, K. K. Rao, D. O. Hall, J. J. G. Moura, A. V. Xavier, M. Bruschi, J. LeGall, A. Deville, and J.-P. Gayda, *Biochim. Biophys. Acta*, **490**, 311 (1977).
149. D. Ghosh, S. O'Donnell, W. Furey, Jr., A. H. Robbins, and C. D. Stout, *J. Mol. Biol.*, **158**, 73 (1982).
150. M. Bruschi and F. Guerlesquin, *FEMS Microbiol. Rev.*, **54**, 155 (1988).
151. D. W. Plank and J. B. Howard, *J. Biol. Chem.*, **263**, 8184 (1988).
152. H. Beinert and M. C. Kennedy, *Eur. J. Biochem.*, **186**, 5 (1989).
153. M. Werst, M. C. Kennedy, H. Beinert, and B. M. Hoffman, manuscript in preparation.
154. J. B. Howard, T. W. Lorsch, D. Ghosh, K. Melis, and C. D. Stout, *J. Biol. Chem.*, **258**, 508 (1983).
155. T. V. Morgan, P. J. Stephens, B. K. Burgess, and C. D. Stout, *FEBS Lett.*, **167**, 137 (1984).
156. T. V. Morgan, P. J. Stephens, F. Devlin, B. K. Burgess, and C. D. Stout, *FEBS Lett.*, **183**, 206 (1985).
157. P. J. Stephens, T. V. Morgan, F. Devlin, J. E. Penner-Hahn, K. O. Hodgson, R. A. Scott, C. D. Stout, and B. K. Burgess, *Proc. Natl. Acad. Sci. USA*, **82**, 5661 (1985).
158. I. Moura, J. J. G. Moura, E. Münck, V. Papaefthymiou, and J. LeGall, *J. Am. Chem. Soc.*, **108**, 349 (1986).
159. K. K. Surerus, E. Münck, I. Moura, J. J. G. Moura, and J. LeGall, *J. Am. Chem. Soc.*, **109**, 3805 (1987).
160. R. H. Holm and E. D. Simhon, in *Molybdenum Enzymes*, T. G. Spiro, Ed., Wiley-Interscience, New York, 1985, Chapter 2.
161. J. A. Kovacs and R. H. Holm, *J. Am. Chem. Soc.*, **108**, 340 (1986); *Inorg. Chem.*, **26**, 702, 711 (1987).
162. S. Ciurli, M. J. Carney, R. H. Holm, and G. C. Papaefthymiou, *Inorg. Chem.*, **28**, 2696 (1989).
163. M. H. Emptage, T. A. Kent, M. C. Kennedy, H. Beinert, and E. Münck, *Proc. Natl. Acad. Sci. USA*, **80**, 4674 (1983).
164. J. Telsner, M. H. Emptage, H. Merkle, M. C. Kennedy, H. Beinert, and B. M. Hoffman, *J. Biol. Chem.*, **261**, 4840 (1986).
165. M. C. Kennedy, M. Werst, J. Telsner, M. H. Emptage, H. Beinert, and B. M. Hoffman, *Proc. Natl. Acad. Sci. USA*, **84**, 8854 (1987).
166. J. V. Schloss, M. H. Emptage, and W. W. Cleland, *Biochemistry*, **23**, 4572 (1984).
167. J. Strouse, S. W. Layten, and C. E. Strouse, *J. Am. Chem. Soc.*, **99**, 562 (1976).
168. J.-L. Dreyer, *Eur. J. Biochem.*, **150**, 145 (1985).

169. R. K. Scopes and K. Griffiths-Smith, *Anal. Biochem.*, **136**, 530 (1984).
170. J. M. Kelly and R. K. Scopes, *FEBS Lett.*, **202**, 274 (1986).
171. R. D. Kuchta, G. R. Hanson, B. Holmquist, and R. H. Abeles, *Biochemistry*, **25**, 7301 (1986).
172. D. H. Flint and M. H. Emptage, *J. Biol. Chem.*, **263**, 3558 (1988).
173. S. J. Vollmer, R. L. Switzer, and P. G. Debrunner, *J. Biol. Chem.*, **258**, 14284 (1983).
174. R. P. Cunningham, H. Asahara, J. F. Bank, C. P. Scholes, J. C. Salerno, K. Surerus, E. Münck, J. McCracken, J. Peisach, and M. H. Emptage, *Biochemistry*, **28**, 4450 (1989).
175. W. H. Orme-Johnson, *Ann. Rev. Biophys. Biophys. Chem.*, **14**, 419 (1985).
176. E. I. Stiefel, H. Thomann, H. Jin, R. E. Bare, T. V. Morgan, S. J. N. Burgmayer, and C. L. Coyle, in *Metal Clusters in Proteins*, L. Que, Jr., Ed., ACS Symposium Series 372, American Chemical Society, Washington, DC, 1988, Chapter 18.
177. D. J. Lowe, R. N. F. Thorneley, and B. E. Smith, *Top. Mol. Struct. Biol.*, **6** (*Metalloproteins*, Part 1), 1985, Chapter 6.
178. B. A. Averill, *Struct. Bonding*, **53**, 59 (1983).
179. R. Zimmermann, E. Münck, W. J. Brill, V. K. Shah, M. T. Henzl, J. Rawlings, and W. H. Orme-Johnson, *Biochim. Biophys. Acta*, **537**, 185 (1978).
180. G. D. Watt, A. Burns, S. Lough, and D. L. Tennent, *Biochemistry*, **19**, 4926 (1980).
181. G. D. Watt, A. Burns, and D. L. Tennent, *Biochemistry*, **20**, 7272 (1981).
182. G. D. Watt and Z.-C. Wang, *Biochemistry*, **25**, 5196 (1986).
183. B. H. Huynh, M. T. Henzl, J. A. Christner, R. Zimmermann, W. H. Orme-Johnson, *Biochim. Biophys. Acta*, **623**, 124 (1980).
184. J. P. Smith, M. H. Emptage, and W. H. Orme-Johnson, *J. Biol. Chem.*, **257**, 2310 (1982).
185. M. K. Johnson, A. J. Thomson, A. E. Robinson, and B. E. Smith, *Biochim. Biophys. Acta*, **671**, 61 (1981).
186. P. A. McLean, V. Papaefthymiou, W. H. Orme-Johnson, and E. Münck, *J. Biol. Chem.*, **262**, 12900 (1987).
187. C. J. Pickett, *J. Chem. Soc. Chem. Commun.*, 322 (1985).
188. C. L. Hill, J. Renaud, R. H. Holm, and L. E. Mortenson, *J. Am. Chem. Soc.*, **99**, 2549 (1977).
189. R. A. Henderson and A. G. Sykes, *Inorg. Chem.*, **19**, 3103 (1980).
190. B. E. Smith, D. J. Lowe, G.-X. Chen, M. J. O'Donnell, and T. R. Hawkes, *Biochem. J.*, **209**, 207 (1983).
191. L. M. Siegel and P. S. Davis, *J. Biol. Chem.*, **249**, 1587 (1974).
192. M. J. Murphy, L. M. Siegel, S. R. Tove, and H. Kamin, *Proc. Natl. Acad. Sci. USA*, **71**, 612 (1974).

193. M. J. Murphy, L. M. Siegel, H. Kamin, and D. Rosenthal, *J. Biol. Chem.*, **248**, 2801 (1973).
194. L. M. Siegel, D. C. Rueger, M. J. Barber, R. J. Krueger, N. R. Orme-Johnson, and W. H. Orme-Johnson, *J. Biol. Chem.*, **257**, 6343 (1982).
195. D. E. McRee, D. C. Richardson, J. S. Richardson, and L. M. Siegel, *J. Biol. Chem.*, **261**, 10277 (1986).
196. J. A. Christner, E. Münck, P. A. Janick, and L. M. Siegel, *J. Biol. Chem.*, **258**, 11147 (1983).
197. J. A. Christner, P. A. Janick, L. M. Siegel, and E. Münck, *J. Biol. Chem.*, **258**, 11157 (1983).
198. J. A. Christner, E. Münck, T. A. Kent, P. A. Janick, J. C. Salerno, and L. M. Siegel, *J. Am. Chem. Soc.*, **106**, 6786 (1984).
199. P. A. Janick and L. M. Siegel, *Biochemistry*, **21**, 3538 (1982); **22**, 504 (1983).
200. J. F. Madden, S. Han, L. M. Siegel, and T. G. Spiro, *Biochemistry*, **28**, 5471 (1989).
201. J. F. Cline, P. A. Janick, L. M. Siegel, and B. M. Hoffman, *Biochemistry*, **24**, 7942 (1985).
202. B. H. Huynh, L. Kang, D. V. DerVartanian, H. D. Peck, Jr., and J. LeGall, *J. Biol. Chem.*, **259**, 15373 (1984).
203. J. R. Lancaster, J. M. Vega, H. Kamin, N. R. Orme-Johnson, W. H. Orme-Johnson, R. J. Krueger, and L. M. Siegel, *J. Biol. Chem.*, **254**, 1268 (1979).
204. M. Hirasawa-Soga and G. Tamura, *Agric. Biol. Chem.*, **45**, 1615 (1981).
205. W. Saak and S. Pohl, *Z. Naturforsch.*, **43b**, 813 (1988).
206. L. L. Nelson, F. Y.-K. Lo, A. D. Rae, and L. F. Dahl, *J. Organometal. Chem.*, **225**, 309 (1982).
207. T. D. P. Stack, Ph.D. Thesis, Harvard University, 1988.
208. D. D. MacNicol, in *Inclusion Compounds*, Vol. 2, J. L. Atwood, J. E. D. Davies and D. D. MacNicol, Eds., Academic Press, New York, 1984, Chapter 5.
209. A. D. U. Hardy, D. D. MacNicol, and D. R. Wilson, *J. Chem. Soc. Perkin Trans. 2*, 137 (1978).
210. C. J. Gilmore, D. D. MacNicol, A. Murphy, and M. A. Russell, *Tetrahedron Lett.*, **23**, 3269 (1983).
211. T. D. P. Stack, J. A. Weigel, and R. H. Holm, *Inorg. Chem.*, in press.
212. R. H. Holm, W. D. Phillips, B. A. Averill, J. J. Mayerle, and T. Herskovitz, *J. Am. Chem. Soc.*, **96**, 2109 (1974).
213. J. G. Reynolds, E. J. Laskowski, and R. H. Holm, *J. Am. Chem. Soc.*, **100**, 5315 (1978).
214. D. J. Cram, *Science*, **219**, 1177 (1983).
215. S. Ciurli and R. H. Holm, *Inorg. Chem.*, **28**, 1685 (1989).
216. T. D. P. Stack, M. J. Carney, and R. H. Holm, *J. Am. Chem. Soc.*, **111**, 1670 (1989).

217. J. A. Weigel, R. H. Holm, K. K. Surerus, and E. Münck, *J. Am. Chem. Soc.*, *111*, 9246 (1989).
218. J. A. Weigel and R. H. Holm, results to be published.
219. S. Ciurli, M. Carrié, J. A. Weigel, M. J. Carney, T. D. P. Stack, G. C. Papaefthymiou, and R. H. Holm, *J. Am. Chem. Soc.*, *112*, 2654 (1990).
220. R. E. Palermo and R. H. Holm, *J. Am. Chem. Soc.*, *105*, 4310 (1983).
221. G. Palmer, in *The Enzymes*, Vol. 22, P. D. Boyer, Ed.; Academic Press, New York, 1975; Part B, Chapter 1.
222. R. C. Prince and M. W. W. Adams, *J. Biol. Chem.*, *262*, 5125 (1987).
223. K. K. Eisenstein and J. H. Wang, *J. Biol. Chem.*, *244*, 1720 (1969).
224. R. N. Mukherjee, T. D. P. Stack, and R. H. Holm, *J. Am. Chem. Soc.*, *110*, 1850 (1988).
225. A. M. Stolzenberg and M. T. Stershic, *Inorg. Chem.*, *24*, 3098 (1985).
226. B. Scharbert and R. H. Holm, results to be published.
227. A. M. Stolzenberg, S. H. Strauss, and R. H. Holm, *J. Am. Chem. Soc.*, *103*, 4763 (1981).
228. A. M. Stolzenberg and M. T. Stershic, *J. Am. Chem. Soc.*, *110*, 5397 (1988).
229. L. J. Young and L. M. Siegel, *Biochemistry*, *27*, 2790 (1988).
230. R. Hille, T. Yoshida, G. E. Tarr, C. H. Williams, Jr., M. L. Ludwig, J. A. Fee, T. A. Kent, B. H. Huynh, and E. Münck, *J. Biol. Chem.*, *258*, 13008 (1983).
231. B. H. Huynh, D. S. Patil, I. Moura, M. Teixeira, J. J. G. Moura, D. V. DerVartanian, M. H. Czechowski, B. C. Pickrill, H. D. Peck, Jr., and J. LeGall, *J. Biol. Chem.*, *262*, 795 (1987).
232. L. L. Nelson, F. Y.-K. Lo, A. D. Rae, and L. F. Dahl, *J. Organometal. Chem.*, *225*, 309 (1982).
233. T. Herskovitz, B. A. Averill, R. H. Holm, J. A. Ibers, W. D. Phillips, and J. F. Weiher, *Proc. Natl. Acad. Sci. USA*, *69*, 2437 (1972).

Indoleamine 2,3-Dioxygenase: Properties and Functions of a Superoxide Utilizing Enzyme

**OSAMU HAYAISHI, OSAMU TAKIKAWA, and
RYOTARO YOSHIDA**

*Department of Cell Biology
Osaka Bioscience Institute
Osaka, Japan*

CONTENTS

I. DISCOVERY OF OXYGENASES	76
II. DISCOVERY OF INDOLEAMINE 2,3-DIOXYGENASE	77
III. PURIFICATION OF INDOLEAMINE 2,3-DIOXYGENASE	78
A. Indoleamine 2,3-Dioxygenase from Rabbit Small Intestine	79
B. Indoleamine 2,3-Dioxygenase from Human Placenta	79
IV. PROPERTIES OF INDOLEAMINE 2,3-DIOXYGENASE	80
A. Substrate Specificity	80
B. Participation of O_2^- in the Reaction of Indoleamine 2,3-Dioxygenase	81
1. O_2^- Generation and Indoleamine 2,3-Dioxygenase Activity	81
2. Inhibition of Indoleamine 2,3-Dioxygenase Reaction by Superoxide Dismutase	81
3. Enhancement of Intracellular Indoleamine 2,3-Dioxygenase Activity by Diethylthiocarbamate	82
4. Reaction of Indoleamine 2,3-Dioxygenase with O_2^-	82
C. Reaction Sequence of Indoleamine 2,3-Dioxygenase	84
V. PHYSIOLOGICAL SIGNIFICANCE OF INDOLEAMINE 2,3-DIOXYGENASE	85
A. Induction of Indoleamine 2,3-Dioxygenase under Various Pathological Conditions	85

Progress in Inorganic Chemistry: Bioinorganic Chemistry, Vol. 38, Edited by Stephen J. Lippard.
ISBN 0-471-50397-5 © 1990 John Wiley & Sons, Inc.

B. Establishment of Antiparasitic State by IFN- γ -Mediated Indoleamine 2,3-Dioxygenase Induction	86
C. Tryptophan Depletion: A Mechanism of Antiproliferative Effects of IFN- γ	87
D. <i>In Vivo</i> Induction of Indoleamine 2,3-Dioxygenase in Tumor Cells: An Efficient Mechanism of Self-Defense	89
VI. CONCLUSION	92
REFERENCES	92

I. DISCOVERY OF OXYGENASES

For many years it was generally assumed that the oxygen found in organic substances always came from water. A water molecule could be added to a double bond and the resulting alcohol dehydrogenated. Nevertheless, there were indications that small amounts of O₂ itself were essential, even to anaerobically growing cells (1). In 1955, Hayaishi et al. (2) and Mason et al. (3) independently demonstrated that ¹⁸O was sometimes incorporated into organic compounds directly from ¹⁸O₂. Today, a bewildering variety of oxygenases are known to function in forming such essential metabolites as sterols, prostaglandins, active derivatives of vitamin D, and amino acids. Thus, molecular oxygen in tissues serves two functions. One is to act as the ultimate hydrogen acceptor in the process of the biological oxidation of foodstuffs where the oxygen molecule is reduced to either water, superoxide anion, or hydrogen peroxide. The other is the incorporation of molecular oxygen into dietary nutrients to yield cellular constituents or biologically active substances (4). The enzymes involved in the former process are referred to as oxidases, and those involved in the latter case are referred to as oxygenases. Oxygenases catalyze the incorporation of either one [monooxygenase or mixed-function oxidase, as in the case of phenolase (3)] or two [dioxygenase, as in the case of pyrocatechase (2)] atoms of molecular oxygen into their substrates (Fig. 1). In the former case, molecular oxygen reacts with the substrate, one atom of oxygen is incorporated into the substrate, and the other atom is reduced to water by a reductant.

Monooxygenase



Dioxygenase



Figure 1. Direct incorporation of molecular oxygen atoms into organic compounds. X, substrate; YH₂, reductant.

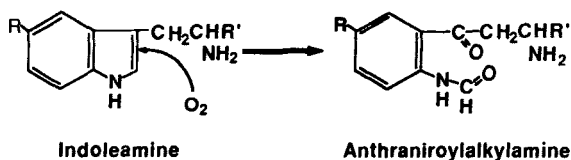


Figure 3. Indoleamine 2,3-dioxygenase-catalyzed reaction.

the rat liver is known to be due to tryptophan 2,3-dioxygenase, which shows a substrate specificity for L-tryptophan (6) [in 1980, hepatic tryptophan 2,3-dioxygenase in certain species of animals was found to cleave the pyrrole ring of the D isomer (7)], they postulated the existence of an enzyme in rabbit tissues that catalyzes the oxidative ring cleavage of D-tryptophan. About 30 years later, Higuchi et al. discovered an enzyme capable of oxidizing D-tryptophan to *N*-formyl-D-kynurenine in a homogenate of rabbit small intestine (8). Because the purified enzyme from rabbit small intestine catalyzes the oxidative cleavage of the indole ring of tryptophan and other indoleamine derivatives such as 5-hydroxytryptophan, tryptamine, and serotonin to yield new types of biogenic amines, the name indoleamine 2,3-dioxygenase was proposed (Fig. 3) (9).

III. PURIFICATION OF INDOLEAMINE 2,3-DIOXYGENASE

The standard assay mixture contained 100 mM potassium phosphate buffer, pH 7.8, 0.025 mM methylene blue, 10 mM ascorbic acid, 50 μ g of catalase, various indoleamines as substrate and enzyme in a total volume of 0.2 mL. Incubation was carried out at 37°C and the reaction was terminated by the addition of 0.2 mL of 5% zinc acetate and 0.2 mL of 0.18*N* sodium hydroxide. After centrifugation at 1000 \times *g* for 5 min, an aliquot (0.4 mL) of the solution was added to 1 mL of 1*M* Tris-HCl buffer, pH 7.0. Any of the previously mentioned indoleamine substrates, for example, serotonin, is incubated with the enzyme. When the indole ring is cleaved, the absorbance maximum shifts by about 40 nm to a longer wavelength. When formamidase is included in the reaction mixture and the formyl group is hydrolyzed, the absorbance maximum shifts by another 40 nm. These spectral properties can be utilized for spectrophotometric determination of these products. This procedure has been employed for the assay of purified enzyme preparations (10). For the assay of crude systems including homogenates, the assay methods with L-[methylene-¹⁴C] indoleamines or L-[ring-2-¹⁴C] tryptophan have been employed, as described (11–13).

A. Indoleamine 2,3-Dioxygenase from Rabbit Small Intestine

Starting from crude extracts of rabbit small intestine, the enzyme was purified about 500-fold with an overall yield of about 11% by the conventional procedure as shown in Table I (10). The most highly purified enzyme preparation is essentially homogeneous upon polyacrylamide gel electrophoresis and analytical ultracentrifugation. The native enzyme is a monomeric protein with a molecular weight of $41,000 \pm 1000$ with an $S_{20,w}^0$ value of 3.45 S. It has a relative abundance of hydrophobic amino acids such as valine, leucine and isoleucine, and contains ~5% carbohydrate by weight. The content of sugar residues per mole of enzyme is galactose, 1.2; mannose, 2.6; *N*-acetylglucosamine, 5.2; and sialic acid, 0.8. One mole of enzyme contains 0.8 mol of protoheme **IX** as a sole prosthetic group. Brady suggested from the experiments with copper chelators that indoleamine 2,3-dioxygenase is a copper-containing hemoprotein (14). Copper, however, is not detected in a significant amount and the ratio of copper to heme is less than 0.03. The turnover number of this enzyme toward *L*-tryptophan is $\sim 100 \text{ mol} \cdot \text{min}^{-1} \cdot \text{mol}^{-1}$ of enzyme at 24°C under the standard assay conditions.

B. Indoleamine 2,3-Dioxygenase from Human Placenta

Human indoleamine 2,3-dioxygenase is most abundant in the placenta, followed by the lung and small intestine (15). Even in the placenta, however, the content ($0.25 \text{ nmol} \cdot \text{min}^{-1} \cdot \text{mg}^{-1}$ of protein) is about 5% of that ($5.6 \text{ nmol} \cdot \text{min}^{-1} \cdot \text{mg}^{-1}$ of protein) in rabbit intestine, and a 10,000-fold purification is required, starting from the crude extract of the placenta.

TABLE I
Purification of Indoleamine 2,3-Dioxygenase from Rabbit Intestine

Steps	Specific Activity ($\text{nmol} \cdot \text{min}^{-1} \cdot \text{mg}^{-1}$ of Protein)	Yield (%)	Purification (-fold)
Crude extracts	5.6	100	1.0
Streptomycin	7.0	106	1.3
Ammonium sulfate	18.2	81	3.3
P-cellulose	24.1	80	4.3
Hydroxyapatite	155.8	62	28.0
Sephadex G-100	1,243	41	222.0
Isoelectric focusing	2,680	16	479.0
Sephadex G-100	2,850	11	509.0

TABLE II
Purification of Indoleamine 2,3-Dioxygenase from Human Placenta

Steps	Specific Activity (nmol · min ⁻¹ · mg ⁻¹ of Protein)	Yield (%)	Purification (-fold)
Crude extracts	0.25	100	1
P-cellulose	2.15	75	4
Hydroxyapatite	6.18	55	24
P-cellulose	43.2	17	172
Sephadex G-100	136	11	536
Isoelectric focusing	1,530	8	6,122
CM Affi-Gel Blue	1,675	3	6,700
TSK CM-3SW	2,525	0.9	10,116

The summary of purification is shown in Table II (16). The purified enzyme has a molecular weight of $\sim 40,000$ on SDS-polyacrylamide gel electrophoresis irrespective of either the presence or absence of SH reagents. Analytical gel filtration with Sephadex G-100 indicated that the native enzyme is a monomeric protein with a molecular weight of $\sim 40,000$. The turnover number ($101 \text{ nmol} \cdot \text{min}^{-1} \cdot \text{mol}^{-1}$ of enzyme) of the purified enzyme toward L-tryptophan was almost the same as that of the rabbit enzyme under the standard assay conditions described above.

IV. PROPERTIES OF INDOLEAMINE 2,3-DIOXYGENASE

A. Substrate Specificity

Substrate specificity of the purified indoleamine 2,3-dioxygenase from rabbit intestine was examined spectrophotometrically at 24°C. The spectra of the reaction products in either the absence or presence of formamidase were compared with those of authentic compounds. A single enzyme protein catalyzed the oxygenative ring cleavage of D- and L-tryptophan, 5-hydroxy-D- and -L-tryptophan, tryptamine, and serotonin (10). The maximal turnover number was obtained with L-tryptophan ($99 \text{ mol} \cdot \text{min}^{-1} \cdot \text{mol}^{-1}$ of enzyme at 24°C), and the lowest K_m value was with 5-hydroxy-L-tryptophan ($20 \mu M$). A marked substrate inhibition is observed by the L isomers of tryptophan and 5-hydroxytryptophan above 0.2 and 0.06 mM, at pH 6.6, respectively. The compounds including skatole, indole, indoleacetic acid, 5-hydroxyindoleacetic acid, N-acetyltryptophan, melatonin, and α -methyl-DL-tryptophan, are all inert as substrate.

Just like the rabbit enzyme (10), the purified human enzyme exhibited a broad substrate specificity; it oxidized L-tryptophan, D-tryptophan, 5-hydroxy-L-tryptophan, 5-hydroxy-D-tryptophan, and tryptamine (16). Unlike the rabbit enzyme, serotonin did not serve as the substrate for the human enzyme.

These results, described above, indicate that the human indoleamine 2,3-dioxygenase is essentially identical to the rabbit enzyme in terms of molecular [size, structure (monomeric) and turnover number toward L-tryptophan, etc.] and catalytic (substrate specificity, etc.) properties.

B. Participation of O_2^- in the Reaction of Indoleamine 2,3-Dioxygenase

One of the most interesting features of indoleamine 2,3-dioxygenase is that the purified enzyme is totally inactive by itself and requires both methylene blue and ascorbic acid for maximum activity (17). The concentrations required for half-maximal activity are 2 μM and 2 mM, respectively. So far, we have not been able to replace methylene blue by any natural cofactors, metals, or other compounds except for toluidine blue and some other closely related dyes. On the other hand, ascorbic acid can be replaced by some enzymes known to generate O_2^- .

1. O_2^- Generation and Indoleamine 2,3-Dioxygenase Activity

With the standard assay mixture containing substrate, enzyme, buffer, catalase, and methylene blue, the reaction can proceed only in the presence of either ascorbic acid, xanthine oxidase, or glutathione reductase with their substrates (Table III) (18). Ascorbic acid, the xanthine oxidase system and the glutathione reductase system are all known to generate O_2^- as well as H_2O_2 (19). However, neither H_2O_2 as such, nor the glucose oxidase or D-amino acid oxidase system, were able to replace ascorbic acid at all. These two enzymes were reported to generate H_2O_2 but not O_2^- (19). These results provided the first clue that O_2^- may be involved in this reaction.

2. Inhibition of Indoleamine 2,3-Dioxygenase Reaction by Superoxide Dismutase

When superoxide dismutase purified from erythrocytes was added to the reaction mixture, either at the beginning or during the steady state phase of the reaction, almost instantaneous inhibition was observed (18). This inhibition was dose dependent and could be completely abolished by superoxide dismutase inhibitors. Furthermore, superoxide dismutase preparations from bovine erythrocytes, green peas, spinach leaves, and *Esch-*

TABLE III
Replacement of Ascorbate by O_2^- or the H_2O_2 Generating System

Addition	Product formation ^a (nmol)
Ascorbic acid	28.0
Xanthine oxidase system ^b	30.0
Glutathione reductase system ^c	25.4
H_2O_2	0
Glucose oxidase system ^d	0
L-Amino acid oxidase system ^e	0

^aThe assay was carried out with 14 μ g of dioxygenase for 10 min under standard assay conditions as described (10).

^bThe xanthine oxidase system consisted of 20 μ g (60 nM) of xanthine oxidase and 1 mM hypoxanthine.

^cThe glutathione reductase system consisted of 1 μ g of glutathione reductase, 2 μ g of glucose 6-phosphate dehydrogenase, 5 mM glucose 6-phosphate, 10 mM $MgCl_2$, and 50 μ M NADPH.

^dThe glucose oxidase system contained 10 μ g of glucose oxidase and 50 mM glucose.

^eThe L-amino acid oxidase system contained 10 μ g of L-amino acid oxidase and 1 mM L-leucine.

erichia coli were all inhibitory regardless of their origins and functional metals. These results strongly suggested that the inhibition by these dismutase preparations was attributable to their specific activity to disproportionate O_2^- rather than to nonspecific protein-protein interactions.

3. Enhancement of Intracellular Indoleamine 2,3-Dioxygenase Activity by Diethyldithiocarbamate

The intracellular indoleamine 2,3-dioxygenase activity in the dispersed enterocytes of rabbit small intestine was markedly enhanced by the addition of 5 mM diethyldithiocarbamate (DDC), an inhibitor of superoxide dismutase (Fig. 4) (20). This agent, however, did not show any activating effect on the purified indoleamine 2,3-dioxygenase *in vitro*. These results seemed to support a possible conclusion that indoleamine 2,3-dioxygenase is a unique enzyme that utilizes the superoxide anion rather than molecular oxygen as the oxidizing agent.

4. Reaction of Indoleamine 2,3-Dioxygenase with O_2^-

Since all these experiments described above indicated that O_2^- is involved in the catalytic process of indoleamine 2,3-dioxygenase, the interaction

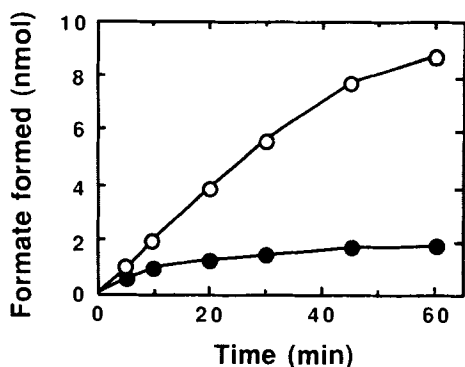


Figure 4. Effects of diethyldithiocarbamate (DDC) on the formation of formate from tryptophan. \circ , +DDC; \bullet , -DDC.

between O_2^- and the dioxygenase was spectroscopically investigated. The native enzyme purified from rabbit small intestine shows an absorbance spectrum typical of a high-spin ferric (Fe^{3+}) hemoprotein having absorbance peaks at 406 nm in the Soret region and 500 and 632 nm in the visible regions at pH 6.0 (21). Upon infusion of O_2^- into the reaction mixture in the presence of catalase, the spectrum of the ferric enzyme changes to that of the oxygenated form of the enzyme, which has absorbance peaks at 415, 542, and 576 nm (Fig. 5) (22). The formation of this new spectral species was completely abolished in the presence of superoxide dismutase, indicating that this process involved the binding of superoxide anion to the ferric form of the enzyme. This spectrum is similar to that of oxygenated hemoglobin (23) or myoglobin (24), peroxidase compound III (25), or the enzyme-substrate- O_2 ternary complex of tryptophan 2,3-dioxygenase (26). This apparent enzyme- O_2 complex can be reversibly converted to the ferrous form of the enzyme and oxygen by degassing. When an excess amount of substrate, such as D-tryptophan, was introduced into a reaction mixture containing enzyme- O_2 complex, free enzyme and the product were im-

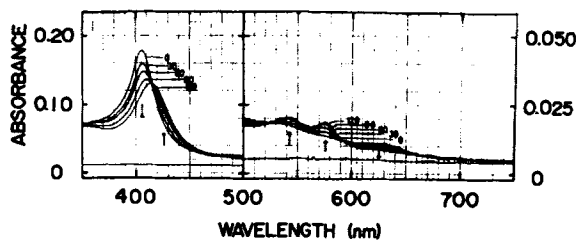


Figure 5. Spectral changes of indoleamine 2,3-dioxygenase by its reaction with O_2^- . The successive infusion of KO_2 (for 30 s) into the ferric state of the enzyme causes decrement in the absorbance at 406 nm and increment at 415, 542, and 576 nm.

mediately released. These results are consistent with the interpretation that the native ferric form of the enzyme binds to the superoxide anion to form the oxygenated enzyme ($\text{Fe}^{3+}\text{O}_2^-$), which then reacts with the substrate to form the endo product of the reaction.

C. Reaction Sequence of Indoleamine 2,3-Dioxygenase

The incorporation of the ^{18}O -labeled oxygen atoms derived from $^{18}\text{O}_2^-$ (K^{18}O_2) was not quantitative (not 100%) and the fractions of the ^{18}O -labeled oxygen atoms of all the oxygen atoms incorporated into the products were about 49 and 77% under aerobic and anaerobic conditions, respectively (27). In order further to understand the reaction mechanism of indoleamine 2,3-dioxygenase, Taniguchi et al. have determined the following rate constants (28); k_1 for the binding of O_2^- to the ferric enzyme, k_2 for the binding of O_2 to the ferrous enzyme, k_3 for the conversion of the ternary complex to the ferric enzyme, k_4 for the product formation, and k_5 for the direct oxidation of the ferrous enzyme to the ferric form. The rate constants k_1 and k_2 were $3.3 \times 10^6 \text{ M}^{-1}\text{s}^{-1}$ and $7.4 \times 10^6 \text{ M}^{-1}\text{s}^{-1}$, respectively, in the absence of L-tryptophan, both values being in the same order of magnitude. The addition of 0.2 mM L-tryptophan significantly decreased the rate constants in both cases. The k_3 value was calculated to be 0.03 s^{-1} in the presence of 0.2 mM L-tryptophan. The k_4 value for the product formation was determined to be 2.0 s^{-1} , which is the same as that obtained from the steady state kinetics. The rate constant k_5 for the direct oxidation of the ferrous enzyme to the ferric form was calculated to be 22 s^{-1} . The relative amount of O_2 and O_2^- used in the catalytic reaction is therefore assumed to depend simply on the ratio of k_3 to k_4 . Relative concentration of O_2 and O_2^- , and also that of the organic substrate, may significantly affect the ratio, *in vivo* and *in vitro*. A possible reaction sequence of indoleamine 2,3-dioxygenase is proposed, as shown in Fig. 6.

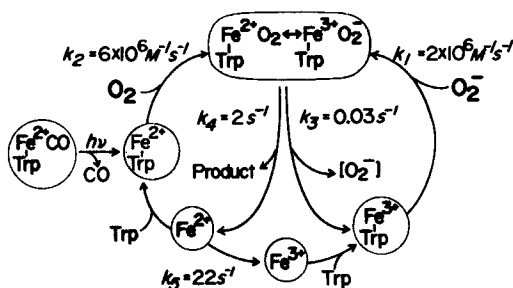


Figure 6. A possible reaction sequence of indoleamine 2,3-dioxygenase.

From the experimental results on the equilibrium reactions of the tryptophan binding to the enzyme, it was strongly suggested that tryptophan binding to the ferric enzyme is rather directly correlated to the substrate inhibition observed only for the L isomers of tryptophan and 5-hydroxytryptophan (21). It is also suggested that the binding of tryptophan to the ferrous enzyme ($K_d \approx K_m$), rather than that of tryptophan to the oxygenated enzyme ($K_d \neq K_m$), is involved in a steady state of the catalytic reaction, assuming that the CO-bound enzyme (Fe^{2+}CO) has a tryptophan binding property similar to the oxygenated enzyme ($\text{Fe}^{3+}\text{O}_2^-$). Thus, the sequence is analogous to that reported with *pseudomonad* tryptophan 2,3-dioxygenase (26).

V. PHYSIOLOGICAL SIGNIFICANCE OF INDOLEAMINE 2,3-DIOXYGENASE

A. Induction of Indoleamine 2,3-Dioxygenase Under Various Pathological Conditions

The indoleamine 2,3-dioxygenase activity in various tissues of mice is relatively stable under various physiological conditions, but it exhibits a daily rhythmic cycle and age-dependent changes (29). Under some pathological conditions, however, the enzyme was dramatically (20- to 120-fold) induced. During *in vivo* influenza virus infection, the pulmonary indoleamine 2,3-dioxygenase activity increased linearly from the 5th day after influenza virus infection, reached the highest level (~120-fold) around the 11th day, and then gradually decreased to normal values in ~3 weeks (Fig. 7) (30). The time course of the increase in the enzyme activity was quite different from that (a peak obtained by the 3rd day and persisted until the 9th day) of virus replication in the lung or that (started to rise on the 9th day) of the serum antibody content. Rather, it closely related to the perivascular and peribronchial infiltrations of mononuclear and lymphocytic cells.

The marked induction of pulmonary enzyme was also found *in vivo* in mice treated with endotoxin (lipopolysaccharide, LPS) (31) or poly(I)poly(C) (a double-stranded RNA) (32), both of which are known to be interferon (IFN) inducers. In contrast, C3H/HeJ mice, totally LPS-nonresponders, were unable in induction of both IFN and indoleamine 2,3-dioxygenase after LPS treatment (32). *In vitro* incubation of mouse lung slices with IFN also caused the enzyme induction (Fig. 8) (33), suggesting that IFN mediates the enzyme induction by LPS or viruses.

To determine the *in vivo* substrate of indoleamine 2,3-dioxygenase, the

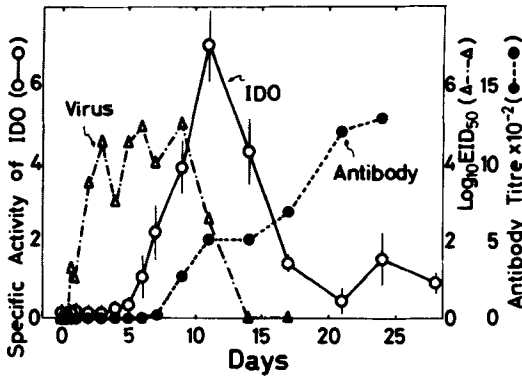


Figure 7. Virus titer (Δ) and indoleamine 2,3-dioxygenase activity in mouse lung (\circ) and serum antibody content (\bullet) at intervals after infection with PR8 influenza virus.

changes in the metabolites of various indoleamines in plasma or urine were estimated after LPS treatment. When mice were treated with LPS, the increase in the enzyme activity caused an increase in the plasma kynurenine (a metabolite of tryptophan) level (Fig. 9) (34). Furthermore, the time courses of change in the enzyme levels in the lung and several other tissues examined such as the cecum, colon, and epididymis paralleled that in plasma kynurenine level. Under the same condition, however, other metabolites on the pyrrole ring cleavage pathway of various indoleamine derivatives were undetectable. These results suggest that indoleamine 2,3-dioxygenase oxidizes an essential amino acid, tryptophan, *in vivo* in mice infected with viruses or treated with LPS.

B. Establishment of Antiparasitic State by IFN- γ -Mediated Indoleamine 2,3-Dioxygenase Induction

Induction of indoleamine 2,3-dioxygenase by IFN *in vitro* was also reported in human lung tissue (35) and peripheral blood mononuclear cells (36), where IFN- γ was found to be more active than IFN- α . In human

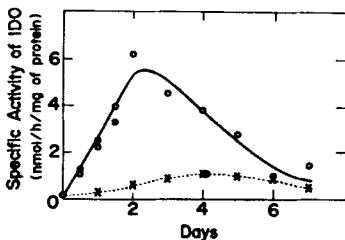


Figure 8. Effect of mouse IFN- α/β on the indoleamine 2,3-dioxygenase activity of mouse lung slices. \circ , +IFN (1.4×10^6 U/mg protein); \bullet , +IFN (2×10^6 U/mg protein); x, no addition.

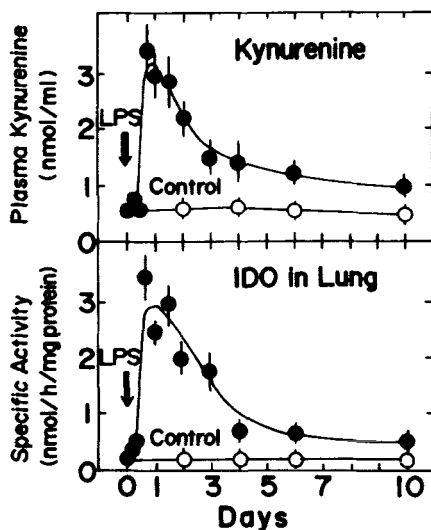


Figure 9. Effects of LPS treatment on plasma kynurenine level (*upper*) and the activity of indoleamine 2,3-dioxygenase in the lung (*lower*).

fibroblasts IFN- γ blocked the growth of *Toxoplasma gondii* by inducing the host cells to degrade tryptophan (Fig. 10) (37); the concentration of tryptophan in the medium markedly affected the antitoxoplasma activity of IFN- γ at the minimal inhibitory concentration ($16 \text{ units} \cdot \text{mL}^{-1}$) in Eagle's medium ($10 \text{ } \mu\text{g} \cdot \text{mL}^{-1}$ of tryptophan). Doubling the $10 \text{ } \mu\text{g}$ of tryptophan found per milliliter of this medium completely blocked the effect of the IFN- γ . These results provided the first clue to solve the question of the physiological significance of indoleamine 2,3-dioxygenase-initiated tryptophan deprivation. In 1986, Byrne et al. (38) demonstrated that the mechanism of human IFN- γ -mediated inhibition of *chlamydia psittaci* growth in T24 cells was reversed by the addition of tryptophan. Furthermore, Shemer et al. (39) reported that recombinant human IFN- γ inhibited the growth of *chlamydia trachomatis* (L2/434 serovar) in HEp-2 cells to the same extent as natural human IFN- γ that was purified from human lymphocytes. These results taken together suggested that IFN- γ -mediated indoleamine 2,3-dioxygenase induction appeared to block the growth of intracellular parasites, *Toxoplasma gondii* (37), *chlamydia psittaci* (38), and *chlamydia trachomatis* (39), by depleting tryptophan in the infected cells.

C. Tryptophan Depletion: A Mechanism of Antiproliferative Effects of IFN- γ

In addition to the antiparasitic activities described above, IFN- γ has a potent antiproliferative activity against many cultured cell lines (40, 41). Tryptophan is one of the essential amino acids for cell growth, and it is

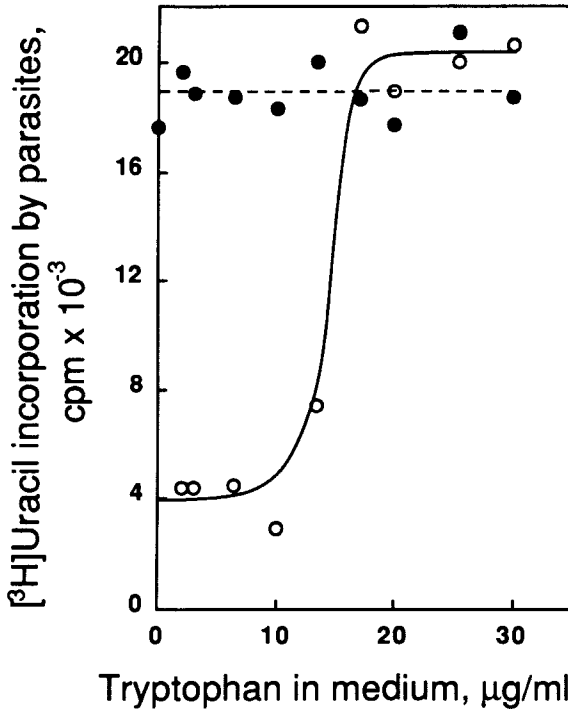


Figure 10. Effect of tryptophan concentration on the inhibition of the growth of *Toxoplasma gondii* in human foreskin fibroblasts treated with IFN- γ . ●, control cultures; ○ cultures treated with IFN- γ .

therefore likely that the tryptophan degradation by indoleamine 2,3-dioxygenase induced by IFN- γ reduces the intracellular level of the amino acid, which consequently leads to a suppression of the growth of cells. To test this possibility, the relationship between the enzyme-mediated tryptophan degradation and the antiproliferative effect of IFN- γ has been studied with several human cell lines (16). When the two lines of cells (HeLa and OKK cells) were cultured in the presence of IFN- γ , the growth of cells was strongly inhibited as shown in Fig. 11B. This growth inhibition accompanied a complete depletion of tryptophan and an accumulation of the metabolite, kynurenine, in the medium (Fig. 11A). Supplementation of the culture medium with tryptophan reversed in part the growth inhibition (Fig. 11B). These results clearly demonstrated that the indoleamine 2,3-dioxygenase-catalyzed tryptophan depletion is significantly responsible for the antiproliferative effect of IFN- γ . De la Meza and Peterson (42) have also reported that the growth inhibition caused by IFN- γ was counteracted

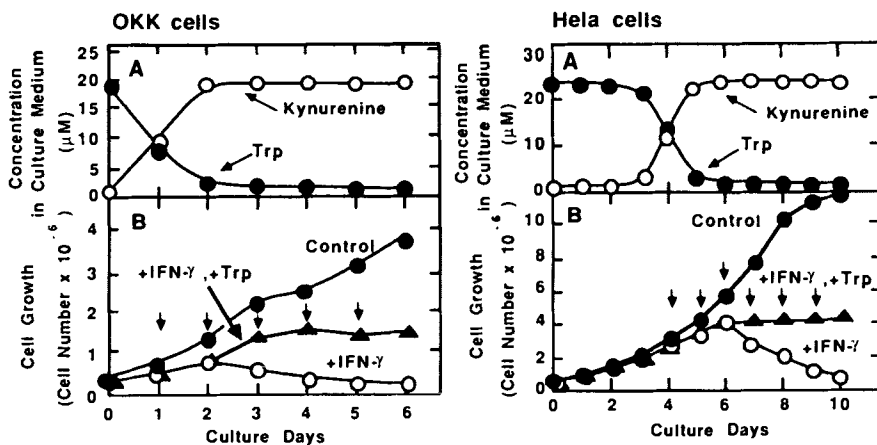


Figure 11. Role of the indoleamine 2,3-dioxygenase-mediated tryptophan depletion in anticellular activity of IFN- γ . Panel A represents the change in level of tryptophan (●) and kynurenine (○) in the medium cultured with IFN- γ . Panel B: growth curves of OKK cells (left) and HeLa cells (right).

by the increase in tryptophan in culture medium for four human cell lines, HeLa229, A549, HEP-2, and T24. Moreover, Ozaki et al. (43) have found a similar mechanism is operative in human KB cells. The responsibility (induction of indoleamine 2,3-dioxygenase) of various human cells to IFN- γ is summarized in Table IV (12, 16, 38, 39, 42–50).

D. *In vivo* Induction of Indoleamine 2,3-Dioxygenase in Tumor Cells: An Efficient Mechanism of Self-Defense

The depletion of an essential amino acid, tryptophan, caused by indoleamine 2,3-dioxygenase induction *in vitro*, has been suggested to be due to a mechanism that is used in self-defense against inhaled microorganisms and tumor growth. In the case of *in vivo* transplantation of tumor cells, the cells continue to grow in a syngeneic strain of mice but are rejected from allogeneic animals. Under such conditions, if the cytotoxicity occurred in the tumor cells but not in host cells, and if tryptophan depletion by indoleamine 2,3-dioxygenase is a type of cytotoxicity, it would be of considerable interest since this mechanism is specific for tumor cells and not host cells.

When Meth-A cells (2×10^6 cells/mouse) were given intraperitoneally to an allogeneic (C57BL/6J) strain of mice, the growth of Meth-A cells began within 24 h after the transplantation, as observed with syngeneic

TABLE IV
Induction of Indoleamine 2,3-Dioxygenase by IFN- γ in Various Human Cells

Indoleamine 2,3-Dioxygenase Induction by IFN- γ	
(+)	(-)
<i>Nonhematopoietic Cells</i>	
Fibroblastic Cells	
HK-2351 (scalp)	IMR-32 (neuroblastoma)
Skin fibroblasts (a biopsy)	
HEL (normal embryonic lung)	
MRC-5 (normal fetal lung)	
FS ₄ (foreskin)	
Epithelial Cells	
HeLa (cervical carcinoma)	A-427 (colon adenocarcinoma)
HeLa 229 (cervical carcinoma)	SW-480 (colon adenocarcinoma)
A-549 (lung carcinoma)	NCI-H128 (small cell lung carcinoma)
HEp-2 (lung carcinoma)	NCI-H69 (small cell lung carcinoma)
FL (amnion)	MCF-7 (breast carcinoma)
A-431 (epidermoid carcinoma)	HLEC-1 (liver carcinoma)
OKK (maxillary gland carcinoma)	
KATO-III (stomach carcinoma)	
KB (oral carcinoma)	
WiDr (colon adenocarcinoma)	
I-407 (normal embryonic intestine)	
A-22 (arachnoid)	
NY (osteosarcoma)	
T-2346 (meningeoma)	
T-24 (bladder carcinoma)	
<i>Hematopoietic Cells</i>	
Monocytes/Macrophages (peripheral)	T-cells (peripheral)
THP-1 (monocytic leukemia)	MOLT-4 (T-cell lymphoma)
	CCR-CEM (T-cell lymphoma)
	CCRF-SB (B-cell lymphoma)
	HL-60 (promyelocytic leukemia)
	U-937 (promonocytic leukemia)
	Raji (Burkitt lymphoma)
	RPMI1788 (lymphoma)

animals, but the tumor cells ceased to grow on the 9th day (Fig. 12) (51). Rapid elimination of the tumor cells from the peritoneal cavity commenced around the 12th day and on the 20th day none was found. Indoleamine 2,3-dioxygenase was induced only when the tumor cells were being rejected from allogeneic animals and no change was observed when the cells continued to grow in syngeneic animals. Furthermore, when the syngeneic

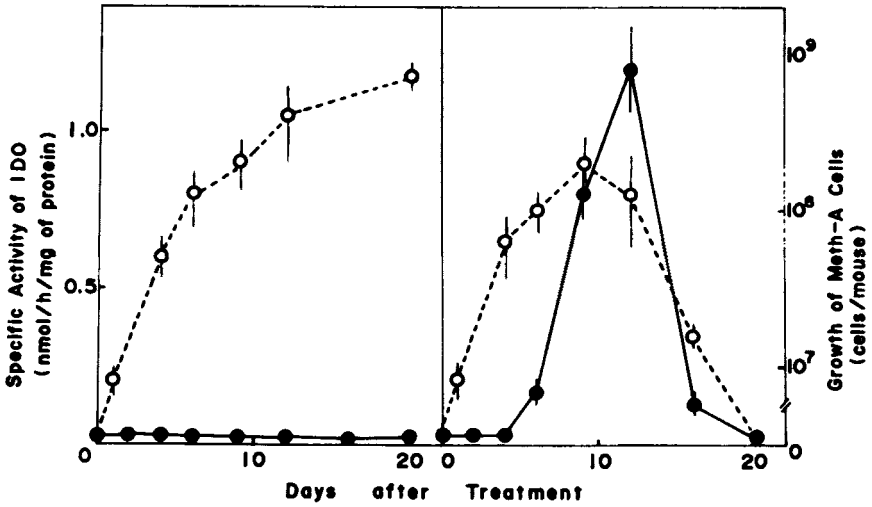


Figure 12. Indoleamine 2,3-dioxygenase induction (●) and growth of Meth-A cells (○) in peritoneal cavity of syngeneic (BALB/c) (left) or allogeneic (C57BL/6) (right) mice.

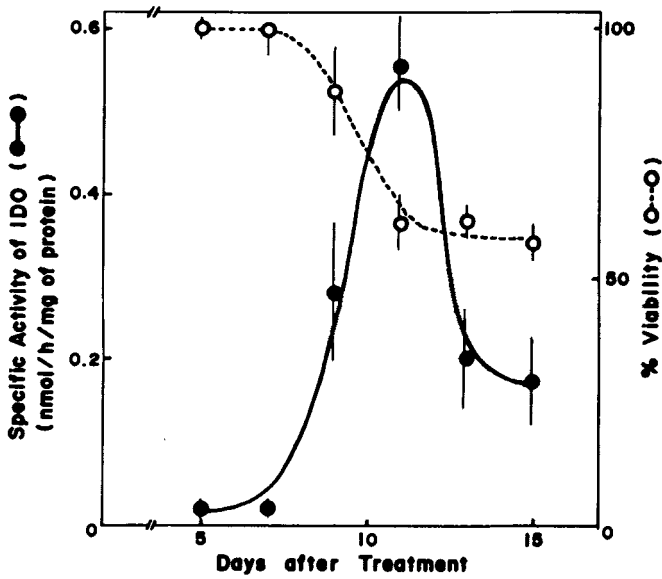


Figure 13. Induction of indoleamine 2,3-dioxygenase (●) in the transplanted syngeneic tumor (3LL) cells undergoing rejection from BALB/c mice. ○, cell (3LL) viability.

tumor cells in a diffusion chamber were intraperitoneally transplanted simultaneously with intraperitoneal injection of allogeneic tumor cells, the enzyme was induced not only in allografted tumor cells but also in the syngeneic tumor cells (Fig. 13). Under these conditions, the tumor cells in the diffusion chamber ceased to grow and 50% of the cells were rejected. The peritoneal exudate cells consisted of tumor cells and host cells, mostly small lymphocytes, and the localization of indoleamine 2,3-dioxygenase in the tumor cells was identified by differential centrifugation or by complement-dependent lysis with specific antibodies against tumor and host cells. These results indicate (a) that indoleamine 2,3-dioxygenase was dramatically induced in allogeneic or syngeneic tumor cells undergoing rejection, but not in host cells, (b) that the enzyme (or the antitumor state) was induced by factor(s) released through the interaction of allografted tumor cells with host cells, and (c) that such factor(s) are permeable through a membrane filter. Investigations into the cellular mechanism (identification of the type of host cells, etc.) of this enzyme induction by tumor transplantation, establishment of an *in vitro* system of enzyme induction in the tumor cytotoxicity, and isolation of soluble factors are presently underway in our laboratory.

VI. CONCLUSION

It has been almost 35 years since the discovery of oxygenases, and extensive studies have been carried out on their properties and functions. Indoleamine 2,3-dioxygenase is a unique heme-containing oxygenase, because it requires the superoxide anion for the initiation of the reaction and for maintenance of the catalytic cycle during the steady state. Under various *in vivo* pathological conditions (influenza virus infection, tumor transplantation, etc.) or by addition of IFN- γ to the culture medium of various types of cells, indoleamine 2,3-dioxygenase is induced 20- to 120-fold. After the enzyme induction, the growth of viruses and transplanted tumor cells *in vivo*, parasites in fibroblasts, or the cells cultured with IFN- γ is completely inhibited. In some *in vitro* systems, this inhibition could be reversed by the addition of tryptophan (a substrate of indoleamine 2,3-dioxygenase). These results imply that the inhibition of virus, parasite, or tumor growth may be caused by the depletion of the essential amino acid, tryptophan, through the induction of indoleamine 2,3-dioxygenase by IFN- γ or other as yet unidentified *in vivo* factor(s).

REFERENCES

1. O. Hayaishi, H. in O. Hayaishi, Ed. *Oxygenases* Academic Press, New York, 1962, pp. 1-29.

2. O. Hayaishi, M. Katagiri, and S. Rothberg, *J. Am. Chem. Soc.*, **77**, 5450–5451 (1955).
3. H. S. Mason, W. L. Fowlks, and L. Peterson, *J. Am. Chem. Soc.*, **77**, 2914–2915 (1955).
4. O. Hayaishi and M. Nozaki, *Science*, **164**, 388–396 (1969).
5. Y. Kotake and N. Ito, *J. Biochem. (Tokyo)*, **25**, 71–77 (1937).
6. P. Feigelson and D. Greengerd, *J. Biol. Chem.*, **237**, 1903–1907 (1962).
7. Y. Watanabe, M. Fujiwara, R. Yoshida, and O. Hayaishi, *Biochem. J.*, **189**, 393–405 (1980).
8. K. Higuchi, S. Kuno, and O. Hayaishi, *Arch. Biochem. Biophys.*, **120**, 397–403 (1967).
9. F. Hirata and O. Hayaishi, *Biochem. Biophys. Res. Commun.*, **47**, 1112–1119 (1972).
10. T. Shimizu, S. Nomiyama, F. Hirata, and O. Hayaishi, *J. Biol. Chem.*, **253**, 4700–4706 (1978).
11. M. Fujiwara, M. Shibata, Y. Watanabe, T. Nukiwa, F. Hirata, N. Mizuno, and O. Hayaishi, *J. Biol. Chem.*, **253**, 6081–6085 (1978).
12. B. Peterkofsky, *Arch. Biochem. Biophys.*, **128**, 638–645 (1968).
13. W. E. Knox, in S. P. Colovick and N. O. Kaplan, Eds. *Methods in Enzymology*, Vol. 2, Academic Press, New York, 1955, pp. 242–246.
14. F. O. Brady, *FEBS Lett.*, **57**, 237–240 (1975).
15. F. Yamazaki, T. Kuroiwa, O. Takikawa, and R. Kido, *Biochem. J.*, **230**, 635–638 (1985).
16. O. Takikawa, T. Kuroiwa, F. Yamazaki, and R. Kido, *J. Biol. Chem.*, **263**, 2041–2048 (1988).
17. S. Yamamoto and O. Hayaishi, *J. Biol. Chem.*, **242**, 5260–5266 (1967).
18. F. Hirata and O. Hayaishi, *J. Biol. Chem.*, **250**, 5960–5966 (1975).
19. V. Massey, S. Strickland, S. OT. Mayhew, L. G. Howell, P. C. Engel, R. G. Mathews, M. Schuman, and P. A. Sullivan, *Biochem. Biophys. Res. Commun.*, **36**, 891–897 (1969).
20. T. Taniguchi, F. Hirata, and O. Hayaishi, *J. Biol. Chem.*, **252**, 2774–2776 (1977).
21. M. Sono, T. Taniguchi, Y. Watanabe, and O. Hayaishi, *J. Biol. Chem.*, **255**, 1339–1345 (1980).
22. F. Hirata, T. Ohnishi, and O. Hayaishi, *J. Biol. Chem.*, **252**, 4637–4642 (1977).
23. A. E. Sidwell, Jr., R. H. Munch, E. S. G. Barron, and R. T. Hogness, *J. Biol. Chem.*, **123**, 335–350 (1938).
24. I. Yamazaki, K. Yokota, and K. Shikama, *J. Biol. Chem.*, **239**, 4151–4153 (1964).
25. K. Yokota, and I. Yamazaki, *Biochem. Biophys. Res. Commun.*, **18**, 48–53 (1965).
26. Y. Ishimura, M. Nozaki, O. Hayaishi, T. Nakamura, M. Tamura, and I. Yamazaki, *J. Biol. Chem.*, **245**, 3593–3602 (1970).

27. O. Hayaishi, F. Hirata, T. Ohnishi, J. P. Heury, I. Rothenthal, and A. Katoh, *J. Biol. Chem.*, **252**, 3548–3550 (1977).
28. T. Taniguchi, M. Sono, F. Hirata, O. Hayaishi, M. Tamura, K. Hayashi, T. Iizuka, and Y. Ishimura, *J. Biol. Chem.*, **254**, 3288–3294 (1979).
29. R. Yoshida, T. Nukiwa, Y. Watanabe, M. Fujiwara, F. Hirata, and O. Hayaishi, *Arch. Biochem. Biophys.*, **203**, 343–351 (1980).
30. R. Yoshida, Y. Urade, M. Tokuda, and O. Hayaishi, *Proc. Natl. Acad. Sci. USA*, **76**, 4084–4086 (1979).
31. R. Yoshida and O. Hayaishi, *Proc. Natl. Acad. Sci. USA*, **75**, 3998–4000 (1978).
32. R. Yoshida, T. Oku, J. Imanishi, T. Kishida, and O. Hayaishi, *Arch. Biochem. Biophys.*, **249**, 596–604, (1986).
33. R. Yoshida, J. Imanishi, T. Oku, T. Kishida, and O. Hayaishi, *Proc. Natl. Acad. Sci. USA*, **78**, 129–132 (1981).
34. O. Takikawa, R. Yoshida, R. Kido, and O. Hayaishi, *J. Biol. Chem.*, **261**, 3648–3653 (1986).
35. H. Yasui, K. Takai, R. Yoshida, and O. Hayaishi, *Proc. Natl. Acad. Sci. USA*, **83**, 6622–6626 (1986).
36. Y. Ozaki, M. P. Edelstein, and D. S. Duch, *Biochem. Biophys. Res. Commun*, **144**, 1147–1153 (1987).
37. E. R. Pfefferkorn, *Proc. Natl. Acad. Sci. USA*, **81**, 908–912 (1984).
38. G. I. Byrne, L. K. Lehmann, and G. J. Landry, *Infect. Immun.*, **53**, 347–351 (1986).
39. Y. Shemer, R. Kol, and I. Sarov, *Curr. Microbiol.*, **16**, 9–13 (1987).
40. P. Lengyel, *Ann. Rev. Biochem.*, **51**, 251–282 (1982).
41. M. J. Clemens and M. A. McNurlan, *Biochem. J.*, **226**, 345–360 (1985).
42. L. M. De la Maza and E. M. Peterson, *Cancer Res.*, **48**, 346–350 (1988).
43. Y. Ozaki, M. P. Edelstein, and D. S. Duch, *Proc. Natl. Acad. Sci. USA*, **85**, 1242–1246 (1988).
44. G. I. Byrne, L. K. Lehmann, J. G. Kirschbaum, E. C. Borden, C. M. Lee, and R. R. Brown, *J. Interferon Res.*, **53**, 347–351 (1986).
45. Y. Ozaki, M. P. Edelstein, and D. S. Duch, *Biochem. Biophys. Res. Commun*, **144**, 1147–1153 (1987).
46. J. M. Carlin, E. C. Borden, P. M. Sondel, and G. I. Byrne, *J. Immunol.*, **139**, 2414–2418 (1987).
47. E. R. Werner, G. Bitterlich, D. Fuchs, A. Hausen, G. Reibnegger, G. Szabo, M. P. Dierich, and H. Wachter, *Life Sciences*, **41**, 273–280 (1987).
48. E. R. Werner, G. Werner-Felmayer, D. Fuchs, A. Hausen, G. Reibnegger, and H. Wachter, *Biochem. J.*, **256**, 537–541 (1988).
49. E. R. Werner, M. Hirsch-Kauffmann, D. Fuchs, A. Hausen, G. Reibnegger, M. Schweiger, and H. Wachter, *Biol. Chem. Hoppe-Seyler*, **368**, 1407–1412 (1988).

50. B. Y. Rubin, S. L. Anderson, G. R. Hellermann, N. K. Richardson, R. M. Lunn, and J. E. Valinsky, *J. Interferon Res.*, *8*, 691-702 (1988).
51. R. Yoshida, S. W. Park, H. Yasui, and O. Takikawa, *J. Immunol.*, *141*, 2819-2823 (1988).

Dinuclear Iron- and Manganese-Oxo Sites in Biology

LAWRENCE QUE, JR., and ANNE E. TRUE

*Department of Chemistry
University of Minnesota
Minneapolis, MN*

CONTENTS

I. INTRODUCTION	98
II. DIIRON PROTEINS THAT INTERACT WITH DIOXYGEN	99
A. Diferric Forms	103
1. Methemerythrin and Its Synthetic Analogues	103
2. Ribonucleotide Reductase	120
3. Methane Monooxygenase	125
B. Diferrous Forms	127
C. Mixed-Valence Forms	131
D. Mechanistic Considerations	138
1. Reversible Dioxygen Binding by Hemerythrin	139
2. Redox Chemistry of Hemerythrin	142
3. Oxygen Activation Chemistry	144
4. Models	147
III. THE PURPLE ACID PHOSPHATASES	149
A. Biochemistry	150
B. Properties of the Diiron(II,III) Active Site	151
C. Fe(III)M(II) Derivatives	154
D. Anion Interactions	155
E. The Puzzle of the Oxidized Diiron Enzymes	161
F. Relevant Synthetic Analogues	162
IV. OTHER (μ -OXO)DIIRON CENTERS IN PROTEINS	164
A. Rubrerythrin	164
B. 3-Deoxy-D-Arabetriose-7-Phosphate Synthase	165

Progress in Inorganic Chemistry: Bioinorganic Chemistry, Vol. 38, Edited by Stephen J. Lippard.

ISBN 0-471-50397-5 © 1990 John Wiley & Sons, Inc.

V. DIMANGANESE CENTERS IN PROTEINS	166
A. Manganese-catalase	166
B. Ribonucleotide Reductase	167
C. The Oxygen Evolving Center from Photosystem II	169
D. Models	169
1. Structural Aspects	170
2. Electronic Spectra	177
3. EPR Properties	178
4. Magnetic Properties	179
5. Redox Properties	180
VI. PERSPECTIVES	182
ACKNOWLEDGMENTS	182
ADDENDUM	182
REFERENCES	184

I. INTRODUCTION

(μ -Oxo)dimetal units have recently emerged as the demonstrated or proposed structural motifs for the active sites of a number of proteins (1). In several cases, there is evidence for additional ligands that bridge the M-O-M unit. The (μ -oxo)bis(μ -carboxylato)diiron(III) core is well established in the crystal structures of methemerythrin and its anion complexes (2, 3). This structural unit is but a wedge of the familiar (μ_3 -oxo)trimetal cluster found in basic metal acetates, $[M_3O(O_2CR)_6]$ (4), and the thermodynamic stability of this tribridged diiron core is demonstrated by the synthesis of $[L_2Fe_2O(O_2CR)_2]$ complexes with a variety of tridentate ligands. This structural motif may be modified in protein active sites and synthetic complexes by protonation or alkylation of the oxo bridge and/or substitution of the carboxylate bridges. This chapter focuses on the proteins that have been proposed or demonstrated to have (μ -oxo)dimetal centers including hemerythrin (Fe_2) (5, 6), ribonucleotide reductase (Fe_2 or Mn_2) (7, 8), purple acid phosphatase (FeM) (9, 10), methane monooxygenase (Fe_2) (11, 12), rubrerythrin (Fe_2) (13), and Mn-catalase (Mn_2) (14, 15). Our understanding of the properties of these protein active sites has been greatly facilitated by the explosion of activity associated with the generation of appropriate synthetic analogues for such sites. This chapter would be incomplete without an extensive discussion of these model compounds.

II. DIIRON PROTEINS THAT INTERACT WITH DIOXYGEN

Three dinuclear iron proteins are known to interact with dioxygen: hemerythrin (Hr), methane monooxygenase (MMO), and the B2 subunit of ribonucleotide (RRB2) reductase. Hemerythrin, an invertebrate dioxygen carrier, cycles between a diferrous deoxy form and an oxy form, which is formulated as a diferric hydroperoxide complex (5, 6). Methane monooxygenase catalyzes the hydroxylation of methane to methanol in methanotrophs (16). It is proposed to utilize a dioxygen binding mechanism similar to that found in hemerythrin and to activate the resulting oxy complex for the difficult alkane hydroxylation chemistry (11). Ribonucleotide reductase converts ribonucleotides into deoxyribonucleotides in the first committed step in DNA biosynthesis (7). The dinuclear iron center appears not to be directly involved in the catalytic mechanism but instead is responsible for the generation of the tyrosyl radical that is essential for activity (17). The tyrosyl radical is obtained in a dioxygen-dependent reaction that presumably involves dioxygen activation by the diiron center. The diiron site in this enzyme is thus part of the regulatory apparatus rather than the actual catalytic apparatus.

Hemerythrin, being the best characterized of the group, is the prototype of this class of proteins (5, 6). The circulatory protein consists of oligomers of an ~ 17 kDa subunit that contains the dinuclear site. The number of subunits that constitute the holoprotein varies from 3 to 8 among the species studied (6). A monomeric form, myohemerythrin, which has been isolated from muscle tissue (18), is presumably related to hemerythrin in its function just as myoglobin is to hemoglobin.

Two forms of hemerythrin and one of myohemerythrin have been crystallographically characterized (2, 3, 19). Crystal structures of metHr, metHrN₃, and metmyoHrN₃ show the diiron active site of each subunit to be placed within the confines of four parallel alpha helices and bound to each helix by amino acid side chains (Fig. 1). The irons are held in close proximity by a triple bridge consisting of an oxo group and two carboxylates from aspartate and glutamate residues (Fig. 2). These bridges constitute the central ligands of a bioctahedron. Five of the six remaining coordination sites are occupied by histidines from the polypeptide chain; the sixth site may be vacant as in metHr or occupied by an exogenous ligand such as azide or hydroperoxide as in metHrN₃ or oxyHr, respectively. When dioxygen is released from oxyHr to yield deoxyHr, the general protein structure apparently is retained on the basis of difference Fourier maps, and the O₂ binding site is now vacant (19).

There are four types of ribonucleotide reductases currently known: the

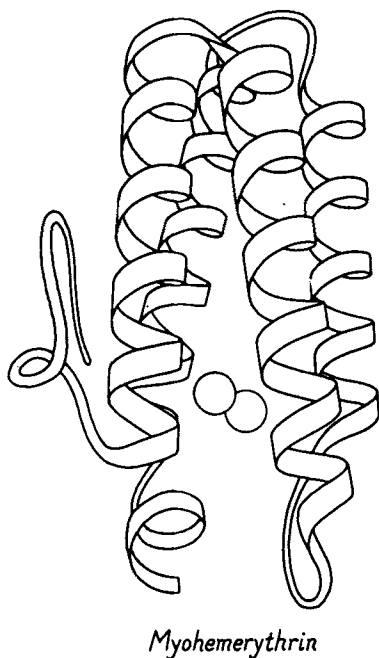


Figure 1. Schematic drawing of the structure of metmyohemerythrin azide. Reprinted with permission. © 1979 Professor Jane S. Richardson.

coenzyme B₁₂-dependent enzymes found in many bacteria (20); the diiron enzymes from mammals, *Escherichia coli*, and viruses (7); the dimanganese enzyme from *Brevibacterium ammoniagenes* and related species (8); and the enzyme from *E. coli* observed during anaerobiosis (21). The diiron enzymes are discussed in this section, while the dimanganese enzyme will be covered in Section V.B.

Of the diiron enzymes, the one from *E. coli* is the best characterized and consists of two components. Subunit B1 ($\alpha\alpha'$, 70 kDa) contains the nucleotide binding site, the thiols required for the reduction, and several effector sites (22). Subunit B2 (β_2 , 87.5 kDa) contains the catalytically essential tyrosyl 122 radical (23) and the dinuclear iron site (24). Both subunits were cloned separately and overexpressed in *E. coli*, thereby affording enzyme of sufficient quantities for biophysical studies (25).

Until recently, the prevailing model for the B2 subunit consisted of one dinuclear iron unit coordinated at the interface of the two polypeptides to ligands from both chains (26). Only one of the potentially two tyrosyl 122 radicals was observed. This model was based on an iron analysis of slightly more than 2/RRB2 and a tyrosyl radical concentration of approximately 1/RRB2. More recent experiments indicate that these stoichiometries should

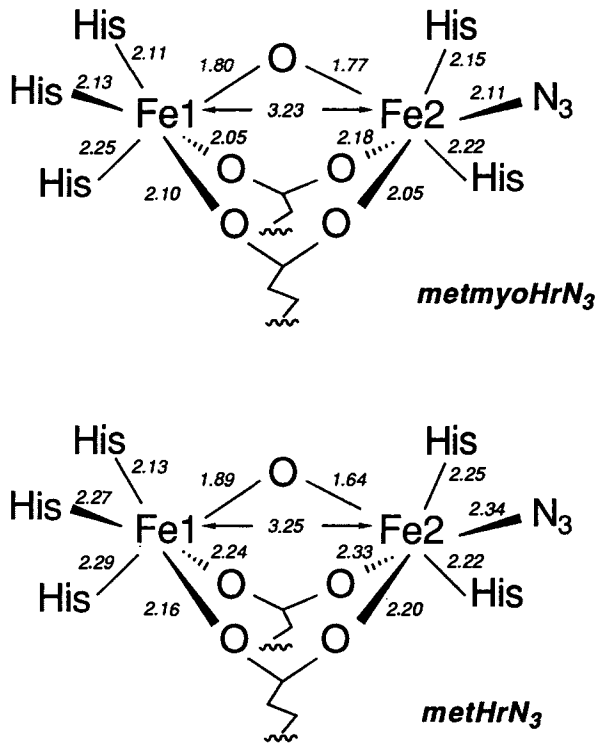


Figure 2. Comparison of the first coordination spheres of the diiron sites in metmyoheme-rythrin azide and methemerythrin azide based on their respective crystal structures. Adapted from Refs. 2 and 3.

be doubled (27). These numbers have been adjusted upward because of a combination of circumstances: (a) the nucleotide sequencing studies have determined the subunit molecular weight to be 87.5 kDa, a value 12% higher than the previously determined number (28); (b) the trichloroacetic acid (TCA) precipitation technique does not release all the bound iron and so repeated extraction of the TCA precipitate with dilute HCl or complete hydrolysis of the polypeptide chain yielded higher iron contents; (c) complete peptide hydrolysis and subsequent amino acid analysis yielded a new ϵ_{280} , which is 17% higher than the original value. When all these factors are taken into account, RRB2 has 3.9 Fe and 1.4 Tyr radical per 87.5-kDa subunit (27). These values support a model of one dinuclear iron cluster per peptide chain with each tyrosine 122 radical being associated with its own cluster; this model has been recently confirmed by X-ray crystallog-

raphy (Fig. 3) (29) (see also color plate). Though the tyrosyl radical concentration, as determined by EPR, is greater than one per RRB2 unit, it does not approach two radicals per subunit, the number suggested by the above model. The circumstances that govern the formation and stability of the radical, however, are currently poorly understood.

Methane monooxygenase is the most recent addition to this class of dinuclear iron-oxo proteins, the best characterized enzymes being obtained from *Methylococcus capsulatus* (Bath) (12, 30) and *Methylosinus tricho-*

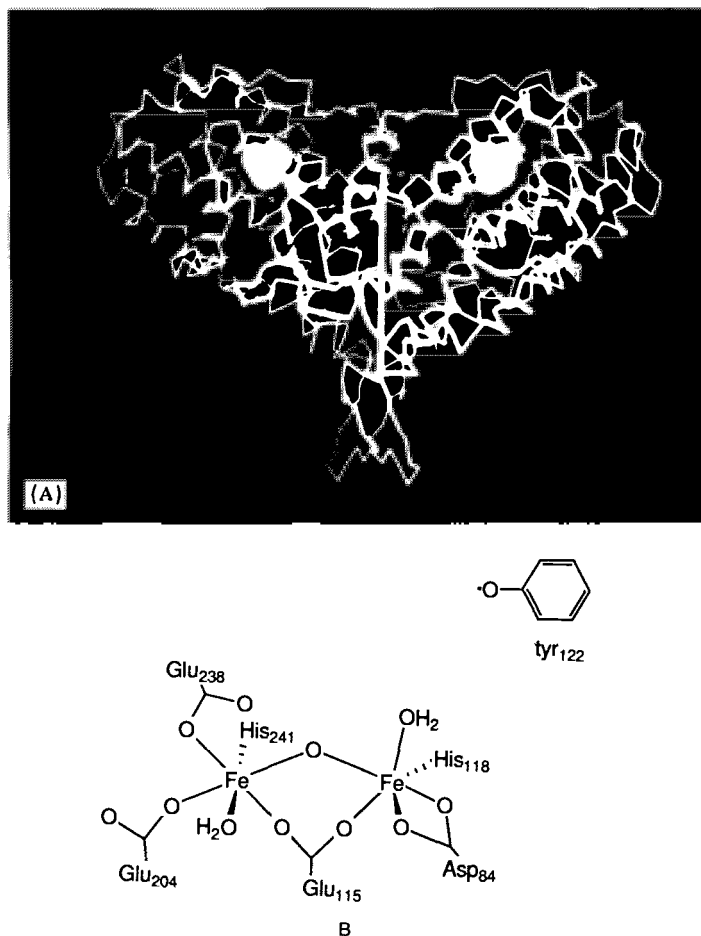
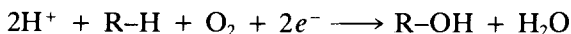


Figure 3. (a) Representation of the structure of the B2 subunit of the *E. coli* ribonucleotide reductase. Courtesy of Prof. Hans Eklund. (b) Schematic of the binuclear iron site in the B2 subunit of ribonucleotide reductase showing the dissimilar iron sites in the μ -oxo bridged core. The relative position of the tyr₁₂₂ radical that is 5 Å from the diiron site is indicated.

sporium OB3b (11, 31). As a result of an improvement in cell culturing and protein purification methods, substantial amounts of enzyme can be isolated with specific activities that are as much as 25-fold higher than those of earlier preparations. The higher activities now attainable derive from the realization that enzyme inactivation during purification could be reversed by the addition of Fe(II) and cysteine to the buffers (11). The enzyme consists of three components—a hydroxylase, a reductase, and a third protein component B, which appears to be required for coupling the reductase and hydroxylase activities. The hydroxylase component has an $\alpha_2\beta_2\gamma_2$ composition with a molecular weight of 245 kDa and contains 1–2 dinuclear iron units (11, 16). Its reaction stoichiometry is similar to that of cytochrome P-450, that is,



where RH is methane for the cellular reaction; however, the enzyme is capable of hydroxylating a variety of alkanes and also effecting the monooxygenations of alkenes, amines, and sulfides (32).

A. Diferric Forms

The diferric oxidation state is the best understood form of the Fe–O(R)–Fe unit. (μ -Oxo)diferric complexes have been known for many years (33), but only recently has intense attention been concentrated on the detailed properties of these complexes as they pertain to corresponding sites in the proteins.

1. Methemerythrin and Its Synthetic Analogues

The physiologically important diferric form of Hr is oxyhemerythrin (5, 6) (discussed in Section II.D.1), but the best characterized form is methemerythrin (metHr). Methemerythrin also contains a diferric site; it does not bind dioxygen but instead avidly binds small anions such as N_3^- , SCN^- , OCN^- , CN^- , and Cl^- . The crystal structures of metHr, metHrN₃, and metmyoHrN₃ demonstrate that the metal sites in these complexes consist of a (μ -oxo)bis(μ -carboxylato-*O,O'*)diiron(III) core unit (2, 3). The Fe–O_{oxo} bonds average 1.78 Å, while the Fe–Fe separation ranges from 3.21 to 3.25 Å, giving rise to an Fe–O–Fe angle of 127–135°.

The cores of metHrN₃ and metmyoHrN₃ are compared in Fig. 2. The core of metmyoHrN₃ features similar but distinct Fe– μ -O bond lengths ($\Delta r = 0.03$ Å), lengthened Fe–N bonds for the histidines trans to the oxo bridge, and unsymmetrically bridged carboxylates (3). Although similar in gross features, the cores of metHr and metHrN₃ differ in detail from that

TABLE I
Properties of Binuclear Iron-Oxo Proteins

	References	Fe- μ -O ^a (Å)	Fe-Fe ^a (Å)	Fe-O-Fe ^a (degree)	Fe-O ₂ N ^a (Å)	J (cm ⁻¹)	δ (mm · s ⁻¹)	ΔE_Q (mm · s ⁻¹)
Fe ^{III} Fe ^{III} methHrN ₃	2, 36, 38	1.78 ^b	3.25 ^b	134.5 ^b	2.24 ^b		0.51	1.95
							0.51	1.47
myometHrN ₃	39	1.80	3.13	127	2.13			
	40	1.80	3.19	125	2.13			
	3	1.79 ^b	3.23 ^b	130 ^b	2.14			
metHr	2, 34, 36	1.80 ^b	3.21 ^b	127 ^b	2.17 ^b	-134	0.46	1.57
	39	1.82	3.13	118	2.11			
oxyHr	34, 36, 39	1.82	3.24	128	2.16	-77	0.51	1.96
							0.52	0.95
metHrCl native RRB2	38	1.78	3.22	130	2.06	-108	0.50	2.04
	24, 26, 40						0.53	1.65
metRRB2	41	1.78	3.37 ± 0.11	127	2.04		0.45	2.45
	26, 40	1.78	3.19		2.05		0.50	1.70
MMO Uf ₆	31, 42	1.92	3.05	105	1.92		0.55	1.65
	43, 44					≤ -40 ^c	0.46	2.12
Uf ₆ -P ₇	1a, 45, 46	3.1-3.2			1.96 ^d		0.52	1.02
					2.10		0.55	1.38

BSPAP _{o-P}	47, 48	3.00		1.98 ^d 2.13	≤ -150	0.51 0.54 0.52	1.03 1.36 1.47
Rubrerithrin Fe ^{II} Fe ^{II}	13						
deoxyHr	35, 36, 39 49	1.98	128	2.19	-13 ± 2 ^c -25 ± 13 ^c >0 ^c	1.14	2.76
deoxyHrN ₃	49						
RRB2 _{red}	27, 50					1.26	3.13
MMO _{red}	31					1.30	3.14
Rubrerithrin _{red}	13					1.30	3.14
Fe ^{III} Fe ^{II}							
semimetHrN ₃	35, 40 51	1.87	135	2.14	-20 ^c -15 ^f		
MMO _{mv}	52, 53						
Uf _{red}	1a, 44, 54	3.41		2.06 2.02 ^d 2.13	-29 ^f -9.9	0.53 1.22	1.78 2.63
Uf-P _r	45, 54				-3	0.54	0.78
BSPAP _r	47, 48			2.02 ^d 2.12	-5 ^f	1.23	2.76

^aUnless otherwise noted, structural parameters are obtained from EXAFS measurements.

^bStructural parameters were obtained from X-ray crystallography measurements.

^cValues are obtained from NMR measurements.

^dEXAFS simulations were obtained using 3 Fe-O and 3 Fe-N ligands per iron.

^eValues are obtained from MCD measurements.

^fValues are obtained from EPR measurements.

of metmyoHrN₃ (2). The most striking difference is the asymmetry of the Fe–O–Fe unit. The Fe–μ–O bonds differ in length by 0.24–0.25 Å, although the average Fe–O bond length is exactly what an Fe–oxo bond should be. The crystallographers advise caution in accepting this asymmetry because of the difficulty of accurately locating a single O atom in two Fe atoms; however, this pattern appears in eight protein subunits in two separate structural determinations, so the asymmetry may be real and imposed by the protein structure.

Properties associated with this core unit include (a) strong antiferromagnetic coupling between the two high-spin ferric centers as indicated by the weak paramagnetism and anti-Curie temperature dependence exhibited by the magnetic susceptibility (34) and NMR isotropic shifts (35), (b) large Mössbauer quadrupole splittings (36–38) (Table I), and (c) distinctive near UV and visible absorption features around 300–500 nm and a broad band near 700 nm (37, 55, 56). These are clearly properties associated with the oxo bridge modulated by the presence of the carboxylate bridges. The availability of synthetic analogues of this site has greatly enhanced our understanding of this structural motif.

(μ-Oxo)bis(μ-carboxylato)diiron(III) complexes are readily synthesized by spontaneous self-assembly using tridentate amine ligands (Fig. 4) (57). Representative structures are shown in Fig. 5. Armstrong and Lippard were first to demonstrate the synthesis of such complexes with hydrotris(pyrazolyl)borate, HBpz₃ (Fig. 5A) (58–60), followed closely thereafter by Wieghardt and co-workers with 1,4,7-triazacyclononane, TACN (61). Besides pyrazole and amine functionalities, pyridine, imidazole, and benzimidazole ligating groups have been shown to assemble this core structure by treating the appropriate tridentate ligand with Fe(III) and carboxylate (72–74, 82). A tribridged complex with all oxygen ligands has also been reported using the novel CpCo[OP(OEt)₂]₃ face capping ligand (67). In a more directed synthesis, Christou and co-workers treated the tetranuclear complex [Fe₄O₂(OAc)₇(bipy)₂](CO₄) with chloride to generate Fe₂O(OAc)₂(bipy)₂Cl₂ (68), which has N₂Cl terminal faces. The presence of the monodentate chloride ligands in the last complex models the anion binding site found in methemerythrin, and the synthesis of the corresponding azide complex has also been briefly mentioned (68). In a more recent report, Lippard and co-workers demonstrated the self-assembly of [Fe₂O(O₂CR)₂L₂Cl₂] complexes (where L is a bidentate nitrogen ligand) by using *m*-phenylenedipropionic acid, a diacid whose span between the two carboxylates allows them to occupy the appropriate positions of a (μ-oxo)bis(μ-carboxylato)dimetal core (69). Relevant structural and physical properties of these complexes are compared in Table II.

All (μ-oxo)bis(μ-carboxylato) complexes in Table II are similar from a

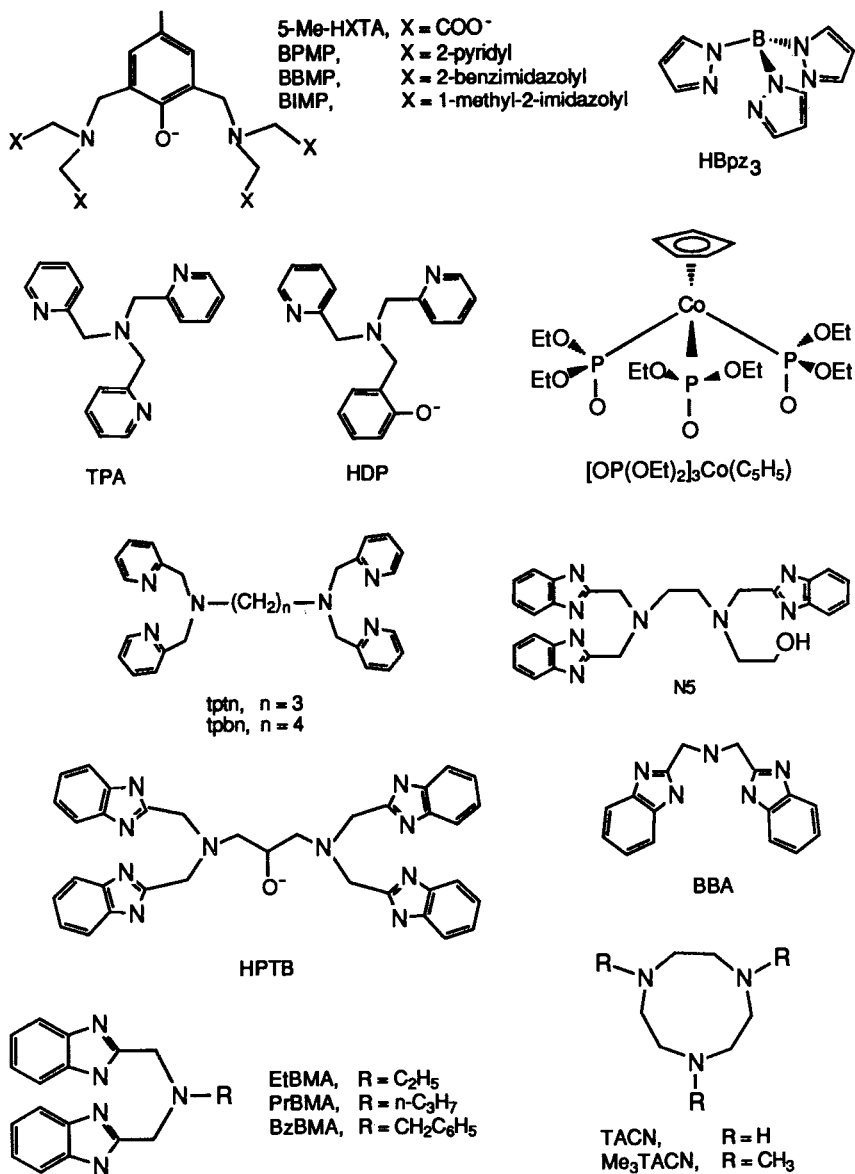


Figure 4. Structures of ligands and their abbreviations.

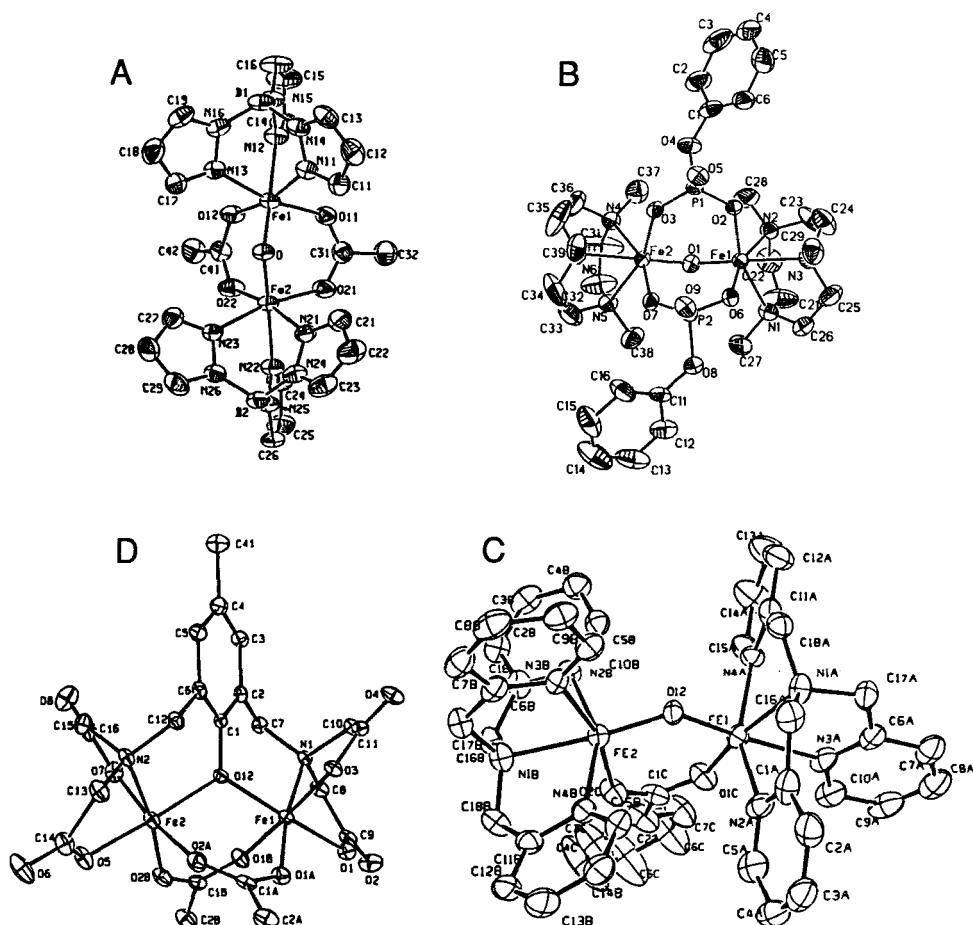


Figure 5. Representative crystal structures of synthetic diiron complexes. (a) $[\text{Fe}_2\text{O}(\text{OAc})_2(\text{HBPz}_3)_2]$, (b) $[\text{Fe}_2\text{O}(\text{O}_2\text{P}(\text{OPh}))_2(\text{Me}_3\text{TACN})_2]$, (c) $[\text{Fe}_2\text{O}(\text{OBz})(\text{TPA})_2](\text{ClO}_4)_3$, (d) $(\text{Me}_4\text{N})[\text{Fe}_2(5\text{-Me-HXTA}(\text{OAc})_2)]$. Reprinted with permission from Refs. 59, 62, 77, 81, © American Chemical Society.

structural perspective. In all cases, some effective symmetry element, either a twofold axis or a plane, relates the two halves of the molecule to give two essentially equivalent iron sites. Thus the inequivalence of the iron sites in metHr and metHrX is not modeled by these complexes. The $\text{Fe}-\text{O}_{\text{oxo}}$ bond falls in the range of 1.77–1.80 Å, not unlike those found in $(\mu\text{-oxo})$ diiron(III) complexes that have no additional bridges (33). Where the three groups of the tridentate ligand are identical, the ligand trans to

TABLE II
Structural and Magnetic Properties of Oxo-Bridged Diron Complexes

Compound	References	Fe- μ -O (Å)	Fe-Fe (Å)	Fe-O-Fe (degrees)	Fe-O _{ax} (Å)	Fe-N _{bas} (Å)	Fe-N _{trans} (Å)	J (cm ⁻¹)	δ (mm · s ⁻¹)	ΔE_0 (mm · s ⁻¹)
(μ -oxo)bis(μ -carboxylato)										
[Fe ₂ O(OAc) ₂ (HBpz) ₂]	58, 59	1.78	3.146	123.6	2.04	2.15	2.19	-121	0.52	1.60
[Fe ₂ O(O ₂ CH) ₂ (HBpz) ₂]	59	1.78	3.168	125.5	2.05	2.14	2.18		0.53	1.66
[Fe ₂ O(MPDB)(HBpz) ₂]	69	1.795	3.161	123.4	2.05	2.14	2.21		0.46	1.72
[Fe ₂ O(OAc) ₂ (TACN) ₂] ₂	70, 71	1.78	3.063	118.7	2.04	2.16	2.20	84 ^a	0.47	1.50
[Fe ₂ O(OAc) ₂ (Me ₃ TACN) ₂](ClO ₄) ₂	70	1.80	3.12	119.7	2.03	2.20	2.27	-115		
[Fe ₂ O(OBz) ₂ (BBA) ₂](ClO ₄) ₂	72	1.79	3.078	118.7	2.04	2.11	2.29	-117		
[Fe ₂ O(OAc) ₂ (bipy) ₂ Cl ₂]	68	1.785	3.151	123.9	2.08	2.15	2.21	-132	0.37	1.80
[Fe ₂ O(MPDP)(4,4'-Me ₃ ppy) ₂ Cl ₂]	69	1.772	3.130	123.0	2.03	2.16	2.20	-119	0.51	1.66
[Fe ₂ O(MPDP)(BIPMe) ₂ Cl ₂]	69	1.78.6	3.183	125.9	2.08	2.12	2.16	-122	0.52	1.94
[Fe ₂ O(MPDP)(TMICMe) ₂ Cl ₂]	69					2.42 ^b				
[Fe ₂ O(OAc) ₂ [(OP(OEt) ₂] ₂ Co(C ₃ H ₇) ₂] ₂]	67	1.80	3.174	124.4	2.028	2.06	2.13	-124	0.54	1.78
[Fe ₂ O(OAc) ₂ (tpbn) ₂ (NO ₃) ₂]	73	1.794	3.129	121.3	2.03	2.14	2.31	-108	0.56	1.78
[Fe ₂ O(OAc) ₂ (tpn) ₂ (ClO ₄) ₂ · 2 H ₂ O]	73									
[Fe ₂ O(OAc) ₂ (R-BMA) ₂](ClO ₄) ₂ ^c	74							-120	0.48	1.39
(μ -oxo)bis(μ -oxoantiro)								-113 ± 4		
[Fe ₂ O(O ₂ P(OPh) ₂)(HBpz) ₂]	75, 76	1.81	3.335	134.7	2.04	2.13	2.21	-98		
[Fe ₂ O(O ₂ P(Ph) ₂)(HBpz) ₂]	76	1.812	3.292	130.6	2.013	2.17	2.18	-93		
[Fe ₂ O(O ₂ P(OPh) ₂)(Me ₃ TACN) ₂]	77	1.818	3.198	123.2	1.98	2.28	2.29	-98		
[Fe ₂ O(HPO) ₂ (Me ₃ TACN) ₂]	77							-80		
[Fe ₂ O(HAsO) ₂ (Me ₃ TACN) ₂]	77							-85		
[Fe ₂ O(CrO) ₂ (Me ₃ TACN) ₂]	77	1.82	3.285	129.1	1.96	2.24	2.27	-112		
[Fe ₂ O(CO) ₂ (Me ₃ TACN) ₂]	78	1.820	3.048	113.8	1.95	2.235	2.29	-91		
[Fe ₂ O(SO) ₂ (Me ₃ TACN) ₂]	79	1.824	3.191	122.1	2.00	2.23	2.27	-97		
[Fe ₂ O(SO) ₂ (Me ₃ TACN) ₂]	79	1.817	3.166	121.1	1.985	2.25	2.282	-104		
(μ -oxo)(μ -carboxylato)										
[Fe ₂ O(OBz)(HDP) ₂](BPh ₄)	80	1.78	3.218	128.3	2.07	2.17	2.27	-118	0.45	1.52
[Fe ₂ O(OBz)(TPA) ₂](ClO ₄) ₃	81	1.79	3.241	129.6	2.01	2.14	2.20	-114	0.45	1.45
[Fe ₂ O(OAc)(TPA) ₂](ClO ₄) ₃	81	1.79	3.243	129.3	2.01	2.14	2.22	-114	0.45	1.45

Fe^{III}Fe^{III} Models

TABLE II (Continued)

Compound	References	Fe- μ -O (Å)	Fe-Fe (Å)	Fe-O-Fe (degrees)	Fe-O _{ar} -Fe (Å)	Fe-N _{inns} (Å)	Fe-N _{inns} (Å)	J (cm ⁻¹)	δ (mm · s ⁻¹)	ΔE_0 (mm · s ⁻¹)
(μ -oxo)(μ -oxoanion)										
[Fe ₂ O ₂ P(OPh) ₂ (TPA) ₂](ClO ₄) ₂	82	1.80	3.357	138.1	2.00	2.13	2.21	-104		
[Fe ₂ O(CO ₂ (HPTA)) ₂ N ₄ · 2 H ₂ O (μ -hydroxo)bis(μ -carboxylato)	83	1.83	3.37	136.4	1.99	2.04 ^d	2.20	63.4		
[Fe ₂ (OH)(OAc) ₂ (HPbz) ₂](ClO ₄) (μ -phenoxo)-bis(M-carboxylato)	60	1.96	3.439	124	2.00	2.10	2.10	-17	0.47	0.25
[Fe ₂ (5-Me-HXTA)(OAc) ₂](Me ₃ N) [Fe ₂ (BPMP)(OBz) ₂](ClO ₄) ₂	62, 84a 64	2.01	3.442	117.9	2.01	2.15	1.98 ^d	-12	0.66	0.52
[Fe ₂ (BBMP)(OAc) ₂](ClO ₄) ₂ (μ -alkoxo)bis(μ -carboxylato)	64							-8.8	0.27	0.71
[Fe ₂ (HPTB)(OBz) ₂](ClO ₄) ₂ (μ -alkoxo)(μ -carboxylato)	85							-26		
{[Fe ₂ (HPTB)(OBz) ₂ (O) ₂](ClO ₄) ₂ [Fe ₂ (HPTB-Et)(OAc) ₂ (O) ₂](ClO ₄) ₂ tris(O, O', μ -XO ₂)	85 85	2.00 2.01	3.539 3.488	123.7 120.9	2.02 1.98	2.24 2.24	2.16 2.16			
[Fe ₂ (O ₂ P(OPh)) ₂ (Me ₃ TACN) ₂] [Fe ₂ (HPO ₃) ₂ (Me ₃ TACN) ₂]	77 77							-3.5 -4.0		
[Fe ₂ (HAsO ₄) ₂ (Me ₃ TACN) ₂] [Fe ₂ (MoO ₄) ₂ (Me ₃ TACN) ₂]	77 86		4.456		1.92	2.24 ^e		-1.0 -4.4		
[Fe ₂ (CrO ₄) ₂ (Me ₃ TACN) ₂]	86		4.552		1.89	2.22 ^e		-7.5		
<i>Fe^{II}Fe^{III} Models</i>										
(μ -hydroxo)bis(μ -carboxylato)										
[Fe ₂ (OH)(OAc) ₂ (Me ₃ TACN) ₂](ClO ₄) (μ -phenoxo)bis(μ -carboxylato)	70, 87	1.99	3.32	113.2	2.13	2.28	2.30	-13	1.16	2.83
[Fe ₂ (BPMP)(OPr) ₂](BPh ₄) (μ -O, O'-carboxylato)bis(μ -O, O'-carboxylato)	66	2.06	3.35	108.9	2.09	2.25	2.17		1.20	2.72
[Fe ₂ (BIPhMe) ₂ (O ₂ CH) ₄]	88	2.15 ^f	3.585	113.1	2.11	2.13	2.045 ^d 2.104		1.26 1.25	2.56 3.30
<i>Fe^{II}Fe^{III} Models</i>										
(μ -oxo)bis(μ -carboxylato)										
[Fe ₂ O(OAc) ₂ (Me ₃ TACN) ₂] ⁺	70, 89							-15 ^g	0.48 1.19	0.42 3.38

the oxo bridge exhibits a longer Fe–N bond. The two Fe–O_{oxo} bonds in a complex can differ in length by as much as 0.04 Å. Where the three groups on the tridentate ligand are different, the weakest base is trans to the oxo group. This trans influence is understandable in view of the strength of the iron–oxo bond.

In general, the iron–ligand bond lengths found in the synthetic complexes match well with those determined for metmyoHrN₃, thus emphasizing the veracity of these compounds as models and confirming the reliability of the protein crystal structure analysis. On the other hand, the structural parameters found for metHr and metHrN₃ appear to be longer than corresponding mean distances observed for the models, with the exception of the extremely short Fe–O_{oxo} bond. This mismatch is troubling, particularly in light of the metmyoHrN₃ data, and needs further scrutiny.

The addition of carboxylate bridges to the (μ-oxo)diiron(III) unit restricts the Fe–O–Fe angle to $120 \pm 5^\circ$ and the Fe–Fe separation to 3.12 ± 0.05 Å. It is interesting that all the (μ-oxo)bis(μ-carboxylato)diiron(III) complexes in Table II exhibit Fe–Fe distances that are significantly shorter than the 3.21–3.25 Å values found for metHr. It has been argued that the “trigonal bite” of the ligands may give rise to the shorter Fe–Fe separation (1a), but the recent addition of Fe₂O(OAc)₂Cl₂(bipy)₂ to this family of compounds renders this argument invalid because this complex still has a 3.15 Å Fe–Fe distance despite having a bidentate and a monodentate terminal ligand on each iron (68). The rationale for the difference in Fe–Fe separations between the synthetic complexes and the protein structures should be further investigated.

Mössbauer spectra of metHrX complexes consist of quadrupole doublets at liquid helium temperatures with isomer shifts of ~ 0.5 mm · s⁻¹, indicating that the ferric centers are in the high-spin state and antiferromagnetically coupled (36–38). These complexes also exhibit large quadrupole splittings (ΔE_Q) and, in some, are distinguished by two different ΔE_Q values, presumably due to the inequivalence of the two iron sites (Table I). The synthetic complexes also exhibit large ΔE_Q values (Table II). Although it has not been established by single-crystal Mössbauer experiments, the large ΔE_Q values are likely to be due to the short Fe–O_{oxo} bond, which is expected to distort significantly the electric field gradient about the ⁵⁷Fe nucleus.

The antiferromagnetic coupling found by magnetic susceptibility methods in metHr is strong with $J = -134$ cm⁻¹ ($H = -2JS_1 \cdot S_2$) (34). The NMR shifts of the solvent exchangeable protons on the histidine residues coordinated to the irons of metHr also corroborate the presence of strong coupling. They are found between 13–25 ppm (35) and are considerably less than the NH shifts in mononuclear high-spin ferric imidazole complexes (~ 100 ppm) (43, 96). The contact shift is directly proportional to the

electron-nuclear hyperfine splitting constant, A , and to the magnetic susceptibility of the complex. Assuming that the hyperfine coupling remains relatively constant in the various coupled spin states, the contact shift in a coupled system is expected to decrease as J increases (43). For comparison, the synthetic complexes exhibit J values that range from -108 to -132 cm^{-1} . The values are somewhat larger than those found for oxo-bridged nonheme iron complexes with no additional bridges (97) and suggest that the carboxylates introduce additional pathways for coupling.

The electronic spectra of metHr (37, 55, 56) and the synthetic $(\mu\text{-oxo})\text{bis}(\mu\text{-carboxylato})\text{diiron(III)}$ complexes are similar (Fig. 6 and Ta-

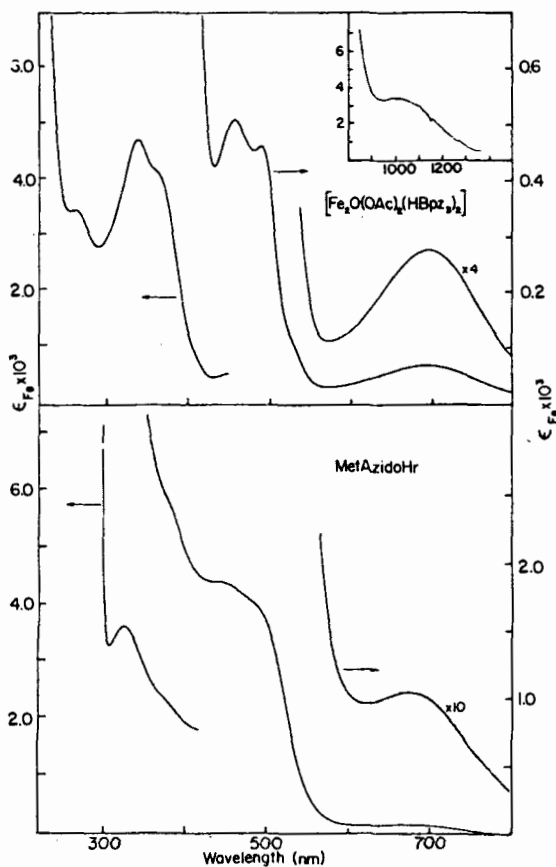


Figure 6. Comparison of the electronic spectra of metHrN₃ and $[\text{Fe}_2\text{O}(\text{OAc})_2(\text{HBpz})_2]$. Reprinted with permission from W. H. Armstrong, A. Spool, G. C. Papaefthymiou, R. B. Frankel, and S. J. Lippard, *J. Am. Chem. Soc.*, 106, 3653-3667 (1984). Copyright © (1984) American Chemical Society.

ble III). Based on variable temperature circular dichroism (CD) and polarized single-crystal absorbance studies, Solomon and co-workers (98) recently assigned many of the intense UV transitions as oxo-to-Fe(III) charge transfer in nature and strongly argued against their assignment as simultaneous pair excitation of ligand field bands as earlier suggested by Gray, Schugar, and their co-workers (101). The lower energy bands in the visible region are assigned to ligand-field transitions, whose intensities are enhanced by low symmetry mixing with their intense low energy oxo bands. These spectral features are not found in complexes with linear oxo bridges (58) and appear characteristic of complexes with bent Fe–O–Fe bonds.

Laser excitation into these absorption features, particularly in the near UV, gives rise to resonance Raman features associated with the Fe–O–Fe unit. In general, the symmetric stretch is found near 500 cm^{-1} , while the asymmetric stretch occurs near 800 cm^{-1} (58, 102–104). In accordance with a simple triatomic model, these values depend on the Fe–O–Fe angle. Indeed, the positions of ν_s and ν_{as} together with their ^{18}O isotope shifts have been used to estimate Fe–O–Fe and the correspondence is reasonable for complexes with known crystal structures (104).

In a survey of tribridged (μ -oxo)diiron(III) complexes with N3 face-capping ligands (104), Sanders-Loehr et al. noted an interesting correlation—that the enhancement of ν_s relative to a standard depends on the nature of the ligands cis and trans to the oxo bridge (Fig. 7 and Table IV). Complexes with only amine nitrogen ligands exhibit weak enhancements of <30 . This enhancement increases to ~ 75 when aromatic nitrogen ligands cis to the oxo bridge are present and to >300 when aromatic nitrogen ligands are both cis and trans to the oxo bridge. Not surprisingly, with its histidine-rich coordination environment, metHrX complexes fall in the last category. The exact mechanism for this enhancement is not established. Perhaps the presence of ligands capable of π -delocalization can enhance the intensity of the oxo-to-Fe(III) charge-transfer transition, which then translates into a substantially larger resonance Raman enhancement. The tribridged complex with $\text{CpCo}[\text{OP}(\text{OEt})_2]_3$ capping ligands has recently been shown to be among the complexes that exhibit strongly enhanced ν_s vibrations (67); its all-oxygen ligand environment, while not contradicting the above correlation, demonstrates that ligands besides aromatic heterocycles can engender such an enhancement.

One aspect of the Raman spectra of metHrX complexes not modeled by the synthetic complexes discussed thus far is the enhancement of the asymmetric Fe–O–Fe stretch, ν_{as} . The ν_{as}/ν_s intensity ratios for metHrX complexes range from 0.18 to 0.4, whereas the ratios in these models are 0.09 or less, <0.04 for most cases (104). The synthetic complexes all have twofold symmetry, while the metHrX complexes lack twofold symmetry,

TABLE III
Electronic Transitions for Fe^{III}O Centers in Proteins and Models

Complex	λ_{\max} in nm (ϵ in $M^{-1} \text{ cm}^{-1}$ per diiron center)			
	LMCT and ${}^6A \rightarrow {}^4A_1, {}^4E$	${}^6A \rightarrow {}^4T_2$	${}^6A \rightarrow {}^4T_1$	
metHrOH ^a	320 (6800) 362 (5900)	480 (sh, 550)	610 (150)	990 (8)
oxyHr ^a	330 (6800) 360 (sh, 5500)	500 (1100)	750 (200)	990 (10)
metHrN ₃ ^a	326 (6800) 380 (sh, 4300)	445 (br, 3700)	680 (190)	1010 (10)
metHrCl ^a	329 (6600) 380 (6000)	490 (sh, 750)	655 (180)	1020 (11)
metRRB2 ^b	325 (4700) 370 (3600)	500 (400)	600 (150)	
rubrerythrin ^c	365 (~5300)	460 (750)		
[Fe ₂ O(OAc) ₂ (HBpz ₃) ₂] ^d	339 (9300) 358 (sh)	457 (1010) 492 (920) 528 (sh)	695 (140)	995 (7)
[Fe ₂ O(O ₂ CH) ₂ (HBpz ₃) ₂] ^d	342 (10200)	460 (1080) 489 (980)	692 (140)	
[Fe ₂ O(OBz) ₂ (HBpz ₃) ₂] ^d	336 (9000)	455 (960) 490 (860)	691 (130)	
[Fe ₂ O(OAc) ₂ (TACN) ₂] ²⁺ (e)	323 (7760) 368 (sh)	468 (1300) 492 (sh) 544 (sh)	745 (71)	
[Fe ₂ O(OAc) ₂ (Me ₃ TACN) ₂] ²⁺ (f)	345 (10,500)	424 (960) 472 (1400) 513 (1100)	729 (140)	1031 (7)
[Fe ₂ O(OBz) ₂ (BBA) ₂] ²⁺ (g)	355 (8000)	485 (sh, 610) 525 (220) 560 (sh, 100)	620 (100)	
[Fe ₂ O(OAc) ₂ tpbn] ²⁺ (h)	348 (7400)	470 (1100) 505 (990)	730 (157)	
[Fe ₂ O(OAc) ₂ Cl ₂ (bipy) ₂] ⁱ	329 (6060)	464 (sh, 387)		
[Fe ₂ O(OAc)(TPA) ₂] ³⁺ (j)	332 (10000) 366 (sh)	458 (1200) 492 (1000) 504 (940) 534 (sh)	700 (140)	1054 (9)
[Fe ₂ O(OBz)(TPA) ₂] ³⁺ (j)	328 (12000) 368 (sh)	460 (1200) 492 (1000) 504 (980) 534 (sh)	700 (160)	1054 (10)

^aCompiled from Refs. 37, 98, and 99.

^bValues corrected for 2 dinuclear centers per mole; Ref. 24.

^cReference 12.

^dReference 58.

^eReference 71.

^fReference 100.

^gReference 72.

^hReference 73.

ⁱReference 68.

^jReference 81.

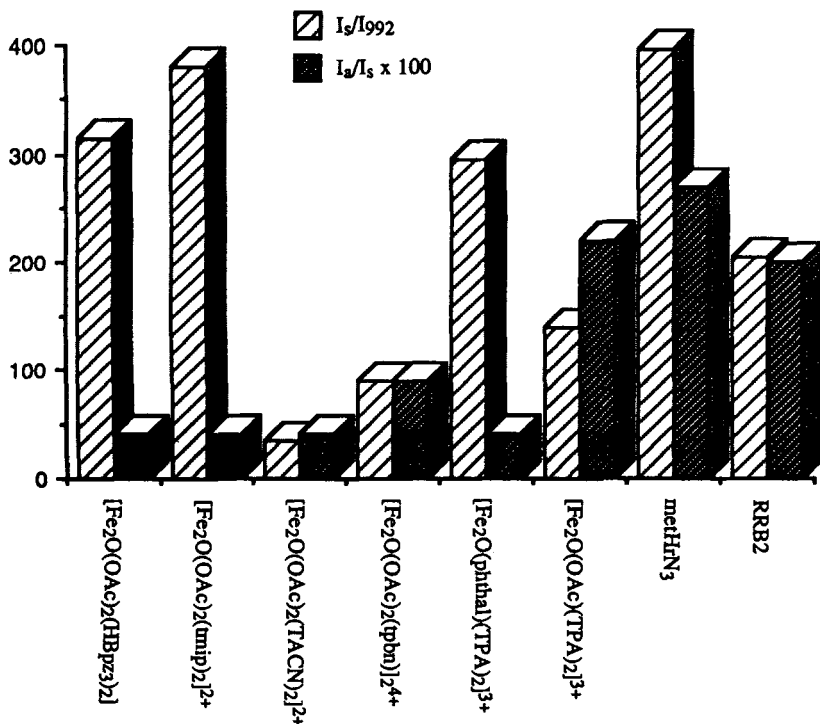


Figure 7. Comparison of the resonance Raman intensities of the $\nu(\text{Fe-O-Fe})$ and the $\nu_{\text{as}}(\text{Fe-O-Fe})$ features for a series of (μ -oxo)diiron(III) synthetic complexes and proteins. Data used is from Refs. 82 and 104.

which may enhance the ν_{as} intensity and depress the ν intensity. Examples of such intensity ratios in synthetic complexes will be discussed shortly.

In addition to the electronic features associated with the Fe-O-Fe group, some metHrX complexes also exhibit X-to-Fe(III) charge-transfer transitions (98, 99, 105). For example, the azide complex shows a broad band near 445 nm, which in single-crystal absorbance data is polarized perpendicular to the Fe-Fe axis and becomes resolved into two features at 485 and 442 nm at 77 K (98). Upon laser excitation into the visible band, vibrations associated with an Fe-N₃ stretch and intra-azide stretches are observed (106, 107).

Synthetic complexes where the bridging groups have been varied are known; these complexes serve to ascertain the properties that have been ascribed to the (μ -oxo)bis(μ -carboxylato)diiron(III) unit. For example, the oxo bridge can be replaced by hydroxo, alkoxo, or phenoxo groups. When $[\text{Fe}_2(\text{HBpz}_3)_2\text{O}(\text{OAc})_2]$ is treated with one equivalent of HBF_4 in CH_2Cl_2 , the conjugate acid $[\text{Fe}_2(\text{OH})(\text{OAc})_2(\text{HBpz}_3)_2]^+$ is formed (60). Protonation of the oxo bridge results in the lengthening of the Fe-O_{bridge}

TABLE IV
Resonance Raman Properties of the $\nu(\text{Fe-O-Fe})$ Features
of (μ -Oxo)diiron(III) Units in Proteins and Models^a

	ν_s (cm^{-1})	ν_{as} (cm^{-1})	I_s/I_{992}^b	I_s/I_{as}
oxyHr	486	753	210	0.17
metHrN ₃	507	768	295	0.27
metHrOCN	509	782	1250	0.09
RRB2	493	756	>205	0.20
[Fe ₂ O(OAc) ₂ (HBpz ₃) ₂]	528	751	315	<0.04
[Fe ₂ O(OAc) ₂ {[OP(OEt) ₂] ₃ CoCp ₂ }] ^c	510		320	
[Fe ₂ O(OBz)(TPA) ₂](ClO ₄) ₃	497	772	160	0.33
[Fe ₂ O(OAc)(TPA) ₂](ClO ₄) ₃	499	770	140	0.30
[Fe ₂ O(O ₂ P(OPh) ₂)(TPA) ₂](ClO ₄) ₃	458	782	220	0.18
[Fe ₂ O(phthal)(TPA) ₂](ClO ₄) ₂ ^d	433	787	>150	<0.04
[Fe ₂ O(OBz)(HDP) ₂](BPh ₄)	494	763	5	<0.04
[Fe ₂ O(O ₂ P(OPh) ₂)(HDP) ₂](BPh ₄)	461		15	<0.04
[Fe ₂ O(OAc) ₂ (TMIP) ₂] ²⁺			380	<0.04
[Fe ₂ O(OAc) ₂ (TACN)]I ₂	540	749	35	<0.04
[Fe ₂ O(OAc) ₂ (Me ₃ TACN) ₂](ClO ₄) ₂	537			<0.04
[Fe ₂ O(OAc) ₂ (tpbn)] ₂ (NO ₃) ₄	525	727	90	0.09

^aAll values unless noted are from Ref. 104.

^bValues obtained with 410-nm excitation.

^cReference 67.

^dReference 84b.

bond to 1.95 Å and the Fe-Fe distance to 3.44 Å, leaving the Fe-O-Fe angle at 125°. In turn, the visible absorption features bleach, ΔE_O diminishes to 0.5 $\text{mm} \cdot \text{s}^{-1}$, and $-J$ decreases to 17 cm^{-1} . The weakening of antiferromagnetic coupling between the metal centers may be attributed to the loss of one of the π -type orbitals on the oxo bridge available for superexchange and the consequent lengthening of the Fe-O_{bridge} bonds.

Although dinuclear complexes with μ -alkoxo bridges have been reported, for example, Fe₂(HPTB)(NO₃)₅ (108) and [Fe₂(HPTB)(OBz)₂](ClO₄)₃ (85), neither one has been crystallographically characterized. The J values for the two complexes are -22 and -25 cm^{-1} , respectively (85, 109). Based on structures of the tetranuclear complexes [Fe₄(HPTB)₂O₂(O₂CR)₂], the Fe-O_{bridge} distance is estimated to be ~ 1.9 Å and the Fe-O-Fe angle $\sim 140^\circ$ (85).

A (μ -phenoxo)bis(μ -carboxylato)diiron(III) complex, (Me₄N)[Fe₂(5-MeHXTA)(OAc)₂] has been crystallographically characterized (Fig. 5d) (62). It exhibits Fe-O_{bridge} bonds of 2.01 Å, an Fe-Fe separation of 3.44 Å, an Fe-O-Fe angle of 118°, and asymmetrically bridged acetates ($\Delta r_{\text{Fe-OAc}} = 0.02\text{-}0.03$ Å). The further lengthening of the Fe-O_{bridge} bonds

results in further weakening of the antiferromagnetic coupling [$J \sim -10 \text{ cm}^{-1}$ for the 5-Me-HXTA complex (84) and -12 cm^{-1} for the analogous BPMP complex (64)] as the bridge oxygen orbitals are now involved in both σ and π bonding to the phenyl group. Visible absorption properties of these compounds are not relevant because their spectra are dominated by the phenolate LMCT band.

This series of μ -oxo, μ -hydroxo, μ -alkoxo, and μ -phenoxo complexes thus demonstrates the effect of the oxygen bridge on the properties of these dinuclear centers. Increasing demand of the bridge substituents on the available oxygen electrons results in the lengthening of the Fe–O_{bridge} bonds and the weakening of the antiferromagnetic coupling between the two Fe(III) centers.

Alterations in the carboxylate bridges also affect the properties of the (μ -oxo)diiron(III) core. A variety of oxoanions has been demonstrated to form the tribridged diiron core (Fig. 5b) (75–77). Because of their potential relevance to the anion complexes of the purple acid phosphatases, detailed discussion will be made in Section III.F. Wieghardt and co-workers have undertaken a systematic study with complexes of Me₃TACN with oxoanions that vary in charge, bite angle, and affinity (basicity) for the iron centers. In general, the substitution of carboxylate with other oxoanions results in the increase of both Fe–O_{bridge} bond lengths and the Fe–Fe distance with concomitant weakening of the antiferromagnetic interaction (77).

A different variation on the bridging carboxylates is to provide circumstances that allow the coordination of only one carboxylate bridge. This modification is easily accomplished with the use of tetradentate tripodal ligands, of which there are three examples: TPA, HDP, and HPTA. With TPA and HDP, complexes of the type [Fe₂O(O₂CR)₂]₂X₃ can be formed (Fig. 5c) (80–82). The (μ -oxo)(μ -carboxylato)diiron(III) core is structurally similar to the tribridged core, but differs in some respects. The Fe–O_{bridge} distances are comparable, but the Fe–O–Fe angles and, consequently, the Fe–Fe distances are bigger, $(129 \pm 1)^\circ$ and $(3.23 \pm 0.01) \text{ \AA}$, respectively. The reasons for the latter values are not established, although Norman et al. (82) have pointed out that the increases are a natural consequence of transforming a face-shared bioctahedron to an edge-shared one, at the same time maintaining similar Fe–ligand bond lengths. It is interesting to note, however, that the Fe–O–Fe angles and the Fe–Fe distances found in the dibridged complexes have values closer to those found in metHr and metHrN₃ than those of the tribridged complexes (Tables I and II).

The loss of one carboxylate bridge does not appear to alter significantly the properties of the (μ -oxo)diiron(III) unit. [Fe₂O(OAc)(TPA)₂](ClO₄)₃ exhibits a visible spectrum very similar to that of [Fe₂O(OAc)₂(HBpz₃)₂] (81). The J value for the TPA complex is -114 cm^{-1} and ΔE_{O} is 1.52

$\text{mm} \cdot \text{s}^{-1}$, values analogous to the tribridged (μ -oxo)diiron(III) complexes.

The third example of a dibridged core was actually the first such complex reported; it is a tetranuclear iron complex of HPTA involving two (μ -alkoxo)diiron(III) units, which are attached together by oxide and carbonate bridges between iron pairs to yield a nearly square array of iron atoms (83). The (μ -oxo)(μ -carbonato)diiron(III) substructure shows Fe–O_{bridge} bonds of 1.83 Å, an Fe–O–Fe angle of 136.4°, and an Fe–Fe separation of 3.37 Å. All these structural parameters are larger than those found for the TPA and HBPz₃ complexes with acetate bridges and most likely result from the high negative charge of the complex. The complex exhibits stronger paramagnetism than the other complexes as would be expected from the structural data; temperature dependence of the magnetization is complicated by the presence of two antiferromagnetic pathways among the four irons and a fit to the data gives $J_{\text{oxo}} = -63 \text{ cm}^{-1}$ and $J_{\text{alkoxo}} = -11 \text{ cm}^{-1}$.

A (μ -alkoxo)(μ -benzoato)diiron(III) substructure is present in the tetranuclear iron complex $[\text{Fe}_4(\text{HPTB})_2\text{O}_2(\text{OBz})_2]^{4+}$, with Fe–O_{alkoxo} bonds of 2.0 Å, an Fe–Fe distance of 3.54 Å, and an Fe–O–Fe angle of 124° (85). Unfortunately, magnetic properties of this unit are complicated by the presence of stronger coupling via oxo bridges to another (μ -alkoxo)(μ -benzoato)diiron(III) unit, and no value for J could be obtained. In general, properties of dibridged complexes are similar to tribridged complexes; these dibridged structures are thus also suitable candidates for the active sites of dinuclear iron proteins that are not yet characterized crystallographically.

The TPA complexes provide yet another variation on these structural themes—the two iron sites are inequivalent (Fig. 5*d*) (81, 82). On Fe2, the amine nitrogen is trans to the oxo bridge, while a pyridine is trans on Fe1. The oxo bridge exerts its trans influence, and these Fe–N bonds are longer than the corresponding Fe–N bonds cis to the oxo group. The carboxylate bridge consequently is trans to a pyridine on Fe1 and to the tertiary amine on Fe2, giving rise to an asymmetrically bridged unit ($\Delta r_{\text{Fe-O}} = 0.06 \text{ Å}$). The inequivalence of the iron atoms is now established for six TPA complexes with different three-atom bridges, and it persists in solution as indicated by NMR spectra (82). It is not clear what gives rise to the inequivalence, but molecular modeling suggests that the symmetric structure may have unfavorable H–H interactions between pyridine C–H atoms on the two TPA ligands (82).

This inequivalence neither significantly affects the visible absorption properties of the (μ -oxo)diiron(III) unit, nor changes the antiferromagnetic interaction as the values for J are similar in the TPA and HDP compounds. However, the inequivalence makes the resonance Raman properties of these complexes different from those of the symmetric ones (Fig. 7). For

the TPA complexes, the resonance Raman enhancements of the $\nu_s(\text{Fe-O-Fe})$ expressed as I_s/I_{992} are 140–230, which are significantly smaller than that found for the HBpz_3 complex, presumably due to the presence of only one pyridine trans to the oxo bridge (82). More interestingly, the I_{as}/I_s ratio, the relative amount of resonance enhancement of the asymmetric Fe-O-Fe stretch compared to the symmetric Fe-O-Fe stretch, is 0.18–0.33, a value similar to those of metHrX complexes (104). That the increased I_{as}/I_s ratio is due to the inequivalence of the Fe ligand trans to the oxo bridge is emphatically affirmed by the I_{as}/I_s value of $[\text{N}_5\text{Fe-O-FeCl}_3]\text{X}$ (110), the first well-characterized unsymmetric (μ -oxo)diiron(III) complex, which exhibits an intense ν_{as} and a weak ν_s ($I_{as}/I_s = 2.7$). Thus, the I_{as}/I_s ratio would appear to be a useful indicator of the asymmetry of dinuclear iron-oxo complexes. Other oxo-bridged complexes with inequivalent metal sites include PFe-O-FeP' (111), PFe-O-CrP (112), and $[\text{FeMnO}(\text{OAc})_2(\text{TACN})_2]^{2+}$ (113).

2. Ribonucleotide Reductase

We can apply many of the insights derived from the synthetic complexes to the interpretation of the spectroscopic data for the iron centers of the ribonucleotide reductase from *E. coli*. That the dinuclear iron centers in RRB2 consist of (μ -oxo)diiron(III) units similar to that found in methemerythrin is based on several observations. The EXAFS analysis clearly shows the presence of short Fe–O bonds of 1.8 Å (40, 41). The presence of such short μ -oxo bonds in the presence of longer distances typical of amino acid ligation is qualitatively indicated by a diminished intensity of the Fourier-filtered first shell EXAFS at low k values (Fig. 8). Figure 9 illustrates the differences in the first shell EXAFS spectra of $[\text{Fe}(\text{acac})_3]$, $[\text{Fe}_2\text{OH}(\text{OAc})_2(\text{HBpz}_3)_2]^+$, and $[\text{Fe}_2\text{O}(\text{OAc})_2(\text{HBpz}_3)_2]$. The short Fe–O bond gives rise to a frequency component that is nearly 180° out of phase from the component due to the longer Fe–(O,N) bonds at low k values and effects a partial reduction of the longer Fe–(O,N) absorption intensity by destructive interference (40).

Mössbauer spectra of native RRB2 reveals two quadrupole doublets of equal intensity with δ values of 0.5 $\text{mm} \cdot \text{s}^{-1}$, which are typical of high-spin ferric centers and ΔE_O values of 1.65 and 2.45 $\text{mm} \cdot \text{s}^{-1}$ (26). These large quadrupole splittings are expected of (μ -oxo)diiron(III) complexes. The appearance of two iron centers with distinct ΔE_O values was difficult to rationalize in the RRB2 model proposed by Reichard and co-workers (24) of a diiron site located between the two polypeptide chains of the B2 subunit because of its implied twofold symmetry, but is completely understandable in the new model of two diiron sites per B2 subunit when the two iron atoms of each dinuclear site have different environments (27).

The Mössbauer spectra of RRB2 at 4.2 K in large applied fields are indicative of a diamagnetic ground state. This result implies that the two iron centers in the dinuclear unit are coupled antiferromagnetically. Variable temperature magnetic susceptibility measurements yield a J of $(-108 \pm 20) \text{ cm}^{-1}$ as expected for an oxo bridged diiron complex (24).

The presence of additional bridges like carboxylate is suggested by the electronic and EXAFS spectra of RRB2. Besides the spectral features of the tyrosyl radical, which can be eliminated by hydroxyurea reduction (24), the UV/vis spectrum of RRB2 shows features at 325, 390, and 600 nm, akin to those found for metHr and its synthetic analogues (Fig. 10) and indicative of a bent Fe–O–Fe unit. EXAFS data show an Fe–Fe distance

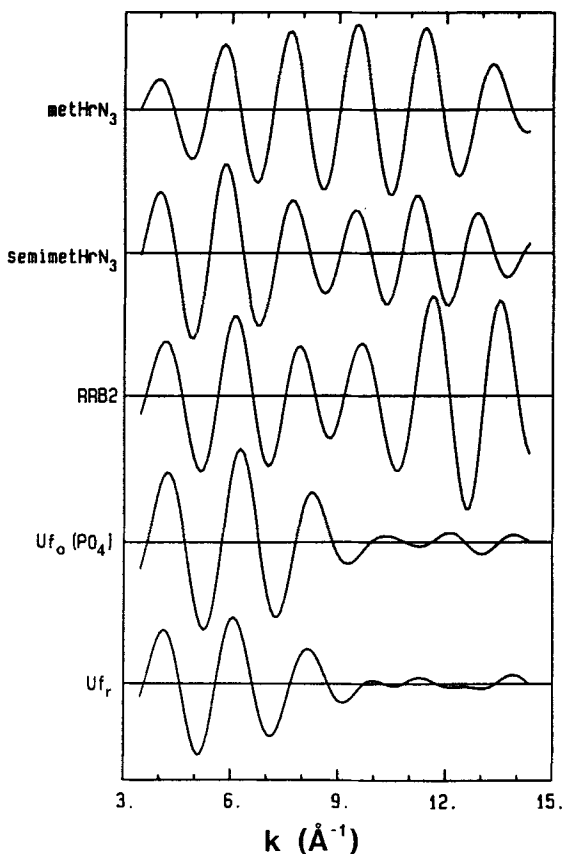


Figure 8. Fourier-filtered first shell EXAFS data for several diiron proteins. Reprinted with permission from L. Que, Jr., R. C. Scarrow, in *Metal Clusters in Proteins*, L. Que, Jr., Ed., American Chemical Society, Washington, DC, 1988, pp. 152–178. Copyright © (1988) American Chemical Society.

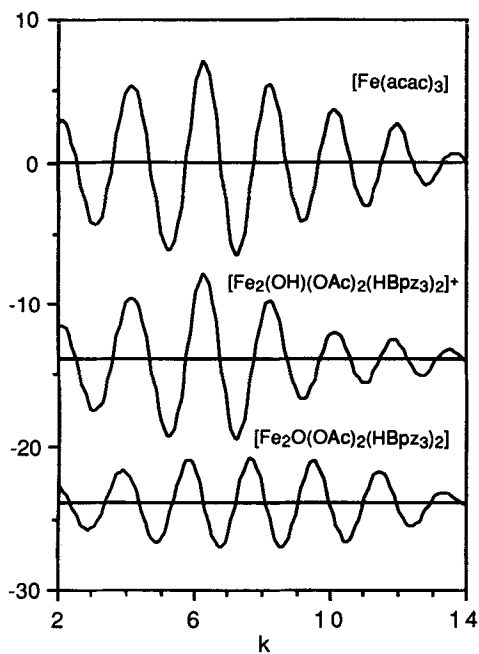


Figure 9. Fourier-filtered first shell EXAFS data for representative model compounds.

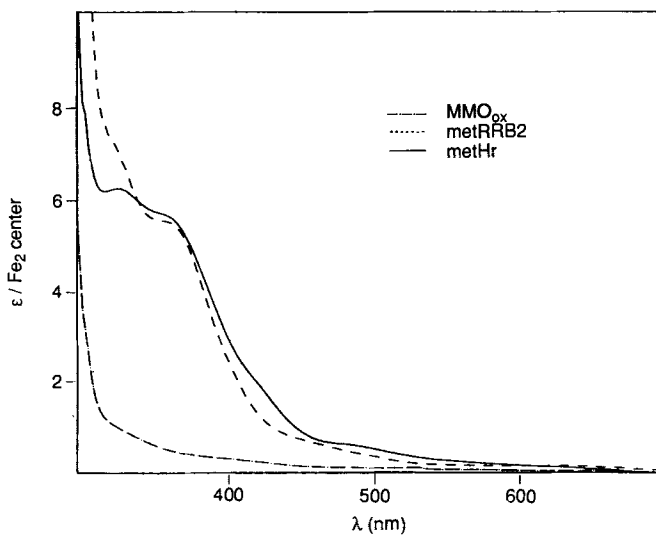


Figure 10. Electronic spectra of metHr, metRRB2, and MMO_{ox} .

of 3.22 Å (40), or 3.26 Å (41), which together with the short Fe–O bonds of 1.80 Å, yield an Fe–O–Fe angle of 127–129°. This angle is smaller than what is seen in complexes with only a μ -oxo bridge and suggests at least one additional bridge(s). Thus, the data point to a (μ -oxo)diiron(III) complex with one or two carboxylate bridges.

The nature of other ligands in this dinuclear complex can be deduced from other spectroscopic data. It is clear that the tyrosyl radical is NOT a ligand. Reduction of the tyrosyl radical with hydroxyurea does not alter the features of the Mössbauer (26) and EXAFS (40) data. Indeed, the only hint that the radical is in the vicinity of the dinuclear iron unit is the temperature dependence of the EPR relaxation properties of the radical signal. At liquid helium temperatures, the tyrosyl radical behaves like an isolated organic radical. But, at temperatures where the dinuclear iron complex becomes paramagnetic, the radical signal becomes harder to saturate relative to an isolated radical (114). Based on these effects, the radical is estimated to be within 10 Å of the diferric site.

Site-directed mutagenesis experiments have identified Tyr-122 as the residue that is oxidized (23). The tyrosyl radical can be observed by EPR spectroscopy at $g = 2.0$ as a doublet ($A = 19$ G) of triplets. In a beautiful study using *E. coli* tyrosine auxotrophs and specifically deuteriated tyrosines, Sjöberg et al. (115) showed that the major splitting arose from one of the β -CH₂ protons, which can be rationalized by a CH₂ conformation, wherein one C–H bond is nearly coaxial with the tyrosine π orbitals and the other is nearly perpendicular. Such a conformation would result in the transfer of significant unpaired spin density to one C–H but not to the other. An EPR signal with similar properties has been ascribed to the tyrosyl radical D in Photosystem II (116). The minor splittings, on the other hand, arise from interactions with 3,5-ring protons. By laser excitation into the tyrosyl electronic bands near 400 nm, a Raman feature at 1498 cm⁻¹ is observed (117). The energies of this vibration, as well as its insensitivity to D₂O, strongly suggest that the radical is present as a neutral species. The spectroscopic properties are also reproduced by neutral synthetic phenoxy radicals.

Resonance Raman studies on the dinuclear iron centers of RRB2 reveal features at 496 and 756 cm⁻¹. Due to their isotope shifts with H₂¹⁸O and to their similarity to bands seen in hemerythrin, these features are assigned to $\nu_s(\text{Fe-O-Fe})$ and $\nu_{as}(\text{Fe-O-Fe})$, respectively (118, 119). The low energy of these vibrations may be due to hydrogen bonding of the μ -oxo bridge, which would decrease ν_s from the expected value of 510 cm⁻¹. Indeed, in D₂O buffer, ν_s shifts by +3 cm⁻¹ as deuterium exchange into the putative hydrogen bond results in a weaker D–O interaction and results in a smaller perturbation of the ν_s value from the expected one.

The I_s/I_{992} ratio for RRB2 is ≥ 205 , smaller than that found for metHr (104, 119). Based on the model studies discussed earlier, it is inferred that there are fewer histidine ligands and the two ligands trans to the oxo bridge may be aromatic nitrogen ligands. In addition, the I_{as}/I_s ratio of 0.27 implies an asymmetry comparable to those found in the metHrX and TPA complexes (Table IV), consistent with the Mössbauer results indicating two distinct iron centers (27).

Comparisons of EXAFS data on RRB2 and metHrN₃ show that the average first shell Fe-(O,N) distance *excluding* the Fe-O_{oxo} bonds is significantly shorter for RRB2 (2.06 vs. 2.13 Å, respectively) (40, 41). A survey of crystal structures for high-spin Fe(III) complexes reveals that Fe(III)-O bonds are typically 1.9–2.0 Å while Fe(III)-N bonds are longer at 2.1–2.2 Å. Corroboration of the bond length shortening in a tribringed complex has recently been obtained with an O3 facecapping ligand (67). In this complex, the Fe-O bonds to the tridentate ligand average 2.06 Å compared to 2.15 Å for the corresponding HBpz₃ complex. The shorter average Fe-(O,N) distance in RRB2 thus suggests that the coordination environment of this dinuclear iron site is more oxygen rich than that of metHrN₃. Minimally, the shorter average distance would require the substitution of a histidine on each iron atom of metHrN₃ with an oxyanion ligand (e.g., OH⁻, carboxylate, phenolate) to generate the EXAFS spectrum of RRB2, a conclusion consistent with resonance Raman data.

Evidence for a hydroxide ligand was inferred from Raman spectra showing a band at 596 cm⁻¹ with appropriate H₂¹⁸O and D₂O isotope shift behavior (119). This feature, however, has recently been demonstrated to arise from a species due to laser decomposition of the protein (117).

Evidence for histidine as a ligand can be obtained from EXAFS and NMR data. The presence of second and third shell features at 3.0 and 4.3 Å in the EXAFS spectrum is usually indicative of imidazole coordination (41). Among protein ligands, the imidazole ring is most likely to be coordinated in such a way as to enhance the contributions of these more distant scatterers via multiple scattering pathways. These outer-shell features are weaker in RRB2 than in metHrN₃, consistent with the suggestion of fewer histidine ligands for RRB2.

The NMR spectra of native RRB2 show a feature at 24 ppm, which disappears upon D₂O exchange (120). The observed shift and solvent exchange behavior is as expected for N-H groups of imidazoles coordinated to (μ-oxo)diiron(III) complexes. Methemerythrin exhibits such a peak at 24 ppm (35), and a variety of model complexes show features associated with imidazole N-H in the 14–20 ppm region (72, 85, 96). When compared to those found for mononuclear high-spin Fe(III)-imidazole complexes at

~100 ppm (43), the significantly smaller values found for the dinuclear complexes reflect the strong antiferromagnetic coupling between the Fe(III) centers, which drastically decreases the magnetic susceptibility of the complex. There is also some variation in the electron–nuclear hyperfine splitting constant A in the various complexes, reflecting differences in the strengths of the Fe–imidazole bonds.

In addition to the D₂O-exchangeable feature, the NMR spectra of RRB2 also exhibit a nonexchangeable feature at 19 ppm with approximately three times the intensity of the 22-ppm peak (120). This peak is currently not assigned, but presumably arises from a coordinated ligand.

The crystal structure of the B2 protein of ribonucleotide reductase for *E. coli* has recently been solved (29); it confirms the presence of one dinuclear iron site per subunit, with each site being associated with its own tyrosine 122 radical. The diferric active site is shown in Fig. 3b.

This diiron site differs from that of hemerythrin by having only two bridges, one μ -oxo and one μ -carboxylato, between the two ferric ions, and by the two irons being in a more oxygen-rich coordination sphere. Contrary to what was expected from the resonance Raman data, the histidines are located cis to the μ -oxo bridge, and, in fact, carboxylate ligands are located trans to the μ -oxo bridge. The coordination environments of the two irons in the dinuclear unit are quite different, in accord with the Mössbauer data. One iron has two monodentate glutamate residues, a histidine, and water as terminal ligands in an approximately octahedral array, while the other iron has a bidentate aspartate residue replacing the two monodentate glutamates. The chelated carboxylate on the latter site results in an environment considerably distorted from an ideal octahedron, which may account for the large Mössbauer quadrupole splitting ($2.45 \text{ mm} \cdot \text{s}^{-1}$) seen for one of the irons in RRB2 (26). Tyrosine 122 is located 5 Å away from the iron site and 10 Å from the protein surface. This placement raises questions regarding the role of the tyrosyl radical in effecting H-atom abstraction.

3. Methane Monooxygenase

The hydroxylase component of methane monooxygenase (MMO) contains the diiron active site (11, 12, 30, 31). The properties of the diferric form of MMO differ from those of metHr and RRB2. This enzyme is essentially colorless with an electronic spectrum that exhibits a weak absorption tail in the region of 300–400 nm (Fig. 10). It exhibits only one quadrupole doublet in the Mössbauer spectrum with a splitting of $1.07 \text{ mm} \cdot \text{s}^{-1}$, a value that is intermediate between (μ -oxo)diiron complexes

of the metHr sort and mononuclear high-spin ferric complexes (31). The quadrupole doublet persists even at liquid helium temperatures and high field studies at 4.2 K indicate a diamagnetic ground state (Fig. 11). However, some paramagnetism can already be detected at 20 K, implicating population of an $S = 1$ excited state at this temperature (53, 121). Although the 4.2 K Mössbauer spectrum shows the presence of an antiferromagnetically coupled diiron unit, the other observations suggest some modification of the putative oxo bridge to account for the lack of visible spectral features and the weaker coupling. Since the conversion to the μ -oxo group

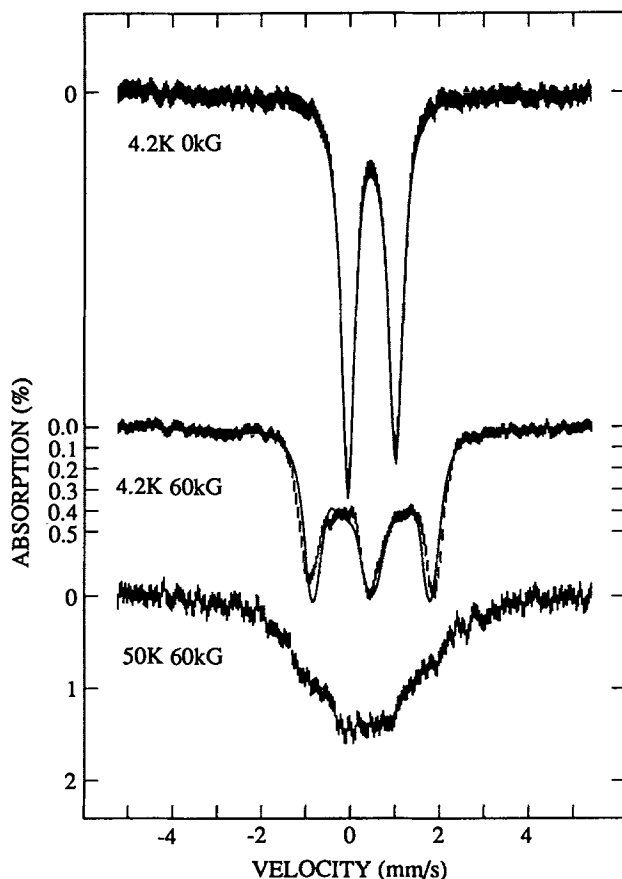


Figure 11. Mössbauer spectra of the oxidized hydroxylase component of MMO at pH 7.0 at 4.2 K and zero applied field (top), 4.2 K and 60 kG applied field (middle), and 50 K and 60 kG applied field (bottom). The *solid* line in the middle spectrum is a spectral simulation assuming that the diiron(III) unit is diamagnetic. Reprinted with permission from Ref. 53.

to a μ -hydroxo bridge entails a decrease of $-J$ to $\sim 20 \text{ cm}^{-1}$ in the synthetic complex (60), a (μ -hydroxo or μ -alkoxo)diiron(III) unit is a likely feature of the MMO active site.

There is an EXAFS report on the hydroxylase component of the MMO from *Methylobacterium* CRL-26 that shows an average Fe–L distance of 1.92 Å and an Fe–Fe separation of 3.05 Å (42). The lack of a short Fe– μ -O bond is consistent with the apparent absence of an oxo bridge based on other techniques, while the presence of a Fe scatterer at 3.05 Å corroborates the dinuclear nature of the site. However, the apparent lower purity of the sample as indicated by the observation of metalloporphyrin-like absorption features in the visible spectrum and the later report by Ericson et al. (52) that MMO from *M. capsulatus* (Bath) is photoreduced in the synchrotron beam raise doubts about the reliability of these results.

B. Diferrous Forms

The two-electron reduction of the diferric forms of hemerythrin (51), ribonucleotide reductase (27, 50), and methane monooxygenase (31) yields dioxygen-sensitive diferrous forms of the proteins. All three can be generated by dithionite treatment of the corresponding diferric forms, although the RRB2 reduction requires methyl viologen as mediator. The Fe(II) oxidation state is more difficult to probe spectroscopically, and only recently have methods been developed that allow this state to be characterized further.

The iron centers in all three diferrous proteins appear to interact with each other magnetically. For deoxyHr, the iron centers are coupled antiferromagnetically based on the magnetic circular dichroism (MCD) observation of a diamagnetic ground state (49). The J is estimated to be -15 cm^{-1} from Evans susceptibility experiments (35) and -12 to -36 cm^{-1} from MCD data (49). Estimates of the energy of the first excited state by MCD are complicated by the zero-field splitting of the ferrous ions, which is comparable in magnitude to the coupling. NMR spectra of deoxyHr show His N–H resonances at 43, 46, and 62 ppm in a 1:1:3 intensity ratio (35). The shifts are comparable to those found for high-spin Fe(II)–imidazole complexes (43, 122) and thus consistent with the observed weak antiferromagnetic coupling.

The addition of azide to deoxyHr yields deoxyHrN₃, which has a paramagnetic ground state based on MCD spectra (49). The MCD analysis suggests that the iron centers have become weakly ferromagnetically coupled. Its NMR spectrum shows His N–H resonances at 47, 67, and 78 ppm in a 1:3:1 intensity ratio (35). Presumably, the spectral changes are a result of the difference in the coupling interaction and the presumed alteration

in anisotropy of the Fe(II) site to which azide coordinates. The change from an antiferromagnetically coupled deoxyHr to a ferromagnetically coupled deoxyHrN₃ is proposed to result from protonation of the single atom bridge upon azide binding. DeoxyHr is believed to have a hydroxo bridge; deoxyHrN₃ would thus have an aqua bridge (49).

The ferrous centers in MMO_{red} and RRB2_{red} are weakly interacting at best, based on high field Mössbauer data (121). As with deoxyHr, however, the interpretation of the spectra is complicated by the comparable magnitudes of J (magnetic coupling) and D (zero-field splitting); our understanding of these competing effects on electronic structure is still quite rudimentary. For RRB2_{red}, J is estimated to be -5 cm^{-1} by Evans susceptibility, and His N-H NMR signals are observed at 60 ppm, consistent with the observed weak coupling (50). The solvent-nonexchangeable resonance, observed in RRB2_{ox} at 19 ppm, is found at 44 ppm in RRB2_{red}.

Mössbauer parameters for all three proteins are all typical of high-spin ferrous centers in oxygen-nitrogen ligand environments. DeoxyHr exhibits a δ value of $1.14 \text{ mm} \cdot \text{s}^{-1}$ (36, 38), while RRB2_{red} and MMO_{red} have δ values of 1.26 and $1.30 \text{ mm} \cdot \text{s}^{-1}$, respectively (27, 31), the larger isomer shifts being consistent with their presumed more oxygen-rich environments. RRB2_{red} and MMO_{red} also exhibit similar ΔE_Q values, which are distinct from that of deoxyHr. This comparison serves to emphasize the similarities between the two diiron sites involved in oxygen activation and to distinguish them from the diiron site whose function is reversible dioxygen binding.

The newest and perhaps most convenient probe discovered thus far for these sites is EPR spectroscopy (Fig. 12). Though deoxyHr is EPR silent, deoxyHrN₃ exhibits a signal at $g = 13$, first reported by Reem and Solomon (49). MMO_{red} has a similar signal at $g = 15$ (31), while RRB2_{red} shows broader signals at low field (27). These are signals derived from transitions within doublets of an integer spin system. For these proteins, either isolated $S = 2$ centers or a coupled system may give rise to these low field signals.

The early work on integer spin systems was done by Hagen (123); more recently, Hendrich and Debrunner have investigated a variety of high-spin Fe(II) complexes and found signals for FeSO₄, Fe^{II}(EDTA), and deoxymyoglobin (124). Figure 13 illustrates a plausible origin of these signals for an $S = 4$ system with a negative zero-field splitting. The diagram for a similar $S = 2$ system would involve only the $|0\rangle$, $|\pm 1\rangle$, and $|+2\rangle$ levels of the $S = 4$ manifold. In such an $S = 4$ spin manifold with axial symmetry, the $|\pm 4\rangle$ doublet is the ground state. No $\Delta m_s = 1$ transitions would be possible between the $|0\rangle$, $|\pm 1\rangle$, $|\pm 2\rangle$, $|\pm 3\rangle$, and $|\pm 4\rangle$ levels because of the large zero-field splitting and no transitions are possible within the doublet levels because of their degeneracy. In the presence of a small rhombic distortion, however, these doubly degenerate

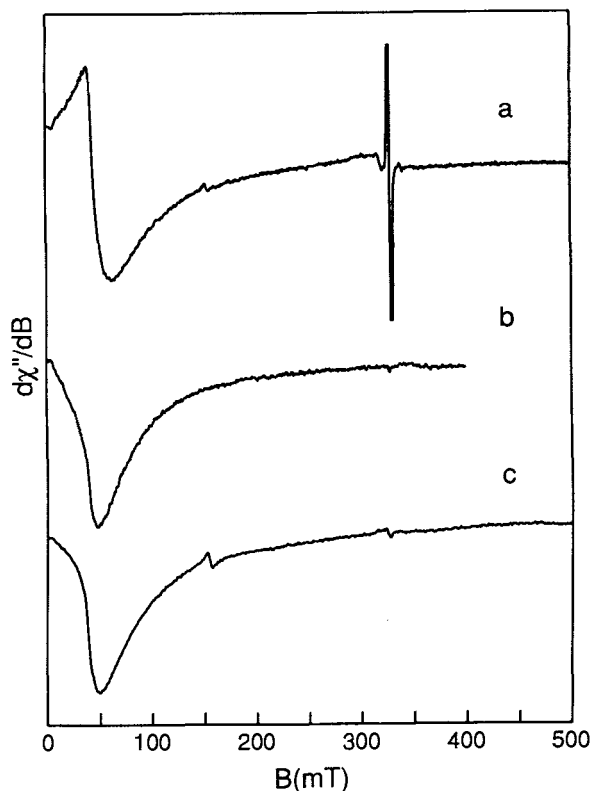


Figure 12. Low-field EPR spectra at ~ 4 K of the diferrous sites in (a) MMO_{red} , (b) deoxyHrN_3 , and (c) $[\text{Fe}_2(\text{BPMP})(\text{OPr})_2]^+$. Courtesy of Dr. Michael P. Hendrich.

levels will split and some mixing of the spin functions will occur; $\Delta m_s = 0$ transitions can then be observed. These are allowed in perpendicular mode ($B_1 \perp B_0$, the normal configuration for EPR experiments) but enhanced in parallel mode ($B_1 \parallel B_0$). $\Delta m_s = 1$ transitions, on the other hand, are allowed only in perpendicular mode, so a parallel mode experiment is a good test for ascertaining the nature of these $\Delta m_s = 0$ transitions.

Transitions within the $|\pm 4\rangle$ levels would be expected at $g \sim 16$, since $\Delta E \sim 8g_0\beta B$ (125). As the rhombic splitting increases the energy difference between the two levels, the resonance condition will shift to lower fields. Signals may be observed from the $|\pm 2\rangle$ doublet at $g \sim 8$. The theory for these integer spin systems is not fully understood and is still in the development stage. These EPR signals can, however, be used as convenient diagnostic probes of this oxidation state.

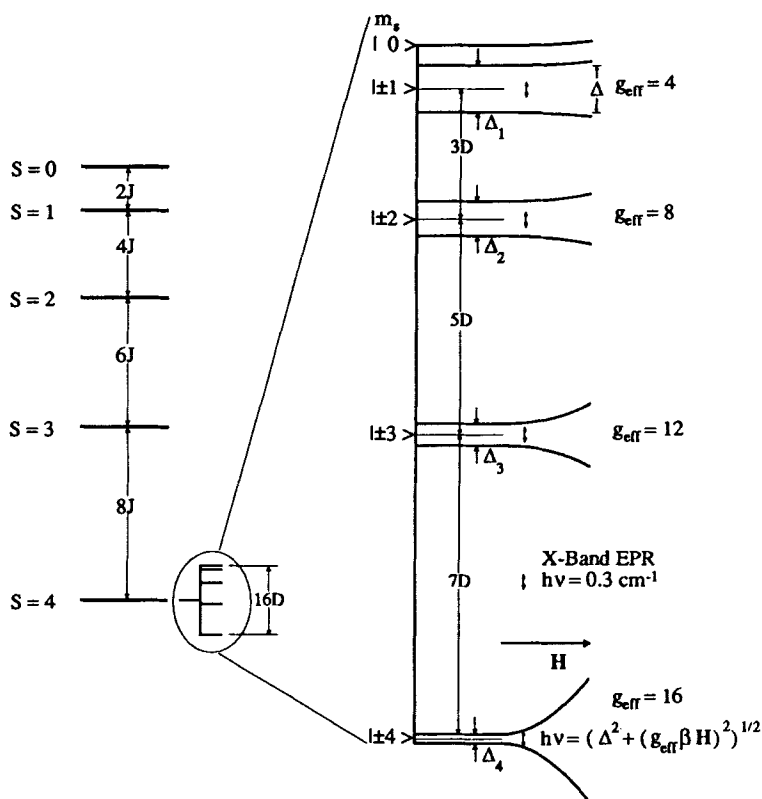


Figure 13. Simplified energy level diagram for a ferromagnetically coupled diferrous system where $|J| \gg |D|$, $E/D = 0$, and $D < 0$ for the $S = 4$ ground state.

Details of the ferrous coordination environments are available only for deoxyHr. A difference electron density map from X-ray diffraction studies of deoxyHr and metHr suggests only small structural differences between the two forms (19). Although the crystal structure of deoxyHr is of low resolution (3.9 \AA), there appears to be a decrease in the correlated motions of the two iron atoms suggesting a weakening of the Fe- μ -O bonds and an increase in the Fe-Fe distance. These changes in core dimensions are confirmed by an EXAFS analysis of deoxyHr ($r_{\text{Fe-O}} = 1.98 \text{ \AA}$, $r_{\text{Fe-Fe}} = 3.57 \text{ \AA}$) (39); they suggest that the oxo bridge has become protonated in deoxyHr, in line with the diminished Lewis acidity of Fe(II).

Near IR CD spectroscopy allows ligand-field transitions of the Fe(II) centers to be more readily observed. For deoxyHr, three bands near $10,000 \text{ cm}^{-1}$ and one near 5000 cm^{-1} are observed (49). This spectrum is consistent

only with one five-coordinate iron (bands near 5000 and 10,000 cm^{-1}) and one six-coordinate iron (two bands near 10,000 cm^{-1}). Addition of anions such as azide, cyanate, and fluoride causes the 5000- cm^{-1} band to be replaced by a fourth band near 10,000 cm^{-1} , suggesting that the anions bind at the vacant site on the five-coordinate iron resulting in two six-coordinate iron atoms (49).

Structurally characterized models for the diferrous oxidation state thus far number only three. The first reported by Wiegardt, $[(\text{Fe}_2(\text{OH})(\text{OAc})_2(\text{Me}_3\text{TACN})_2)(\text{ClO}_4)]$ (70, 87), has a (μ -hydroxo)bis(μ -carboxylato)diiron(II) core. Its structure is closely related to that of the diferric form, but the Fe- μ -O and Fe-Fe distances of 1.99 and 3.32 Å, respectively, are longer than their ferric counterparts. The Fe(II) ions in this complex are antiferromagnetically coupled with a J of -13 cm^{-1} and the complex is thus EPR silent. The J value of the complex is comparable to that found for deoxyHr, suggesting that deoxyHr is likely to have a hydroxide bridging the iron centers.

$[\text{Fe}_2(\text{BPMP})(\text{OPr})_2](\text{BPh}_4)$ has a (μ -phenoxo)bis(μ -carboxylato)-diiron(II) core with Fe- μ -O and Fe-Fe distances of 2.06 and 3.35 Å, respectively (66, 126). $[\text{Fe}_2(\text{BIPhMe})_2(\text{O}_2\text{CH})_4]$, on the other hand, has a (μ -*O, O*-formato)bis(μ -*O, O'*-formato)diiron core with Fe- μ -O and Fe-Fe distances of 2.15 and 3.585 Å, respectively (88). The two iron sites differ; while bidentate BIPhMe ligands coordinate to both irons, one iron has a monodentate terminal formate and the other has the carbonyl oxygen of the *O, O*-bridging formate 2.79 Å away occupying the sixth position in an octahedral environment. This complex models some of the asymmetry found in the putative deoxyHr site and affords a potential site for dioxygen binding.

Both complexes exhibit a low field EPR signal at $g = 16$, presumably derived from a coupled diferrous system (88, 126). These complexes thus serve as models for deoxyHrN₃ and MMO_{red} . What structural and electronic factors determine the appearance of an integer spin EPR signal from diferrous complexes is not understood at present, but the availability of such models provides opportunities to explore the effects of the coordination chemistry of the diferrous state on the properties of this signal.

C. Mixed-Valence Forms

Mixed-valence forms of the dinuclear iron unit have been observed for hemerythrin and MMO. These are characterized by EPR signals, which are observable only near liquid helium temperatures, with $g_{\text{av}} \sim 1.7$ – 1.8 and arise from the $S = \frac{1}{2}$ state of an antiferromagnetically coupled high-spin Fe(III)–high-spin Fe(II) pair (Fig. 14) (127). Similar signals are found

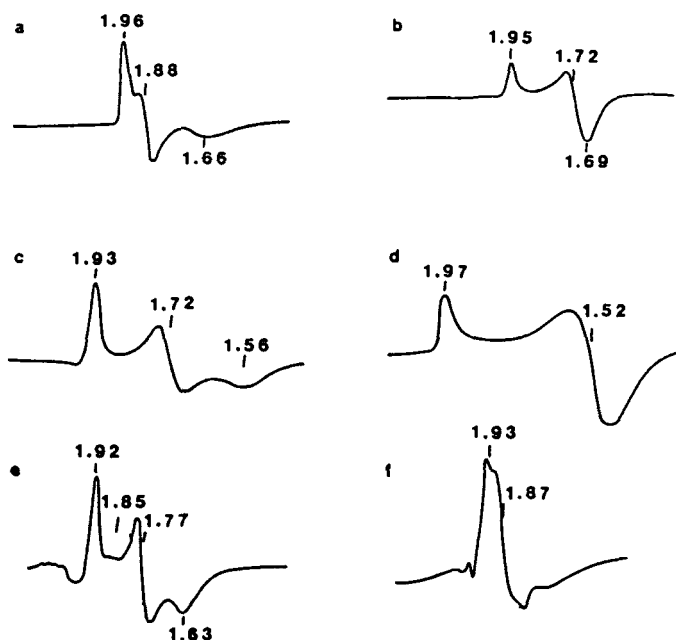


Figure 14. EPR spectra of mixed-valence forms of the diiron proteins: (a) semimet_rHr, (b) semimet_oHr, (c) Uf_r, (d) Uf_r·MoO₄, (e) bovine spleen PAP, (f) MMO_m. Reprinted with permission from Ref. 6. Copyright © 1987 Elsevier.

in iron-sulfur proteins, but g_{av} is typically 1.94 for these latter proteins (128). The vector coupling model for the antiferromagnetic interaction of an $S = \frac{3}{2}$ center with an $S = 2$ center predicts that (129)

$$g_0(S' = \frac{1}{2}) = \frac{7}{3}g_0(S = \frac{3}{2}) - \frac{4}{3}g_0(S = 2)$$

Qualitatively speaking, since g_0 for the orbitally nondegenerate Fe(III) = 2, the deviation from 2 for the $g_0(S' = \frac{1}{2})$ value principally derives from orbital contributions that make $g_0[\text{Fe(II)}] > 2$. Such contributions are expected to be more significant for the five- and six-coordinate (O,N) sites in Hr and MMO than for the tetrahedral S_4 sites in iron-sulfur proteins.

The physiological significance of the mixed-valence forms of Hr and MMO is unclear, although Kurtz et al. (130) have observed EPR signals typical of the mixed-valence form in sipunculid erythrocytes that have been allowed to become anoxic.

The mixed-valence forms of Hr, or semimetHr's, can be obtained by treatment of metHr with dithionite to form (semimet)_RHr or by treatment

of deoxyHr with ferricyanide to form (semimet)_OHr (6, 127). These two forms are distinguished by differences in their visible spectra and EPR *g* values (*g* = 1.96, 1.88, and 1.67 for (semimet)_RHr and *g* = 1.95, 1.72, and 1.68 for (semimet)_OHr) (131). These differences may reflect which iron atom is reduced (51), but proof for this hypothesis is lacking. The differences may also result from the different protein conformations of the parent states and a substantial barrier for interconversion. The two semimetHr's are metastable states and thus prone to disproportionation (*t*_{1/2} ~ 0.5 h).

Either of these semimetHr's binds small anions to form semimetHrX complexes (where X = N₃⁻, OCN⁻, CN⁻, F⁻, Cl⁻, etc.) which are more stable. SemimetHrN₃ is the best characterized of the mixed-valence forms of Hr. It exhibits EPR signals at *g* = 1.94, 1.85, and 1.57 (131). An estimate of the antiferromagnetic coupling can be obtained by measuring the temperature dependence of the power saturation of the EPR signals. The *J* value for semimetHrN₃ is (-15 ± 1) cm⁻¹ if an Ohrbach relaxation process is assumed to be dominant, that is, electron spin lattice relaxation occurs by accessing the nearest excited state, which for a coupled ($\frac{5}{2}$, 2) system would be the *S'* = $\frac{3}{2}$ state. The *J* values for (semimet)_RHr and (semimet)_OHr are comparable at (-15 ± 1) and (-16 ± 1) cm⁻¹, respectively (51, 89).

It is clear from various spectroscopic studies that the azide in semimetHrN₃ is bound to the Fe(III) of the mixed-valence dinuclear unit. The optical spectrum of semimetHrN₃ is dominated by a band at 470, which is similar in shape to that observed in metHrN₃ and assigned to an azide-to-Fe^{III} LMCT transition (98, 132, 133). This assignment is corroborated by the observation of enhanced Raman vibrations due to the Fe-N₃ moiety (133).

NMR studies of semimetHrN₃ show two paramagnetically shifted resonances at 72 and 54 ppm with a relative integration of 2:3 (35). These resonances disappear in D₂O, identifying them as the N-H protons of the coordinated imidazoles. Comparisons with the N-H shifts of imidazoles coordinated to mononuclear Fe(III) and Fe(II) centers at 100 and 65 ppm, respectively (43, 96), permits the assignment of the 72 and 54 ppm peaks to imidazole N-H groups coordinated to the Fe(III) and Fe(II) atoms of semimetHrN₃, respectively. The shifts in semimetHrN₃ are diminished relative to the mononuclear standards because of antiferromagnetic coupling. The temperature dependence of these shifts can be used to estimate a *J* of (-20 ± 2) cm⁻¹ (35), a value comparable to that estimated from EPR (51).

The relative integration of the two N-H peaks observed would be consistent with the Fe(III) center coordinated to 2 His and the N₃⁻ and the Fe(II) center coordinated to 3 His. Resonances from the presumed bridging carboxylates have not been observed thus far. Similar conclusions can be drawn from NMR studies of other semimetHrX complexes (35).

EXAFS data on semimetHrN₃ suggest that the dinuclear cluster retains most of the structural features associated with the cluster in the met form except for the oxo bridge (Fig. 8) (40). The short Fe- μ -O bonds have lengthened and, consequently, the Fe-Fe separation has increased to 3.46 Å. The fit to the first shell suggests the presence of one Fe-O bond in the dinuclear cluster at 1.87 Å, presumably associated with the Fe(III)- μ -O, with the remaining 11 Fe-(O,N) bonds at an average of 2.14 Å.

The structural features of the dinuclear unit in semimetHrN₃ can be best interpreted in light of the changes observed upon protonating the (μ -oxo)diiron(III) moiety in [Fe₂O(OAc)₂(HBpz₃)₂] to form a (μ -hydroxo)diiron(III) complex (60). Although these are diferric complexes, they are the best models currently available. The protonation of the oxo bridge results in the lengthening of the Fe- μ -O bonds from 1.78 to 1.96 Å and an increase in the Fe-Fe separation from 3.15 to 3.44 Å. The resulting gain in the Lewis acidity of the Fe(III) centers when protonated shortens the remaining iron-ligand bonds from an average of 2.11 to 2.06 Å.

Thus, the increases in the Fe- μ -O and Fe-Fe distances in semimetHrN₃ appear likely to result from protonation of the μ -oxo group upon 1 electron reduction of the diiron core. The conversion of an Fe(III) to the less Lewis acidic Fe(II) in a (μ -oxo)diiron unit should increase the basicity of the bridging oxide and strengthen the remaining Fe(III)- μ -O bond, that is, either shortening it, or, more likely, causing the oxide to pick up a proton. The observed 1.87 Å Fe- μ -O bond length in semimetHrN₃ is inconsistent with the retention of an Fe(III)- μ -O bond; however, an Fe(III)- μ -OH bond would be expected to be intermediate between the observed 1.96 Å length for the Fe(III)- μ -OH bond in [Fe₂OH(OAc)₂(HBpz₃)₂](ClO₄) (60) and the 1.83 Å length found for the Fe-OEt bond in [FeN₅(OEt)]²⁺ (110c). These arguments need substantiation from crystallographic data on appropriate synthetic mixed-valence complexes.

The similarity of the non-Fe- μ -O first shell distances in metHrN₃ and semimetHrN₃ (2.13 and 2.14 Å, respectively) deserves some comment. Reduction of an Fe(III) center should give rise to longer iron-ligand bonds at the Fe(II) center. This lengthening can be counterbalanced by the expected shortening of iron-ligand bonds at the Fe(III) center if the oxo bridge becomes protonated. Thus the EXAFS analysis on semimetHrN₃ is wholly consistent with an active site structure similar to that found in metHrN₃ save for the protonation of the oxo bridge (39, 40).

Spectroscopic comparisons between semimetHr's and the mixed-valence form of MMO are just beginning to emerge. EPR signals at liquid helium temperatures are found at $g = 1.94, 1.86, \text{ and } 1.75$ for MMO_{mv} (30b, 31), so g_{av} is somewhat higher (1.85 for MMO_{mv} vs. 1.79 for semimetHrN₃). The J value determined on the basis of the temperature dependence of the

power saturation of this signal is $(-29 \pm 3) \text{ cm}^{-1}$ (53), a value significantly different from those found for the semimetHr's. The implications of this difference have not yet been addressed.

EXAFS data on MMO_{mv} have been reported by Ericson et al. (52). Although MMO in the diferric state was introduced into the synchrotron beam, it is clear that photoreduction of the sample occurred during the experiment as an $\sim 1.5\text{-eV}$ edge shift was observed. Like semimetHrN₃, there is no short Fe- μ -O bond length. The first shell data analysis yields an average Fe-(O,N) distance of 2.06 Å, a value shorter than corresponding distances in metHrN₃ and semimetHrN₃ but comparable to that of native RRB2 (39-41). As with the RRB2 data, the 2.06 Å average Fe-(O,N) distance indicates a coordination environment that is more oxygen rich than what is found in Hr. The similarities between MMO and RRB2 suggest that such coordination environments may be more appropriate for the oxygen activation chemistry required of these enzymes and that the more nitrogen rich environment of Hr is better adapted for reversible dioxygen binding.

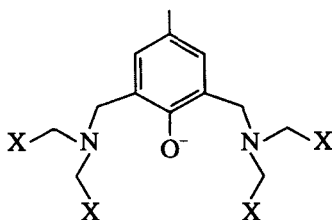
Models for the mixed-valence forms have been difficult to characterize because of their instability. Cyclic voltammetry of $[\text{Fe}_2\text{O}(\text{OAc})_2(\text{HBpz}_3)_2]$ shows an irreversible one-electron reduction at -760 mV vs. SCE that leads to the breakdown of the dinuclear unit (58). On the return, a new reversible wave is observed at 260 mV vs. SCE characteristic of the mononuclear $[\text{Fe}(\text{HBpz}_3)_2]^+$ complex. On the other hand, $[\text{Fe}_2\text{O}(\text{OAc})_2(\text{Me}_3\text{TACN})_2](\text{PF}_6)$ exhibits a quasireversible reduction at -374 mV vs. SCE ($\Delta E_p = 80 \text{ mV}$) corresponding to the formation of the $\text{Fe}^{\text{II}}\text{Fe}^{\text{III}}$ species (70). The reversibility of this process is attributed to the presence of the methyl groups that prevent formation of the mononuclear bis(ligand) complex, thus eliminating a primary decomposition pathway for the mixed-valence complex. The mixed-valence Me_3TACN complex generated either electrochemically or by cobaltocene reduction is metastable and exhibits a nearly isotropic EPR signal at $g = 1.92$, which quantitates to nearly 60% of the initial dinuclear complex (70). The temperature dependence of its power saturation corresponds to an estimated J of -15 cm^{-1} (89). The unsymmetric $[\text{Fe}_2\text{TPA}_2\text{O}(\text{OAc})](\text{ClO}_4)_3$ complex also exhibits a reversible $\text{Fe}^{\text{III}}_2/\text{Fe}^{\text{II}}\text{Fe}^{\text{III}}$ couple at -68 mV vs. SCE ($\Delta E_p = 62 \text{ mV}$) (89). One-electron reduction of the diferric complex yields a mixed-valence species with a nearly isotropic EPR signal at $g = 1.95$ with an estimated J of -15 cm^{-1} .

The Me_3TACN and TPA complexes are thus far the only examples of mixed-valence complexes derived from oxo- and carboxylato-bridged diferric complexes. Their EPR properties are remarkably similar to each other and the J values estimated are close to those found for the semimetHr complexes. Unfortunately, structural information on these models is lack-

ing because of their thermodynamic instability. It would be useful to determine, for example, the Fe- μ -O bond lengths or whether the oxo bridge may have become protonated in the one-electron reduced form.

One related complex that is structurally characterized is the reduction product of $[\text{Fe}(\text{acacen})]_2\text{O}$ with Na, $\{[\text{Fe}(\text{acacen})]_2\text{ONa}\}_2$ (93). The reduced complex, obtained as air-sensitive red brown crystals, exhibits a downshift of the $\nu_{\text{as}}(\text{Fe}-\text{O}-\text{Fe})$ from 840 cm^{-1} in the parent complex to 780 cm^{-1} and an increase in μ_{eff} from $1.80\ \mu_{\text{B}}$ in the parent complex to $3.64\ \mu_{\text{B}}$ at 290 K. The latter value allows us to estimate a J of $(-30 \pm 5)\text{ cm}^{-1}$, which is intriguingly in the range observed for MMO_{mv} . The structure of the mixed-valence complex shows the Fe- μ -O bonds to be 1.999 and 2.069 Å; this asymmetry appears too small to indicate a valence-trapped species. Indeed, the Fe-(O,N) bonds to the tetradentate ligands are not much different on the two Fe(acacen) units. Whether the similarity of the two units is due to valence detrapping or crystallographic disorder is unclear at present. What is clear is that the one-electron reduction of $[\text{Fe}(\text{acacen})_2]$ results in a significant lengthening of the Fe- μ -O bonds, from 1.77 to 2.03 Å and a decrease of the Fe-O-Fe angle from 150.7° to 134.9° . The coordination of the Na atom to the oxo bridge undoubtedly contributes to the observed structural alterations and may be considered somewhat analogous to protonation of the bridge. Further characterization of the physical properties of the mixed-valence complex would undoubtedly be helpful.

Stable mixed-valence complexes of the type $[\text{Fe}_2\text{L}(\text{O}_2\text{CR})_2]$ can be obtained with the use of dinucleating ligands having phenolate oxygen atoms as bridging groups, that is, where X = pyridine (BPMP) (66, 91, 134), benzimidazole (BBMP) (64, 91, 92), imidazole (BIMP) (65), and carboxylate (5-Me-HXTA) (90, 135).



The complexes where X is an aromatic nitrogen ligand have been characterized crystallographically, and the metal valences appear localized in the crystalline state as evidenced by the distinct differences in iron-ligand bond lengths (Table II). Typically the $\text{Fe}^{\text{III}}-\mu-\text{O}$ bond is 1.95 Å, while the $\text{Fe}^{\text{II}}-\mu-\text{O}$ bond is 2.10 Å. These longer Fe- μ -O distances result in a larger Fe-Fe separation of $\sim 3.4\ \text{Å}$, which is comparable to those observed for semimetHrN₃ and MMO_{mv} from EXAFS spectra.

In solution, the complexes behave like type II mixed-valence compounds in the Robin–Day scheme (136). At room temperature, a near-IR feature at ~ 1300 nm can be found and assigned as an intervalence charge-transfer band. The extinction coefficient of this band varies from 200 to $700 M^{-1} \text{cm}^{-1}$ depending on the nature of X and may relate to the barrier for valence detrapping. Mössbauer spectra of the BPMP, BIMP, and HXTA complexes indicate valence trapped species at temperatures below 100 K where quadrupole doublets due to the Fe(III) and the Fe(II) centers are observed. While the BPMP complex remains valence trapped in the crystalline state even at room temperature (134), valence detrapping is observed for the BIMP complex above 100 K (65); such behavior is believed to be related to the solid-state mobility of the counterions.

The NMR spectra of these complexes under ambient conditions exhibit sharp, paramagnetically shifted features that can span up to 400 ppm (90, 134). Electron exchange is fast on the NMR time scale, so there is an effective twofold symmetry, which approximately halves the number of distinct features observed. The sharpness of the resonances is due to the short electron spin-lattice relaxation time of the Fe(II) center, which allows even the CH_2 protons adjacent to the coordinated nitrogen atoms to be observed.

The coupling between the metal centers is weak, ranging from -3 to -7 cm^{-1} (Table II), which is not unexpected for a μ -phenoxo group relative to a μ -oxo or μ -hydroxo group as observed in the diferric complexes. The weak coupling is now comparable in magnitude to the Fe(II) zero-field splitting, and this combination gives rise to EPR signals that are broader and more anisotropic. All four complexes exhibit EPR signals with $g_{av} < 2$ as predicted by the vector coupling model; they are difficult to saturate, consistent with the easy accessibility of an excited state for Orbach relaxation due to the small $-J$ values. Of the four complexes, the BIMP complex has the sharpest features at $g = 2.18, 1.90,$ and 1.44 (65). Indeed, the BPMP and HXTA complexes were initially reported to be apparently EPR silent because of the broadness of the spectral features, which made observation difficult (66, 90). A similar problem plagued the observation of the EPR spectrum from the reduced uteroferrin–phosphate complex (cf. Section III.D).

Two other mixed-valence diiron complexes deserve brief mention, $[\text{Fe}_2(\text{salmp})_2]^-$ (94) and $[\text{Fe}_2(\text{OH})_3(\text{Me}_3\text{TACN})_2]^{2+}$ (95). $[\text{Fe}_2(\text{salmp})_2]^-$ has a crystallographically characterized $\text{Fe}_2(\text{OPh})_2$ core with Fe– μ -O bonds of 2.09 \AA and an Fe–Fe separation of $3.08\text{--}3.12 \text{ \AA}$. $[\text{Fe}_2(\text{OH})_3(\text{Me}_3\text{TACN})]^{2+}$ is proposed to have a tris(μ -hydroxo)diiron core based on an Fe–Fe distance of 2.5 \AA from EXAFS. Both mixed-valence complexes exhibit ferromagnetic coupling. $[\text{Fe}_2(\text{salmp})_2]^-$ has a J value of $+8.6 \text{ cm}^{-1}$ (94); it is valence trapped at 4.2 K and becomes detrapped at higher temperatures

(94). $[\text{Fe}_2(\text{OH})_3(\text{Me}_3\text{TACN})_2]^{2+}$ is the first example of a delocalized valence pair derived from double exchange with the double exchange parameter $B = 1300 \text{ cm}^{-1}$ (95). Although yet unobserved, complexes with similar magnetic properties may be recognized in proteins as the dinuclear iron-oxo proteins are investigated further.

D. Mechanistic Considerations

The common thread that relates hemerythrin, MMO, and ribonucleotide reductase is the involvement of dioxygen with a diiron active site. For hemerythrin, reversible dioxygen binding is its function and much is known of this chemistry. For MMO and ribonucleotide reductase, the role of dioxygen and its mechanism of activation is just beginning to emerge.

1. Reversible Dioxygen Binding by Hemerythrin

OxyHr has been crystallized and difference electron density maps indicate that there is little change in active site structure relative to metHrN₃, save for the substitution of the dioxygen ligand for azide (19). Mössbauer spectroscopy of oxyHr shows two quadrupole doublets with isomer shifts typical of high-spin Fe(III) (0.51 and 0.52 mm · s⁻¹, respectively) and large but distinct quadrupole splittings (1.96 and 0.95, respectively) (36, 38). The significant difference in the ΔE_{O} values probably reflects the effect of the dioxygen ligand on the electronic environment of the iron to which it is bound. Based on a comparison of the ΔE_{O} values of metHrX and model peroxide complexes, it seems reasonable to associate the smaller ΔE_{O} with the iron atom with the coordinated peroxide; however, this assignment has not been established unequivocally.

EXAFS comparisons of oxyHr with metHrN₃ suggest that the Fe- μ -O bonds may be slightly longer in oxyHr (1.82 Å vs. 1.76–1.80 Å) (39), implying that the coordination of dioxygen has subtle effects on the Fe-O-Fe unit. The Fe...Fe distance has been estimated at 3.24 Å for oxyHr, comparable to that for metHrN₃. In any case, there appears to be a strong similarity between oxyHr and metHrX. Together with spectroscopic data to be discussed, the structural features found for oxyHr suggest that it can be considered as a metHrOOH complex.

OxyHr is purple in color, associated with a λ_{max} near 500 nm, which is polarized perpendicular to the Fe-Fe axis in single-crystal absorbance data (98, 99). Resonance Raman spectroscopy unequivocally assigns this electronic spectral feature to a peroxide-to-Fe(III) charge-transfer band (137–139). Vibrational features at 503 and 884 cm⁻¹ are assigned to $\nu(\text{Fe}-\text{O}_2)$ and $\nu(\text{O}-\text{O})$, based on their sensitivity to ¹⁸O substitution. Their enhance-

ment profiles track that of the visible band (actually matching the CD maximum at 520 nm) (138). When $^{16}\text{O}^{18}\text{O}$ is used, four new features can be discerned indicating that the O_2 is bound unsymmetrically (139).

Excitation into the near-UV bands enhances the iron–ligand vibrations, and stretching modes due to the Fe-O_2 and Fe-O-Fe moieties are observed (137, 138). Interestingly, the Fe-O-Fe symmetric stretch appears at 492 cm^{-1} , a value somewhat lower than those observed for the metHrX complexes. When the experiment is conducted in D_2O , the vibration upshifts by 4 cm^{-1} (Fig. 15). This behavior has been attributed to the effect of hydrogen bonding to the Fe-O-Fe unit which is expected to weaken the Fe-O-Fe bonds and thus downshifts $\nu_s(\text{Fe-O-Fe})$ relative to the metHrX

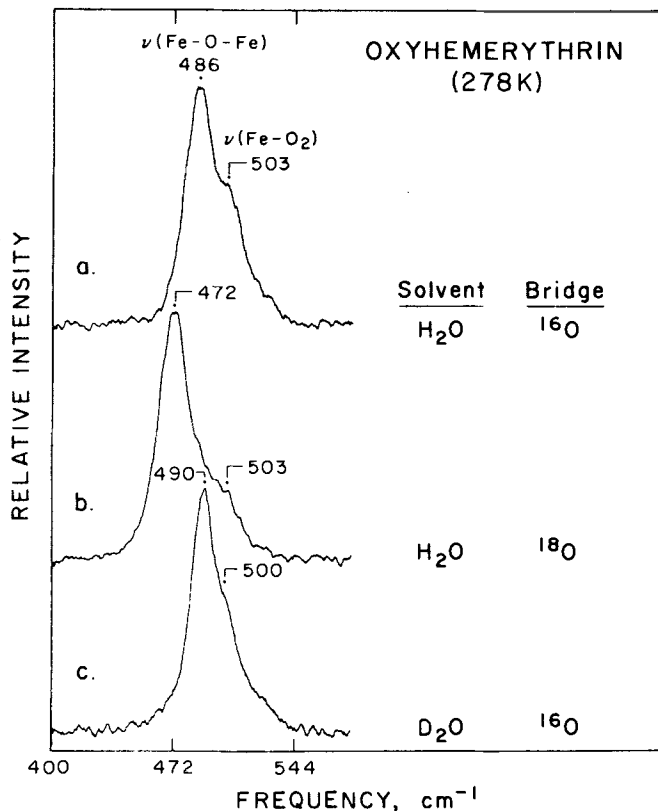


Figure 15. Resonance Raman spectrum of oxyHr showing the effect of H_2^{18}O and D_2O on the $\nu_s(\text{Fe-O-Fe})$ feature. Reprinted with permission from A. K. Shiemke, T. M. Lochr, and J. Sanders-Lochr, *J. Am. Chem. Soc.*, 108, 2437–2443 (1986). Copyright © 1988 American Chemical Society.

complex. However, D_2O introduces a deuterium bond in place of the hydrogen bond and downshifts the $\nu_s(\text{Fe}-\text{O}-\text{Fe})$ to a smaller extent due to its weaker acidity; thus the upshift relative to H_2O . The hydrogen is likely to be associated with the peroxide moiety and the downshift of the $\nu(\text{Fe}-\text{O}_2\text{H})$ in D_2O corroborates this suggestion.

The proposed hydrogen bonding on the $\text{Fe}-\text{O}-\text{Fe}$ moiety is consistent with the observed lengthening of the $\text{Fe}-\mu-\text{O}$ bonds in the EXAFS spectra of oxyHr and should also be reflected in its magnetic properties. The antiferromagnetic coupling for hydrogen-bonded $\text{Fe}-\text{O}-\text{Fe}$ units should be intermediate between those of $[\text{Fe}_2\text{O}(\text{OAc})_2(\text{HBpz}_3)_2]$ and $[\text{Fe}_2\text{OH}(\text{OAc})_2(\text{HBpz}_3)_2]^+$. Magnetic susceptibility measurements on oxyHr support this suggestion; J for oxyHr is -77 vs. -134 cm^{-1} for metHr (34).

Based on the X-ray diffraction and spectroscopic studies, Stenkamp et al. (19) have proposed a mechanism for dioxygen binding to hemerythrin (Fig. 16). What is presented below incorporates our reflections and those of Solomon (1a, 98). Dioxygen binds to the five-coordinate $\text{Fe}(\text{II})$ atom in deoxyHr, which has a $(\mu\text{-hydroxo})\text{bis}(\mu\text{-carboxylato})\text{diiron}(\text{II})$ active site. Electron transfer from the dinuclear unit to dioxygen occurs via one of two possible pathways—either (a) sequential one-electron transfers from each of the two iron atoms coupled with proton transfer from the $\mu\text{-hydroxo}$ group to the incipient bound peroxide or (b) initial one electron transfer from the “five-coordinate” iron to O_2 followed by hydrogen atom transfer from the $\mu\text{-OH}$ to the incipient *superoxide* and electron reorganization within the dinuclear unit. In either case, the metHrOOH (oxyHr) complex

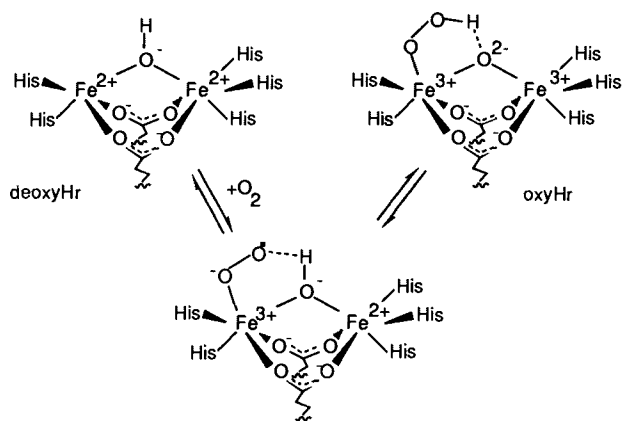


Figure 16. Proposed mechanism for reversible dioxygen binding in hemerythrin. Adapted from Ref. 2.

results with the HO_2^- group hydrogen bonded to the oxo bridge. It would appear that nature has utilized various factors to devise this diiron reversible dioxygen carrier: (1) The facile proton transfer between the Fe–O–Fe unit and the O_2 ligand allows electrons to flow in either direction within the active site. Thus the μ -OH proton of deoxyHr neutralizes the incipient charge of the bound dioxygen and promotes formation of the hydroperoxide. The hydroperoxide is further stabilized by ligation to Fe(III) and by hydrogen bonding to the oxo bridge, which inhibits the undesirable loss of HO_2^- , thereby preventing the irreversible production of metHr. The hydrophobicity of the active site enhances such interactions and insulates the dioxygen binding machinery from external factors. Of course, the use of protons to stabilize oxy complexes in hydrophobic active sites is a strategy that is used in myoglobin and hemoglobin (140, 141). (2) The Fe–O–Fe unit in Hr appears to be designed as an acid–base center. It adopts the bent configuration required for a (μ -hydroxo)diiron(II) species but not disfavored by a (μ -oxo)diiron(III) species. The bent $\text{Fe}^{\text{III}}_2\text{O}$ moiety would tend to be more basic (relative to a linear unit), thus favoring hydrogen-bond formation from the hydroperoxide; such an arrangement would facilitate eventual proton abstraction and peroxide reduction of the iron in the deoxygenation process. Perhaps it is the function of the carboxylate bridges to maintain the bent Fe–O–Fe unit. (3) The formation of a hydrogen bond from the hydroperoxy ligand to the (μ -oxo) bridge in oxyHr would be expected to increase the Fe– μ -oxo bond from the 1.8-Å distance seen in metHrN₃ towards the 1.98-Å value postulated for deoxyHr. This longer bridge might reduce the Franck–Condon reorganization barrier to electron transfer due to the decrease in the Fe– μ -oxo bond length during the oxidation of deoxyHr to oxyHr (1b). All these factors enhance the two-electron process required for reversible dioxygen binding, which is facile for Hr in contrast to its one-electron redox chemistry (cf. Section II.D.2).

The only other ligand to change in oxidation state upon binding to deoxyHr is NO; it binds to deoxyHr generating deoxyHrNO, which is formulated as $\text{Fe}^{\text{II}}\text{-OH-Fe}^{\text{III}}\text{-NO}^-$ (142, 143). This complex thus serves as an analogue to the putative “semimetHr superoxide” intermediate in the oxygenation of deoxyHr. The binding of NO is reversible as evidenced by its ready conversion to oxyHr on exposure to O_2 ; ligands such as azide and cyanate can also displace NO. DeoxyHrNO exhibits an EPR spectrum with g_{\parallel} at 2.77 and g_{\perp} at 1.84, and a Mössbauer spectrum with two quadrupole doublets at 100 K having $\delta(\Delta E_Q)$ values of 0.68(0.61) and 1.21(2.65) $\text{mm} \cdot \text{s}^{-1}$. Taken together, these features are ascribed to an antiferromagnetically coupled diiron unit consisting of an $S = \frac{3}{2}$ $\{\text{FeNO}\}^7$ and an $S = 2$ Fe^{II} center. Resonance Raman studies on deoxyHrNO show features

at 433 and 421 cm^{-1} associated with stretching and bending modes, respectively, of the $\{\text{FeNO}\}^7$ unit (143). The bending mode is sensitive to D_2O , suggesting that the bound NO participates in hydrogen bonding, like the hydroperoxide ligand in oxyHr.

2. Redox Chemistry of Hemerythrin

The facile interconversion between deoxyHr and oxyHr upon O_2 binding ($k = 7.4 \text{ M}^{-1} \text{ s}^{-1}$) (144) is in sharp contrast to the deoxyHr–metHr redox chemistry, which is a slow, multistep process. The only other redox process that gives clean uniphase kinetics is the oxidation of deoxyHr to metHr by H_2O_2 . The form of the resultant metHr complex is a matter of disagreement (145, 146).

DeoxyHr can be oxidized to metHr with one-electron oxidants such as ferricyanide, and metHr can be converted to deoxyHr with reductants such as dithionite. In either direction, three phases are observed and semimetHr intermediates are involved (51, 132, 146–148). Recently, Pearce et al. (51) proposed the scheme shown in Fig. 17 for the one-electron redox chemistry of Hr. For the reduction of metHr, it is proposed that only the iron atom closest to the outer surface of each subunit in the octamer is directly reduced by “outer-sphere” reducing agents to form $(\text{semimet})_{\text{R}}\text{Hr}$. The atom reduced in $(\text{semimet})_{\text{R}}\text{Hr}$ is the same as the reduced iron in semimetHrN_3 (35). In the rate-limiting step, $(\text{semimet})_{\text{R}}\text{Hr}$ undergoes a conformational change to a $(\text{semimet})_{\text{O}}$ -like species and this complex either undergoes a

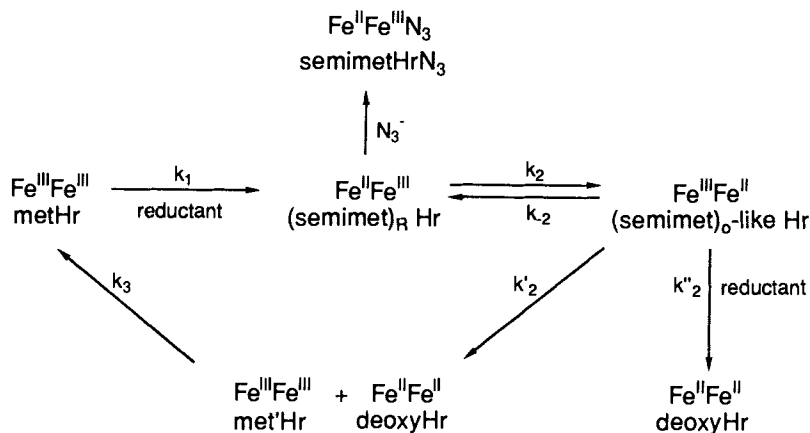


Figure 17. Redox chemistry of methemerythrin. Adapted from Ref. 51.

direct reduction to deoxyHr by inorganic reducing agents or disproportionates to met'Hr and deoxyHr. The nature of the met'Hr species is unknown. This species does not bind N_3^- and exhibits unusual Mössbauer parameters. It has been postulated to be metHrOH based on the kinetics of its conversion to metHr, which are similar to those seen for other metHrX species (149). The oxidation of deoxyHr to metHr is proposed to follow a similar scheme in the opposite direction.

The nature of the structural changes in the conversion of (semimet)_RHr to (semimet)_O-like Hr is of great interest. The EPR spectrum of (semimet)_RHr is more rhombic than that of (semimet)_OHr (131, 132), and while the exact nature of the difference between these two species has not been established, a small difference in the rhombic distortion of the ferrous site is apparent, sufficient to account for the differences in the EPR spectra (150). Pearce et al. (51) proposed that the (semimet)_RHr to (semimet)_O-like Hr conformational change is accompanied by a reversal of the oxidation states of the two iron sites. Only then can further "outer-sphere" reduction by external agents occur to produce deoxyHr. There is no D₂O effect on the rate of reduction of metHr to (semimet)_RHr suggesting that the μ -oxo bridge is not protonated in this step (51). Consequently, part of the conformational change in the (semimet)_RHr to (semimet)_O-like Hr conversion may be protonation of the μ -oxo bridge. The antiferromagnetic coupling between the two irons, which is greatly reduced upon reduction of metHr to (semimet)_RHr, does not significantly change, however, upon conversion of (semimet)_RHr to (semimet)_OHr (51, 89). As protonation of the μ -oxo bridge has been shown to decrease the magnitude of antiferromagnetic coupling, this behavior argues that there is a μ -hydroxo bridge in both forms of semimetHr.

The redox potentials of hemerythrin and myohemerythrin have been determined (Table V). They can be compared with available data from model complexes; however, it must be noted that the latter studies were performed in aprotic media. A perusal of the data shows that the redox potentials of the synthetic complexes can be easily rationalized in terms of ligand basicity. In general, (μ -oxo)diiron complexes have potentials more negative than those of μ -phenoxo complexes. Note that the metHr-to-(semimet)_RHr potential is significantly more positive than those of the (μ -oxo)bis(μ -acetato)diiron(III) complexes obtained in aprotic media. Since it is unequivocal that metHr has a μ -oxo bridge, the observed potential would suggest that the semimet form is stabilized in the active site, possibly by protonation of the oxo-bridge as suggested by studies on semimetHrN₃. With regard to the (semimet)_OHr/deoxyHr couple, there is insufficient data from model compounds to make useful inferences.

TABLE V
 Redox Potential of Diiron Centers in Proteins and Models

Compound	References	Fe ^{III} Fe ^{III} /Fe ^{II} Fe ^{III} (mV vs. NHE)	Fe ^{II} Fe ^{II} /Fe ^{II} Fe ^{II} (mV vs. NHE)
Hemerythrin	151	+110 ^a	+310 ^b
Myohemerythrin	151	+70 ^a	+350 ^b
[Fe ₂ O(OAc) ₂ (HBpz ₃) ₂]	58	-520 ^{c,d}	
[Fe ₂ O(OAc) ₂ (Me ₃ TACN) ₂](PF ₆) ₂	70	-130 ^{c,e}	-1260 ^{c,d}
[Fe ₂ O(OAc) ₂ {[OP(OEt) ₂] ₂ Co(C ₅ H ₅) ₂ }]	67	-200 ^{c,f}	-600 ^{d,e,g}
[Fe ₂ O(OAc)(TPA) ₂](ClO ₄) ₃	89	+180	
[Fe ₂ (BBMP)(OAc) ₂](BF ₄) ₂	64	+800 ^c	+120 ^c
[Fe ₂ (BBMP)(OBz) ₂](BF ₄) ₂	64	+900 ^c	+240
[Fe ₂ (BPMP)(OAc) ₂](BF ₄) ₂	91	+920 ^c	+210 ^c
[Fe ₂ (BPMP)(OPr) ₂](BPh ₄) ₂	134	+932 ^c	+230 ^c
[Fe ₂ (BPMP)(OBz)](BF ₄) ₂	91	+970 ^c	+190 ^c
[Fe ₂ (BPMP)(OAc)(OH)](BF ₄) ₂	91	+910 ^{c,d}	+160 ^{c,d}

^aMet/(semimet)_R.

^b(Semimet)_O/deoxy.

^cOriginally reported as vs. SCE (+0.24-V correction factor).

^dIrreversible.

^eQuasireversible.

^fOriginally reported as vs. Ag/AgCl (+0.20 correction factor).

^gAssignment tentative.

3. Oxygen Activation Chemistry

The redox behavior of MMO and RRB2 is just beginning to be characterized. As isolated, both enzymes occur as the diferric form. The diiron(III) unit in MMO can be reduced by dithionite titration to yield the diferrous form via a mixed-valence intermediate (11, 12, 31, 152). The redox potentials for the hydroxylase component of the *M. capsulatus* enzyme are estimated to be +350 and -25 mV vs. NHE, while the values are apparently closer to each other for the *M. trichosporum* enzyme since the EPR signal of the diferrous form can already be observed even before a full electron equivalent has been added to the diferric MMO (11a). When an EPR sample of MMO containing both diferrous and mixed-valence forms is exposed to dioxygen, only the $g = 16$ signal due to the diferrous form disappears (11a). This observation implicates the diferrous form in the oxygen binding and activation chemistry and may exclude the mixed-valence form from a significant role in enzyme function.

Stopped flow kinetic studies (30a) show that the reductase component of MMO is responsible for transferring the reducing equivalents of NADH to the hydroxylase component and that the electron-transfer steps from

NADH through the reductase to the hydroxylase all occur faster than the turnover rate of the enzyme. The function of protein B, the third component of MMO, appears to be to facilitate electron transfer between the reductase and hydroxylase only in the presence of substrate. Single turnover experiments with the fully reduced hydroxylase component show that oxygenations of substrates can occur in the absence of the reductase and component B (11a). Thus the hydroxylase is solely responsible for the oxygen activation chemistry. Competition experiments with mixtures of CH_4 and CD_4 show a large isotope effect with $k_{\text{H}}/k_{\text{D}}$ between 5 and 12, indicating that C–H bond cleavage is probably the rate-limiting step of the MMO reaction (153).

RRB2 can also be reduced to the diferrous form with dithionite, but only under certain conditions, such as the presence of a mediator like benzyl viologen or a “deforming” buffer like imidazole (27, 50). No mixed-valence form has thus far been observed. When the diferrous form is exposed to dioxygen, the dinuclear unit is oxidized to the diferric state, the tyrosine radical appears, and active RRB2 is produced. The stoichiometry of this oxidation process remains to be sorted out, since dioxygen is presumably a four-electron oxidant and only three electrons need to be removed to convert a diferrous complex and one tyrosine to a diferric complex and a tyrosyl radical.

The redox chemistry observed in the RRB2 interconversions supports the proposed role of the diiron center in ribonucleotide reductase. The diiron center is postulated to perform a regulatory function, rather than a catalytic function (17). Ribonucleotide reductase activity has been directly correlated with the amount of tyrosyl radical present (114). It has been observed by following the EPR of whole cells that the tyrosyl radical content varies in the life cycle of the cell, which means that there must be some mechanism for regenerating a radical (154). The diiron center is proposed to serve this function. Indeed Reichard and co-workers (17) have recently demonstrated the presence of components in the crude extract capable of converting metRRB2 into native RRB2 (Fig. 18). Among these components is an NAD(P)H:flavin oxidoreductase, which presumably provides the reducing equivalents from the reduction of metRRB2 to RRB2_{red} . Exposure to O_2 then transforms RRB2_{red} to native RRB2.

The mechanisms for O_2 utilization by MMO_{red} and RRB2_{red} are not established. The diferrous complex in either protein presumably serves to bind dioxygen, as in hemerythrin, forming a diferric peroxide complex (Fig. 19). This putative intermediate has been observed in neither the MMO nor the RRB2 cycle. Unlike in oxyHr, the peroxide intermediates of MMO and RRB2 must become activated to perform the required oxidation chemistry. This activation may derive from the ligand environments

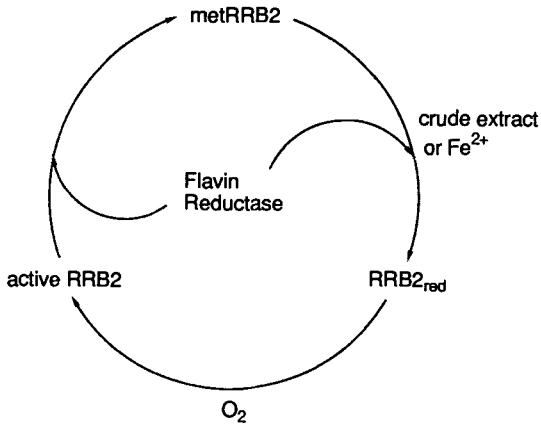


Figure 18. Redox cycle for the diiron unit of RRB2. Adapted from Ref. 17.

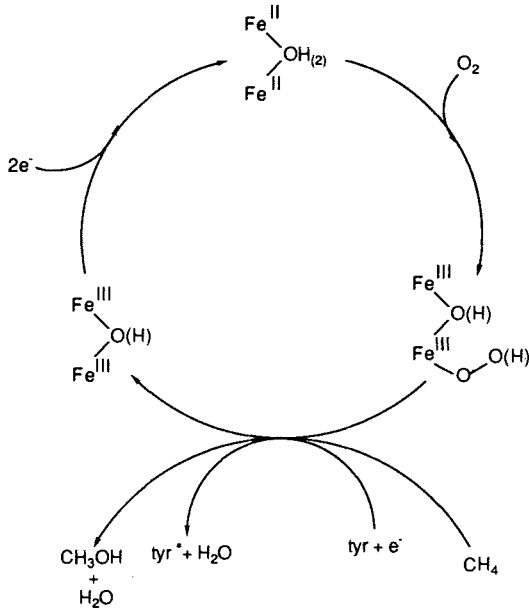


Figure 19. Proposed dioxygen activation mechanism for the diiron sites in MMO and RRB2. In RRB2, the diiron site is responsible for the generation of the tyrosine radical. The diiron site of MMO oxidizes methane to methanol; no evidence for the production of a tyrosine radical is seen in this system.

of the diiron centers. EXAFS and Mössbauer studies appear to indicate that the iron ligands are similar for the two enzymes and more oxygen rich than in hemerythrin (27, 31, 40, 52). The protein residues in the vicinity of the diiron complexes may also play a role in dioxygen activation analogous to those postulated for active site residues in horseradish peroxidase and cytochrome *c* peroxidase (155, 156).

4. Models

There are few peroxide adducts of synthetic non-heme iron complexes that are well characterized (Table VI). Perhaps the best known adduct is that derived from $\text{Fe}^{\text{III}}(\text{EDTA})$ under basic conditions. This purple complex has an absorption maximum near 520 nm (ϵ 528 $M^{-1}\text{cm}^{-1}$) (163). These are absorptions characteristics associated with the peroxide-to- Fe^{III} charge-transfer band in oxyHr; however, the coordination mode of peroxide in the complex appears to be different from that in oxyHr. After some debate in the literature, it has been concluded that the peroxide is η^2 -bound on the basis of isotope effects observed in the Raman spectrum of the complex (158, 164). The $\nu(\text{O}-\text{O})$ of the $\text{H}_2^{16}\text{O}_2$ complex is found at 815 cm^{-1} . When $\text{H}_2^{16}\text{O}^{18}\text{O}$ is used, the $\nu(\text{O}-\text{O})$ shifts to 794 cm^{-1} and appears as a peak of comparable line width. Were the peroxide only η^1 -bound, two peaks due to the $\text{Fe}-\text{O}^{16}-\text{O}^{18}$ and the $\text{Fe}-^{18}\text{O}-^{16}\text{O}$ isotopomers would have been expected, as in oxyHr. An η^2 -peroxo structure is also proposed for $[\text{Fe}(\text{TPP})\text{O}_2]^-$ and has been determined for the corresponding $[\text{Mn}(\text{TPP})\text{O}_2]^-$ complex (165).

Synthetic diiron(III) peroxide complexes all exhibit electronic spectral features in the region of 500–600 nm associated with peroxide-to- $\text{Fe}(\text{III})$ charge-transfer transitions (Table VI). In the cases studied, resonance enhanced $\nu(\text{O}-\text{O})$ features are observed near $(860 \pm 30) \text{ cm}^{-1}$. These complexes are presumably μ -1,2-peroxo-bridged species, but definitive isotopic

TABLE VI
Properties of Iron Peroxo Complexes

Complex	References	λ_{max}	$\nu_{\text{O-O}}$
oxyHr	139, 157	500(ϵ 2300)	845
$[\text{Fe}^{\text{III}}(\text{EDTA})\text{O}_2]^{2-}$	158	520(ϵ 530)	815
$\{[\text{Fe}(\text{pyN5})_2\text{O}_2]^{3+}$	159	540(ϵ 190)	
$[\text{Fe}_2(\text{HPTB})\text{O}_2]^{3+}$	108, 160	600(ϵ 2600)	890
$[\text{Fe}_2(5\text{-Cl-HXTA})(\text{OAc})\text{O}_2]^{2-}$	62	470(ϵ 1750)	884
$\{[\text{Fe}(\text{Ph}_3\text{PO})_4]_2\text{O}_2\}^{4+}$	161	576(ϵ 3540)	882
$[\text{Fe}_6(\text{O})_2(\text{O}_2)(\text{OBz})_{12}(\text{OH}_2)_2]$	162	534(ϵ 1590)	853

data confirming the structural assignment is not available. One of these complexes is derived from oxygenation of the parent $\text{Fe}^{\text{II}}(\text{pyN5})$ complex and thus serves as the only model of dioxygen uptake related to hemerythrin (159). This system has not been characterized in detail, however.

The two complexes based on dinucleating ligands result from peroxide addition to the parent diferric complexes. The HPTB complex is proposed to be a dibridged species with an RO bridge from the dinucleating ligand forming a five-membered $\text{Fe}_2\text{O}(\text{O}_2)$ ring (160). Although it has only limited stability, excess H_2O_2 maintains a high steady state concentration of the complex in methanol solution. It seems likely that the decomposition of the complex results in methanol oxidation and regeneration of the parent species (109).

The 5-Me-HXTA complex, on the other hand, is formulated on the basis of NMR as a tribridged species with the diiron unit connected by μ -phenoxy, μ -1,2-peroxo, and μ - O, O' -acetato moieties (62). The parent $[\text{Fe}_2(5\text{-Me-HXTA})(\text{OAc})_2]$ has twofold symmetry relating the two acetates and the two meta phenyl protons, respectively, to yield two resonances with a 6:2 intensity ratio. Peroxide binding results in the loss of one acetate and the twofold symmetry axis.

The Ph_3PO complex has a novel parentage. It is formed by the reaction of PhIO or other oxygen atom donors with $[\text{Fe}^{\text{II}}(\text{Ph}_3\text{PO})_4]^{2+}$ in CH_3CN , presumably via the O, O' -coupling of two $[\text{Fe}^{\text{IV}}\text{O}(\text{Ph}_3\text{PO})_4]$ moieties (161). If verified, this reaction would be the reverse of a proposed dioxygen activation mechanism involving homolytic cleavage of a μ -1,2-peroxide. When PhI^{18}O is used, the $^{18}\text{O}_2$ complex is formed. Interestingly, and perhaps not surprisingly because of how it is formed, this complex does not readily effect oxygenation of substrates such as PPh_3 , Ph_2SO , PhCH_2OH , and cyclohexene.

The hexanuclear complex (Table VI), although somewhat beyond the scope of this review, deserves mention inasmuch as it is the only structurally characterized synthetic iron peroxide complex thus far (162). It contains a μ -peroxo species coordinated to two Fe_3O units via two of the three iron atoms in each trinuclear unit. The peroxide in this complex appears to be sufficiently stabilized as to be unreactive.

Of the diiron peroxide complexes discussed thus far, only the HPTB and HXTA complexes have been reported to effect oxidation chemistry. The HPTB complex is claimed to convert 2,4-di-*tert*-butylphenol to 3,5-di-*tert*-butylbenzoquinone (4 days, 5% yield) (160), while the 5-Me-HXTA complex can disproportionate H_2O_2 , epoxidize olefins, and hydroxylate aromatics (62). The mechanistic details for these reactions are not well developed and require further study.

Nonheme iron complexes capable of hydroxylating unactivated alkane C–H bonds are also beginning to emerge (166). There are three cases where a (μ -oxo)diferric species is involved in alkane hydroxylation. The complex $[\text{Fe}_2\text{O}(\text{OAc})_2(\text{HBpz}_3)_2]$ (167) was demonstrated to oxidize adamantane and cyclohexane to their respective alcohols and ketones in the presence of Zn, HOAc, and O_2 [Gif-like conditions (168)]. $[\text{Fe}(\text{PA})_2]$ has been shown to be a catalyst that activates HOOH for the selective ketonization of methylenic carbon atoms (169). This reaction was proposed to proceed through an intermediate that is a (μ -oxo)diiron(III)-peroxide adduct. Fish, Christou, and co-workers (68) have reported that oxo-bridged diiron and tetrairon complexes, $[\text{Fe}_2\text{O}(\text{OAc})_2(\text{bipy})_2\text{Cl}_2]$ and $[\text{Fe}_4\text{O}_2(\text{OAc})_7(\text{bipy})_2](\text{ClO}_4)$, can catalyze the hydroxylation of alkanes with *t*-butylhydroperoxide. About 120 turnovers of cyclohexane oxidation can be effected by the diiron complex over a 3-day period, while the tetrairon complex can accomplish this in 5 h. These systems are reminiscent of models designed to mimic cytochrome P-450 reactivity (170). The range of (μ -oxo)diiron(III) complexes available should enhance the likelihood of obtaining mechanistic insight into how nonporphyrin iron centers may generate the high potential intermediate analogous to the oxoiron(IV) porphyrin cation radical species that is capable of attacking unactivated C–H bonds.

III. THE PURPLE ACID PHOSPHATASES

The purple acid phosphatases (PAP) catalyze the hydrolysis of phosphate esters under acidic pH conditions (pH optimum 5) (9, 10). They differ from other acid phosphatases in having a distinct purple color due to the presence of iron or manganese and in being uninhibited by tartrate. Diiron units have been found in the active sites of the enzymes from mammalian spleen (171–173) and uterus (173, 174), while a heterodinuclear FeZn unit has been characterized for the enzyme from red kidney bean (175). Either the Fe_2 or the FeZn unit is catalytically competent in these enzymes, since the enzymes from porcine uterus and bovine spleen can be converted into active FeZn forms and the kidney bean enzyme can be transformed into an active Fe_2 form (176). There are also enzymes from other plant sources (particularly sweet potato) that have been reported to have either a mononuclear Mn(III) or Fe(III) active site (177), but these are beyond the scope of the review. This section will focus on the enzymes from porcine uterus (also called uteroferrin), bovine spleen, and red kidney bean.

A. Biochemistry

The mammalian purple acid phosphatases with bimetallic active sites are glycoproteins with molecular weights of 35–40 kDa. Uteroferrin (Uf) consists of a single polypeptide chain (173, 174), while the bovine enzyme consists of two chains of 15 and 24 kDa, although the latter may be artifactual and result from proteolysis during the purification process (171b, 173). The kidney bean enzyme, on the other hand, is a homodimer of 120 kDa (175). The amino acid sequences of the two mammalian enzymes have been determined and substantial sequence homology is found (178). The homology is interesting, considering that the bovine enzyme is intracellular, while the porcine enzyme is secreted into the allantoic fluid after progesterone induction during the estrus cycle of the sow.

The biological role of these enzymes remains unclear. Uteroferrin has been postulated to play a key role in providing iron for the fetal pig by transfer to apotransferrin (179), but strong evidence for this role is lacking (180). With respect to the phosphatase activity, it is clear that the enzymes show a preference for activated phosphate esters and anhydrides, and one potential role is hydrolysis of phosphotyrosine bonds in proteins (171b, 181). The bovine enzyme has been localized by histochemical methods to be only in lysosome-like organelles of cells belonging to the reticulophagocytic system of the spleen and is proposed to play a role in the degradation of aged blood cells by dephosphorylating phosphoproteins of the erythrocyte membranes and the cytoskeleton (182). Interestingly, calcineurin, a known phosphoprotein phosphatase from bovine brain contains one atom of iron and one atom of zinc per molecule, but a detailed study of its metallobiochemistry has not been carried out (183). Finally, there are intriguing homologies between the sequences of PAPs and those of a number of phosphoprotein phosphatases (184); these studies are being pursued and should shed further light on the biological role of these enzymes.

The purple acid phosphatases are typically assayed by their ability to hydrolyze *p*-nitrophenylphosphate. The K_m values for this substrate are in the millimolar range (171b, 174). The product phosphate and its analogue arsenate are weak competitive inhibitors ($K_i \sim mM$); in addition, they potentiate the conversion of the diiron enzymes under aerobic conditions to an irreversibly inactivated, oxidized form (45, 185–187). Other tetraoxo anions such as molybdate and tungstate, on the other hand, are tightly bound inhibitors ($K_i \sim \mu M$) which do not potentiate the oxidation of the diiron enzymes (185, 186). Interestingly, the FeZn forms are similarly inhibited by these anions with comparable K_i values, but are not susceptible to the oxidative inactivation observed for the diiron derivatives (185).

B. Properties of the Diiron(II,III) Active Site

The first indication that associated the purple acid phosphatases with the dinuclear iron-oxo proteins was their EPR spectra with $g_{av} \sim 1.75$ (Fig. 14). This typically rhombic spectrum has been observed for the diiron forms of the bovine (188), porcine (189), and kidney bean enzymes (176) and is reminiscent of the Fe(II)Fe(III) states of Hr and MMO. The mixed-valence nature of the diiron unit has been confirmed by Mössbauer spectroscopy in all three cases (44, 45, 47, 190, 191). As discussed in an earlier section, the low g_{av} value is characteristic of an $S = \frac{1}{2}$ system derived from an antiferromagnetically coupled Fe(II)Fe(III) unit. The fact that these signals can be observed only at temperatures below 40 K suggests an efficient electron relaxation mechanism and a small antiferromagnetic interaction. Initial estimates by the temperature dependences of the EPR signals (47), and the NMR isotropic shifts (43) established a range of 6–10 cm^{-1} for the $-J$ value. Subsequent magnetic susceptibility measurements on uteroferrin yielded a J value of $-(9.9 \pm 0.3) \text{ cm}^{-1}$ (54). This value is smaller than those estimated for the semimetHr complexes and the mixed-valence species derived from synthetic (μ -oxo)diiron(III) complexes (Table II). Based on this J value, it has been proposed that a hydroxo bridge mediates the coupling between the Fe(III) and the Fe(II) centers (43, 47).

EXAFS studies on the active diiron PAP forms estimate the Fe–Fe distance to be 3.0–3.2 Å (1a, 46, 48), which is significantly shorter than those found for semimetHrN₃ (40), MMO_{mv} (52), and synthetic (μ -phenoxo)bis(μ -carboxylato)diiron(II,III) complexes (Table II). The shorter Fe–Fe distance in the PAPs either requires a smaller Fe–O–Fe angle for the tribridged diiron core or consideration of alternative diiron units. An Fe₂(μ -OR)₂ core unit would be consistent with the observed Fe–Fe separation. Examples of such cores are readily found among diferric complexes (94, 192), but there is only one example that is in the mixed-valence oxidation state. The complex [Fe₂(salmp)₂][−] has an Fe₂(μ -OPh)₂ core with Fe–Fe distances of 3.081 and 3.116 Å (94). The metal centers in [Fe₂(salmp)₂][−] are *ferromagnetically* coupled to an $S = \frac{3}{2}$ ground state in this complex, however. A *ferromagnetically* coupled ground state can clearly be ruled out for the PAP_r values based on the EPR and magnetic data, so further synthetic work will be required to test whether other mixed-valence complexes with Fe₂(μ -OR)₂ core units have properties consistent with the PAP_r active site.

Endogenous ligands to the dinuclear unit have been identified by using a combination of spectroscopic methods. The active diiron enzyme exhibits a visible absorption maximum at 510 nm (ϵ_M 4000), the large extinction coefficient being associated with a charge-transfer band (47, 173). Laser

excitation into the absorption band gives rise to enhanced vibrations at 1164, 1287, 1498, and 1600 cm^{-1} (Fig. 20), which are characteristic to tyrosinate deformations; these bands unequivocally identify the chromophore as a tyrosinate-to-Fe(III) charge-transfer transition (47, 193, 194). In corroboration, features assignable to an Fe(III)-bound tyrosinate are observed in the ^1H NMR spectrum of uteroferrin [cf. Fig. 21: 3,5-H, peaks c and d; 2,6-H, peak y; $\beta\text{-CH}_2$, peaks a and j (not shown)] (43, 195). No features due to an Fe(II)-bound tyrosinate could be identified. Thus, like the diiron units in Hr and RRB2, the diiron complex in the purple acid phosphatases is inherently unsymmetric.

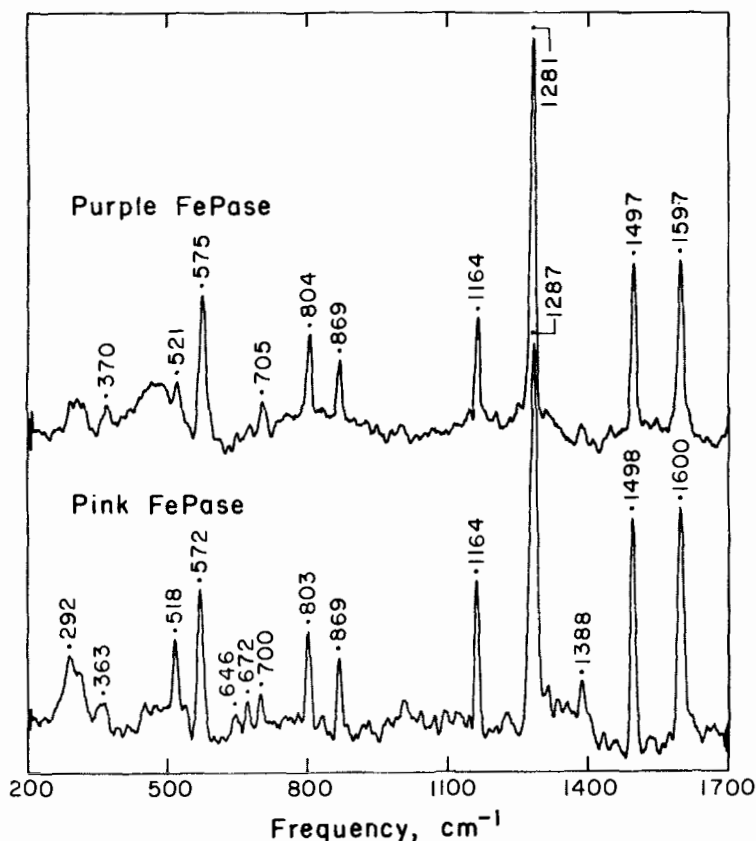


Figure 20. Resonance Raman spectra of PAP from bovine spleen. Reprinted with permission from B. A. Averill, J. C. Davis, S. Burman, T. Zirino, J. Sanders-Loehr, T. M. Loehr, J. T. Sage, and P. G. Debrunner, *J. Am. Chem. Soc.*, 109, 3760-3767 (1987). Copyright © (1987) American Chemical Society.

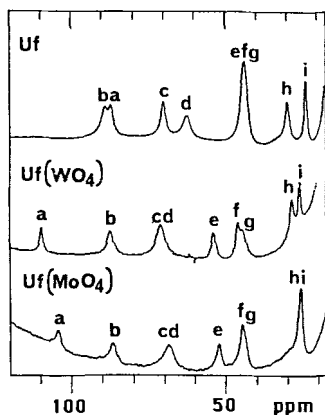


Figure 21. ^1H NMR spectra of reduced uteroferrin and its tungstate and molybdate complexes. Reprinted with permission from R. C. Scarrow, J. W. Pyrz, and L. Que, Jr., *J. Am. Chem. Soc.*, 112, 657–665 (1990). Copyright © (1990) American Chemical Society.

It has been suggested that there are two Tyr residues coordinated to the Fe(III) center on the basis of the ϵ_M of 4000 (43, 47). Model complexes typically exhibit ϵ_M values of 1000–2000 per iron(III)–phenolate bond (196). This proposed number would require, however, that the two Tyr's be in essentially identical environments to give rise to the reported NMR and Raman spectra, since both phenolate NMR isotropic shifts and the tyrosinate Raman $\nu_{(\text{CO})}$ peaks are quite sensitive to differences in protein environment. The $\nu_{(\text{CO})}$ modes in recently obtained Raman spectra are sharp features and show no evidence of tyrosine heterogeneity (47, 185). Furthermore, absolute integration of the NMR signals relative to an internal standard supports the presence of only *one* Tyr coordinated to the Fe(III) center (195). The variability of the ϵ_M values in synthetic iron–phenolate complexes suggests that there may be circumstances under which one iron(III)–phenolate bond would give rise to a larger ϵ_M value; recent model studies indicate that this behavior is possible (80).

The ^1H NMR spectra of uteroferrin also provide evidence for His coordination to the diiron unit; solvent exchangeable resonances at shifts expected for Fe(III)-His-N-H (peak b in Fig. 21) and Fe(II)-His-N-H (peak e in Fig. 21) protons are observed (195). The presence of nitrogen-containing ligands is also indicated by ENDOR and ESEEM data (197, 198). From the NMR integration, the Tyr[Fe(III)]:His[Fe(III)]:His[Fe(II)] ratio is 1:1:1 (195). The nature of the remaining endogenous ligands to the diiron unit is at best speculative. The possibility of carboxylates as ligands is attractive. There are unassigned features in the NMR spectrum (peaks f and g) that may be consistent with the CH_2 protons of a carboxylate terminally bound to the Fe(II) center (195). The coordination of a carboxylate would also be consistent with the larger Mössbauer isomer shift

associated with the Fe(II) site in Uf, (44, 45, 47) relative to those of deoxyHr (37, 38). Evidence for a bridging carboxylate is not available from NMR spectroscopy because the CH₂ protons of such a bridge are expected to be too broad to be observable (195). The present picture of the purple acid phosphatase active site (Fig. 22) thus leaves room for a variety of potential ligands. Not to be overlooked is the possibility of solvent water, particularly because of the hydrolytic function of the enzymes. ENDOR (electron nuclear double resonance) and ESEEM (electron spin echo envelope modulation) studies reveal the presence of solvent-exchangeable features, some of which may be ascribed to coordinated water molecules (197, 198). One of these coordinated solvent molecules may be displaced when substrate or inhibitor binds, while another may serve as the nucleophile in the hydrolysis reaction as proposed for the alkaline phosphatases (199).

C. Fe(III)M(II) Derivatives

The heterobimetallic derivatives of the purple acid phosphatases presumably retain much of the coordination chemistry deduced for their diiron counterparts; however, comparative studies are just beginning. In the Fe(III)Zn(II) forms, the replacement of Fe(II) with the diamagnetic Zn(II) ion eliminates the antiferromagnetic interaction between the metal centers

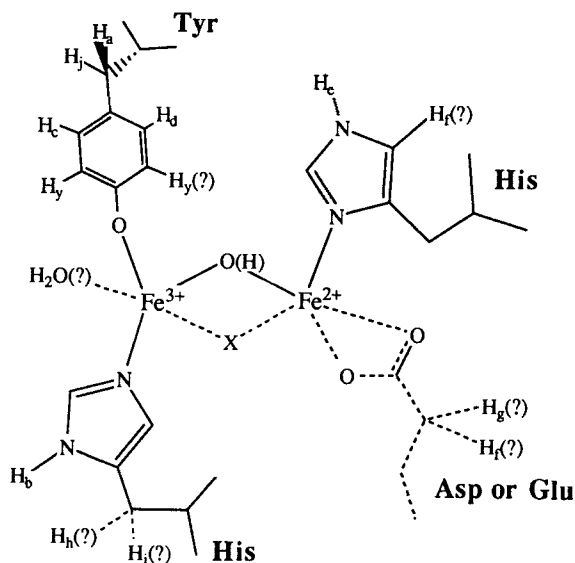


Figure 22. Proposed active site for reduced uteroferrin based on ¹H NMR data. Adapted from Ref. 195.

(171a, 185). The EPR signals at $g = 4.3$ are thus observed (171a, 176, 185), which are typical of a high-spin Fe(III) center in rhombic symmetry. The Mössbauer spectrum of FeZnUf shows a six-line pattern at 4.2 K with an overall splitting associated with a hyperfine coupling ($a/g_n\beta_n$) of -21 T (190), which is comparable to that of protocatechuate 3,4-dioxygenase, another non-heme iron protein with coordinated tyrosines (200).

The purple color is retained (λ_{\max} 530 nm) in the FeZn forms (171a, 185, 201), and Raman spectra exhibit the characteristic tyrosinate deformations (185). There are disagreements in the reported ϵ_M values for the purple chromophore that are not yet resolved. Zerner and co-workers (201) report an ϵ_M of 3650 for FeZnUf and the kidney bean enzyme, while Averill and his co-workers (171a) find ϵ_M to be 2100 for the bovine enzyme. Recent studies in Que's lab on FeZnUf concur with Averill's value (185). While there may be a possibility of Fe and Zn site scrambling in preparations with lower ϵ_M values, the high specific activities reported and the sharp EPR signals of the FeZnUf in the Que preparations would appear to argue against site heterogeneity. Clearly, more studies are needed to resolve the matter.

Other Fe(III)M(II) PAP derivatives where M is Mn(II), Co(II), Ni(II), Cu(II), Cd(II), and Hg(II) have been reported with variable amounts of catalytic activity observed (201, 202). The phosphatase activity is retained even after treatment with H_2O_2 , indicating that the activity observed is not due to contaminating Fe(II)Fe(III) enzyme but to the Fe(III)M(II) derivatives themselves. Studies of their coordination chemistry are at an early stage.

D. Anion Interactions

Insights into how substrate interacts with the active site of the PAPs may be gleaned from an investigation of the tetraoxo anion inhibitor complexes. These studies have focused on the effects of the substrate analogue and product phosphate, but comparative data on arsenate and molybdate are also informative. The various observations are summarized in Table VII. Note that phosphate and arsenate are weak binding inhibitors, while molybdate binds tightly (45, 185, 186, 203). These observations apply to both the Fe_2 and the FeZn forms, suggesting that the anion interaction site is independent of the divalent metal ion (185). Note also that anion binding elicits similar changes of rhombicity in the EPR spectra of the Fe_2 and the FeZn enzymes. In particular, molybdate binding generates sites of axial symmetry in both enzymes relative to their rhombic anion-free states. Again, these observations show that the Fe(III) site appears quite sensitive to anion binding.

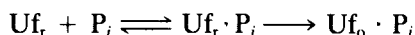
The effect of phosphate on the purple acid phosphatases is complex and

TABLE VII
 Properties of Uf-Anion Complexes

Complex	References	K_i	λ_{\max}	EPR	J (cm^{-1})
Uf _{red} + Phosphate	54, 185	12 mM	536	1.06, 1.51, 2.27	-3
Uf _{red} + Arsenate	185, 186	1.3 mM	505	1.41, 1.56, 1.93	-6
Uf _{red} + Molybdate	185, 186	4 μ M	525	1.52, 1.97	-8
FeZnUf + Phosphate	185	3.5 mM	550	4.25, 4.28, 4.32 9.6	
FeZnUf + Arsenate	185	2.5 mM	510	3.81, 4.17, 4.31 8.77, 5.98	
FeZnUf + Molybdate	185	2 μ M	510	5.94 5.28, 6.92	

has been the subject of some controversy (45, 54, 186, 203, 204). When phosphate is added to Uf_r, there is an immediate red shift in its visible spectrum and an immediate loss of its characteristic EPR signals, rendering it apparently EPR silent, but catalytic activity diminishes slowly ($t_{1/2} \sim 1$ h) (45, 203). Upon standing in air, the oxidized uteroferrin-phosphate complex is formed, which is purple in color, EPR silent, and catalytically inactive. The phosphate in this complex is tightly (essentially irreversibly) bound as demonstrated by gel filtration experiments with ³²P-phosphate (203). Indeed, the tightly bound phosphate was a major factor in the misdetermination of iron content in uteroferrin; samples containing phosphate yielded only 1 Fe/holoprotein under acid extraction conditions as opposed to 2Fe/holoprotein when the protein was dry ashed (205).

Thus, with respect to color and EPR activity, the initial uteroferrin-phosphate complex resembles the oxidized uteroferrin-phosphate complex, but the two complexes differ significantly in catalytic activity and phosphate affinity. Whereas the oxidized uteroferrin-phosphate complex is irreversibly formed (203), the initial uteroferrin-phosphate complex can be dissociated by gel filtration to regenerate native enzyme (185). An appropriate scheme to rationalize the above observations involving two distinct phosphate complexes is shown below.



The initial complex is reversibly formed with a K_D in the millimolar range as determined by inhibition kinetics; this species would be the reduced uteroferrin-phosphate complex shown by Mössbauer studies to contain a mixed-valence diiron unit (45). This complex oxidizes to the diferric state upon standing in air, forming the oxidized uteroferrin phosphate

complex (45, 203). Phosphate binding dramatically alters the ΔE_0 of the Fe(III) site in Uf_r , while only slightly perturbing that of the Fe(II) site. On the other hand, the ΔE_0 values of both iron sites in Uf_o are significantly affected by phosphate binding. The EPR silence of $Uf_r \cdot P_i$ was initially puzzling until its spectrum was observed under somewhat more stringent power and temperature conditions (54). The $Uf_r \cdot P_i$ complex exhibits signals that are broad and quite anisotropic (Fig. 23). Although this spectrum could be discerned even in the initial experiments, the use of low temperatures (2–4 K) and high modulation amplitudes greatly enhances the signals. Magnetic susceptibility studies on $Uf_r \cdot P_i$ show that the J value for the mixed-valence diiron unit is -3 cm^{-1} (54), so that there is significant depopulation of the $S = \frac{1}{2}$ ground state at temperatures (10–12 K) typically used for liquid helium studies. The small coupling is now comparable to the zero-field splitting of the Fe(II) ion; such a situation can complicate the description of the electronic structure of the mixed-valence diiron unit and lead to the large anisotropy observed (54, 125a). The details of this situation are not well understood and will require further investigation.

The interaction of phosphate with the bovine PAP appears uncomplicated by the intermediacy of the reduced enzyme–phosphate complex, since the red shift and the loss of EPR signal both parallel the loss of catalytic activity (187). Nevertheless, the reduced enzyme–phosphate complex must still be involved because phosphate is a known competitive inhibitor of the bovine enzyme (171). In the bovine case, conversion of the reduced enzyme–phosphate complex to its oxidized counterpart may occur at a rate significantly faster than that observed for the porcine enzyme. The differences between the two enzymes are intriguing and should be examined more closely.

We have proposed a mechanism for how phosphate interacts with the diiron unit (Fig. 24) (185). At pH 5, phosphate is wholly in its monobasic form, $H_2PO_4^-$. It binds to the Fe(III) ion as suggested by the Mössbauer data and donates one of its protons to (or strongly hydrogen bonds with) the hydroxo bridge, thus forming $Uf_r \cdot P_i$. The weakening of the antiferromagnetic interaction in $Uf_r \cdot P_i$ necessitates some mechanism to remove an oxygen orbital on the μ -OH bridge from mediating coupling, and the protonation (or hydrogen bonding) of the hydroxo bridge provides a suitable mechanism. In the rate-determining step, the terminal phosphate ligand becomes bridging, thereby potentiating the oxidation of the diiron unit and fixing the anion into the dinuclear complex.

Arsenate similarly potentiates the oxidation of uteroferrin, but its binding to the enzyme induces only a slight *blue* shift in the visible spectrum (185, 186), a slight broadening of the EPR signals (185), and little change in the J value as determined by the temperature dependence of the power

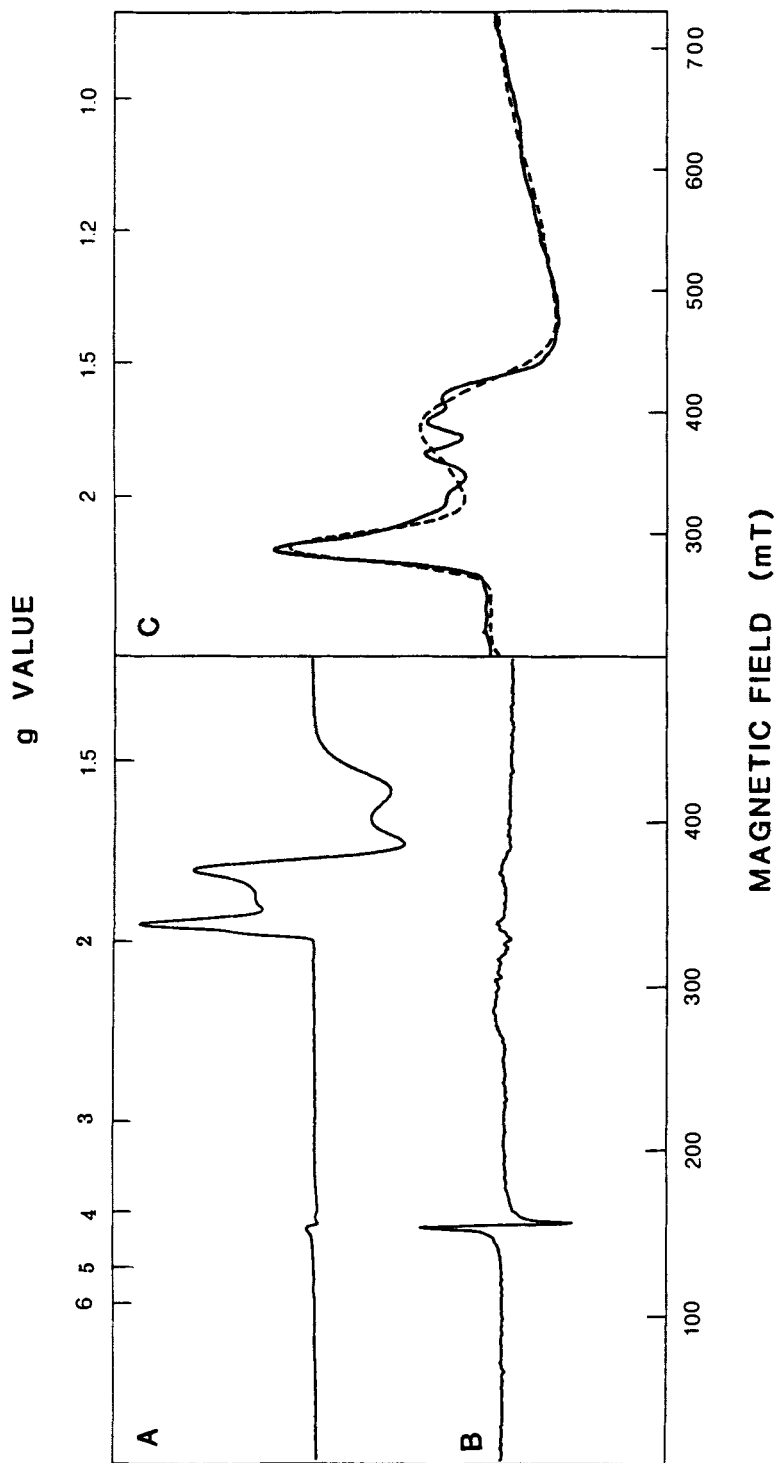


Figure 23. EPR spectra of (a) reduced uteroferrin and (b) its phosphate complex at 8 K and 10 G modulation amplitude and (c) the phosphate complex at 2 K and 40 G modulation amplitude. Reprinted with permission from Ref. 54. © American Society of Biochemistry and Molecular Biology.

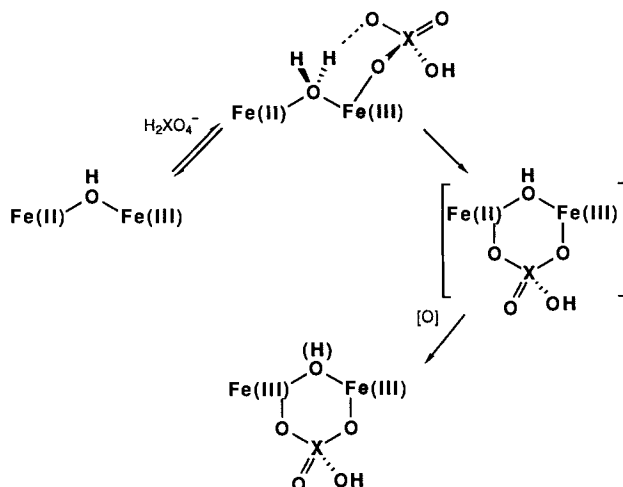


Figure 24. Proposed interaction of phosphate with the diiron site in reduced uteroferrin.

saturation of the EPR signal (185). These observations suggest that arsenate binding does not significantly alter the hydroxo bridge, unlike phosphate binding. However, H_2AsO_4^- appears to hydrogen bond to the hydroxo bridge based on EPR experiments in H_2O and D_2O . The EPR signals of $\text{Uf}_r \cdot \text{AsO}_4^-$ in D_2O buffer shift to lower field and sharpen relative to the complex in H_2O buffer (Fig. 25a) (185). These spectral changes are ascribed to the strengthening of the antiferromagnetic coupling in D_2O due to the weaker acidity of D_2AsO_4^- relative to H_2AsO_4^- ; the observations thus support the model proposed in Fig. 24.

The model also postulates anion coordination to the dinuclear active site. That anions bind to the Fe(III) ion is suggested by the UV/vis, EPR, and Mössbauer spectral changes observed upon binding of the different anions to Uf_r and FeZnUf (45, 185, 186). But direct evidence for anion coordination to the dinuclear active site comes from studies on $\text{Uf}_r \cdot ^{95}\text{MoO}_4^-$ and $\text{FeZnUf} \cdot \text{P}^{17}\text{O}_4^-$. Coupling of the electronic spin to the ^{95}Mo nucleus ($I = \frac{5}{2}$) was detected from the ESEEM spectrum (198), demonstrating that molybdate coordinates to the diiron unit but not specifying to which metal center it is bound. Broadening of the very sharp $g = 4.3$ signal of the $\text{FeZnUf} \cdot \text{P}_i$ complex was observed when $\text{P}^{17}\text{O}_4^-$ was used (Fig. 25b) (185), showing that phosphate coordinates to the Fe(III) center of the dinuclear active site in the active enzyme; coordination to the Zn center is not excluded, however.

Evidence for a bridging phosphate in the oxidized enzyme-phosphate complex comes from EXAFS studies on the bovine and porcine enzymes

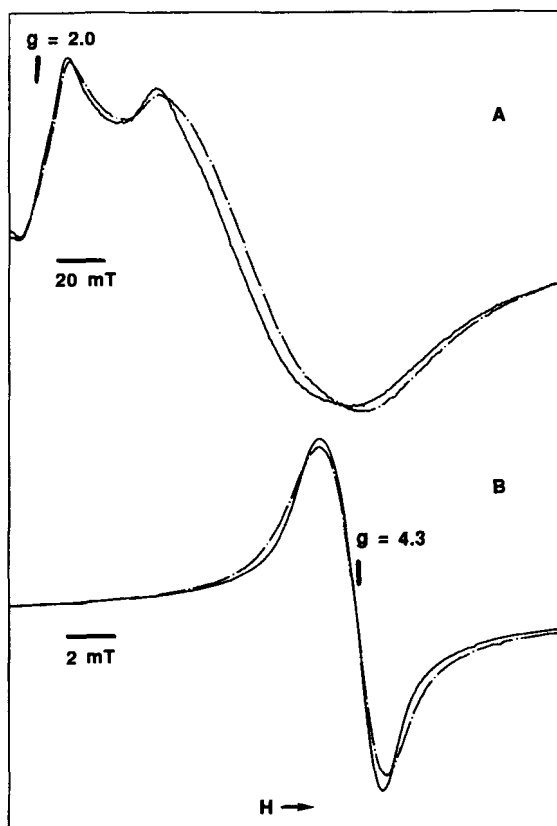


Figure 25. EPR spectra of (a) $Uf_7 \cdot AsO_4$ in H_2O (---) and D_2O (—) and (b) $FeZnUf$ coordinated with $P^{16}O_4$ (—) and $P^{17}O_4$ (---).

(46, 48). Features due to one Fe-P component per iron at 3.1–3.2 Å can be observed. Since only one phosphate is bound to each enzyme molecule, the EXAFS fits require that it be bridging the diiron unit. Que and Scarrow favored an O,O'-bridging mode for the phosphate in the porcine enzyme (1a, 46), by analogy to the several examples of O,O'-bridging phosphates in synthetic complexes. In contrast, Kauzlarich et al. (48) proposed a terminally bound phosphate for the bovine enzyme, but did not address the discrepancy between the model and the coordination number determined for P in the fit.

The above studies provide a working model for how anions, particularly phosphate, interact with the dinuclear active site. It may be conjectured that substrate interacts in a similar manner to initiate the catalytic process.

E. The Puzzle of the Oxidized Diiron Enzyme

The purple acid phosphatases can occur in two diferric forms—one as the tightly bound phosphate complex (characterized for the bovine and porcine enzymes) (45, 171, 203) and the other derived from peroxide or ferricyanide oxidation of the reduced enzyme (thus far accessible for only the porcine enzyme) (206). These oxidized forms are catalytically inactive. They are EPR silent because of antiferromagnetic coupling of the two Fe(III) ions and exhibit visible absorption maxima near 550–570 nm associated with the tyrosinate-to-Fe(III) charge-transfer transition. The unchanging value of the molar extinction coefficient between the oxidized and reduced enzymes indicates that the redox-active iron does not contribute to the visible chromophore and that tyrosine is coordinated only to the iron that remains ferric in agreement with the NMR spectrum of U_f (45).

These diferric forms are analogous to metHr and RRB2, but evidence for a (μ -oxo)diiron(III) unit in the PAP active site is equivocal. The strongest argument for the presence of an oxo bridge comes from magnetic susceptibility measurements that show strong antiferromagnetic coupling (43, 47, 171, 189, 207). For the bovine oxidized phosphate complex, there is so little paramagnetic susceptibility detected that $-2J$ is estimated to be $\sim 300 \text{ cm}^{-1}$ (47). This measurement needs to be corroborated inasmuch as magnetic susceptibility data on the reduced bovine enzyme from the same study also suggested strong coupling in the mixed-valence state (171), a conclusion clearly contradicted by a variety of other studies discussed earlier. For the oxidized porcine enzyme, $-2J$ is estimated at 200 cm^{-1} from SQUID susceptibility measurements (207) and at $>80 \text{ cm}^{-1}$ from Evans' susceptibility measurements (43). These large values favor an oxo bridge, but more work clearly needs to be carried out to reconcile the different values.

Mössbauer studies on U_{f_0} and $U_{f_0} \cdot P_i$ show antiferromagnetically coupled Fe(III) centers with large ΔE_Q values (45, 190). The ΔE_Q values for U_{f_0} are among the larger ones known for this class of proteins and phosphate binding does diminish the splittings significantly. These values, however, all indicate a large asymmetry in the electric field about the ^{57}Fe nucleus that is consistent with the presence of an oxo bridge. Recently, Sage et al. (190) have reported variable temperature high field measurements on U_{f_0} . Whereas the spectra at 4 K clearly demonstrate the diamagnetic character of the ground state, the spectra at 100 K show hints of a paramagnetic excited state. In the $\frac{5}{2}, \frac{5}{2}$ coupling scheme, this result would suggest population of the $S = 1$ state near 100 K or a J value comparable to that determined by Evans' susceptibility measurements.

Resonance Raman and EXAFS studies, on the other hand, are unable

to demonstrate the presence of an oxo bridge. No $\nu_s(\text{Fe-O-Fe})$ has been observed (47), but its absence may be rationalized by one of two arguments: (a) that the oxo-to-Fe(III) charge-transfer band is blue shifted so that it cannot be probed by the laser lines used for the Raman study or (b) that the oxo bridge is trans to ligands that do not enhance the intensity of the $\nu_s(\text{Fe-O-Fe})$ mode, thus rendering it difficult to observe.

With EXAFS, no evidence for a short Fe-O bond has been found. Analysis of the first shell EXAFS data of both the bovine and the porcine oxidized phosphate complexes reveals 3 Fe-O components at 1.95–1.98 Å and 3 Fe-N components at 2.12–2.15 Å (46, 48). A comparison of the first shell EXAFS data on metHrN₃, RRB2, and Uf_o·P_i (Fig. 8) shows clearly that the Uf_o·P_i coordination shell differs from those of the other two, particularly in the destructive interference at high *k* values. Kauzlarich et al. (48) have suggested that the short Fe-O bond may be masked by the slightly longer Fe-O(Tyr) bond(s). However, Scarrow and Que (46) have tested this hypothesis with two synthetic complexes having both Fe-μ-O and Fe-OPh bonds and found that the short Fe-O bond can be discerned in the EXAFS spectra of the models. Thus the presence of the oxo bridge is a matter yet to be resolved.

In summary, the active site structure of the oxidized diiron phosphatases remains a puzzle because of the seemingly conflicting experimental observations. In of itself, the diferric phosphatases represent an inactive form of these enzymes and are thus of less biochemical interest than the active Fe(III)Fe(II) and Fe(III)Zn(II) forms. The details of the diferric active site are intriguing from a bioinorganic perspective, however, mainly in terms of its relationship to the active sites of Hr, MMO, and RRB2.

F. Relevant Synthetic Analogues

Model compounds to date have addressed three properties of the purple acid phosphatases: the visible chromophore, anion interactions, and EPR signals of the Fe(III)M(II) state. Work on the visible chromophore focused on whether the purple color could be consistent with the presence of an oxo bridge. Complexes with salicyaldimine ligands are among the best known (μ-oxo)diiron(III) complexes (33, 97c). The prototypical [Fe(salen)]₂O exhibits only visible tailing of near-UV absorptions resulting in its characteristic yellow color (33). Other salicyaldimine complexes exhibit similar spectra features, as does [Fe(8-mequin)]₂O, indicating that iron centers with an oxo bridge and two phenolates per iron typically have blue-shifted phenolate-to-iron(III) charge-transfer transitions. The blue shift is consistent with a high-spin ferric center of diminished Lewis acidity (208). Removing either the oxo bridge or one of the phenolates should increase the Lewis acidity of the iron center and red shift the charge-transfer band.

There are several examples of bis(phenolate)iron(III) complexes, with $[\text{Fe}(\text{salhis})_2]^+$ (209) and $[\text{Fe}(\text{salen})\text{Im}_2]^+$ (196b) among those having appropriate λ_{max} values. $[\text{Fe}_2\text{O}(\text{OBz})(\text{HDP})_2]^+$ is the only example of a structurally characterized (μ -oxo)diiron(III) complex with one phenolate per iron (80). Its λ_{max} is at 522 nm (CH_2Cl_2), so an active site analogous to this complex would be consistent with the purple color of the oxidized phosphatases. More interestingly, the hdp complex exhibits an ϵ_{M} near 3000 $\text{M}^{-1}\text{cm}^{-1}$ per Fe.

With regard to anion interactions, Lippard, Wieghardt, and Que have explored the effects of replacing carboxylate bridges with other anions in their respective model systems. Relevant structural and physical properties are summarized in Table II. Prominent among these complexes are the μ -phosphato derivatives for which crystal structures are known for the HBpz_3 (75, 76), Me_3TACN (77), and TPA (82) series. In addition, Wieghardt and his co-workers (77) obtained a series of complexes with bridging phosphate, phosphate monoester, and phosphate diester to reveal the effect that charge may have on the properties of the (μ -oxo)diiron(III) unit.

The structural consequences of substituting phosphate for carboxylate are a slight elongation of the Fe- μ -O bonds and an increase in the Fe-O-Fe angles. The lengthening of the Fe- μ -O bonds is presumably due to the greater basicity of the phosphate ligands, which would engender stronger Fe-O (phosphate) bonds and weaken the Fe- μ -O bonds, while the larger Fe-O-Fe angles (and consequently longer Fe-Fe distances) may be ascribed to the larger bite of the phosphate ligand. These structural differences are reflected in changes in magnetic behavior and electronic properties. There is a clear weakening of the antiferromagnetic coupling between the ferric centers with $-2J$ decreasing from ~ 240 to ~ 200 cm^{-1} when acetate is replaced by diphenyl phosphate; this effect may be correlated with the lengthening of the Fe- μ -O bonds (75, 77, 82). The coupling further weakens on going from a $\text{O}_2\text{P}(\text{OR})_2^-$ bridge to a $\text{O}_3\text{P}(\text{OH})_2^{2-}$ bridge ($2J = -160$ cm^{-1}) in the Me_3TACN series (77). Unfortunately, the latter has not been characterized crystallographically, so the structural changes implied by the weaker coupling cannot yet be confirmed. Such effects of the phosphate bridge may provide clues for clarifying the puzzle of the oxidized phosphatase active site. For example, it may be possible to weaken the coupling of the (μ -oxo)diiron unit to the extent implied by the Mössbauer and Evans susceptibility measurements by a combination of a bridging phosphate and strong hydrogen bonding to the oxo bridge. Such a hypothesis remains to be tested.

Me_3TACN complexes with bridging arsenate, molybdate, and tungstate have also been reported and may serve as models for their respective PAP-anion complexes (77). Tris($O, O' - \mu\text{-XO}_2$) complexes can be obtained; of these, the tris(chromato) and tris(arsenato) complexes are structurally de-

terminated and found to have Fe-Fe distances of 4.456 and 4.552 Å, respectively (77). Thus, it is apparent that the tetraoxo anions can act as bridges in dinuclear complexes; what remains to be determined is whether they may coordinate with a single iron center.

The EPR properties of some synthetic mixed-valence complexes have been discussed in an earlier section with references to analogous signals found in semimetHr's and MMO_{mv}. The earlier comments apply to the PAPs in their catalytically active Fe(III)Fe(II) forms as well. What needs further comment is the effect of phosphate binding in U_r, which engenders an EPR signal that spans almost 0.4 T (Fig. 23). Similar anisotropic signals are observed in complexes of dinucleating ligands with (μ-phenoxo)bis(μ-carboxylato)diiron(II,III) cores (64, 65, 134). It is clear that the phenoxo bridge, like the aqua bridge proposed for U_r·PO₄, mediates weak coupling between the metal centers ($-J \sim 5 \text{ cm}^{-1}$, Table II), which is now comparable to the zero-field splitting (D) of the Fe(II) center. It is this relationship between D and J (i.e., $|D| \sim |J|$) that is believed to give rise to such anisotropic EPR signals, but the detailed spin physics of these systems is not yet well understood.

One other property for the dinucleating ligands that is useful for modeling the PAPs is their ability to form Fe(III)M(II) complexes. Because of the affinity of Fe(III) for phenolate, a monoferric complex of the dinucleating ligand can be obtained; subsequent addition of a divalent ion and carboxylates forms $[\text{Fe(III)M(II)L(O}_2\text{CR)}_2]^{2+}$. To date, complexes with Fe(III)Zn(II), Fe(III)Cu(II), Fe(III)Mn(II), and Ga(III)Fe(II) (with a slight synthetic modification) units have been synthesized (91, 134, 210). The Fe(III)Zn(II) and Ga(III)Fe(II) complexes are useful for the determination of the electronic properties of the Fe(III) and Fe(II) centers separately in the absence of antiferromagnetic coupling; this information is being used to sort out the Mössbauer and magnetic properties of the corresponding mixed-valence complexes. The Fe(III)M(II) complexes will also be useful as spectroscopic models for the Fe(III)M(II) PAP derivatives as their properties are determined.

IV. OTHER (μ-OXO)DIIRON CENTERS IN PROTEINS

A. Rubrerythrin

Recently, a protein of unknown function was isolated from the periplasmic fraction of *D. vulgaris* and found to contain two "rubredoxin-like" FeS₄ centers and one "hemerythrin-like" center (13). Thus, it was named, *rubrerythrin*. Rubrerythrin is a dimer of identical subunits of 21.9 kDa. Crystals of this protein have been grown and preliminary X-ray crystal-

lography results indicate a twofold symmetry in the protein (211). Since there is only one diiron center in the protein, retention of this symmetry predicts a model where each polypeptide coordinates one rubredoxin-like Fe with four cysteines and shares the diiron site at an interface between the two subunits.

Mössbauer data on the oxidized protein show a six-line magnetic spectrum attributed to the two rubredoxin-like FeS_4 centers, as well as a quadrupole doublet which has parameters (δ , $0.52 \text{ mm} \cdot \text{s}^{-1}$; ΔE_Q , $1.47 \text{ mm} \cdot \text{s}^{-1}$) that are typical of (μ -oxo)diiron(III) sites (13). High field studies indicate that the latter two irons are in a diamagnetic environment and suggest that the two ferric irons are antiferromagnetically coupled to produce an $S = 0$ ground state. The observed quadrupole splitting suggests the presence of an oxo bridge, similar to that seen in metHrN₃ and RRB2, but the strength of the coupling interaction has not yet been determined. The diiron center can be reduced and has Mössbauer parameters (δ , $1.30 \text{ mm} \cdot \text{s}^{-1}$; ΔE_Q , $3.14 \text{ mm} \cdot \text{s}^{-1}$) that are nearly identical with those of reduced MMO and reduced RRB2.

The UV/vis spectrum of rubrerythrin shows maxima at 365 and 490 nm with shoulders at 350 and 570 nm. This spectrum is similar to that seen in rubredoxin except that there is a higher A_{365}/A_{492} ratio in rubrerythrin. When the spectrum of Rd from *D. vulgaris* is subtracted from that of rubrerythrin, the resultant spectrum shows a λ_{max} at 365 nm (ϵ $5.3 \text{ mM}^{-1}\text{cm}^{-1}$) and shoulder at 460 nm, similar to that of metHr, which has a λ_{max} at 355 nm (ϵ $6.4 \text{ mM}^{-1}\text{cm}^{-1}$) and shoulders at 480 and 580 nm.

Besides strong signals at $g = 9.4$ and 4.3 associated with the isolated high-spin ferric centers, the EPR spectrum of rubrerythrin shows a weak signal with g values of 1.98, 1.76, and 1.57. This rhombic signal with $g < 2$ is characteristic of an antiferromagnetically coupled $\text{Fe}^{\text{II}}\text{Fe}^{\text{III}}$ site similar to those seen in the semimet forms of hemerythrin and MMO and may correspond to a small portion of the diiron site that has been reduced to the mixed-valence form. It would thus appear that rubrerythrin belongs to this new subclass of iron proteins. Efforts are underway to compare the properties of the diiron site with those of other members of the subclass and to establish what biological role this novel protein plays.

B. 3-Deoxy-D-Arabino-Heptulosonate 7-Phosphate Synthase

3-Deoxy-D-arabino-heptulosonate 7-phosphate (DAHP) synthase is the first enzyme of the common aromatic biosynthetic pathway in bacteria and plants (212). Three such isozymes have been identified in *E. coli*, which are sensitive to phenylalanine, tyrosine, and tryptophan, respectively. The tyrosine-sensitive DAHP synthase has been found to contain approximately one iron per mole of enzyme and to exhibit an absorption maximum at

350 nm (ϵ 3500 $M^{-1}cm^{-1}$) (213). There is some interesting homology in the carboxy terminal amino acid sequence of DAHP synthase with those of an iron-binding region of hemerythrin (residues 50–70 of the *P. gouldii* protein (214a), but sequences determined later for other DAHP synthases do not match (214b,c). The sequence homology, the iron content, and the absorption characteristics all hint that DAHP synthase may belong to this class of iron-oxo proteins, but this evidence is circumstantial at best and needs stronger corroboration.

V. DIMANGANESE CENTERS IN PROTEINS

Recently, proteins with proposed (μ -oxo)dimanganese active sites have emerged. In this group are the ribonucleotide reductases found in coryneform bacteria (8, 215) and catalases found in aerobic lactic acid bacteria (14). These enzymes have been proposed to have manganese analogues of the hemerythrin active site based on spectroscopic similarities of the enzymes with corresponding dimanganese models. This analogy is reasonable since Mn(III) and Fe(III) have similar ionic radii and form similar complexes. Indeed, there is a growing list of metalloenzymes where the active site can involve iron in one system and manganese in another. The best example is superoxide dismutase, which has been crystallographically characterized in its iron and manganese forms and shown to have very similar metal coordination environments (216). Other examples that are much less well characterized include homoprotocatechuate 2,3-dioxygenase (217), catalase (218), and ribonucleotide reductase; one difference between iron and manganese is the latter's greater accessibility to higher valent oxidation states. This property is presumably utilized by the oxygen evolving complex of Photosystem II in the oxidation of water, a topic formally beyond the scope of this chapter. Since much of the synthetic work on dimanganese complexes has been initiated with the oxygen evolving complex as the rationale, however, we will discuss the system briefly. Many excellent reviews on the subject have been published recently (219–222).

A. Manganese-catalase

The enzyme catalase mediates the conversion of hydrogen peroxide to water and dioxygen. While most catalases have a heme center as the prosthetic group (218), the aerobic lactic acid bacteria and their close relatives cannot produce heme, and instead, utilize a non-heme, manganese-containing "pseudocatalase" (14). Unlike heme catalases, these Mn-containing catalases are only weakly inhibited by cyanide or azide. Manganese-catalase

has been isolated from three different bacterial sources and consists of an aggregate of either four (*Thermoleophilum album*) (223), five (*Lactobacillus plantarum*) (14), or six (*Thermus thermophilus*) (224) identical subunits of 34 kDa.

Manganese-catalase exhibits a visible spectrum with λ_{\max} at 470 nm (ϵ 1350 $M^{-1}\text{cm}^{-1}$) and shoulders at 395 and 500 nm (225). That it contains dimanganese sites is indicated by crystallographic and EPR studies (15, 224, 226). The crystal structure of the *T. thermophilus* enzyme shows a bundle of four α helices with the dimanganese unit located in the center, in amazing homology to the structure of hemerythrin (2, 3). The Mn–Mn separation is estimated to be 3.6 Å; however, the resolution at this stage of structure refinement is insufficient to determine the nature of the bridging groups.

EPR studies on Mn-catalase show a multiline signal centered at $g = 2.0$ (15, 227). Below 50 K, the enzyme from *T. thermophilus* shows a dominant 18-line signal that can be fit using parameters characteristic of a $\text{Mn}^{\text{II}}\text{Mn}^{\text{III}}$ unit; this signal is strongly temperature dependent and not detectable above 50 K. At 50 K the spectrum is a superposition of a 22 line and a 16-line pattern attributed to $\text{Mn}^{\text{II}}\text{Mn}^{\text{II}}$ and $\text{Mn}^{\text{III}}\text{Mn}^{\text{IV}}$ forms, respectively (227). The EPR studies on the enzyme from *L. plantarum* reveal only the 16-line signal associated with the $\text{Mn}^{\text{III}}\text{Mn}^{\text{IV}}$ species, which is observed even at 6 K (Fig. 26) (15). This spectrum has parameters ($g = 2.0075$, $A_1 = 154$ G, $A_2 = 81$ G), which are nearly identical with those of the 16-line pattern of the enzyme from *T. thermophilus* (227). The disagreement in the two EPR studies is not resolved. Nevertheless, it is clear that there is a new active site for biological peroxide disproportionation and new mechanistic possibilities must be considered.

B. Ribonucleotide Reductase

Recently, a new type of ribonucleotide reductase that did not require coenzyme-B12 or iron for activity was discovered in the coryneform bacteria *Brevibacterium ammoniagenes* and *Micrococcus luteus* (228); this enzyme requires manganese instead. Like the diiron-containing enzyme from *E. coli*, the enzyme from *B. ammoniagenes* consists of two components, a 30 kDa B1 subunit that binds the nucleotides and 100 kDa B2 subunit consisting of two 50-kDa chains with at least one Mn per chain (8). Enzyme from Mn-deficient cells showed no ribonucleotide reductase activity but could be activated by addition of Mn^{2+} (215). Furthermore, ^{54}Mn was incorporated into the B2 subunit when the bacteria were grown on $^{54}\text{MnCl}_2$ -enriched medium (8). These experiments strongly implicate a manganese containing active site.

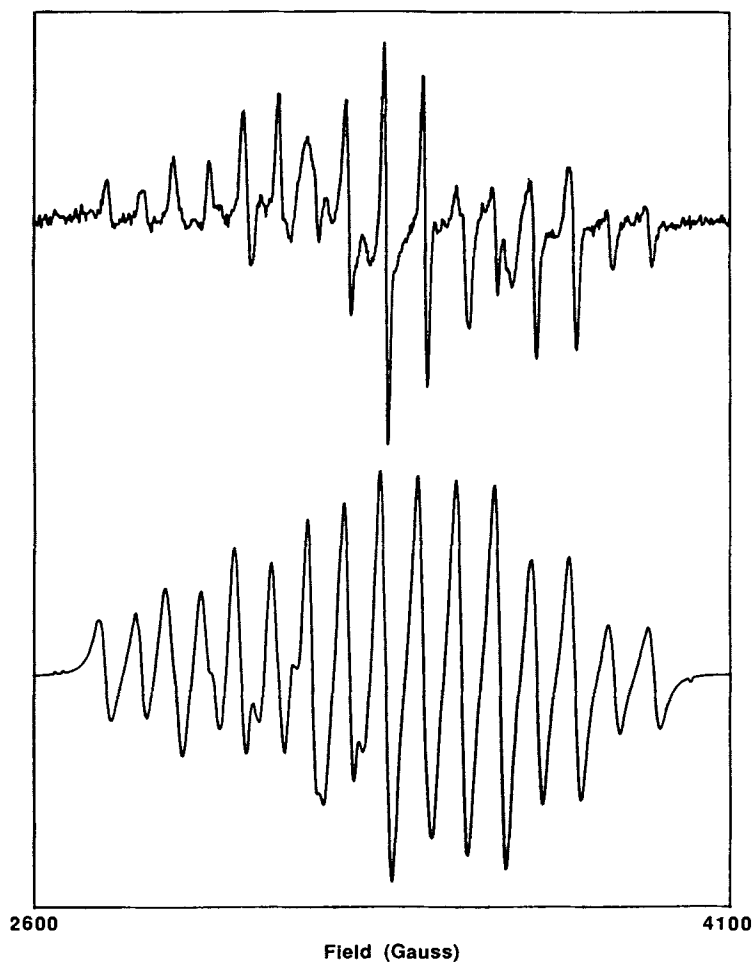


Figure 26. EPR spectrum of the manganese catalase from *L. plantarum*. Reprinted with permission from R. M. Fronko, J. E. Penner-Hahn, and C. J. Bender, *J. Am. Chem. Soc.*, 110, 7554-7555 (1988). Copyright © (1988) American Chemical Society.

The electronic spectrum of the B2 subunit ($\lambda_{\max} = 455, 485, \text{ and } 615$ nm) closely resembles those of Mn-catalase and synthetic tribridged $\text{Mn}^{\text{III}}\text{O}$ complexes (8). The metal site was thus proposed (229) to be analogous to the diiron center of the enzyme from *E. coli*. This analogy may be reasonable as iron restores 50-70% of the activity in protein derived from Mn-deprived cells (230). Similar to the enzyme from *E. coli*, the Mn-containing ribonucleotide reductase is inhibited by hydroxyurea and au-

rintricarboxylic acid (230). This result suggests that the Mn-containing enzyme may also use an organic radical in its mechanism; however, none has been detected by EPR studies. The structure of the manganese site, the involvement of a free radical, its nature, and how it is generated remain interesting problems to be solved in the future.

C. The Oxygen Evolving Center from Photosystem II

The most studied of the manganese enzymes is the oxygen evolving center from Photosystem II (PS II), which involves four Mn ions in the active site and catalyzes the four-electron oxidation of water to dioxygen in photosynthesis (219–222). Kok et al. (231) showed that the O₂-evolving complex in PS II is oxidized in four one-electron oxidation processes. The five states of this protein are designated as S₀–S₄ with S₀ being the totally reduced form. The S₄ state is only transiently stable and rapidly converts to S₀ with concomitant O₂ evolution. A complete review of this work is beyond the scope of this chapter, but several points should be made in relation to the other oxo-bridged Mn species.

EPR studies on the S₂ state of the manganese aggregate reveal a pattern at $g = 1.96$ consisting of at least 16 hyperfine lines with possibly more lines in the wings (232). This 16-line pattern was originally simulated with a pair of antiferromagnetically coupled manganese atoms (232). When the wings of the spectrum are included, however, the pattern can be reasonably fit using parameters characteristic of three Mn^{III} and one Mn^{IV} (233).

EXAFS studies on the S₁ and S₂ states of the oxygen evolving center of PS II show that each Mn atom has one Mn neighbor at 2.7 Å (234). There were also three O,N scatterers at 1.75 Å and three O,N scatterers at 1.98 Å characteristic of bridging and terminal ligands, respectively. A longer Mn–Mn interaction may also be present at 3.3 Å (220). The short Mn–ligand distances have been observed in manganese coordination chemistry only for complexes containing bridging oxide species, while the 2.7-Å Mn–Mn distance is characteristic of Mn₂(μ-O)₂ cores. Thus proposed structures for the tetramanganese center incorporate the Mn₂O₂ structural motif, including a distorted cubane-like Mn₄O₄ cluster and an Mn₄O₂ butterfly structure, both of which have been found in synthetic complexes (235).

D. Models

The emergence of dimanganese units as potential metalloprotein active sites has resulted in an intense synthetic effort to model such sites. Since the metalloproteins are not structurally well characterized, there are few

benchmarks with which to compare the synthetic analogues. Among these include the visible spectrum (Mn-catalase and ribonucleotide reductase) (8, 236), the multiline EPR signal (Mn-catalase and the oxygen evolving center) (15, 227, 233) and the Mn–Mn separation (~ 3.6 Å in Mn-catalase and 2.7 and probably 3.3 Å for the oxygen evolving complex).

1. Structural Aspects

A large number of dimanganese complexes has been synthesized and structurally characterized. They can be classified according to the nature of their bridging units, as illustrated in Fig. 27 and listed in Table VIII. Figure 28 shows the structure of the ligands. As expected, Mn–O_{oxo} bonds are short, averaging about 1.8 Å, irrespective of whether the complex contains Mn^{III} or Mn^{IV}. The Mn–Mn separation depends on the number

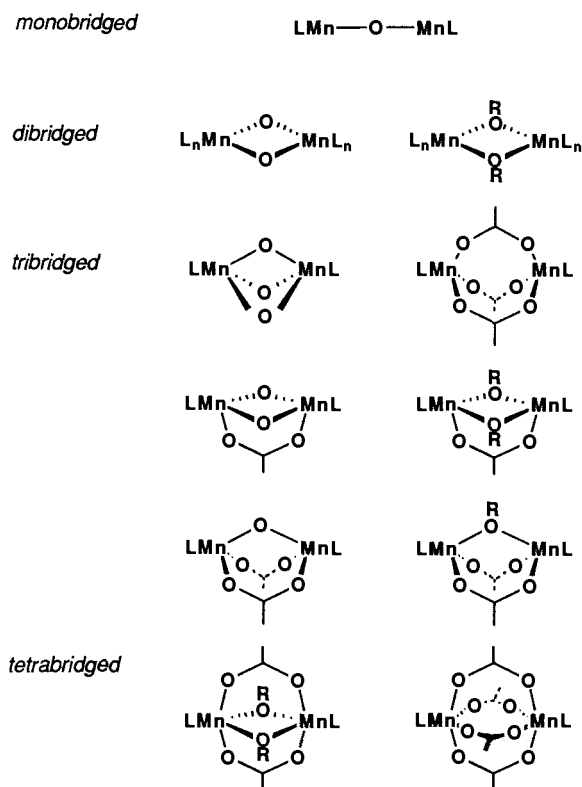


Figure 27. Structural core motifs of the synthetic dimanganese complexes.

of bridges and the nature of these bridges. The only two examples of (μ -oxo)dimanganese complexes with no additional bridges have tetradentate macrocyclic ligands and linear or nearly linear Mn–O–Mn bonds. The Mn–Mn distances are thus the sum of the Mn– μ -O bond lengths, 3.42 Å for the phthalocyanine complex (263) and 3.54 Å for the tetraphenylporphin complex (274). The presence of additional bridges serves to decrease the Mn–O–Mn angle and shorten the Mn–Mn distance. Additional carboxylate bridges result in Mn–O–Mn angles of $\sim 120^\circ$ and Mn–Mn distances of 3.1–3.2 Å (264). A second oxo bridge decreases the Mn–O–Mn angle to near 90° and the Mn–Mn distance to 2.6–2.7 Å, respectively (Table VIII), while a third oxo bridge further reduces the angle and the distance to 78° and 2.3 Å (238). It is conjectured that a metal–metal bond may be present in the tris(μ -oxo) complex, but firm evidence is lacking. The 2.6–2.7 Å Mn–Mn distance found for the bis(μ -oxo) complexes make the Mn_2O_2 unit the favored structural motif to account for the 2.7-Å distance found for the oxygen evolving complex in Photosystem II (234).

Modification of the oxo bridge invariably lengthens the Mn– μ -O bond and increases the Mn–Mn distance. The tribridged (μ -oxo)bis(μ -carboxylato)dimanganese(III) core illustrates this point well. The parent unit, of which there are seven examples, has an Mn–Mn separation of ~ 3.1 Å (229, 237, 254–257). One-electron oxidation without altering the bridges lengthens the Mn– μ -O bonds slightly and increases the Mn–Mn separation to 3.23 Å (264). In the corresponding dimanganese(II) complex, the oxo bridge is protonated, thereby increasing the Mn– μ -O bond lengths to 2.05 Å and the Mn–Mn distance to 3.35 Å (237, 238). Further protonation to a μ -aqua derivative yields Mn– μ -O bonds of 2.22 Å and a Mn–Mn distance of 3.74 Å (239). Replacement of the μ -oxo bridge to a μ -phenoxo group as in the $Mn^{II}Mn^{III}$ complexes affords Mn–Mn distances of ~ 3.5 Å. These are trends paralleled by similar tribridged diiron complexes.

The TACN and Me_3TACN complexes of Wieghardt constitute the most versatile series of compounds, affording a range of oxidation states and bridging arrangements. In total, six different core combinations can be obtained and structurally characterized, namely, $Mn_2^{II}(\mu-OH)(\mu-OAc)_2$ (237), $Mn_2^{III}(\mu-O)(\mu-OAc)_2$ (237, 254), $Mn^{III}Mn^{IV}(\mu-O)(\mu-OAc)_2$ (264), $Mn^{III}Mn^{IV}(\mu-O)_2(\mu-OAc)$ (272), $Mn_2^{IV}(\mu-O)_3$ (238), and $Mn_2^{II}(\mu-OAc)_3$ (238).

Details of the coordination chemistry about the Mn atoms are as expected from data on mononuclear complexes, with Mn(III) showing the effects of the Jahn–Teller distortion and oxo groups exerting their trans bond lengthening effects. The consequences of these occasionally competing effects are illustrated in the structures of $[Mn^{III}Mn^{IV}O_2L_2]$ and $[Mn_2^{III}O(OAc)_2L_2]$ complexes. There are two examples of mixed-valence

TABLE VIII
Properties of Dinuclear Manganese-Oxo Complexes

Compound	References	Mn- μ -O (Å)	Mn-Mn (Å)	Mn-O-Mn (degrees)	Mn-O ^{carb} (Å)	Mn-L ^{trans} ^a (Å)	Mn-L ^{cis} ^a (Å)	J (cm ⁻¹)
(μ -hydroxo)bis(μ -carboxylato) [Mn ₂ OH(OAc) ₂ (Me ₃ TACN) ₂](PF ₆) (μ -aquo)bis(μ -carboxylato)	237, 238	2.053	3.351	109.4	2.17	2.329	2.31	-9 ^b
[Mn ₂ (H ₂ O) ₃ (F ^{prop}) ₄ (NITEt) ₂] tris(μ -carboxylato)	239	2.22	3.739	114.6	2.12	2.18 ^c	2.16 ^c	-1.7
[Mn ₂ (OAc) ₃ (Me ₃ TACN) ₂](BPh) ₄ (μ -phenoxo)bis(μ -carboxylato)	238		4.034		2.12	2.35		-1.7
[Mn ₂ (BPMP)(OAc) ₂](ClO ₄) ₂	240							-4.9
[Mn ₂ (BPMP)(OBz) ₂](ClO ₄) ₂	240							-5.5
bis(μ -phenoxo) [Mn ₂ (BPEAP) ₂ (THF) ₂](ClO ₄) ₂	241	2.13	3.256	99.9		2.31 ^d	2.20	> -0.18
[Mn ₂ (BPNP) ₂ (NCS) ₂]	242	2.17	3.422	104.1		2.26	2.21	
[Mn ₂ (saldien) ₂]	243, 244							-0.63
[Mn ₂ (salps) ₂]	245	2.13	3.300	101		2.26	2.04 ^e	-1.88
[Mn ₂ (L)Cl ₂]	246	2.12	3.324	103.2		2.18	2.35 ^e	+0.24
[Mn ₂ (L')Cl ₂]	247							+0.20
tetrakis(μ -carboxylato) [Mn ₂ (C ₆ F ₅ CO ₂) ₄ (bipy) ₂]	248		3.679		2.19	2.28 ^f		-2.6
(μ -alkoxo)(μ -chloro) [Mn ₂ (HPTB)(Cl) ₂]	249		3.3 ^g					~ -1 ^g

	$Mn^{II}Mn^{III}$							
(μ -phenoxo)bis(μ -carboxylato) [Mn ₂ (BPMP)(OAc) ₂](ClO ₄) ₂	244, 250	2.193	3.447	114.4	2.12	2.21	2.30	-6.0
[Mn ₂ (BCMP)(OAc) ₂](ClO ₄) ₂	250, 251	1.903	3.422	112.1	2.01	2.05	2.15	-7.7
[Mn ₂ (BIMP)(OAc) ₂](ClO ₄) ₂	252	1.957	3.54	116.8	2.11	2.22	2.24	-4.5
bis(μ -phenoxo) [Mn ₂ (biphen) ₂ (biphenH)(bipy) ₂] bis(μ -phenoxo)(μ -chloro) [Mn ₂ (L)Cl ₂ Br]	253 246, 250	2.08 2.26 1.94	3.182 3.168	100 93.6 102.5	2.15 ^b 2.11	2.02 ^c 2.67 ^{a,j}	+0.89 -1.7	
		$Mn^{III}-Mn^{III}$						
(μ -oxo)bis(μ -carboxylato) [Mn ₂ O(OAc) ₂ (Me ₃ TACN) ₂](ClO ₄) ₂	237, 254	1.810	3.15	120.9	2.047	2.131	2.232	+9
[Mn ₂ O(OAc) ₂ (TACN) ₂] _{1,1}	237	1.788	3.096	119.9	2.06	2.068	2.18	+10
[Mn ₂ O(OAc) ₂ (TACN) ₂](ClO ₄) ₂	254	1.80	3.084	117.9	2.00	2.06	2.24	-0.5
[Mn ₂ O(OAc) ₂ (HBpz) ₂]	229	1.780	3.159	125.1	2.07	2.06	2.17	>0 ^a
[Mn ₂ O(OAc) ₂ (bipy) ₂ (N ₃) ₂]	255	1.802	3.153	122.0	2.09	2.092	2.13	<0 ^a
[Mn ₂ O(OAc) ₂ (bipy) ₂ Cl ₂]	255	3.153						-3.4
[Mn ₂ O(OAc) ₂ (bipy) ₂ (H ₂ O) ₂](PF ₆) ₂	256	1.78	3.132	122.9	1.938	2.06	2.05	+1.72
[Mn ₂ O(OAc) ₂ (BBAE) ₂](ClO ₄) ₂	257							
bis(μ -oxo) [Mn ₂ O ₂ (BMPEA) ₂](ClO ₄) bis(μ -hydroxo) [Mn ₂ (OH) ₂ (salpn) ₂] bis(μ -alkoxo)(μ -carboxylato) [Mn ₂ (salDP)(OCH ₃)(OAc)(HOCH ₃)](ClO ₄)	258 259 260	1.84 2.72 1.94	2.676 2.931	93 97.2	2.11 2.17	2.43 2.362 1.849 ^c	-10.6	

TABLE VIII (Continued)

Compound	References	Mn- μ -O (\AA)	Mn-Mn (\AA)	Mn-O-Mn (degrees)	Mn-O _{carb} (\AA)	Mn-L _{trans} ^a (\AA)	Mn-L _{cis} ^a (\AA)	J (cm^{-1})
bis(μ -alkoxo)bis(μ -carboxylato) [Mn ₂ (OAc) ₂ (spa) ₂]	261	1.92	2.869	96.34	2.23	2.006		-19.1
bis(μ -phenoxo) [Mn ₂ (sal) ₂ (py) ₂][Mn(EtOH) ₄]	262	1.911	3.247	99.78		2.299 1.863 ^c	1.91 ^c	$\leq 0^k$
(μ -oxo) [Mn ₂ O(Pc) ₂ (py) ₂]	263	1.71		178		2.15	1.97	
<i>Mn^{III}-Mn^{IV}</i>								
(μ -oxo)bis(μ -carboxylato) [Mn ₂ O(OAc) ₂ (Me ₃ TACN) ₂](ClO ₄) ₃	264	1.948 1.826	3.230	125.1	1.98	2.12	2.12	-40
bis(μ -oxo) [Mn ₂ O ₂ (tren) ₂](CF ₃ SO ₃) ₃	265	1.85 1.77	2.679	95.2 82.5		2.11 2.09	2.28 2.05	
[Mn ₂ O ₂ (phen) ₄](PF ₆) ₃	266	1.81	2.700	96.0		2.10	2.13	-148
[Mn ₂ O ₂ (bipy) ₄](ClO ₄) ₃	267	1.81	2.716	96.6		2.10	2.12	-150
[Mn ₂ O ₂ (bispcen) ₂](ClO ₄) ₃	268	1.833 1.793	2.659	94			2.169 2.092	
[Mn ₂ O ₂ (BPG) ₂]	269	1.80	2.656	94	1.96 ^c 2.08	2.14		
[Mn ₂ O ₂ (TPA) ₂](S ₂ O ₃) _{3/2}	270, 271	1.84 1.78	2.643	94		2.08 2.05	2.23 2.01	-159

	<i>MnIV-Mn^{IV}</i>						
bis(μ -oxo)(μ -carboxylato)							
[Mn ₂ O ₂ (OAc)(TACN) ₂](BPh ₄) ₂	272	1.81	2.588	91.1	2.079	2.11	2.13 ^c
[Mn ₂ O ₂ (OAc)(bipy) ₂ Cl ₂]	253	1.82	2.667	94	2.203	2.33 ^e	2.15
					2.047	2.10	2.05
tris(μ -oxo)							
[Mn ₂ O ₃ (Me ₃ TACN) ₂](PF ₆)	238	1.82	2.296	78		2.11	-390
bis(μ -oxo)							
[Mn ₂ O ₃ (phen) ₄](ClO ₄) ₄	266	1.80	2.748	99.5		2.08	-144
[Mn ₂ O ₂ (TPA) ₂](ClO ₄) ₄	271						-137
[Mn ₂ O ₂ (bispicen) ₂](ClO ₄) ₄	273	1.81	2.672	95.1		2.06	-126
[Mn ₂ O ₃ (OH) ₂ (TACN) ₂]	238	1.83	2.625	91.9		2.06	$\leq 0^*$
[Mn ₃ (C ₂ O ₄) ₄ (OH) ₂] (μ -oxo)							1.881 ^c
[Mn ₂ O(TPP) ₂ (N ₃) ₂]	274	1.77	3.537	180		2.00	$\leq 0^*$

^aThe Mn-L distances refer to Mn-N distances unless otherwise noted.

^bClO₄ salt.

^cThis is a Mn-O distance.

^dThere are 1N and 1O ligands trans to the phenoxo bridges.

^eThis is a Mn-Cl distance.

^fThere is no trans and cis distinction in the nonbridging ligands.

^gBased on EPR measurements.

^h3N and 1O.

ⁱ2O and 1N.

^jThis is a Mn-Br distance.

^k>0 means weakly ferromagnetic, <0 means weakly antiferromagnetic, ≤ 0 means strongly antiferromagnetic.

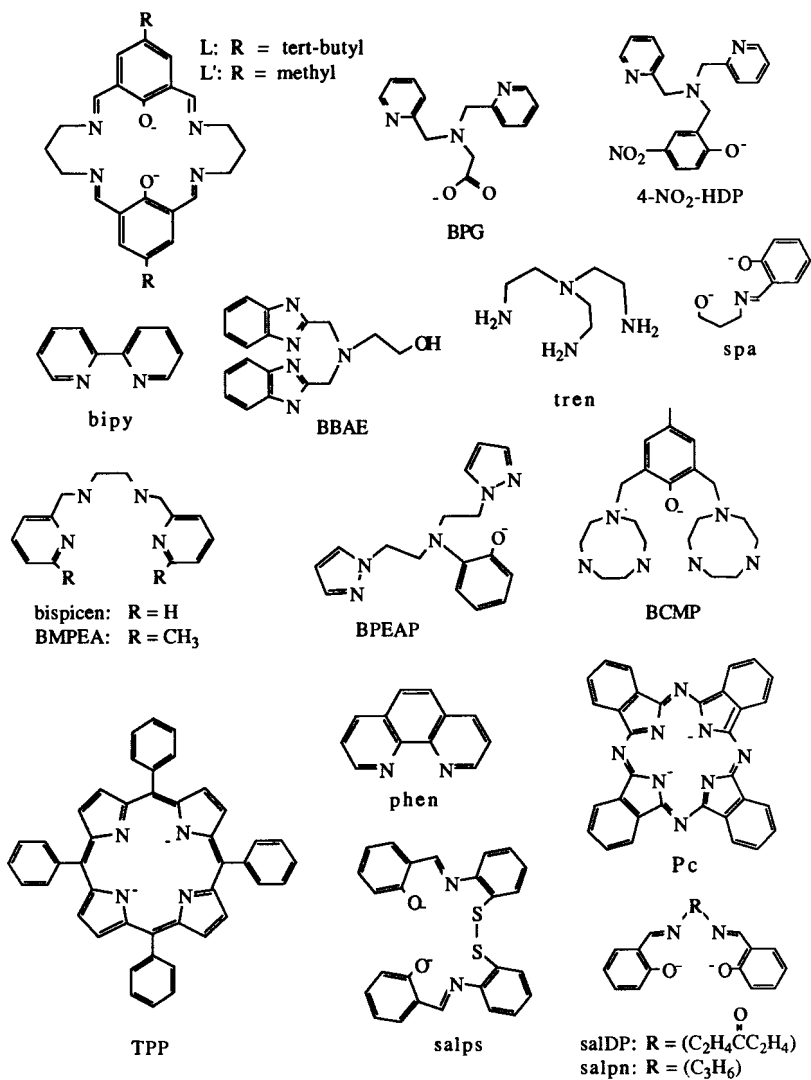


Figure 28. Structures of additional ligands and their abbreviations.

Mn_2O_2 complexes where the oxidation states of the metal atoms can be assigned (L = TPA, tren) (265, 270). In these cases, the $Mn^{IV}-O_{oxo}$ bonds are clearly shorter than the corresponding $Mn^{III}-O_{oxo}$ bonds by 0.06–0.08 Å. On the Mn^{IV} ion, the Mn–N bonds trans to the oxo groups are slightly longer than those cis to the oxo groups; on the Mn^{III} ion, the Mn–N bonds trans to the oxo groups are significantly shorter than those cis to the oxo groups, the dramatic elongation of the latter bonds being ascribed to Jahn–

Teller effects. In the $[\text{Mn}_2^{\text{III}}\text{O}(\text{OAc})_2\text{L}_2]$ complexes, the Mn–N bonds trans to the oxo groups do not differ much in length from their cis analogues, in contrast to what is observed for the iron derivatives. Wieghardt argues that this result is due to Jahn–Teller compression along the $\text{O}_{\text{oxo}}\text{–Mn–N}$ axis congruent with the requirement for a short Mn– O_{oxo} bond (237). The compression should shorten the Mn– N_{trans} bond, but this effect is canceled by the trans effect of the oxo group, thus yielding an Mn–N bond comparable in length to the others.

2. Electronic Spectra

Detailed comparisons of the electronic spectral properties of the various dimanganese complexes have not yet been carried out and undoubtedly will contribute to our understanding of their electronic structures. The $(\mu\text{-oxo})\text{bis}(\mu\text{-carboxylato})\text{dimanganese(III)}$ complexes exhibit spectra (Fig. 29) that are remarkably similar to those of Mn-catalase and ribonucleotide reductase. The features in the visible region are probably ligand-field transitions by analogy to mononuclear Mn(III) complexes; however, some intensity may be due to charge-transfer transitions of the $[\text{Mn}_2\text{O}(\text{OAc})_2]^{2+}$ core, because Mn–O–Mn vibrations at 558 and 717 cm^{-1} are observed with 406.7 nm excitation and Mn(OAc) modes at $\sim 340\text{ cm}^{-1}$ are enhanced with 457–488 nm excitation (229).

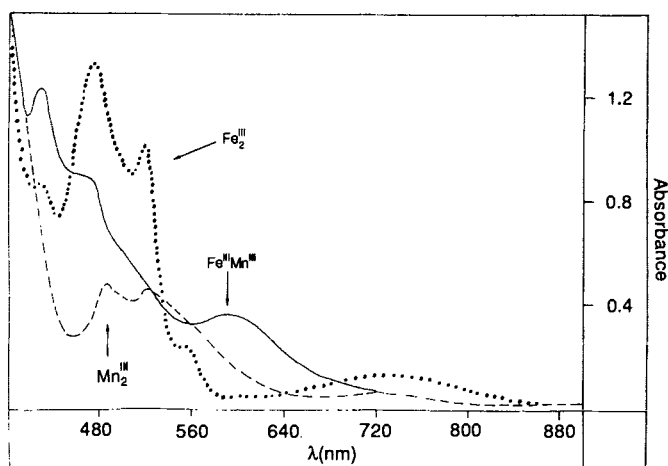


Figure 29. Electronic spectra of $[\text{MM}'\text{O}(\text{OAc})_2(\text{Me}_3\text{TACN})_2]^{2+}$. Reprinted with permission from Ref. 113. Copyright © 1989 The Chemical Society.

3. EPR Properties

Multiline EPR signals are observed for all the mixed-valence complexes. These signals arise from $S = \frac{1}{2}$ states derived from antiferromagnetic coupling of Mn(III) and Mn(II) or Mn(IV) ions, the multiplicity of the signals resulting from distinct ^{55}Mn ($I = \frac{5}{2}$) nuclei. In general, the $\text{Mn}^{\text{III}}\text{Mn}^{\text{IV}}\text{O}_2$ complexes exhibit a 16-line signal (Fig. 30*b*), which is observable even

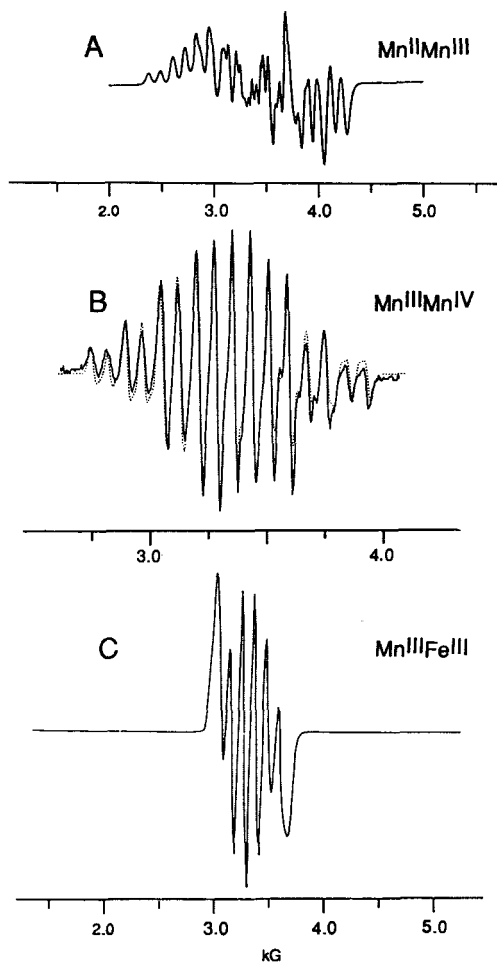


Figure 30. EPR spectra of (a) $[\text{Mn}_2(\text{BCMP})(\text{OAc})_2](\text{ClO}_4)_2$, (b) $[\text{Mn}_2\text{O}_2(\text{tren})_2](\text{ClO}_4)_3$, and (c) $[\text{FeMnO}(\text{OAc})_2(\text{Me}_3\text{TACN})](\text{ClO}_4)_2$. Reprinted with permission from Refs. 113, 250, 265. © American Chemical Society and The Chemical Society.

above liquid nitrogen temperatures because of their large J values (cf. Section V.D.4). A values of 160 ± 10 and 78 ± 3 G for the two inequivalent ^{55}Mn nuclei can be derived from the spectra (265, 269, 272, 275), and these match the 16-line spectrum of Mn-catalase well (15).

The $\text{Mn}^{\text{II}}\text{Mn}^{\text{III}}(\text{OPh})(\text{OAc})_2$ complexes typically have a 29-line EPR signal (Fig. 30a) (240, 250, 252). Because of the weak antiferromagnetic coupling between the metal centers, these signals are more difficult to simulate. The d^4 – d^5 system requires a 30×30 spin Hamiltonian energy matrix that includes the effects of magnetic exchange, the single ion zero-field splittings, and the Zeeman interaction. Hendrickson and his co-workers (250, 251) provide a detailed report of these efforts.

The weak antiferromagnetic coupling found in the $\text{Mn}^{\text{II}}\text{Mn}^{\text{III}}$ complexes also allows the population of higher states of the spin manifold at fairly low temperatures. Thus, broad features at $g \sim 4$ observed even at 7.5 K are ascribed to the $S = \frac{3}{2}$ state, and signals near $g \sim 8$ can be discerned at 30 K that may arise from the $S = \frac{5}{2}$ state (250).

EPR signals of one other complex deserves brief mention. Christou and his co-workers (253) report that $\text{Mn}_2(\text{biphen})_2(\text{biphenH})(\text{bipy})_2$ with a $\text{Mn}^{\text{II}}\text{Mn}^{\text{III}}(\mu\text{-OPh})_2$ core exhibits signals at $g = 12$, 5.1 (with ^{55}Mn splitting), 2.01, and 1.47. These signals may derive from a ferromagnetically coupled $\text{Mn}^{\text{II}}\text{Mn}^{\text{III}}$ unit ($J = 0.89 \text{ cm}^{-1}$) and needs further investigation.

4. Magnetic Properties

In general, the magnetic interactions between manganese ions in a dinuclear complex are strongest at higher oxidation states and decrease as the metal centers become more reduced (Table VIII). The $\text{Mn}_2^{\text{IV}}\text{O}_3$ core shows by far the largest antiferromagnetic coupling ($J = -390 \text{ cm}^{-1}$), very likely enhanced by the short Mn–Mn distance and the multiple superexchange pathways (238). The $\text{Mn}_2^{\text{IV}}\text{O}_2$ and $\text{Mn}_2^{\text{IV}}\text{O}$ cores also exhibit strong antiferromagnetic coupling; J values for $[\text{Mn}_2\text{O}_2(\text{phen})_4]^{4+}$ and $[\text{Mn}_2\text{O}_2(\text{TPA})_2]^{4+}$ are -144 and -137 cm^{-1} , respectively (266, 271).

The addition of one electron into the Mn_2O_2 core does not appear to alter the coupling. All dibridged $\text{Mn}^{\text{III}}\text{Mn}^{\text{IV}}\text{O}_2$ complexes exhibit J values of $(-150 \pm 10) \text{ cm}^{-1}$ (see Table VIII). The presence of an additional carboxylate, however, has unpredictable effects. The TACN complex has a J value of -220 cm^{-1} (272), while the (bipy,Cl) complex has a J value of -114 cm^{-1} (253). The conversion of a $\text{Mn}^{\text{III}}\text{Mn}^{\text{IV}}\text{O}_2(\text{OAc})$ core to a $\text{Mn}^{\text{III}}\text{Mn}^{\text{IV}}\text{O}(\text{OAc})_2$ core leads to a significant weakening of the coupling to -40 cm^{-1} (264). But, more interestingly, reduction of the $\text{Mn}^{\text{III,IV}}\text{O}(\text{OAc})_2$ core by one electron almost eliminates any magnetic interaction. Indeed, of the six examples with the $\text{Mn}_2^{\text{II}}\text{O}(\text{OAc})_2$ core, three exhibit weak an-

tiferromagnetic coupling while the other three show weak ferromagnetic coupling.

The weakness of the magnetic interaction in the $\text{Mn}_2^{\text{III}}\text{O}(\text{OAc})_2$ core, particularly as compared to the strong antiferromagnetic coupling observed for the corresponding $\text{Fe}_2^{\text{III}}\text{O}(\text{OAc})_2$ core (cf. Section II.A.1), has been the subject of some discussion. Sheats et al. (229) suggested that, since the $\text{M}-\text{O}_{\text{oxo}}$ bond is the shortest bond in both Mn and Fe complexes, the d_z^2 orbital would be expected to be the most destabilized among the five $3d$ orbitals of each metal center. Coupling might then be expected to result from a $d_z^2-d_z^2$ interaction via the oxo bridge. The fact that this orbital would be occupied in the Fe case and unoccupied in the Mn case would explain the difference in magnetic interactions.

This hypothesis was put to test with the synthesis of the heterobimetallic $[\text{Fe}^{\text{III}}\text{Mn}^{\text{III}}\text{O}(\text{OAc})_2(\text{Me}_3\text{TACN})]^{2+}$ (113). Although not crystallographically characterized, the FeMn complex exhibits an optical spectrum that is distinct from an equimolar mixture of the two homodinuclear complexes (Fig. 29). More compelling is the observation of an EPR signal from the expected $S = \frac{1}{2}$ ground state showing six ^{55}Mn hyperfine lines (Fig. 30c, $A_{\text{Mn}}(S = \frac{1}{2})$, 110 G or $a_{\text{Mn}}^{\text{III}}$, 82.5 G). If a $d_z^2-d_z^2$ interaction were the dominant pathway for antiferromagnetic coupling, then the FeMn complex should be weakly coupled; however, a J value of -72 cm^{-1} is observed. In an analysis of the magnetic orbitals of the $\text{M}_2^{\text{III}}\text{O}(\text{OAc})_2$ core, Girerd and his co-workers (113, 276) proposed that the dominant pathway for antiferromagnetic coupling must be the $d_z^2-d_{xz}$ pathway to explain the magnetic properties of all three complexes. Indeed, J_{MnFe} is predicted to be approximately 60% of J_{FeFe} based on the fact that there are two $d_z^2-d_{xz}$ pathways in the diiron case and only one in the FeMn case and that the diiron case has 25 microstates while the FeMn case has only 20 $[(1/20)/(2/25)]$. This relationship is observed. Other Mn_2^{III} , $\text{Mn}^{\text{II}}\text{Mn}^{\text{III}}$, and Mn_2^{II} complexes exhibit weak coupling; but these complexes have not been compared in sufficient detail to yield insights.

5. Redox Properties

The redox properties of the dimanganese model complexes are listed in Table IX. In general, three redox states can be accessed electrochemically. For oxo-bridged complexes, the Mn_2^{IV} , $\text{Mn}^{\text{III}}\text{Mn}^{\text{IV}}$, and Mn_2^{III} can be attained with the $\text{Mn}_2^{\text{IV}}/\text{Mn}^{\text{III}}\text{Mn}^{\text{IV}}$ couple at about 1–1.8 V vs. NHE and the $\text{Mn}^{\text{III}}\text{Mn}^{\text{IV}}/\text{Mn}_2^{\text{III}}$ couple 0.6–0.9 V lower. The phenoxo-bridged complexes, on the other hand, access the Mn_2^{III} , $\text{Mn}^{\text{II}}\text{Mn}^{\text{III}}$, and Mn_2^{II} states in the same potential range. This positive shift in potential when the oxo bridge

TABLE IX
 Redox Potentials of Dimanganese Complexes^a

Complex	References	IV,IV/III,IV	III,IV/III,III	III,III/II,III	II,III/II,II
μ-Oxo-complexes					
[Mn ₂ O ₂ (bipy) ₄]	277	+ 1.56 ^b	+ 0.60 ^b		
[Mn ₂ O ₂ (phen) ₄]	266	+ 1.280	+ 0.340		
[Mn ₂ O ₂ (tren) ₂]	265	+ 1.030 ^{c,d}	+ 0.282 ^c		
[Mn ₂ O ₂ (TPA) ₂]	270	+ 1.14 ^{b,e}	+ 0.44 ^{b,d}		
	271	+ 1.28 ^b	+ 0.48 ^b		
[Mn ₂ O ₂ (bispicen) ₂]	268	+ 0.99 ^{b,d}	+ 0.38 ^{b,d}		
[Mn ₂ O ₂ (BPG) ₂]	269	+ 1.00 ^b	+ 0.220 ^b		
[Mn ₂ O ₂ (BMPEA) ₂]	258	+ 1.534 ^{c,d}	+ 0.765 ^{c,d}		
[Mn ₂ O ₂ (cyclam) ₂](ClO ₄) ₃	278	+ 1.22 ^f	+ 0.22 ^f		
[Mn ₂ O ₂ (cyclen) ₂](ClO ₄) ₃	278	+ 1.12 ^f	+ 0.37 ^f		
[Mn ₂ O(OAc) ₂ (Me ₃ TACN) ₂]	238, 264	+ 1.76 ^g	+ 1.10 ^g	+ 0.02 ^g	
[Mn ₂ O(OAc) ₂ (HBpz ₃) ₂]	229	+ 1.77 ^{d,g}	+ 1.06 ^{d,g}		
[Mn ₂ O(OAc) ₂ Cl ₂ (bipy) ₂]	255	+ 1.50 ^{d,g}	+ 0.93 ^g		
[Mn ₂ O(OAc) ₂ (N ₃) ₂ (bipy) ₂]	255		+ 0.95 ^g		
μ-Phenoxo complexes					
[Mn ₂ (BPMP)(OAc) ₂]	240			+ 1.44 ^b	+ 0.71 ^{b,c}
	250b			+ 1.146 ^{d,g}	+ 0.616 ^{d,g}
[Mn ₂ (BPMP)(OBz) ₂]	240a			+ 1.31 ^b	+ 0.77 ^b
[Mn ₂ (BCMP)(OAc) ₂]	250, 251			+ 0.896 ^{d,g}	+ 0.415 ^{d,g}
[Mn ₂ (BIMP)(OAc) ₂]	252			+ 1.210 ^{e,d}	+ 0.632 ^{c,d}
[Mn ₂ LCI ₂]	246			+ 1.20	+ 0.596
[Mn ₂ LBr ₂]	246			+ 1.30	+ 0.629
μ-Hydroxo complexes					
[Mn ₂ OH(OAc) ₂ (Me ₃ TACN) ₂]	264			+ 1.05 ^{d,g}	+ 0.70 ^{d,g}

^aAll potentials reported vs. NHE.

^bOriginally reported as vs. SCE (+ 0.24-V correction factor).

^cOriginally reported as vs. Ag/AgCl (+ 0.20-V correction factor).

^dQuasireversible.

^eIrreversible.

^fOriginally reported as vs. Ag/Ag⁺ (+ 0.57-V correction factor).

^gOriginally reported as vs. Fc⁺/Fc (+ 0.55-V correction factor).

is replaced by phenoxide is also observed in iron chemistry (cf. Section II.D.2).

There is not much work thus far modeling the reaction chemistry of the dimanganese proteins; more will undoubtedly be published in the near future. Dismukes and his co-workers (249) have found that [Mn₂(HPTB)Cl₃] decomposes H₂O₂ catalytically with an initial rate proportional to [H₂O₂]²[complex], while mononuclear Mn(II) is ineffective. It is proposed that the reaction proceeds through the initial formation of a Mn^{III}(μ-O)

intermediate; this observation may serve as a basis for an analogous mechanism for the function of the Mn-catalase but will need further investigation.

VI. PERSPECTIVES

M–O–M units are emerging as important structural motifs in metalloproteins. Besides the diiron and dimanganese proteins discussed in this review, such structures are likely for dicopper centers (279, 280) and possible for the nickel sites in urease (281). There has been an explosion of literature relating to this area, and this high level of activity will undoubtedly continue, given the interest in and importance of the various systems that contain such sites in proteins. What we would like to emphasize is the breadth of expertise that has been needed for our understanding of these active sites to the present stage, which include physics, spectroscopy, synthetic chemistry, mechanistic chemistry, biochemistry, molecular biology, and microbiology; these talents will be required to uncover further secrets that nature has hidden in the chemistry of these fascinating metalloproteins.

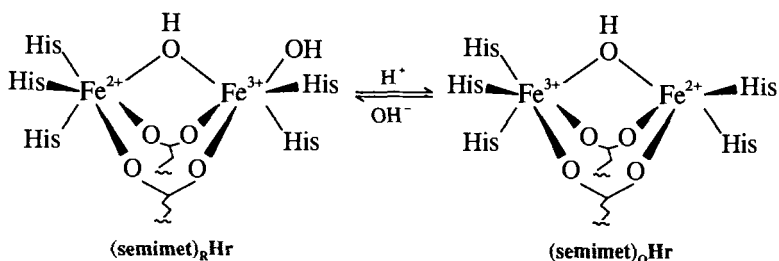
ACKNOWLEDGMENTS

This review was written with the support of the National Institutes of Health (GM-38767) and the National Science Foundation (DMB-8804458). These agencies have also supported the work from the Que laboratory that is cited in this manuscript. A. E. T. is grateful for a National Research Service Fellowship from the N. I. H. (GM-12792). We thank our colleagues in the Minnesota Metalloprotein Interest Group for their enthusiastic support and stimulating discussions, including Eckard Münck, John Lipscomb, Edmund Day, Bridget Brennan, Andy Borovik, Sheila David, Brian Fox, Michael Hendrich, Ted Holman, Randy Leising, John Lynch, Stephane Menage, Vasilios Papaefthymiou, Linda Pearce, Richard Norman, and Robert Scarrow. We would also like to thank Professor Stephen J. Lippard, Professor Joann Sanders-Loehr, and Professor Karl Wieghardt for valuable input.

ADDENDUM

SemimetHr. Based on recent CD and MCD data, McCormick and Solomon (282) found that the Fe^{II} sites in (semimet)_RHr and (semimet)_OHr differ substantially. They propose that the Fe^{III} sites are six coordinate in

both semimet forms while the Fe^{II} sites are six and five coordinate in $(\text{semimet})_{\text{R}}\text{Hr}$ and $(\text{semimet})_{\text{O}}\text{Hr}$, respectively. Furthermore, the two forms appear to be related by a pH equilibrium. Together with previous observations on the redox kinetics of hemerythrin (51) and the similarity of the antiferromagnetic interactions in both semimet forms (51, 89), the new data suggest the following scheme:



It has been previously noted that electron transfer is facile for the $\text{metHr}/(\text{semimet})_{\text{R}}\text{Hr}$ and $(\text{semimet})_{\text{O}}\text{Hr}/\text{deoxyHr}$ couples (6, 148). With the five-coordinate Fe^{II} site, $(\text{semimet})_{\text{O}}\text{Hr}$ can be readily reduced to deoxyHr without significant structural rearrangement (282). On the other hand, the presence of hydroxide as an exogenous ligand for the Fe^{III} site in $(\text{semimet})_{\text{R}}\text{Hr}$ allows the facile deprotonation of the hydroxo bridge to form the oxo-bridged metHr . This scheme also accounts for the lack of pH dependence for the $\text{metHr}/(\text{semimet})_{\text{R}}\text{Hr}$ couple (147). The transfer of the second electron in either direction becomes relatively more difficult because of the structural reorganization required for the intramolecular electron-transfer process.

MMO_{red} . Further analysis of the integer spin EPR signal of the diferrous form of MMO indicates that the scheme in Fig. 13, which depicts an axial system with $D < 0$ and $J \gg D$, cannot apply to this particular system (283). For MMO_{red} , the EPR signal can be accounted for quantitatively with either of two models: (1) $|J| \gg |D|$, $D > 0$, $E/D = 0.16$ or (2) $|J| < |D|/3$, $D < 0$. In the first case, the resonance would still be from an $S_{\text{T}} = 4$ multiplet similar to that depicted in Fig. 13, except that the multiplet must be inverted. In the second case, however, the total spin, S_{T} , is not a valid quantum number and Fig. 13 would not apply. Currently, the spectroscopic data cannot differentiate between the two models; nevertheless, the analysis concludes that the $g = 16$ signal that is observed for MMO is a consequence of a ferromagnetic interaction between the two Fe^{II} centers.

Manganese-Catalase. A recent ESEEM study by Dikanov et al. (284) on the manganese-catalase from *T. thermophilus* reports evidence for an

imidazole group near the dimanganese active site. The value of the isotropic hyperfine coupling interaction ($A = 2.3 \pm 0.5$ MHz) and the magnitude of the anisotropic component of this coupling indicates a nitrogen atom that is not directly coordinated by manganese but one further removed from the region of principal unpaired electron density. Dikanov et al. suggest that this effect is from the uncoordinated nitrogen of a ligated histidine residue.

Recent Results. Noteworthy papers have recently appeared regarding the generation of tyrosyl radical from metRRB2 (285, 286) and the formation of dioxygen complexes from nonheme ferrous precursors (287, 288).

REFERENCES

1. Other recent reviews on the subject: (a) L. Que, Jr., and R. C. Scarrow, in *Metal Clusters in Proteins*, L. Que, Jr., Ed., American Chemical Society, Washington, DC, 1988, pp. 152–178. (*ACS Symp. Ser.*, Vol 372). (b) S. J. Lippard, *Angew. Chem. Intl. Ed. Engl.*, 27, 344–361 (1988). (c) J. Sanders-Loehr, in *Iron Carriers and Iron Proteins*, T. M. Loehr, Ed., VCH, New York, 1989, pp. 375–466.
2. R. E. Stenkamp, L. C. Sieker, and L. H. Jensen, *J. Am. Chem. Soc.*, 106, 618–622 (1984).
3. S. Sheriff, W. A. Hendrickson, and J. L. Smith, *J. Mol. Biol.*, 197, 273–296 (1987).
4. F. A. Cotton and G. Wilkinson, *Advanced Inorganic Chemistry*, 5th ed.; Wiley, New York, 1988, pp. 466–467.
5. I. M. Klotz and D. M. Kurtz, Jr., *Acct. Chem. Res.*, 17, 16–22 (1984).
6. P. C. Wilkins and R. G. Wilkins, *Coord. Chem. Rev.*, 79, 195–214 (1987).
7. B.-M. Sjöberg and A. Gräslund, *Adv. Inorg. Biochem.*, 5, 87–110 (1983).
8. A. Willing, H. Follmann, and G. Auling, *Eur. J. Biochem.*, 170, 603–611 (1988).
9. B. C. Antanaitis and P. Aisen, *Adv. Inorg. Biochem.*, 5, 111–136 (1983).
10. K. Doi, B. C. Antanaitis, and P. Aisen, *Struct. Bonding (Berlin)*, 70, 1–26 (1988).
11. (a) B. G. Fox, W. A. Froland, J. E. Dege, and J. D. Lipscomb, *J. Biol. Chem.*, 264, 10023–10033 (1989). (b) B. G. Fox and J. D. Lipscomb, *Biochem. Biophys. Res. Commun.*, 154, 165–170 (1988).
12. M. P. Woodland and H. Dalton, *J. Biol. Chem.*, 259, 53–59 (1984).
13. J. LeGall, B. C. Prickrill, I. Moura, A. V. Xavier, J. J. G. Moura, and B.-H. Huynh, *Biochemistry*, 27, 1636–1642 (1988).
14. W. F. Beyer, Jr. and I. Fridovich, *Biochemistry*, 24, 6460–6467 (1985).

15. R. M. Fronko, J. E. Penner-Hahn, and C. J. Bender, *J. Am. Chem. Soc.*, *110*, 7554–7555 (1988).
16. (a) H. Dalton, in *Microb. Growth Cl Compd., Proc. Int. Symp.*, 3rd meeting date 1980, H. Dalton, Ed., Heyden, London, 1981, pp. 1–10. (b) H. Dalton and D. J. Leak, *Spec. Publ. Soc. Gen. Microbiol.*, *14*, 173–213 (1985).
17. M. Fontecave, R. Eliasson, and P. Reichard, *J. Biol. Chem.*, *264*, 9164–9170 (1989).
18. C. Manwell and C. M. A. Baker, *Comp. Biochem. Physiol. B. Comp. Biochem.*, *89B*, 453–463 (1988).
19. R. E. Stenkamp, L. C. Sieker, L. H. Jensen, J. D. McCallum, and J. Sanders-Loehr, *Proc. Natl. Acad. Sci. USA*, *82*, 713–716 (1985).
20. G. W. Ashley, G. Harris, and J. Stubbe, *J. Biol. Chem.*, *261*, 3958–3964 (1986).
21. (a) T. Barlow, *Biochem. Biophys. Res. Commun.*, *155*, 747–753 (1988). (b) M. Fontecave, R. Eliasson, and P. Reichard, *Proc. Natl. Acad. Sci. USA*, *86*, 2147–2151 (1989).
22. A. Aberg, S. Hahne, M. Karlsson, Å. Larsson, M. Ormö, A. Åhgren, and B.-M. Sjöberg, *J. Biol. Chem.* *264*, 12249–12252 (1989).
23. A. Larsson and B.-M. Sjöberg, *EMBO J.*, *5*, 2037–2040 (1986).
24. L. Petersson, A. Gräslund, A. Ehrenberg, B.-M. Sjöberg, and P. Reichard, *J. Biol. Chem.*, *255*, 6706–6712 (1980).
25. (a) B.-M. Sjöberg, S. Hahne, M. Karlsson, H. Jörnvall, M. Göransson, and B. E. Uhlin, *J. Biol. Chem.*, *261*, 5658–5662 (1986). (b) S. P. Salowe and J. Stubbe, *J. Bacteriol.*, *165*, 363–366 (1986).
26. C. L. Atkin, L. Thelander, P. Reichard, and G. Lang, *J. Biol. Chem.*, *248*, 7464–7472 (1973).
27. J. B. Lynch, C. Juarez-Garcia, E. Münck, and L. Que, Jr., *J. Biol. Chem.*, *264*, 8091–8096 (1989).
28. J. Carlson, J. A. Fuchs, and J. Messing, *Proc. Natl. Acad. Sci. USA*, *81*, 4294–4297 (1984).
29. P. Nordlund, B.-M. Sjöberg, and H. Ecklund, *Nature (London)*, *345*, 593–598 (1990).
30. (a) J. Green and H. Dalton, *Biochem. J.*, *259*, 167–172 (1989). (b) M. P. Woodland, D. S. Patil, R. Cammack, and H. Dalton, *Biochim. Biophys. Acta*, *873*, 237–242 (1986).
31. B. G. Fox, K. K. Surerus, E. Münck, and J. D. Lipscomb, *J. Biol. Chem.*, *263*, 10553–10556 (1988).
32. H. Dalton, *Adv. Appl. Microbiol.*, *26*, 71–87 (1980).
33. (a) K. S. Murray, *Coord. Chem. Rev.*, *12*, 1–35 (1974). (b) D. M. Kurtz, Jr., *Chem. Rev.*, *90*, 585–606 (1990).
34. J. W. Dawson, H. B. Gray, H. E. Hoenig, G. R. Rossman, J. M. Schredder, and R.-H Wang, *Biochemistry*, *11*, 461–465 (1972).

35. M. J. Maroney, D. M. Kurtz, Jr., J. M. Nocek, L. L. Pearce, and L. Que, Jr., *J. Am. Chem. Soc.*, *108*, 6871–6879 (1986).
36. P. E. Clark and J. Webb, *Biochemistry*, *20*, 4628–4632 (1981).
37. K. Garbett, D. W. Darnall, I. M. Klotz, and R. J. P. Williams, *Arch. Biochem. Biophys.*, *103*, 419–434 (1969).
38. M. Y. Okamura, I. M. Klotz, C. E. Johnson, M. R. C. Winter, and R. J. P. Williams, *Biochemistry*, *8* 1951–1958 (1969).
39. K. Zhang, E. A. Stern, F. Ellis, J. Sanders-Loehr, and A. K. Shiemke, *Biochemistry*, *27*, 7470–7479 (1988).
40. (a) R. C. Scarrow, M. J. Maroney, S. M. Palmer, L. Que, Jr., A. L. Roe, S. P. Salowe, J. Stubbe, *J. Am. Chem. Soc.*, *109*, 7857–7864 (1987). (b) R. C. Scarrow, M. J. Maroney, S. M. Palmer, L. Que, Jr., S. P. Salowe, and J. Stubbe, *J. Am. Chem. Soc.*, *108*, 6832–6834 (1986).
41. G. Bunker, L. Petersson, B.-M. Sjöberg, M. Sahlin, M. Chance, B. Chance, and A. Ehrenberg, *Biochemistry*, *26*, 4708–4716 (1987).
42. R. C. Prince, G. N. George, J. C. Savas, S. P. Cramer, and R. N. Patel, *Biochim. Biophys. Acta*, *952*, 220–229 (1988).
43. R. B. Lauffer, B. C. Antanaitis, P. Aisen, and L. Que, Jr., *J. Biol. Chem.*, *258*, 14212–14218 (1983).
44. P. G. Debrunner, M. P. Hendrich, J. de Jersey, D. T. Keough, J. T. Sage, and B. Zerner, *Biochim. Biophys. Acta.*, *745*, 103–106 (1983).
45. J. W. Pyrz, J. T. Sage, P. G. Debrunner, and L. Que, Jr., *J. Biol. Chem.*, *261*, 11015–11020 (1986).
46. R. C. Scarrow and L. Que, Jr., unpublished observations.
47. B. A. Averill, J. C. Davis, S. Burman, T. Zirino, J. Sanders-Loehr, T. M. Loehr, J. T. Sage, and P. G. Debrunner, *J. Am. Chem. Soc.*, *109*, 3760–3767 (1987).
48. S. M. Kauzlarich, B. K. Teo, T. Zirino, S. Burman, J. C. Davis, and B. A. Averill, *Inorg. Chem.*, *25*, 2781–2785 (1986).
49. (a) R. C. Reem and E. I. Solomon, *J. Am. Chem. Soc.*, *106*, 8323–8325 (1984). (b) R. C. Reem and E. I. Solomon, *J. Am. Chem. Soc.*, *109*, 1216–1226 (1987).
50. M. Sahlin, A. Graslünd, L. Petersson, A. Ehrenberg, and B.-M. Sjöberg, *Biochemistry*, *28*, 2618–2625 (1989).
51. L. L. Pearce, D. M. Kurtz, Jr., Y.-M. Xia, and P. G. Debrunner, *J. Am. Chem. Soc.*, *109*, 7286–7293 (1987).
52. A. Ericson, B. Hedman, K. O. Hodgson, J. Green, H. Dalton, J. G. Bentsen, R. H. Beer, S. J. Lippard, *J. Am. Chem. Soc.*, *110*, 2330–2332 (1988).
53. B. G. Fox, *Mechanistic Studies of the Catalytic Cycle of Methane Monooxygenase from Methylosinus trichosporium OB3b*, Ph.D. Thesis, University of Minnesota (1989).
54. E. P. Day, S. S. David, J. Peterson, W. R. Dunham, J. J. Bonvoisin, R. H. Sands, and L. Que, Jr., *J. Biol. Chem.*, *263*, 15561–15567 (1988).

55. S. Keresztes-Nagy and I. M. Klotz, *Biochemistry*, **4**, 919–930 (1965).
 56. J. Sanders-Loehr, T. M. Loehr, A. G. Mauk, and H. B. Gray, *J. Am. Chem. Soc.*, **102**, 6992–6996 (1980).
 57. List of Abbreviations Used in this Text

Abbreviation	Name
BBA	bis(2-benzimidazolymethyl)amine
BBAE	2-bis(2-benzimidazolymethyl)aminoethanol
BBMP	2,6-bis[bis(2-benzimidazolymethyl)aminomethyl]-4-methylphenol
BCMP	2,6-bis(1,4,7-triazacyclonon-1-ylmethyl)-4-methylphenol
BIMP	2,6-bis[bis(1-methyl-2-imidazolyl)aminomethyl]-4-methylphenol
BIPhMe	2,2'-bis(1-methylimidazolyl)-phenylmethoxymethane
bipy	2,2'-bipyridine
bispicen	<i>N,N'</i> -bis(2-pyridylmethyl)-1,2-diaminoethane
BMPEA	<i>N,N'</i> -bis(2,6-dimethylpyridyl)-1,2-diaminoethane
BPEAP	<i>o</i> -(bis(2-(1-pyrazolyl)ethyl)amino)phenol
BPMP	2,6-bis[bis(2-pyridylmethyl)aminomethyl]-4-methylphenol
BPG	<i>N,N'</i> -bis(2-pyridylmethyl)glycine
biphenH ₂	2,2'-biphenol
(F ₃ prop)	pentafluoropropionate
cyclam	1,4,8,11-tetra-azacyclotetradecane
cyclen	1,4,7,10-tetra-azacyclododecane
EDTA	ethylenediaminetetraacetic acid
HBpz ₃	hydrotris(pyrazolyl)borate
HEDTA	<i>N</i> -hydroxyethyl-1,2-diaminoethane- <i>N,N',N'</i> -triacetic acid
H ₂ MPDP	<i>m</i> -phenylene diproponic acid
HPTA	2-hydroxy-1,3-diaminopropanetetraacetic acid
HPTB	1,3-bis[<i>N,N</i> -bis(2-benzimidazolymethyl)amino]-2-hydroxypropane
L	the Schiff base derived from two 1,3-diaminopropanes and two 2,6-diformyl-4- <i>tert</i> -butylphenols
L'	the Schiff base derived from two 1,3-diaminopropanes and two 2,6-diformyl-4-methylphenols
4,4'-Me ₂ bpy	4,4'-dimethyl-2,2'-bipyridine
5-Me-HXTA	<i>N,N'</i> -(2-hydroxy-5-methyl-1,3-xylylene)bis(<i>N</i> -carboxymethylglycine)
Me ₃ TACN	1,4,7-trimethyl-1,4,7-triazacyclononane
N5	<i>N,N'</i> -hydroxyethyl- <i>N,N',N'</i> -tris(2-benzimidazolymethyl)-1,2-diaminoethane
NITet	4,4,5,5-tetramethyl-2-ethyl-4,5-dihydro-1 <i>H</i> -imidazolyl-1-oxo-3-oxide
4-NO ₂ -HDP	2-[bis(2-pyridyl)methyl]aminomethyl]-4-nitrophenol
OAc	acetate
OBz	benzoate

Abbreviation	Name
OPr	propionate
PA	picolinic acid
Pc	phthalocyanine
phen	1,10-phenanthroline
py	pyridine
pyN5	3,6,10,13,19-pentaazabicyclo[13.3.1]nonadeca-1(19),15,17-triene
R-BMA saldien	<i>N</i> -alkyl- <i>N,N</i> ,-bis(2-benzimidazolylmethyl)amine the Schiff base derived from diethylenetriamine and salicylaldehyde
salDP	the Schiff base derived from salicylaldehyde and 1,5-diamino-3-pentanol
salmp	2-bis(salicylideneamino)methylphenol
salpn	<i>N,N'</i> -trimethylene bis(salicyladimine)
salps	<i>N,N'</i> -[1,1'-dithiobis(phenylene)]bis(salicylideaneamin)
spa	the Schiff base derived from salicylaldehyde and 3-amino-1-propanol
TACN	1,4,7-triazacyclononane
THF	tetrahydrofuran
TMICMe	2,2',2''-tris(1-methylimidazolyl)methoxymethane
TMP	tetramesitylporphrin
TmTP	tetrakis(<i>m</i> -tolyl)porphrin
TPA	tris(2-pyridylmethyl)amine
tpbn	<i>N,N,N',N'</i> -tetrakis(2-pyridylmethyl)-1,4-diaminobutane
TPP	tetraphenylporphrin
tptn	<i>N,N,N',N'</i> -tetrakis(2-pyridylmethyl)-1,3-diaminopropane
tren	tris(2-aminoethyl)amine

58. W. H. Armstrong, A. Spool, G. C. Papaefthymiou, R. B. Frankel, and S. J. Lippard, *J. Am. Chem. Soc.*, *106*, 3653–3667 (1984).
59. W. H. Armstrong and S. J. Lippard, *J. Am. Chem. Soc.*, *105*, 4837–4838 (1983).
60. W. H. Armstrong and S. J. Lippard, *J. Am. Chem. Soc.*, *106*, 4632–4633 (1984).
61. K. Wieghardt, K. Pohl, and W. Gebert, *Angew. Chem. Intl. Ed. Engl.*, *22*, 727 (1983).
62. B. P. Murch, F. C. Bradley, and L. Que, Jr., *J. Am. Chem. Soc.*, *108*, 5027–5028 (1986).
63. M. Suzuki, A. Uehara, and K. Endo, *Inorg. Chim. Acta*, *123*, L9–L10 (1986).
64. M. Suzuki, H. Oshio, A. Uehara, K. Endo, M. Yanaga, S. Kida, and K. Saito, *Bull. Chem. Soc. Jpn.*, *61*, 3907–3913 (1988).
65. M. S. Mashuta, R. J. Webb, K. J. Oberhausen, J. F. Richardson, R. M. Buchanan, and D. N. Hendrickson, *J. Am. Chem. Soc.*, *111*, 2745–2746 (1989).

66. A. S. Borovik and L. Que, Jr., *J. Am. Chem. Soc.*, *110*, 2345–2347 (1988).
67. X. Feng, S. G. Bott, and S. J. Lippard, *J. Am. Chem. Soc.*, *111*, 8046–8047 (1989).
68. J. B. Vincent, J. C. Huffman, G. Christou, Q. Li, M. A. Nanny, D. N. Hendrickson, R. H. Fong, and R. H. Fish, *J. Am. Chem. Soc.*, *110*, 6898–6900 (1988).
69. R. H. Beer, W. B. Tolman, S. G. Bott, and S. J. Lippard, *Inorg. Chem.*, *28*, 4557–4558 (1989).
70. J. R. Hartman, R. L. Rardin, P. Chaudhuri, K. Pohl, K. Wieghardt, B. Nuber, J. Weiss, G. C. Papaefthymiou, R. B. Frankel, and S. J. Lippard, *J. Am. Chem. Soc.*, *109*, 7387–7396 (1987).
71. A. Spool, I. D. Williams, and S. J. Lippard, *Inorg. Chem.*, *24*, 2156–2162 (1985).
72. P. Gómez-Romero, N. Casan-Pastor, A. Ben-Hussein, and G. B. Jameson, *J. Am. Chem. Soc.*, *110*, 1988–1990 (1988).
73. H. Toftlund, K. S. Murray, P. R. Zwack, L. F. Taylor, and O. P. Anderson, *J. Chem. Soc., Chem. Commun.*, 191–193 (1986).
74. Y. Nishida, S. Haga, and T. Tokii, *Chem. Lett.*, 109–112 (1989).
75. W. H. Armstrong and S. J. Lippard, *J. Am. Chem. Soc.*, *107*, 3730–3731 (1985).
76. P. N. Turowski, W. H. Armstrong, M. E. Roth, and S. J. Lippard, *J. Am. Chem. Soc.*, *112*, 681–690 (1990).
77. S. Drüeke, K. Wieghardt, B. Nuber, J. Weiss, H.-P. Fleischhauer, S. Gehring, and W. Haase, *J. Am. Chem. Soc.*, *111*, 8622–8631 (1989).
78. S. Drüeke, K. Wieghardt, B. Nuber, and J. Weiss, *Inorg. Chem.*, *28*, 1414–1417 (1989).
79. K. Wieghardt, S. Drüeke, P. Chaudhuri, U. Flörke, H.-J. Haupt, B. Nuber, and J. Weiss, *Z. Naturforsch.*, *44b*, 1093–1101 (1989).
80. S. Yan, L. Que, Jr., L. F. Taylor, and O. P. Anderson, *J. Am. Chem. Soc.*, *110*, 5222–5224 (1988).
81. S. Yan, D. D. Cox, L. L. Pearce, C. Juarez-Garcia, L. Que, Jr., J. H. Zhang, and C. J. O'Connor, *Inorg. Chem.*, *28*, 2507–2509 (1989).
82. R. E. Norman, S. Yan, L. Que, Jr., J. Sanders-Loehr, G. Backes, J. Ling, J. H. Zhang, and C. J. O'Connor, *J. Am. Chem. Soc.*, *112*, 1554–1562 (1990).
83. D. L. Jameson, C.-L. Xie, D. N. Hendrickson, J. A. Potenza, and H. J. Schugar, *J. Am. Chem. Soc.*, *109*, 740–746 (1987).
84. (a) B. P. Murch, *The Structure and Reactivity of Non-Heme Iron(III) Proteins and Model Complexes*, Ph.D. Thesis, Cornell University (1987). (b) R. E. Norman, unpublished observations.
85. Q. Chen, J. B. Lynch, P. Gomez-Romero, A. Ben-Hussein, G. B. Jameson, C. J. O'Connor, L. Que, Jr., *Inorg. Chem.*, *27*, 2673–2681 (1988).
86. P. Chaudhuri, M. Winter, K. Wieghardt, S. Gehring, W. Haase, B. Nuber, and J. Weiss, *Inorg. Chem.*, *27*, 1564–1569 (1988).

87. P. Chaudhuri and K. Wieghardt, *Angew. Chem. Int. Ed. Engl.* **24**, 778–779 (1985).
88. W. B. Tolman, A. Bino, and S. J. Lippard, *J. Am. Chem. Soc.*, **111**, 8522–8523 (1989).
89. L. L. Pearce, S. S. David, and S. M. Menage, unpublished observations.
90. A. S. Borovik, B. P. Murch, L. Que, Jr., V. Papaefthymiou, and E. Münck, *J. Am. Chem. Soc.*, **109**, 7190–7191 (1987).
91. M. Suzuki, A. Uehara, H. Oshio, K. Endo, M. Yanaga, S. Kida, and K. Saito, *Bull. Chem. Soc. Jpn.*, **60**, 3547–3555 (1987).
92. A. Ben-Hussein, N. L. Morris, P. Gómez-Romero, and G. B. Jameson, unpublished results.
93. F. Arena, C. Floriani, A. Chiesi-Villa, and C. Guastini, *J. Chem. Soc., Chem. Commun.* 1369–1371 (1986).
94. (a) B. S. Snyder, G. S. Patterson, A. J. Abrahamson, and R. H. Holm, *J. Am. Chem. Soc.*, **111**, 5214–5223 (1989). (b) K. K. Surerus, E. Münck, B. S. Snyder, and R. H. Holm, *J. Am. Chem. Soc.*, **111**, 5501–5502 (1989).
95. (a) S. Drüeke, P. Chaudhuri, K. Pohl, K. Wieghardt, X.-Q. Ding, E. Bill, A. Sawaryn, A. X. Trautwein, H. Winkler, and S. J. Gurman, *J. Chem. Soc., Chem. Commun.*, 59–62 (1989). (b) X.-Q. Ding, E. L. Bominaar, E. Bill, H. Winkler, A. X. Trautwein, S. Drüeke, P. Chaudhuri, K. Wieghardt, *J. Chem. Phys.*, **92**, 178–186, (1990).
96. F.-J. Wu and D. M. Kurtz, Jr., *J. Am. Chem. Soc.*, **111**, 6563–6572 (1989).
97. (a) J. Adler, J. Ensling, P. Gütlich, E. L. Bominaar, J. Guillin, and A. X. Trautwein, *Hyperfine Interactions*, **42**, 869–872 (1988). (b) C. Ercolani, M. Gardini, K. S. Murray, G. Pennesi, and G. Rossi, *Inorg. Chem.*, **25**, 3972–3976 (1986). (c) R. N. Mukherjee, T. D. P. Stack, and R. H. Holm, *J. Am. Chem. Soc.*, **110**, 1850–1861 (1988).
98. R. C. Reem, J. M. McCormick, D. E. Richardson, F. J. Devlin, P. J. Stephens, R. L. Musselman, and E. I. Solomon, *J. Am. Chem. Soc.*, **111**, 4688–4704 (1989).
99. R. R. Gay and E. I. Solomon, *J. Am. Chem. Soc.*, **100**, 1972–1973 (1978).
100. K. Wieghardt, K. Pohl, and D. Ventur, *Angew. Chem. Int. Ed. Engl.*, **24**, 392–393 (1985).
101. H. J. Schugar, G. R. Rossman, C. G. Barraclough, and H. B. Gray, *J. Am. Chem. Soc.*, **94**, 2683–2690 (1972).
102. J. E. Plowman, T. M. Loehr, C. K. Schauer, and O. P. Anderson, *Inorg. Chem.*, **23**, 3553–3559 (1984).
103. R. S. Czernuszewicz, J. E. Sheats, and T. G. Spiro, *Inorg. Chem.*, **26**, 2063–2067 (1987).
104. J. Sanders-Loehr, W. D. Wheeler, A. K. Shiemke, B. A. Averill, and T. M. Loehr, *J. Am. Chem. Soc.*, **111**, 8084–8093 (1989).
105. T. M. Loehr and A. K. Shiemke, in *Oxygen Complexes Oxygen Act. Transition*

- Met.*, 5th meeting date 1987, A. E. Martel, and D. T. Sawyer, Eds., Plenum, New York, 1988, pp. 17–32.
106. J. B. R. Dunn, D. F. Shriver, and I. M. Klotz, *Biochemistry*, *14*, 2689–2695 (1975).
 107. D. M. Kurtz, Jr., D. F. Shriver, and I. M. Klotz, *Coord. Chem. Rev.*, *24*, 145–178 (1987).
 108. Y. Nishida, M. Takeuchi, H. Shimo, S. Kida, *Inorg. Chim. Acta*, *96*, 115–119 (1984).
 109. B. A. Brennan, L. Que, Jr., and C. J. O'Connor, unpublished observations.
 110. (a) P. Gómez-Romero, G. C. DeFotis, and G. B. Jameson, *J. Am. Chem. Soc.*, *108*, 851–853 (1986). (b) P. Gómez-Romero, E. H. Witten, W. M. Reiff, G. Backes, J. Sanders-Loehr, and G. B. Jameson, *J. Am. Chem. Soc.*, *111*, 9039–9047 (1989). (c) G. B. Jameson, unpublished observations.
 111. A. Wyslouch, L. Latos-Grazynski, M. Grzeszczuk, K. Drabent, and T. Bartczak, *J. Chem. Soc., Chem. Commun.*, 1377–1378 (1988).
 112. D. J. Liston, B. J. Kennedy, K. S. Murray, and B. O. West, *Inorg. Chem.*, *24*, 1561–1567 (1985).
 113. U. Bossek, T. Weyhermüller, K. Wieghardt, J. Bonvoisin, and J.-J. Girerd, *Chem. Commun.*, 633–636 (1989).
 114. A. Ehrenberg and P. Reichard, *J. Biol. Chem.*, *247*, 3485–3488 (1972).
 115. B.-M. Sjöberg, P. Reichard, A. Gräslund, and A. Ehrenberg, *J. Biol. Chem.*, *253*, 6863–6865 (1978).
 116. B. A. Barry and G. T. Babcock, *Proc. Natl. Acad. Sci. USA*, *84*, 7099–7103 (1987).
 117. G. Backes, M. Sahlin, B.-M. Sjöberg, T. M. Loehr, and J. Sanders-Loehr, *Biochemistry*, *28*, 1923–1929 (1989).
 118. B.-M. Sjöberg, T. M. Loehr, and J. Sanders-Loehr, *Biochemistry*, *21*, 96–102 (1982).
 119. B.-M. Sjöberg, J. Sanders-Loehr, and T. M. Loehr, *Biochemistry*, *26*, 4242–4247 (1987).
 120. M. Sahlin, A. Ehrenberg, A. Gräslund, and B.-M. Sjöberg, *J. Biol. Chem.*, *261*, 2778–2780 (1986).
 121. A. S. Borovik, M. P. Hendrich, T. R. Holman, E. Münck, V. Papaefthymiou, and L. Que, Jr., *J. Am. Chem. Soc.*, *112*, 6031–6038 (1990).
 122. T. Inubushi and T. Yonetani, *FEBS Lett.*, *160*, 287–290 (1983).
 123. W. R. Hagen, *Biochim. Biophys. Acta*, *708*, 82–98 (1982).
 124. M. P. Hendrich and P. G. Debrunner, *Biophys. J.*, *56*, 489–506 (1989).
 125. (a) A. Abragam and B. Bleaney, *Electron Paramagnetic Resonance of Transition Ions*, Dover Publications, New York, 1970. (b) J. W. Whittaker and E. I. Solomon, *J. Am. Chem. Soc.*, *108*, 835–836 (1986).
 126. A. S. Borovik, M. P. Hendrich, T. R. Holman, E. Münck, V. Papaefthymiou, and L. Que, Jr., *J. Am. Chem. Soc.*, *112* (to appear in Aug. issue) (1990).

127. L. M. Babcock, Z. Bradic, P. C. Harrington, R. G. Wilkins, and G. S. Yoneda, *J. Am. Chem. Soc.*, *102*, 2849–2850 (1980).
128. P. Bertrand, B. Guigliarelli, J.-P. Gayda, P. Beardwood, and J. F. Gibson, *Biochim. Biophys. Acta*, *831*, 261–266 (1985).
129. G. Palmer, in *Iron Sulfur Proteins*, Vol. II, W. Lovenberg, Ed., Academic Press, New York and London, pp. 285–325 (1973).
130. R. E. Utecht and D. M. Kurtz, Jr., *Biochim. Biophys. Acta*, *953*, 164–178 (1988).
131. B. B. Muhoberac, D. C. Wharton, L. M. Babcock, P. C. Harrington, and R. G. Wilkins, *Biochim. Biophys. Acta*, *626*, 337–345 (1980).
132. R. G. Wilkins and P. C. Harrington, *Adv. Inorg. Biochem.*, *5*, 52–85 (1983).
133. M. J. Irwin, L. L. Duff, D. F. Shriver, and I. M. Klotz, *Arch. Biochem. Biophys.*, *224*, 473–478 (1983).
134. A. S. Borovik, V. Papaefthymiou, L. F. Taylor, O. P. Anderson, and L. Que, Jr., *J. Am. Chem. Soc.*, *111*, 6183–6195 (1989).
135. B. P. Murch, P. D. Boyle, and L. Que, Jr., *J. Am. Chem. Soc.*, *107*, 6728–6729 (1985).
136. M. B. Robin and P. Day, *Adv. Inorg. Chem. Radiochem.*, *10*, 247–422 (1967).
137. A. K. Shiemke, T. M. Loehr, and J. Sanders-Loehr, *J. Am. Chem. Soc.*, *108*, 2437–2443 (1986).
138. A. K. Shiemke, T. M. Loehr, and J. Sanders-Loehr, *J. Am. Chem. Soc.*, *106*, 4951–4956 (1984).
139. D. M. Kurtz, Jr., D. F. Shriver, and I. M. Klotz, *J. Am. Chem. Soc.*, *98*, 5033–5035 (1976).
140. C. R. Cantor and P. R. Schimmel, *Biophysical Chemistry. Part 1: The Conformation of Biological Macromolecules*, W. H. Freeman, San Francisco, 1980, pp. 14–15.
141. M. Brunori, A. Bellelli, B. Giardina, S. Condo, and M. F. Perutz, *FEBS Lett.*, *221*, 161–166 (1987).
142. (a) J. M. Nocek, D. M. Kurtz, Jr., R. A. Pickering, and M. P. Doyle, *J. Biol. Chem.*, *259*, 12334–12338 (1984). (b) J. M. Nocek, D. M. Kurtz, Jr., J. T. Sage, P. G. Debrunner, M. J. Maroney, and L. Que, Jr., *J. Am. Chem. Soc.*, *107*, 3382–3384 (1985).
143. J. M. Nocek, D. M. Kurtz, Jr., J. T. Sage, Y.-M. Xia, P. G. Debrunner, A. K. Shiemke, J. Sanders-Loehr, T. M. Loehr, *Biochemistry*, *27*, 1014–1024 (1988).
144. D. J. A. deWaal and R. G. Wilkins, *J. Biol. Chem.*, *251*, 2339–2343 (1976).
145. Z. Bradic, P. C. Harrington, and R. G. Wilkins, in *Biochemical and Clinical Aspects of Oxygen*, W. S. Caughey, Ed., Academic Press, New York, 1979, pp. 459–474.
146. G. D. Armstrong and A. G. Sykes, *Inorg. Chem.*, *25*, 3514–3516 (1986).

147. P. C. Harrington, D. J. A. deWaal, and R. G. Wilkins, *Arch. Biochem. Biophys.*, *191*, 444–451 (1978).
148. G. D. Armstrong, T. Ramasami, and A. G. Sykes, *Inorg. Chem.*, *24*, 3230–3234 (1985).
149. E. Olivas, D. J. A. deWaal, and R. G. Wilkins, *J. Inorg. Biochem.*, *11*, 205–212 (1979).
150. P. Bertrand, B. Guigliarelli, and J. P. Gayda, *Arch. Biochem. Biophys.*, *245*, 305–307 (1986).
151. F. A. Armstrong, P. C. Harrington, and R. G. Wilkins, *J. Inorg. Biochem.*, *18*, 83–91 (1983).
152. R. N. Patel and J. C. Savas, *J. Bacteriol.*, *169*, 2313–2317 (1987).
153. (a) D. J. Leak and H. Dalton, *Biocatalysis*, *1*, 23–36 (1987). (b) A. I. Pelyashenko-Novokhatny, A. N. Grigoryan, A. P. Kovalyov, V. S. Belova, and R. I. Gvozdev *Dokl. Akad. Nauk. SSSR*, *245*, 1501–1503 (1979).
154. G. Lassman, B. Liermann, W. Lehmann, H. Graetz, A. Koberling, and P. Langen, *Biochem. Biophys. Res. Commun.*, *132*, 1137–1143 (1985).
155. J. T. Groves and Y. Watanabe, *J. Am. Chem. Soc.*, *110*, 8443–8452 (1988).
156. T. L. Poulos, S. T. Freer, R. A. Alden, N. H. Xuong, S. L. Edwards, R. C. Hamlin, and J. Kraut, *J. Biol. Chem.*, *253*, 3730–3735 (1978).
157. J. B. R. Dunn, A. W. Addison, R. E. Bruce, J. Sanders-Loehr, and T. M. Loehr, *Biochemistry*, *16*, 1743–1749 (1977).
158. S. Ahmad, J. D. McCallum, A. K. Shiemke, E. H. Appelman, T. M. Loehr, and J. Sanders-Loehr, *Inorg. Chem.*, *27*, 2230–2233 (1988).
159. E. Kimura, M. Kodama, R. Machida, and K. Ishizu, *Inorg. Chem.*, *21*, 595–602 (1982).
160. Y. Nishida and M. Takeuchi, *Z. Naturforsch.*, *42b*, 52–54 (1987).
161. D. T. Sawyer, M. S. McDowell, L. Spencer, and P. K. S., Tsang, *Inorg. Chem.*, *28*, 1166–1170 (1989).
162. (a) W. Micklitz, T. G. Boh, J. G. Bentsen, and S. J. Lippard, *J. Am. Chem. Soc.*, *111*, 372–379 (1989). (b) W. Micklitz and S. J. Lippard, *Inorg. Chem.*, *27*, 3067–3068 (1988).
163. C. Walling, M. Kurz, and H. J. Schugar, *Inorg. Chem.*, *9*, 931–937 (1970).
164. (a) C. Bull, G. J. McClune, and J. A. Fee, *J. Am. Chem. Soc.*, *105*, 5290–5300 (1983). (b) K. C. Francis, D. Cummins, and J. Oakes, *J. Chem. Soc., Dalton Trans.*, 493–501 (1985).
165. (a) E. McCandlish, A. R. Miksztal, M. Nappa, A. Q. Sprenger, J. S. Valentine, J. D. Stong, and T. G. Spiro, *J. Am. Chem. Soc.*, *102*, 4268–4271 (1980). (b) R. B. VanAtta, C. E. Strouse, L. K. Hanson, and J. S. Valentine, *J. Am. Chem. Soc.*, *109*, 1425–1434 (1987). (c) J. N. Burstyn, J. A. Roe, A. R. Miksztal, B. A. Shaevitz, G. Lang, and J. S. Valentine, *J. Am. Chem. Soc.*, *110*, 1382–1388 (1988).
166. J. T. Groves and M. Van der Puy, *J. Am. Chem. Soc.*, *98*, 5290–5297 (1976).

167. N. Kitajima, H. Fukui, and Y. Moro-oka, *J. Chem. Soc., Chem. Commun.*, 485–486 (1988).
168. D. H. R. Barton, F. Halley, N. Ozbalik, M. Schmitt, E. Young, and G. Balavoine, *J. Am. Chem. Soc.*, *111*, 7144–7149 (1989).
169. C. Sheu, S. A. Richert, P. Cofré, B. R. Ross, Jr., A. Sobkowiak, D. T. Sawyer, and J. R. Kanofsky, *J. Am. Chem. Soc.*, *112*, 1936–1942 (1990).
170. T. J. McMurry and J. T. Groves, in *Cytochrome P450. Structure, Mechanism, and Biochemistry*, P. R. Ortiz de Montellano, Ed., Plenum, New York, 1986, Chapter 1.
171. (a) J. C. Davis and B. A. Averill, *Proc. Natl. Acad. Sci. USA*, *79*, 4623–4627 (1982). (b) J. C. Davis, S. S. Lin, and B. A. Averill, *Biochemistry*, *20*, 4062–4067 (1981).
172. (a) C. M. Ketcham, G. A. Baumbach, F. W. Bazer, and R. M. Roberts, *J. Biol. Chem.*, *260*, 5768–5776 (1985). (b) A. Hara, H. Sawada, T. Kato, T. Nakayama, H. Yamamoto, and Y. Matsumoto, *J. Biochem. (Tokyo)*, *95*, 67–74 (1984).
173. H. D. Campbell, D. A. Dionysius, D. T. Keough, B. E. Wilson, J. de Jersey, and B. Zerner, *Biochem. Biophys. Res. Commun.*, *82*, 615–620 (1978).
174. D. C. Schlosnagle, F. W. Bazer, J. C. M. Tsibris, and R. M. Roberts, *J. Biol. Chem.*, *249*, 7574–7579 (1974).
175. J. L. Beck, L. A. McConachie, A. C. Summors, W. N. Arnold, J. de Jersey, and B. Zerner, *Biochim. Biophys. Acta*, *869*, 61–68 (1986).
176. J. L. Beck, J. de Jersey, B. Zerner, M. P. Hendrich, and P. G. Debrunner, *J. Am. Chem. Soc.*, *110*, 3317–3318 (1988).
177. (a) Y. Sugiura, H. Kawaba, H. Tanaka, S. Fujimoto, and A. Ohara, *J. Biol. Chem.*, *256*, 10644–10670 (1981). (b) S. K. Heffler and B. A. Averill, *Biochem. Biophys. Res. Commun.*, *146*, 1173–1177 (1987). (c) H. Kawabe, Y. Sugiura, M. Terauchi, and H. Tanaka, *Biochim. Biophys. Acta*, *784*, 81–89 (1984).
178. D. F. Hunt, J. R. Yates, J. Shabanowitz, N.-Z. Zhu, T. Zirino, B. A. Averill, S. T. Daurat-Larroque, J. G. Shewale, R. M. Roberts, and K. Brew, *Biochem. Biophys. Res. Commun.*, *144*, 1154–1160 (1987).
179. W. C. Buhi, C. A. Ducsay, F. W. Bazer, and R. M. Roberts, *J. Biol. Chem.*, *257*, 1712–1723 (1982).
180. K. Doi, B. C. Antanaitis, and P. Aisen, *J. Biol. Chem.*, *261*, 14936–14938 (1986).
181. R. M. Roberts and F. W. Bazer, *Biochem. Biophys. Res. Commun.*, *68*, 450–455 (1976).
182. J. Schindelmeister, D. Munstermann, and H. Witzel, *Histochemistry*, *87*, 13–19 (1987).
183. M. M. King and C. Y. Huang, *J. Biol. Chem.*, *259*, 8847–8856 (1984).
184. J. B. Vincent and B. A. Averill, *FEBS Lett.*, *263*, 265–268, (1990).
185. S. S. David and L. Que, Jr., *J. Am. Chem. Soc.*, *112* (to appear in Aug. issue) (1990).

186. B. C. Antanaitis and P. Aisen, *J. Biol. Chem.*, *260*, 751–756 (1985).
187. S. Burman, J. C. Davis, M. J. Weber, and B. A. Averill, *Biochem. Biophys. Res. Commun.*, *136*, 490–497 (1986).
188. B. C. Antanaitis and P. Aisen, *J. Biol. Chem.*, *257*, 5330–5332 (1982).
189. B. C. Antanaitis, P. Aisen, and H. R. Lilienthal, *J. Biol. Chem.*, *258*, 3166–3172 (1983).
190. J. T. Sage, Y.-M. Xia, P. G. Debrunner, D. T. Keough, J. de Jersey, and B. Zerner, *J. Am. Chem. Soc.*, *111*, 7239–7247 (1989).
191. K. Cichutek, H. Witzel, and F. Parak, *Hyperfine Interactions*, *42*, 885–888 (1988).
192. (a) K. Spartalain, J. A. Bonadies, and C. J. Carrano, *Inorg. Chim. Acta*, *152*, 135–138 (1988). (b) B. Chiari, O. Piovesana, T. Tarantelli, and P. F. Zanazzi, *Inorg. Chem.*, *23*, 3398–3404 (1984).
193. B. C. Antanaitis, T. Streckas, and P. Aisen, *J. Biol. Chem.*, *257*, 3766–3770 (1982).
194. B. P. Gaber, J. P. Sheridan, F. W. Bazer, and R. M. Roberts, *J. Biol. Chem.*, *254*, 8340–8342 (1979).
195. R. C. Scarrow, J. W. Pyrz, and L. Que, Jr., *J. Am. Chem. Soc.*, *112*, 657–665 (1990).
196. (a) R. H. Heistand, R. B. Lauffer, E. Fikrig, and L. Que, Jr., *J. Am. Chem. Soc.*, *104*, 2789–2796 (1982). (b) E. W. Ainscough, A. M. Brodie, J. E. Plowman, K. L. Brown, A. W. Addison, and A. R. Gainsford, *Inorg. Chem.*, *19*, 3655–3663 (1980).
197. B. C. Antanaitis, J. Peisach, W. B. Mims, and P. Aisen, *J. Biol. Chem.*, *260*, 4572–4574 (1985).
198. K. Doi, J. McCracken, J. Peisach, and P. Aisen, *J. Biol. Chem.*, *263*, 5757–5763 (1988).
199. (a) J. E. Coleman and J. F. Chlebowski, *Adv. Inorg. Biochem.*, *1*, 1–66 (1979). (b) J. E. Coleman and P. Gettins, *Met. Ions Biol.* *5*, 153–217 (1983).
200. (a) L. Que, Jr., J. D. Lipscomb, E. Zimmermann, E. Münck, N. R. Orme-Johnson, and W. H. Orme-Johnson, *Biochim. Biophys. Acta*, *452*, 320–334 (1976). (b) J. W. Whittaker, J. D. Lipscomb, T. A. Kent, and E. Münck, *J. Biol. Chem.* *259*, 4466–4475 (1984).
201. (a) D. T. Keough, D. A. Dionysius, J. de Jersey, and B. Zerner, *Biochem. Biophys. Res. Commun.* *94*, 600–605 (1980). (b) J. L. Beck, D. T. Keough, J. de Jersey, and B. Zerner, *Biochim. Biophys. Acta*, *791*, 357–363 (1984).
202. J. L. Beck, M. J. McArthur, J. de Jersey, and B. Zerner, *Inorg. Chim. Acta*, *153*, 39–44 (1988).
203. D. T. Keough, J. L. Beck, J. de Jersey, and B. Zerner, *Biochem. Biophys. Res. Commun.*, *108*, 1643–1648 (1982).
204. K. Doi, R. Gupta, and P. Aisen, *J. Biol. Chem.*, *262*, 6982–6985 (1987).
205. B. C. Antanaitis and P. Aisen, *J. Biol. Chem.*, *259*, 2066–2069 (1984).
206. B. C. Antanaitis and P. Aisen, *J. Biol. Chem.*, *257*, 1855–1859 (1982).

207. E. Sinn, C. J. O'Connor, J. de Jersey, and B. Zerner, *Inorg. Chim. Acta*, **78**, L13-L15 (1983).
208. J. W. Pyrz, A. L. Roe, L. J. Stern, and L. Que, Jr., *J. Am. Chem. Soc.*, **107**, 614-620 (1985).
209. (a) L. Que, Jr., R. H. Heistand, II, R. Mayer, and A. L. Roe, *Biochemistry*, **19**, 2588-2593 (1980). (b) J. C. Davis, W.-J. Kung, and B. A. Averill, *Inorg. Chem.*, **25**, 394-396 (1986).
210. A. S. Borovik, L. Que, Jr., V. Papaefthymiou, E. Münck, L. F. Taylor, and O. P. Anderson, *J. Am. Chem. Soc.*, **110**, 1986-1988 (1988).
211. L. C. Sieker, S. Turley, B. C. Prickrill, and J. LeGall, *Proteins: Struct., Funct. Genet.*, **3**, 184-186 (1988).
212. P. R. Srinivasan and D. B. Sprinson, *J. Biol. Chem.*, **234**, 716-722 (1959).
213. R. J. McCandliss and K. Hermann, *Proc. Natl. Acad. Sci. USA*, **75**, 4810-4813 (1978).
214. (a) K. M. Hermann, J. Schultz, and M. A. Hermodson, *J. Biol. Chem.*, **255**, 7079-7081 (1980). (b) J. Shultz, M. A. Hermodson, C. C. Gardner, and K. M. Hermann, *J. Biol. Chem.*, **259**, 9655-9661 (1984). (c) T. Baasov and J. R. Knowles, *J. Bacteriol.*, **171**, 6155-6160 (1989).
215. J. Plönzig and G. Auling, *Arch. Microbiol.*, **146**, 396-401 (1987).
216. W. C. Stallings, K. A. Patridge, R. K. Strong, and M. L. Ludwig, *J. Biol. Chem.*, **259**, 10695-10699 (1984).
217. (a) M. P. Jamaluddin, *J. Bacteriol.*, **129**, 690-697 (1977). (b) Y.-L. T. Lee and S. Dagley, *J. Bacteriol.*, **131**, 1016-1017 (1977). (c) L. Que, Jr., J. Widom, and R. L. Crawford, *J. Biol. Chem.*, **256**, 10941-10944 (1981). (d) M. Ono-Kamimoto and S. Senoh, *J. Biochem. (Tokyo)*, **75**, 321-331 (1974). (e) D. M. Arciero, A. M. Orville, and J. D. Lipscomb, *J. Biol. Chem.*, **260**, 14035-14044 (1985).
218. Y. Kono and I. Fridovich, *J. Biol. Chem.*, **257**, 5751-5754 (1982).
219. J. Ames, *Biochim. Biophys. Acta*, **726**, 1-12 (1983).
220. J. B. Vincent and G. Christou, *Adv. Inorg. Chem.*, **33**, 197-257 (1989).
221. G. W. Brudvig, in *Metal Clusters in Proteins*, L. Que, Jr., Ed., American Chemical Society, Washington, DC, 1988, *ACS Symp. Ser.*, **372**, pp. 221-237.
222. G. W. Brudvig, W. F. Beck, and J. C. dePaula, *Ann. Rev. Biophys. Biophys. Chem.*, **18**, 25-46 (1989).
223. G. S. Allgood and J. J. Perry, *J. Bacteriol.*, **186**, 563-567 (1986).
224. V. V. Barynin, A. A. Vagin, V. R. Melik-Adamyanyan, A. I. Grebenko, S. V. Khangulov, A. N. Popov, M. E. Andrianova, B. K. Vainshtein, *Dokl. Akad. Nauk SSSR*, **288**, 877-880 (1986).
225. Y. Kono, and I. Fridovich, *J. Biol. Chem.*, **258**, 13646-13648 (1983).
226. B. K. Vainshtein, V. R. Melik-Adamyanyan, V. V. Barynin, and A. A. Vagin, in *Progress in Bioorganic Chemistry and Molecular Biology*, Y. A. Ovchin-

- nikov, Ed., Elsevier, Amsterdam, pp. 117–125 (1984).
227. S. V. Khangulov, V. V. Barynin, V. R. Melik-Adamyanyan, A. I. Grebenko, N. V. Voerodskaya, L. A. Blumenfeld, S. N. Dobryakov, and V. B. Il'Yasova, *Bioorg. Khim.*, *12*, 741–748 (1986).
 228. G. Schimpff-Weiland and H. Follmann, *Biochem. Biophys. Res. Commun.*, *102*, 1276–1282 (1981).
 229. J. E. Sheats, R. S. Czernuszewicz, G. C. Dismukes, A. L. Rheingold, V. Petrouleas, J. Stubbe, W. H. Armstrong, R. H. Beer, and S. J. Lippard, *J. Am. Chem. Soc.*, *109*, 1435–1444 (1987).
 230. H. Follmann, A. Willing, G. Auling, and J. Plönzig, in *Thioredoxin and Glutaredoxin Systems: Structure and Function*, A. Holmgren, C. I. Braenden, H. Joernvall, and B.-M. Sjöberg, Eds., Raven Press, New York, 1986, 217–226.
 231. B. Kok, B. Forbush, and M. McGloin, *Photochem. Photobiol.*, *11*, 457–475 (1970).
 232. G. C. Dismukes and Y. Siderer, *Proc. Natl. Acad. Sci. USA*, *78*, 274 (1981).
 233. G. C. Dismukes, K. Ferris, and P. Watnick, *Photobiochem. Photobiophys.*, *3*, 243–256 (1982).
 234. (a) V. K. Yachandra, R. D. Guiles, A. McDermott, R. D. Britt, S. L. Dexheimer, K. Sauer, and M. P. Klein, *Biochim. Biophys. Acta*, *850* 324–332 (1986). (b) A. E. McDermott, V. K. Yachandra, R. D. Guiles, J. L. Cole, S. L. Dexheimer, R. D. Britt, K. Sauer, and M. P. Klein, *Biochemistry*, *27*, 4021–4031 (1988).
 235. (a) R. J. Kulawiec, R. H. Crabtree, G. W. Brudvig, and G. K. Schulte, *Inorg. Chem.*, *27*, 1309–1311 (1988). (b) J. B. Vincent, C. Christmas, H.-R. Chang, Q. Li, P. D. W. Boyd, J. C. Huffman, D. N. Hendrickson, and G. Christou, *J. Am. Chem. Soc.*, *111*, 2086–2097 (1989). (c) G. W. Brudvig and R. H. Crabtree, *Proc. Natl. Acad. Sci. USA*, *83*, 4586–4588 (1986).
 236. W. F. Beyer, Jr. and I. Fridovich, in *Manganese Metab. Enzyme Funct.*, V. L. Schramm and F. C. Wedler, Eds., Academic Press, Orlando, Florida, pp. 193–219 (1986).
 237. U. Bossek, K. Wiegardt, B. Nuber, and J. Weiss, *Inorg. Chim. Acta*, *165*, 123–129, (1989).
 238. K. Wiegardt, U. Bossek, B. Nuber, J. Weiss, J. Bonvoisin, M. Corbella, S. E. Vitols, and J.-J. Girerd, *J. Am. Chem. Soc.*, *110*, 7398–7411 (1988).
 239. A. Caneschi, F. Ferraro, D. Gatteschi, M. C. Melandri, P. Rey, and R. Sessoli, *Angew. Chem. Int. Ed. Engl.*, *28*, 1365–1367 (1989).
 240. (a) M. Suzuki, M. Mikuriya, S. Murata, A. Uehara, H. Oshio, S. Kida, and K. Saito, *Bull. Chem. Soc. Jpn.*, *60*, 4305–4312 (1987). (b) M. Suzuki, S. Murata, A. Uehara, and S. Kida, *Chem. Lett.*, 281–284 (1987).
 241. D. J. Hodgson, B. J. Schwartz, and T. N. Sorrell, *Inorg. Chem.*, *28*, 2226–2228 (1989).

242. Y. Nishida, *Chem. Lett.*, 2151–2152 (1987).
243. B. Mabad, P. Cassoux, J.-P. Tuchagues, and D. N. Hendrickson, *Inorg. Chem.*, *25*, 1420–1431 (1986).
244. B. Mabad, J.-P. Tuchagues, Y. T. Hwang, and D. N. Hendrickson, *J. Am. Chem. Soc.*, *107*, 2801–2802 (1985).
245. D. M. Kessissoglou, W. M. Butler, and V. L. Pecoraro, *Inorg. Chem.*, *26*, 495–503 (1987).
246. H.-R. Chang, S. K. Larsen, P. D. W. Boyd, C. G. Pierpont, and D. N. Hendrickson, *J. Am. Chem. Soc.*, *110*, 4565–4576 (1988).
247. S. L. Lambert and D. N. Hendrickson, *Inorg. Chem.*, *18*, 2683–2686 (1979).
248. S. Menage, *Contribution à la modélisation structurale et fonctionnelle du système de dégagement d'oxygène des plantes: synthèse, étude des propriétés électroniques et de la réactivité de complexes contenant le coeur [Mn(III)₂O(RCO₂)₂]²⁺*, Ph.D. Thesis, University of Paris-Sud (Orsay) (1988).
249. P. Mathur, M. Crowder, and G. C. Dismukes, *J. Am. Chem. Soc.*, *109*, 5227–5233 (1987).
250. (a) H. Diril, H.-R. Chang, X. Zhang, S. K. Larsen, J. A. Potenza, C. G. Pierpont, H. J. Schugar, S. S. Isied, and D. N. Hendrickson, *J. Am. Chem. Soc.*, *109*, 6207–6208 (1987). (b) H. Diril, H.-R. Chang, M. J. Nilges, X. Zhang, J. A. Potenza, H. J. Schugar, S. S. Isied, and D. N. Hendrickson, *J. Am. Chem. Soc.*, *111*, 5102–5114 (1989).
251. H.-R. Chang, H. Diril, M. J. Nilges, X. Zhang, J. A. Potenza, H. J. Schugar, D. N. Hendrickson, and S. S. Isied, *J. Am. Chem. Soc.*, *110*, 625–627 (1988).
252. R. M. Buchanan, K. J. Oberhausen, and J. F. Richardson, *Inorg. Chem.*, *27*, 971–973 (1988).
253. J. S. Bashkin, A. R. Schake, J. B. Vincent, H.-R. Chang, Q. Li, J. C. Huffman, G. Christou, and D. N. Hendrickson, *J. Chem. Soc., Chem. Commun.*, 700–702 (1988).
254. K. Wiegardt, U. Bossek, D. Ventur, and J. Weiss., *J. Chem. Soc., Chem. Commun.*, 347–349 (1985).
255. J. B. Vincent, K. Folting, J. C. Huffman, and G. Christou, *Biochem. Soc. Trans.*, *16*, 822–823 (1988).
256. S. Menage, J.-J. Girerd, and A. Gleizes, *J. Chem. Soc., Chem. Commun.*, 431–432 (1988).
257. Y. Nishida, N. Oshino, and T. Tokii, *Z. Naturforsch.*, *43b*, 637–638 (1987).
258. P. A. Goodson and D. J. Hodgson, *Inorg. Chem.*, *28*, 3606–3608 (1989).
259. H. S. Maslen and T. N. Waters, *J. Chem. Soc., Chem. Commun.*, 760–761 (1973).
260. Y. Nishida, N. Oshino, and T. Tokii, *Z. Naturforsch.*, *43b*, 472–474 (1988).
261. (a) N. Torihara, M. Mikuriya, H. Okawa, and S. Kida, *Bull. Chem. Soc. Jpn.*, *53*, 1610–1613 (1980). (b) M. Mikuriya, N. Torihara, H. Okawa, and S. Kida, *Bull. Chem. Soc. Jpn.*, *54*, 1063–1067 (1981).

262. J. B. Vincent, K. Folting, J. C. Huffman, and G. Christou, *Inorg. Chem.*, **25**, 996–999 (1986).
263. L. H. Vogt, A. Zalkin, and D. H. Templeton, *Inorg. Chem.*, **6**, 1725–1730 (1967).
264. K. Wieghardt, U. Bossek, J. Bonvoisin, P. Beauvillain, J.-J. Girerd, B. Nuber, J. Weiss, and J. Heinze, *Angew. Chem. Int. Ed. Engl.*, **25**, 1030–1031 (1986).
265. K. S. Hagen, W. H. Armstrong, and H. Hope, *Inorg. Chem.*, **27**, 967–969 (1988).
266. M. Stebler, A. Ludi, and H.-B. Bürgi, *Inorg. Chem.*, **25**, 4743–4750 (1986).
267. P. M. Plaskin, R. C. Stoufer, M. Mathews, and G. J. Palenik, *J. Am. Chem. Soc.*, **94**, 2121–2122 (1972).
268. M. A. Collins, D. J. Hodgson, K. Michelsen, and D. K. Towle, *J. Chem. Soc., Chem. Commun.*, 1659–1660 (1987).
269. M. Suzuki, H. Senda, Y. Kobayashi, H. Oshio, and A. Uehara, *Chem. Lett.*, 1763–1766 (1988).
270. D. K. Towle, C. A. Botsford, and D. J. Hodgson, *Inorg. Chim. Acta*, **141**, 167–168 (1988).
271. M. Suzuki, S. Tokura, M. Suhara, and A. Uehara, *Chem. Lett.*, 477–480 (1988).
272. K. Wieghardt, U. Bossek, L. Zsolnai, G. Huttner, G. Blondin, J.-J. Girerd, and F. Babonneau, *J. Chem. Soc. Chem. Commun.*, 651–653 (1987).
273. P. A. Goodson, J. Glerup, D. J. Hodgson, K. Michelsen, and E. Pederson, *Inorg. Chem.*, **29**, 503–508 (1990).
274. B. C. Schardt, F. J. Hollander, and C. L. Hill, *J. Am. Chem. Soc.*, **104**, 3964–3972 (1982).
275. S. R. Cooper, G. C. Dismukes, M. P. Klein, and M. Calvin, *J. Am. Chem. Soc.*, **100**, 7248–7252 (1978).
276. J.-J. Girerd, unpublished results.
277. (a) T. Matsushita, L. Spencer, and D. T. Sawyer, *Inorg. Chem.*, **27**, 1167–1173 (1988). (b) M. M. Morrison, and D. T. Sawyer, *J. Am. Chem. Soc.*, **99**, 237–238 (1977).
278. K. J. Brewer, A. Liegeois, J. W. Otvos, M. Calvin, and L. O. Spreer, *J. Chem. Soc., Chem. Commun.*, 1219–1220 (1988).
279. (a) E. I. Solomon, D. Allendorf, L. S. Kau, J. E. Pate, D. Spira-Solomon, D. Wilcox, and A. G. Porras, *Life Chem. Rep.*, **5**, 37–89 (1987). (b) Z. Tyeklar and K. D. Karlin, *Acc. Chem. Res.*, **22**, 241–248 (1989).
280. (a) A. Volbeda and W. G. J. Hol, *Prog. Clin. Biol. Res.*, **274**, 291–304 (1988). (b) N. M. Soeter, P. A. Jekel, J. J. Beintema, A. Volbeda, and W. G. J. Hol, *Eur. J. Biochem.*, **169**, 323–332 (1987). (c) A. Messerschmidt, A. Rossi, R. Ladenstein, R. Huber, M. Bolognesi, G. Gatti, A. Marchesini, R. Petruzzelli, and A. Finazzi-Agro, *J. Mol. Biol.*, **206**, 513–529 (1989).
281. P. A. Clark and D. E. Wilcox, *Inorg. Chem.*, **28**, 1326–1333 (1989).

282. J. M. McCormick and E. I. Solomon, *J. Am. Chem. Soc.*, *112*, 2005–2007 (1990).
283. M. P. Hendrich, B. G. Fox, J. D. Lipscomb, and E. Münck, *J. Am. Chem. Soc.*, *112*, 5861–5865 (1990).
284. S. A. Dikanov, Yu. D. Tsvetkov, S. V. Khangulov, and M. G. Gol'dfel'd, *Dokl. Akad. Nauk. SSSR*, *302*, 174–177 (1988).
285. M. Sahlin, B.-M. Sjöberg, G. Backes, T. Loehr, and J. Sanders-Loehr, *Biochem. Biophys. Res. Comm.*, *167*, 813–818 (1990).
286. M. Fontecave, C. Gerez, M. Atta, and A. Jeunet, *Biochem. Biophys. Res. Comm.*, *168*, 659–664 (1990).
287. N. Kitajima, H. Fukui, Y. Moro-oka, Y. Mizutani, and T. Kitagawa, *J. Am. Chem. Soc.*, *112* (1990).
288. S. Menage, B. A. Brennan, C. Juarez-Garcia, E. Münck, and L. Que, Jr., *J. Am. Chem. Soc.*, *112* (1990).

Metal Ion Promoted Reactions of Phosphate Derivatives

PHILIP HENDRY and **ALAN M. SARGESON**

*Research School of Chemistry
Australian National University
Canberra, A.C.T.
Australia*

CONTENTS

I. INTRODUCTION	202
II. REACTIONS OF PHOSPHATES IN THE ABSENCE OF METAL IONS	203
A. The Dissociative Reactions, $S_N1(P)$	203
B. The Associative Reaction, $S_N2(P)$	206
C. Cyclic Phosphates	207
D. Intramolecular Reactions	209
III. REACTIONS OF PHOSPHATES IN THE PRESENCE OF LABILE METAL IONS	209
IV. REACTIVITY OF SUBSTITUTION INERT METAL ION PHOSPHATE COMPLEXES	213
A. Introduction	213
B. Intermolecular Attack of Nucleophiles	214
C. Intermolecular Attack of Hydroxide Ion: Cobalt(III) Complexes	216
D. Intramolecular Attack of Hydroxide Ion: Iridium(III) Complexes	221
E. Intramolecular Attack of Amido Ion: Cobalt(III) Complexes	225
F. Intramolecular Attack of Amido Ion: Iridium(II) Complexes	229
G. Activation by More than One Metal Ion	231
H. Chelation of the Phosphate Esters and Phosphate Ion	233
I. Conclusions	236

Progress in Inorganic Chemistry: Bioinorganic Chemistry, Vol. 38, Edited by Stephen J. Lippard.

ISBN 0-471-50397-5 © 1990 John Wiley & Sons, Inc.

V. RELATIONSHIPS BETWEEN MODEL STUDIES AND ENZYME MECHANISMS	237
A. <i>Escherichia coli</i> Alkaline Phosphatase and Related Enzymes	237
B. Yeast Inorganic Pyrophosphatase	240
C. Pyrophosphate Cleavage	242
D. Triphosphate Hydrolyses	244
E. Kinases	247
F. Nonenzymic Hydrolysis of ATP and ADP	249
VI. CONCLUSIONS	251
ABBREVIATIONS	252
REFERENCES	253

I. INTRODUCTION

The biological utilization of phosphate derivatives is of utmost importance. Phosphate diesters form part of the backbone of DNA. The phosphate derivatives and anhydrides, in particular ATP, are the main method of energy transduction in the cell and phosphorylation of proteins is a key step in the regulation of some metabolic pathways. In contrast to their reactivity in biological systems, phosphate derivatives are generally unreactive in laboratory conditions. A striking feature of many of the enzymes in this area is that most of them are metalloenzymes or require metal ion cofactors (108). This observation prompts the question, Do metal ions have a special effect on the reactivity of phosphate derivatives or are they merely used in a structural role (140)? A number of mechanisms by which metal ions could conceivably facilitate the reactions of phosphate derivatives are fairly obvious and include the six modes listed below.

1. Electrophilic activation of the phosphorus center.
2. Charge neutralization of the phosphate moiety.
3. Provision of an efficient nucleophile at biological pH, for example, coordinated OH^- ion.
4. Organization of the reactants for an intramolecular reaction.
5. Orientation of the substrate for the enzyme.
6. Activation of the substrate in a strained chelate.

This chapter reviews some of the work that has been conducted in an effort to evaluate the efficacy of the above mentioned potential activating modes and other more specific questions that have arisen in the course of these investigations.

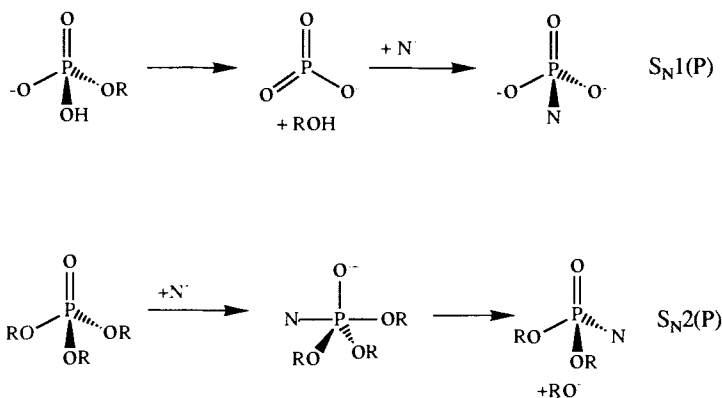
II. REACTIONS OF PHOSPHATES IN THE ABSENCE OF METAL IONS

Nucleophilic substitution of phosphates appears to proceed via two basic mechanisms (115, 144), Scheme 1; the dissociative mechanism [$S_N1(P)$] and the associative mechanism [$S_N2(P)$]. The dissociative mechanism proceeds via an extremely reactive three-coordinate metaphosphate intermediate and the associative mechanism proceeds via a five-coordinate phosphorane or equivalent, which may or may not be an intermediate.

A. The Dissociative Reaction, $S_N1(P)$

The elimination–addition reaction for phosphate esters was first proposed to account for the shape of the pH-rate profile of alkyl monoesters (40), which are most reactive at the maximum concentration of the mono-anion, that is, \sim pH 4. The explanation for this observation was that the reaction proceeded via a metaphosphate “intermediate” by the expulsion of an alcohol group with the proton for the alcohol being transferred from the phosphate as the reaction proceeds. Further studies of the reactions of monoesters have implied that the above mechanism operates for all alkyl and aryl monoesters where the pK_a of the leaving group exceeds about 5.5. In these instances, the alcohol or phenol needs to be protonated to be an effective leaving group. In contrast, phosphate monoesters with a phenolic leaving group with a $pK_a < 5.5$ show rate maxima where the dianion predominates (18, 94). In this situation, the phenolate ion appears to be an effective leaving group and therefore does not require protonation.

Since the mid-1950s many experiments have been performed lending support to the thesis that metaphosphate was involved in the hydrolysis of



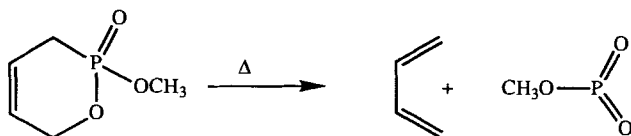
Scheme 1. Hydrolysis of phosphate esters.

ionized phosphate monoesters. These include studies showing that the products of solvolysis of monoesters carried out in mixed alcoholic-aqueous media are alkylphosphate and phosphate in a ratio that is close to that of the molar ratio of the solvent (86). The interpretation is that a phosphorylating agent is produced that is not selective towards the two nucleophiles present. Also, 2,4-dinitrophenylphosphate phosphorylates the sterically hindered tertiary butyl alcohol in acetonitrile at almost the same rate as it is hydrolyzed in that solvent, implying a dissociative-type mechanism (114). The oxygen kinetic isotope effect in the hydrolysis of 2,4-dinitrophenylphosphate, with the ^{18}O atom on the phenol group, ($k_{\text{O}^{18}}/k_{\text{O}^{16}}$) is 1.02 ± 0.004 , which is indicative of substantial P-O bond cleavage in the rate limiting step (66). The three phase test (120) in which the reactive phosphate is anchored to insoluble polymer beads and the receptor is attached to another type of bead, both in an inert solvent shows that the reactive phosphorylating agent has migrated through the solvent to the receptor molecule. A bimolecular reaction between the reactant and receptor is precluded by the fact that they are attached to separate insoluble polymers.

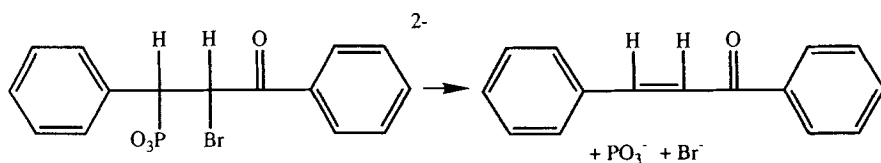
Experiments have been performed that appear to demonstrate the production of the metaphosphate fragment from other than a phosphate derivative. The pyrolysis of an appropriate precursor molecule, for example, methyl-2-butenylphosphonate (Scheme 2) yields products attributable to the reaction products of methylmetaphosphate (146).

Recently, Westheimer and co-worker (22, 23) re-examined the Conant-Swan fragmentation of β -halophosphonates and have presented evidence for the fragmentation proceeding via metaphosphate (Scheme 3). The PO_3^- anion so generated can be trapped by the addition of a suitable reagent (22, 23).

The monomeric metaphosphate anion has also been directly observed in the gas phase by mass spectrometry (107). Ramirez and co-workers have utilized the negative ion chemical ionization technique to study the fragmentation of phosphotriesters. In many of these spectra, a prominent peak occurs at $m/e = 79$; exact mass measurements of this peak confirm that it is PO_3^- . It is important to note, however, that all reactions where the metaphosphate anion has apparently been trapped have been conducted in nonaqueous media.



Scheme 2. Pyrolysis of methyl-2-butenylphosphonate.



Scheme 3. The Conant-Swan fragmentation (according to Westheimer (22, 23)).

Knowles and co-workers have studied the stereochemical consequences of the presumed $S_N1(P)$ reaction. They have shown that the methanolysis of chiral $^{16}\text{O}^{17}\text{O}^{18}\text{O}$ -substituted phenol- and 2,4-dinitrophenylphosphate and phosphocreatine (13, 14), under conditions where they were expected to react by the metaphosphate pathway, all undergo complete inversion of configuration at phosphorus. This result implies that the putative metaphosphate is not a free intermediate; that it is not even long-lived enough to equilibrate with the solvent cage in which it is formed. It was concluded that the reaction must be preassociative at least in aqueous-alcoholic media. A recent report (24) has shown that the Conant-Swan fragmentation described earlier also occurs with inversion about the phosphorus atom.

In acetonitrile solution, the transfer of the phosphoryl group of the monoanion of phenylphosphate to *tert*-butanol proceeds largely with racemization at the P center (61) indicating that under these conditions the metaphosphate anion has a lifetime long enough at least to equilibrate with its environment. A second possibility is that the PO_3^- intermediate undergoes multiple transfer reactions with the solvent before ultimately transferring to the final acceptor. Likewise the terminal phosphate in ADP is transferred to a variety of alcohols in acetonitrile with racemization about the phosphorus center (43).

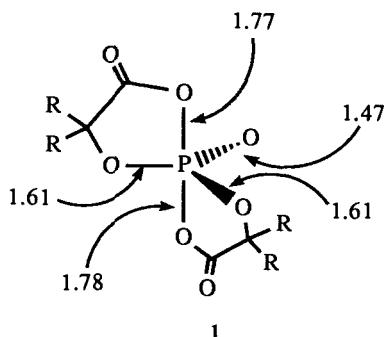
Unlike its phosphate parent, the dianion of chiral (^{18}O substituted) 4-nitrophenyl-*thio*-phosphate undergoes solvolysis in ethanol to yield ethylthiophosphate, which is completely racemic (44, 45), implying that *thio*-metaphosphate has a longer lifetime than metaphosphate in protic solvents. The monoanion is largely racemized in ethanol (80%) and aqueous ethanol (70%).

The volume of activation for the hydrolysis of 2,4-dinitrophenylphosphate in aqueous solution is $-4.8 \text{ cm}^3 \cdot \text{mol}^{-1}$ (116) and this has been interpreted as a reaction that involves some associative nature. In contrast, the activation volume for the hydrolysis of 2,4-dinitrophenyl-*thio*-phosphate is $+10 \text{ cm}^3 \cdot \text{mol}^{-1}$, which is indicative of a more dissociative pathway (19).

These are all experiments that indicate the short life of the “ PO_3^- intermediate” and display a spectrum of knowledge about its properties without being exhaustive.

B. The Associative Reaction, $S_N2(P)$

The addition–elimination reaction proceeds via addition of a nucleophile at phosphorus to generate a five-coordinate intermediate or activated complex. The phosphorus atom is readily able to use its *d* orbitals to expand its coordination number and it is argued that an attacking nucleophile such as OH^- adds to the four-coordinate phosphorus to form a pentacoordinate phosphorane (143). It appears that generally the pentacoordinate intermediate will have a trigonal bipyramidal structure, although spirocyclic phosphoranes seem to favor square pyramidal structures (80).



(Bond lengths in Å, $R = \text{C}_6\text{H}_5$)

Phosphate di- and triesters appear to react exclusively via this $S_N2(P)$ mechanism. Phosphate monoesters can react via either mechanism depending on their state of protonation (115), but the neutral diprotonated monoesters always appear to react via the $S_N2(P)$ pathway.

X-ray crystallographic analyses of available trigonal bipyramidal phosphoranes show that, usually, apical bonds are longer (see, e.g., **1**) and, as a corollary, weaker than the equatorial bonds (54, 117).

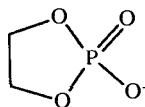
X-ray structures determined for trigonal bipyramidal phosphoranes with mixed alkyl–alkoxy substituents invariably show that the alkoxy groups prefer apical coordination and alkyl groups prefer the equatorial sites (138). An approximate scale of apicophilicities, a measure of a substituent's preference for an apical position in the trigonal bipyramid, has been deduced for phosphoranes from NMR studies of these compounds (137). The scale spans F^- to alkyl groups in order of decreasing apicophilicity. Phosphoranes appear to be stabilized by the presence of four-, five- and six-membered rings incorporating the phosphorus atom as witnessed by the relative paucity of X-ray structures for nonring phosphoranes (117).

Phosphoranes, however, are not coordinatively saturated. There are

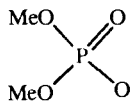
many examples of hexacoordinate phosphorus compounds, for example, PF_6^- , $\text{P}(\text{OCH}_3)_6^-$, and $\text{P}(\text{OC}_6\text{H}_5)_6^-$ (49), it can be concluded that like phosphoranes, hexacoordinate phosphorus compounds are also stabilized by electronegative substituents (49). Therefore, it is evident that four-coordinate phosphorus has no problem expanding its coordination number to five or six.

C. Cyclic Phosphates

Much pioneering work on the mechanism of hydrolysis of phosphate esters was done by Westheimer and co-workers in the 1950s and 1960s. They observed that the five-membered ring cyclic phosphates were hydrolyzed millions of times faster than their acyclic analogues in both acid and base (143). Thus **2** is hydrolyzed in base $\sim 10^7$ -fold faster than **3** (100).

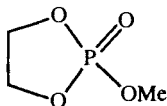


2



3

Significantly, in the acid hydrolysis of ethylene phosphate, **2**, oxygen exchange in the reactant occurred at almost the same rate as hydrolysis. Similarly, the hydrolysis of methylethylenephosphate, **4**, in acidic solution took place with both ring opening and loss of the methoxy group, but in basic conditions only ring opening was observed (38). Prior to these observations the explanation for the rapid hydrolysis was simply the strain relief in the product (39), however, similar rates for exocyclic and endocyclic hydrolysis invalidated this argument.



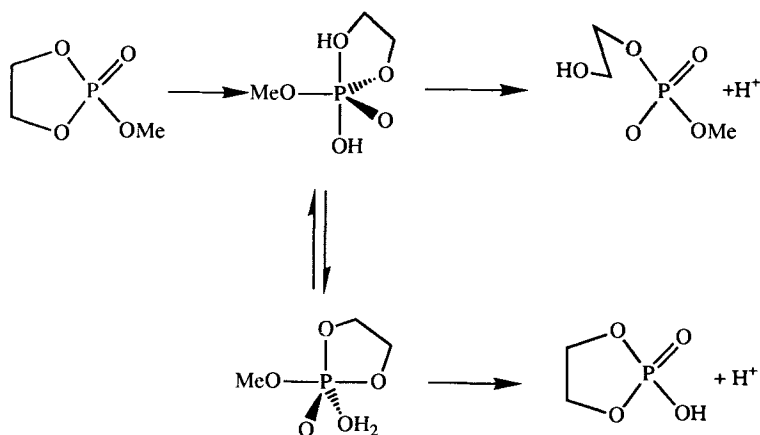
4

During the 1960s Westheimer proposed a reaction mechanism that accounted for all of these observations and that had predictive value as well (143). It was postulated that hydrolysis of these cyclic phosphates pro-

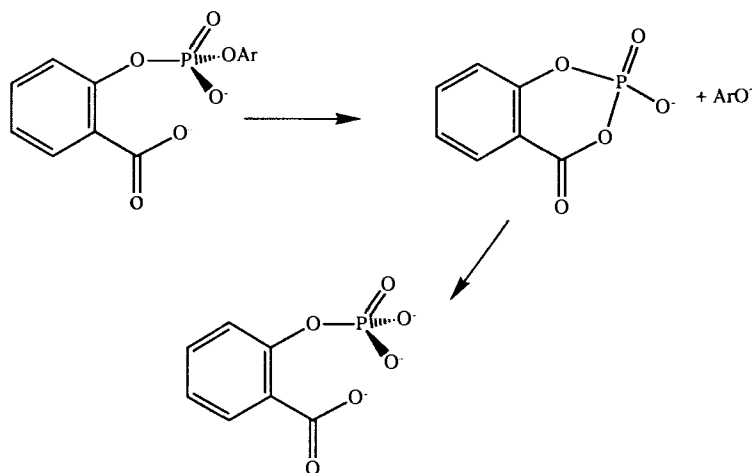
ceeded via a phosphorane which, because of the presence of the ring, was much lower in energy than the corresponding acyclic phosphorane relative to the starting phosphate esters. The extent of the exocyclic cleavage was dependent on whether the intermediate phosphorane could pseudorotate or not (113). Westheimer's theory can be summarized by a number of *rules*:

1. The reaction proceeds via a trigonal bipyramidal phosphorane intermediate.
2. The nucleophile and leaving group enter and depart the phosphorane at the axial position.
3. The trigonal bipyramidal intermediate may pseudorotate, with certain restrictions (see rules 4 and 5).
4. Four- and five-membered rings may only span axial-equatorial positions.
5. Orientation of substituents in the intermediate is dependent on the relative apicophilicities of the substituents.

The theory is best illustrated by the acid hydrolysis of methylethylenephosphate. Scheme 4 shows how pseudorotation of the phosphorane intermediate can accommodate exocyclic hydrolysis. The rate enhancement of the five-membered cyclic phosphate arises from two effects of the ring. The cyclic phosphate ester is strained in spanning the tetrahedral angle of 109° , which raises the strain energy of the cyclic phosphate relative to that of the acyclic phosphate (65). In going from the phosphate ester to the intermediate, the angle that the ring is required to span is reduced to 90° ,



Scheme 4. The acid hydrolysis of methylethylenephosphate (143).



Scheme 5. Hydrolysis of phenylsalicylphosphate ($\text{Ar} = \text{C}_6\text{H}_5$).

the strain is thereby relieved in the formation of the intermediate. In addition, the presence of the ring in the trigonal bipyramidal intermediate helps stabilize the structure (65), which also favors formation of the intermediate from the cyclic phosphate. These effects are reflected in a lowering of the energy of the transition state for the reaction.

D. Intramolecular Reactions

With a few notable exceptions the di- and triesters of phosphates are generally hydrolyzed quite slowly. These exceptions include the five-membered ring phosphate esters described previously and phosphate esters, which have available to them an intramolecular pathway, that is, phosphate esters that have a pendant nucleophilic functional group in a suitable position to attack the phosphorus atom. Alcohol (12), amine (101), or carboxylic functional groups (1) able to form four- five-, or six-membered rings by nucleophilic attack at phosphorus react relatively rapidly. For example, the hydrolysis of phenylsalicylphosphate (Scheme 5), is accelerated 10^7 – 10^8 -fold over the analogous intermolecular path (92).

III. REACTIONS OF PHOSPHATES IN THE PRESENCE OF LABILE METAL IONS

Simple metal ions have been known for some time to promote polyphosphate and phosphate ester hydrolysis (135). Several proposals for the

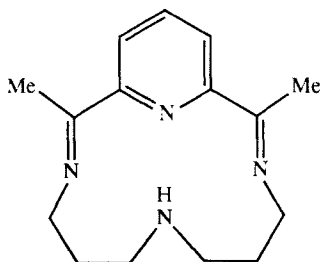
mechanisms by which metal ions act have been advanced (127, 128, 131). A major problem with experimental systems of this kind is that the divalent metal ions are substitutionally labile, and form numerous complexes, most of which are in rapid equilibrium. This situation makes it extremely difficult to unravel the system and to say with certainty that any particular complex or binding mode is wholly or partly responsible for the rate enhancement. It is axiomatic, however, that substitution lability is an essential requirement for efficient catalysis and presumably this is the reason enzymes choose mostly first-row divalent metal ions as cofactors.

Lanthanide hydroxide gels have been known for about 50 years to catalyze the hydrolysis of polyphosphates and phosphate esters (20). However, the study of these systems is fraught with similar difficulties to those mentioned previously, that is, the inability to be able to identify the complexes responsible for the activation. Butcher and Westheimer (20) in 1955 investigated the hydrolysis of a variety of phosphate esters by $\text{La}(\text{OH})_3$ gels. The gel promotes the hydrolysis of the esters by up to 10^3 -fold. The reaction is at the P-center as shown by tracer studies. In that communication, the mechanism by which the metal ion promotes hydrolysis could not be specified although a mechanism involving the intermediacy of the metaphosphate anion was suggested as a possibility.

Sigel and co-workers have over a number of years investigated the hydrolysis of a variety of nucleoside 5'-triphosphates and the effects of divalent metal ions. A significant result is that for the hydrolysis of ϵ -ATP (ϵ -ATP is 1, N^6 -ethenoadenosine 5'-triphosphate) in the presence of both Zn^{2+} and Cu^{2+} , the most active species is a 2:1 complex metal ion: ϵ -ATP (122). It was also proposed that a metal ion bound OH^- ion effected the hydrolysis. The effect of a number of divalent metal ions on the rates of dephosphorylation of a number of nucleotide triphosphates has also been investigated (128). The ability to dephosphorylate ATP decreased in the order $\text{Cu}^{2+} > \text{Cd}^{2+} > \text{Zn}^{2+} > \text{Ni}^{2+} > \text{Mn}^{2+} > \text{Mg}^{2+}$. It was suggested that since the pH maximum for the hydrolytic reaction for a particular metal ion paralleled the tendency for that metal ion to form hydroxo complexes (i.e., the $\text{p}K_a$ of the coordinated water molecule) that a metal bound hydroxide ion was involved in the reaction. The most reactive species of the pyrimidine triphosphates could be formulated as $[\text{M}_2(\text{NTP})(\text{OH})]$, although the structure of the active complex could only be speculated upon. The reactivity of the purine NTPs was attributed to the dimeric species $[\text{M}_2(\text{NTP})_2(\text{OH})]$. In both cases, however, two divalent metal ions and a bound hydroxide ion seem to be required to activate the NTPs to hydrolysis.

Breslow and co-workers (64) studied the hydrolysis of diphenyl-4-nitrophenylphosphate (DPNPP) by the Zn^{2+} complex of macrocycle **5** (112). Wooley had studied this complex and found that it catalyzed the hydration

of acetaldehyde analogously to the enzyme carbonic anhydrase (148, 149). The complex **5** also catalyzed the hydrolysis of DPNPP in 50% acetonitrile in a reaction that was probably dependent on the deprotonation of the coordinated water ligand. Interestingly, the coordinated hydroxide ion is more effective than free OH^- at promoting the hydrolysis of the triester. This result presumably reflects the effectiveness of an intramolecular pathway as compared to an intermolecular route. The kinetic $\text{p}K_a$ found for this reaction is 8.7, identical to the value found independently for the aqua complex. In addition, slightly higher amounts of phenol than normal were liberated as well as the expected *p*-nitrophenol. The reaction proceeds at pH 8 only ~50-fold faster in the presence of 1 mM of the zinc complex of **5** as compared to its absence. No estimate of the equilibrium constant for coordination of the DPNPP by the zinc complex of **5** was made and therefore no estimate of the actual rate of attack of the coordinated hydroxide ion on the P center could be made. The complex behaves as a true catalyst, with a turnover number in the region of several hundred; however, the reaction is eventually inhibited by the major diester product of the reaction, diphenylphosphate.

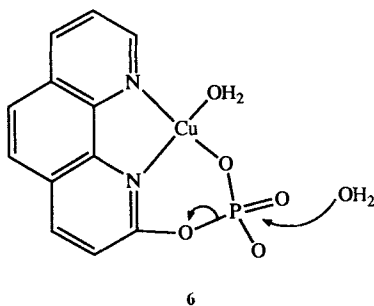


5

Morrow and Trogler (109) have studied the hydrolysis of two phosphate diesters by $[\text{Cu}(\text{bipy})]^{2+}$ (bipy = 2,2'-bipyridine) in aqueous solution at 75°C in the pH range 5.8–8.3. For both bis(4-nitrophenyl)phosphate and ethyl-4-nitrophenylphosphate the reaction was proposed to proceed via coordination of the diester to the $[\text{Cu}(\text{bipy})]^{2+}$ moiety followed by attack of a cis coordinated OH^- ion at the P center. Maximal rate enhancements of $\sim 10^3$ - to 10^4 -fold were reported. The reaction was accompanied by incorporation of a single ^{18}O label in the product ethylphosphate when the reaction was conducted in ^{18}O labeled water. Saturation kinetics were observed for the hydrolysis of ENPP (ethyl-4-nitrophenylphosphate). The reaction obeyed Michaelis–Menton kinetics with a k_m for the ENPP ion of $4.7 \times 10^{-2} M$ and a first-order reaction rate constant of $5.6 \times 10^{-4} \text{ s}^{-1}$

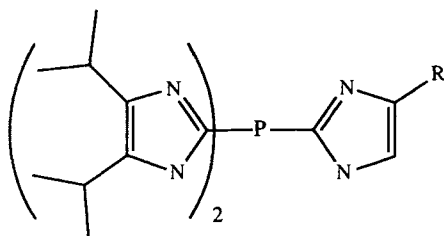
for attack of the coordinated hydroxide ion on the complexed diester at 75 °C. The kinetic pK_a (7.0) observed for the hydrolysis of ENPP by this complex ion is close to the measured pK_a (7.1) for $[\text{Cu}(\text{bipy})(\text{OH}_2)_2]^{2+}$. This result is rather surprising in view of the reduced overall charge on the complex when the phosphate diester is coordinated.

The hydrolysis of 2-(1,10-phenanthrolyl)phosphate not unexpectedly shows a catalytic effect for a variety of metal ions (59). The metal ions Cu^{2+} , Ni^{2+} , Co^{2+} , and Zn^{2+} have some effect on the rate of its hydrolysis, but only Cu^{2+} has a large effect. The ester binds all four metal ions very well, with saturation kinetics observed above 1 mM for all the metal ions involved. The Cu^{2+} ion was most effective at promoting hydrolysis of the ester. The rate enhancement is not great, however, amounting to ~ 300 -fold at pH 8 and 85 °C. The reaction was proposed to proceed via attack of H_2O on complex **6** or its kinetic equivalent, for example, attack of hydroxide ion on the protonated form of complex **6**. Apparently, the Cu^{2+} coordinated OH^- ion, when formed as expected at $\sim \text{pH}$ 7, is sterically restrained from attack at the P center.



Brown and Zamkane (11) have reported that the Co(II) complexes of **7** act as nucleophilic catalysts towards the hydrolysis of several phosphate triesters and a phosphonate diester. For **7a** the nucleophile is a Co(II) bound hydroxide ion, for **7b** the Co(II) coordinated alcoholate anion is suggested to be the nucleophile. The complexes were not significantly superior to the Co(II) ion alone except they remained soluble at higher pH. There was no evidence that the phosphate derivatives are bound to the Co center during the reaction.

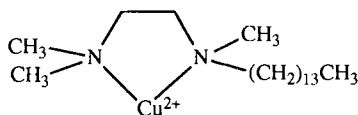
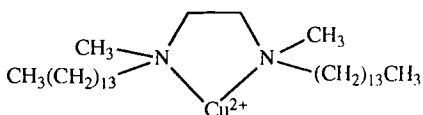
The use of several long-chain copper chelates, **8a** and **b**, to hydrolyze DPNPP has been reported (104). These complexes form micelles in water to which the triester is bound reasonably strongly ($K_{\text{assoc}} = 2.6 \times 10^5 \text{ M}^{-1}$). Once bound the triester is hydrolyzed. The observed rate constant reaches a maximum at a concentration of 0.6 mM in **8a**. The reaction is almost



7

R = H = **7a**, R = CH₂CH₂OH = **7b**.

independent of pH in the region of pH 6–8, and it is claimed that this independence implies that the pK_a of the Cu–OH₂ moiety in the micelle is less than pH 6, and that the reaction proceeds via attack of the coordinated hydroxide ion on the micelle bound ester. It is estimated that the rate enhancement over the uncatalyzed reaction is up to 10⁵, which is very

**8a****8b**

substantial compared to that usually observed for divalent metal ions; micelle formation seems to play a very important role in the reaction. The reaction is catalytic, at least up to two turnovers. The complex **8a** also hydrolyzes a number of other phosphate derivatives including BNPP and the nerve agent GD, a fluorophosphonate ester. Another complex, **8b**, with hydrolytic properties similar to **8a** was also prepared. The solubility of the complex in water was rather limited, however.

IV. REACTIVITY OF SUBSTITUTION INERT METAL ION COMPLEXES

A. Introduction

The problems encountered with the study of labile metal ions, that is, the difficulty of assigning a “configuration” to the complex responsible for

the rate enhancement, can be resolved by the use of well-defined substitution inert complexes. The use of such complexes has yielded important information, particularly with respect to the activation of the P center to attack by inter- and intramolecular nucleophiles. The major part of this chapter therefore, is concerned with an analysis of the reactivity of such robust complexes, because there is a need to establish what the effective paths are in order to design good catalysts to promote the reactions. A consequence of such catalysis is that turnover ensues and by implication the rate limiting steps become more difficult to define.

B. Intermolecular Attack of Nucleophiles

The first topic discussed in this section is the intermolecular attack of nucleophiles on the P center of coordinated phosphate derivatives. This method is probably the simplest by which a metal ion can influence the reactivity of the phosphate moiety, since it does not necessarily involve any change in the mechanism. Coordination of a metal ion to a phosphate derivative will have two immediate effects; one is to increase the positive charge on the phosphate and the other is to make the P center more electrophilic. The effects are mutually dependent and cannot be readily separated. For anionic or polar nucleophiles both effects will tend to increase the rate of attack of the nucleophile at the P center.

The first clear example of activation of a phosphate exclusively by this mode was the reaction involving intermolecular attack of hydroxide ion on trimethylphosphate (TMP) coordinated to the pentaammineiridium(III) moiety (75). This complex was chosen because the Ir-O bond is not readily broken and survives the reaction at the P center. The reaction of the free TMP in hydroxide ion solution presumably occurs by direct attack of hydroxide ion on the P center to give the five-coordinate oxyphosphorane and ultimately methanol and dimethylphosphate. Similarly, the reaction of the complex occurs exclusively by attack of OH⁻ at the P center yielding finally dimethylphosphatopentaammineiridium(III) ion and methanol, as shown by an ¹⁸O tracer experiment. Both reactions have the same rate law:

$$v = k_1[\text{phosphate ester}][\text{OH}^-]$$

Free TMP has a rate constant k_1 of $1.6 \times 10^{-4} \text{ L}\cdot\text{mol}^{-1} \text{ s}^{-1}$ in aqueous conditions at 25 °C (3). The Ir(III) complex has a rate constant k_1 of $6.7 \times 10^{-2} \text{ L}\cdot\text{mol}^{-1} \text{ s}^{-1}$ at 25 °C, a rate enhancement of 400-fold. This effect is significant but not exciting in relation to the enzymic catalysis.

The analogous Rh(III) complex has also been synthesized and its reactivity studied (77). Like the Ir(III) complex, the P center is attacked by

OH^- to produce the coordinated dimethylphosphate (DMP) anion and methanol; in this case, however, the reaction is accompanied by considerable Rh–O bond cleavage. This reaction presumably occurs by the characteristic dissociative conjugate base, $\text{S}_{\text{N}}1(\text{cb})$, mechanism (136) for metal–ligand bond rupture, which also has a first-order dependence on hydroxide ion concentration. At zero buffer concentration the rate follows the rate law:

$$v = k_{\text{p}}[\text{complex}][\text{OH}^-] + k_{\text{cb}}[\text{complex}][\text{OH}^-]$$

where k_{p} is $6.9 \times 10^{-2} \text{ L}\cdot\text{mol}^{-1} \text{ s}^{-1}$ at 25°C and refers to the production of methanol and coordinated DMP; k_{cb} has the value $0.42 \text{ L}\cdot\text{mol}^{-1} \text{ s}^{-1}$ and refers to the $\text{S}_{\text{N}}1(\text{cb})$ reaction to produce free TMP and pentaamminehydroxorhodium(III). The reaction was actually followed in 1-butylamine buffers and a significant effect of free amine was observed. The amine actually attacked the carbon of the methyl groups to demethylate the coordinated TMP and produce methylated butylamine.

The rates for attack of hydroxide ion on the P center of TMP coordinated to both metal ions are identical within experimental error, indicating that the metal ions Ir(III) and Rh(III) have very similar inductive and charge modification effects on the TMP ester.

The other member of this triad of metals, [pentaamminetrimethylphosphatocobalt] $^{3+}$, was first synthesized by Taube and co-workers in the 1960s (90, 123). They reported that the hydrolysis of the TMP complex produced only the aquapentaamminecobalt(III) complex and free TMP and that the reaction occurred predominantly with Co–O bond cleavage but with some P–O bond cleavage, 20% in neutral solution and 12% in alkaline solution. Later, however, the experiment was repeated and shown to occur with at least 97% Co–O bond cleavage by the $\text{S}_{\text{N}}1(\text{cb})$ mechanism (52). We can presume that the attack of hydroxide ion on the P center of trimethylphosphatopentaamminecobalt(III) occurs with a similar rate constant to that observed for the analogous Rh(III) and Ir(III) complexes since similar effects have been demonstrated for the members of the cobalt triad with intermolecular reactions of coordinated amides and nitriles (15, 16, 46, 151). The rate constant for the $\text{S}_{\text{N}}1(\text{cb})$ (ligand loss) reaction for the Co(III) complex is $78 \text{ L}\cdot\text{mol}^{-1} \text{ s}^{-1}$ at 25°C (52) and therefore the reaction of the P center is too slow to compete effectively.

It has, however, proved possible to demethylate the pentaammine-TMPcobalt complex by the use of “softer” nucleophiles such as SCN^- , I^- and $\text{S}_2\text{O}_3^{2-}$ (83). The reaction occurs exclusively at the carbon center of the methyl group. The rate enhancement over the same reaction on the

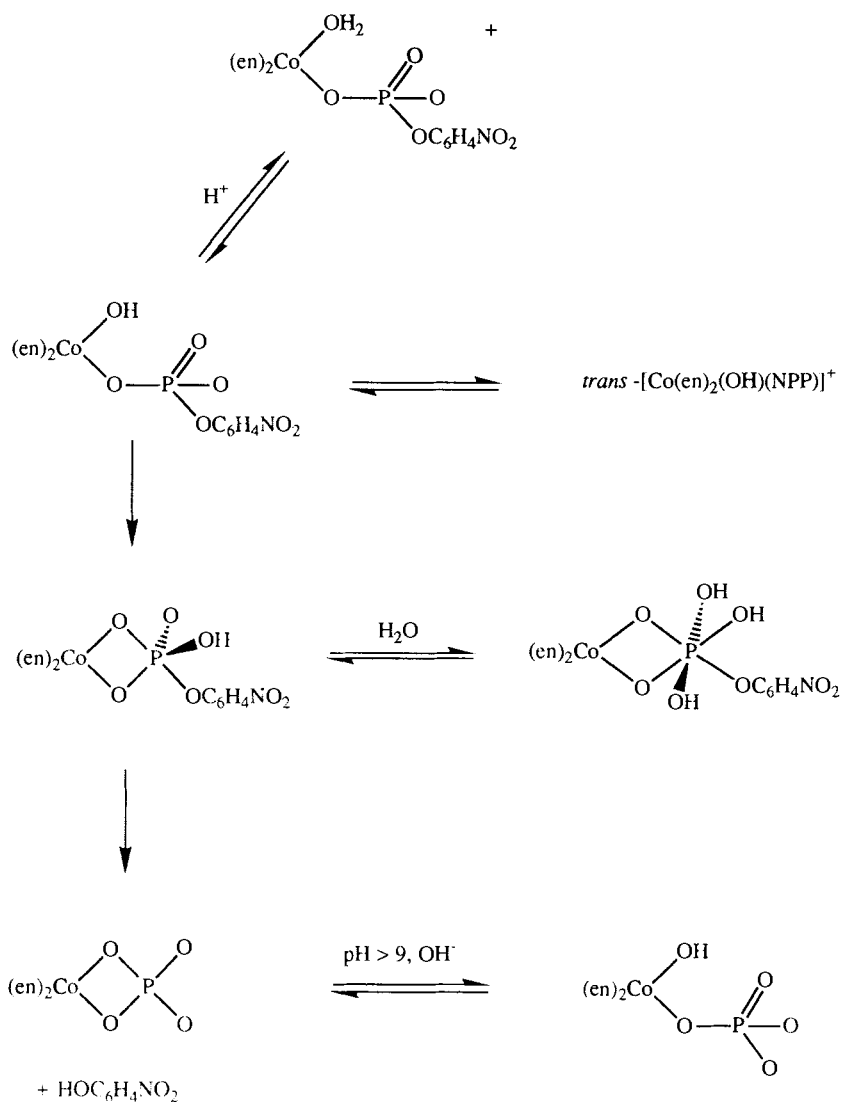
uncoordinated TMP is ~ 150 -fold for all three nucleophiles, and similar to that observed for attack of OH^- on the P center of TMP.

The net result is that, in these intermolecular reactions mediated by the metal ion, the rate enhancements can be appreciable but not dramatic and certainly not anywhere near the enzymic activation.

C. Intramolecular Attack of Hydroxide Ion: Cobalt(III) Complexes

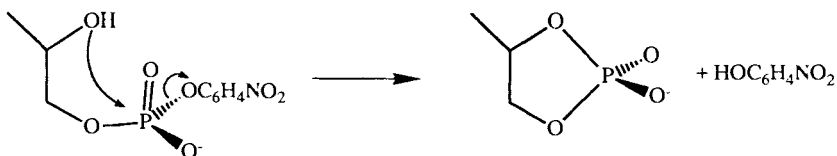
The efficiency of the intramolecular nucleophile OH^- in causing hydrolysis was examined initially through the reactivity of the 4-nitrophenylphosphate ion in the complex ion $\text{cis}[(\text{en})_2\text{Co}(\text{OH}_2)(\text{NPP})]^+$ (87). In that study, it was shown that the labeled cis coordinated hydroxide ion attacked the P center to yield 4-nitrophenolate and the chelated phosphate ion as the P-containing product. An initial rate increase over the pH range 6–8 coincides with deprotonation of the coordinated water molecule to give the coordinated hydroxide ion. The pH independent region (pH 8–12) corresponds to the reactivity of the hydroxo complex and yields 86% NP and 14% NPP as the products. Tracer studies (^{18}O) show that the former derives solely from the attack of the coordinated nucleophile and the latter by Co–O rupture of NPP from isomerized $\text{trans}[(\text{en})_2\text{Co}(\text{OH})(\text{NPP})]$ via the usual $\text{S}_{\text{N}}1(\text{cb})$ path, Scheme 6. The kinetic $\text{p}K_{\text{a}}$ for the reaction was 7.6, as was the directly measured $\text{p}K_{\text{a}}$ for the aqua group proton. Between pH 8 and 12 the rate constant for production of NP was $\sim 10^{-3} \text{ s}^{-1}$ at 25 °C. This intramolecular path yields initially the intermediate five-coordinate phosphorane that has a lifetime long enough to exchange oxygen (17–20%) with the solvent water; this result in turn implies the involvement of a six-coordinate species as an activated complex or intermediate. The five-coordinate phosphorane decays rapidly to the chelate phosphate complex whose ring opens at $\text{pH} > 9$ to yield some of the monodentate phosphato complex (17, 102). The rate enhancement of the reaction over the uncoordinated NPP ion is $> 10^5$ -fold at pH 9 since the rate constant for hydrolysis of NPP in aqueous solution at pH 9 is estimated to be $2 \times 10^{-9} \text{ s}^{-1}$ at 25 °C (57).

The essential feature of the reaction is relatively rapid hydrolysis of the ester moiety by the intramolecular nucleophile at near neutral conditions. This rate enhancement occurs despite the formation of a strained four-membered ring and despite the reduction of basicity of OH^- on coordination to the metal ion. Coordinated OH^- is in this system some 10^7 – 10^8 -fold less basic than free OH^- , yet it is a more efficient nucleophile by a factor of 10^5 – 10^6 . The comparison clearly attests to the efficiency of the intramolecular pathway.



Scheme 6

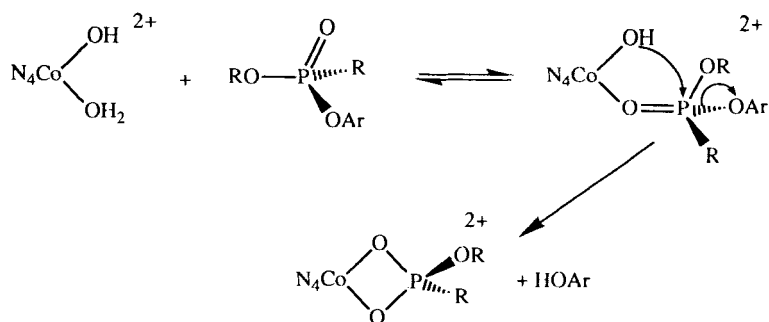
Other primary features of this chemistry are that it demonstrates facile O-to-O phosphoryl transfer and that the mode of reaction of the monoester is by the phosphorane path and not via the metaphosphate intermediate. Both the tracer experiments and the chelate product require this conclusion.



Scheme 7

It is of interest to compare the metal centered chemistry with that of an organic analogue such as that shown in Scheme 7. The reaction is first order in OH^- in the pH range 8–14 with $k = 0.21 \text{ L}\cdot\text{mol}^{-1} \text{ s}^{-1}$ at 25°C and $\mu = 1.0 \text{ M}$ (12). It follows that at pH 8 coordinated OH^- is much more efficient than the alcohol in effecting the hydrolysis. By implication, however, the alkoxide ion would be superior to coordinated OH^- in an intramolecular role if allowance were made for the difference in ring size. This conclusion follows from the relative basicities of the two nucleophiles. In this context, it is clear that metal ions can provide a source of efficient nucleophiles (coordinated OH^-) at biological pH, whereas an alcohol group would be in more difficulty on this count and would require a general base to remove the proton and create the nucleophile.

Substitutionally labile hydroxo(aqua)tetraaminocobalt(III) complexes may also be used in a catalytic or semicatalytic role (Scheme 8) and by inference the bound OH^- ion is the effective nucleophile. Rapid water exchange in these complexes is the key step followed by competitive coordination of the substrate. $[\text{Co}(\text{tn})_2(\text{OH})(\text{OH}_2)]^{2+}$ ion was an early reagent effective in regard of its ability to hydrolyze 4-nitrophenylphosphate (2), polyphosphates (73, 74, 87), nitriles (47) and to hydrate olefins (62). The strategy has since been taken up and used effectively for a variety of substrates. Various cobalt(III) complexes of the general formula $[\text{N}_4\text{Co}(\text{OH})(\text{OH}_2)]^{2+}$ [where N_4 represents a bis-bidentate or tetradentate N donor ligand(s)] have been used to hydrolyze the phosphonate esters 4-nitrophenyl-methylphosphonate and ethyl-4-nitrophenyl-methylphosphonate (91). The complexes include, $\text{N}_4 = \text{tn}_2, \text{tmen}_2, \text{trien}$, and bipy_2 ($\text{tn} = 1,3$ -propanediamine, $\text{tmen} = 2,3$ -dimethyl-2,3-butanediamine, $\text{trien} = 1,8$ -diamino-3,6-diazaoctane, $\text{bipy} = 2,2'$ -bipyridine). The rate of the reaction to produce 4-nitrophenolate from both phosphonates parallels the reactivity of the complexes with regard to exchange of the coordinated water ($\text{tmen}_2 > \text{tn}_2 > \text{trien} > \text{bipy}_2$), indicating that the rate-limiting step in the reaction is probably the substitution step shown in Scheme 8. The intramolecular attack of the cis coordinated hydroxide ion upon the P center proceeds rapidly. The rate constant observed for liberation of NP is thus related to the rate of exchange of water on the complex. The reactions



Scheme 8

appear to be catalytic at least for several turnovers. The most reactive complex, *cis*-[(trpn)₂Co(OH)(OH₂)]²⁺, yields an apparent second-order rate constant for the reaction with PMP of $1.47 \times 10^{-1} \text{ L} \cdot \text{mol}^{-1} \text{ s}^{-1}$.

Hydrolysis of the monoester 2,4-dinitrophenylphosphate (DNPP) by the complexes [(trpn)Co(OH)(OH₂)]²⁺ (trpn = 4-(3-propylamine)-4-azaheptane-1,7-diamine) and [(tn)₂Co(OH)(OH₂)]²⁺ occurs relatively rapidly (119). The trpn complex reacts by a mechanism that appears to be a reversible binding of the phosphate to the Co(III) ion followed by intramolecular attack of the *cis* coordinated hydroxide ion. The equilibrium and first-order rate constants required to describe the system are 216 mol^{-1} and 0.106 s^{-1} , respectively. The reaction promoted by the (tn)₂ complex is more complex and apparently involves both a 1:1 complex analogous to that above and a 2:1 Co:P complex. The constants describing the system were given as $K_1 = 314 \text{ mol}^{-1}$, $K_2 = 212 \text{ mol}^{-2}$ and $k_1 = 1.39 \times 10^{-4} \text{ s}^{-1}$ and $k_2 = 2.81 \times 10^{-3} \text{ s}^{-1}$. The results imply that the amine ligands have a marked effect on the rates of the intramolecular reactions, that is, a 10^3 -fold difference for the hydrolysis of the *cis* coordinated phosphate esters. It is not likely that the $\text{p}K_a$ values of the coordinated water molecules differ by more than one unit but it is likely as a result of the compression from the chelate rings that the angle between the bound substrate and the *cis* OH⁻ is less for the trpn complex than for the tn₂ complex.

Similarly, Chin and co-workers have studied the hydrolysis of a number of phosphate esters by several complexes of the type [N₄Co(OH)(OH₂)]²⁺ (25–28). Cyclic-AMP is estimated to be hydrolyzed 10^8 -fold faster, at pH 7 and 50 °C, in the presence of [(trien)Co(OH)(OH₂)]²⁺ than in its absence (25). The mechanism proposed is that described above. In later reports (27, 28) the effect of changing the N₄ ligand is described. The cyclen, tren, and trpn complexes (which are all *cis* complexes) hydrolyze bis(4-nitro-

phenyl)phosphate (BNPP) with apparent second-order rate constants that parallel their rates of anation by phosphate ion. The differences, however, which amount to some 300-fold are explained solely in terms of differences in the rates in intramolecular attack of hydroxide ion. In another paper (26), however, the importance of the rate of formation of the phosphate ester complex with the less labile cobalt ions was acknowledged to be important. This uncertainty highlights the problem of using even well-behaved pseudolabile metal ion complexes when investigating reaction mechanisms of this type; that is, it is difficult to separate the various reaction steps and equilibria.

Irrespective of these uncertainties, rate enhancements using these procedures are substantial. The reagents are useful to do the chemistry required on a reasonable time scale, pH and temperature, and they add significantly to the chemical armory. Moreover, there are interesting stereochemical facets to be explored. For example, recent work in this laboratory (147) has shown that different complexes of this type have different reactivities towards 3',5'-cyclic AMP; the complex $[\text{trienCo}(\text{OH})(\text{OH}_2)]^{2+}$ yields predominantly 3'-AMP as the major (~90%) product. The complex $[(\text{tn})_2\text{Co}(\text{OH})(\text{OH}_2)]^{2+}$, however, yields ~80% of

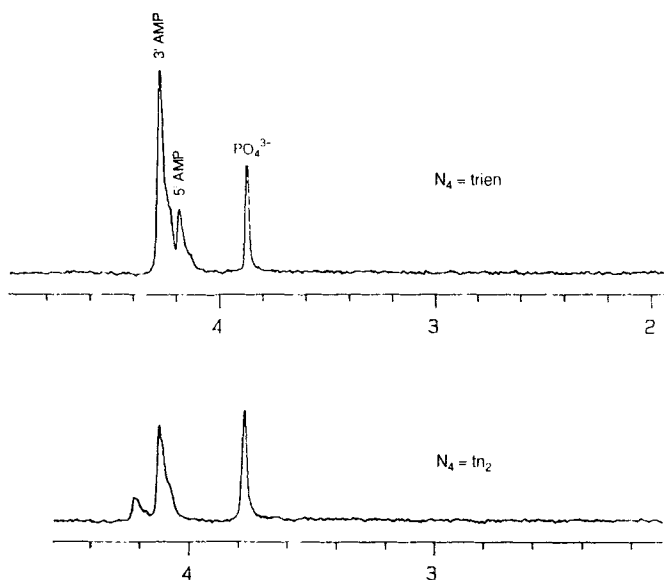
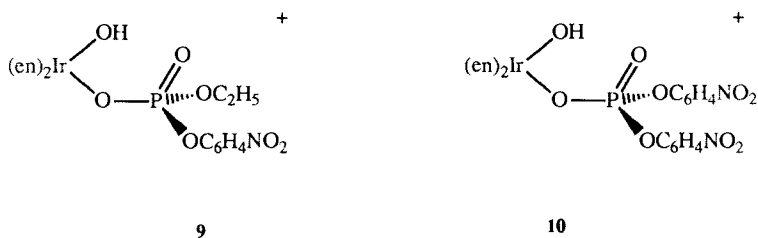


Figure 1. ^{31}P NMR of the products of hydrolysis of cyclic-AMP by $[\text{N}_4\text{Co}(\text{OH})(\text{OH}_2)]^{2+}$ after reduction of Co(III).

the 5'-AMP (Fig. 1). This difference can be interpreted in terms of differing steric demands of the two complexes when bound to the substrate. The implication in this study is that reagents of this type may selectively cleave DNA or RNA at the 3' or 5' sites.

D. Intramolecular Attack of Hydroxide Ions: Iridium(III) Complexes

The use of the coordinated hydroxide ion as an intramolecular nucleophile has also been explored for Ir(III) bound phosphate esters. The complexes **9** and **10** were synthesized and their behavior studied over the pH range 5–14 (78). As the pH was increased from 5 for both complexes, the rate of release of nitrophenolate increased as the aqua group was deprotonated. Both the complexes had kinetic pK_a values of around 7.0 as expected for dicationic Ir(III) complexes. Above \sim pH 8 the reaction reaches a plateau region and the rate of production of NP is independent of pH. As the concentration of hydroxide ion is increased above pH \sim 11 the rate of release of NP increases again.



The rate of hydrolysis of both complexes over the entire pH range follows the rate law:

$$v = \{k_1 K_a / (K_a + [\text{H}^+])\} + k_2 [\text{OH}^-] + k_3 [\text{OH}^-]^2.$$

For the ENPP complex the values of the rate constants were $4.6 \times 10^{-5} \text{ s}^{-1}$, $2.7 \times 10^{-4} \text{ L}\cdot\text{mol}^{-1} \text{ s}^{-1}$ and $6.6 \times 10^{-4} \text{ L}^2\cdot\text{mol}^{-2} \text{ s}^{-1}$ for k_1 , k_2 , and k_3 , respectively. Likewise for the BNPP complex the rate constants are $3.95 \times 10^{-4} \text{ s}^{-1}$, $2 \times 10^{-2} \text{ L}\cdot\text{mol}^{-1} \text{ s}^{-1}$, and $6 \times 10^{-2} \text{ L}^2\cdot\text{mol}^{-2} \text{ s}^{-1}$ (79).

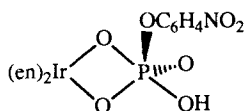
^{31}P NMR spectra recorded while the reaction was in progress indicated that a single species was produced over the entire pH range. In the ^{31}P NMR for both complexes only the ring opened monodentate monoester was observed. Apparently the chelate monoester that must be formed in the initial reaction is hydrolyzed rapidly. The metal ion *locus* for the reaction, Ir(III), is an extremely inert cation with respect to ligand exchange;

indeed, this reason is why it was chosen and, unlike the reactions of the Co(III) complexes in the previous section, no cis-to-trans isomerization was observed. It follows that the Ir(III) ion should also limit the rate of any metal centered reaction, for example, Ir–O cleavage. It was therefore of considerable interest to determine whether the ring-opening of the chelate ester occurred with P–O or Ir–O cleavage. An ^{18}O tracer study was conducted using the ^{31}P NMR isotope shift method and the reaction was judged to occur at least predominantly with P–O cleavage. Thus although the chelate ester is not observed, its presence as a short lived intermediate is not in doubt. The fact that the chelate ester is present and is rapidly hydrolyzed, presumably via an $\text{S}_{\text{N}}2(\text{P})$ -type mechanism, is of interest. No reaction was observed for the monodentate ethylphosphate even in 1 M NaOH over 50 days at 20 °C. This result implies a maximal rate constant of $\sim 10^{-8} \text{ s}^{-1}$ for the conditions. The rate constant for the generation of the chelate at pH 8 is $\sim 5 \times 10^{-5} \text{ s}^{-1}$, so ring opening must occur at least as fast. If the chelate monoester is hydrolyzed by intermolecular attack of hydroxide ion then a second-order rate constant of $\geq 10 \text{ L}\cdot\text{mol}^{-1} \text{ s}^{-1}$ is required to produce an observed rate of the correct magnitude. This value represents a rate enhancement for attack of OH^- on the P center of some 10^9 . If the reaction proceeds by attack of water, then the rate need only be $\sim 5 \times 10^{-5} \text{ s}^{-1}$; however, this value represents still a very substantial increase in the susceptibility of the ester towards P–O cleavage upon chelation to the Ir(III) ion but not towards exohydrolysis.

Similarly, for the BNPP complex (**10**) hydrolysis and generation of the chelate occurs with a rate constant of $4 \times 10^{-4} \text{ s}^{-1}$ at pH 8 and 25 °C. Intermolecular attack of hydroxide ion on the uncoordinated ester NPP occurs with a rate constant of $2 \times 10^{-9} \text{ s}^{-1}$ in 0.5M NaOH at 25 °C. If the ring opening of the product chelate NPP occurs by intermolecular attack of OH^- then to achieve a rate of $4 \times 10^{-4} \text{ s}^{-1}$ at pH 8 a second-order rate constant of $4 \times 10^2 \text{ L}\cdot\text{mol}^{-1} \text{ s}^{-1}$ is required. This value represents a rate increase of 10^{11} -fold for P–O bond rupture over that for the uncoordinated ester.

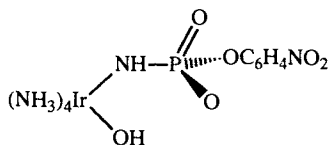
Therefore, the chelation of the phosphate ester does have a very significant effect on its reactivity. The reaction, however, is ring opening and no loss of the exocyclic ester group is observed even for the 4-nitrophenol group. By applying Westheimer's criteria for a $\text{S}_{\text{N}}2(\text{P})$ reaction, namely, that the nucleophile and leaving group enter and depart, respectively, from the apical positions of the trigonal bipyramid (TBP) and that the small ring must span axial-equatorial positions in the TBP, it is apparent that the entering nucleophile occupies one apical position, and one of the oxygen atoms of the chelate ring occupies the other. Consequently, the ester group must always be equatorially oriented in the TBP, **11**. For loss of this

ester group to occur, the TBP intermediate must undergo some form of rearrangement, for example, pseudorotation, to place the ester group in an axial position. That this reorientation does not occur even with the nitrophenolate leaving group implies that the TBP intermediate is either not able to rearrange or that the lifetime of this intermediate is too short to allow such a process to take place. Since all the substituents of the TBP intermediate are of similar apicophilicity and there are examples of phosphoranes containing four-membered rings (50) that are able to pseudorotate readily, there seems no reason why the TBP should not be able to pseudorotate. It seems simply that chelate P–O rupture for decay of the TBP intermediate is faster than pseudorotation.



11

The major product of the hydrolysis of *cis*-[(*en*)₂Ir(OH)(BNPP)]⁺ (**10**) the corresponding monoester, is also hydrolyzed by attack of the *cis* coordinated hydroxide ion with a rate constant of $8 \times 10^{-6} \text{ s}^{-1}$ at 40 °C, or $\sim 2 \times 10^{-6} \text{ s}^{-1}$ at 25 °C in the pH independent region. The product of this reaction is the ring opened monodentate phosphato complex *cis*-[(*en*)₂Ir(OH)(OPO₃)]⁻. Thus, unlike the corresponding Co(III) complex, the chelate is not thermodynamically stable even at pH 9. The rate of attack of the *cis* coordinated hydroxide ion on the P center is also ~ 500 -fold slower than that reported for the analogous Co(III) reaction.



12

The major product of the hydrolysis of [(NH₃)₅IrBNPP]²⁺ (see below), complex **12**, undergoes intramolecular attack of hydroxide ion to yield the chelated phosphoramidate ion, which is observed in the ³¹P NMR spectra of the reaction products along with the ring opened species, N-coordinated

phosphoramidate. The coordination of the N of the phosphoramidate to the Ir(III) ion greatly increases the acidity of the protons on that atom, as observed previously for Co(III) chelated phosphoramidate ($pK_a = 13.1$) and the tetraammineiridium-*N*-ethylphosphoramidate ($pK_a = 12.5$). As expected, the deprotonated nitrophenylphosphoramidate is less susceptible to nucleophilic attack at the P center than the protonated complex. Thus the first-order rate constant for attack of coordinated hydroxide ion on the N-protonated complex is $3.1 \times 10^{-3} \text{ s}^{-1}$ at 25 °C but, as the pH is increased to above pH 11, the rate drops to $2 \times 10^{-5} \text{ s}^{-1}$. The kinetic pK_a and the pK_a determined from the ^{31}P NMR chemical shift dependence are both ~ 9.8 (see Fig. 2). The effect of the nitrophenyl group as compared to the ethyl group lowers the pK_a by 2.7.

The attack of the *cis* coordinated hydroxide ion on the P center of complex **12** occurs more rapidly than for the reaction of the BNPP complex, **10**. Interestingly, the chelated phosphoramidate product is observed transiently in the ^{31}P NMR spectrum of the reacting ions at pH 10.4. At pH 6.1 it is relatively long lived, perhaps indicating that the ring-opening reaction is dependent on $[\text{OH}^-]$. The product in both cases was the monodentate N-coordinated phosphoramidate.

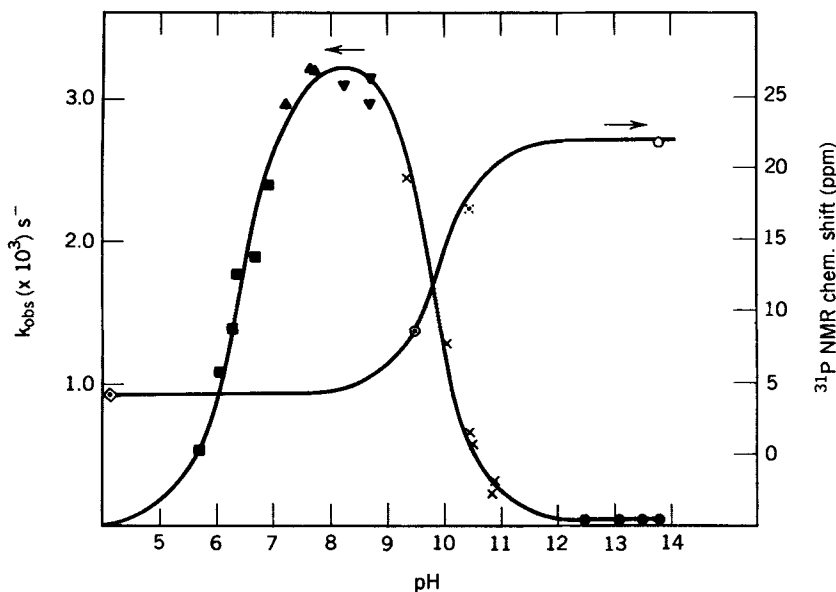
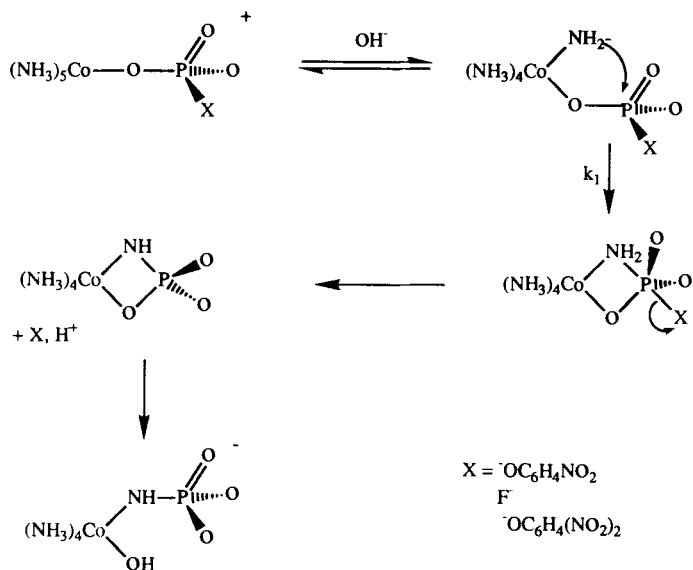


Figure 2. pH vs. rate and ^{31}P NMR chemical shift for the reaction of **12**. Buffers; ■ mes, ▲ hepes, ▼ tris, × caps, ● OH^- , ◇ acetate, ○ NH_3 .

E. Intramolecular Attack of Amido Ion: Cobalt(III) Complexes

The transfer of the phosphoryl group from oxygen to oxygen has been demonstrated by the preceding experiments, but one of the important biological pathways is facile transfer of a phosphoryl group from an oxygen to nitrogen. This section addresses that issue. The hydrolysis of 4-nitrophenylphosphate coordinated to the pentaamminecobalt(III) moiety has been studied, Scheme 9 (70). The reaction proceeds via two competing pathways, the $S_N1(cb)$ path resulting in loss of the NPP ligand, and the other involving attack of coordinated amido ion (NH_2^-) at the P center. Deprotonation of an ammonia cis to the ester leads to rapid reaction and ester hydrolysis (estimated $k_1 = 0.4 \text{ s}^{-1}$ at 25°C). It is not clear at this time if the process is concerted or if the aminophosphorane has a lifetime long enough for its intermediacy to be probed. If it is an intermediate, however, it does not have a lifetime long enough to exchange its oxygen atoms with the solvent H_2O . What it achieves relatively rapidly is the elimination of the nitrophenol with the production of the phosphoramidate ion. The phosphoramidate ion is presumably chelated initially and undergoes rapid Co-O ring opening to give the hydroxo-*N*-bound phosphoramidate complex, which is the first observed (^{31}P NMR) product of the reaction.

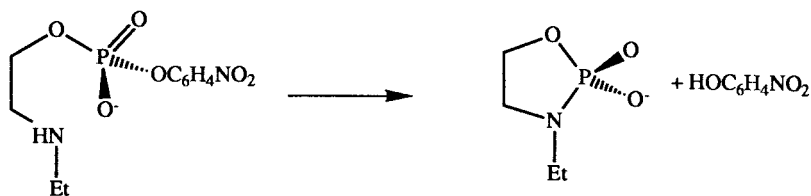


Scheme 9

In addition to hydrolysis in order to produce nitrophenolate, this reaction involves rapid transfer of a phosphoryl group from O to N. If the amido ion concentration is taken into account, then the ester hydrolysis and O-to-N phosphoryl transfer are enhanced at least 10^8 -fold relative to the uncoordinated ester reacting with OH^- or NH_3 (the $\text{p}K_a$ of the coordinated ammonia is estimated as ~ 17). If the concentration of the intramolecular nucleophile is ignored ($k_{\text{OH}} = 3.6 \times 10^{-4} \text{ L}\cdot\text{mol}^{-1} \text{ s}^{-1}$ at 25°C) then the rate enhancement factor is still 10^5 -fold. The enhancement for the intramolecular reaction is surprisingly large when it is borne in mind that a strained four-membered ring is formed. The strain in a trigonal bipyramid about the P atom is, however, not as great as that expected in the tetrahedral ground state provided that the chelate spans the axial-equatorial positions. Therefore, it can be inferred that the reaction is concerted or that addition of the nucleophile is rate limiting and not decay of the aminophosphorane.

The metal ion chemistry may be compared with the related intramolecular organic substitutions using the substrate shown in Scheme 10. This process is also first order in OH^- up to the $\text{p}K_a$ of the amine moiety, after which a limiting rate is reached ($k = 2.7 \times 10^{-3} \text{ s}^{-1}$ at 35°C , $\mu = 1.0 \text{ M}$) (111). Clearly the process is much slower than that estimated for the complex. Correspondingly, however, the $\text{p}K_a$ of the amine is much lower than that for the complex, 9.4 vs. ~ 17 . The different reactivities reflect in part this difference in $\text{p}K_a$ and in part the strain difference in formation of the ring systems. The four-membered chelate should be considerably more difficult to form than the five-membered organic ring.

The reaction of fluorophosphate in the $[(\text{NH}_3)_5\text{CoO}_3\text{PF}]^+$ moiety proceeds in an analogous manner (41), with loss of F^- and a rate enhancement of $>10^7$ over the uncoordinated fluorophosphate. The rate constant for attack of the coordinated amido ion on the P center is $1.7 \times 10^{-3} \text{ L}\cdot\text{mol}^{-1} \text{ s}^{-1}$ at 25°C , as is the rate constant for the parallel reaction resulting in the loss of the O_3PF^{3-} anion from the complex. The rate constant for hydrolysis of fluorophosphate ion in 0.6 M NaOH at 80°C is $8.2 \times 10^{-7} \text{ s}^{-1}$ (51) and is estimated to be $\sim 10^{-10} \text{ L}\cdot\text{mol}^{-1} \text{ s}^{-1}$ at 25°C (41). If the



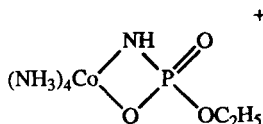
Scheme 10

proportion of the complex in the deprotonated state is taken into account, a rate enhancement of some 10^{10} -fold is estimated. Despite the fact that this reaction proceeded ~ 10 -fold faster than the analogous NPP reaction the chelate phosphoramidate was still not observed.

The observation of the elusive chelate phosphoramidate was achieved, however, by using an even more reactive analogue, the 2,4-dinitrophenylphosphate complex $[(\text{NH}_3)_5\text{CoDNPP}]^+$ (76). The second-order rate constant for the production of 2,4-dinitrophenolate ion was $1.8 \times 10^{-2} \text{ L}\cdot\text{mol}^{-1} \text{ s}^{-1}$ at 25°C , ~ 100 -fold faster than that observed for the NPP complex. The N,O chelate was observed by ^{31}P NMR to grow in and decay over the course of the overall reaction. This observation supported the inference that the chelate phosphoramidate was an intermediate in this and the previous reactions. The chelate phosphoramidate complex displayed a substantial pH dependence of its ^{31}P NMR chemical shift; at an OH^- ion concentration of 0.15M the chemical shift was 22.1 ppm and at 0.98M it was 30.6 ppm. A plot of pH vs. chemical shift for the chelate followed a titration curve for a single ionizable proton with a $\text{p}K_a$ of 13.1 and chemical shifts of 18 and 34 ppm for the fully protonated and deprotonated complexes, respectively. As expected from the previous studies the chelate was observed to decay to the monodentate *N*-phosphoramidate complex with a rate constant ($1 \times 10^{-3} \text{ s}^{-1}$) apparently independent of $[\text{OH}^-]$ in the range $0.15\text{--}0.5\text{M}$ NaOH but increasing to $\sim 2 \times 10^{-3} \text{ s}^{-1}$ in 1.0M NaOH at 25°C . When compared to the rate of attack of NH_3 on the P center in 1M NH_3 solution [$1.5 \times 10^{-5} \text{ L}\cdot\text{mol}^{-1} \text{ s}^{-1}$ (76)] the rate of attack of the cis coordinated NH_2^- ion on the P center represents a rate enhancement of 10^3 -fold, but if the amount of nucleophile in the deprotonated form is considered, this value rises to $\sim 10^6$.

The observation of the chelate phosphoramidate in the previous series of experiments pointed the way to investigate the reactivity of a chelated phosphoramidate ester. This opportunity arises by coordinating a phosphate diester to the $[(\text{NH}_3)_5\text{Co}]^{3+}$ moiety. After attack of the coordinated amido ion at the P center, the aminophosphorane should decay to the chelate phosphoramidate monoester. Such an imidoester would contain essentially a very strained chelate ring including the phosphorus atom and an exocyclic ester group and the reactivity of such systems has been the subject of considerable speculation ever since Westheimer rationalized the reactivity of the cyclic organic phosphate esters. The ester chosen for this study was the ethyl-4-nitrophenylphosphate ion (ENPP) (79). As expected, the hydrolysis reaction was first order in hydroxide ion and complex. The familiar pattern of some ligand loss was also observed. Below 25°C , the dominant reaction produced nitrophenolate, the $\text{S}_{\text{N}}1(\text{cb})$ reaction produced free ENPP, which increased relatively at higher temperatures. The phos-

phorus containing product of the NP producing reaction was found to be the chelate phosphoramidate ester **13** and the rate constant for production of the chelate was $0.29 \text{ L}\cdot\text{mol}^{-1} \text{ s}^{-1}$ in hydroxide ion solution at 25°C . The free ligand is hydrolyzed in hydroxide ion solution with a rate constant of $3.3 \times 10^{-7} \text{ L}\cdot\text{mol}^{-1} \text{ s}^{-1}$ at 25°C and $\mu = 1.0M$. Thus the cleavage of NP from the ester is enhanced 10^6 -fold upon coordination to the $[(\text{NH}_3)_5\text{Co}]^{3+}$ moiety, or 10^8 -fold if the concentration of the nucleophile is taken into account [estimated $\text{p}K_a = 16$ (5)].



13

In base the chelate, **13**, decomposed to the free ethylphosphoramidate ion; no intermediate in the reaction between the chelate and the free ethylphosphoramidate was observed. The ^{18}O tracer studies showed that the reaction proceeded with Co-ligand cleavage, that is, no reaction occurred at the P center. The rate of decomposition of the phosphoramidate ester chelate was estimated to be 10^{-3} s^{-1} and was independent of hydroxide ion concentration in strongly basic solution, almost identical to the rate of ring opening of the chelate phosphoramidate complex under the same conditions. The base independent ring-opening reactions of these chelates is interesting from the point of view of the $\text{S}_{\text{N}}1(\text{cb})$ mechanism for metal-ligand bond rupture. Under the conditions of the ring-opening reactions for both the chelate phosphoramidate and the phosphoramidate ester, the nitrogen in the chelate ring is largely deprotonated, and is probably acting to labilize the adjacent site, that is, the oxygen of the chelate ring in the manner usually ascribed to the deprotonated amine group in the $\text{S}_{\text{N}}1(\text{cb})$ reaction.

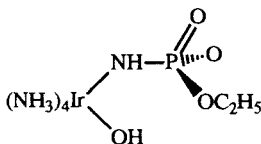
The hydrolysis of ethylene phosphate in hydroxide ion solution proceeds with a rate constant of $5 \times 10^{-4} \text{ L}\cdot\text{mol}^{-1} \text{ s}^{-1}$ (100). The O-P-O angle in the ring of ethylene phosphate of 99° is expected to be rather similar to that for the four-membered ring incorporating the cobalt and phosphorus centers. Therefore it is likely that reaction at the strained P center of the complex is eclipsed by a more rapid metal-ligand cleavage reaction. This problem can be circumvented by the use of metal ion complexes of Ir(III) where the metal-ligand bonds are more inert as the locus for the reaction.

F. Intramolecular Attack of Amido Ion: Iridium(III) Complexes

With the above arguments in mind the reactivity of two pentaammineiridium(III) phosphodiester complexes was investigated (79a). The first of these, the ethyl-4-nitrophenylphosphate complex, $[(\text{NH}_3)_5\text{IrENPP}]^{2+}$, hydrolyzed in aqueous hydroxide ion solution by a reaction consisting of two paths, both paths yielded the same products. The reaction obeyed the rate law;

$$v = k_1[\text{complex}][\text{OH}^-] + k_2[\text{complex}][\text{OH}^-]^2$$

The rate constants for the reaction were $k_1 = 2.4 \times 10^{-4} \text{ L}\cdot\text{mol}^{-1} \text{ s}^{-1}$ and $k_2 = 2.9 \times 10^{-4} \text{ L}^2\cdot\text{mol}^{-2} \text{ s}^{-1}$. Both paths produced two phosphorus containing metal complexes in the same relative yields. The minor species (19% yield) was readily identified as the ethylphosphate complex $[(\text{NH}_3)_5\text{IrEP}]^+$. The major species, however, was not the chelate phosphoramidate ester, but the ring opened species, N-coordinated monodentate ethylphosphoramidate, **14**. Both products were indefinitely stable in hydroxide ion solution. The reaction proceeds some 10^3 -fold slower than the reaction of the analogous Co(III) complex, which is rather significant and will be discussed in detail later. The slower rate of production of the 4-nitrophenolate ion also accounts for the failure to see the chelate phosphoramidate esters.



The major product of the reaction obviously arises from attack of a cis coordinated amido ion on the P center of the phosphate ester since there is no other source of nitrogen in the reaction, the minor product, however, the $[(\text{NH}_3)_5\text{IrEP}]^+$ ion could come from a variety of sources. The most obvious route is by intermolecular attack of hydroxide ion on the coordinated ester. Such is probably not the case, however. The yield of the product is constant over the range of hydroxide ion concentrations studied where the contribution of the overall third-order reaction accounts for ~ 10

to ~60% of the reaction products. It seems likely, therefore, that the two products are produced from some intermediate common to both pathways after the rate-limiting step. The obvious choice for such an intermediate is the chelate ethylphosphoramidate. Attack of OH^- on the chelate could produce both the observed reaction products depending on whether the reaction proceeded with P–N or P–O cleavage by analogy with the iridium chelate ester chemistry (Section IV.D). The origin of the pathway second order in hydroxide ion is less clear. There are at least two possibilities; either the reaction is occurring via a hexacoordinate intermediate or it may reflect deprotonation of the intermediate phosphorane. These alternatives are not able to be evaluated on the basis of the current data.

The major product of the reaction displayed a variable ^{31}P NMR chemical shift with pH. This variation is ascribed to deprotonation of the bridging nitrogen. The $\text{p}K_a$ of that proton was ~12.5, and the chemical shift for the fully protonated and fully deprotonated species was 9.0 and 27.0 ppm, respectively. These values are similar to those observed for related Co(III) complexes.

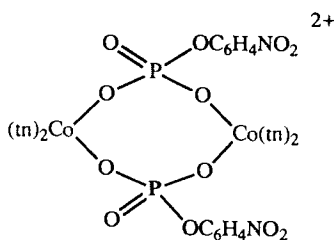
The bis-4-nitrophenylphosphate analogue $[(\text{NH}_3)_5\text{IrBNPP}]^+$ reacts in a similar manner (79). The same rate law obtains and the rate constants are, $k_1 = 4.8 \times 10^{-3} \text{ L}\cdot\text{mol}^{-1} \text{ s}^{-1}$ and $k_2 = 1.2 \times 10^{-1} \text{ L}^2\cdot\text{mol}^{-2} \text{ s}^{-1}$ at 25 °C. Despite the increased rate of production of the chelate phosphoramidate ester, it was still not observed by ^{31}P NMR. Again, two products were observed by ^{31}P NMR in constant ratio, independent of hydroxide concentration. They were the $[(\text{NH}_3)_5\text{IrNPP}]^+$ ion and the complex **12**, which reacted further by attack of the cis coordinated hydroxide ion on the phosphate ester. The $[(\text{NH}_3)_5\text{IrNPP}]^+$ ion does not react further in the time scale of this experiment. This finding is in accord with our observations on the relative reactivity of the Co(III) and Ir(III) complexes, which lead us to predict a half-life for hydrolysis of the $[(\text{NH}_3)_5\text{IrNPP}]^+$ ion in 1M NaOH at 25 °C of ~200 h.

The rate constant for attack of OH^- on the chelated phosphoramidate ester must be at least of the order of $2 \times 10^{-2} \text{ L}\cdot\text{mol}^{-1} \text{ s}^{-1}$ at 25 °C, which is the rate constant for its production in 1M NaOH solution. This value represents an enormous rate enhancement for attack of OH^- on the P center of free 4-nitrophenylphosphoramidate due largely to relief of strain engendered by the chelation of the ester. Similarly, the rate constant for attack of OH^- on the chelate ethylphosphoramidate must be at least $5 \times 10^{-4} \text{ L}\cdot\text{mol}^{-1} \text{ s}^{-1}$ in order for the chelate not be observed in that system.

Thus all attempts to observe the exocyclic cleavage of the ester group have thus far been thwarted by the more rapid ring-opening reaction for phosphoramidate esters.

G. Activation by More than One Metal Ion

A study of the reactivity of the supposed chelate $[(\text{tn})_2\text{CoO}_2\text{P}(\text{O})\text{-OC}_6\text{H}_4\text{NO}_2]^+$ (**2**) concluded that chelation of the NPP ester activates it toward hydrolysis by induction of strain in the four-membered ring. It was later shown, however, that the object of the study was not a chelate but a rather unusual dimer, **15**. At the time there were compelling reasons for assuming the chelate structure, but it will not help the present analysis to go over that ground again. It suffices to say that the problem has been resolved and the dimer leads to interesting phosphate ester hydrolysis.

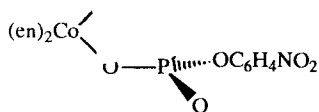


15

The reactivity of the more inert “en” analogue of this dimer complex was elucidated by Jones et al. (88). The complex undergoes a rapid ring opening of the eight-membered ring followed by two competing reactions, attack of a cis coordinated OH^- on the bridging phosphate ester moiety, and further cleavage of the dimer by $\text{S}_{\text{N}}1(\text{cb})$ Co–O bond rupture. The reaction proceeds as shown in Scheme 11 with rate constants $k_2 = 2 \times 10^{-2} \text{ s}^{-1}$ at 25 °C for the (en)₂ analogue and $\sim 4 \times 10^{-1} \text{ s}^{-1}$ for the (tn)₂ analogue.

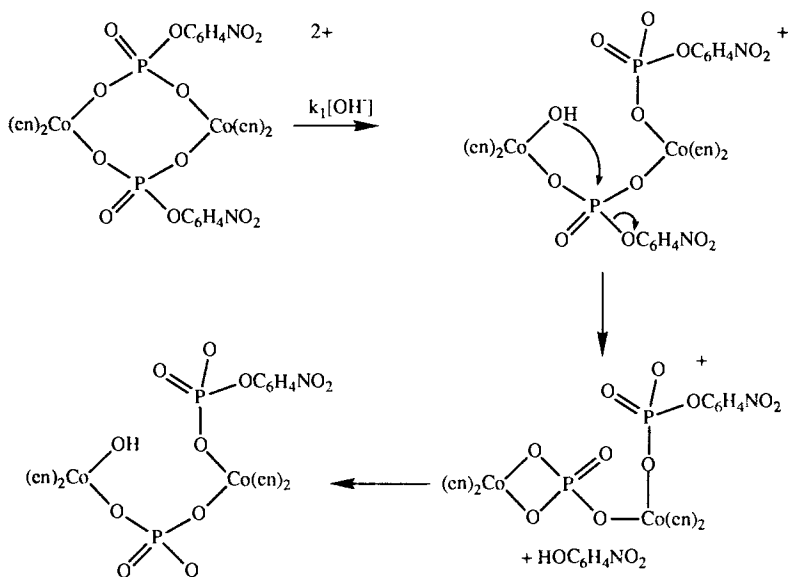
These rate constants are of interest when compared to the rate constant for attack of coordinated OH^- at the P center of the mononuclear complex **16**, namely, $\sim 8 \times 10^{-4} \text{ s}^{-1}$ at 25 °C (87). Clearly, the dimeric complex **15** leads to hydrolysis of the ester some 25-fold faster than **16** and the (tn)₂ analogue is ~ 500 -fold faster. It follows that coordination of a second metal ion complex to the phosphate ester results in a modest but significant rate enhancement and that the N ligands on the Co(III) ion can modulate the effect.

Similar effects are observed for the NH_2^- ion as an intramolecular nucleophile. The complex $[(\text{NH}_3)_5\text{CoNPP}]^+$ retains a single basic oxygen on

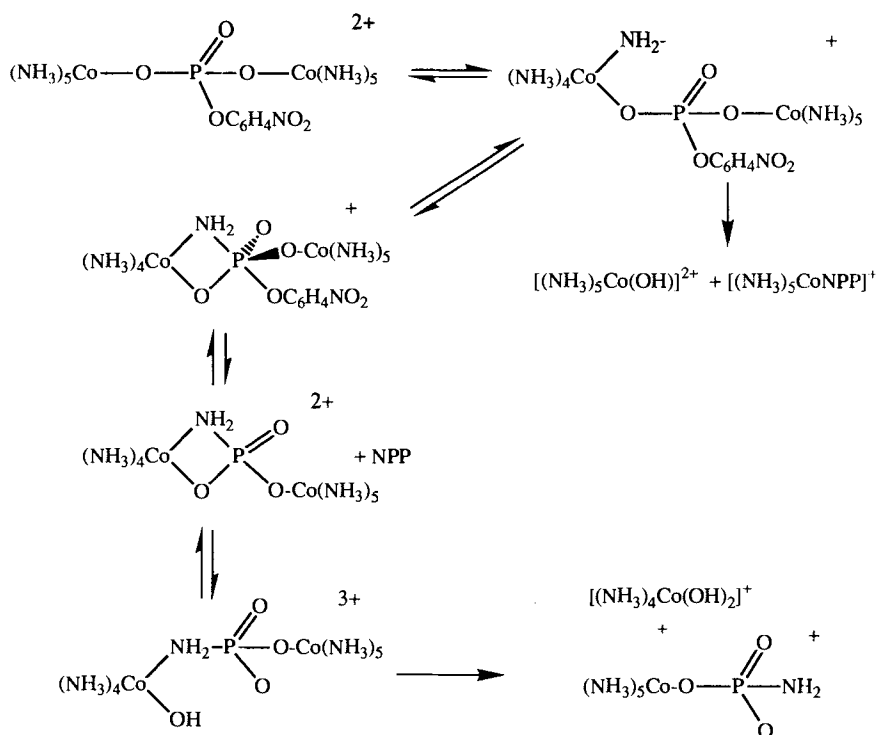


16

the phosphate moiety which is available for coordination to another metal ion. When that site is occupied by another $[(\text{NH}_3)_5\text{Co}]^{3+}$ moiety the complex $[(\text{NH}_3)_5\text{CoNPPCo}(\text{NH}_3)_5]^{4+}$ is formed. This complex hydrolyzes in a reaction that is first order in hydroxide ion and complex concentration, and like the analogous mononuclear reactions, two competing pathways are present (79). The dominant pathway at temperatures below 35°C is that producing the 4-nitrophenolate ion and the competing pathway, involving Co–O rupture, produces the complexes $[(\text{NH}_3)_5\text{CoNPP}]^+$ and $[(\text{NH}_3)_5\text{Co}(\text{OH})]^{2+}$ (Scheme 12). The reaction proceeds 100-fold faster than that for the mononuclear complex $[(\text{NH}_3)_5\text{CoNPP}]^+$, which provides clear evidence that the role of the second metal ion complex is significant but much less significant than that of the first. These effects arise because one metal ion institutes the intramolecular pathway, whereas the second metal



Scheme 11



Scheme 12

only enhances the rate of the reaction by charge neutralization and withdrawal of electron density from the P at much the same level as described for the TMP hydrolysis with intermolecular nucleophiles (Section IV.B).

The implication in these studies is that multiple metal ions and/or protons will assist nucleophilic attack at the anionic phosphorus residues at a significant level (≥ 100 -fold per addition).

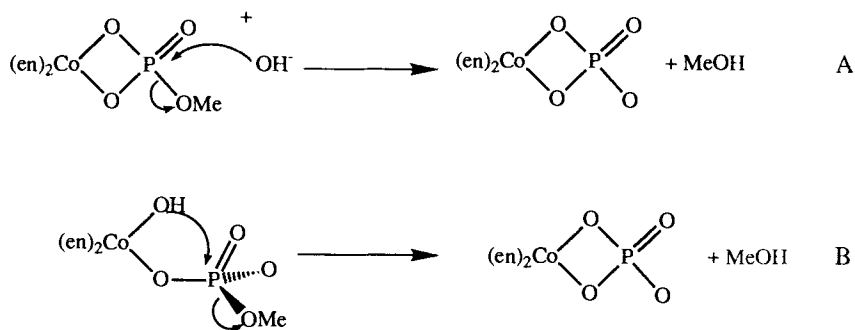
H. Chelation of the Phosphate Esters and Phosphate Ion

The chelation of phosphate ion itself needs some discussion. Lincoln and Stranks (102) have published an extensive series of papers on the phosphato complexes of a series of Co(III) complexes. They showed that the chelate is the thermodynamically favored species in the pH range 5–

9, for both the tetraammincobalt and bis(ethylenediamine)cobalt complexes. Subsequent investigations by Jones et al. (87) and Buckingham et al. (17) have shown that the chelation and ring opening of the chelate both occur exclusively with Co–O bond cleavage over the entire pH range. The same situation should hold for labile metal ion complexes but may not obtain for the more inert complexes of iridium(III), for example.

Independently, and after Westheimer's explanation of the reactivity of cyclic phosphate esters, Farrell et al. (58) and Harrowfield (71) investigated the reactivity of Co(III) complexes of methyl phosphate. Some enhancement of the reactivity of methyl phosphate was observed, but it was not possible to discriminate between the perceived options for the reaction at the time, Scheme 13. Moreover, it is very likely that the complexes made in this manner are not four-membered chelates but are dimers like **15**, which react by ring opening and intramolecular attack of the coordinated nucleophile as in Scheme 11. Many attempts to synthesize such Co(III) chelates have been unsuccessful (58, 71, 72), which is surprising given the ease with which the chelate phosphate complexes can be made. So far such chelates have only been observed or deduced as intermediates and some of the previous discussion points to the lack of reactivity with respect to exo-ester hydrolysis in such authentic chelates of phosphate esters and phosphoramidate esters. This result can be attributed to lack of pseudorotation relative to ring opening by P–O cleavage in the phosphorane or ring opening of the metal ion chelate. Regardless of the reason for lack of reactivity in this mode, it does not seem likely that this is a fruitful path for exo-ester hydrolysis in enzymic systems containing phosphate derivatives coordinated to a metal ion.

Some discussion of the relative rates of the intramolecular reactions



involving the Co(III) and Ir(III) metal ions is relevant. In all instances where formation of a four-membered ring was involved, the reaction centered around the Ir(III) ion occurred $\sim 10^3$ -fold slower than for the corresponding Co(III) complex. The reason for this decrease cannot be a different degree of activation of the phosphate ester by the two metal ions, because this effect has been shown to be small for the hydrolysis of TMP and other coordinated substrates (15, 16, 46, 151). Moreover, nucleophiles bound to Ir(III) are somewhat more basic than for Co(III). The reason for the rate difference most likely lies in the fact that the two metal ions are quite different in size. The effective ionic radii of the two ions are 0.55 Å and 0.68 Å for Co(III) and Ir(III), respectively (125). This large difference must influence the energy required to form the strained four-membered ring. X-ray crystallographic analyses of the complexes $[(en)_2CoO_2PO_2]$ (2) and $[(NH_3)_4CoO_2PO_2]$ (105) show that the in-ring bond angles and lengths are almost identical for both complexes. In both cases, the four-membered ring containing the Co(III) and the phosphorus atom is strained (Fig. 3). In the case of the bis(ethylenediamine) complex, the nonbonded interatomic distance between the Co and P is only 2.554 Å, which is close to the sum of the covalent radii of the two atoms involved. The large Ir(III) ion must cause further strain in this ring. Simple geometric considerations dictate that if the metal–O bond lengths are increased to 2.1 Å, a reasonable estimate for the Ir–O bond, and the bond angles and lengths about the phosphorus center are invariant, the O–M–O bond angle would be decreased to 69° , much more strained than the angle subtended at the Co(III) center. If these critical bond angles, O–M–O and O–P–O, were increased to relieve the strain the metal–phosphorus nonbonded interaction would increase.

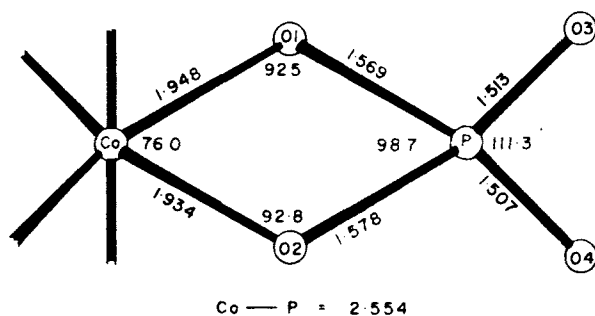


Figure 3. The bond lengths (Å) and angles in the chelate phosphate ring in the complex $[(en)_2CoO_2PO_2]$ (2).

Molecular mechanics calculations imply that, in addition to the fact that the longer bond lengths increase the separation of the nucleophile and the P center, the intrinsic resistance to deformation of the O–M–O bond angle will be greater for Ir(III) than for Co(III). From an inspection of molecular geometries, it has been anticipated that the O–Ir–O bond angle may need to compress to nearly 70° to achieve a reasonable activated complex geometry for the reaction involving the intramolecular attack of hydroxide ion on a coordinated phosphate derivative, see above. In contrast to this expectation, a suitable activated complex geometry for the corresponding Co(III) complex would be closer to 78° – 80° , for the O–Co–O angle based on the geometry in the product ground state (2, 105). The strain difference between the Co(III) and Ir(III) complexes is also apparent in the stability of the chelate phosphate ion, for Co(III) the chelate is the thermodynamically favored complex at neutral pH (102) but for Ir(III) the chelate phosphate has yet to be observed at any pH. This strain effect must influence the stability of the chelated esters and it is quite possible that the Co(III) chelated phosphate esters may behave quite differently to their Ir(III) analogues.

The strain involved in closure of the four-membered ring thus depends on the size of the metal ion for the d^2 ions, Co(III) and Ir(III). However it does not necessarily follow that because, for example, the Zn(II) ion is larger than Ir(III), that the ring closing will be even more sterically restrained. The Zn(II) ion is a d^{10} metal ion and does not possess a large ligand-field stabilization energy so it is able more readily to accommodate severe deformation of bond angles. In fact, the structure of zinc phenylphosphonate (103) possesses a four-membered chelate ring with an in-ring angle of 64.5° at the distorted octahedral Zn(II) center and a Zn–O bond length of 2.28 Å. The flexibility of coordination at the Zn(II) center is also evident from the relatively small distortion at the P center, O–P–O in-ring angle 105° and an O–P bond length of 1.54 Å. It is also evident in the high-resolution structures of at least two Zn²⁺ phosphatases (60, 81).

I. Conclusions

The studies described in this section indicate that;

1. Coordination of a trivalent metal ion to a phosphate ester has only a modest effect on the electrophilic nature of the P center. The combined effect of the electron withdrawal and reduction in net negative charge amounts to a rate enhancement of the order of 10 – 10^3 for attack by OH^- .

2. One of the most effective ways that metal ion can promote reactions of phosphate esters is to provide an intramolecular nucleophile; that is, it is able to coordinate the phosphate in a position that is accessible to an adjacent coordinated nucleophile. This effect is dependent on the nature of the metal ion and, in particular, the ease of formation of the requisite four-membered ring. The intramolecular effect cannot be dissected precisely from the electrophilic activation, but it can be argued to add at least $\sim 10^4$ to the rate enhancement.
3. Provision of an available nucleophile at physiological pH is an important role for the metal ion in the model chemistry, and it is a likely role for the metal ion in enzymes.
4. Chelation of phosphate monoesters has not to date been effective at promoting the exocyclic hydrolysis of an ester group. For Ir(III) complexes, however, the four-membered chelate ring is reactive in another way, namely, by chelate ring opening with P-O cleavage. With the Co(III) complexes, however, this ring opening occurs with Co-O rupture.
5. Addition of multiple metal ions enhances the reactivity of phosphate esters by a variety of methods. For example, one metal ion may be able to provide the intramolecular nucleophile and electrophilic activation while another activates the phosphate ester by further withdrawal of electron density and charge neutralization.

In the following section the relevance of these effects is considered in the light of what is known of mechanisms of appropriate phosphatase and polyphosphatase enzymes.

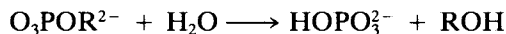
V. RELATIONSHIP BETWEEN MODEL STUDIES AND ENZYME MECHANISMS

A. *Escherichia coli* Alkaline Phosphatase and Related Enzymes

Recent developments in the structural analyses of enzymes that cleave phosphate esters have revealed a common property for the reaction center (60, 81, 93, 130), namely, more than one metal ion, usually Zn^{2+} , is involved. The first example of this kind to be identified was *E. coli* alkaline phosphatase, an isologous dimer of molecular weight 94,058, which contains $4.0 (\pm 0.3)$ g atoms of tightly bound Zn^{2+} per mole and $1.3 (\pm 0.2)$ g atoms of Mg^{2+} per mole (130). Recent refinements of the structure of this enzyme (93) containing PO_4^{3-} ion show that two phosphate oxygen atoms

are separately bound to two Zn^{2+} ions. These observations imply that both Zn^{2+} ions are involved in binding and activating the substrate monoesters.

The enzyme is used in nature to hydrolyze phosphate monoesters in general:

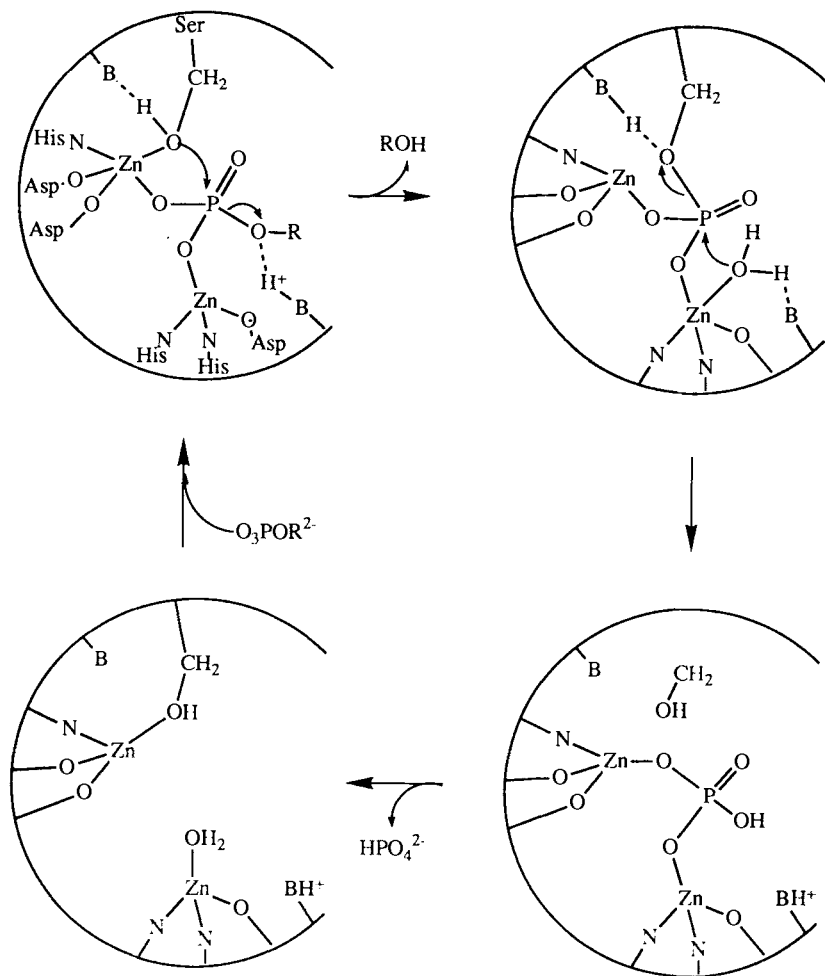


Also, it is clearly established that the process occurs by first phosphorylating a serine residue of the enzyme and then by hydrolysis of the phosphoseryl enzyme (33). The enzyme will also transfer the phosphoryl group to another alcohol as well as to water, and it has been shown by using chiral ^{16}O , ^{17}O , ^{18}O , 4-nitrophenylphosphate that the phosphoryl transfer to 1,2-propanediol occurs with net retention of chirality (89). Implicit in this observation are two inversion-substitution processes at the P center, that is, inversion in the PO_3 transfer to the enzyme and again in the PO_3 transfer to water (98).

The model studies imply mechanistic paths in the enzyme that would accommodate much of the rate enhancement and are consistent with the observations above. These are displayed in Scheme 14. The phosphate ester binds to both Zn^{2+} ions, which activates the P center to attack by the coordinated deprotonated serine nucleophile. Binding the serine hydroxyl to the metal ion enhances its deprotonation and gives an efficient intramolecular nucleophile, as we have seen from model studies. Such a process would also be assisted by an enzyme base to remove the proton intramolecularly and protonation of the alkoxide leaving group by an enzyme acid would be helpful. In addition, inversion of configuration would ensue at the P center. A coordinated water at the second Zn^{2+} ion could then be deprotonated to function as the intramolecular nucleophile which eliminates the serine alkoxide ion. Both aspects would be assisted by an enzyme base and acid, respectively. The stereochemistry of the processes would lead to inversion and therefore to net retention overall consistent with the expectation from the experiments by Jones et al. (89).

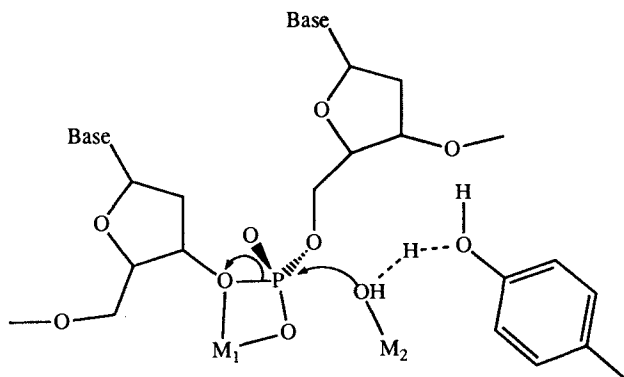
It can be seen from the models that the combination of binding the substrate to two metal ions plus the intramolecular nucleophile can lead to rate increases of at least 10^8 , which is a large component of the enzymic activation. The remainder of the rate enhancement could readily be accounted for by the assistance of the enzyme acids and bases strategically placed to donate and accept protons at the appropriate sites in a synchronous manner.

It is striking that at least two other enzymes, which carry out similar hydrolysis functions for phosphate esters, show related constellations of metal ions in the active site (60, 81). The high-resolution structure (1.5 Å) of phospholipase C from *Bacillus cereus* (81) shows three five-coordinate



Scheme 14

Zn²⁺ ions bound to a mixture of histidine, aspartate, glutamate residues, and water ligands. The phosphate ion replaces two water molecules. Two Zn²⁺ ions are bound to one oxygen of the PO₄³⁻ ion and another oxygen is bound to the remaining Zn²⁺. Also, high-resolution structures of editing complexes of single-stranded DNA bound to the large fragment of DNA polymerase I (Klenow fragment) from *E. coli* (60) shows two divalent metal ions (Mg²⁺, Mn²⁺, or Zn²⁺) interacting with the phosphodiester to be hydrolyzed. The proposed mechanism for the 3'-5'-exonuclease reaction is shown in Scheme 15. It may be possible, however, that metal ion M₂ could



Scheme 15

also bind the phosphoryl group and make the intramolecular attack of the nucleophile more intimate. Certainly, the model chemistry would support such a role and the present structural detail does not seem to exclude it. Moreover, an advantage in using the Zn^{2+} ion is its ability to accommodate the optimum juxtaposition of the nucleophilic OH^- ion and the phosphate ester for efficient hydrolysis. This flexibility is also seen in its capacity to coordinate four, five, and six ligands quite readily depending on steric demands of the system. It is not likely that the tyrosine hydroxyl group will function as a base to remove H^+ from Zn-OH_2 , however.

B. Yeast Inorganic Pyrophosphatase

Yeast inorganic pyrophosphatase (YIP) is an enzyme consisting of two identical subunits giving a molecular weight for the dimer of 64,000. Yeast inorganic pyrophosphatase catalyses the reversible hydrolysis of pyrophosphate. In the presence of Mg^{2+} , YIP appears to be specific for pyrophosphate; however, when other activating metal ions are employed, the enzyme becomes less specific and will hydrolyze a number of pyrophosphate esters (21). There is even a possibility that a mixture of enzymes is present in some preparations (55).

The native dimer binds divalent metal ions in the absence of phosphate, but in the presence of phosphate three divalent metal ions are bound with high affinity. These metal ions include Mg^{2+} , Mn^{2+} , Co^{2+} , Zn^{2+} , Ni^{2+} , Fe^{2+} , and Cd^{2+} , all of which activate the enzyme, and Ba^{2+} and Ca^{2+} which inhibit YIP (95). *In vivo*, Mg^{2+} appears to be the ion that is bound to the enzyme. NMR studies of ^{113}Cd substituted YIP show that, in the presence of phosphate, three separate ^{113}Cd resonances are observed, all of which

are different from free Cd^{2+} in solution (142). The chemical shifts of all three Cd^{2+} signals indicate that the ligands to the metal ions are almost all oxygen donors as might be expected for sites that normally bind Mg^{2+} (142).

The enzyme seems to have two binding sites for phosphate per subunit, one high affinity site and another site of lower affinity. The substrate for the enzyme in the hydrolytic direction is the Mg^{2+} pyrophosphate complex. There is still some discussion as to whether the substrate is a P_1, P_2 chelate (95) or a monodentate species (142). Cooperman (34) is of the opinion that it is more likely that the natural substrate for the enzyme is the monodentate pyrophosphate. This conclusion is based on the observation that, for the $(\text{Cd}^{2+})_3$ enzyme in the presence of phosphate, apparently only one of the two bound phosphates interacts with the Cd^{2+} ion. This conclusion is supported by an increase in the ^{31}P NMR line width following a change from ^{112}Cd ($I = 0$) to ^{113}Cd ($I = \frac{1}{2}$).

Evidence in favor of the chelate as the substrate has come from studies of the $\text{Mg}^{2+} - \text{P}_2\text{O}_7^{2-}$ equilibrium, which indicate that the chelate is the most abundant species (96). More compelling evidence has come from the observation that the stable chelates $[(\text{H}_2\text{O})_4\text{CrP}_2\text{O}_7]^-$, $[(\text{NH}_3)_4\text{CoP}_2\text{O}_7]^-$, and $[(\text{H}_2\text{O})_4\text{RhP}_2\text{O}_7]^-$ are substrates for the enzyme in the presence of added divalent metal ions (4, 95, 126). Moreover, the monodentate complex $[(\text{NH}_3)_5\text{CoOP}_2\text{O}_6]^-$ is not a substrate for the enzyme (96). The Cr(III) and Rh(III) aqua complexes and Co(III) amine complexes, unlike Mg(II) complexes, are substitution inert, allowing separation, purification, and characterization of specific complexes. The $[(\text{H}_2\text{O})_4\text{CrP}_2\text{O}_7]^-$, $[(\text{H}_2\text{O})_4\text{RhP}_2\text{O}_7]^-$, and $[(\text{NH}_3)_4\text{CoP}_2\text{O}_7]^-$ complex ions have therefore been purified and unambiguously characterized as the P_1, P_2 chelate by X-ray crystallographic analyses (105, 106, 126).

These observations indicate that one metal ion is required to chelate the substrate and at least one other divalent metal ion is required for activity. More recent work employing paramagnetic probes provides evidence that three metal ions are involved in the catalytic cycle of the enzyme (4, 97). Also, when $[(\text{NH}_3)_4\text{CoP}_2\text{O}_7]^-$ was used as a substrate, the initial product of the reaction was *cis*- $[(\text{NH}_3)_4\text{Co}(\text{PO}_4)_2]^{3-}$ (69).

There is an essential arginine located in the active site (34), which is required to be protonated for activity. Competitive inhibitors of the reaction such as phosphate, $[\text{CaP}_2\text{O}_7]^{2-}$ and $[\text{MgO}_3\text{PCH}(\text{OH})\text{PO}_3]^{2-}$ also competitively inhibit the inactivation of the arginine 77 residue by phenylglyoxal (34). This result implies that the protonated arginine residue is involved in substrate binding presumably by hydrogen bonding.

Any consideration of the mechanism for the hydrolysis of pyrophosphate must account for the following observations: The substrate is a Mg^{2+} -

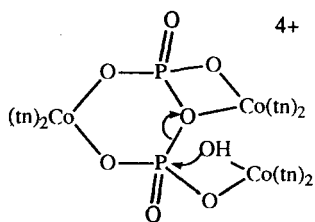
pyrophosphate complex, two more divalent metal ions are required for activity, and there appears to be an essential arginine residue in the active site.

Two proposals for the mechanism of YIP are quite similar (34, 95), both include metal ion binding to pyrophosphate to produce a substrate, both have proposed a metal bound hydroxo ligand as a nucleophile (the hydroxo ligand is produced by deprotonation of an aqua ligand by an adjacent basic amino acid residue), both involve stabilization of the substrate by interaction with the protonated arginine residue. The mechanisms differ in the spatial arrangement of the substrate, the various metal ions, and essential amino acid residues.

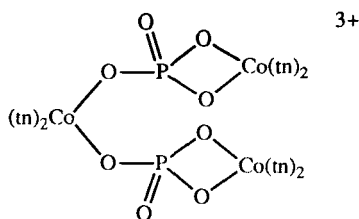
C. Pyrophosphate Cleavage

Pyrophosphate is extremely inert at neutral pH in laboratory conditions. Its hydrolysis can be enhanced mildly by the presence of a variety of metal ions (135, 141). Certain Co(III) reagents, however, are able to accelerate its hydrolysis up to 10^7 -fold (42, 67, 82). These reagents are *cis*-[(hydroxo)(aqua)tetraamminecobalt(III)]²⁺ complexes such as *cis*-[(tn)₂Co(OH)(OH₂)]²⁺. The function of the amine groups is to stabilize the Co(III) oxidation state while at the same time allowing the aqua group to exchange relatively rapidly. The hydroxo group also has two functions; one is to assist the labilization of the water ligand, the other is to act as an intramolecular nucleophile towards a *cis* coordinated phosphate residue.

The addition of 3 mol of [(tn)₂Co(OH)(OH₂)]²⁺ to 1 mol of pyrophosphate or 2 mol of [(tn)₂Co(OH)(OH₂)]²⁺ to 1 mol of [(en)₂CoP₂O₇]⁻ results in an almost maximal rate of hydrolysis of P₂O₇⁴⁻ ($k = 2.8 \times 10^{-4} \text{ s}^{-1}$ at pH 7) (42), compared to the rate in the presence simply of sodium ions of $\sim 10^{-9} \text{ s}^{-1}$ at pH 7 and 25°C (141). For a ratio of 1:1 [(tn)₂Co(OH)(OH₂)]²⁺:P₂O₇⁴⁻ very little hydrolysis of the pyrophosphate occurs; for a 2:1 ratio hydrolysis occurs, but at a greatly reduced rate as compared to that observed for the 3:1 ratio. The proposed active species is complex **17**. The outline of the mechanism derived from ³¹P NMR studies is as follows: first, the stable [(tn)₂CoP₂O₇]⁻ ion forms rapidly and completely. The second and third cobalt complexes add to produce complex **17**. It has not been clarified yet whether the reactivity of the 2:1 system is due to the reactivity of the 2:1 complex or whether it is due to a small amount of the 3:1 complex. This second possibility seems likely since the 2:1 reaction appears not to proceed to completion. The major product of the 3:1 reaction is complex **18**. It appears that two extra chelatable complexes are required for relatively rapid cleavage of the initially formed chelated pyrophosphate because less rapid cleavage is observed for complex

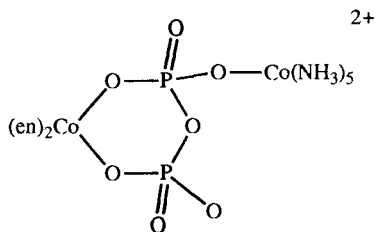


17



18

19 plus 1 mol of $[(tn)_2Co(OH)(OH_2)]^{2+}$. The results imply that chelation of the leaving phosphate residue is important and aids the P–O bond rupture as shown in **17**. The bis(chelate) product is also significant since hydrolysis of the stable $CoP_2O_7^-$ chelate would not be a thermodynamically favored process without the formation of two stable Co chelate rings in the product to affect the rupture of the stable $CoP_2O_7^-$ chelate.



19

The whole reaction sequence can be modeled reasonably well for cleavage of the $P_2O_4^{4-}$ ion in $[(en)_2CoP_2O_7]^-$ using 2 mol of $[Co(tamen)(OH)(OH_2)]^{2+}$ [tamen = 6-methyl-6-(4-amino-2-azabutyl)-1,4-diazacycloheptane] as the effective reagent. The mechanistic outline

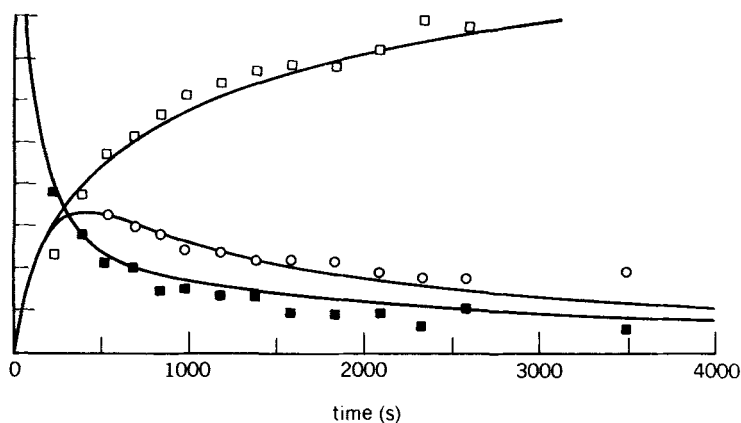


Figure 4. [Species] vs. time plot, solid lines are calculated from rate constants given in Scheme 16. □ = 33 ppm, ■ = 11 ppm, and ◆ = 14 ppm, $[(en)_2P_2O_7] = 0.025M$, $[Co(tamen)(OH)(OH_2)] = 0.05M$

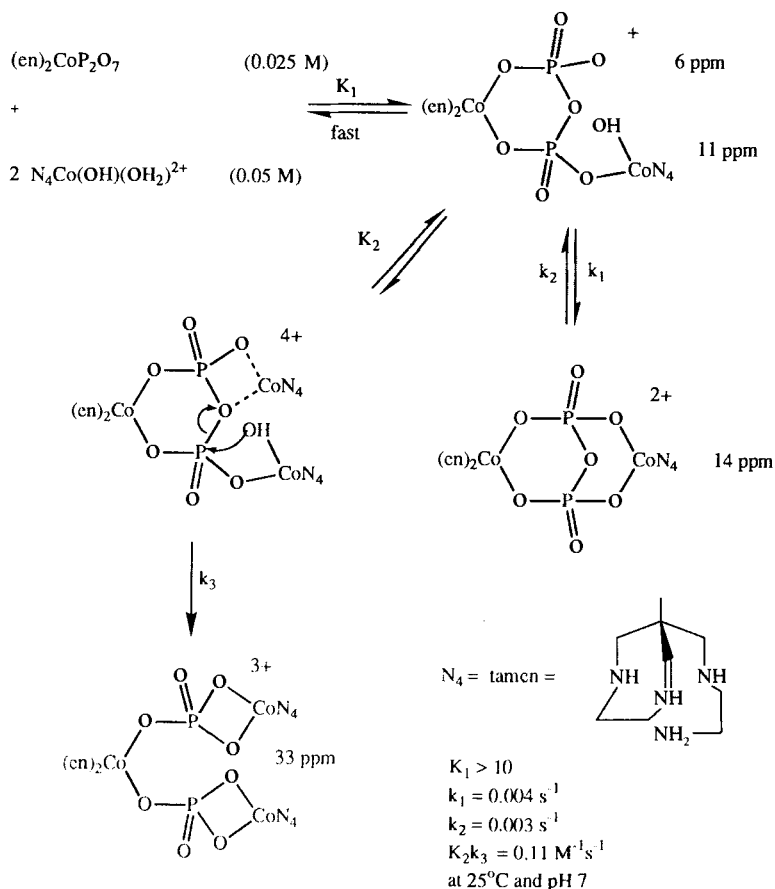
and fitting for the derived rate constants for the reactions are given in Fig. 4 and Scheme 16. A condition approximating the steady state applies and it is evident that if the nonreactive mixed chelate complex $[(en)_2CoP_2O_7Co(tamen)]^{2+}$ could be avoided then the hydrolysis rate would be even more rapid (steps K_2k_3).

The hydrolysis of pyrophosphate is also enhanced in the presence of *cis*- $[(NH_3)_2Pt(OH_2)_2]^{2+}$ (9, 10). The reaction profile appears to be much more complex than that for the *cis*- $[(tn)_2Co(OH)(OH_2)]^{2+}$ promoted reactions, although again multinuclear species (2:1, Pt:P₂O₇) seem to be involved and the participation of a *cis* coordinated hydroxide ion seems likely. The reaction is also complicated by a change of oxidation state of the platinum in the reaction and some Pt(IV) and mixed-valence species appear to be involved.

These model systems imply an important role for the multiple metal ions in the yeast inorganic pyrophosphatase reaction. A plausible mechanism consistent with its known properties and requirements is shown in Scheme 17. Clearly, the metal ions would reduce the charge on the phosphate residues and activate the P centers to nucleophilic attack. They also probably provide "intramolecular" hydroxide nucleophiles.

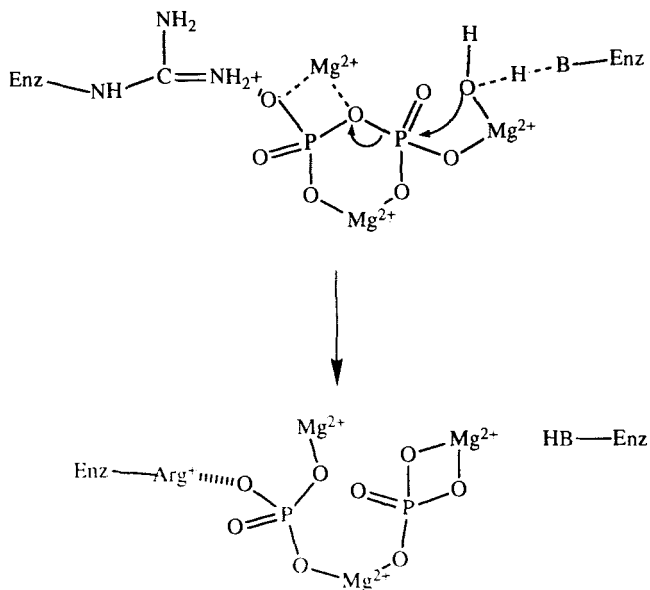
D. Triphosphate Hydrolysis

Like pyrophosphate, linear triphosphate is hydrolyzed by *cis*- $[(tn)_2Co(OH)(OH_2)]^{2+}$ and similar Co(III) reagents (67). Bidentate coordination



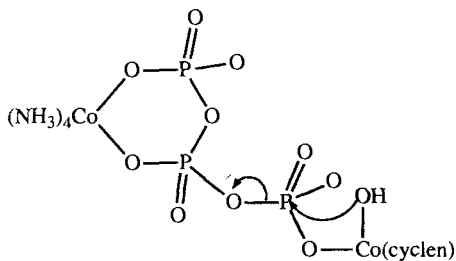
Scheme 16

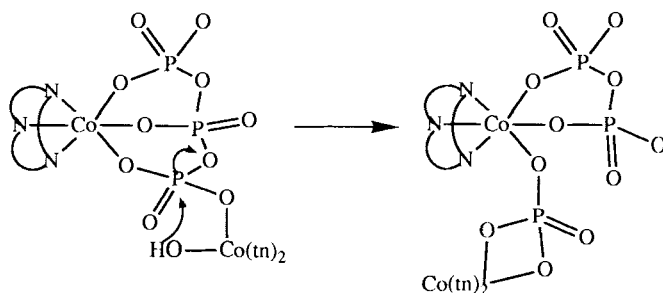
in the complex $[(\text{NH}_3)_4\text{CoP}_3\text{O}_{10}]^{2-}$ (α, β coordination) has a small effect on the rate of cleavage at neutral pH (36). Addition of $[(\text{NH}_3)_5\text{CoOH}_2]^{3+}$ accelerates the reaction slightly but still only ~ 25 -fold over the uncoordinated triphosphate (37). Addition of the complex $[(\text{NH}_3)_4\text{Co}(\text{OH}_2)_2]^{3+}$ results in a hydrolysis rate enhancement of 700-fold over that for the free triphosphate (37). Addition of the complex *cis*- $[(\text{cyclen})\text{Co}(\text{OH})(\text{OH}_2)]^{3+}$ results in a rate enhancement of some 5×10^5 -fold over that for free triphosphate and 3×10^4 -fold over that for the bidentate complex (110). The reaction depends on a deprotonation with a $\text{p}K_a$ of 7.9 for optimal reaction rates, which corresponds to the deprotonation of the aqua group of the cyclen complex to yield the *cis* coordinated hydroxide ion required for the reaction as shown in 20.



The α,γ -coordinated triphosphate complex $[(\text{NH}_3)_4\text{CoP}_3\text{O}_{10}]^{2-}$ has also been synthesized (121), but little has been reported on its hydrolytic reactivity.

The α,β,γ -tridentate complex $[(\text{tacn})\text{CoP}_3\text{O}_{10}]^{2-}$ (68), on the other hand, shows greatly enhanced reactivity. In the presence of 1 mol of $[(\text{tn})_2\text{Co}(\text{OH})(\text{OH}_2)]^{2+}$ the triphosphate is cleaved to pyrophosphate and phosphate with a half-life of 3 min at 25 °C and pH 7.3, an increase of 10^6 -fold over the free triphosphate (Scheme 18). The rate of the cleavage is





Scheme 18

independent of the additional $[(tn)_2Co(OH)(OH_2)]^{2+}$, but the extent of the reaction is dependent on the amount of reagent. The reaction only goes to completion in the presence of 3 mol of reagent. It proceeds at a maximal rate when only a single mole of $[(tn)_2Co(OH)(OH_2)]^{2+}$ is added to the α -phosphate, however, and this result is ascribed largely to the difference in leaving group capabilities of PO_3^{3-} vs. $P_2O_7^{4-}$. Additional metal ion is not needed to help $P_2O_7^{4-}$ depart.

E. Kinases

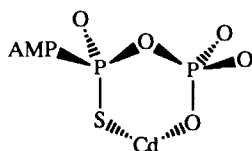
As a major source of energy for chemical reactions in biology, nucleoside 5'-triphosphates (NTPs) are involved in many enzyme catalyzed reactions that involve transfer of the terminal PO_3^- group to an acceptor molecule. The class of enzymes that catalyze these reactions are named NTP^oases when the acceptor molecule is water, or kinases, when the acceptor molecule is other than water. An outstanding feature of this group of enzymes is that, with one possible exception, all require at least one divalent metal ion (frequently Mg^{2+}) for activity (108). The metal ion appears to participate in the reaction as the NTP complex and in some cases additional metal ions may be required by the enzyme. The thesis that the substrate for some kinases is the β,γ -chelate Mg^{2+} -NTP complex has been supported by the fact that the substitution inert complexes β,γ - $[(NH_3)_4CoATP]^-$, β,γ - $[(H_2O)_4CrATP]^-$, and/or $[(H_2O)_4RhADP]$ (126) can also serve as substrates for some kinases. β,γ -bidentate coordination of NTP to a metal ion causes the β phosphorus center to become chiral. The two diastereoisomers thus produced (since the nucleoside is chiral) have been designated, somewhat misleadingly, Δ and Λ (35). This nomenclature is confusing since these symbols are the standard nomenclature used to describe the chirality at the metal centers of multidentate metal ion complexes. Here we will use the standard (*R,S*) nomenclature to describe the stereochemistry of

the tetrahedral centers. All the enzymes investigated thus far utilize only one of the diastereoisomers as a substrate. Thus yeast hexokinase will hydrolyze only the (*R*) isomer of β,γ -[(NH₃)₄CoATP]⁻ ion (35). These complexes are inferior substrates for a variety of enzymes: the β,γ -[(NH₃)₄CoATP]⁻ complex is a poor substrate for the Ca²⁺ and Mg²⁺ ATPases (63) β,γ -[(H₂O)₄CrATP]⁻ is a substrate for glycerokinase[(*R*)isomer], pyruvate kinase (*S*), phosphofructokinase (*R*), creatine kinase (*R*), myokinase (*R*), and arginine kinase (*R*) (29). In addition to their substrate activity, they also act as competitive inhibitors of kinases utilizing their natural substrates. In cases where the inert complex is both a substrate and a competitive inhibitor it is often found that the k_m and k_i values are quite similar (63), thus reinforcing the notion that these molecules are reasonable substrate analogues.

Sulfur substituted ATP analogues have also been used as substrates for certain kinases (30, 84, 85). When a sulfur atom is stereospecifically substituted for oxygen in a nonbridging position on the α or β phosphorus of ATP, that phosphorus center becomes chiral and the molecule becomes diastereoisomeric. These diastereoisomers have been separated and tested as substrates for some kinases including arginine kinase (30), 3-phosphoglycerate kinase (85), hexokinase (84), and pyruvate kinase (84). As shown previously, the substrate for most kinases is actually a metal ion NTP complex. When Mg²⁺ is the activating metal ion, one of the diastereoisomers is preferred, that is, one of the diastereoisomers has a lower K_m (stronger binding), and a higher V_{max} than the other. When Cd²⁺ is the activating metal ion, however, the other diastereoisomer is preferred. The rationale for these observations is that Mg²⁺ prefers to bind oxygen, whereas Cd²⁺, being a "softer" cation, preferentially coordinates to sulfur. This disparity necessarily generates two different diastereoisomers for the Mg²⁺ and Cd²⁺ 6-chelates and since the enzyme takes one absolute configuration of the substrate, it follows that the two thiopyrophosphate moieties must be enantiomeric.

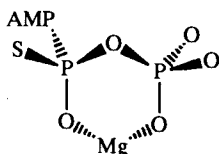
It appears that, from the large number of kinases investigated by these two techniques, the enzymes will utilize only one conformation of the complex, that is, they are typically stereospecific. It is also apparent from these studies that the kinases require the NTP substrate to be coordinated to a metal ion for activity.

A recent report (129) on the utilization of the (*R*)_(P) and (*S*)_(P) isomers of ADP(α -S) (α thio substituted ADP) by Mn²⁺ substituted creatine kinase has shown that the enzyme binds the (*R*)_(P) substrate with the Mn²⁺ bound to the O but, with the (*S*)_(P) substrate, the enzyme bound form is predominantly coordinated via the sulfur atom. Both these complexes result in the



21

The complex preferentially formed between ATP(R-βS) and Cd^{2+}



22

The complex preferentially formed between ATP(R-βS) and Mg^{2+}

α,β -chelate ring having the same required conformation. This finding concurs with earlier studies using Mg^{2+} and Cd^{2+} .

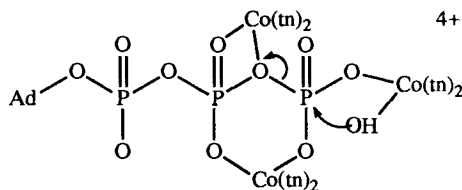
The stereochemical courses of many enzymic reactions involving phosphate derivatives have been investigated, and they have been reviewed by Westheimer (145) and Knowles (99). The individual steps in all enzymic reactions so far investigated have been found to proceed with inversion about the phosphorus center.

F. Nonenzymic Hydrolysis of ATP and ADP

ATP and ADP are hydrolyzed in neutral aqueous solution by the familiar $[\text{N}_4\text{Co}(\text{OH})(\text{OH}_2)]^{2+}$ ions. Milburn and co-workers have made a detailed study of the effect of these complexes on the dephosphorylation and dephosphorylation of these nucleotide phosphates (73, 74, 133, 134). The most reactive complexes contain more than one metal ion. Similar observations were made by Sigel and co-workers (122, 128). The hydrolysis of ATP by $[(\text{tn})_2\text{Co}(\text{OH})(\text{OH}_2)]^{2+}$ proceeds measurably faster than for ATP alone only when the amount of $[(\text{tn})_2\text{Co}(\text{OH})(\text{OH}_2)]^{2+}$ added exceeds that required to form the 1:1 Co:ATP complex. The 1:1 complex formed is almost exclusively the β,γ six-membered chelate and shows no detectable increase in the rate of hydrolysis compared to free ATP. Addition of more $[(\text{tn})_2\text{Co}(\text{OH})(\text{OH}_2)]^{2+}$ results in relatively rapid hydrolysis of ATP,

up to 10^5 -fold enhancement at pH 7 in the presence of 3 mol of $[(tn)_2Co(OH)(OH_2)]^{2+}$ per ATP. Presumably, the reaction proceeds via attack of the cis coordinated hydroxide ion on the P center, probably the center to which that $[(tn)_2Co(OH)(OH_2)]^{2+}$ moiety is coordinated. The rate constants estimated for the 2:1 and 3:1 complexes are 6×10^{-4} and $4 \times 10^{-3} \text{ s}^{-1}$, respectively, at 25 °C and pH 7.

The structure of the first $[N_4Co(OH)(OH_2)]^{2+}$ moiety, that is, the complex that forms the β, γ chelate, is not important in determining the reactivity of the system upon addition of more $[N_4Co(OH)(OH_2)]^{2+}$. The preformed complexes $[(trpn)Co(ATP)]$ react at identical rates when equivalent amounts of $[(tn)_2Co(OH)(OH_2)]^{2+}$ are added (133). When 1 mol of $[(trpn)Co(OH)(OH_2)]^{2+}$ is added to either of the above preformed ATP complexes, however, the rate of hydrolysis of ATP is almost 100 times faster than that for the analogous reaction with added $[(tn)_2Co(OH)(OH_2)]^{2+}$. The reason for this behavior is probably two-fold, first, the rates of water exchange for the $[(trpn)Co(OH)(OH_2)]^{2+}$ are significantly higher than for $[(tn)_2Co(OH)(OH_2)]^{2+}$ (118) and, secondly, the trpn complex is constrained to be cis, which is the geometry required for hydrolytic activity. The $[(tn)_2Co(OH)(OH_2)]^{2+}$ complex can also coordinate in trans configuration, which would be inactive.



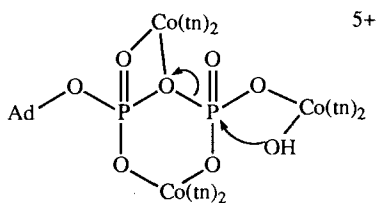
23

A Possible Structure of the Active 3:1 $[(tn)_2Co(OH)(OH_2)]^{2+}/ATP$ complex.

All of the above reactions involve predominantly dephosphorylation of the ATP; however, when Cu^{2+} or Ca^{2+} is added to preformed $[N_4Co(ATP)]$ significant amounts of pyrophosphate are produced (134). This result is ascribed to the fact that Cu^{2+} at least has a reasonably strong affinity for the N7 of the adenine moiety and from this position a Cu^{2+} bound OH^- ion is able to attack the α -phosphorus. No reasonable explanation for the reaction involving the $[N_4Co(OH)(OH_2)]^{2+}$ species not attacking the α -phosphorus was advanced despite the fact that these complexes undoubtedly coordinate to the α -phosphate residue.

Like ATP the hydrolysis of ADP is promoted by $[(tn)_2Co(OH)(OH_2)]^{2+}$ and other $[N_4Co(OH)(OH_2)]^{2+}$ reagents (73, 118). The reactivity of the system is dependent on the amount of Co(III) reagent added in excess of that required to form the 1:1 α,β -chelate complex. The reactive complex may be as drawn in 24.

In all these examples, both enzymic and model systems, it can be seen that the role of the metal ions is an active one. They do not merely hold the pieces together. Moreover, the model studies, especially on the pre-formed robust complexes, give clear indications on how the metal ion activates the substrate, provides a potent nucleophile at neutral pH, and helps the leaving group depart.



24

A Possible active complex in the hydrolysis of ADP

VI. CONCLUSIONS

This chapter collates data from various sources so that the roles the metal ions play in the enzymic manipulation of phosphate derivatives might be assessed. The use of model systems has allowed an estimation of the degree of activation (rate enhancement) expected for particular modes of metal ion-phosphate derivative interaction. In the enzymic systems, some of the roles proposed from the model systems seem to be especially relevant and it is no coincidence that the multiple metal ions required for high activity in the models are reflected in the clusters of metal ions in the reaction centers of some enzymes apparent when high-resolution structural analyses have been carried out. Clearly, charge neutralization, polarization, intramolecular nucleophiles, and effects on the leaving groups are all pertinent aspects for the metal ion's role in the natural systems. They are certainly important in the model systems. Moreover, much, but not all, of the rate enhancement in the metalloenzymes can be accounted for by these effects. Also, the role of intramolecular acids and bases in the enzyme systems is probably important. Certainly, the structures imply intimate

involvement. Duplication of these last effects is still at a primitive stage in model chemistry and in chemistry in general, although the community is aware of the possible value of such interactions in assisting reaction rates. More and better molecular engineering is clearly required in this area.

The presence of metal ions in the metabolism of phosphate derivatives seems to be quite general and the role of Zn^{2+} in alkaline phosphatase (31, 33) was discussed in some detail. The roles of Fe^{2+} and Zn^{2+} in the purple acid phosphatases (6, 7, 8, 48, 53) is still under active investigation, however, and the role of metal ions, in particular Zn^{2+} , in the metabolism of RNA and DNA and in gene expression generally is receiving some attention (56, 124). Vallee (139) has shown, for example, that Zn^{2+} deficient *Euglena gracillis* develop abnormally. Many enzymes involved in the replication and transcription of DNA have been shown or suggested to be Zn^{2+} metalloenzymes (32, 150), and given the fact that DNA and RNA are long-chain phosphate esters and negatively charged, it is not surprising that metal ions are so intimately involved in their metabolism. These areas at least will be fruitful for exploration. Moreover, some of the metal complexes may be useful in dissecting the polynucleotide polymers in a controlled way (synthetic restriction agents) and as reagents for molecular biology in general as well as for mechanistic studies in particular.

ABBREVIATIONS

ADP	Adenosine 5'-diphosphate
AMP	Adenosine 5'-monophosphate
ATP	Adenosine 5'-triphosphate
bipy	2,2'-Bipyridine
BNPP	Bis(4-nitrophenyl)phosphate
cyclen	1,4,7,10-Tetraazacyclododecane
DMP	Dimethylphosphate
DNA	Deoxyribonucleic acid
DNPP	2,4-Dinitrophenylphosphate
DPNPP	Diphenyl-4-nitrophenylphosphate
en	1,2-Ethanediamine
ENPP	Ethyl-4-nitrophenylphosphate
EP	Ethylphosphate
N	Any amine donor ligand
NMR	Nuclear magnetic resonance
NP	4-Nitrophenol(ate)
NPP	4-Nitrophenylphosphate
NTP	Nucleoside 5'-triphosphate

phen	1,10-Phenanthroline
PMP	4-Nitrophenylmethylphosphonate
RNA	Ribonucleic acid
tamen	6-Methyl-6-(4-amino-2-azabutyl)-1-4-diazacycloheptane
TBP	Trigonal bipyramid
tmen	2,3-Dimethyl-2,3-butanediamine
TMP	Trimethylphosphate
tn	1,3-Propanediamine
trien	3,6-Diazaoctane-1,8-diamine
trpn	4-(3-Propylamine)-4-azaheptane-1,7-diamine
YIP	Yeast inorganic pyrophosphatase

REFERENCES

1. K. W. Y. Abel and A. J. Kirby, *J. Chem. Soc. Perkin Trans. 2*, 1171 (1980).
2. B. Anderson, R. M. Milburn, J. MacB. Harrowfield, G. B. Robertson, and A. M. Sargeson, *J. Am. Chem. Soc.*, *99*, 2652 (1977).
3. P. W. C. Barnard, C. A. Bunton, D. R. Llewellyn, C. A. Vernon, and V. A. Welch, *J. Chem. Soc.*, 2670 (1961).
4. R. J. Barry and D. Dunaway-Mariano, *Arch. Biochem. Biophys.*, *259*, 196 (1987).
5. F. Basolo and R. G. Pearson, *Mechanisms of Inorganic Reactions*, 2nd Ed., Wiley, New York, 1967, pp. 183-184.
6. J. L. Beck, D. T. Keough, J. de Jersey, and B. Zerner, *Biochim. Biophys. Acta*, *791*, 357 (1984).
7. J. L. Beck, J. de Jersey, B. Zerner, M. P. Hendrich, and P. G. Debrunner, *J. Am. Chem. Soc.*, *110*, 3317 (1988).
8. J. L. Beck, M. J. McArthur, J. de Jersey, and B. Zerner, *Inorg. Chim. Acta*, *153*, 39 (1988).
9. R. N. Bose, R. D. Cornelius, and R. E. Viola, *Inorg. Chem.*, *23*, 1182 (1984).
10. R. N. Bose, R. D. Cornelius, and R. E. Viola, *Inorg. Chem.*, *24*, 3989 (1985).
11. R. S. Brown and M. Zamkanej, *Inorg. Chim. Acta*, *108*, 201 (1985).
12. D. M. Brown and D. A. Usher, *J. Chem. Soc.*, 6558 (1965).
13. S. C. Buchwald and J. R. Knowles, *J. Am. Chem. Soc.*, *104*, 1438 (1982).
14. S. C. Buchwald, J. M. Friedman, and J. R. Knowles, *J. Am. Chem. Soc.*, *106*, 4911 (1984).
15. D. A. Buckingham, F. R. Keene, and A. M. Sargeson, *J. Am. Chem. Soc.*, *95*, 5649 (1973).
16. D. A. Buckingham, J. MacB. Harrowfield, and A. M. Sargeson, *J. Am. Chem. Soc.*, *96*, 1726 (1974).

17. N. E. Brasch, D. A. Buckingham, J. Simpson, and I. Stewart, *Inorg. Chem.*, **29**, 371 (1990).
18. C. A. Bunton, E. J. Fendler, and J. H. Fendler, *J. Am. Chem. Soc.*, **89**, 1221 (1966).
19. J. Burgess, N. Blundell, P. M. Cullis, C. D. Hubbard, and R. Misra, *J. Am. Chem. Soc.*, **110**, 7900 (1988).
20. W. W. Butcher and F. H. Westheimer, *J. Am. Chem. Soc.*, **77**, 2420 (1955).
21. L. G. Butler, *The Enzymes*, Vol. 4, 3rd ed., P. D. Boyer, Ed., Academic Press, New York, (1973), pp. 529–541.
22. K. C. Calvo and F. H. Westheimer, *J. Am. Chem. Soc.*, **105**, 2827 (1983).
23. K. C. Calvo and F. H. Westheimer, *J. Am. Chem. Soc.*, **106**, 4205 (1984).
24. K. Calvo, *J. Am. Chem. Soc.*, **107**, 3690 (1985).
25. J. Chin and X. Zou, *Can. J. Chem.*, **65**, 1882 (1987).
26. J. Chin and X. Zou, *J. Am. Chem. Soc.*, **110**, 223 (1988).
27. J. Chin, M. Banaszczyk, and V. Jubian, *J. Chem. Soc. Chem. Commun.*, 735 (1988).
28. J. Chin, M. Banaszczyk, V. Jubian, and X. Zou, *J. Am. Chem. Soc.*, **111**, 186 (1989).
29. W. W. Cleland and A. S. Mildvan, *Advances in Inorganic Biochemistry*, Vol. 1, G. L. Eichorn and L. G. Marzilli, Eds., Elsevier, New York, 1979, pp. 163–191.
30. M. Cohn, N. Shih, and J. Nick, *J. Biol. Chem.*, **257**, 7646 (1982).
31. J. E. Coleman and P. Gettins, *Metal Ions in Biological Systems*, Vol. 5, T. G. Spiro, Ed., Wiley-Interscience, New York, 1983, pp. 153–217.
32. J. E. Coleman, *Metal Ions in Biological Systems*, Vol. 5, T. G. Spiro, Ed., Wiley-Interscience, New York, 1983, pp. 219–252.
33. J. E. Coleman and P. Gettins, *Advances in Enzymology*, Vol. 55, A. Meister, Ed., Interscience, New York, 1983, pp. 381.
34. B. S. Cooperman, *Methods in Enzymology*, Vol. 87, D. L. Purich, Ed., Academic Press, New York, 1982, pp. 526–548.
35. R. D. Cornelius and W. W. Cleland, *Biochem.*, **17**, 3279 (1978).
36. R. D. Cornelius, *Inorg. Chem.*, **19**, 1286 (1980).
37. R. D. Cornelius, *Inorg. Chim. Acta*, **46**, L109 (1980).
38. F. Covitz and F. H. Westheimer, *J. Am. Chem. Soc.*, **85**, 1773 (1963).
39. J. R. Cox, R. E. Wall, and F. H. Westheimer, *Chem. Ind.*, 929 (1959).
40. J. R. Cox and O. B. Ramsay, *Chem. Rev.*, **64**, 317 (1964).
41. I. I. Creaser, R. V. Dubs, and A. M. Sargeson, *Aust. J. Chem.*, **37**, 1999 (1984).
42. I. I. Creaser, G. P. Haight, R. Peachey, W. T. Robinson, and A. M. Sargeson, *J. Chem. Soc. Chem. Commun.*, 1568 (1984).
43. P. M. Cullis and A. J. Rous, *J. Am. Chem. Soc.*, **108**, 1298 (1986).

44. P. M. Cullis and A. Iagrossi, *J. Am. Chem. Soc.*, *108*, 7870 (1986).
45. P. M. Cullis, R. Misra, and D. J. Wilkins, *J. Chem. Soc. Chem. Commun.*, 1594 (1987).
46. N. J. Curtis and A. M. Sargeson, *J. Am. Chem. Soc.*, *106*, 625 (1984).
47. N. J. Curtis, unpublished observations.
48. E. P. Day, S. S. David, J. Peterson, W. R. Dunham, J. J. Bonivoisin, R. H. Sands, and L. Que, *J. Biol. Chem.*, *263*, 15561 (1988).
49. D. B. Denney, D. Z. Denney, P. J. Hammond, and Y-P. Wang, *J. Am. Chem. Soc.*, *103*, 1785 (1981).
50. D. Z. Denney, D. W. White, and D. B. Denney, *J. Am. Chem. Soc.*, *93*, 2066 (1971).
51. L. N. Devonshire and H. H. Rowley, *Inorg. Chem.*, *1*, 680 (1962).
52. N. E. Dixon, W. G. Jackson, W. Marty, and A. M. Sargeson, *Inorg. Chem.*, *21*, 688 (1982).
53. K. Doi, B. C. Anatanaitis, and P. Aisen, *Structure and Bonding*, Vol. 70, Springer-Verlag, Berlin, (1888), pp. 1-26.
54. A. Dubourg, R. Roques, G. Germain, J-P. Declercq, B. Garrigues, D. Boyer, A. Munoz, A. Klæbe, and M. Comtat, *J. Chem. Res. (S)*, 180 (1982).
55. D. Dunaway-Mariano, private communication.
56. G. L. Eichorn, *Metal Ions in Biological Systems*, Vol. 10, H. Sigel, Ed., Marcel Dekker, New York, (1980), pp. 1-21.
57. Extrapolated from the data in A. J. Kirby and W. P. Jencks, *J. Am. Chem. Soc.*, *87*, 3209 (1965).
58. F. J. Farrell, W. A. Kjellstrom, and T. G. Spiro, *Science*, *164*, 320 (1969).
59. T. H. Fife and M. P. Pujari, *J. Am. Chem. Soc.*, *110*, 7790 (1988).
60. P. S. Freemont, J. M. Friedman, L. S. Beese, M. R. Sanderson, and T. A. Steitz, *Proc. Natl. Acad. Sci. USA*, *85*, 8924 (1988).
61. J. M. Friedman and J. R. Knowles, *J. Am. Chem. Soc.*, *107*, 6126 (1985).
62. L. R. Gahan, J. MacB. Harrowfield, A. J. Herlt, L. F. Lindoy, P. O. Whimp, and A. M. Sargeson, *J. Am. Chem. Soc.*, *107*, 6231 (1985).
63. M. L. Gantzer, C. Klevickis, and C. M. Grisham, *Biochemistry*, *21*, 4083 (1982).
64. S. H. Gellman, R. Petter, and R. Breslow, *J. Am. Chem. Soc.*, *108*, 2388 (1986).
65. J. A. Gerlt, F. H. Westheimer, and J. M. Sturtevant, *J. Biol. Chem.*, *250*, 5059 (1975).
66. D. G. Gorenstein, Y-G. Lee, and D. Kar, *J. Am. Chem. Soc.*, *99*, 2264 (1977).
67. G. P. Haight, *Coord. Chem. Rev.*, *79*, 293 (1987).
68. G. P. Haight, T. W. Hambley, P. Hendry, G. A. Lawrance, and A. M. Sargeson, *J. Chem. Soc. Chem. Commun.*, 488 (1985).

69. T. P. Haromy, W. B. Knight, D. Dunaway-Mariano, and M. Sundaralingham, *Biochemistry*, *21*, 6950 (1982).
70. J. MacB. Harrowfield, D. R. Jones, L. F. Lindoy, and A. M. Sargeson, *J. Am. Chem. Soc.*, *102*, 7733 (1980).
71. J. MacB. Harrowfield, unpublished work.
72. R. W. Hay and R. Bembi, *Inorg. Chim. Acta*, *78*, 143 (1983).
73. M. Hediger and R. M. Milburn, in *Phosphorus Chemistry*, ACS Symposium Series No. 171, (1981), Chapter 43, pp. 211–216.
74. M. Hediger and R. M. Milburn, *J. Inorg. Biochem.*, *16*, 165 (1982).
75. P. Hendry and A. M. Sargeson, *J. Chem. Soc. Chem. Commun.*, 164 (1984).
76. P. Hendry and A. M. Sargeson, *Inorg. Chem.*, *25*, 865 (1986).
77. P. Hendry and A. M. Sargeson, *Aust. J. Chem.*, *39*, 1177 (1986).
78. P. Hendry and A. M. Sargeson, *J. Am. Chem. Soc.*, *111*, 2521 (1989).
79. P. Hendry and A. M. Sargeson, *Inorg. Chem.*, *29*, 92 (1990). (a) P. Hendry and A. M. Sargeson, *Inorg. Chem.*, *29*, 97 (1990).
80. R. R. Holmes, *J. Am. Chem. Soc.*, *96*, 4143 (1974).
81. E. Hough, L. K. Hansen, B. Birkner, K. Junge, S. Hansen, A. Hordvik, C. Little, E. Dodson, and Z. Derevenda, *Nature (London)*, *388*, 357 (1989).
82. P. W. A. Hubner and R. M. Milburn, *Inorg. Chem.*, *19*, 1267 (1980).
83. W. G. Jackson and B. C. McGregor, *Inorg. Chim. Acta*, *83*, 115 (1984).
84. E. K. Jaffe and M. Cohn, *J. Biol. Chem.*, *253*, 4823, (1978).
85. E. K. Jaffe, J. Nick, and M. Cohn, *J. Biol. Chem.*, *257*, 7650, (1982).
86. W. P. Jencks and M. Gilchrist, *J. Am. Chem. Soc.*, *86*, 1410 (1964).
87. D. R. Jones, L. F. Lindoy, and A. M. Sargeson, *J. Am. Chem. Soc.*, *105*, 7327 (1983).
88. D. R. Jones, L. F. Lindoy, and A. M. Sargeson, *J. Am. Chem. Soc.*, *106*, 7807 (1984).
89. R. S. Jones, A. L. Kindman, and J. R. Knowles, *Nature (London)*, *275*, 564 (1978).
90. R. B. Jordan, A. M. Sargeson, and H. Taube, *Inorg. Chem.*, *4*, 1091 (1965).
91. R. A. Kenley, R. H. Fleming, R. M. Laine, D. S. Tse, and J. S. Winterle, *Inorg. Chem.*, *23*, 1870 (1984).
92. S. A. Khan, A. J. Kirby, M. Wakselman, D. P. Horning, and J. M. Lawlor, *J. Chem. Soc. B*, 1182 (1970).
93. E. E. Kim and H. W. Wyckoff, to be published.
94. A. J. Kirby and A. G. Varvoglis, *J. Am. Chem. Soc.*, *89*, 415 (1966).
95. W. B. Knight, S. W. Fitts, and D. Dunaway-Mariano, *Biochemistry*, *20*, 4079 (1981).
96. W. B. Knight, S-J. Ting, S. Chuang, D. Dunaway-Mariano, T. Haromy, and M. Sundaralingam, *Arch. Biochem. Biophys.*, *227*, 320 (1983).

97. W. B. Knight, D. Dunaway-Mariano, S. C. Ranson, and J. J. Villafranca, *J. Biol. Chem.*, **259**, 2886, (1984).
98. J. R. Knowles, *Ann. Rev. Biochem.*, **49**, 877 (1980).
99. J. R. Knowles, *Methods Enzymol.*, **87**, 279 (1982).
100. J. Kumamoto, J. R. Cox, and F. H. Westheimer, *J. Am. Chem. Soc.*, **78**, 4858 (1956).
101. R. A. Lazarus, P. A. Benkovic, and S. J. Benkovic, *J. Chem. Soc. Perkin Trans. 2*, 373 (1980).
102. S. F. Lincoln and D. R. Stranks, *Aust. J. Chem.*, **21**, 37, 57, 67, 1733, and 1745 (1968).
103. K. J. Martin, P. J. Squattrito, and A. Clearfield, *Inorg. Chim. Acta*, **155**, 7 (1989).
104. F. M. Menger, L. H. Gan, E. Johnson, and D. H. Durst, *J. Am. Chem. Soc.*, **109**, 2800 (1987).
105. T. P. Merritt and M. Sundaralingam, *Acta Cryst.*, **B36**, 2576 (1980).
106. E. A. Merrit, M. Sundaralingam, and D. Dunaway-Mariano, *J. Am. Chem. Soc.*, **103**, 3565 (1981).
107. S. Meyerson, D. J. Harvan, J. R. Hass, F. Ramirez, and J. F. Marecek, *J. Am. Chem. Soc.*, **106**, 6977 (1984).
108. J. F. Morrison and E. Heyde, *Ann. Rev. Biochem.*, **41**, 29, (1972).
109. J. R. Morrow and W. C. Trogler, *Inorg. Chem.*, **27**, 3387 (1988).
110. P. R. Norman and R. D. Cornelius, *J. Am. Chem. Soc.*, **104**, 2356 (1982).
111. M. I. Page and W. P. Jencks, *Proc. Natl. Acad. Sci. USA*, **68**, 1678 (1971).
112. R. H. Prince, D. A. Stolter, and P. Wooley, *Inorg. Chim. Acta*, **9**, 51 (1974).
113. Pseudorotation is a ligand reorganizational isomerization in which two of the equatorial ligands replace the axial ligands that become equatorial. See, for example, Ref. 38.
114. F. Ramirez and J. F. Marecek, *J. Am. Chem. Soc.*, **101**, 1460 (1975).
115. F. Ramirez and J. F. Marecek, *Pure Appl. Chem.*, **52**, 1021 (1980).
116. F. Ramirez, J. Marecek, J. Minore, S. Srivastava, and W. J. le Noble, *J. Am. Chem. Soc.*, **108**, 348 (1986).
117. F. Ramirez and I. Ugi, *Advances on Physical Organic Chemistry*, V. Gold, Ed., Academic Press, London, 1971, pp. 25–126.
118. G. Rawji, M. Hediger, and R. M. Milburn, *Inorg. Chim. Acta*, **79**, 247 (1983).
119. G. H. Rawji and R. M. Milburn, *Inorg. Chim. Acta*, **150**, 227 (1988).
120. J. Rebek, F. Gavina, and C. J. Navarro, *J. Am. Chem. Soc.*, **100**, 8113 (1978).
121. J. Reibenspies and R. D. Cornelius, *Inorg. Chem.*, **23**, 1563 (1984).
122. V. Scheller-Krattiger and H. Sigel, *Inorg. Chem.*, **25**, 2638 (1986).
123. W. Schmidt and H. Taube, *Inorg. Chem.*, **2**, 698 (1963).
124. See, for example, *Metal Ions in Biological Systems*, Vol. 25, "Interactions

- between metal ions, enzymes and gene expression." H. Sigel and A. Sigel, Eds., Marcel Dekker, New York, 1989.
125. R. D. Shannon, *Acta Cryst. A.*, **A32**, 751 (1976).
 126. A. L. Shorter, T. P. Haromy, T. Scalzo-Brush, W. B. Knight, D. Dunaway-Mariano, and M. Sundaralingam, *Biochemistry*, **26**, 2060 (1987).
 127. H. Sigel and P. E. Amsler, *J. Am. Chem. Soc.*, **98**, 7390 (1976).
 128. H. Sigel, F. Hofstetter, R. B. Martin, R. M. Milburn, V. Scheller-Krattiger, and K. H. Scheller, *J. Am. Chem. Soc.*, **106**, 7935 (1984).
 129. G. W. Smithers, R. D. Sammons, P. J. Goodhart, R. LoBrutto, and G. H. Reed, *Biochemistry*, **28**, 1597 (1988).
 130. J. M. Sowadski, M. D. Handschumacher, H. M. Krishna-Murthy, B. A. Foster, and H. W. Wyckoff, *J. Mol. Biol.*, **186**, 417 (1985).
 131. T. G. Spiro, W. A. Kjellstrom, M. Zeydel, and R. A. Butow, *Biochemistry*, **7**, 859 (1968).
 132. D. D. Swank, C. N. Caughlan, F. Ramirez, and J. F. Pilot, *J. Am. Chem. Soc.*, **93**, 5236 (1971).
 133. F. Tafesse, S. S. Massoud, and R. M. Milburn, *Inorg. Chem.*, **24**, 2591 (1985).
 134. F. Tafesse and R. M. Milburn, *Inorg. Chim. Acta*, **135**, 119 (1987).
 135. M. Tetas and J. M. Lowenstein, *Biochemistry*, **2**, 350, (1963).
 136. M. L. Tobe, *Advances in Inorganic and Bioinorganic Mechanisms*, Vol. 2, A. G. Sykes, Ed., Academic Press, London, 1983, pp. 1-94.
 137. S. Trippett, *Pure Appl. Chem.*, **40**, 595 (1974).
 138. M. Ul-Haque, C. N. Caughlan, F. Ramirez, J. F. Pilot, and C. P. Smith, *J. Am. Chem. Soc.*, **93**, 5229 (1971).
 139. B. L. Vallee, *Metal Ions in Biological Systems*, Vol. 5, T. G. Spiro, Ed., Wiley-Interscience, New York, 1983, pp. 1-24.
 140. B. L. Vallee and R. J. P. Williams, *Inorg. Chim. Acta Rev.*, **5**, 137 (1971).
 141. J. R. Van Wazer, E. J. Griffith, and J. F. McCullough, *J. Am. Chem. Soc.*, **77**, 287 (1955).
 142. K. M. Welsh, I. M. Armitage, B. S. Cooperman, *Biochemistry*, **22**, 1046 (1983).
 143. F. H. Westheimer, *Acc. Chem. Res.*, **1**, 70, (1968).
 144. F. H. Westheimer, *Pure Appl. Chem.*, **49**, 1059 (1977).
 145. F. H. Westheimer, *Rearrangements in Ground and Excited States*, Vol. 2, P. de Mayo, Ed., Academic Press, New York, 1980, pp. 229-271.
 146. F. H. Westheimer, *Chem. Rev.*, **81**, 313 (1981).
 147. R. Wijesekera, unpublished observations.
 148. P. Wooley, *Nature (London)*, **258**, 677 (1975).
 149. P. Wooley, *J. Chem. Soc. Perkin Trans. 2*, 318 (1977).
 150. F. Y-H. Wu and C-W. Wu, *Metal Ions in Biological Systems*, Vol. 15, H. Sigel, Ed., Marcel Dekker, New York, 1983, pp. 157-192.
 151. A. Zanella and P. C. Ford, *Inorg. Chem.*, **14**, 700 (1975).

Long-Range Electron Transfer in Donor (Spacer) Acceptor Molecules and Proteins

**BRUCE E. BOWLER, ADRIENNE L. RAPHAEL, and
HARRY B. GRAY**

*Arthur Amos Noyes Laboratory
California Institute of Technology
Pasadena, California*

CONTENTS

I. INTRODUCTION	260
II. ELECTRON TRANSFER IN INORGANIC AND ORGANIC SYSTEMS	261
A. Free-Energy Dependence	261
B. Distance Dependence	267
III. ELECTRON TRANSFER BETWEEN PROTEINS AND INORGANIC COMPLEXES	281
A. Cytochrome <i>c</i>	282
B. Blue Copper Proteins	284
C. Iron-Sulfur Proteins	288
IV. ELECTRON TRANSFER IN MODIFIED PROTEINS	289
A. Modification Procedures	290
B. Characterization of Modified Proteins	293
C. Kinetic Methods	294
D. Modified Heme Proteins	296
1. Distance Dependence	297
2. Driving-Force Dependence	301
3. Reversibility	304
E. Modified Blue Copper Proteins	304
F. Modified Iron-Sulfur Proteins	307

Progress in Inorganic Chemistry: Bioinorganic Chemistry, Vol. 38, Edited by Stephen J. Lippard.

ISBN 0-471-50397-5 © 1990 John Wiley & Sons, Inc.

V. ELECTRON TRANSFER IN PROTEIN-PROTEIN COMPLEXES	308
A. (Fe,Zn)-Hybrid Hemoglobins	308
B. Cytochrome <i>c</i> -Cytochrome <i>b</i> ₅	310
C. Cytochrome <i>b</i> ₅ -(Fe,Zn)Hemoglobin	311
D. Cytochrome <i>c</i> -Cytochrome <i>b</i> ₂	311
E. Cytochrome <i>c</i> -Cytochrome <i>c</i> peroxidase	311
GLOSSARY OF TERMS	313
ACKNOWLEDGMENTS	314
REFERENCES	314

I. INTRODUCTION

The study of electron transfer (ET) in metalloproteins has taken advantage of the foundation laid by research on simple chemical systems (173, 174, 189). It was recognized early that parameters such as ET distance and driving force would have to be carefully controlled in order to provide experimental information that could be used in a meaningful way to evaluate theoretical models (108-110). Since it proved to be difficult to accomplish this goal through intermolecular ET studies, attention turned to measurements of intramolecular ET rates in systems in which the donor and acceptor are separated by a fixed and known distance.

Work on intramolecular ET complexes has included investigations of intervalence spectra in binuclear complexes (29, 160, 178). Recent research has been focused on measurements of the distance and driving force dependence of intramolecular ET rates in donor-acceptor complexes. Concurrently, methods to monitor ET in metalloproteins and protein-protein complexes have been developed. Our aim in this chapter is to compare and contrast ET data from proteins and donor-acceptor complexes in an attempt accurately to represent the current level of understanding of ET processes as they relate to biological systems. Our emphasis will be on the potential control of ET by variation in fundamental parameters such as the ET distance, driving force, and intervening medium.

Because of the vast quantity of published ET research, we have had to neglect several important areas of current interest. Many investigators have built systems to try to mimic the first steps of photosynthesis as well as the low-temperature (4.2 K) ET seen in photosynthetic reaction centers. Efficient ET has been observed down to 10 K in certain complexes (19, 184), and studies of ET across membranes using model systems have been made (59, 135, 137, 167). A relatively new area related to photosynthetic charge separation encompasses the study of ET in polymers that have been func-

tionalized with redox-active metal complexes and organic molecules. The main goal of this research is to exploit the diffusion properties of polymers to achieve long-lived charge separation (98, 127, 128).

II. ELECTRON TRANSFER IN INORGANIC AND ORGANIC SYSTEMS

A. Free-Energy Dependence

An unusual dependence of ET rate on reaction free energy (ΔG°) was predicted by Marcus over 30 years ago (109). Inspection of Eq. 1 (108–110),

$$k_{\text{et}} = (\pi/\hbar^2\lambda k_{\text{B}} T)^{1/2}[H_{\text{ab}}]^2 \exp[-(\Delta G^\circ + \lambda)^2/4\lambda k_{\text{B}} T] \quad (1)$$

shows that k_{et} will increase as $-\Delta G^\circ$ increases, reaching a maximum value when $-\Delta G^\circ = \lambda$. When $-\Delta G^\circ$ becomes larger than λ , the rate will decrease. A plot of $\log(k_{\text{et}})$ vs. $-\Delta G^\circ$ should have the shape of an upside-down parabola; the portion of the parabola where k_{et} is increasing with increasing driving force is known as the “normal” region, and the part where k_{et} is decreasing with increasing driving force is known as the Marcus “inverted” region. Whereas Marcus theory treats the free-energy dependence of k_{et} classically, several theories have been developed that take into account the quantum nature of the vibrational states of the electronic levels involved. Typically, the donor is treated as being in its vibrational ground state and is allowed to interact with the quantized vibrational levels of the acceptor. One such expression for k_{et} is given in Eq 2 (21, 42, 91), where the

$$k_{\text{et}} = (\pi/\hbar^2\lambda_s k_{\text{B}} T)^{1/2}[H_{\text{ab}}]^2 \times \sum (e^{-S} S^w/w!) \exp[-(\lambda_s + \Delta G^\circ + wh\omega)^2/4\lambda_s k_{\text{B}} T] \quad (2)$$

summation is over the vibrational quantum levels of the acceptor and $S = \lambda_v/h\omega$. As with Marcus theory, the equation predicts that the rate will be a maximum when $-\Delta G^\circ = \lambda = \lambda_s + \lambda_v$. The exponential term in Eq. 1 (or the summation in Eq. 2) often is referred to as the nuclear or Franck-Condon term. Many early experiments failed to reveal the inverted behavior predicted by Eqs. 1 and 2. At best the rate of ET between donors and acceptors in solution was seen to increase with increasing driving force and then level off. A typical example of this behavior is the quenching of the first excited triplet state of $[\text{Ir}(\mu\text{-pz})(\text{cod})]_2$ (pz = pyrazolyl and cod = 1,5-cyclooctadiene) with a series of alkylated pyridinium acceptors. The rate rises as $-\Delta G^\circ$ increases, but levels off at the diffusion limit (115).

A thorough study of the inverted region utilized pulse radiolysis on frozen methyltetrahydrofuran (MTHF) solutions of biphenyl as donor, with a range of organic acceptors ($-\Delta G^\circ$ from 0.01 to 2.75 eV) (129). The increase in rate with $-\Delta G^\circ$ in the normal region was observed to be steeper than the decrease with $-\Delta G^\circ$ in the inverted region. This phenomenon was related to the difficulty in maintaining a constant λ across a series of acceptors as $-\Delta G^\circ$ increases. It was noted that the reduction potentials of the high-driving-force acceptors were probably overestimates, and that λ was higher for these acceptors due to their chemical nature. Both these factors would lead to a slower apparent decrease of rate in the inverted region (129). Using a frozen matrix was key to observing the inverted region, since it eliminated diffusion effects that had previously obscured inverted behavior.

Rigidly bridged donor-acceptor compounds have allowed the free-energy dependence of k_{et} to be studied without obfuscation by diffusion limitations. A convincing account of inverted behavior was achieved for a series of compounds where a steroid was used to bridge between biphenyl as donor and a series of organic acceptors (Fig. 1) (130). The plot of $\log(k_{\text{et}})$ vs. $-\Delta G^\circ$ in Fig. 1 is consistent with the predictions of Marcus theory. This system prevents diffusion control of the overall reaction from obscuring the intrinsic nature of the ET reaction, and the acceptors cannot form excited-state products that would lead to anomalously fast rates in the inverted region. The effect of solvent polarity on the dependence of rate on free energy also was studied in this system. Fitting the data to Eq. 2, it was found that the value of λ_s was 0.75, 0.45, and 0.15 eV ($\lambda_v = 0.45$ eV) in MTHF, di-*n*-butyl ether, and isooctane, respectively (20, 21, 130). The λ_s value decreased as the solvent became less polar, as expected from a dielectric continuum model for λ_s (see Eq. 7, Section II,B). A similar dependence of λ_s on solvent polarity was observed in an investigation of the ΔG° dependence of k_{et} for a zinc porphyrin linked to a series of substituted quinones by the rigid spacer bicyclooctane (84). The value of λ increased in the series benzene < MTHF < butyronitrile < acetonitrile. A fit of the benzene data to Eq. 2 gave $\lambda_v = 0.3$ and $\lambda_s = 0.3$ eV.

Another method of varying the driving force of an ET reaction involves using different excited-state donors. Typically, the forward ET reaction (usually a charge separation, CS) is followed by CR with a much larger driving force (see Fig. 2). If a porphyrin is the donor in the photoinduced ET reaction, the driving force of both the electron transfer and the charge recombination may be varied by metal substitution into the porphyrin. It is possible to vary the driving force of reactions involving charge separation by varying the solvent polarity. Weller (187) has developed an expression that describes the effects of solvation on the free energy of CS (Eq. 3),

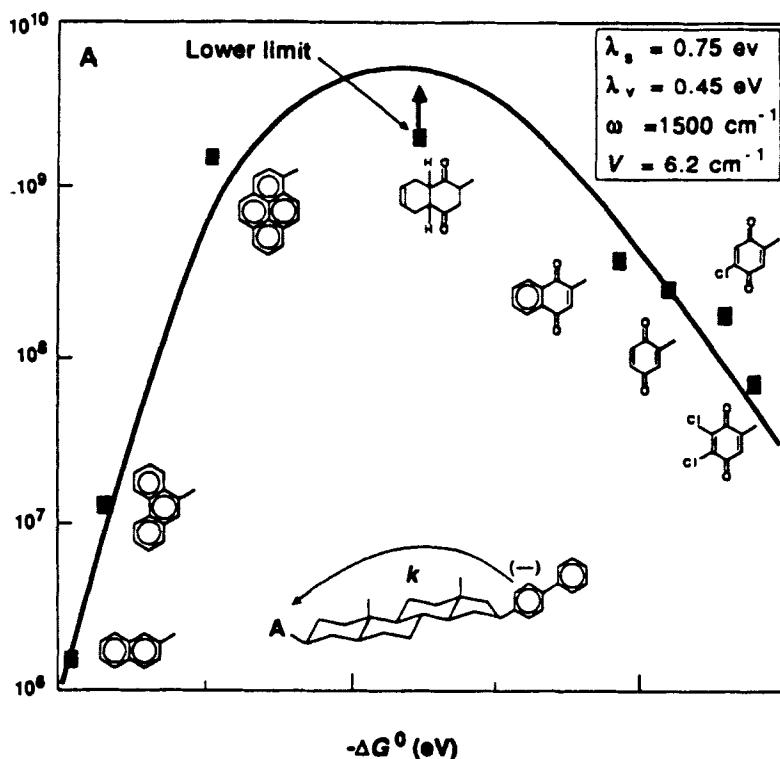


Figure 1. $\log k_{et}$ vs. $-\Delta G^\circ$ plot showing inverted behavior from the data of Closs and Miller (20, 21) for a donor and acceptor bridged by a sterical spacer.

$$\Delta G^\circ(\epsilon) = (E_D^{\text{ox}} - E_A^{\text{red}})^{\text{MeCN}} + [(e_0^2/\epsilon)(1/r - 1/a)] - (e_0^2/37r) \quad (3)$$

where $(E_D^{\text{ox}} - E_A^{\text{red}})^{\text{MeCN}}$ is the difference in the electrochemical potential of donor and acceptor in acetonitrile, r is the average radius of the donor and the acceptor, a is the donor-acceptor separation, and ϵ is the static dielectric constant of the solvent.

A combination of these methods (Zn and metal free porphyrin donor, three quinone acceptors, and toluene and butyronitrile as solvents) was used in a system in which a porphyrin was linked to a quinone via a rigid triptycene spacer. The spacer maintains a constant edge-edge separation of 6–7 Å between the donor and the acceptor (185, 186). These techniques allowed a $-\Delta G^\circ$ range of 0–0.8 eV for photoinduced charge separation (CS) and 1.2–1.8 eV for charge recombination (CR) to be studied. The $\log(k_{et})$ vs. $-\Delta G^\circ$ plots for photoinduced ET and CR when fit separately to the best parabola (Eq. 1) both maximize at $-\Delta G^\circ = \lambda = 0.9$ eV and

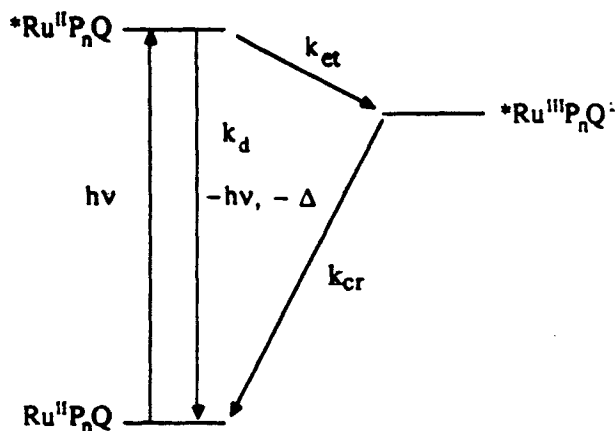


Figure 2. Energy level diagram for a photoinduced ET reaction in a donor–acceptor compound. k_{et} is the forward ET rate, k_{cr} is the rate of charge recombination (cr), and k_d is the natural decay rate of the excited donor in the absence of an acceptor (161).

$k_{et} = 2.5 \times 10^{11} s^{-1}$. The photoinduced CS reactions show normal (k_{et} increases with increasing $-\Delta G^\circ$) behavior; for CR, the rates are inverted (k_{cr} decreases with increasing $-\Delta G^\circ$). These data indicate that, in spite of the different electronic states involved in photoinduced CS and CR, the rearrangements of solvent and donor–acceptor structure must be similar.

In a system in which a porphyrin was capped by a quinone or methyl viologen with flexible alkyl ester straps, metal substitution (Mg^{2+} , metal free) and solvent variation (CCl_4 , toluene, chlorotoluene–toluene, CH_2Cl_2 , CH_3CN) established a $-\Delta G^\circ$ range of -0.07 – 1.1 eV for photoinduced CS and 1.13 – 2.07 eV for CR (73). A much steeper increase in rate with $-\Delta G^\circ$ was observed in the normal region than the decrease of rate with $-\Delta G^\circ$ in the inverted region. The data could not be fit well using the Marcus equation; however, a reasonable fit was obtained using a displaced oscillator quantum mechanical model.

A recent observation of inverted behavior has come from studies of photoinduced CS from singlet and triplet excited states and CR using an iridium dimer donor bound to a series of *N*-alkylpyridinium acceptors via a phosphonite ligand (43, 44). The plot of $\ln k_{et}$ vs. $-\Delta G^\circ$ gave an excellent fit (almost no scatter of data points away from the theoretical curve) to the Marcus equation (Eq. 1) with $\lambda = 1.1$ eV. It was assumed that the same values of λ_s , λ_v , and H_{ab} could be used for all three types of reactions, an assumption not *a priori* evident given the different spatial extent and polarizabilities of singlet states, triplet states, and radicals. The surprisingly good fit to the Marcus equation suggests, however, that λ_s , λ_v , and H_{ab} do

not vary significantly for the three different reactions in this particular complex.

Interestingly, inverted behavior has been observed for reactions in solution between donors and acceptors that are not attached by molecular bridges. In a novel approach, the diffusion-control problem was avoided by monitoring charge recombination in geminate radical pairs (see Fig. 3). It is possible to extract the CR rate constant, k_{cr} , from the quantum yield of radicals escaping from the geminate radical pair (Eq. 4), where Φ_{sep} is monitored with a cation radical trap such as dimethoxystilbene (DMS).

$$\Phi_{sep} = k_{sep}/(k_{sep} + k_{cr}) \quad (4)$$

With 2,6,9,10-tetracyanoanthracene (TCA) and 9,10-dicyanoanthracene (DCA) as acceptors and a range of two-ring aromatic compounds as donors, k_{cr} was found to decrease by a factor of 100 as $-\Delta G^\circ$ increased from 2.03 to 2.90 eV (49). A fit to Eq. 2 gave $\lambda_s = 0.95$ eV, $\lambda_v = 0.6$ eV, and $H_{ab} = 11$ cm⁻¹ (with ω set to 1500 cm⁻¹). In another study, several redox-active systems, including [Rh(dp-phen)₃]^{3+.2+} (dp-phen = diphenylphenanthroline), [Cr(dp-phen)₃]^{3+.2+}, disodium tetraiodofluorescein (Er²⁻), and zinc octaethylporphyrin (Zn(OEP)), were studied with aromatic amines, methoxybenzenes, and quinone acceptors (143). For Cr^{II} and Rh^{II} donors, inverted behavior for k_{cr} was observed for $-\Delta G^\circ > 1.7$ eV. Interestingly, although $\lambda = 1.7$ eV for both the Cr and the Rh systems, the steepness of the driving-force dependence of k_{cr} was much greater in the normal

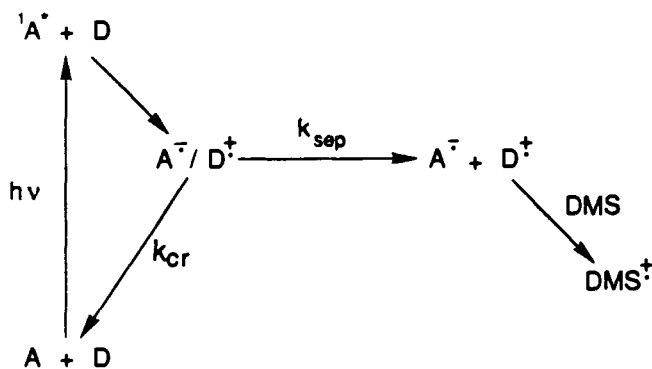


Figure 3. Schematic representation of the reactions involved in geminate radical pair recombination, showing the ground state, the excited state, the geminate radical pair, and the separated radical pair. k_{cr} is the geminate radical pair recombination rate, k_{sep} is the rate of separation (diffusion) of the geminate radical pair, and DMS is dimethoxystilbene, a cation radical scavenger (49).

region for Cr donors than for the Rh donor. Marcus theory predicts that a steeper $-\Delta G^\circ$ dependence should lead to a smaller λ . In the normal $-\Delta G^\circ$ region, the slope of the $\log(k_{cr})$ vs. $-\Delta G^\circ$ plot followed the order $\text{Cr}^{\text{II}}\text{-aromatic amine}^{+\cdot} > \text{Er}^{\text{III}}\text{-quinone}^{\cdot-} > \text{Rh}^{\text{II}}\text{-aromatic amine}^{+\cdot} > \text{Zn}(\text{OEP})^{+\cdot}\text{-quinone}^{\cdot-}$, for the geminate radical pair systems studied. This order is the same as that expected from estimates of the electronic coupling matrix element, H_{ab} , based on orbital overlap arguments. It was proposed that the value of H_{ab} , not just the value of λ , influenced the slope of the $\log(k_{cr})$ vs. $-\Delta G^\circ$ plot (143).

Several other interesting results have been obtained from work with geminate radical pairs of DCA and TCA with aromatic donors. Two-ring and one-ring donors fall on separate $\log(k_{cr})$ vs. $-\Delta G^\circ$ curves with $\lambda_s = 1.6$ and 1.45 eV, respectively (52). This observation is in accord with previous data, indicating one-ring aromatics are better solvated than two-ring aromatics (53). The $\log(k_{cr})$ vs. $-\Delta G^\circ$ plots of contact pairs vs. solvent-separated pairs gave dramatically different λ_s values, 0.55 and 1.6 eV, respectively (51). This result accords with the distance dependence of λ_s (Eq. 7). For acetonitrile, $\Delta\lambda_s = 7.63[(1/r_0) - (1/r)]$, so that if 7 \AA is taken as the separation distance of a solvent-separated radical pair with a $\Delta\lambda_s$ of approximately 1 eV, a reasonable separation distance ($r_0 = 3.6 \text{ \AA}$) for a contact radical pair is obtained. A study of the differences between charge-shift reactions (CSH) vs. CR reactions was carried out by comparing 9-methylacridinium (9-MA^+) geminate radical pairs with TCA and DCA geminate radical pairs (52). In contrast to a theory developed by Kakitani and Mataga (86–88), the $\log(k_{cr})$ vs. $-\Delta G^\circ$ plot in the inverted region was found to be steeper for the CSH reaction than for the CR reaction, mainly due to the smaller λ_s for CSH, 1.4 vs. 1.6 eV for CR. Studies of k_{cr} as a function of $-\Delta G^\circ$ between DCA, TCA, and deuterated alkylbenzene donors demonstrated that high-frequency C–H vibrations have a significant effect on ET rates (50). This work indicates that the assumption that only carbon skeletal vibrations are important in ET processes (using $\omega = 1500 \text{ cm}^{-1}$ when fitting Eq. 2) may not always be appropriate, and that high-frequency vibrations must be included in the analysis in some circumstances.

The very important result achieved with both rigidly bridged donor-acceptor model systems and geminate radical pairs is that an inverted region exists for ET reactions having $-\Delta G^\circ > \lambda$. The data also provide insight into a strategy that could be used in nature to achieve charge separation in the proteins involved in photosynthesis. In particular, it is now established that charge separation can occur at fast rates at low driving forces, and that charge recombination from the charge-separated state could be much slower if the driving force is large enough to be in the inverted

region. The data of Closs and Miller (20, 21, 130) on the solvent dependence of λ_s also suggest a possible reason for the choice of a nonpolar protein environment for photosynthesis. As λ_s decreases in less polar environments, optimal charge separation will be achieved at small $-\Delta G^\circ$ values (wasting less of the photoexcitation energy) and the recombination reaction will be further into the inverted region (slower rate).

Caution, however, is advised when comparing the absolute values of λ reported. Closs and Miller have pointed out that varying the structure of the donor or the acceptor can affect the value of λ of ET reactions [see above (20, 21, 130)]. Also, since λ_s is solvent dependent (Eq. 7), using solvent to vary ΔG° will affect λ of the reaction as well. In some studies, donor-acceptor compounds with spacers of unequal length have been used on the same $\log(k_{et})$ vs. $-\Delta G^\circ$ plot. Given the distance dependence of λ_s (Eq. 7), such a practice will produce unreliable λ values. Such effects may account in part for the scatter of data points observed in some $\log(k_{et})$ vs. $-\Delta G^\circ$ plots and may indeed affect the shape of those curves so that conclusions based on curve shape should be made carefully. Inverted behavior for ET reactions, however, is now on firm experimental (as well as theoretical!) ground.

B. Distance Dependence

According to standard theory (Eq. 1 and 2), the ET rate is proportional to the square of the electronic coupling matrix element, H_{ab}

$$k_{et} \propto [H_{ab}]^2$$

To a first approximation, electronic coupling results from overlap of the donor and acceptor orbital wave functions. Since orbital wave functions decay exponentially with distance, H_{ab} also is expected to decay exponentially with distance. Two common ways to express this decay are shown in Eqs. 5 and 6 (21, 110).

$$H_{ab} = (H_{ab})_0 \exp[-\beta(r - r_0)/2] \quad (5)$$

$$k_{et} = k_{op} \exp[-\beta(r - r_0)] \quad (6)$$

The value of β reflects the efficacy of the medium in coupling the donor and the acceptor. Since electronic coupling between donors and acceptors is often treated in terms of a superexchange model, the decay of electronic coupling is sometimes reported per bond rather than per unit distance. In the bond-coupling model, the exponent in Eq. 5 becomes $[-\beta'(N - 1)/2]$,

where N is the number of bonds separating the donor and the acceptor and $(H_{ab})_0$ becomes $(H_{ab})'_0$. The term $(H_{ab})_0$ reflects how well the donor and the acceptor couple to the medium that bridges them. Both $(H_{ab})_0$ and β must be favorable for the overall coupling of the donor and acceptor to be substantial.

The nuclear term in Eqs. 1 and 2, which is replaced by k_{op} in Eq. 6, has a distance dependence of its own. In particular, λ_s , derived assuming a dielectric continuum, is dependent on the donor-acceptor separation, r_{DA} (Eq. 7). Therefore, if β is to reflect only the rate of decay of electronic

$$\lambda_s = -e^2(1/2r_A + 1/2r_B - 1/r_{DA})(1/\epsilon_s - 1/\epsilon_{op}) \quad (7)$$

coupling with distance, k_{ct} values at different distances must be corrected using Eq. 7 to account for changes in the free energy of activation, ΔG^* ($\Delta G^* = [(\Delta G^\circ + \lambda)^2/4\lambda]$ in Eq. 1), due to λ_s . Equation 8 has been employed

$$k = k_0 \exp[-(\beta + \gamma)(r - r_0)] \quad (8)$$

by Sutin (76), where β represents the decay with distance due to the electronic term and γ is the decay with distance due to the nuclear or Franck-Condon term (ΔG^* , λ_s). It is possible to extract β and γ values from ET activation parameters (76).

Many compounds containing a donor and an acceptor joined by a flexible linker have been synthesized (see Ref. 185 for an extensive list of references). The difficulty in using such compounds to study the distance dependence of ET is that the flexibility of the linker precludes knowing the donor-acceptor separation precisely. Distances have been estimated from fluorescence quenching volumes (61) and NMR conformational studies (60) with such compounds. NMR studies indicated that the methylene linker between the porphyrin and the quinone in carotenoid-porphyrin-quinone triads is in an extended (all-anti) conformation (60). The calculated value of β , based on this conformation for the series of methylene linkers, was 0.6 \AA^{-1} . If one methylene in each chain is in a gauche conformation, however, the predicted β would be 1.7 \AA^{-1} . So, even under the best conditions, ambiguities exist when flexible linkers are used to study the distance dependence of ET rates.

The first experiments to examine reliably the distance dependence of ET involved suspension of donor and acceptor molecules in a rigid matrix at variable concentrations so that the average separation of donor and acceptor could be varied (129). Since then, many complexes of sophisticated design have been synthesized in order to extract information about

electronic coupling from Eqs. 5, 6, and 8. Common to the design of all these compounds is a donor and an acceptor joined by an electrochemically inert molecular bridge. The molecular bridge is typically composed of discrete synthetic units so that the distance between the donor and the acceptor can be changed by altering the number of units in the bridge. In most instances, the bridge is designed to be rigid so that the distance

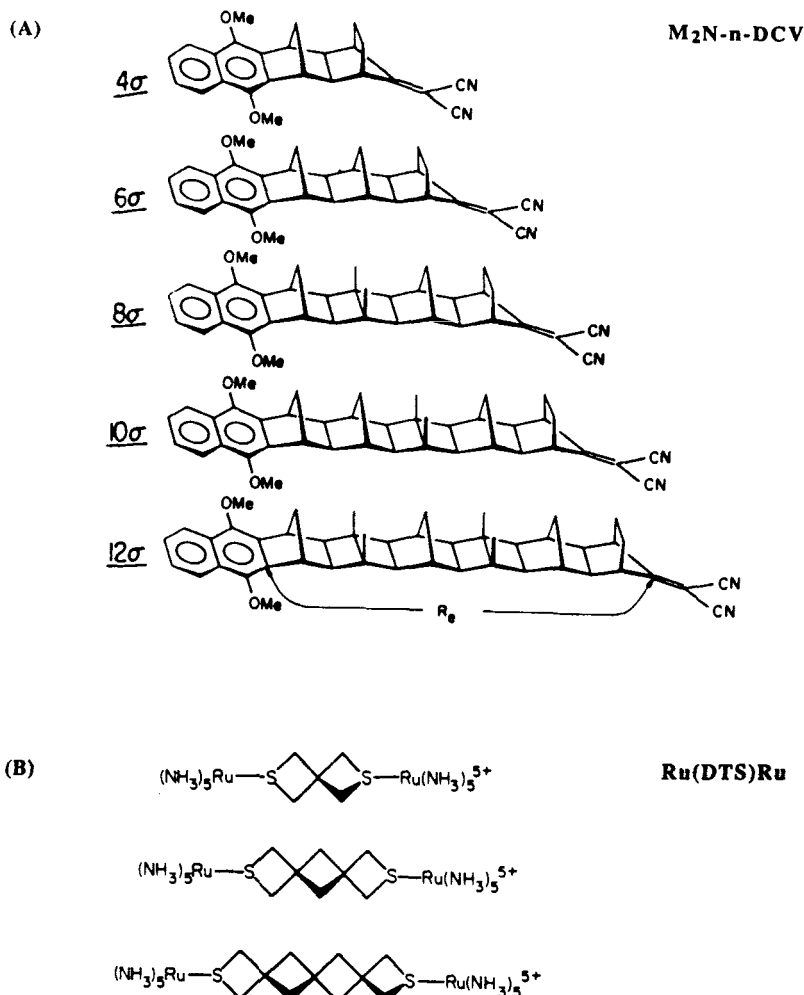
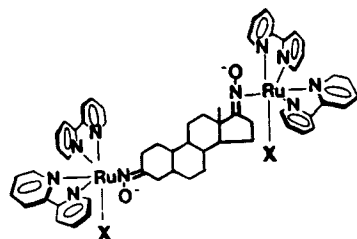
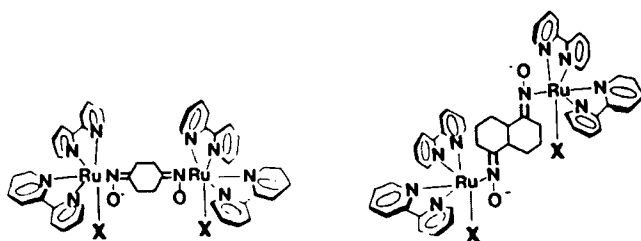


Figure 4. Donor-acceptor complexes with saturated-carbon bridges: (a) norbornyl bridges (72); (b) cyclobutane bridges (171, 172); (c and d) fused cyclohexane or steroid bridges (20, 21, 33, 45, 46); (e and f) bicyclobutane bridges (4, 85).

(C)



(D)

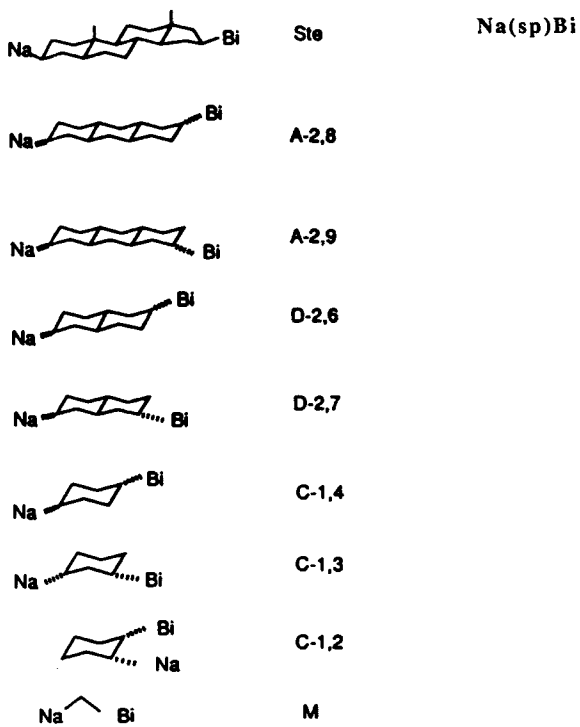


Figure 4. (Continued)

between the donor and the acceptor is known precisely. It is evident from Figs. 4–6 that an impressive array of molecular bridges has been utilized. The saturated-carbon bridges (Fig. 4) include strained norbornyl (**4a**) (72, 142, 147, 149, 181–183) and cyclobutane rings (**4b**) (171), fused cyclohexane rings [**4c** (33, 45, 46) and **4d** (20, 21)], and connected bicyclooctane units [**4e** (84, 85, 99) and **4f** (4)]. In Fig. 5, the donor–acceptor compounds use peptide bridges (75, 76, 161) that contain a mixture of saturated and unsaturated chemical groups. Finally, the compounds in Fig. 6 are bridged by polyenes (**6a**) (192) or aromatic groups (**6b**) (41, 64, 65).

Maintaining the donor and acceptor at a fixed distance is an important attribute of the compounds in Figs. 4–6. However, the overall electronic coupling is expected to depend not only on the length of the bridge but also on the orientation of the donor and the acceptor relative to the bridge. It is therefore advantageous to control this parameter as well. The orientation of the donor and acceptor relative to the bridge is known precisely only for the norbornyl-bridged compounds (72).

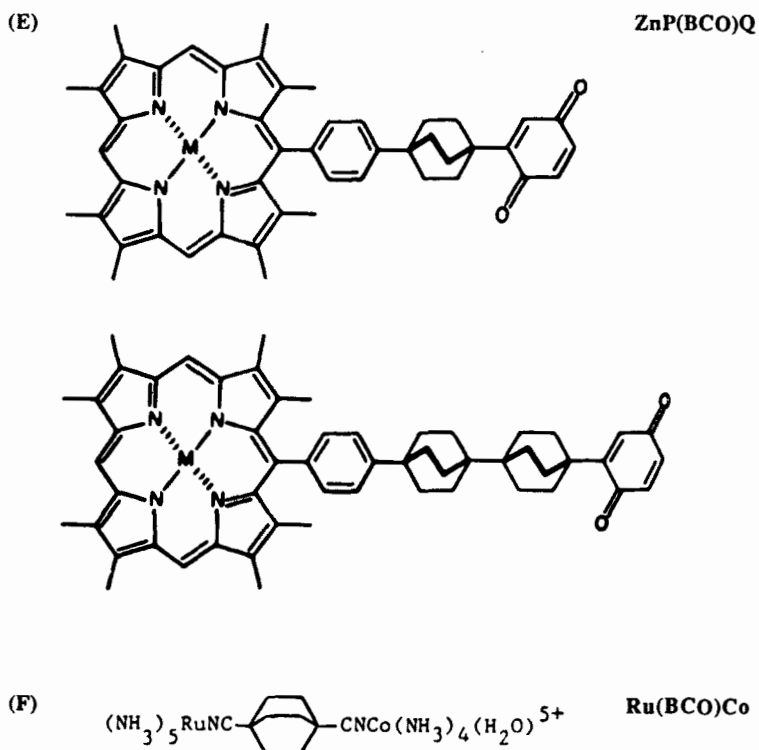
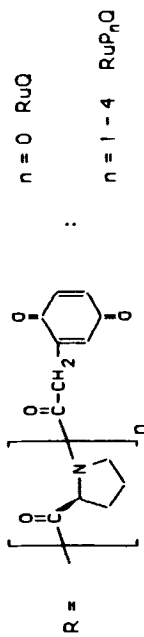
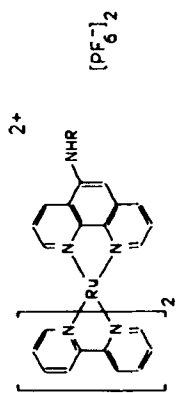


Figure 4. (Continued)

(A) RuP_nQ



(B) OsP_nRu

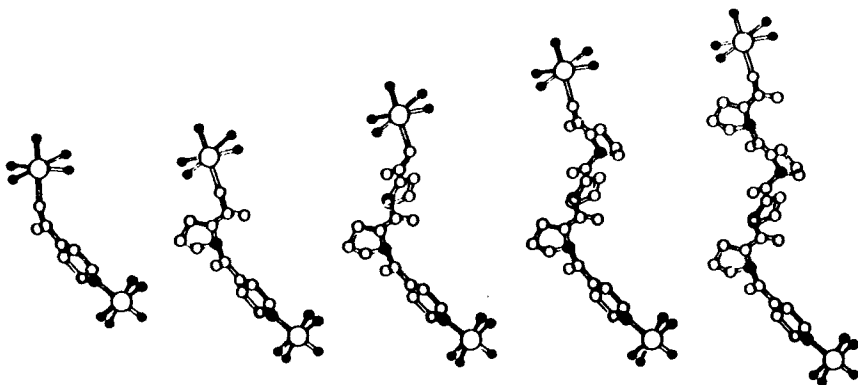


Figure 5. Donor-acceptor complexes bridged by peptide units composed of polyproline units: (a) ruthenium donor, quinone acceptor (161); (b) osmium donor, cobalt acceptor (75, 76).

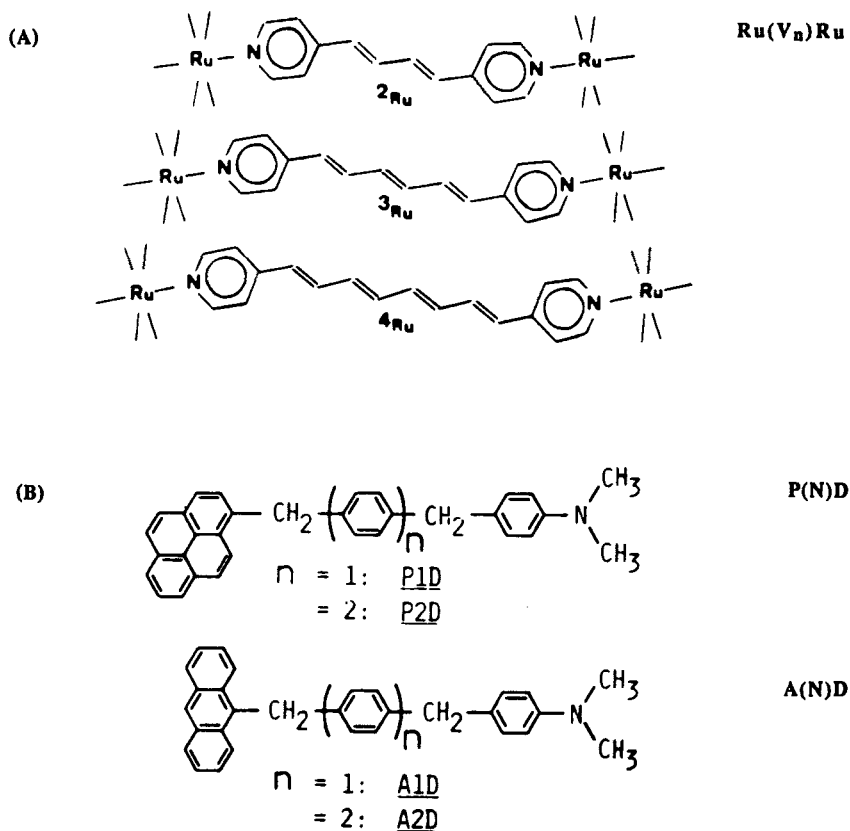


Figure 6. Donor–acceptor complexes bridged by aromatic groups: (a) polyene bridges (192); (b) polyphenyl bridges (41, 64, 65).

There are two common methods for estimating electronic couplings in donor–acceptor molecules. Values of H_{ab} and β may be obtained from ET kinetics using Eqs. 5, 6, or 8, or from intervalence absorption spectra using a theory developed by Hush (71). Tables I and II give estimates of the donor–acceptor electronic couplings in the molecules depicted in Figs. 4–6, using ET kinetics and intervalence spectra, respectively. Considering only data that have been corrected for the distance dependence of ΔG^* , β values span the range of 0.14–1.2 \AA^{-1} . Thus, depending on the composition of the bridge, the difference in the decay of the ET rate over 4 \AA can amount to almost two orders of magnitude. In most cases, the decay in k_{et} due to the distance dependence of the nuclear factor (γ) is relatively small (a factor of 2–3 over 4 \AA ; $\gamma = 0.2\text{--}0.3 \text{\AA}^{-1}$, see Tables I and II),

TABLE I
Electronic Coupling Parameters Derived from ET Rates

D-A System	Experiment	β (\AA^{-1})	$(H_{ab})_0$ (cm^{-1})	β' (bond $^{-1}$)	$(H_{ab})'_0$ (cm^{-1})	$[H_{ab}(r)/H_{ab}(r + 4 \text{\AA})]^2$	$[k(r)/k(r + 4 \text{\AA})]$	References
P(N)D	Photoinduced ET	0.50				7.7	27	41, 65
A(N)D	Photoinduced ET	0.56				9.3	22	41, 65
Os ₂ P ₂ Ru	Pulse radiolysis	0.68				15.2	578 ^a	76
RuP ₂ Q	Photoinduced ET	0.75 ^{b,c}					20 ^d	161
M ₂ N- <i>n</i> -DCV	Photoinduced ET	0.85		0.98		30	78 ^d	142
M ₂ N- <i>n</i> -DCV	Charge recombination	0.88 ^c		1.00			34	147
Na(Sp)Bi	Pulse radiolysis	0.95	1900 ^e	1.12	1100	44	92	20, 21
Bi-D MTHF glass	Pulse radiolysis	1.20	314			122		129
D-A Sucrose							305 ^f	34
Octaacetate glass ^f	Photoinduced ET	1.43 ^g						
ZnP(BCO)Q	Photoinduced ET	1.5-1.86 ^g					500-1600	99
Ru(BCO)Co	Thermal Et	>2.3 ^g					>3 × 10 ^h	4

^a $\gamma = 0.91 \text{\AA}^{-1}$.

^bLower limit.

^cUncorrected value.

^dEstimated value.

^eCalculated using center-center distance.

^fD = pentacene; A = duroquinone.

TABLE II
Electronic Coupling Parameters Derived from Intervalence Absorption Spectra

D-A System	β^a (\AA^{-1})	$(H_{ab})_0$ (cm^{-1})	β' (bond^{-1})	$(H_{ab})'_0$ (cm^{-1})	$\{H_{ab}(r)/$ $H_{ab}(r + 4 \text{\AA})\}^2$	$\{k(r)/$ $k(r + 4 \text{\AA})\}^2$	References
Ru(V_n)Ru	0.14		0.17		1.8		192
[M_2N - <i>n</i> -DCV]	0.57	1855 ^b	0.84	4355	9.7		149
Ru(dioxA)Ru	0.75	1160 ^b			20.1		33, 45
Ru(DTS)Ru	0.78 ^c		0.85	484 ^d	22.6	1100 ^d	161

^aCalculated from H_{ab} values.

^bCalculated using r_c values.

^c H_{ab} calculation (Ref. 70); assumed a 2.2- \AA spirobutane width.

^dSulfur-to-sulfur bond count.

but in some instances it is very significant (a factor of up to 30–50 over 4 \AA ; $\gamma = 0.9$ – 1.0\AA^{-1} , see Tables I and II). Hence, to evaluate the role of electronic coupling in determining ET rates at various distances, the distance dependence of the nuclear factor must be taken into account.

Some trends are apparent in the β values of the various bridging groups (Figs. 4–6). In particular, the smallest values of β (0.14 – 0.56\AA^{-1}) occur when the bridging group contains mainly π orbitals. Several theoretical treatments of bridged donor–acceptor compounds indicate that aromatic or polyene bridges should be much better conductors than aliphatic bridges (83, 96, 97). Experimentally, a direct comparison has been made between k_{et} of an (Os, Co) dimer bridged with cyclohexyldione dioxime and k_{et} for the same dimer bridged with the aromatic analogue of this bridge, benzoquinone dioxime (33). The rate of ET from Os(II) to Co(III) increased by almost a factor of 100, from 7.2×10^{-5} to $6.3 \times 10^{-3} \text{s}^{-1}$, upon replacing the aliphatic bridge with its aromatic analogue (33). Peptide bridges, which have a mixture of saturated and unsaturated units, also provide a good medium ($\beta = 0.68$ – 0.75\AA^{-1}) for ET. The β value for proteins is about 0.7 – 1.0\AA^{-1} (uncorrected for the distance dependence of the nuclear factor) (76, 118), in close agreement with peptide model systems. Surprisingly, aliphatic bridges provide strong electronic coupling as well ($\beta = 0.57$ – 0.95\AA^{-1}). Molecular orbital calculations for the thiaspirobutane bridge have shown that the alignment of the orbitals in the HOMO provides a good hyperconjugative pathway for electronic coupling (see Fig. 7) (172), thereby explaining the relatively favorable β (0.78\AA^{-1}) for this bridge despite the spiro linkages.

A recent study allows a direct comparison of peptide and aliphatic groups bridging the same donor–acceptor pair (162). Two different amide bridges were compared to a bicyclooctane bridge. The ET rate for the amide bridges was 10–100-fold higher than for the bicyclooctane bridge. These data suggest that peptide linkages provide better electronic coupling than

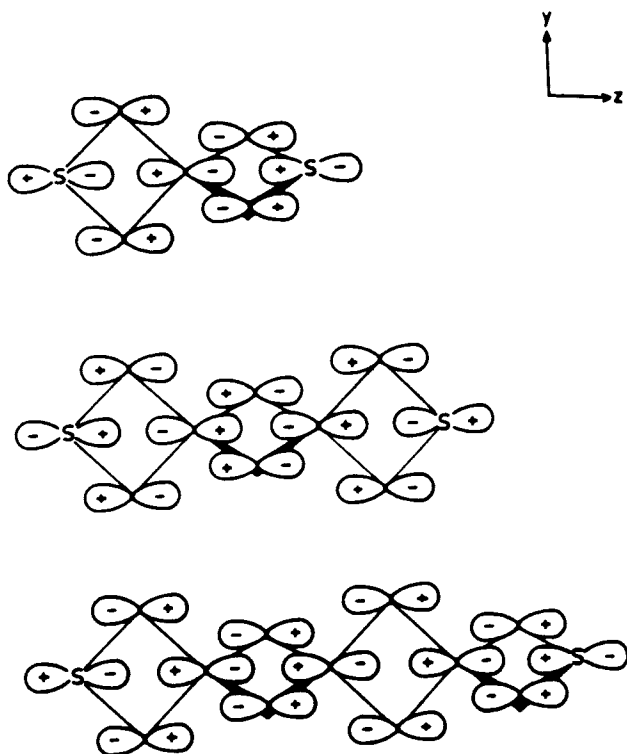


Figure 7. Pictures of the highest occupied molecular orbitals (HOMO) for dithiaspiro bridges (172).

simple aliphatic bridges; however, inspection of the data in Table I shows that there is significant overlap of the ranges of β values for peptide and aliphatic linkers. The slower ET rate for the bicyclooctane-bridged compound may be intrinsic to coupling through bicyclooctane and not through aliphatic spacers in general. The β values for bicyclooctane(BCO)-bridged donor-acceptor compounds suggest that this inference is true; however, neither β value has been corrected for the distance dependence of the nuclear factor.

An important factor controlling electronic coupling through aliphatic bridges has been elucidated recently. Two isomers of the norbornyl-bridged donor-acceptor system have been synthesized, in which the all-trans linkages of the original series have been replaced partially with cis linkages (see Fig. 8) (94, 145). The ET rates through these bent bridges were approximately 10-fold slower than for the corresponding all-trans com-

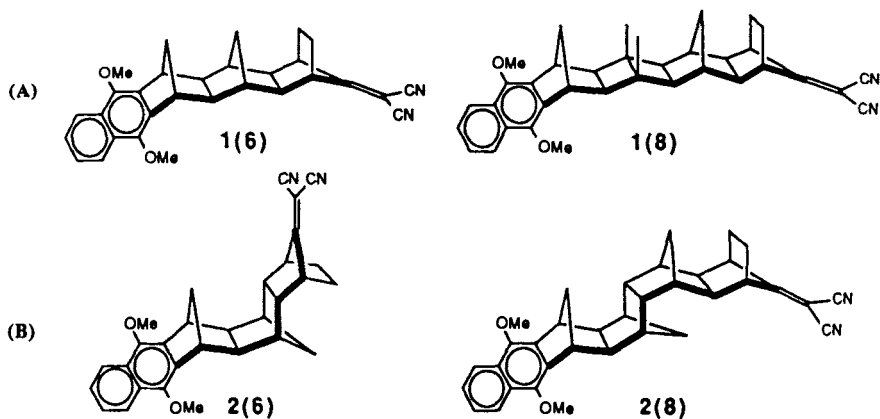


Figure 8. Norbornyl-bridged donor-acceptor complexes: (a) all-trans linkages; (b) with one cis linkage in the bridge (145).

pounds, despite a slightly decreased through-space edge-edge distance. These data indicate that Hoffmann's through-bond interaction theory, which predicts that an all-trans, antiperiplanar alignment of σ bonds is the optimum conformation for electronic coupling in aliphatic systems (68, 69), is applicable to ET reactions.

The data for the trans vs. the cis norbornyl bridges support the postulate that ET in this case occurs by a superexchange (bond-mediated) mechanism in preference to a direct through-space mechanism. Despite the shorter through-space distance for the bent compounds, their ET rates relative to the all-trans compounds are slower. This result demonstrates that specifics of the bridge and not the through-space separation control the ET rate. Closs and Miller similarly found that their rate data for a series of bridged donor-acceptor molecules correlated better with the number of bonds separating the donor and the acceptor rather than with the through-space distance (20, 21). Strikingly, the electronic coupling matrix elements, H_{ab} , for the 2,7-ee and 2,7-aa isomers of decalin-bridged donor-acceptor compounds, were almost identical (same number of bonds separating donor and acceptor) despite a difference of 6.3 Å in the through-space separation distance (see Fig. 9). Thus, superexchange coupling mechanisms are strongly implicated in long-range ET reactions.

A much stronger solvent dependence was noted for the ET rates in the case of the bent norbornyl-bridged compounds. The distance dependence of the electronic coupling also was similar to that observed in rigid glasses ($\beta = 1.20 \text{ \AA}^{-1}$, see Table I). A tentative proposal was put forth suggesting that solvent-mediated superexchange could compete with bridge-mediated

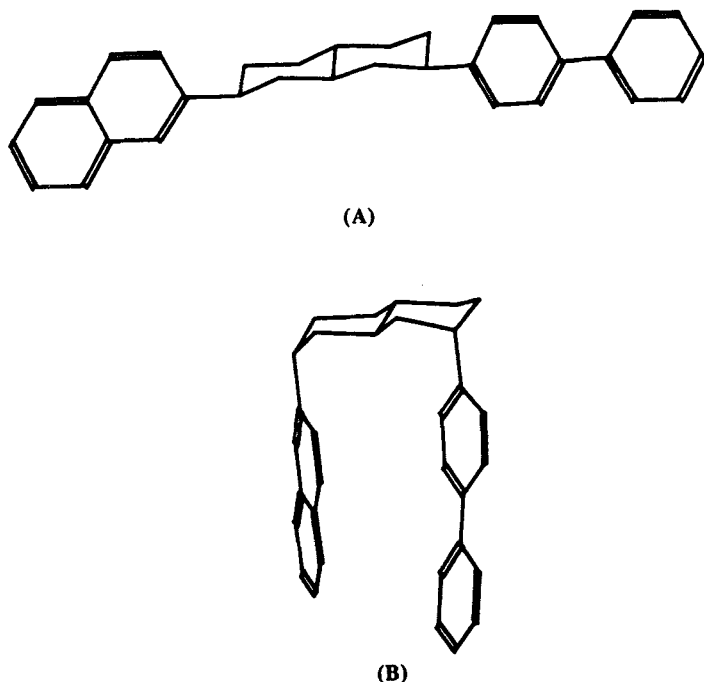


Figure 9. (a) 2, 7 equatorial-equatorial and (b) 2, 7 axial-axial decalin-bridged donor-acceptor complexes. The donor-acceptor center-center separation distance is 12.5 Å for the equatorial-equatorial isomer and 6.5 Å for the axial-axial isomer (21).

superexchange when bridge coupling was not optimal. A crude correlation of rate with solvent polarizability was obtained (94). On this point, it is of interest that a β of 1.8 \AA^{-1} was extracted from an *ab initio* theoretical treatment of ET in the $[\text{Fe}^{2+}:\text{Fe}^{3+}]$ -hexaquo couple (139). The β for ET in a rigid organic glass ($1.2\text{--}1.4 \text{ \AA}^{-1}$; see Table I) is significantly below this value, thereby indicating that organic solvents, although they do not provide a fully bonded pathway, can provide better pathways than water for ET. This observation could be useful in thinking about electronic coupling through proteins, since fully bonded pathways are often circuitous (28), whereas much more direct pathways involving one or two hydrogen-bond interactions, and possibly through-space interactions between nonbonded atoms, often exist (11, 28).

Some interesting electronic coupling data have been obtained from $\log(k_{\text{et}})$ vs. $-\Delta G^\circ$ plots for charge recombination within geminate radical pairs. It was found that $H_{\text{ab}} = 10.7 \text{ cm}^{-1}$ when the donor is a one-ring aromatic and that $H_{\text{ab}} = 7.8 \text{ cm}^{-1}$ when the donor is a two-ring aromatic (53). Since

the MOs of a one-ring aromatic are less nodal than those of a two-ring aromatic, it is not surprising that electronic coupling is also better for one-ring aromatics. The distance dependence of electronic coupling was demonstrated in geminate radical pairs. The value of H_{ab} was 200 cm^{-1} for contact radical pairs and 11 cm^{-1} for solvent-separated radical pairs (51).

Tables I and II also contain values for $(H_{ab})_0$ and $(H_{ab})'_0$. The matrix elements $(H_{ab})_0$ and $(H_{ab})'_0$ can be understood as the coupling of the donor and the acceptor to the molecular bridge or as the intrinsic coupling of the donor with the acceptor at van der Waals contact. The largest $(H_{ab})'_0$ value is observed for $[\text{M}_2\text{N}-n\text{-DCV}]^-$. The very good coupling of the donor-acceptor to the bridge in the $[\text{M}_2\text{N}-n\text{-DCV}]^-$ compounds has been attributed to the existence of two equivalent pathways through the bridge, the small size of the acceptor (DCV), and the large II coefficient (0.7) on the acceptor atom attached to the bridge (149).

Binuclear metal complexes often exhibit unusually low ET rates (33, 46, 75). And, at comparable separation distances, the rates of ET in ruthenium-modified proteins are well below those of bridged organic donor-acceptor compounds (90, 118, 126). It is of interest to consider how much of this difference is due to electronic coupling factors. For example, in the complex $\text{Os(II)(dioxA)Co(III)}$, $k_{et}(\text{Os to Co})$ is $7.2 \times 10^{-5} \text{ s}^{-1}$ (33, 46). Similarly, Ru(BCO)Co has a rate of less than $3.6 \times 10^{-6} \text{ s}^{-1}$ (4). The Na(Sp)Bi compounds of Closs and Miller having a similar-sized spacer and a smaller driving force have ET rates of approximately $1 \times 10^9 \text{ s}^{-1}$ (20, 21). The Co is probably responsible for much of this effect, since reduction of Co(III) to Co(II) places an electron in a $\sigma^*(e_g)$ orbital, leading to large changes in Co-to-ligand bond lengths and hence a large reorganization energy (159). In the normal region, a larger λ for a given driving force will slow down the rate by decreasing the value of the nuclear term. The electronic coupling of Co to the bridge may be affected as well (159). Unfortunately, with the current data, it is not possible to separate the nuclear and electronic effects for these Co-containing binuclear complexes. For the related complexes, Ru(dioxA)Ru , the observed electronic coupling parameters (see Table II) are comparable to those reported for the Na(Sp)Bi compounds; hence, poor coupling to the intervening medium is not intrinsic to metals. The maximum ET rate ($\lambda = -\Delta G^\circ$) of $1.1 \times 10^{11} \text{ s}^{-1}$ for an Ir dimer linked to a series of alkylated pyridinium derivatives (edge-edge separation distance, r_e , of 5.8 \AA) is relatively large (44). The value of $H_{ab} = 21 \text{ cm}^{-1}$ calculated from the $\log(k_{et})$ vs. $-\Delta G^\circ$ plots is about one-third the value of H_{ab} (54 cm^{-1}) observed for the Na(Sp)Bi compound with $r_e = 6.4 \text{ \AA}$. The Ru(DTS)Ru complexes with $(H_{ab})_0 = 484 \text{ cm}^{-1}$ (see Table II) also couple somewhat less well to the bridge than the Na(Sp)Bi complexes. Turning to comparisons at longer donor-acceptor distances,

ET rates in ruthenium-modified horse heart cytochrome *c* (Ru-Fe-cyt *c*) indicate that $H_{ab} = 0.03 \text{ cm}^{-1}$ ($r_e = 11.7 \text{ \AA}$) (126). This value is a factor of 200 smaller than the $H_{ab} = 6.2 \text{ cm}^{-1}$ observed for Na(Ste)A ($r_e = 10.2 \text{ \AA}$ for naphthalene bridged by a steroid to a series of acceptors) (20, 21). Given that β values for proteins ($0.7\text{--}1.0 \text{ \AA}^{-1}$) (6, 118) and Na(Sp)Bi (0.95 \AA^{-1}) are about the same, the longer distance through the intervening medium for Ru-Fe-cyt *c* can only account for about a factor of 2 decrease in H_{ab} . In this analysis, then, the remaining factor of 100 is attributable to poorer donor-acceptor coupling to the intervening medium (smaller $(H_{ab})_0$). Confirmation of such a low $(H_{ab})_0$ awaits studies of the distance dependence of ET in cytochrome *c*.

An important factor in the coupling of the donor-acceptor to the intervening bridge is the orientation of the donor and the acceptor orbitals relative to the relevant bridge orbitals. Molecular orbital calculations on the Na(Sp)Bi compounds (20, 144) show that the value of H_{ab} can vary as much as a factor of 15, corresponding to a factor of 225 in rate, depending on the orientation of the donor and the acceptor relative to the bridge. Molecular mechanics calculations demonstrated that, for the equatorial-equatorial Na(Sp)Bi isomers, the lowest energy conformation corresponded to maximum H_{ab} . Calculations also indicated that the energy well was not steep enough to prevent other less favorable conformations from being sampled, thereby decreasing H_{ab} from its maximum value. Similarly, for the A(N)D and P(N)D compounds (see Fig. 6), the values of H_{ab} calculated using extended Hückel methods (65) were about a factor of 4 larger than the experimentally determined values (41). Whereas the MO calculation was carried out for the conformation giving maximum electronic interaction, in reality the donor and acceptor can readily rotate relative to the bridge, sampling many conformations with less favorable electronic coupling. Hence, the observed H_{ab} is smaller than the calculated H_{ab} . The importance of maintaining the optimum conformation for electronic coupling is evident and may be another reason for the strong electronic coupling observed for the norbornyl-bridged donor-acceptor compounds, in which the donor and the acceptor are rigidly attached to the bridge (27, 147, 149, 181-183).

Investigation of the effect of the orientation of donors and acceptors is of great importance in understanding electronic coupling. Very few ET systems exist in which the donor and acceptor are held absolutely rigidly. There are several molecules, however, in which the orientation of the donor and the acceptor is constrained within certain limits. A porphyrin-porphyrin-quinone trimer has been synthesized in which the porphyrins are held in a "flat" (1,4-phenyl linkage) or "gabled" (1,3-phenyl linkage) orientation (165, 166). Consistently faster rates are observed for ET from the

distal porphyrin to the quinone for "gabled" vs. "flat" isomers (166). Whether or not this effect is purely orientational is unclear, since the through-space distance and the number of bonds separating the distal porphyrin and the quinone are less for the "gabled" isomers than for the "flat" isomer. Two isomers of a porphyrin-porphyrin-pyromellitide trimer also have been synthesized, a side-by-side arrangement and a stacked one (27). Both photoinduced ET from the porphyrins to the pyromellitide and charge recombination back to the porphyrins are a factor of at least 100 faster for the stacked versus the side-by-side isomer. A definite orientation effect seems to be operative in this case, since the number of bonds separating donor and acceptor is the same in both isomers; however, the average through-space distance may be shorter. Compounds in which two porphyrins are held roughly parallel or perpendicular to each other by steric constraints also have been described (63, 122). To date, kinetic data are available only for the parallel isomer. Very few investigations relevant to the question of orientation effects on ET in proteins have appeared; one indicated that the relatively slow intraprotein ET rate in cytochrome *cd*₁ could result from a perpendicular heme-heme orientation (107).

Many important conclusions have been reached using inorganic and organic donor-acceptor molecules to study ET. The relative efficacy of different kinds of intervening media in coupling donors and acceptors is beginning to be evaluated, and the role of the conformation of the bridging medium is beginning to be understood. Experiments also have shown that a through-bond (superexchange) mechanism for ET may be more important than direct through-space coupling in many instances, and data from several sources have indicated that the intrinsic coupling of the donor and the acceptor to the bridging unit can be as important in controlling ET rates as the propagation of the coupling through the intervening medium.

III. ELECTRON TRANSFER BETWEEN PROTEINS AND INORGANIC COMPLEXES

Studies of interactions between ET proteins and inorganic redox agents have been extensive and have provided valuable information with respect to the relative importance of electrostatics, size, and the nature of the redox partner, and often have located redox-active protein sites. Rate saturation in these systems indicates that a precursor complex is formed and that a specifically bound complex is reacting with the metal center. Analysis generally is in terms of Eq. 9:

$$k = Kk_{\text{ct}} \quad (9)$$

where K is the equilibrium constant for formation of the precursor complex, and k_{et} is the intracomplex ET rate constant. Recent investigations of ET reactions of proteins with inorganic complexes will be reviewed in this section, in order to provide a framework for the discussions of ET in modified proteins and protein-protein complexes in Sections IV and V.

A. Cytochrome *c*

Extensive ET studies carried out on cytochrome *c* (132, 134) have demonstrated that the reactivity of the protein is dominated by the high positive charge ($\text{Fe(III)} = +7$) due to lysine residues. The charge distribution is very uneven and leads to a dipole moment of 310 D, which contributes significantly to the reactivity of cytochrome *c* at biological ionic strengths (158). In addition, the heme edge (pyrrole rings II and III) is partially exposed to solvent, and is thought to be involved in interprotein ET (92), whereas the thioether of Met-80 may increase reactivity with smaller ET reagents (180).

Further studies of ET between the protein and inorganic complexes have defined three sites for binding. Site I is positioned at the top left as pictured in Fig. 10 (17, 175), and includes residues Met-65, and Lys-89, -5, -86, -87 (92). This site is preferred by physiological protein partners (92). Site II includes Val-11, Ala-15, Thr-19, and Lys-7, -25, -27. Site III, to the left of the heme edge, may include Ile-81, Phe-82, Ala-83, and Lys-13, -72, -86; sites I and III have high affinities for anionic reactants. Cationic oxidants such as $[\text{Co}(\text{phen})_3]^{3+}$ interact mainly at site II, possibly a result of the presence of Glu-21 and fewer positively charged side chains in this region (16, 35).

Second-order rate constants have been obtained for a series of inorganic oxidants and reductants over a range of pH values where the rate = $k[\text{cyl } c][\text{complex}]$; or $k = (k_1K + k_2[\text{H}^+])/(K + [\text{H}^+])$ (5, 32, 35). Representative values are listed in Table III. A $\text{p}K_a$ value of 6.9 was calculated, indicative of His-33 protonation; the latter inhibits reaction with cationic oxidants. Interestingly, no effect of pH on rates of cytochrome *c* reduction was found. It is difficult to analyze the ET rates in terms of a straightforward driving force or distance analysis, since the binding sites are not the same for each complex (the ET distances vary) and the charges and hydrophobicities change. In comparable cases, such as $[\text{Co}(\text{phen})_3]^{3+}$ and $[\text{Co}(\text{terpy})_2]^{3+}$, the ET rate increases at higher driving force (133).

A recent study by Rush et al. (157) indicates that inorganic complexes can serve as both structural and ET probes. Oxidation of horse heart ferrocyanochrome *c* by $[\text{Co}(\text{bpy})_3]^{3+}$ and $[\text{Co}(\text{phen})_3]^{3+}$ at low ionic strengths (6–60 mM) was found to be independent of the concentration of the Co

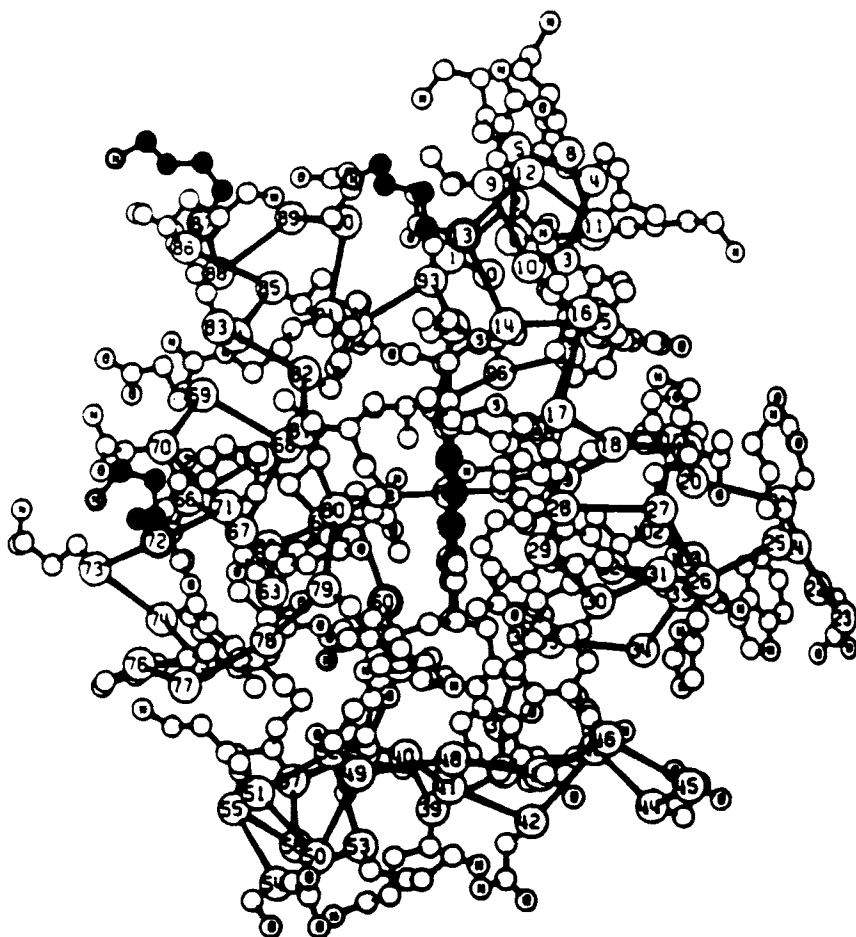


Figure 10. Front view of the structure of tuna ferricytochrome *c* (17). The larger circles are α carbon atoms; the smaller circles represent side-chain atoms.

complex, and to occur much faster than the second-order process observed at higher ionic strength (μ 0.1M, $k_1 = 1.5 \times 10^3 M^{-1}s^{-1}$). It was proposed that a conformational change of the protein occurs, leading to an open (accessible heme crevice) form that reacts much faster with certain reagents than the closed form. In support of this suggestion, $[\text{Cr}(\text{phen})_3]^{3+}$ was found by NMR to bind to the open form. The enhancement of the rate of oxidation may reflect both greater kinetic accessibility and a higher intrinsic rate constant for ET if the reorganization energy [from Fe(II) to Fe(III)]

TABLE III
Reactions of Cytochrome *c* with Inorganic Complexes

Reaction	Complex	pH	E° (mV vs. NHE)	k ($M^{-1}s^{-1}$)	References
Oxidation	[Co(phen) ₃] ³⁺	8.0	370	1.8×10^3	35
	[Co(phen) ₃] ³⁺	5.0		1.1×10^3	35
	[Co(terpy) ₂] ³⁺	8.0	270	9.2×10^2	35
	[Co(terpy) ₂] ³⁺	5.0		6.3×10^2	35
	[Fe(CN) ₆] ³⁻	5-8	410	9.0×10^5	35
	[Co(dipic) ₂] ³⁻	5-8	747	1.0×10^4	35
Reduction	[Co(terpy) ₂] ²⁺	5-8		1.0×10^3	35
	[Ru(NH ₃) ₅ py] ²⁺	5-8	253	4.1×10^3	32, 35
	[Co(sep)] ²⁺	5-8	-260	3.4×10^5	5, 35

forms] is lowered by the change in the conformation of the reduced form (157).

Electron-transfer rate constants for reactions between [Ru(NH₃)₆]²⁺ and [Ru(NH₃)₅(His)]²⁺ and Fe(III) and Zn-substituted cytochrome *c* are summarized in Table IV (36). K is estimated to be $0.4M^{-1}$ for Ru(II) and Fe(III)-cyt *c* reactions, and $K \sim 0.24M^{-1}$ for Zn-cyt *c*^{*} reactions. Electron-transfer rate constants span 10^5 – $10^8 M^{-1}s^{-1}$, probably due to the large reaction driving forces (note that the calculated rates are within a factor of 10 of the measured reaction rates) (36).

B. Blue Copper Proteins

Plastocyanin is the best characterized of the blue copper ET proteins; it is a small protein ($M_m = 10,500$ Da) containing a single type 1 copper site. The Cu(II) form exhibits a strong charge-transfer band at 600 nm. The overall charge of the plant protein at pH 7.0 is -9 . Plastocyanin is

TABLE IV
Reactions of Fe and Zn Cytochrome *c*^e

Reaction	$-\Delta G^\circ$ (eV)	k_{obsd} ($M^{-1}s^{-1}$)	E_a (kcal/mol)	k_{calcd} ($M^{-1}s^{-1}$)
[Ru(NH ₃) ₆] ²⁺ + Fe(III)-cyt <i>c</i>	0.20(1)	$6.7(1) \times 10^4$	1.5(2)	1.2×10^5
[Ru(NH ₃) ₅ (His)] ²⁺ + Fe(III)-cyt <i>c</i>	0.18(1)	$8.5(1) \times 10^4$	0.8(2)	8.4×10^4
[Ru(NH ₃) ₆] ²⁺ + Zn-cyt <i>c</i> [*]	0.84(10)	$1.5(2) \times 10^8$	3.2(4)	1.4×10^8
[Ru(NH ₃) ₅ (His)] ²⁺ + Zn-cyt <i>c</i> [*]	0.82(10)	$3.6(5) \times 10^8$		1.2×10^8
Zn-cyt <i>c</i> [*] + [Ru(NH ₃) ₆] ³⁺	0.86(10)	$1.4(1) \times 10^7$	3.3(4)	1.6×10^8
Zn-cyt <i>c</i> [*] + [Ru(NH ₃) ₅ (His)] ³⁺	0.88(10)	$2.4(3) \times 10^7$	2.4(3)	1.7×10^8

^eReference 36.

found in algae and the chloroplasts of higher plants, and its function is to transfer electrons from cytochrome *f* (360 mV) to P-700⁺ in photosystem I (176).

Extensive structural information has been obtained for plastocyanins from plants and algae (58, 81). In general, as pictured in Fig. 11 (57), the copper atom is located at one end of the protein in a hydrophobic pocket formed by loops in the peptide backbone. The higher plant plastocyanins have two histidines, His-37 and His-87, both of which coordinate to copper. Cys-84 and Met-92 serve as the other Cu ligands.

The algal plastocyanins from *Anabaena variabilis* (*A.v.*) and *Scenedesmus obliquus* (*S.o.*) possess, in addition, a single uncoordinated surface

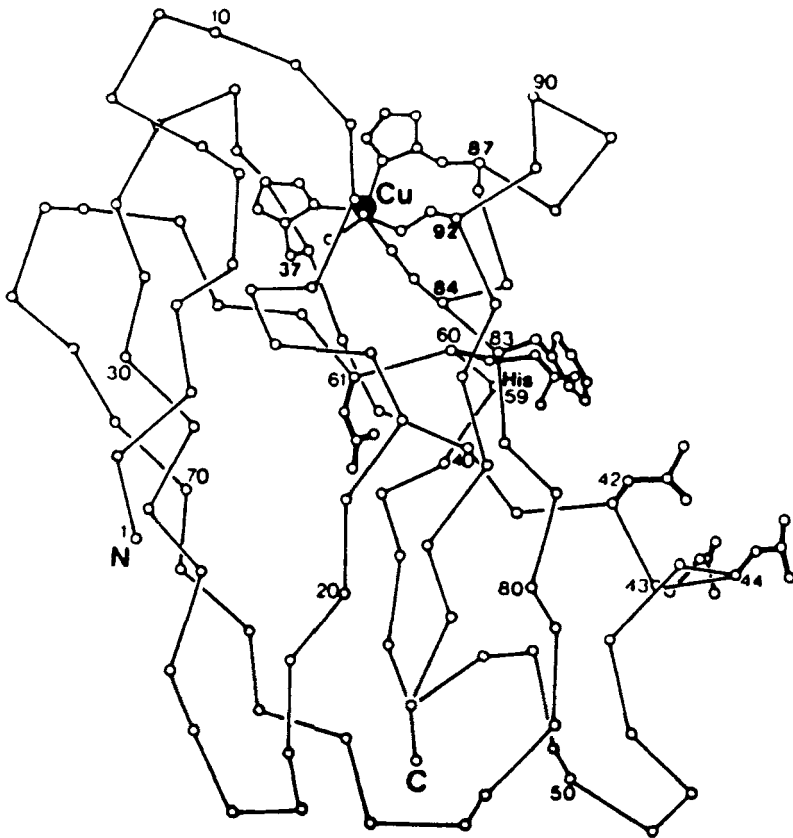


Figure 11. Structure of poplar Cu^{II}-plastocyanin showing the α -carbon framework and selected side chains (57).

histidine at position 59 (80). The *A.v.* protein has a charge of +1 [Cu(I)] at pH 7.0, and the *S.o.* protein has a charge of -9 at pH 7.0, and residues 57 and 58, proximal to His-59, are not present in the latter protein. Although residues 57 and 58 are deleted in *S.o.* (and also in parsley and *Chlorella fusca*) plastocyanin, the standard notation used is that of the poplar protein containing Met-57 and Ser-58. The His residue adjacent to Ser-56 is therefore referred to as His-59 in the *S.o.* protein.

Studies carried out on the reactions of plastocyanin with inorganic complexes have indicated that ET takes place in two regions on the surface of the protein. The first site is close to the exposed His-87 (one of the Cu ligands), allowing approach at the surface of the protein only $\sim 6 \text{ \AA}$ from the Cu atom; this region is called the "north site." The "east site" is on the right-hand side of the protein as pictured in Fig. 11, and includes the negative patch of acidic residues 42-45, close to Tyr-83. The distance between the carboxylate of Asp-42 and sulfur of Cys-84 is $\sim 14 \text{ \AA}$ (80). Another region of ET activity may be acidic residues 59-61 in higher plants; it is not known whether this is an independent binding site or somehow associated with the 42-45 region. The binding sites of several oxidants are known: Negatively charged $[\text{Fe}(\text{CN})_6]^{3-}$ binds to the His-87 site, and positively charged $[\text{Cr}(\text{phen})_3]^{3+}$, $[\text{Co}(\text{phen})_3]^{3+}$, ferricenium complexes, and cytochrome *f* bind to the east site (24, 116, 154). Second-order rate constants for the reactions of plastocyanin with $[\text{Co}(\text{phen})_3]^{3+}$ and $[\text{Fe}(\text{CN})_6]^{3-}$ are summarized in Table V (81, 120). It has been estimated that the small inorganic reagents also react 15-45% of the time at other sites (119). A pH dependence of ET activity is consistently seen with $\text{pK} \sim 5.0$ due to His-87 protonation and dissociation from copper; the resulting Cu(I) is planar and three coordinate (58).

In studies of reactions with inorganic complexes, it has been shown that small sequence differences in plastocyanins can lead to observable changes in ET rates. For example, in *S.o.* plastocyanin, a slight decrease in ET

TABLE V
Rates of Reactions of Plastocyanin with Inorganic Complexes^a

Plastocyanin	$[\text{Fe}(\text{CN})_6]^{3-}$ $k (M^{-1}s^{-1})$	$[\text{Co}(\text{phen})_3]^{3+}$ $k (M^{-1}s^{-1})$
Parsley	9.4×10^4	3.0×10^3
Spinach	8.5×10^4	2.5×10^3
French bean	5.8×10^4	4.7×10^3
Poplar	6.9×10^4	2.9×10^3
<i>Scenedesmus obliquus</i>	9.0×10^4	1.85×10^3
<i>Anabena variabilis</i>	6.5×10^5	6.8×10^2

^aFrom Refs. 81 and 120.

second-order rate constants is seen due to reduced 42–45 charge (–3 compared to –4 for plant plastocyanins), and at alkaline pH, His-59 deprotonation causes a 10% decrease in rate ($pK_a = 7.83$). The pK_a of the active-site His-87 was found to be 5.45, in general higher than active-site pK values of plant proteins, due to the deletion of residues 57 and 58, which alters the peptide chain conformation in this area. Indeed, in the parsley protein, also missing 57 and 58, the same perturbed active-site pK is seen (120).

Plastocyanin from the blue-green alga *A.v.* has an overall charge of +1 for Cu(I). Rates of reduction and oxidation by inorganic complexes are significantly affected by the overall charge (rate constants for the $[\text{Co}(\text{phen})_3]^{3+}$ and $[\text{Fe}(\text{CN})_6]^{3-}$ reactions are given in Table V). Saturation kinetics are not observed for $[\text{Co}(\text{phen})_3]^{3+}$. NMR experiments suggest two possible binding sites for $[\text{Cr}(\text{CN})_6]^{3-}$, one located near His-59, and the other near Lys-9 and 33 (81).

Excited-state ET rates have been calculated from $[\text{Cr}(\text{phen})_3]^{3+*}$ and $[\text{Ru}(\text{bpy})_3]^{2+*}$ emission quenching by plastocyanin and azurin (15). For $[\text{Ru}(\text{bpy})_3]^{2+*}$ quenching by reduced plastocyanin, $k_q = 1.9 \times 10^9 \text{ M}^{-1}\text{s}^{-1}$ at $-\Delta G^\circ = 0.48 \text{ eV}$, and for $[\text{Cr}(\text{phen})_3]^{3+*}$ quenching in this system, $k_q = 3.5 \times 10^9 \text{ M}^{-1}\text{s}^{-1}$ at $-\Delta G^\circ = 1.06 \text{ eV}$. For $[\text{Ru}(\text{bpy})_3]^{2+*}$ quenching by reduced azurin, $k_q = 6.5 \times 10^8 \text{ M}^{-1}\text{s}^{-1}$ at $-\Delta G^\circ = 0.53 \text{ eV}$, and for $[\text{Cr}(\text{phen})_3]^{3+*}$ quenching, $k_q = 4.0 \times 10^8 \text{ M}^{-1}\text{s}^{-1}$ at $-\Delta G^\circ = 1.11 \text{ eV}$. The effect of driving force on the rate constant for $[\text{CrL}_3]^{3+*}$ quenching by reduced azurin was studied using $[\text{Cr}(\text{phen})_3]^{3+*}$, with $E^\circ(\text{Cr}^{3+*}/\text{Cr}^{2+}) = 1.42 \text{ V}$, $[\text{Cr}(5\text{-Clphen})_3]^{3+*}$ with $E^\circ = 1.53 \text{ V}$, and $[\text{Cr}(4,7\text{-(CH}_3)_2\text{phen})_3]^{3+*}$, with $E^\circ = 1.23 \text{ V}$. The three quenching constants were found to be within 10% of each other.

A two-site ET mechanism (adjacent and remote sites) was used to explain the resulting kinetics. From NMR results and computer modeling, $[\text{Cr}(\text{phen})_3]^{3+}$ and $[\text{Co}(\text{phen})_3]^{3+}$ are thought to bind near Tyr-83 in plastocyanin and azurin via hydrophobic interactions. The ET distance from cysteine sulfur to phenanthroline was calculated from the data (12 Å) and was found to be in close agreement with the modeling results (10.3 Å) (15, 54).

Rhus vernicifera stellacyanin is a blue copper glycoprotein that reacts rapidly with many inorganic redox agents (37, 117, 169). In the chromous reduction of the protein (37), ET is believed to involve binding of Cr(II) to $\gamma\text{-CO}_2^-$ of Asp-49 and $\epsilon\text{-NH}_3$ of Lys-50; the Cr(II) to Cu(II) ET would then take place over a Cr–Cu distance of $\sim 11 \text{ \AA}$. Since a model of the structure of stellacyanin indicates that there are no other negative residues near Asp-49, it can be concluded that the labeling is primarily due to favorable ET reactivity at the 49–50 site (190).

C. Iron-Sulfur Proteins

The most thoroughly investigated high-potential iron-sulfur protein (HiPIP) is that isolated for *Chromatium vinosum* (a purple photosynthetic bacterium). The reduction potential of the iron-sulfur cluster is 350 mV, and the overall charge on the protein is -3 ; the Fe_4S_4 cluster is buried within the 9500-Da protein, ligated to cysteines at positions 43, 45, 63, and 77 (Fig. 12) (1, 18). Several studies have been made of the oxidation and reduction of HiPIP by inorganic complexes (40, 62, 131, 153).

Oxidation of reduced HiPIP by $[\text{Co}(\text{phen})_3]^{3+}$ (370 mV) and $[\text{Fe}(\text{CN})_6]^{3-}$ at pH 7.0 occurs with rates of 3.04×10^3 and $2.09 \times 10^3 \text{ M}^{-1}\text{s}^{-1}$ (62). Using a set of substituted ferricenium complexes (0.3–0.44 V) as oxidants,

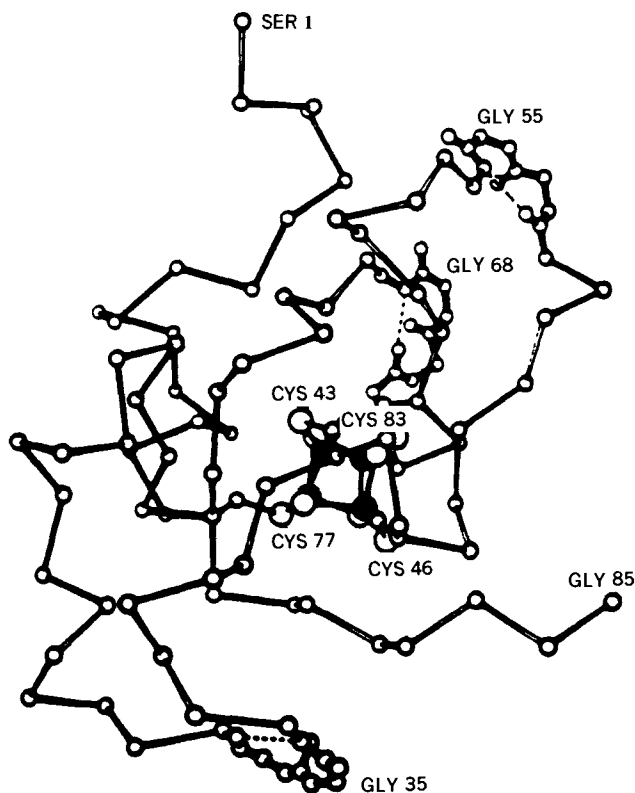


Figure 12. The HiPIP main chain, showing the position of all α -carbon atoms and the location of the cluster. The amino terminal Ser-1 is at the upper left, and the carboxyl terminal Gly-85 is at the lower right. Filled circles represent iron atoms (18).

ET rates from 0.35×10^6 to $14 \times 10^6 M^{-1}s^{-1}$ were measured, increasing with increasing driving force (153). Rate saturation was not observed for any of the oxidants, and the pH dependences of the reactions gave pK_a values of 7.0 and 6.9 in the two studies.

The pK_a is assigned to His-42, which through Cys-43 is directly attached to the Fe_4S_4 cluster. The reduction potential of HiPIP increases by 30 mV upon protonation of this residue, and the Fe-S bond lengths increase from 2.22 to 2.38 Å upon reduction (62). It is suspected that a conformational change takes place upon protonation of His-42; the protonated HiPIP_{red} is approximately one-half as reactive as the unprotonated form with the positively charged oxidants.

Rate variations for HiPIP oxidation by the above reagents are similar in many respects to those seen in the redox reactions with several other inorganic complexes (40, 62, 131). However, using $[Co(4,7-DPSphen)_3]^{3+}$ (DPSphen = 4,7-bis(phenyl-4-sulfonate)1,10-phenanthroline) as the oxidant, saturation kinetics were seen, consistent with an association constant $K(25^\circ C) = 3420 M^{-1}$, and $k_{et} = 0.02 s^{-1}$. It was demonstrated that the binding site for this complex is distinct from the binding site for $[Fe(CN)_6]^{3-}$ (2).

The surface binding locations of the inorganic oxidants and reductants are unknown. Two areas proposed for the ET reaction are (a) a hydrophobic patch at Cys-46 (bound to Fe_4S_4), near the surface residues Phe-48, Thr-81, and Ile-65, with a corresponding distance from the active site to the protein surface of ~ 4 Å, and (2) the area near His-42, where the distance from ϵN -His-42 to the sulfur of cysteine is ~ 7.9 Å (62, 153).

IV. ELECTRON TRANSFER IN MODIFIED PROTEINS

Synthetic molecular bridges provide a very simple method to study intramolecular ET between an oxidant and a reductant separated by a fixed distance. Another useful spacer (in fact the one nature prefers!) for electron donors and acceptors is a protein. In 1982, long-range ET at a known distance through a protein was achieved using cytochrome *c* as a spacer (Fig. 13) (77, 191). Attachment of a redox-active species to a specific amino acid at the surface of a structurally characterized protein has several advantages. Surface modification of a protein is expected to be nonperturbative (3, 7, 48), so it can be assumed that the structure of the modified protein is the same as that of the native protein. Hence, the distance and the intervening medium involved in ET between the native and synthetic protein redox sites are known (see Fig. 13). Altering the site of attachment allows both the distance and the intervening medium for ET to be varied.

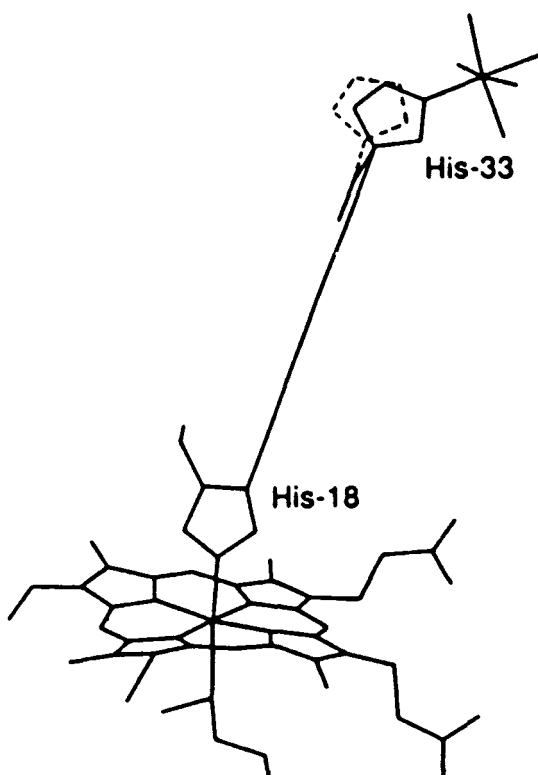


Figure 13. Schematic representation of $a_3\text{Ru}(\text{His-33})$ -modified horse heart cytochrome *c*, showing the ruthenated histidine and the heme with its axial ligands (His-18 and Met-80). The ET distance (edge-edge) is 11.7 Å (118).

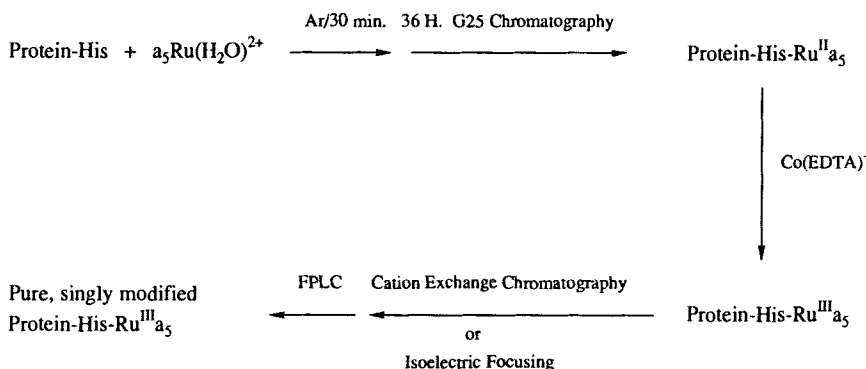
Orientation effects on ET can be examined by varying the site of attachment of the surface redox complex relative to the protein redox center, while maintaining the same site-site separation. Changing the modification reagent also permits driving-force effects on the rate of the reaction to be studied. Modified proteins thus are extremely versatile molecules for studying biologically relevant ET (13, 54, 55, 104, 105, 118, 163).

A. Modification Procedures

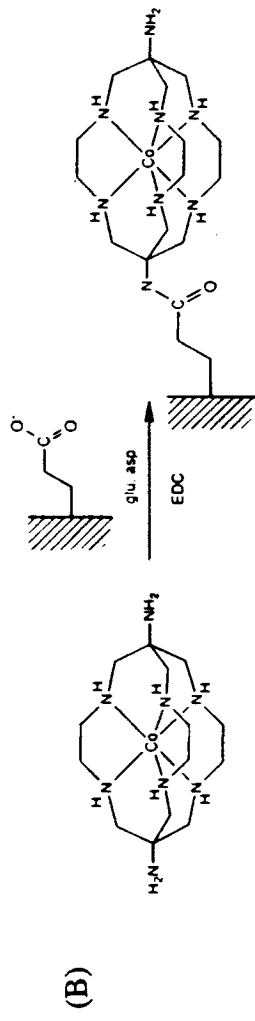
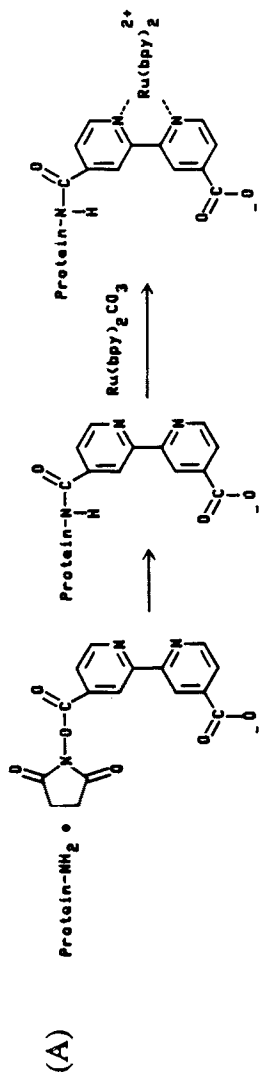
Histidine, glutamate, aspartate, and lysine side chains accessible on the protein surface have been used as sites for modification by redox-active metal species. The original modification procedure involved direct reaction

of aquopentaammineruthenium(II) (a_5Ru^{2+}) with the imidazole of a surface histidine (30, 113, 193). Reaction times vary from 30 min (30) to 24–72 h (193), depending on the accessibility of the particular histidine. The yield of the reaction also can be buffer dependent (140). Scheme I outlines the reaction and purification procedure. The a_5Ru (histidine)-modified proteins are stable in both the Ru(II) and the Ru(III) oxidation states and, although a_5Ru^{2+} slowly dissociates from surface histidines (146), the a_5Ru^{3+} complex stays attached for at least 2 months under appropriate conditions (194). One disadvantage of the ruthenium modification method is that there are relatively few surface-exposed histidines in the structurally characterized ET proteins. This limitation has recently been overcome, however, by specifically placing a histidine on the surface of yeast iso-1-cytochrome *c* using site-directed mutagenesis and modifying that histidine with a_5Ru^{2+} (14).

Surface lysine residues of horse heart cytochrome *c* have been modified through reaction with a mono-*N*-hydroxysuccinimide ester 4,4'-dicarboxy-2,2'-bipyridine followed by reaction with $[Ru(bpy)_2CO_3]$ (see Scheme IIA) (148). An advantage of this technique is that the driving force of the photoinduced Ru(II)-to-Fe(III) ET reaction can be altered readily by changing the substituents on the bipyridine rings. Surface-exposed glutamate and aspartate side chains have been reacted with $[Co(diAMsar)]^{3+}$ using 1-ethyl-3-[3-(dimethylamino)propyl]carbodiimide (EDC) to activate the carboxylate groups of glutamate or aspartate (see Scheme IIB) (23). Both techniques have the advantage that surface accessible lysines, glutamates, and aspartates are much more prevalent than histidines. Therefore, many more ET reactions can be studied for a given crystallographically characterized protein.



Scheme I. Preparation and Purification of a_5Ru (His) Modified Proteins.



Scheme II. (a) Method for the modification of surface lysines with redox-active metal complexes (148). (b) Method for the modification of surface glutamates and aspartates with a redox-active metal complex (23).

B. Characterization of Modified Proteins

After a modified protein is prepared, the site of modification must be determined rigorously. It also is necessary to ensure that the structure of the protein has not been perturbed by the modification. Several methods have been used to determine the number and position of metal atoms affixed to the protein surface. The number of metal atoms is commonly determined by atomic absorption analysis (194) or by inductively coupled plasma (ICP) atomic emission analysis (23, 146). Under favorable circumstances, the metal ratios in modified derivatives can be determined by UV/vis spectroscopy (23, 113). Another method for quantifying ruthenium attached to histidines is to compare the reactions of the native and modified proteins with diethyl pyrocarbonate (146), which is a histidine specific reagent.

Two methods have been used extensively to determine the site of modification, peptide mapping (8, 14, 23, 30, 89, 148, 164, 193, 194) and NMR spectroscopy (8, 89, 114, 146, 193). Peptide mapping typically involves cleavage of the protein with a protease, followed by high-performance liquid chromatography (HPLC) purification of the fragments. A change in mobility indicates a fragment that has a metal complex attached to it. The fragment is then identified by amino acid analysis. The presence of the metal complex is determined by UV/vis spectroscopy (8, 164, 193, 194) or fast atom bombardment mass spectrometry (FABMS) (23). The attachment of a Ru(III) complex to a histidine causes paramagnetic shifting and broadening of the C-2 and C-4 protons in the ^1H NMR spectrum of a protein. The paramagnetism results in loss of these histidine protons from the aromatic chemical-shift region and their reappearance upfield of TMS (89, 164). For proteins containing multiple surface histidines, however, such as myoglobin (89) and *Candida krusei* cytochrome *c* (164), ambiguities can remain in the assignment of which histidine is modified, based solely on the NMR spectrum.

A variety of physical methods has been used to ascertain whether or not surface ruthenation alters the structure of a protein. UV/vis, CD, EPR, and resonance Raman spectroscopies have demonstrated that myoglobin (30, 89), cytochrome *c* (74, 164, 193, 194), and azurin (113) are not perturbed structurally by the attachment of a ruthenium complex to a surface histidine. The reduction potential of the metal redox center of a protein and its temperature dependence are indicators of protein structure as well. Cyclic voltammetry (113, 193), differential pulse polarography (30, 31, 140), and spectroelectrochemistry (30, 31, 194) are commonly used for the determination of the ruthenium and protein redox center potentials in modified proteins. The reduction potential and thermodynamic parameters

for reduction of the protein redox center in both the native and the modified protein tend to be similar (E° within 12 mV), indicating no significant structural perturbation near the protein redox site upon ruthenation (113, 140, 193, 194). Much more variation in the reduction potential of the $a_5\text{Ru}(\text{histidine})$ complex is seen, which may be due to local protein-environment effects on the redox properties of ruthenium (see Table VI).

High-resolution structural data for modified proteins can be obtained from NMR and X-ray crystallographic studies. Extensive NMR studies of $[\text{a}_5\text{Ru}]_3\text{myoglobin}$ (179) and *Chromatium gracile* high-potential iron-protein ruthenated at either His-20 or His-42 (170) demonstrate at most only slight chemical-shift changes. The X-ray crystal structure of $a_5\text{Ru}(\text{His-48})\text{Mb}$ also has been determined; it is virtually identical with that of the native protein (136). These observations confirm that surface ruthenation does not significantly alter the conformation of a protein.

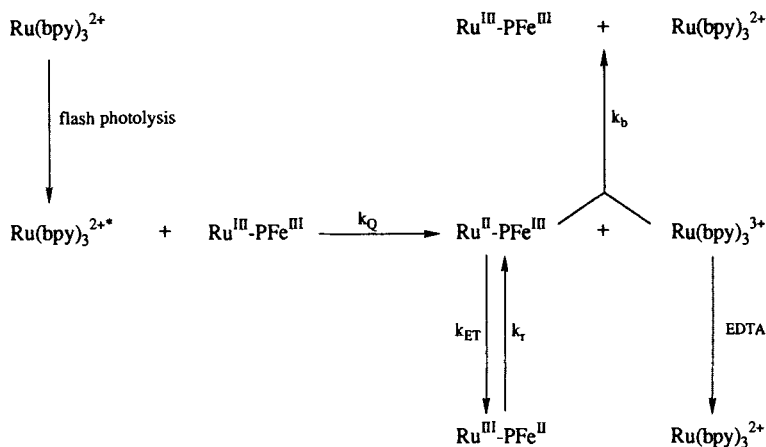
C. Kinetic Methods

As with donor-acceptor model complexes, ET reactions in proteins have been induced by photoexcitation and pulse radiolysis. In pulse radiolysis experiments, it has been found that the ratio of reduction of the surface metal center to the internal protein redox center can be manipulated, depending on the choice of the mediator. With $a_5\text{Ru}^{\text{III}}(\text{His-33})\text{Fe}^{\text{III}}\text{cytochrome } c$, reduction of the Ru(III) site was 35% efficient with isopropanol as mediator and 95% efficient with pentaerythritol as mediator (74).

Two flash photolysis techniques have been developed to study ground-state ET in modified proteins. A method that allows study of ET from a surface $a_5\text{Ru}(\text{III})(\text{histidine})$ to a protein redox center is outlined in Scheme

TABLE VI
 $a_5\text{Ru}(\text{histidine})$ Reduction Potentials

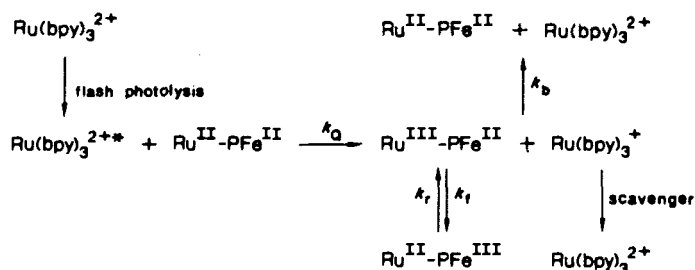
Complex	$E^\circ(\text{Ru}^{3+,2+})$ (mV vs. NHE)	References
$a_5\text{Ru}(\text{histidine})$	106	194
$a_5\text{Ru}(\text{imidazole})$	105	194
$a_5\text{Ru}(\text{His-33})\text{Cyt } c$	80(5)	140
$a_5\text{Ru}(\text{His-39})\text{Cyt } c$	120(5)	164
$a_5\text{Ru}(\text{His-83})\text{Az}$	50	113
$a_5\text{Ru}(\text{His-48})\text{Mb}$	86(2)	30
$a_5\text{Ru}(\text{His-81})\text{Mb}$	61	28
$a_5\text{Ru}(\text{His-116})\text{Mb}$	70	28
$a_5\text{Ru}(\text{His-12})\text{Mb}$	75	28



Scheme III. Method for studying $\text{Ru}^{\text{II}} \rightarrow \text{Fe}^{\text{III}}$ electron transfer in ruthenium-modified heme proteins.

III (140). The ET reaction is initiated by photogenerated $[\text{Ru}(\text{bpy})_3]^{2+*}$, which rapidly reduces the surface ruthenium. The $[\text{Ru}(\text{bpy})_3]^{3+}$ is then scavenged by EDTA before it can back react with $a_5\text{Ru}(\text{II})(\text{histidine})$. Electron transfer to the protein metal center is then monitored spectroscopically. In the case of a heme (FeP), a fast increase in absorbance because of direct reduction of $\text{Fe}(\text{III})\text{P}$ by $[\text{Ru}(\text{bpy})_3]^{2+*}$ is followed by a slower increase in absorbance due to reduction of $\text{Fe}(\text{III})\text{P}$ by the $\text{Ru}(\text{II})$ on the protein surface. Control flash experiments with unmodified proteins show only the fast initial increase in absorbance resulting from $\text{Fe}(\text{III})\text{P}$ reduction by $[\text{Ru}(\text{bpy})_3]^{2+*}$. Such control experiments demonstrate for horse heart cytochrome *c* (140), azurin (93), and sperm whale myoglobin (30) that slow reduction of the heme by the EDTA radical produced in the scavenging step does not occur in competition with intramolecular ET. For *C. krusei* cytochrome *c*, however, the control experiment shows evidence for slow EDTA radical reduction of the heme after initial fast reduction by $[\text{Ru}(\text{bpy})_3]^{2+*}$ (164).

A method for the study of ET from a protein metal center to a surface ruthenium is given in Scheme IV (103). In this method, $[\text{Ru}(\text{bpy})_3]^{2+*}$ acts as an oxidant, selectively removing an electron from a surface $a_5\text{Ru}(\text{II})(\text{histidine})$. A Ni-RBr scavenger system $[\text{Ni}(\text{II})\text{hexamethyltetraazacyclododecane}$ and an alkyl bromide] oxidizes the $[\text{Ru}(\text{bpy})_3]^+$ before it can back react with the $a_5\text{Ru}(\text{III})(\text{histidine})$ complex. Electron transfer from the reduced protein metal center to the oxidized ruthenium can be monitored spectroscopically.



Scheme IV. Method for studying $\text{Fe}^{\text{II}} \rightarrow \text{Ru}^{\text{III}}$ electron transfer in ruthenium-modified heme proteins (103).

D. Modified Heme Proteins

The first studies of ground-state ET in modified proteins gave ET rates of $0.02\text{--}53 \text{ s}^{-1}$ for ET distances of $11.7\text{--}12.7 \text{ \AA}$ (see Table VII). The activation enthalpy for cytochrome *c* is lower than that for myoglobin. Equation 10 (111) was used to evaluate the reorganization enthalpy due to the heme center in each of these proteins. In Eq. 10, ΔH_{12}^* is the reorganization enthalpy for

$$\Delta H_{12}^* = (\Delta H_{11}^* + \Delta H_{22}^* + \Delta H_{12}^{\circ})/2 \quad (10)$$

the intramolecular ET reaction, ΔH_{11}^* and ΔH_{22}^* are the reorganization enthalpies of the $\text{Ru}^{3+,2+}$ and $\text{FeP}^{3+,2+}$ self-exchange reactions, respectively, and ΔH_{12}° is the standard enthalpy of the intramolecular ET reaction. The reorganization enthalpy for the $[\text{a}_5(\text{Rupy})]^{3+,2+}$ self-exchange ($6.9 \text{ kcal} \cdot \text{mol}^{-1}$) along with measured values of ΔH_{11}^* and ΔH_{12}° were used to calculate ΔH_{22}^* values for cytochrome *c* ($7\text{--}8 \text{ kcal} \cdot \text{mol}^{-1}$) (140) and myoglobin ($20 \text{ kcal} \cdot \text{mol}^{-1}$) (30, 31). The larger ΔH_{22}^* for myoglobin

TABLE VII
ET Reactions of Modified Proteins

Reaction	$-\Delta G^{\circ}$ (ev)	k_{et} (s^{-1})	ΔH^* (kcal/mol)	ΔS^* (eu)	References
$\text{Ru}^{\text{II}}(\text{His-33})\text{Fe}^{\text{III}}\text{Cyt } c \rightarrow$	0.180	$30 \pm 3, 53 \pm 2$	$1.1 \pm 0.4,$	$-48 \pm 2,$	74, 140
$\text{Ru}^{\text{III}}(\text{His-33})\text{Fe}^{\text{II}}\text{Cyt } c$			3.5 ± 0.2	-39 ± 1	
$\text{Ru}^{\text{II}}(\text{His-48})\text{Fe}^{\text{III}}\text{Mb} \rightarrow$					
$\text{Ru}^{\text{III}}(\text{His-48})\text{Fe}^{\text{II}}\text{Mb}$	-0.02	0.019 ± 0.0025	7.4		30, 31
$\text{Ru}^{\text{III}}(\text{His-48})\text{Fe}^{\text{II}}\text{Mb} \rightarrow$					
$\text{Ru}^{\text{II}}(\text{His-48})\text{Fe}^{\text{III}}\text{Mb}$	0.02	0.041 ± 0.003	19.5		30, 31

was attributed to the loss of the axially ligated water upon reduction of the heme, whereas both axial ligands are retained upon reduction of cytochrome *c*. The ΔH_{12}^* values for photoinduced ET from $^3\text{ZnP}^*$ (6) and $^3\text{MgP}^*$ (25) to $a_5\text{Ru}(\text{His-48})^{3+}$ are 1.7 and 2.2 kcal · mol⁻¹, respectively. The reorganization enthalpy ΔH_{22}^* is smaller for these myoglobin reactions, in accord with less rearrangement of the water structure in the porphyrin region.

1. Distance Dependence

The distance dependence of ET in proteins has been studied in ruthenated sperm whale myoglobin, where there are four surface histidines at different edge-edge distances from the metal porphyrin (see Table VIII and Fig. 14). The driving force (0.02 eV) for ET from the Fe(II)heme to $a_5\text{Ru}(\text{III})(\text{histidine})$ is too small to allow observable ET rates for the three long distance histidines (His-81, His-116, His-12). To increase the driving force for the ET reaction, the iron porphyrin was replaced by zinc mesoporphyrin IX diacid (ZnP) (6) and magnesium mesoporphyrin IX diacid and diester (MgP and MgP_{de}, respectively) (25, 26, 28). Photoinduced ET

TABLE VIII
Photoinduced ET in $a_5\text{Ru}^{\text{III}}(\text{His})(\text{MP})\text{Mb}$

Reaction	r_c (Å)	k_{et} (s ⁻¹)	ΔH^* (kcal/mol)	ΔS^* (eu)	References
$^3\text{ZnP}^* \rightarrow$					
$a_5\text{Ru}^{\text{III}}(\text{His-48})$	12.7	$70 \pm 8 \times 10^3$	1.7 ± 1.6		6
$a_5\text{Ru}^{\text{III}}(\text{His-81})$	19.3	86 ± 12	5.6 ± 2.5		6
$a_5\text{Ru}^{\text{III}}(\text{His-116})$	20.1	89 ± 3	5.4 ± 0.4		6
$a_5\text{Ru}^{\text{III}}(\text{His-12})$	22.0	101 ± 11	4.7 ± 0.9		6
$^3\text{MgP}^*(\text{diacid}) \rightarrow$					
$a_5\text{Ru}^{\text{III}}(\text{His-48})$	12.7	$57 \pm 4 \times 10^3$	2.2 ± 0.3	-11 ± 7	26, 28
$a_5\text{Ru}^{\text{III}}(\text{His-81})$	19.3	82 ± 12	5.8 ± 0.5	1 ± 6	26, 28
$a_5\text{Ru}^{\text{III}}(\text{His-116})$	20.1	69 ± 3	5.2 ± 0.5	3 ± 7	26, 28
$a_5\text{Ru}^{\text{III}}(\text{His-12})$	22.0	67 ± 11	5.2 ± 0.5	-1 ± 6	26, 28
$^3\text{MgP}^*(\text{diester}) \rightarrow$					
$a_5\text{Ru}^{\text{III}}(\text{His-48})$	12.7	$32 \pm 5 \times 10^3$			26, 28
$a_5\text{Ru}^{\text{III}}(\text{His-81})$	19.3	48 ± 1			26, 28
$a_5\text{Ru}^{\text{III}}(\text{His-116})$	20.1	49 ± 8			26, 28
$a_5\text{Ru}^{\text{III}}(\text{His-12})$	22.0	39 ± 9			26, 28

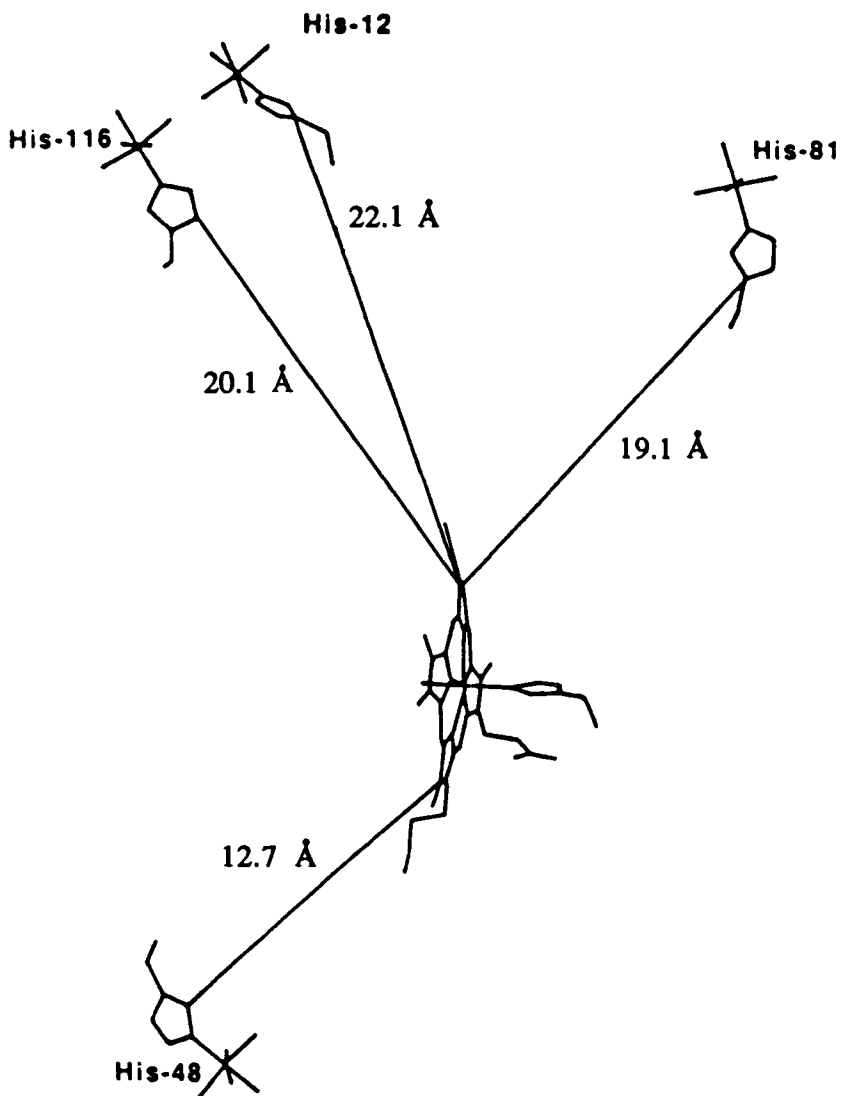


Figure 14. Schematic representation of sperm whale myoglobin showing the ruthenated histidines 12, 48, 81, and 116, and the heme with its axial histidine. The edge-edge ET distances are shown for each histidine (118).

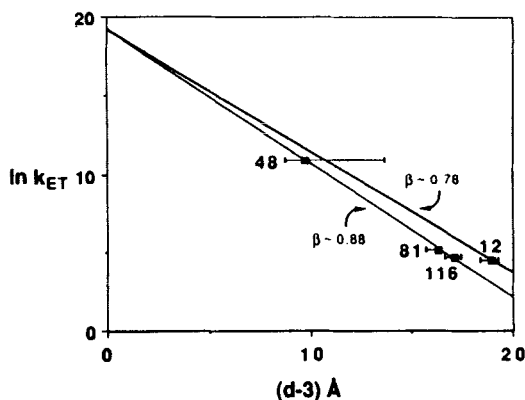


Figure 15. $\ln k_{ET}$ vs. distance plot for sperm whale myoglobin, showing that the ET rate for His-12 scales with a β of 0.78 \AA^{-1} compared to the value of 0.88 \AA^{-1} for the ET rates of His-81 and His-116. Data are for ET from the excited triplet of Mg-mesoporphyrin to $a_5\text{Ru}(\text{His})^{3+}$ (28).

was then observed from $^3\text{MP}^*$ to the $a_5\text{Ru}(\text{III})(\text{histidine})$ on the protein surface. The driving force for this ET reaction is approximately 0.8 eV (slightly less for the mesoporphyrin IX diester) (28, 36). In Table VIII, it can be seen that the ET rates scale with edge-edge distance, r_e , and a plot of $\log(k_{et})$ vs. distance (Fig. 15) gives β values in the $0.8\text{--}0.9\text{-\AA}^{-1}$ range for all three metal-porphyrin systems (25, 28). Corrected ET rates (for ΔG° differences) for $a_5\text{Ru}(\text{His-33})$ cytochrome *c* and porphyrin-substituted hemoglobin (see below) fall near the lines in Fig. 15. It also has been found that luminescence quenching rates (probably ET rates) for $[\text{Ru}(\text{bpy})_3]^{2+*}$ attached to surface lysines in horse heart cytochrome *c* scale roughly with r_e (148).

One notable observation is that the ET rate to $a_5\text{Ru}(\text{His-12})$ is higher than expected based on its edge-edge distance to the metal porphyrin (see Fig. 15 and Table VIII). Since Trp-14 lies directly on the through-space ET pathway (6, 25, 28) between His-12 and the porphyrin, it may play a role in enhancing the ET rate. One possibility is that β is approximately 0.1 \AA^{-1} less for His-12 than for the other myoglobin pathways (Fig. 15) (28). Unusual ET rate enhancement effects of aromatic amino acids also have been observed in protein-protein complexes (see Section V). Theoretical treatments of protein ET have indicated no special advantage for ET pathways through aromatic groups, however (95). Recently, ET from $a_5\text{Ru}(\text{II})(\text{His-62})$ to Fe(III) in a yeast iso-1-cytochrome *c* mutant, produced by site-directed mutagenesis methods, showed no apparent rate enhance-

ment despite having the polarizable Trp-59 and Met-64 side chains in the ET pathway (14). It remains to be seen whether aromatic amino acid residues play a special role in conducting electrons through a protein medium.

Not all data in the literature are consistent with ET rates scaling with r_c . Cytochrome c_{551} has been ruthenated at His-47; the Ru(II)-to-Fe(III) ET rate is 13 s^{-1} for $r_c = 7.9 \text{ \AA}$. The driving force for ET is the same as for horse heart cytochrome c modified at His-33, and yet ET is slower (13 vs. 30 s^{-1}) for an r_c that is 3.8 \AA shorter (146). Several other unusually slow rates for short edge-edge separation distances have been observed for ruthenium-modified blue copper and iron-sulfur proteins (see below).

A theory has been developed that suggests that ET in proteins is regulated by pathways that are optimal combinations of through-bond, hydrogen-bond, and through-space links (10, 11, 28). In this model, the molecular orbitals of the protein matrix mediate ET by a superexchange mechanism analogous to that proposed for donor-acceptor model compounds (see above). A computerized procedure (12) was employed to search for such pathways (see Fig. 16), and the ET data for His-33 of horse heart cytochrome c and His-62 of yeast iso-1-cytochrome c were found to

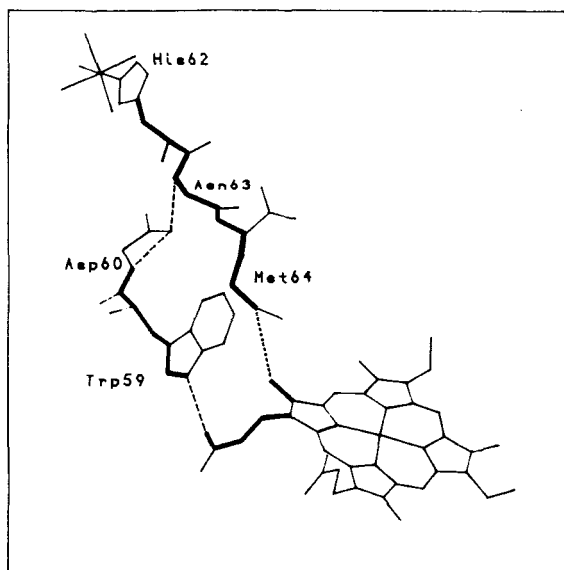


Figure 16. Diagram showing two pathways (10, 11, 28) for ET from ruthenated His-62 to the heme in a His-62 mutant yeast iso-1-cytochrome c (14).

be consistent with the pathway model, although a dependence of electronic coupling on r_e also fits the data (14). Pathways generated for the four ruthenated histidines of myoglobin fit the experimental data fairly well, but there are some significant discrepancies (10, 28). Significantly, a calculation of H_{ab} based on the His-48 pathway predicted by the model is in reasonable agreement with the experimentally measured value (10, 28). Electron transfer rate data for a ruthenated Fe-S protein, however, do not support the pathway model (see below).

Neither the pathway model nor the edge-edge correlation of electronic coupling can explain all the ET rate data. Issues such as the role of aromatic groups in long-range coupling must be clarified before the data can be understood properly using either model. It also is likely that ET rate data from different proteins may not be directly comparable using either the pathway model or an r_e dependence, since the intrinsic donor-acceptor coupling between ruthenium and a protein redox center may vary from one protein to another.

2. Driving-Force Dependence

It is common to write an activationless ET rate as a product of a nuclear frequency factor, ν_n ($\sim 10^{13} \text{ s}^{-1}$), and an electronic factor κ_e :

$$\nu_n \kappa_e = (\pi/h^2 \lambda k_B T)^{1/2} [H_{ab}]^2 \quad (11)$$

In this framework, the full expression for the ET rate at any ΔG° is

$$k_{et} = \nu_n \kappa_e \exp[-(\Delta G^\circ + \lambda)^2/4\lambda k_B T] \quad (12)$$

$$\kappa_e = \kappa_e^0 \exp[-\beta(r_e - 3)] \quad (13)$$

In Eq. 13, κ_e^0 is the value of κ_e when the donor and acceptor are in close contact ($r_e = 3 \text{ \AA}$).

Two methods for varying the ET driving force in proteins are commonly used. One way is to vary the reduction potential at ruthenium by replacing an ammine ligand with a substituted pyridine (see Table IX) (126) and the other is to vary the energy of the $^3\text{MP}^*$ state by varying the metal (see Table X) (28). Some difficulty has been encountered in evaluating $E(\text{MP}^+ / ^3\text{MP}^*)$. A self-consistent method of determining $E(\text{MP}^+ / ^3\text{MP}^*)$ has been developed, however, so that reliable ΔG° values for photoinduced ET in proteins are now available (26).

Driving-force studies have been carried out for both His-33-modified horse heart cytochrome *c* (36, 126) and His-48-modified sperm whale myoglobin (28, 90). In early work, relatively high values for λ were obtained,

TABLE IX
Electron-Transfer Data for $a_4(L)Ru^{III}(\text{His-33})(\text{MP})\text{Cytochrome } c^a$

Reaction	$-\Delta G^\circ$ (eV)	k_{et} (s^{-1})	λ (eV)	$\nu_n \kappa_c$ (s^{-1})	H_{ab} (cm^{-1})
<i>Charge Separation</i>					
${}^3ZnP^* \rightarrow a_5Ru^{III}$	0.7	7.7×10^5			
${}^3ZnP^* \rightarrow a_4(\text{py})Ru^{III}$	0.97	3.3×10^6	1.15	3.9×10^6	0.13
${}^3ZnP^* \rightarrow a_4(\text{isn})Ru^{III}$	1.05	2.9×10^6			
<i>Charge Recombination</i>					
$a_4(\text{isn})Ru^{III} \rightarrow ZnP^{+\cdot}$	0.66	2.0×10^5			
$a_4(\text{py})Ru^{III} \rightarrow ZnP^{+\cdot}$	0.74	3.5×10^5	1.24	2.5×10^6	0.10
$a_5Ru^{II} \rightarrow ZnP^{+\cdot}$	1.01	1.6×10^6			
<i>Ru/Fe ET</i>					
$a_5Ru^{II} \rightarrow Fe^{III}P$	0.18	3.0×10^1	1.20	2.0×10^5	0.03

^aFrom Ref. 126.

consistent with data from porphyrin-substituted hemoglobin (see Section V). In driving-force studies with horse heart cytochrome *c*, fits of $\log(k_{et})$ vs. $-\Delta G^\circ$ to Eq. 12, in which $\nu_n \kappa_c^0 = 10^{13} s^{-1}$ was assumed, gave either $\beta = 1.8 \text{ \AA}^{-1}$ for $\lambda = 1.2 \text{ eV}$ or $\lambda = 1.85 \text{ eV}$ for $\beta = 1.2 \text{ \AA}^{-1}$ (36). Reasonable values for λ or β gave unreasonable values for the other parameter. Similar evaluation of driving-force data for myoglobin, setting

TABLE X
Electron-Transfer Data for $a_5Ru^{III}(\text{His-48})\text{Mb}({}^3\text{MP}^*)^a$

Mb(${}^3\text{MP}^*$)	$-\Delta G^\circ$ (eV)	k_{et} (s^{-1})
ZnMb	0.88	$7.0 \pm 1.0 \times 10^4$
MgMb	0.87	$5.7 \pm 0.4 \times 10^4$
CdMb	0.85	$6.3 \pm 0.5 \times 10^4$
PtMb	0.73	$1.2 \pm 0.1 \times 10^4$
PdMb	0.70	$0.91 \pm 0.1 \times 10^4$
H ₂ Mb	0.53	$0.076 \pm 0.006 \times 10^4$
FeMb ^b	0.02	$4.1 \pm 0.3 \times 10^{-2}$

^aFrom Ref. 28.

^bGround-state ET ($Fe^{II} \rightarrow Ru^{III}$).

$\nu_n \kappa_c^0 = 10^{11} - 10^{13} \text{ s}^{-1}$ and $\beta = 0.91 \text{ \AA}^{-1}$, gave $\lambda = 1.9 - 2.45 \text{ eV}$ (90). Both these studies used high values for $\nu_n \kappa_c^0$, which assumes good donor-acceptor coupling at close contact.

In more recent work, $\nu_n \kappa_c^0$ has been varied freely so as to achieve the best fit of Eq. 12 to the $\log(k_{ct})$ vs. $-\Delta G^\circ$ data. With use of a series of metalloporphyrins substituted into myoglobin, a driving-force study for photoinduced ET [${}^3\text{MP}^* \rightarrow a_5\text{Ru(III)(His-48)}$] was accomplished (Table IX) (28). A plot of $\log(k_{ct})$ vs. $-\Delta G^\circ$ gave $\lambda = 1.3 \pm 0.3 \text{ eV}$ and $\nu_n \kappa_c^0 = 10^7 - 10^9 \text{ s}^{-1}$. Extrapolation of $H_{ab} = 0.006 \text{ cm}^{-1}$ ($r_e = 12.7 \text{ \AA}$) between $a_5\text{Ru(His-48)}$ and the metalloporphyrin gave $H_{ab}(r_e = 3 \text{ \AA}) = 0.3 \text{ cm}^{-1}$ (28), indicative of a highly nonadiabatic ET reaction at close contact. For horse heart cytochrome *c*, an extensive driving-force study using both photoinduced ET and CR reactions has been completed (Table X) (126). It was found that the plots of $\log(k_{ct})$ vs. $-\Delta G^\circ$ for photoinduced ET, CR, and Ru(II)-to-Fe(III) electron transfer were best fit separately to Eq. 12. The values of λ range from 1.15 to 1.25 eV (Table X and Fig. 17), slightly smaller than λ for myoglobin. The H_{ab} values derived from $\nu_n \kappa_c$ (Eq. 11) are 0.03–0.13 cm^{-1} . If $\beta = 0.9 \text{ \AA}^{-1}$ is assumed, then extrapolation to close contact gives $H_{ab}(r_e = 3 \text{ \AA}) = 1.5 - 6.5 \text{ cm}^{-1}$. Thus, ET from His-33 of horse heart cytochrome *c* also would be nonadiabatic at close contact; however, the electronic coupling is much better for ET between His-33 and ZnP/FeP in cytochrome *c* than from ${}^3\text{MP}^*$ to His-48 in myoglobin. These studies demonstrate that λ values in protein systems are comparable to λ values (0.9–1.25 eV) in the donor-acceptor model complexes discussed earlier. The electronic coupling estimated for close contact, however, is dramatically smaller than the range (314–1900 cm^{-1}) extracted from data

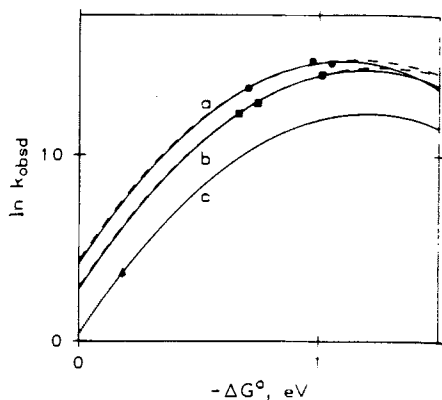


Figure 17. $\ln k_{ct}$ vs. $-\Delta G^\circ$ plots for ET in $a_4\text{LRu(His-33)}^{3+ \cdot 2+}$ horse heart cytochrome *c* ($L = \text{NH}_3$, pyridine, or isonicotinamide). The different plots are for the reactions (a) $\text{ZnP}^* \rightarrow \text{Ru}^{\text{II}}$, (b) $\text{Ru}^{\text{II}} \rightarrow \text{ZnP}^{+ \cdot}$, and (c) $\text{Ru}^{\text{II}} \rightarrow \text{Fe}^{\text{III}}$. See Table IX for the rate data (126).

obtained for the model compounds (Tables I and II). The intrinsic (close contact) electronic coupling also varies significantly from protein to protein.

3. Reversibility of Electron Transfer

Isied and co-workers (9) have reported that ET from $a_5\text{Ru(II)(His-33)}$ to Fe(III)P in cytochrome *c* exhibits a rate of 53 s^{-1} ($-\Delta G^\circ = 0.11 \text{ eV}$), but ET from Fe(II)P to $a_4(\text{isn})\text{Ru(III)(His-33)}$ ($-\Delta G^\circ = 0.18 \text{ eV}$) was not observed, despite the larger driving force. The authors proposed that ET into the oxidized heme was more facile than ET out of the reduced heme. This apparently directional ET in cytochrome *c* was attributed to a conformational change in the protein upon heme reduction. Interestingly, ET between $\text{FeP}^{3+,2+}$ and $a_5\text{Ru(His-48)}^{3+,2+}$ in myoglobin has been shown to be reversible ($-\Delta G^\circ = 0.02 \text{ eV}$) (103), and ET from Fe(II)P to $a_4\text{pyRu(III)(His-48)}$ in myoglobin ($-\Delta G^\circ = 0.24 \text{ eV}$) also occurs (103).

Conformational changes could control ET reactions in proteins. The rates of such changes often are in the same range as ET rates; for example, the T-R transition in hemoglobin occurs at a rate of approximately $2 \times 10^4 \text{ s}^{-1}$ (112). Hoffman and Ratner (66,67) have pointed out that a way to test for conformational control of an ET reaction is to measure the reaction rate at different driving forces. If the rate stays the same, the ET reaction is conformationally controlled. If it does not, it is not conformationally controlled. No evidence for conformation control exists for ET in ruthenium-modified proteins on this basis. Data from both ruthenated His-33 in horse heart cytochrome *c* (126) and ruthenated His-48 in myoglobin (103) show that the rate changes with ΔG° in a manner consistent with Marcus theory.

E. Modified Blue Copper Proteins

A comparative study of intramolecular long-range ET from ruthenium complexes bound to the protein surface to copper in *S.o.* and *A.v.* plastocyanins has been performed (80, 82). The two proteins were modified with $a_5\text{Ru}^{3+}$ at the exposed His-59, as pictured in Fig. 18.

Reduction of $\text{PCu}^{\text{II}}\text{Ru}^{\text{III}}$ was monitored at 597 nm. By using pulse radiolysis generation of CO_2^- to reduce $\text{PCu}^{\text{II}}\text{Ru}^{\text{III}}$, the reduction ($k = 6.7 \times 10^8 \text{ M}^{-1} \text{ s}^{-1}$) partitioned between Cu^{II} (72%) and Ru^{III} (28%), yielding the stable $\text{PCu}^{\text{I}}\text{Ru}^{\text{III}}$ and transient $\text{PCu}^{\text{II}}\text{Ru}^{\text{II}}$. The transient species then decayed both by intra- and intermolecular reactions (k_1 , k_2) to $\text{PCu}^{\text{I}}\text{Ru}^{\text{III}}$: k_1 was found to be $<0.08 \text{ s}^{-1}$ for *A.v.* plastocyanin, and $<0.26 \text{ s}^{-1}$ for *S.o.* plastocyanin (80).

The rates of ET in these proteins are anomalously low with respect to

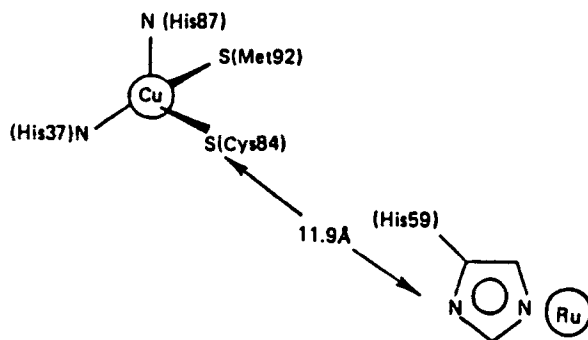


Figure 18. View of the ET donor and acceptor centers in ruthenium-modified *Anabena variabilis* plastocyanin (80).

the other proteins investigated so far (see Table XI). These results indicate that, in this weakly coupled system, the effect of the intervening medium on long-range ET is significant. The inner-sphere reorganization energy for blue copper proteins should be small, since the geometry at the copper site is intermediate between Cu(I) and Cu(II) (54, 56). The outer-sphere reorganization energy is expected to be small as well, since the Cu site is buried (and no solvent molecules are proximal to the metal). In addition, the ruthenium-labeled histidine is thought to be similar in structure to that of the modified histidines in other proteins.

The intervening medium between donor and acceptor therefore may be the most influential factor in ET rate determination. One favorable route for ET in plastocyanin has been found from Tyr-83/Asp-42 to Cu(I), with a 14 Å edge-edge separation; the ET rate in the $[\text{Co}(\text{phen})_3]^{3+}$ -plastocyanin precursor complex was found to be 26 s^{-1} (the driving force, however, is only 20 mV) (80). Importantly, reaction of $[\text{a}_3\text{RuIm}]^{2+}$ with the *A. v.* and *S. o.* proteins results in $k_{\text{et}} > 5 \times 10^3 \text{ s}^{-1}$ (80). Clearly, a_3Ru^{3+} -His-59 is not at an optimal site for ET.

TABLE XI
Electron-Transfer Rates in Ruthenated Proteins

Protein	ET	r_c (Å)	$-\Delta G^\circ$ (eV)	k_{et} (s^{-1})	References
Cytochrome <i>c</i> (horse heart)	$\text{Ru}^{\text{II}} \rightarrow \text{Fe}^{\text{III}}$	11.7	0.18	30	126
Azurin (<i>P. a.</i>)	$\text{Ru}^{\text{II}} \rightarrow \text{Cu}^{\text{II}}$	11.8	0.24	1.9 ± 0.4	93
Azurin (<i>P. a.</i>)	$\text{Ru}^{\text{II}} \rightarrow \text{Cu}^{\text{II}}$	11.8	0.24	2.5 ± 0.8	80
Myoglobin (sperm whale)	$\text{Ru}^{\text{II}} \rightarrow \text{Fe}^{\text{III}}$	12.7	-0.02	0.02	28, 103
Plastocyanin (<i>A. v.</i>)	$\text{Ru}^{\text{II}} \rightarrow \text{Cu}^{\text{II}}$	11.9	0.26	< 0.08	80
Plastocyanin (<i>S. o.</i>)	$\text{Ru}^{\text{II}} \rightarrow \text{Cu}^{\text{II}}$	10-12	0.29	< 0.26	80

Pseudomonas aeruginosa (*P.a.*) azurin has been ruthenated at His-83 ($r_e \sim 11.8 \text{ \AA}$) (54, 93, 113); the donor-acceptor separation is pictured in Fig. 19. Production of $a_5\text{Ru}(\text{His-83})^{2+}\text{-Az}(\text{Cu}^{2+})$ was achieved by flash photolysis in the presence of $[\text{Ru}(\text{bpy})_3]^{2+}$. The reduction of the protein was monitored at 625 nm, and the intramolecular Ru(II)-to-Cu(II) ET rate of 1.9 s^{-1} was found to be independent of temperature. The Cu reorganization enthalpy was estimated to be $<7 \text{ kcal} \cdot \text{mol}^{-1}$ (93, 113), a value confirming that blue copper is structured for efficient ET. Table XI compares ET rates for the blue copper proteins with those for heme proteins; the blue copper rates are low in comparison with the heme protein rates over similar distances and driving forces. This effect could be a result of poor electronic coupling of $a_5\text{Ru}$ with the copper center, possibly owing to unfavorable ET pathways.

Rhus vernicifera stellacyanin has been labeled with $a_5\text{Ru}^{3+}$ at both exposed histidines, His-32 and 100 (38, 39). A pulse radiolysis study was carried out, and both the Ru(III) and Cu(II) sites were reduced by formate radicals on the order of $1 \times 10^9 \text{ M}^{-1}\text{s}^{-1}$, in 55 and 45% proportions. A slower reduction of Cu(II) also was found; this was attributed to Ru(II) to Cu(II) ET, with a rate constant of 0.05 s^{-1} . Since a crystal structure of stellacyanin is not available, the ET distances were estimated from a computer model to be $\sim 16.1 \text{ \AA}$ (39). The relatively low ET rate is in line with the slow ET reactions observed for azurin and plastocyanin.

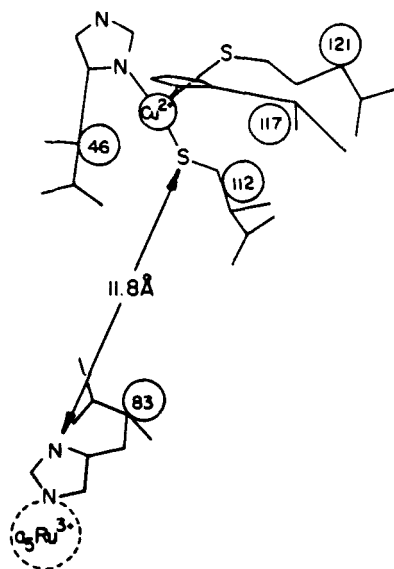


Figure 19. View of the ET donor and acceptor centers in azurin with $a_5\text{Ru}^{3+}$ bonded to the imidazole of His-83 (93).

F. Modified Iron-Sulfur Proteins

For an intramolecular ET study, HiPIP was modified with $a_5\text{Ru}^{3+}$ at His-42. The $a_5\text{Ru}^{3+}$ -His-42 protein has a Fe_4S_4 reduction potential of 350 mV. The protein was reduced using pulse radiolysis to $\text{HiPIP}_{\text{ox}}-\text{Ru}^{\text{II}}$, which then formed $\text{HiPIP}_{\text{red}}-\text{Ru}^{\text{III}}$. This system is interesting, because the estimated through-space distance from the Fe_4S_4 cluster to $a_5\text{Ru}^{3+}$ -His-42 is only 7.9 Å, and the through-bond pathway also is relatively short, as pictured in Fig. 20 (78, 79).

Three distinct kinetic stages are seen at 480 nm for reaction of e_{aq}^- with $\text{HiPIP}_{\text{ox}}-\text{Ru}^{\text{III}}$. Stage 1 is initial reduction, at $1.7 \times 10^{10} \text{ M}^{-1}\text{s}^{-1}$, which partitions to some extent between $\text{HiPIP}_{\text{ox}}-\text{Ru}^{\text{II}}$ and $\text{HiPIP}_{\text{red}}-\text{Ru}^{\text{II}}$. The former then transfers an electron, in stage 2, to give $\text{HiPIP}_{\text{red}}-\text{Ru}^{\text{III}}$, with $k_2 = 18 \pm 2 \text{ s}^{-1}$ at 20 °C. Stage 3 is associated with the presence of $\text{HiPIP}_{\text{red}}-\text{Ru}^{\text{III}}$ resulting from autoreduction, that is, $\text{HiPIP}_{\text{red}}-\text{Ru}^{\text{II}} + \text{HiPIP}_{\text{ox}}-\text{Ru}^{\text{III}} \rightarrow 2\text{HiPIP}_{\text{red}}-\text{Ru}^{\text{III}}$; $k_3 \sim 1 \times 10^5 \text{ M}^{-1}\text{s}^{-1}$ (78).

The process in stage 2 was assigned to intramolecular ET, because k_2 is independent of the concentration of $\text{HiPIP}_{\text{ox}}-\text{Ru}^{\text{III}}$, the decay remains first order after several pulses, and the rate is not affected by the presence of reductant or $[\text{Fe}(\text{CN})_6]^{3-}$ (78).

At a driving force of $\sim 0.27 \text{ eV}$, k_{et} (Ru to the Fe_4S_4 cluster) was found to be 18 s^{-1} . The ET rate is ~ 2 orders of magnitude *lower* than expected by comparison with cytochrome *c* ET rates, assuming an exponential de-

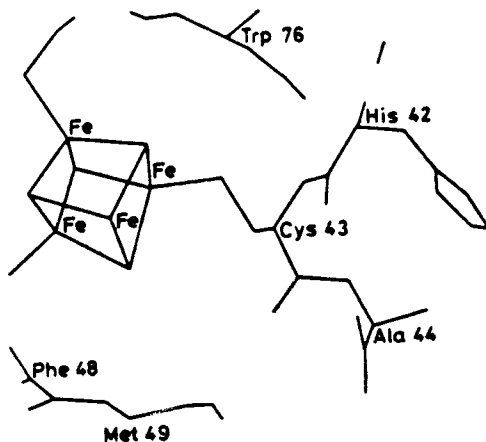


Figure 20. The Fe_4S_4 cluster of HiPIP, which is coordinated by Cys-43; also shown is His-42, which is the site of ruthenium modification (79).

pendence on r_e with $\beta = 0.9 \text{ \AA}^{-1}$. The ET also is disturbingly slow in view of the short through-bond pathway; His-42 is adjacent to Cys-43, which is bonded directly to the iron-sulfur cluster.

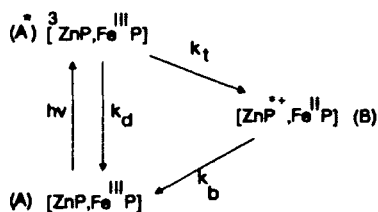
V. ELECTRON TRANSFER IN PROTEIN-PROTEIN COMPLEXES

Recent investigations have begun to provide more detailed information about factors that control ET in protein-protein complexes (122, 150, 188). Several different approaches have been used to vary the ET driving forces in these systems, and in certain cases site-directed mutagenesis has been utilized to change a particular amino acid residue thought to be involved in an ET pathway. In this section, we review work on protein-protein complexes in which the structures of both partners are known.

A. (Fe,Zn)-Hybrid Hemoglobins

In studying ET between proteins, complications may arise because the systems exhibit more than one stable conformational state (66). In hemoglobin (Hb), for example, the $\alpha_2\beta_2$ tetramer exists in two distinct states, T (deoxyhemoglobin) and R (oxyhemoglobin). Electron transfer between subunits in hemoglobin hybrids, $[\alpha_1(\text{Fe}), \beta_2(\text{Zn})]$ and $[\alpha_1(\text{Zn}), \beta_2(\text{Fe})]$, has been studied by Hoffman and co-workers (47, 66, 121, 151). The association of the Fe and Zn subunits has been extensively characterized (121); photogenerated ^3Zn -protoporphyrin* transfers an electron to a ferriheme acceptor, as outlined in Scheme V.

The quaternary structure adopted by the hybrids is the T form, where the metal-metal distance is 25 Å; the porphyrin planes are approximately parallel and the edge-edge distance is ~ 20 Å (Fig. 21). In the deoxyhemoglobin structure, the subunits of closest approach are $\alpha_1\beta_2$. Since $\alpha_1\beta_1$



Scheme V. Proposed kinetic scheme for electron transfer following flash excitation in Zn-substituted protein systems (121).

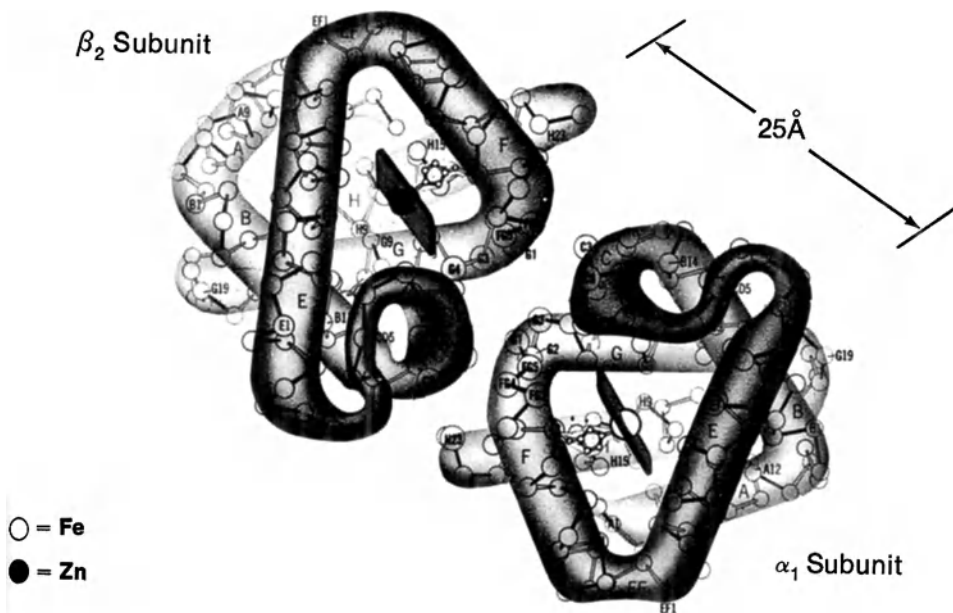


Figure 21. The (α_1, β_2) ET unit in hemoglobin. The metals in the two hemes are separated by roughly 25 Å (150).

distances are much longer (Fe–Zn, 37 Å), the Hb is considered as two independent $\alpha_1\beta_2$ ET pairs. The ET rate [$k_t = 100$ (10) s^{-1} , $k_b > 10^3 \text{ s}^{-1}$ ($\text{Fe}^{\text{II}}\text{P} \rightarrow \text{ZnP}^*$)] is strongly temperature dependent.

Fe(III)-heme ligand replacement with imidazole increases the rate to 175 s^{-1} , CO binding does not affect the rate, and ligand replacement with F^- , CN^- , or N_3^- decreases the rate to 20 s^{-1} . the ET rate constant in hybrid hemoglobin therefore depends strongly on heme ligation. The changes in k_t with axial ligation cannot be explained readily by energetics (ΔG°) or spin state; the trend that emerges is that the *net charge* associated with the ferriheme acceptor correlates with the rate: k_t is large when X is neutral and $\text{Fe}^{\text{III}}\text{X}$ is positive ($\text{X} = \text{H}_2\text{O}$, Im) and ET involves a charge shift. The ET rate is small when $\text{Fe}^{\text{III}}\text{X}$ is neutral ($\text{X} = \text{F}^-$, CN^- , N_3^-) (121). Work also has shown that the rates vary with the metal (Zn or Mg) in the porphyrin donor (138).

The temperature dependences from 77–313 K of the ET rates for [$\alpha_1(\text{Fe})$, $\beta_2(\text{Zn})$] and [$\alpha_1(\text{Zn})$, $\beta_2(\text{Fe})$] Hb hybrids have been determined (151). In these systems, the rate constant for long-range reduction of the aquoferriheme by ${}^3\text{ZnP}^*$ is $k_t = k_{\text{obsd}} - k_D$, where k_D is the rate of ${}^3\text{ZnP}^*$ decay in

reduced Hb hybrids ($\sim 55 \text{ s}^{-1}$). Decay rates (k_D) do not significantly vary over this temperature range. Electron transfer rates for the intersubunit transfer decrease rapidly from the room temperature (300 K) value [$k_1 = 100$ (6) s^{-1}]. At 140–160 K, the rates become temperature independent, and the low-temperature tunneling rate constant for $[\alpha_1(\text{Fe}), \beta_2(\text{Zn})]$ is 9 (2) s^{-1} ; for $[\alpha_1(\text{Zn}), \beta_2(\text{Fe})]$, it is 8 (2) s^{-1} .

For $[\alpha_1(\text{Zn}), \beta_2(\text{Fe})]$, a smooth transition occurred down to the temperature-independent region, whereas for $[\alpha_1(\text{Fe}), \beta_2(\text{Zn})]$, a plateau was found between 230 and 270 K. The evidence suggests that, upon cooling, the heme of $[\alpha_1\text{Fe(III)(H}_2\text{O)}\beta_2\text{Zn}]$ binds a histidine and remains low spin, whereas the $[\alpha_1\text{Zn}\beta_2\text{Fe(III)(H}_2\text{O)}]$ hybrid does not change its coordination.

The reorganization energies extracted from the temperature dependence of the ${}^3\text{ZnP}^* \rightarrow \text{Fe}^{\text{III}}$ reaction ($-\Delta G^\circ \sim 0.8 \text{ eV}$) are as follows: $[\alpha_1(\text{Zn}), \beta_2(\text{Fe})]$, $\lambda = 2.06 \text{ eV}$; $[\alpha_1(\text{Fe}), \beta_2(\text{Zn})]$, $\lambda = 1.79 \text{ eV}$ (151). The λ values are expected to be large, since reduction of Fe(III)-P results in the loss of H_2O , with change in the Fe position with respect to the porphyrin plane, as well as changes in the porphyrin geometry.

B. Cytochrome *c*-Cytochrome *b*₅

Cytochrome *c* and cytochrome *b*₅ form a complex in which the two heme centers are believed to lie in parallel planes separated by a closest edge-edge distance of 8.5 Å, with a center-center separation of 16 Å. With use of pulse radiolysis and flash photolysis, rates were measured in various derivatives under conditions where >90% of the cytochrome *b*₅ was bound to cytochrome *c*. Rates were found to be independent of concentration in this regime. Fe(III)-cyt *b*₅ decay at 428 nm and Fe(II)-cyt *c* growth at 416 nm were coincident. Electron-transfer driving forces and rates are given in Table XII (123, 125). The reorganization energy was estimated to be 0.8 eV (123).

TABLE XII
ET Rates in Cyt *c*-Cyt *b*₅ Complexes^a

Donor-Acceptor	$-\Delta G^\circ$ (eV)	k_{et} (s^{-1})
Fe(II)cyt <i>c</i> -Fe(III)cyt <i>b</i> ₅	0.3	$1.6 \pm 0.7 \times 10^3$
³ porph-cyt <i>c</i> *-Fe(III)cyt <i>b</i> ₅	0.35	5×10^4
³ Zn-cyt <i>c</i> *-Fe(III)cyt <i>b</i> ₅	0.75	5×10^5
H ₂ porphyrin-cyt <i>c</i> *-Fe(III)cyt <i>b</i> ₅	1.1	$8 \pm 1 \times 10^3$

^aFrom Refs. 123 and 125.

Molecular dynamics simulations of the cyt *c*-cyt *b*₅ complex have shown that different heme geometries and relative orientations are sampled over 46 ps; the protein complex may find a configuration that is potentially more favorable for ET than the docked structures (106). Of potential relevance in this connection is the finding that the phenyl side chain of Phe-82 in cyt *c* can be moved to a position in which it bridges the cyt *c* and cyt *b*₅ hemes (188).

C. Cytochrome *b*₅-(Fe, Zn) Hemoglobin

Electron transfer also has been measured between cyt *b*₅ and (Fe, Zn)-hemoglobin (168). The proteins form a noncovalent complex ($K = 3.4 \times 10^5 M^{-1}$); in a model of the complex, the hemes are coplanar with a 7 Å edge-edge distance. The ET rate in ZnHb-cyt *b*₅ (${}^3\text{ZnP}^* \rightarrow \text{Fe(III)}$; $-\Delta G^\circ = 0.75 \text{ eV}$) is $8 \times 10^3 \text{ s}^{-1}$, as compared with $4 \times 10^5 \text{ s}^{-1}$ in Zn-cyt *c*-cyt *b*₅. The reason for the slower rate is not known, but it is possible that the heme orientation in the ZnHb-cyt *b*₅ complex is not optimal for ET (168).

D. Cytochrome *c*-Cytochrome *b*₂

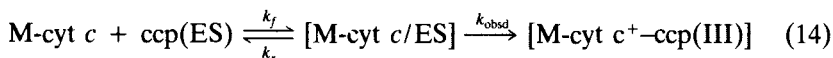
In the cyt *c*-cyt *b*₂ complex, the lack of a strong driving force dependence of the ET rate points to a rate-limiting conformational change (124). The initial reduction of *S. cerevisiae* cytochrome *b*₂ by flavin was followed by ET to horse heart cytochrome *c*. For Fe(III)cyt *c*-cyt *b*₂ ($-\Delta G^\circ \sim 0.2 \text{ eV}$), $k_{\text{et}} = 200(80) \text{ s}^{-1}$ at 25°C (pH 7, 5 mM P_i). Under the same conditions, the rate of photoactivated ET from ${}^3\text{Zn-cyt } c^*$ to cyt *b*₂ ($-\Delta G^\circ = 0.8 \text{ eV}$) is $600(200) \text{ s}^{-1}$; for ${}^3\text{porph-cyt } c^*$ -cyt *b*₂ ($-\Delta G^\circ = 0.4 \text{ eV}$), $k_{\text{et}} = 700(100) \text{ s}^{-1}$.

E. Cytochrome *c*-Cytochrome *c* Peroxidase

Cytochrome *c* and cytochrome *c* peroxidase (ccp) are physiological partners in the ccp reaction cycle; structural, thermodynamic, and kinetic data are available for the protein-protein interaction (141, 155, 177, 195). A model indicates that the cyt *c*-ccp complex is stabilized by specific salt bridges with the hemes in parallel planes; the Fe-Fe distance is $\sim 24 \text{ \AA}$, and the edge-edge distance is 16 \AA (155).

Long-range ET studies have been carried out between Zn-cyt *c* and Fe-ccp (22), monitoring the reaction at 420 nm (ES or Fe^{IV}-ccp absorbance, where ES, the oxidation product of Fe^{II}-ccp and peroxide, has two oxidizing

equivalents, namely, $\text{Fe}^{\text{IV}}\text{O}$ and a protein-based organic radical cation). The process followed is



Electron transfer from cyt *c* to ccp proceeds with a rate of 800 s^{-1} at $-\Delta G^\circ = 0.90(0.15) \text{ eV}$. In order to vary the driving force for ET, rates were measured for Fe-cyt *c*, Zn-cyt *c*, and H_2 -porphyrin-cyt *c* (porph-cyt *c*). For ET from porph-cyt *c* to ES, $k = 0.01 \text{ s}^{-1}$ at $-\Delta G^\circ = 0.05 \text{ eV}$, and from ZnP-cyt *c* to ES, $k = 0.2 \text{ s}^{-1}$ at $-\Delta G^\circ = 0.35 \text{ eV}$ (pH 7.0, 10 mM P_i , 25°C). It has been shown that the binding of porph-cyt *c* and Zn-cyt *c* to ccp is similar to that of cyt *c*; k_f is approximately $10^9 \text{ M}^{-1}\text{s}^{-1}$, and k_r is roughly 10^3 s^{-1} (k_f and k_r are assumed to be the same in all three cases).

The cyt *c*-ccp reorganization energy was estimated to be 1.5 eV, which falls within the range found for other protein-protein complexes. The relatively large reorganization energies obtained for protein complexes may be a result of redox-dependent fluctuations of the protein-protein orientation, since the primary binding mode is electrostatic (salt bridges) (22).

Elucidation of the factors that control ET in the cyt *c*-ccp system has been facilitated by employing yeast iso-1-cytochrome *c* mutants with Phe, Tyr, Gly, Ser, Leu, and Ile at position 82 (in vertebrate numbering); these mutants also have Thr in place of Cys at position 102. The residue at position 82 is important, because Phe-82 is thought to be involved in the ET reaction in the cyt *c*-ccp complex (156). Zn-protoporphrin IX has been substituted for the heme in ccp, and photoinduced long-range ET has been measured from Zn-ccp to cyt *c* (Scheme V) (100-102, 152).

The ET rates are given in Table XIII. All mutants except Gly-82 behave similarly in the excited-state (k_f) reaction, but back ET is very dependent on the residue at position 82. For the Ser, Leu, and Ile mutants, k_b is $\sim 10^4$

TABLE XIII
Electron-Transfer Rates for Position-82 Mutants of Iso-1-Cytochrome *c*^a

Residue-82	${}^3\text{ZnP}^* \rightarrow \text{Fe}^{\text{III}}\text{P}$ $k_f (\text{s}^{-1})$	$\text{ZnP}^+ \leftarrow \text{Fe}^{\text{II}}\text{P}$ $k_b (\text{s}^{-1})$
Phe	166 ± 4	$1.9 \pm 0.6 \times 10^4$
Tyr	173 ± 1	$1.5 \pm 0.6 \times 10^4$
Ser	151 ± 5	2.3 ± 0.5
Leu	93 ± 5	2.0 ± 0.5
Ile	56 ± 3	3.0 ± 0.5
Gly	13 ± 2	1.4 ± 0.3

^aFrom Ref. 101.

less at 0°C than for the position-82 aromatics (101). For the Gly mutant, k_i is reduced as well as k_b , suggesting that the conformation of the complex has changed. The large differences in back ET rates are not well understood.

In summary, studies of long-range ET in protein-protein complexes, both among physiological partners, nonphysiological protein complexes, and subunits of one protein, have shown that rates generally increase with driving force, in Marcus fashion, the exception being the cyt *c*-cyt *b*₂ complex. Reorganization energy values range from 0.8 eV (cyt *c*-cyt *b*₅) to 2.06 eV (Zn, Fe-hybrid hemoglobin). Although much has been learned from the work done to date, it is evident that ET experiments need to be carried out over a larger range of distances and driving forces in complexes in which systematic structural changes can be made. With more information, it should be possible to elucidate at least some of the factors that control ET in natural systems.

GLOSSARY OF TERMS

β	Constant reflecting distance dependence of electronic coupling
β'	Constant reflecting the dependence of electronic coupling on the number of bonds separating donor and acceptor
CS	Charge separation
γ	Constant reflecting distance dependence of the nuclear factor
ϵ_{op}	Optical dielectric constant ($=n^2$; n = refractive index)
ϵ_s	Static dielectric constant
ET	Electron transfer
ΔG°	Reaction free energy
ΔG^*	Activation free energy
ΔH^*	Activation enthalpy
H_{ab}	Electronic coupling matrix element
$(H_{ab})_0$	Electronic coupling matrix element at close contact (r_0) between the donor and acceptor
$(H_{ab})'_0$	Electronic coupling matrix element with one bond separating the donor and acceptor
k_{cr}	Charge recombination rate
k_{et}	ET rate
k_o	ET rate at close contact between donor and acceptor
k_{op}	Optimal (activationless, $-\Delta G^\circ = \lambda$) electron-transfer rate
k_q	Quenching rate
k_{sep}	Rate of radical escape from a geminate radical pair

k_f and k_b	Forward and back ET rates, respectively, for photoinitiated reactions
κ_e	Electronic coupling factor
κ_e°	Electronic coupling factor when donor and acceptor are in closest contact
λ	Reorganization energy ($=\lambda_s + \lambda_v$)
λ_s	Solvent reorganization energy
λ_v	Internal reorganization energy
${}^3\text{MP}^*$	Photoexcited triplet state of metalloporphyrin
ν_n	Nuclear frequency factor
Φ_{sep}	Quantum yield of radical escape from a geminate radical pair
r	ET distance
r_{DA}	Donor-acceptor separation
r_e	Edge-edge ET distance between donor and acceptor
r_o	Close contact distance between donor and acceptor
ΔS^*	Activation entropy
w	Vibrational quantum number
ω	Vibrational frequency

ACKNOWLEDGMENTS

Our work on electron transfer in proteins is supported by grants from the National Science Foundation and the National Institutes of Health. This is contribution No. 8036 from the Arthur Amos Noyes Laboratory.

REFERENCES

1. E. T. Adman, *Biochim. Biophys. Acta*, **549**, 107–144 (1979).
2. I. K. Adzhami, D. M. Davies, C. S. Stanley, and A. G. Sykes, *J. Am. Chem. Soc.*, **103**, 5543–5547 (1981).
3. T. Alber, S. Dao-pin, J. A. Nye, D. C. Muchmore, and B. W. Matthews, *Biochemistry*, **26**, 3754–3758 (1987).
4. B. Anderes and D. K. Lavalley, *Inorg. Chem.*, **22**, 2665–2666 (1983).
5. G. D. Armstrong, J. A. Chambers, and A. G. Sykes, *J. Chem. Soc. Dalton Trans.*, 755–758 (1986).
6. A. W. Axup, M. Albin, S. L. Mayo, R. J. Crutchley, and H. B. Gray, *J. Am. Chem. Soc.*, **110**, 435–439 (1988).
7. R. L. Baldwin and D. Eisenberg, *Protein Engineering*, D. L. Oxender and C. F. Fox, Eds., Alan R. Liss, New York, (1987), pp. 127–148.

8. R. Bechtold, M. B. Gardineer, A. Kazmi, B. van Hemelryck, and S. S. Isied, *J. Phys. Chem.*, *90*, 3800–3804 (1986).
9. R. Bechtold, C. Kuehn, C. Lepre, and S. S. Isied, *Nature (London)*, *322*, 286–288 (1986).
10. D. N. Beratan and J. N. Onuchic, *Photosynthesis Research*, *22*, 173–186 (1989).
11. D. N. Beratan, J. N. Onuchic, and J. J. Hopfield, *J. Phys. Chem.*, *86*, 4488–4498 (1987).
12. J. N. Betts, D. N. Beratan, B. E. Bowler, J. N. Onuchic, and H.B. Gray, *Am. Chem. Soc.*, in press.
13. B. E. Bowler, H. B. Gray, and T. J. Meade, *McGraw-Hill Yearbook of Science and Technology*, McGraw-Hill, New York, 1989, pp. 53–55.
14. B. E. Bowler, T. J. Meade, S. L. Mayo, J. H. Richards, and H. B. Gray, *J. Am. Chem. Soc.*, *111*, 8757–8759 (1989).
15. B. S. Brunshwig, P. J. DeLaive, A. M. English, M. Goldberg, H. B. Gray, S. L. Mayo, and N. Sutin, *Inorg. Chem.*, *24*, 3743–3749 (1985).
16. J. Butler, S. K. Chapman, D. M. Davies, A. G. Sykes, S. H. Speck, N. Osheroff, and E. Margoliash, *J. Biol. Chem.*, *258*, 6400–6404 (1983).
17. J. Butler, D. M. Davies, A. G. Sykes, W. H. Koppenol, N. Osheroff, and E. Margoliash, *J. Am. Chem. Soc.*, *103*, 469–471 (1981).
18. C. W. Carter, Jr., J. Kraut, S. T. Freer, N.-H. Xuong, R. A. Alden, and R. G. Bartsch, *J. Biol. Chem.*, *249*, 4212–4225 (1974).
19. P. Chen, E. Danielson, and T. J. Meyer, *J. Phys. Chem.*, *92*, 3708–3711 (1988).
20. G. L. Closs, L. T. Calcaterra, N. J. Green, K. W. Penfield, and J. R. Miller, *J. Phys. Chem.*, *90*, 3673–3683 (1986).
21. G. L. Closs and J. R. Miller, *Science*, *240*, 440–447 (1988).
22. K. T. Conklin and G. McLendon, *J. Am. Chem. Soc.*, *110*, 3345–3350 (1988).
23. D. W. Conrad and R. A. Scott, *J. Am. Chem. Soc.*, *111*, 3461–3463 (1989).
24. D. J. Cookson, M. T. Hayes, and P. E. Wright, *Nature (London)*, *283*, 682–683 (1980).
25. J. A. Cowan and H. B. Gray, *Chem. Scr.* *28A*, 21–26 (1988).
26. J. A. Cowan and H. B. Gray, *Inorg. Chem.*, *28*, 2074–2078 (1989).
27. J. A. Cowan, J. K. M Sanders, G. S. Beddard, and R. J. Harrison, *J. Chem. Soc. Chem. Commun.*, 55–58 (1987).
28. J. A. Cowan, R. K. Upmacis, D. N. Beratan, J. N. Onuchic, and H. B. Gray, *Ann. New York Acad. Sci.*, *550*, 68–84 (1988).
29. C. Creutz, *Prog. Inorg. Chem.*, *30*, 1–73 (1983).
30. R. J. Crutchley, W. R. Ellis, Jr., and H. B. Gray, *Frontiers in Bioinorganic Chemistry*, A. V. Xavier, Ed., VCH, Weinheim, FRG, 1986, pp. 679–693.
31. R. J. Crutchley, W. R. Ellis, Jr., and H. B. Gray, *J. Am. Chem. Soc.*, *107*, 5002–5004 (1985).
32. D. Cummins and H. B. Gray, *J. Am. Chem. Soc.*, *99*, 5158–5167 (1977).

33. J. H. Dawson, M. J. K. Geno, and E. T. Kintner, *Frontiers in Bioinorganic Chemistry*, A. V. Xavier, Ed., VCH, Weinheim, FRG, 1985, pp. 704–713.
34. R. P. Domingue and M. D. Fayer, *J. Chem. Phys.*, **83**, 2242–2251 (1985).
35. P. L. Drake, R. T. Hartshorn, J. McGinnis, and A. G. Sykes, *Inorg. Chem.*, **28**, 1361–1366 (1989).
36. H. Elias, M. H. Chou, and J. R. Winkler, *J. Am. Chem. Soc.*, **110**, 429–434 (1988).
37. O. Farver, A. Licht, and I. Pecht, *Biochemistry*, **26**, 7317–7321 (1987), and references cited therein.
38. O. Farver and I. Pecht, *FEBS Lett.*, **244**, 376–378 (1989).
39. O. Farver and I. Pecht, *FEBS Lett.*, **244**, 379–382 (1989).
40. B. A. Feinberg and W. A. Johnson, *Biochem. Biophys. Res. Commun.*, **93**, 100–105 (1980).
41. P. Finckh, H. Heitele, M. Volk, and M. E. Michel-Beyerle, *J. Phys. Chem.*, **92**, 6584–6590 (1988).
42. S. F. Fischer and R. P. Van Duyne, *Chem. Phys.*, **26**, 9–16 (1977).
43. L. S. Fox, Ph.D. Thesis, “Intramolecular Electron Transfer in an Iridium d⁸-d⁸ Donor-Acceptor System,” California Institute of Technology (1989).
44. L. S. Fox, H. B. Gray, M. Kozik, and J. R. Winkler, *Science*, **247**, 1069–1071 (1990).
45. M. J. K. Geno and J. H. Dawson, *Inorg. Chem.*, **23**, 1182–1183 (1984).
46. M. J. K. Geno and J. H. Dawson, *Inorg. Chem.*, **24**, 1731–1732 (1985).
47. D. J. Gingrich, J. M. Nocek, M. J. Natan, and B. M. Hoffman, *J. Am. Chem. Soc.*, **109**, 7533–7534 (1987).
48. M. Go and S. Miyazawa, *Int. J. Peptide Protein Res.*, **15**, 211–224 (1980).
49. I. R. Gould, D. Ege, S. L. Mattes, and S. Farid, *J. Am. Chem. Soc.*, **109**, 3794–3796 (1987).
50. I. R. Gould and S. Farid, *J. Am. Chem. Soc.*, **110**, 7883–7885 (1988).
51. I. R. Gould, R. Moody, and S. Farid, *J. Am. Chem. Soc.*, **110**, 7242–7244 (1988).
52. I. R. Gould, J. E. Moser, B. Armitage, S. Farid, J. C. Goodman, and M. S. Herman, *J. Am. Chem. Soc.*, **111**, 1917–1919 (1989).
53. I. R. Gould, J. E. Moser, D. Ege, and S. Farid, *J. Am. Chem. Soc.*, **110**, 1991–1993 (1988).
54. H. B. Gray, *Chem. Soc. Rev.*, **15**, 17–30 (1986), and references cited therein.
55. H. B. Gray and B. G. Malmström, *Biochemistry*, **28**, 7499–7505 (1989).
56. H. B. Gray and B. G. Malmström, *Comments Inorg. Chem.*, **2**, 203–209 (1983).
57. J. M. Guss and H. C. Freeman, *J. Mol. Biol.*, **169**, 521–563 (1983).
58. J. M. Guss, P. R. Harrowell, M. Murata, V. A. Norris, and H. C. Freeman, *J. Mol. Biol.*, **192**, 361–387 (1986).
59. D. Gust and T. A. Moore, *Science*, **244**, 35–41 (1989).

60. D. Gust, T. A. Moore, P. A. Liddell, G. A. Nemeth, L. R. Makings, A. L. Moore, D. Barrett, P. J. Pessiki, R. V. Bensasson, M. Rougee, C. Chachaty, F. C. De Schryver, M. Van der Auweraer, A. R. Holzwarth, and J. S. Connolly, *J. Am. Chem. Soc.*, *109*, 846–856 (1987).
61. A. Harriman, *Inorg. Chim. Acta.*, *88*, 213–216 (1978).
62. R. T. Hartshorn, M.-C. Lim, and A. G. Sykes, *Inorg. Chem.*, *27*, 4603–4606 (1988).
63. D. Heiler, G. McLendon, and P. Rogalskyj, *J. Am. Chem. Soc.*, *109*, 604–606 (1987).
64. H. Heitele and M. E. Michel-Beyerle, *J. Am. Chem. Soc.*, *107*, 8286–8288 (1985).
65. H. Heitel, M. E. Michel-Beyerle, and P. Finckh, *Chem. Phys. Lett.*, *134*, 273–278 (1987).
66. B. M. Hoffman and M. A. Ratner, *J. Am. Chem. Soc.*, *109*, 6237–6243 (1987).
67. B. M. Hoffman and M. A. Ratner, *J. Am. Chem. Soc.*, *110*, 8267 (1988).
68. R. Hoffmann, *Acc. Chem. Res.*, *4*, 1–9 (1971).
69. R. Hoffmann, A. Imamura, and W. Hehre, *J. Am. Chem. Soc.*, *90*, 1499–1509 (1968).
70. J. J. Hopfield, *Biophys. J.*, *18*, 311–321 (1977).
71. N. S. Hush, *Coord. Chem. Rev.*, *64*, 135–157 (1985).
72. N. S. Hush, M. N. Paddon-Row, E. Cotsaris, H. Oevering, J. W. Verhoeven, and M. Heppener, *Chem. Phys. Lett.*, *117*, 8–11 (1985).
73. M. P. Irvine, R. J. Harrison, G. S. Beddard, P. Leighton, and J. K. M. Sanders, *Chem. Phys.*, *104*, 315–324 (1986).
74. S. S. Isied, C. Kuehn, and G. Worosila, *J. Am. Chem. Soc.*, *106*, 1722–1726 (1984).
75. S. S. Isied, A. Vassilian, R. H. Magnuson, and H. A. Schwarz, *J. Am. Chem. Soc.*, *107*, 7432–7438 (1985).
76. S. S. Isied, A. Vassilian, J. F. Wishart, C. Creutz, H. A. Schwarz, and N. Sutin, *J. Am. Chem. Soc.*, *110*, 635–639 (1988).
77. S. S. Isied, G. Worosila, and S. J. Atherton, *J. Am. Chem. Soc.*, *104*, 7659–7661 (1982).
78. M. P. Jackman, M.-C. Lim, G. A. Salmon, and A. G. Sykes, *J. Chem. Soc. Chem. Commun.*, 179–180 (1988).
79. M. P. Jackman, M.-C. Lim, A. G. Sykes, and G. A. Salmon, *J. Chem. Soc. Dalton Trans.*, 2843–2850 (1988), and references cited therein.
80. M. P. Jackman, J. McGinnis, R. Powls, G. A. Salmon, and A. G. Sykes, *J. Am. Chem. Soc.*, *110*, 5880–5887 (1988).
81. M. P. Jackman, J. D. Sinclair-Day, M. J. Sisley, A. G. Sykes, L. A. Denys, and P. E. Wright, *J. Am. Chem. Soc.*, *109*, 6443–6449 (1987).
82. M. P. Jackman, A. G. Sykes, and G. A. Salmon, *J. Chem. Soc. Chem. Commun.*, 65–66 (1987).

83. C. Joachim, *Chem. Phys.*, *116*, 339–349 (1987).
84. A. D. Joran, B. A. Leland, P. M. Felker, A. H. Zewail, J. J. Hopfield, and P. B. Dervan, *Nature (London)*, *327*, 508–511 (1987).
85. A. D. Joran, B. A. Leland, G. G. Geller, J. J. Hopfield, and P. B. Dervan, *J. Am. Chem. Soc.*, *106* 6090–6092 (1984).
86. T. Kakitani and N. Mataga, *J. Phys. Chem.*, *90*, 993–995 (1986).
87. T. Kakitani and N. Mataga, *J. Phys. Chem.*, *91*, 6277–6285 (1987).
88. T. Kakitani and N. Mataga, *Chem. Phys.*, *93*, 381–397 (1985).
89. J. L. Karas, Ph.D. Thesis, "Long-Range Electron Transfer in Ruthenium-Labelled Wyoglobin," California Institute of Technology (1989).
90. J. L. Karas, C. M. Lieber, and H. B. Gray, *J. Am. Chem. Soc.*, *110*, 599–600 (1988).
91. N. R. Kestner, J. Jortner and J. Logan, *J. Phys. Chem.*, *78*, 2148–2165 (1979).
92. W. H. Koppenol and E. Margoliash, *J. Biol. Chem.*, *257*, 4426–4437 (1982).
93. N. M. Kostic, R. Margalit, C.-M. Che, and H. B. Gray, *J. Am. Chem. Soc.*, *105*, 7765–7767 (1983).
94. J. Kroon, A. M. Oliver, M. N. Paddon-Row, and J. W. Verhoeven, *Recl. Trav. Chim. Pays-Bas*, *107*, 509–510 (1988).
95. A. Kuki and P. G. Wolynes, *Science*, *236*, 1647–1652 (1987).
96. S. Larsson, *Chem. Phys. Lett.*, *90*, 136–139 (1982).
97. S. Larsson, *Discuss. Faraday. Soc.*, *74*, 390–392 (1982).
98. J.-M. Lehn, *NATO ASI Series C, Vol. 214: Supramolecular Photochemistry* V. Balzani, Ed., D. Reidel, Boston, 1987, pp. 29–43.
99. B. A. Leland, A. D. Joran, P. M. Felker, J. J. Hopfield, A. H. Zewail, and P. B. Dervan, *J. Phys. Chem.*, *89*, 5571–5573 (1985).
100. N. Liang, C. H. Kang, P. S. Ho, E. Margoliash, and B. M. Hoffman, *J. Am. Chem. Soc.*, *108*, 4665–4666 (1986).
101. N. Liang, A. G. Mauk, G. J. Pielak, J. A. Johnson, M. Smith, and B. M. Hoffman, *Science*, *240*, 311–313 (1988).
102. N. Liang, G. J. Pielak, A. G. Mauk, M. Smith, and B. M. Hoffman, *Proc. Natl. Acad. Sci. USA*, *84*, 1249–1252 (1987).
103. C. M. Lieber, J. L. Karas, and H. B. Gray, *J. Am. Chem. Soc.* *109*, 3778–3779 (1987).
104. C. M. Lieber, J. L. Kras, S. L. Mayo, M. Albin, and H. B. Gray, *Proc. Robert A. Welch Found. Conf. Chem. Res.*, *31*, 9–33 (1987).
105. C. M. Lieber, J. L. Karas, S. L. Mayo, A. W. Axup, M. Albin, R. J. Cruchley, W. R. Ellis, Jr., and H. B. Gray, *Trace Elements in Man and Animals*, *6*, Plenum; New York, 1988, pp. 23–27.
106. G. V. Louie, G. J. Pielak, M. Smith, and G. D. Brayer, *Biochemistry*, *27*, 7870–7876 (1988).
107. M. W. Makinen, S. A. Schichman, S. C. Hill, and H. B. Gray, *Science*, *222*, 929–931 (1983).

108. R. A. Marcus, *Ann. Rev. Phys. Chem.*, *15*, 155–196 (1964).
109. R. A. Marcus, *J. Phys. Chem.*, *24*, 966–978 (1956).
110. R. A. Marcus and N. Sutin, *Biochim. Biophys. Acta*, *811*, 265–322 (1985).
111. R. A. Marcus and N. Sutin, *Inorg. Chem.*, *14*, 213–216 (1975).
112. M. C. Marden, E. S. Hazard, and Q. H. Gibson, *Biochemistry*, *25*, 7591–7596 (1986).
113. R. Margalit, N. M. Kostic, C.-M. Che, D. F. Blair, H.-J. Chiang, I. Pecht, J. B. Shelton, J. R. Shelton, W. A. Schroeder, and H. B. Gray, *Proc Natl. Acad. Sci. USA*, *81*, 6554–6558 (1984).
114. R. Margalit, I. Pecht, and H. B. Gray, *J. Am. Chem. Soc.*, *105*, 301–302 (1983).
115. J. L. Marshall, S. R. Stobart, and H. B. Gray, *J. Am. Chem. Soc.*, *106*, 3027–3029 (1984).
116. A. G. Mauk, E. Bordignon, and H. B. Gray, *J. Am. Chem. Soc.*, *104*, 7654–7657 (1982).
117. A. G. Mauk, R. A. Scott, and H. B. Gray, *J. Am. Chem. Soc.*, *102*, 4360–4363 (1980).
118. S. L. Mayo, W. R. Ellis, Jr., R. J. Crutchley, and H. B. Gray, *Science*, *233*, 948–952 (1986).
119. J. McGinnis, J. D. Sinclair-Day, and A. G. Sykes, *J. Chem. Soc. Dalton Trans.*, 2007–2009 (1986).
120. J. McGinnis, J. D. Sinclair-Day, A. G. Sykes, R. Powls, G. Moore, and P. E. Wright, *Inorg. Chem.*, *27*, 2306–2312 (1988).
121. J. L. McGourty, S. E. Peterson-Kennedy, W. Y. Ruo, and B. M. Hoffman, *Biochemistry*, *26*, 8302–8312 (1987).
122. G. McLendon, *Acc. Chem. Res.*, *21*, 160–167 (1988).
123. G. McLendon and J. R. Miller, *J. Am. Chem. Soc.*, *107*, 7811–7817 (1985).
124. G. McLendon, K. Pardue, and P. Bak, *J. Am. Chem. Soc.*, *109*, 7540–7541 (1987).
125. G. L. McLendon, J. R. Winkler, D. G. Nocera, M. R. Mauk, A. G. Mauk, and H. B. Gray, *J. Am. Chem. Soc.*, *107*, 739–740 (1985).
126. T. J. Meade, H. B. Gray, and J. R. Winkler, *J. Am. Chem. Soc.*, *111*, 4353–4356 (1989).
127. T. J. Meyer, *Acc. Chem. Res.*, *22*, 163–170 (1989).
128. T. J. Meyer, *NATO ASI Series C, Vol. 214: Supramolecular Photochemistry* V. Balzani, Ed., Reidel, Boston, 1987, pp. 103–120.
129. J. R. Miller, J. V. Beitz, and R. K. Huddleston, *J. Am. Chem. Soc.*, *106*, 5057–5068 (1984).
130. J. R. Miller, L. T. Calcaterra, and G. L. Closs, *J. Am. Chem. Soc.*, *106*, 3047–3049 (1984).
131. I. A. Mizrahi, T. E. Meyer, and M. A. Cusanovich, *Biochemistry*, *19*, 4727–4733 (1980).

132. G. R. Moore, G. S. Eley, and G. Williams, *Adv. Inorg. Bioinorg. Mech.*, **3**, 1–96 (1984).
133. G. R. Moore, D. A. Harris, F. A. Leitch, and G. W. Pettigrew, *Biochim. Biophys. Acta*, **764**, 331–342 (1984).
134. G. R. Moore, and G. W. Pettigrew, Eds., in *Cytochromes c: Biological Aspects*, Springer-Verlag; New York, 1987.
135. T. A. Moore, D. Gust, A. L. Moore, R. V. Bensasson, P. Seta, and E. Bienvenue, *NATO ASI Series C, Vol. 214: Supramolecular Photochemistry* V. Balzani, Ed., Reidel, Boston, 1987, pp. 283–297.
136. J. Mottonen, D. Ringe, and G. Petsko, unpublished results.
137. M. Nango, H. Kryu, and P. Loach, *J. Chem. Soc. Chem. Commun.*, 697–698 (1988).
138. M. J. Natan and B. M. Hoffman, *J. Am. Chem. Soc.*, **111**, 6468–6470 (1989).
139. M. D. Newton, *Intl. J. Quantum Chem.: Quant. Chem. Symp.*, **14**, 363–391 (1980).
140. D. G. Nocera, J. R. Winkler, K. M. Yocom, E. Bordignon, and H. B. Gray, *J. Am. Chem. Soc.*, **106**, 5145–5150 (1984).
141. S. H. Northrup, J. O. Boles, and J. C. L. Reynolds, *Science*, **241**, 67–70 (1988).
142. H. Oevering, M. N. Paddon-Row, M. Heppener, A. M. Oliver, E. Cotisaris, J. W. Verhoeven, and N.S. Hush, *J. Am. Chem. Soc.*, **109**, 3258–3269 (1987).
143. T. Ohno, A. Yoshimura, H. Shioyama, and N. Mataga, *J. Phys. Chem.*, **91**, 4365–4370 (1987).
144. K. Ohta, G. L. Closs, K. Morokuma, and N. J. Green, *J. Am. Chem. Soc.*, **108**, 1319–1320 (1986).
145. A. M. Oliver, D. C. Craig, M. N. Paddon-Row, J. Kroon, and J.W. Verhoeven, *Chem. Phys. Lett.*, **150**, 366–373 (1988).
146. P. Osvath, G. A. Salmon, and A. G. Sykes, *J. Am. Chem. Soc.*, **110**, 7114–7118 (1988).
147. M. N. Paddon-Row, A. M. Oliver, J. M. Warman, K. J. Smit, M. P. de Haas, H. Oevering, and J. W. Verhoeven, *J. Phys. Chem.*, **92**, 6958–6962 (1988).
148. L. P. Pan, B. Durham, J. Wolinska, and F. Millett, *Biochemistry*, **27**, 7180–7184 (1988).
149. K. W. Penfield, J. R. Miller, M. N. Paddon-Row, E. Cotisaris, A. M. Oliver, and N. S. Hush, *J. Am. Chem. Soc.*, **109**, 5061–5065 (1987).
150. S. E. Peterson-Kennedy, J. L. McGourty, P. S. Ho, C. J. Sutoris, N. Liang, H. Zemel, N. V. Blough, E. Margoliash, and B. M. Hoffman, *Coord. Chem. Rev.*, **64**, 125–133 (1985).
151. S. E. Peterson-Kennedy, J. L. McGourty, J. A. Kalweit, and B. M. Hoffman, *J. Am. Chem. Soc.*, **108**, 1739–1746 (1986).
152. G. J. Pielak, A. G. Mauk, and M. Smith, *Nature (London)*, **313**, 152–154 (1985).

153. J. R. Pladziewicz, A. J. Abrahamson, R. A. Davies, and M. D. Likar, *Inorg. Chem.*, **26**, 2058–2062 (1987).
154. J. R. Pladziewicz and M. S. Brenner, *Inorg. Chem.*, **26**, 3629–3634 (1987).
155. T. Poulos and B. Finzel, *Peptide and Protein Reviews*, M. T. W. Hearn, Ed., Marcel Dekker, New York, 1984, pp. 115–171.
156. T. L. Poulos and J. Kraut, *J. Biol. Chem.*, **255**, 10322–10330 (1980).
157. J. D. Rush, W. H. Koppenol, E. A. E. Garber, and E. Margoliash, *J. Biol. Chem.*, **263**, 7514–7520 (1988).
158. J. D. Rush, J. Lan, and W. H. Koppenol, *J. Am. Chem. Soc.*, **109**, 2679–2682 (1987).
159. D. Sandrini, M. T. Gandolfi, M. Maestri, F. Bolleta, and V. Balzani, *Inorg. Chem.*, **23**, 3017–3023 (1984).
160. L. J. Schaffer and H. Taube, *J. Phys. Chem.*, **90**, 3669–3673 (1986) and references cited therein.
161. K. S. Schanze and K. Sauer, *J. Am. Chem. Soc.*, **110**, 1180–1186 (1988).
162. J. A. Schmidt, A. P. McIntosh, A. C. Weedon, J. R. Bolton, J. S. Connolly, J. K. Hurley, and M. R. Wasielewski, *J. Am. Chem. Soc.*, **111**, 4353–4356 (1988).
163. R. A. Scott, A. G. Mauk, and H. B. Gray, *J. Chem. Educ.*, **62**, 932–938 (1985).
164. M. Selman, Ph.D. Thesis, “Preparation and Characterization of an Intramolecular Electron Transfer in a Pentaammineruthenium Derivative of *Candida Krusei* Cytochrome C,” California Institute of Technology (1989).
165. J. L. Sessler and M.R. Johnson, *Angew. Chem. Int. Ed.*, **26**, 678–680 (1987).
166. J. L. Sessler, M.R. Johnson, T.-Y. Lin, and S. E. Creager, *J. Am. Chem. Soc.*, **110**, 3659–3661 (1988).
167. P. Seta, E. Bienvenue, A. L. Moore, P. Mathis, R. V. Bensasson, P. Liddell, P. J. Ressiki, A. Joy, T. A. Moore, and D. Gust, *Nature (London)*, **316**, 653–655 (1985).
168. K. P. Simolo, G. L. McLendon, M. R. Mauk, and A. G. Mauk, *J. Am. Chem. Soc.*, **106**, 5012–5013 (1984).
169. M. J. Sisley, M. G. Segal, C. S. Stanley, I. K. Adzamli, and A. G. Sykes, *J. Am. Chem. Soc.*, **105**, 225–228 (1983).
170. M. Sola, J. A. Cowan, and H. B. Gray, *Biochemistry*, **28**, 5261–5268 (1989).
171. C. A. Stein, N. A. Lewis, and G. Seitz, *J. Am. Chem. Soc.*, **104**, 2596–2599 (1982).
172. C. A. Stein, N. A. Lewis, G. Seitz, and A. D. Baker, *Inorg. Chem.*, **22**, 1124–1128 (1983).
173. N. Sutin, *Acc. Chem. Res.*, **15**, 275–282 (1982).
174. N. Sutin, *Prog. Inorg. Chem.*, **30**, 441–498 (1983).

175. R. Swanson, B. L. Trus, N. Mandel, O. B. Kallai, and R. E. Dickerson, *J. Biol. Chem.*, *252*, 759-775 (1977).
176. A. G. Sykes, *Chem. Soc. Rev.*, *14*, 283-315 (1985).
177. V. Taniguchi, W. Ellis, V. Cammarata, J. Webb, F. Anson, and H. B. Gray, *Electrochemical Studies of Biological Redox Components*, K. Kadish, Ed., American Chemical Society, Washington DC, ACS Adv. Chem. Ser. 201, 1982, pp. 51-68.
178. H. Taube, *Ann. N. Y. Acad. Sci.*, *313*, 481-495 (1978).
179. H. Toi, G. N. La Mar, R. Margalit, C.-M. Che, and H. B. Gray, *J. Am. Chem. Soc.*, *106*, 6213-6217 (1984).
180. G. Tollin, L. K. Hanson, M. Caffrey, T. E. Meyer, and M. Cusanovich, *Proc. Natl. Acad. Sci. USA*, *83*, 3693-3697 (1986).
181. J. W. Verhoeven, M. N. Paddon-Row, N. S. Hush, H. Oevering, and M. Heppener, *Pure Appl. Chem.*, *58*, 1285-1290 (1986).
182. J. M. Warman, M. P. de Haas, H. Oevering, J. W. Verhoeven, M. N. Paddon-Row, A. M. Oliver, and N. S. Hush, *Chem. Phys. Lett.*, *128*, 95-99 (1986).
183. J. M. Warman, M. P. de Haas, M. N. Paddon-Row, E. Cotsaris, N. S. Hush, H. Oevering, and J. W. Verhoeven, *Nature (London)*, *320*, 615-616 (1986).
184. M. R. Wasielewski, D. G. Johnson, W. A. Svec, K. M. Kersey, and D. W. Minsek, *J. Am. Chem. Soc.*, *110*, 7219-7221 (1988).
185. M. R. Wasielewski and M. P. Niemczyk, *J. Am. Chem. Soc.*, *106*, 5043-5045 (1984).
186. M. R. Wasielewski, M. P. Niemczyk, W. A. Svec, and E. B. Pewitt, *J. Am. Chem. Soc.*, *107*, 1080-1082 (1985).
187. A. Weller, *Z. Physik. Chem. N.F.*, *133*, 93-98 (1982).
188. J. J. Wendoloski, J. B. Matthew, P. C. Wever, F. R. Salemme, *Science*, *238*, 794-797 (1988).
189. S. Wherland and H. B. Gray, *Biological Aspects of Inorganic Chemistry*, A. W. Addison, W. R. Cullen, D. Dolphin, and B. R. James, Eds., Wiley, New York, 1977, pp. 289-368.
190. S. Wherland, O. Farver, and I. Pecht, *J. Mol. Biol.*, *204*, 407-415 (1988).
191. J. R. Winkler, D. G. Nocera, K. M. Yocom, E. Bordignon, and H. B. Gray, *J. Am. Chem. Soc.*, *104*, 5798-5800 (1982).
192. S. Woitellier, J. P. Launay, and C. W. Spangler, *Inorg. Chem.*, *28*, 758-762 (1989).
193. K. M. Yocom, J. B. Shelton, J. R. Shelton, W. A. Schroeder, G. Worosila, S. S. Isied, E. Bordignon, and H. B. Gray, *Proc. Natl. Acad. Sci. USA*, *79*, 7052-7055 (1982).
194. K. M. Yocom, J. R. Winkler, D. G. Nocera, E. Bordignon, and H. B. Gray, *Chem. Scr.*, *21*, 29-33 (1983).
195. T. Yonetani, *The Enzymes*, Vol. 13, P. D. Boyer, Ed., Academic Press, New York, 1976, pp. 345-361.

Mercury(II)–Thiolate Chemistry and the Mechanism of the Heavy Metal Biosensor MerR

**JEFFREY G. WRIGHT,[†] MICHAEL J. NATAN,[†]
FREDERICK M. MacDONNELL,[†] DIANA M. RALSTON,[§]
and THOMAS V. O'HALLORAN^{†§}**

[†]Department of Chemistry and

*[§]Department of Biochemistry, Molecular Biology, and Cellular
Biology, Northwestern University, Evanston, Illinois*

CONTENTS

I. INTRODUCTION	325
A. Scope of this Chapter	326
B. Background	326
C. Regulation of Gene Expression by Metals	327
D. Metal Ion Sensitivity and Selectivity	328
E. The MerR Protein: An Hg(II)-Sensitive Switch	329
1. Ultrasensitivity to Mercuric Ion	329
2. Metal Ion Selectivity	329
II. STRUCTURAL CHEMISTRY OF MERCURIC–THIOLATE COMPLEXES	331
A. Model Complexes and Scope of Structural Survey	331
B. Primary and Effective Coordination Number	332
1. Definitions	332
2. Thiolate Ligands	334
C. Two-Coordinate Complexes	335
1. Mononuclear Complexes	335
2. Polynuclear Complexes	339
D. Three- and Four-Coordinate Complexes	340
1. Mononuclear Complexes	340
2. Polynuclear Complexes	344

Progress in Inorganic Chemistry: Bioinorganic Chemistry, Vol. 38, Edited by Stephen J. Lippard.

ISBN 0-471-50397-5 © 1990 John Wiley & Sons, Inc.

E. Thioether Complexes	345
F. Statistical Survey of Thiolate-Containing Complexes of Hg(II)	349
G. The Zinc Family Paradox	351
H. EXAFS Characterization of a Hg(Cys) ₃ Binding Site in MerR	352
III. AQUEOUS Hg(II) CHEMISTRY	354
A. Thermodynamics	354
B. Lability of Hg(II)-Thiolate Ligand Complexes	358
IV. ELECTRONIC SPECTROSCOPY OF Hg(II) COMPLEXES	361
V. VIBRATIONAL SPECTROSCOPY OF Hg(SR) _n	366
A. Vibrational Spectroscopy of Hg(II) Halides	368
B. "Linear" Hg(II) Thiolates	369
C. Three- or Four-Coordinate Hg(II) Thiolates	372
VI. ¹⁹⁹ Hg NMR SPECTROSCOPY OF Hg(II)-THIOLATE COMPLEXES	374
A. Solution ¹⁹⁹ Hg NMR	375
B. Solid-State ¹⁹⁹ Hg NMR	379
C. Contributions to the ¹⁹⁹ Hg NMR Chemical Shift	383
D. Shielding Parameters from Solid-State Spectra	384
VII. BIOCHEMISTRY AND SITE-SPECIFIC MUTAGENESIS OF MerR	385
A. Chemical Modification Studies of MerR	387
B. Mutagenesis Studies of MerR	389
C. Impact of Metal Coordination on Mechanism	390
VIII. MOLECULAR BIOLOGY AND MECHANISM OF THE Hg(II)-RESPONSIVE SWITCH	393
A. Background	393
B. Kinetics of Hg(II)-Induced Transcriptional Activation	394
C. Topology of the Transcription Complex	395
D. Hg-MerR-Induced Distortions in DNA Structure	399
E. Overview of the Switching Mechanism	402
IX. SUMMARY	402
ACKNOWLEDGMENTS	403
REFERENCES	404

I. INTRODUCTION

One important example of inorganic molecular recognition is found in the *metalloregulatory* proteins, heavy-metal sensors that mediate metal-responsive gene regulation. These proteins can be differentiated from other metal-containing proteins involved in gene expression by their ability to alter the expression of specific genes in response to changes in metal ion concentration (144). The metalloregulatory proteins characterized to date (Table I) act as heavy-metal ion receptors that bind a specific metal and subsequently undergo some type of structural change that can be communicated to other biopolymers in a genetic control circuit. Physical and inorganic studies of the coordination environment can provide unique insights into the molecular basis of receptor sensitivity and selectivity between heavy metals. The corresponding principles, coupled with the availability of overexpressed proteins, can in turn be applied in the design of metal-specific macrocyclic and chelating ligands, metal ion separation schemes, heavy-metal biosensor devices, and in the development of pharmaceutical

TABLE I
Systems Exhibiting Metal-Responsive Gene Expression

Metal Ion	System	Metalloregulatory Protein	References
<i>Prokaryotes</i>			
Arsenate	Resistance operon		163
Cadmium	Resistance genes		176
	Oxidative stress response		44
Copper	Resistance operon	PcoR	15, 165
Iron	Superoxide dismutase		79
	Uptake regulon	Fur	8
Mercury	Resistance operon	AngR/Taf	166
		MerR	144,185, 200
Molybdenum	Anaerobic respiration		50
	Nitrogenase		98
	Nitrate reductase		96
Tellurium	Resistance operon		100
<i>Eukaryotes</i>			
Iron	Ferritin	IRE-BP	87, 118
	Transferrin receptor	IRE-BP	87, 118
	Respiratory proteins, Cyt-c	HAP1	153
Copper	Metallothionein	ACE1 (CUP2)	68, 93, 203
	Plastocyanin, Cyt-c552		133
Cadmium	Metallothionein		77
	Heat shock response		211
Zinc	Metallothionein	MTF-1	205

agents that capitalize on the differences between metal-responsive gene regulation in microbes and in humans.

One of the best understood metalloregulatory proteins is MerR, an ultrasensitive and specific receptor for mercuric ion. This small, metal-sensing, DNA-binding protein has been purified to homogeneity and shown to act as a switch controlling the expression of mercurial detoxification systems in bacteria. A formidable barrier to understanding the coordination chemistry involved in Hg(II) recognition by the MerR receptor is the absence of well-established relationships between spectroscopic parameters and structural characteristics such as coordination number and geometry in the Hg-thiolate literature.

A. Scope of this Chapter

This chapter focuses on correlating the structural, solution, and spectroscopic properties of mercuric–thiolate complexes in general and incorporates recent models for the mechanism of heavy metal recognition by the MerR receptor. Before the inorganic chemistry of Hg(II) thiolates is addressed, a brief discussion of other members of this recently identified class of metal-activated proteins is provided. Biochemical evidence for the ultrasensitivity of the MerR switch to Hg(II), presented in Section I.D, quantitatively defines recognition in terms of the selectivity for Hg(II) over other soft metal ions. These results are provided at the outset so as to frame a recurring question: What type of coordination environment in MerR allows (a) high binding constants for Hg(II) in the presence of competing cellular thiols; (b) discrimination against other soft metals; and (c) a distinct structural change in protein conformation when the site is occupied? This chapter is a review of mercury thiolate chemistry and does not address sulfide complexes or the interaction of organomercurial species with thiolates but rather focuses on the difficult problem of characterizing Hg–SR complexes with coordination number greater than 2. As will be shown, molecular recognition of mercuric ion by the MerR receptor involves more than simple linear bis-thiolate coordination. This chapter concludes with an overview of the mechanics of Hg–MerR interactions with the macromolecules involved in this metal-responsive switching event.

B. Background

One of the most tantalizing chemical transformations known to ancient practitioners of inorganic chemistry involved roasting of mercuric sulfide ores such as cinnabar to form hydrargyrum or quicksilver (60). As the toxic properties of mercury became more widely appreciated in the middle ages, formulations of the metal and its salts were used in medical applications,

including the treatment of syphilis (120). More recent interest in the chemistry of mercuric ion in biological systems has been stimulated by biochemical studies of the effect of Hg(II) on enzymes and proteins such as metallothioneins (59) and the discovery of specific bacterial processes for Hg(II) detoxification (176, 182, 184, 200).

The chemistry of mercuric ion in a biological medium is dominated by thiolate complexes of low coordination number, yet several other types of coordination environments have been proposed for mercuric complexes of amino acids, proteins, and enzymes. Corresponding small molecule mercuric-thiolate complexes in the solid state frequently exhibit distinct linear geometries with weak but significant secondary bonding interactions. Simple correlations between solid-state structure or stoichiometry with the stereochemistry of solution complexes is complicated by several phenomena. First, complexes of low coordination number tend to form clusters in solution and in the solid state. The barriers to polymerization can be low, and often influenced by the nature of the solvent and the counterion. Second, while the thermodynamics of mercuric thiolate interactions indicate extremely strong bonds, these complexes undergo rapid ligand exchange, complicating attempts to correlate features of NMR spectra with the structure of the ions in solution. Further complicating the elucidation of the solution chemistry of these complexes is the dearth of well-characterized mononuclear mercury-thiolate complexes with coordination number greater than 2. As a result, assignments based on electronic, vibrational, and NMR data are frequently controversial. Recent results correlating solid-state and solution spectroscopy for crystallographically characterized complexes can, in some cases, resolve these controversies. Further progress in elucidating the nature of mercuric ion interactions with biopolymers such as MerR requires an expansion of the structural and spectroscopic data base of three- and four-coordinate mercuric thiolate complexes.

A complementary approach to probing the Hg(II) coordination environment in biopolymers such as MerR involves mutagenesis of amino acid residues involved in metal ion coordination. A great deal of progress has been made in this area in the last three years and these results will be compared to those obtained from physical methods described above. The feasibility of developing additional spectroscopic techniques as probes of mercuric ion coordination environments in small molecules, proteins and solid-state complexes are discussed in Sections IV-VI.

C. Regulation of Gene Expression by Metals

Inorganic stimuli can induce a number of biological responses that are initiated at the genetic level. The molecular mechanisms involved in these

processes are being addressed by using a combination of approaches from the fields of inorganic chemistry, biochemistry, and molecular biology. In the last few years, several members of the class of proteins responsible for regulating metal response have been isolated from both prokaryotic and eukaryotic organisms. Table I, updated from Ref. 159, is a brief list of systems in which metal-responsive gene expression has been demonstrated. Detailed overviews of systems exhibiting metal-responsive gene expression can be found elsewhere (144, 160). Of the systems where metalloregulatory proteins have been isolated, those regulating bacterial mercuric ion resistance (MerR), bacterial iron uptake (Fur), and yeast metallothionein expression (ACE1), are the best understood at the molecular level.

D. Metal Ion Sensitivity and Selectivity

Although metalloregulatory proteins can alter the expression of a target gene in response to more than one type of metal ion, each protein exhibits a different level of metal ion sensitivity and selectivity. The DNA-binding activity of the Fur protein, a repressor of iron uptake genes in bacteria, may be induced not only by Fe(II), but also by Cd(II), Co(II), Cu(II), Mn(II), and Zn(II) (7). Similarly, DNA-binding and transcriptional activation by the ACE1 protein, a regulator of metallothionein genes in yeast, may be induced by Cu(I), Cu(II), and Ag(I) (68). Some of these additional metal ions are called gratuitous inducers in order to distinguish them from the physiologically relevant metal ion, particularly when they are not processed by the gene products that they induce. For example, Fur is activated to bind DNA by the six divalent metal ions listed above but Fe(II) is the primary effector. Cd(II), Cu(II), and Zn(II) do not generally cause repression of iron uptake *in vivo*, and Mn(II) results in the reduction of iron uptake to a level two-thirds of that caused by Fe(II). Similarly, Cu(I) appears to be the primary effector for ACE1 (68). Metalloregulatory proteins may discriminate between metals by using protein side chains to create a coordination environment optimized for a specific metal ion. Alternatively, they may recognize specific complexes of metal ions with small molecules (e.g., iron citrate) instead of binding the metal ion directly; however, this mechanism has not been demonstrated in any of the above systems.

While more than one metal may activate these metalloregulatory proteins, it is important to consider the relative concentration that induces half-maximal activity in each case. As seen below, a receptor-metal ion binding constant may vary over several orders of magnitude depending on the metal, thus providing a thermodynamic basis for efficient discrimination between metal ions with similar properties.

E. The MerR Protein: An Hg(II)-Sensitive Switch

The logic behind the regulation of bacterial detoxification of mercuric ion is simple. In the absence of mercuric ion, the cell does not require that Hg(II) detoxification proteins be present. Thus, these proteins, including mercuric ion reductase, are not synthesized and the genes encoding the proteins are said to be repressed. When Hg(II) concentrations exceed a threshold level (10^{-8} M) the *merTPAD* genes, which encode the detoxification machinery, are rapidly transcribed and subsequently translated into proteins. The change in Hg(II) concentration effectively activates a molecular switch (MerR), turning on transcription of the mercury resistance proteins.

1. Ultrasensitivity to Mercuric Ion

The switching activity of MerR for the stimulation of resistance genes has been shown to be responsive to submicromolar concentrations of mercuric ion but requires higher concentrations of cadmium (159). Using purified protein and the method of abortive transcriptional initiation (130), the metal ion sensitivity and selectivity of MerR has been further delineated. By quantitating levels of transcription in response to a range of 10^{-12} – 10^{-2} M HgCl₂, the half-maximal effective Hg(II) concentration for *in vitro* activation has been determined to be 1.0×10^{-8} M, making MerR an exquisitely sensitive metal sensor (157). This result is even more striking considering that MerR is able to detect these trace levels of Hg(II) in the presence of 10^{-3} M dithiothreitol, a chelating dithiol ligand. In addition to detecting very low mercuric ion concentrations MerR demonstrates ultrasensitivity, shifting from 10 to 90% of transcriptional activation in response to a small increase in Hg(II). This behavior is evident by the apparent Hill slope (n_{app}) of 2.3(0.4) of the transcriptional response to Hg(II) concentration (Fig. 1), in contrast to the expected $n_{app} = 1$ observed for proteins obeying Michaelis–Menten kinetics. The molecular basis of this type of cooperative (or threshold) effect is briefly addressed in Section VIII and elsewhere (157).

2. Metal Ion Selectivity

The ability of metal ions other than Hg(II) to stimulate MerR activation of transcription has been investigated. In addition to Hg(II), varying degrees of activation are observed in response to Cd(II), Zn(II), and Au(I), as shown in Fig. 2 (157). In each case, much higher concentrations of metal ions are necessary for induction, and levels of transcription are never as

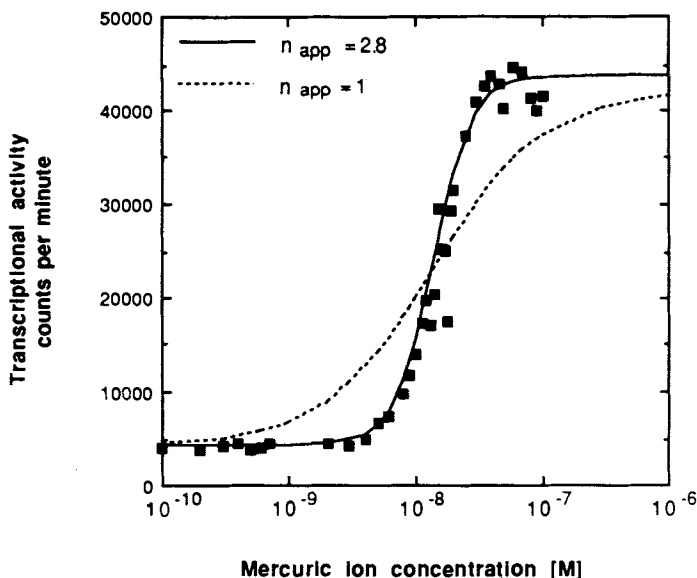


Figure 1. Transcriptional activity of the mercuric ion resistance genes in response to Hg(II) concentration. Transcription is measured in counts per minute of radioactive mRNA (■ = data). Data were fit by a nonlinear least-squares program and curves were generated with apparent Hill slopes (n_{app}) of 1 (dashed line) and 2.8 (solid line).

high as in the presence of Hg(II). Although MerR responds to other metal ions, induction of the *mer* operon does not confer resistance to these metals. Induction by Cd(II), Zn(II), and Au(I) is thus gratuitous. Transcription is also induced by Au(III), although this response may result from reduction to Au(I). It is of interest that extracts of mercury-resistant bacteria have been reported to cause the reduction of Ag(I) and Au(III) to colloidal metal (185). It was not demonstrated, however, whether this activity was a property of cell lysates or specifically of *mer* operon gene products, since mercury-sensitive bacteria were not analyzed. Thus, in the case of MerR, discrimination between the signal, Hg(II), and gratuitous inducers such as Cd(II) is achieved by a receptor site that has a much higher binding constant for Hg(II) and which therefore activates transcription at much lower concentrations of Hg(II) than Cd(II). The coordination environment responsible for the combined sensitivity and selectivity can be addressed by physical and inorganic studies of Hg(II) and Cd(II) forms of the MerR protein described below.

As with the induction of metallothionein (58, 103, 125, 193), there is a correlation between physicochemical properties of the metal ion, such as

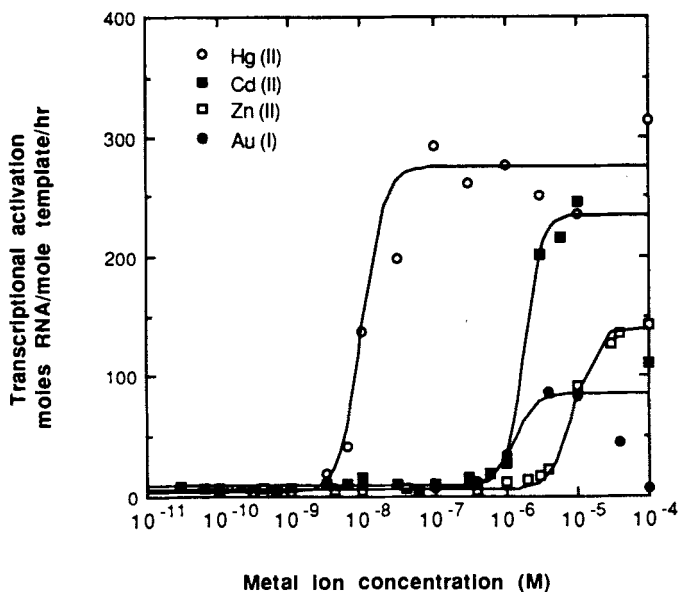


Figure 2. Transcriptional activation of the mercuric ion resistance genes by MerR in response to the concentration of various metal ions. Transcriptional activity is measured as moles of RNA produced per mole of DNA template per hour. Curves are approximate fits of responsiveness data (157).

the Pearson–Mawby softness parameter, σ_p (1), and its ability to induce MerR transcriptional activation. In the latter case, not all soft metals activate transcription and a wide range of maximal activities is observed among those that do. The high degree of Hg(II) sensitivity and discrimination exhibited by the coordination environment of the MerR receptor must have a basis in specific structural preferences and solution chemistry of Hg(II). As is shown below, the coordination chemistry of this d^{10} metal ion is diverse and distinct from the other d^{10} ions in the Zn triad.

II. STRUCTURAL CHEMISTRY OF MERCURIC-THIOLATE COMPLEXES

A. Model Complexes and Scope of Structural Survey

Structural and spectroscopic characterization of simple mercuric coordination compounds containing the ligands available in biological systems (i.e., thiolate, thioether, carboxylate, amine, aquo, and chloride) is crucial

to elucidating and reconstructing the metal-binding sensitivity and selectivity of these various proteins. As elaborated in Section III, the thiolate groups of cysteine side chains in enzymes and polypeptides are the principal biological ligands for Hg(II). Detailed structural knowledge of model complexes facilitates systematic correlation of spectroscopic data with coordination environments in biopolymers. A number of previously characterized bis-thiolate–Hg(II) complexes provide a broad base of structural information. Although there are a large number of HgL₂ complexes that exhibit additional Hg–L interactions at longer distances, mononuclear Hg–thiolate complexes with coordination number >2 and mixed-ligand donor types are rare. Inconsistent use of the term “coordination number” frequently results in confusion in the literature, and for this reason a definition consistent with structural, chemical and spectroscopic properties is outlined here. This section focuses on simple mercuric coordination complexes containing at least one thiolate. Structures with sulfide, dithiocarbamate, dithiolene, or the general R(=S)S[−] ligand type (52) are not examined here. Mercuric–halide complexes are not discussed in detail, except when found with thiols, since the structural chemistry of mercuric halides has been thoroughly discussed (6, 57, 167, 204).

B. Primary and Effective Coordination Number

1. Definitions

Mercuric–thiolate complexes are well known for their unusual coordination environments and predominantly exhibit geometries that are variations on a linear two-coordinate theme. Coordination number four is typically found with bridging thiolates (54). Solid-state structural studies commonly show that additional ligands are found at distances *longer* than would be expected for covalent bonding to mercuric ion, but *shorter* than the sum of their respective van der Waals radii. Frequently, these “long” interactions do not fit simple geometric descriptions and are commonly referred to as secondary bonds. Grdenić proposed two types of coordination number for such complexes (72):

1. The *primary (or characteristic) coordination number*, indicating mercury–ligand bond distances appropriate for the sum of their respective covalent radii.
2. The *effective coordination number*, indicating all mercury–ligand interactions that are less than the sum of their respective van der Waals radii, or simply the total number of primary and secondary bonds.

A simple shorthand notation for referring to the unusually complex coordination of Hg(II) was also suggested by Grdenić. A typical example, Hg(SMe)₂ (25), is denoted as a [2 + 3] complex indicating two short, primary bonds and three longer secondary bonding interactions from adjacent molecules, yielding an effective coordination number of five. This notation provides a simple, efficient way to describe the local Hg(II) coordination environment.

The sums of the respective covalent and van der Waals radii for Hg(II) and relevant donor atoms are given in Table II. An additional 0.2 Å is added to the bridging sulfur covalent radii compared to terminal sulfur radii, as suggested by Bowmaker et al. (23). Although several values for the van der Waals radius of Hg(II) (29, 52, 12, 147) have been reported, the most recent work by Canty and Deacon proposed a value of 1.73 Å with an acceptable range from 1.70 to 2.00 Å, which is used in this chapter (29).

Examination of Table II shows that Hg-L secondary bonding distances typically fall within 1 Å of the covalent bond length. Secondary bonding interactions are important in the solid state and the effective coordination number is often successfully used to explain physical and spectroscopic data (57). In solution, the effective coordination number is less useful as the solvent can play a large role in altering existing secondary bonds. Solvent coordination can also contribute directly to secondary bonding interactions (151). The primary coordination number itself is difficult to determine for Hg(II) complexes in solution due to dissociation processes, ligand exchange, and cluster formation. In X-ray crystallographic studies,

TABLE II
Hg(II)-Ligand Bond Lengths(Å) from Summation of Known Covalent and van der Waals Radii

Ligand ^a	Radii		Hg(II) Covalent	Hg(II) van der Waals
	(Covalent;	van der Waals)(Å)	(1.48 Å) ^b Hg-L(Å)	(1.73 Å) ^c Hg-L(Å)
S	(1.02;	1.80) ^d	2.50	3.53
S*	(1.22; ^e	1.80) ^d	2.70	3.53
O	(0.73;	1.50) ^d	2.21	3.23
N	(0.75;	1.55) ^d	2.23	3.28
Cl	(0.99; ^d	1.73) ^b	2.47	3.43

^aAn * denotes a bridging sulfur.

^bReference 142;

^cReference 29.

^dReference 94.

^eReference 23.

the coordination environment is precisely defined, but shorthand terminology (i.e., bis-coordinate, trigonal, four-coordinate) is frequently carried over from the structural literature into the spectroscopic, chemical, and biological literature without discrimination between primary and secondary bonding. For simplicity, it is preferable to have a single definition of coordination number that is consistent with the physical and chemical properties of the mercuric complexes. As will be shown throughout the course of this chapter, the categorization of coordination based on the sum of the covalent radii consistently delineates the chemical and spectroscopic properties of each group. Thus, throughout this chapter the term coordination number refers to the number of Hg–L bonds that have distances less than or equal to the sum of the covalent radii. Adoption of this convention in the Hg(II) literature may help avoid problematic assignments such as those found for NMR spectra for “four-coordinate” Hg(O₂CCH₃)₂ (78). The crystal structure shows two Hg–O bonds with an angle of 171° and three longer bonds outside the sum of the covalent radii ([2 + 3] coordination) (4), but the NMR spectrum (78) was interpreted as arising from a four-coordinate complex. Based on the Grdenić convention, Hg(O₂CCH₃)₂ is best described as a linear bis-coordinate complex with three secondary bonding interactions. As seen in Section VI. B, this distinction is critical to understanding such spectra.

2. Thiolate Ligands

Thiolate ligands (RS⁻) can be classified as pseudohalides and are usually found in μ_2 -bridging or terminal coordination. Anionic sulfur is a good donor and is easily polarizable, which accounts for its affinity toward large, soft metal ions. The bulk and electronic nature of the R group is easily varied and can exhibit strong effects on the coordination environment. Recent reviews by Dance (54) and Blower and Dilworth (19) on the structural chemistry of metal–thiolate complexes demonstrate the versatility of this class of ligand.

The Hg(II) chemistry of thiolate ligands is dominated by low coordination numbers. The Hg(SR)₂ compounds with MeS⁻ and EtS⁻ prefer linear coordination. Unexpectedly, the bis *n*-BuS⁻ and *t*-BuS⁻ complexes favor a tetrahedral polymeric chain structure, making simple correlations with respect to ligand bulk difficult to rationalize. The complex [Et₄N][Hg(S-*t*-Bu)₃] has a trigonal planar structure (202), whereas the stoichiometrically identical [Et₄N][Hg(SMe)₃] (23) is dimeric with tetrahedral coordination. These structures are easily rationalized on the basis of steric arguments, but other less tangible effects also have considerable influence on the coordination geometry. With the [Hg(SPh)₃]⁻ anion, replacement of the

[Bu₄N]⁺ cation with [Me₄N]⁺ induces formation of the dimeric tetrahedral structure preferentially over the mononuclear trigonal complex (54).

C. Two-Coordinate Complexes

Coordination number (CN) 2 is found in Group IB (+1) ions, and is common for Hg(II). Indeed, two is the most common coordination number for Hg(II), and this phenomenon has been attributed to the ease of forming *d-s-p* hybrid orbitals (61, 146) and/or to the minimization of metal *d* orbital overlap with ligand nonbonding *p* orbitals (190), with relativistic considerations (156) playing an important role in either scheme (discussed in greater detail Section II.G). A number of two-coordinate mercuric-thiolate complexes have been structurally characterized and the pertinent metrical data for both primary and secondary bonding has been summarized in Table III. [Hg(saccharinate)₂(bipy)] and Hg(O₂CCH₃)₂ are the only complexes listed with no sulfur donor ligands. The zwitterionic [2 + 2] [Hg(saccharinate)₂(bipy)] has primary Hg-N bonds at 2.14 and 2.12 Å, and secondary Hg-N interactions at 2.33 and 2.39 Å (90). Similarly, the neutral [2 + 3] Hg(O₂CCH₃)₂ has short primary bonds at 2.06 and 2.09 Å, and secondary bonds at 2.71, 2.75, and 2.76 Å (4). These examples of primary Hg-N and Hg-O bonding are listed for comparison, since there are few such examples in the presence of thiols.

1. Mononuclear Complexes

Mononuclear complexes with a CN = 2 exhibit covalent bond lengths between 2.316 and 2.361 Å and angles in the range of 180.0–167.4° (see Table III). It is interesting to note that all the complexes solved to date have at least one weak secondary bonding interaction.

Simple correlations between the number and strength of secondary bonding interactions, the primary bond distances, and the distortion of the primary S-Hg-S bond angle do exist. Ideally, [2 + 1] and [2 + 2] complexes would have the greatest deviations from linearity (trigonal and tetrahedral distortions), while the [2 + 3] and [2 + 4] would remain linear, since the primary thiolate ligands could occupy short axial positions in flattened trigonal bipyramidal and octahedral structures. Primary bond lengths are expected to increase with the number of secondary bonding interactions. This trend is readily observed in the following series of complexes: the [2 + 1] [Hg(SC₅H₉NH(CH₃))₂][ClO₄]₂ (10) with bond lengths at 2.329 Å and S-Hg-S bond angle of 176.9°; [2 + 2][Hg(penH)₂Cl₂ (37) at 2.335 Å and 171.6°; [2 + 3] Hg(SCH₃)₂ (25) at 2.36(5) Å and 180°; and finally [2

TABLE III
Comparison of Selected Distances and Angles in Two-Coordinate Mercuric-Thiolate Compounds

Compound ^a	Primary Coordination Number ^b	Secondary Bonding Interactions ^c	Ligand ^d	Hg-L(Å)	L-Hg-L(°) ^e	Reference
1. [Hg(cys)cysH]Cl·0.5H ₂ O	2	1	1 S	2.355(3)	169.8(1)°	189
			1 S	2.329(5)		
2. [Hg(SC ₃ H ₆ NH(CH ₃)) ₂]·[ClO ₄] ₂	2	1	1 Cl'	3.232(5)	176.9(1)°	10
			2 S	2.329(4)		
			1 O'	3.08(2)		
3. 2[μ ₃ -Cl(HgpenH) ₃]·3(μ ₂ -Cl)·2(H ₃ O)·(H ₂ O·Cl) ₃ (three equivalent Hg atoms)	2	1	1 S	2.32(2)	167.2(9)	21
			1 Cl	2.371(1)	81.6(5)	
			1 Cl'	3.06(2)		
4. [Hg(saccharinate) ₂ (bipy)]	2	2	2 N	2.141(4)	135.4(2)	90
				2.120(4)	111.1(1)	
			2 N'	2.393(3)	70.7(1)	
				2.328(4)	102.7(2)	
					98.5(1)	
5. [Hg(O ₂ CCH ₃) ₂]	2	3	1 O	2.06(3)	176	4
			1 O	2.09(3)	173	
			1 O'	2.71(3)	112	
			1 O'	2.76(3)	105	
			1 O'	2.75(3)	81	
5. [Hg(penH) ₂]Cl ₂ ·H ₂ O	2	2	1 S	2.335(5)	171.6(1)°	37
			1 S	2.357(4)		
			1 Cl'	2.850(5)		
			1 Cl'	3.323(5)		
					70	
6. [Hg(SSi(O- <i>t</i> -Bu) ₃) ₂]	2	2	2 S	2.316(2)	180.0°	207
			2 O'	2.878(4)		
7. [Hg(SCH ₃) ₂]	2	3	2 S	2.36(5)	180.0(25)°	25
			3 S'	3.25(5)	~90	
8. [Hg(SC ₂ H ₅) ₂]	2	4	2 S	2.45(6)	180°	24
				2.36(2) ^f		
			2 S'	3.53	~90	
			2 S'	3.55	~90	
9. [Hg(SC ₇ H ₅ O ₂)]·C ₄ H ₈ O ₂	2	4	2 S	2.361(7)	180°	5
			2 S'	3.420(7)	88.9(2)	
			2 O'	3.08(2)		
10. {Hg(cysH)Cl ₂ } _n (polymeric chain)	2	2	1 μ ₂ -S	2.490(4)	136.0(1)°	189
			1 μ ₂ -S	2.453(4)	103.8(1)	
			1 Cl'	2.582(4)	91.4	
			1 Cl'	2.645(5)	96.3(1)	
11. {Hg(S(CH ₂) ₃ NH(CH ₃) ₂)Cl ₂ } _n (polymeric chain)	2	2	1 μ ₂ -S	2.464(6)	130.2(3)°	39
			1 μ ₂ -S	2.471(6)	112.5(2)	
			1 Cl'	2.513(6)	99.0(2)	
			1 Cl'	2.634(5)	102.3(2)	
					104.1(3)	
12. [Hg ₄ (S- <i>t</i> -Bu) ₄ (py) ₂ Cl ₄] (tetramer with two independent Hg sites)	2	2	Hg1			32
			1 μ ₂ -S	2.39(1)	159.9(3)°	
			1 μ ₂ -S	2.38(1)	104.2(3)	
			1 Cl'	2.70(1)	92.3(4)	
			1 Cl'	2.81(1)	96.5(3)	

TABLE III (Continued)
Comparison of Selected Distances and Angles in Two-Coordinate Mercuric-Thiolate Compounds

Compound ^a	Primary Coordination Number ^b	Secondary Bonding Interactions ^c	Ligand ^d	Hg-L(Å)	L-Hg-L(°) ^e	Reference
13. [Hg ₄ S- <i>t</i> -Bu] ₄ (picoline) ₂ Cl ₄] (tetramer with two independent Hg sites)	3	1	Hg2			
			1 μ ₂ -S	2.509(9)	127.7(3)*	33
			2 μ ₂ -S	2.488(7)	98.4(5)	
			1 Cl	2.45(1)	115.7(3)	
1 N'	2.44(3)	98.0(7)				
13. [Hg ₄ S- <i>t</i> -Bu] ₄ (picoline) ₂ Cl ₄] (tetramer with two independent Hg sites)	2	2	Hg1			33
			1 μ ₂ -S	2.395(8)	158.1(3)*	
			1 μ ₂ -S	2.379(8)	89.2(3)	
			1 Cl'	2.748(8)	105.9(3)	
13. [Hg ₄ S- <i>t</i> -Bu] ₄ (picoline) ₂ Cl ₄] (tetramer with two independent Hg sites)	3	1	Hg2			33
			1 μ ₂ -S	2.505(8)	130.9(2)*	
			1 μ ₂ -S	2.501(8)	113.2(3)	
			1 Cl	2.479(10)	112.8(3)	
14. {Hg(SMe)(O ₂ CCH ₃) _n } (polymeric sheet)	2	3	1 N'	2.39(2)	95.0(6)	32
			1 μ ₂ -S	2.387(5)	159.0(2)*	
			1 μ ₂ -S	2.405(5)	97.0(3)	
			1 O'	2.42(2)	100.9(4)	
14. {Hg(SMe)(O ₂ CCH ₃) _n } (polymeric sheet)	2	3	1 O'	2.82(2)	99.0(3)	32
			1 O'	2.70(2)	92.2(4)	
			1 μ ₂ -S	2.471(5)	143.0(2)*	
			1 μ ₂ -S	2.432(5)	110.8(4)	
14. {Hg(SMe)(O ₂ CCH ₃) _n } (polymeric chain)	2	3	1 O'	2.43(2)	90.6(4)	32
			1 N'	2.432(5)	95.4(5)	
			1 O'	2.69(2)	101.0(4)	
			1 O'	2.69(2)	101.0(4)	
16. {Hg(SMe)(O ₂ CCH ₃) (γ-picoline) _n } (two independent polymeric strands)	2	3	Hg1			33
			1 μ ₂ -S	2.471(7)	141.3(2)*	
			1 μ ₂ -S	2.414(7)	86.3(5)	
			1 O'	2.44(2)	111.6(5)	
16. {Hg(SMe)(O ₂ CCH ₃) (γ-picoline) _n } (two independent polymeric strands)	2	3	1 N'	2.49(2)	88.2(5)	33
			1 O'	2.66(2)	128.1(6)	
			Hg2			
			1 μ ₂ -S	2.459(7)	136.1(2)*	
16. {Hg(SMe)(O ₂ CCH ₃) (γ-picoline) _n } (two independent polymeric strands)	2	3	1 μ ₂ -S	2.473(6)	107.8(4)	33
			1 O'	2.37(1)	111.5(4)	
			1 N'	2.41(2)	87.1(4)	
			1 O'	2.80(2)	135.3(6)	
17. [Hg(O ₂ CCH ₃) ₂ (SC ₆ H ₅)] (two independent Hg atoms in a polymeric chain)	2	3	Hg1			179
			1 μ ₂ -S	2.445(3)	143.7(1)*	
			1 μ ₂ -S	2.481(3)		
			1 O'	2.378(8)		
17. [Hg(O ₂ CCH ₃) ₂ (SC ₆ H ₅)] (two independent Hg atoms in a polymeric chain)	2	4	1 O'	2.551(10)		179
			1 O'	2.569(8)		
			Hg2			
			1 μ ₂ -S	2.403(3)	162.4(1)*	
17. [Hg(O ₂ CCH ₃) ₂ (SC ₆ H ₅)] (two independent Hg atoms in a polymeric chain)	2	4	1 μ ₂ -S	2.410(3)	104.1(2)	179
			1 O'	2.483(9)	93.4(2)	
			1 O'	2.514(8)	51.9(3)	
			1 O'	2.852(9)		
17. [Hg(O ₂ CCH ₃) ₂ (SC ₆ H ₅)] (two independent Hg atoms in a polymeric chain)	2	4	1 O'	2.873(8)		179

TABLE III (Continued)
Comparison of Selected Distances and Angles in Two-Coordinate Mercuric-Thiolate Compounds

Compound ^a	Primary Coordination Number ^b	Secondary Bonding Interactions ^c	Ligand ^d	Hg-L(Å)	L-Hg-L(°) ^e	Reference
18. {Hg(S- <i>i</i> -Pr)Cl} _n (polymeric chain with two independent Hg sites)	2	4	Hg1			16
			2 μ ₂ -S	2.378(2)	178.2(2)*	
			2 Cl'	2.985(8)	97.2(2)	
	4	0	Hg2			
			2 μ ₂ -S	2.537(6)	119.5(2)*	
			2 μ ₂ -Cl	2.534(8)	115.3(2)	
					100.1(2)	
					111.3(2)	
19. {Hg(S- <i>i</i> -Pr)(O ₂ CCH ₃) _n (polymeric chain)	2	4	1 μ ₂ -S	2.41	156.2*	155
			1 μ ₂ -S	2.40	96.7	
			1 O'	2.42	81.6	
			2 O'	2.76	100.1	
			1 O'	3.14	88.7	
20. {Hg(S- <i>t</i> -Bu)(O ₂ CCH ₃) _n (polymeric chain)	2	4	1 μ ₂ -S	2.40	157.0*	155
			1 μ ₂ -S	2.42	94.1	
			1 O'	2.47	80.3	
			1 O'	2.86	96.8	
			1 O'	2.78	89.5	
			1 O'	2.98	107.8	

^aThe abbreviation for the penicillamine zwitterion, ⁻SC(CH₃)₂CH(NH₃⁺)COO⁻ is penH. (208)

^bPrimary coordination number indicating the number of ligands that fall within a reasonable range of the normal sum of the appropriate covalent radii.

^cSecondary bonding interaction indicates the total number of ligands around the mercuric ion that are bound at a distance greater than the sum of the covalent radii but less than or equal to the sum of the appropriate van der Waals radii.

^d(') indicates secondary bonding interaction.

^e(*) indicates S-Hg-S bond angles for primary Hg-S bonds from independent ligands.

^fEXAFS data (Refs. 191, 209).

+ 4] Hg(C₇H₅O₂S)₂·C₄H₈O₂ (5) at 2.361 Å and 180°. Exceptions, however, are not uncommon. For example, the [2 + 2] [Hg(SSi(O-*t*-Bu)₃)₂] complex (207) (2.316 Å and 180°) has the shortest reported Hg-S bond length, and no distortion of the S-Hg-S angle. Factors such as the unusual Si R group and the chelate effect of the intramolecular ether oxygen atoms weakly bound to the Hg(II) center (Hg-O' 2.88 Å) may explain the unusually short Hg-S bond; however, the lack of distortion in the S-Hg-S angle is more subtle, and possibly steric in nature. The [2 + 2] complex of penicillamine, [Hg(penH)₂]Cl₂ (37) and the [2 + 1] complex [Hg(cys)(cysH)]Cl (189), have primary S-Hg-S angles of 171.6 and 169.8°, respectively. Apparently, the single long Hg-Cl (3.23 Å) secondary bond in [Hg(cys)(cysH)]Cl effects a greater distortion towards trigonal geometry than the two bridging

chlorides (one at the same distance of 3.23 Å, the other significantly shorter at 2.85 Å) towards tetrahedral geometry. Again, it is possible that the steric bulk present in the penicillamine ligand could restrain the S–Hg–S angle. These anomalies demonstrate the rather large steric effect inherent with a soft Hg(II) d^{10} ion and the practical consideration that must be given to any attempt to correlate secondary bonding interactions with bond lengths and angles.

The compound $\text{Hg}(\text{SC}_2\text{H}_5)_2$ has been deliberately left out of this discussion, since there are questions concerning the accuracy of the reported crystallographic data (24). Recent EXAFS data best fits a two-coordinate sulfur ligation with bond distances at 2.36(2) Å (191, 209). These data are consistent with predictions based on the other two-coordinate complexes, whereas the crystallographic data give a Hg–S bond distance of 2.45(6) Å (24). X-ray powder diffraction data, when compared to the powder diffraction pattern calculated from the crystallographic data, also suggest the crystal structure data is incorrect (123).

2. Polynuclear Complexes

Syntheses of 1:1 Hg(SR) complexes invariably lead to polymeric chains or small cluster structures. This class is the most common found within the scope of this chapter and a dozen such structurally characterized compounds are listed in Table III. The general polymeric formula, $\{\text{Hg}(\text{SR})\text{L}_x\}_n$ (where L = acetate, chloride, and/or pyridine bases; $x = 1-3$), indicates the wide selection of mixed-ligand coordination environments accessible. The structure consists of $(-\text{Hg}-\text{S}-)_n$ chains, often cross-linked into sheets by secondary bonding to acetates or halide groups bridging adjacent mercuries. Primary Hg–S bonds are slightly longer than in the mononuclear two-coordinate complexes ($\text{Hg}-\text{S}_{\text{av}} = 2.419$ vs. 2.339 Å, respectively). These compounds often crystallize with two independent Hg sites (see Table III), making spectral assignments more difficult, if not impossible.

The mercuric coordination environment is highly distorted with S–Hg–S primary bond angles ranging from 178.2° to 130.2°; Hg–S primary bonds are usually asymmetric with one bond $\sim 0.01-0.06$ Å longer than the other (Table III). Secondary bonding interactions play a more noticeable role in stabilizing the cationic Hg(II) center. Whereas mononuclear $\text{Hg}(\text{SR})_2$ have average Hg–Cl' and Hg–O' secondary bonds at 3.05 and 3.02 Å, respectively, the polymeric $\{\text{Hg}(\text{SR})\}_x$ average considerably shorter secondary bonds at 2.83 Å (Hg–Cl'), 2.64 Å (Hg–O'), and 2.44 Å (Hg–N') (Table III). Increased secondary bonding interactions and asymmetric primary coordination are directly related to the high S–Hg–S angular distortion,

as seen in $\{\text{Hg}(\text{SMe})(\text{O}_2\text{CCH}_3)(\text{py})\}_n$, which has [2 + 3] mercuric coordination (32) and a S–Hg–S angle of 143° . These distortions, unlike the mononuclear bis complexes, do not behave in any predictable fashion. Complexes such as the [2 + 1] $\{\text{Hg}(i\text{-PrS})\text{Cl}\}_n$ (16), with linear S–Hg–S at 178° , are less distorted than [2 + 3] and [2 + 4] complexes.

D. Three- and Four-Coordinate Complexes

Unlike the neutral 1:1 $\text{Hg}(\text{SR})\text{L}_x$ polymeric compounds and 1:2 $\text{Hg}(\text{SR})_2\text{L}_x$ linear complexes (where L is a nonthiolate ligand), anionic $[\text{Hg}(\text{SR})_{3-4}]^{n-}$ complexes bind Hg(II) in a primary three- or four-coordinate environment, usually with no secondary bonding interactions. A large stoichiometric excess of thiolate ligands apparently overcomes the d – s – p hybrid orbital rearrangement energy allowing more $6p$ participation and stabilization (see Section II.G). The resulting four-coordinate complexes with exclusive thiolate coordination are much like the corresponding cadmium and zinc complexes (52, 139, 187, 194, 196). The Hg(II) center also has a considerable three-coordinate chemistry in solution and the solid state, as determined by IR, Raman, NMR, and X-ray crystallography and discussed throughout this chapter. This structural motif was proposed for the coordination of Hg(II) to the Tn501 MerR metalloprotein (202, 209). A similar site was proposed for the *Bacillus* MerR protein based on site-specific mutagenesis results. (83).

1. Mononuclear Complexes

Table IV contains a summary of the structural data for relevant three- and four-coordinate Hg(II) complexes. These complexes are important as models for the higher coordination environment currently postulated in MerR, which was invoked to explain its high affinity for Hg(II) in a buffer containing excess thiol (144). Only two mononuclear three-coordinate Hg–thiolate complexes have been structurally characterized to date. $[n\text{-Bu}_4\text{N}][\text{Hg}(\text{SC}_6\text{H}_5)_3]$ (45) (Fig. 3) is a distorted trigonal planar complex with two short Hg–S bonds at 2.41 and 2.43 Å and a third longer bond at 2.51 Å. The largest angular deviation from 120° occurs between the two shorter bonds (S–Hg–S of 137°) showing a significant distortion towards linear geometry; however, all Hg–S bond lengths are within the expected covalent bonding distance. The second complex, $[\text{Et}_4\text{N}][\text{Hg}(\text{S}-t\text{-Bu})_3]$ (202) (Fig. 4), is closer to the idealized trigonal planar geometry with the largest S–Hg–S angle at 121.2° and bond distances (2.438, 2.436, and 2.451 Å) fall into narrow range with no distinctly long or short bonds. This structure is a particularly valuable model complex because the alkylthiolate ligands

TABLE IV
Comparison of Selected Distances and Angles in Three- and Four-Coordination Mercuric-Thiolate

Compound	Primary Coordination Number ^d	Secondary Bonding Interactions ^b	Ligand ^{c,d}	Hg-L(Å)	L-Hg-L(°)	Reference
[Et ₄ N][Hg(S- <i>t</i> -Bu) ₃]	3	0	1 S 1 S 1 S	2.438(1) 2.451(1) 2.436(1)	121.24(4) 120.85(4) 117.90(4)	202
[<i>n</i> -Bu ₄ N][Hg(SC ₆ H ₅) ₃]	3	0	1 S 1 S 1 S	2.507(3) 2.407(3) 2.431(3)	120.0(1) 102.9(1) 137.1(1)	45
Hg(II)-substituted poplar plastocyanin	3	1	1 His 1 His 1 Cys	2.34(5) 2.25(3) ^e 2.36(5) 2.25(3) ^e 2.38(5) 2.32(3) ^e	100 133 119 81 112 101	46
[Me ₄ N] ₂ [Hg(<i>p</i> -SC ₆ H ₄ Cl) ₄]	4	0	1 Met' 2 S 2 S	3.02(5) 2.537(1) 2.552(1)	119.79(6) 114.43(7) 109.84(4) 101.76(4)	43
[Et ₄ N] ₂ [Hg(S ₆) ₂]	4	0	1 S 1 S 1 S 1 S	2.505(5) 2.606(8) 2.517(6) 2.527(5)	117.0(2) 109.2(2) 99.6(2) 109.6(2)	138
[Ph ₄ P] ₂ [Hg(S ₄) ₂]	4	0	1 S 1 S 1 S 1 S	2.547(4) 2.538(4) 2.553(5) 2.564(4)	124.4(2) 119.3(1) 113.0(1) 109.4(1) 96.4(1) 96.1(1)	139
[Ph ₄ P] ₂ [Hg ₃ (SCH ₂ CH ₂ S) ₄]	4	0	Hg1 2 μ ₂ -S 2 μ ₂ -S	2.563(2) 2.545(2)	101.1(3) 115.0(1) 116.0(1) 107.6(1)	85
	2	2	2 Hg* 2 S 2 S'	2.371(2) 2.864(2)	159.0(1) 85.6(1) 87.5(1) 107.6(1)	
[Et ₄ N] ₂ [Hg ₂ (SMc) ₆] (two equivalent Hg sites)	4	0	2 Hg* 1 S 1 S 1 μ ₂ -S 1 μ ₂ -S	2.438(2) 2.473(2) 2.629(2) 2.706(2)	121.87(7) 116.09(7) 106.98(6) 104.94(6) 108.68(7) 94.27(5)	23
{Hg(S- <i>t</i> -Bu) ₂ } _n (polymeric chain)	4	0	2 μ ₂ -S 2 μ ₂ -S	2.59(2) 2.66(2)	121(1) 90(1) 87(1)	114

TABLE IV (Continued)
Comparison of Selected Distances and Angles in Three- and Four-Coordination Mercuric-Thiolate

Compound	Primary Coordination Number ^a	Secondary Bonding Interaction ^b	Ligand ^{c,d}	Hg-L(Å)	L-Hg-L(°)	Reference
{Hg(S- <i>n</i> -Bu) ₂ } _n (polymeric chain)	4	0	Hg1			178
			1 μ ₂ -S	2.482(5)	122.2(1)	
			1 μ ₂ -S	2.552(4)	114.5(2)	
			1 μ ₂ -S	2.549(5)	113.0(2)	
			1 μ ₂ -S	2.628(5)	106.4(2)	
					102.4(2)	
					94.3(2)	
	4	0	Hg2			
			1 μ ₂ -S	2.500(5)	117.9(2)	
			1 μ ₂ -S	2.524(5)	115.0(1)	
1 μ ₂ -S			2.535(5)	109.5(2)		
1 μ ₂ -S			2.584(4)	106.1(2)		
				105.0(2)		
				103.7(2)		
{Hg ₂ (SCH ₂ CH ₂ S) ₃ } _n (polymeric chain, two independent Hg sites)	4	0	2 Hg*			85
			1 S	2.420(1)	143.8(1)	
			1 S	2.442(1)	118.8(1)	
			1 μ ₂ -S	2.772(1)	104.4(1)	
			1 μ ₂ -S	2.675(1)	99.3(1)	
					94.2(1)	
				86.4(1)		
[Ph ₃ P][Hg ₃ (SCH ₂ C ₆ H ₄ CH ₂ S) ₄ ·6MeOH (cluster, three equivalent Hg atoms)]	4	0	3Hg*			86
			2 S	2.423	107.5	
			1 μ ₂ -S	2.642	90.3	
			1 μ ₃ -S	2.775	84.3	

^aPrimary coordination number indicating the number of ligands that fall within a reasonable range of the normal sum of the appropriate covalent radii.

^bSecondary bonding interaction indicates the number of ligands around the mercuric ion that are bound at a distance greater than the sum of the covalent radii but less than or equal to the sum of the appropriate van der Waals radii.

^c(^{*}) indicates secondary bonding interaction.

^d(^{*}) Indicates symmetrically equivalent Hg.

^eEXAFS data Ref. 112.

are electronically similar to the biological ligand cysteine. Thiophenolate ligands, on the other hand, have a lower pK_a than the alkylthiolates and ligand-based low energy UV transitions ($\pi \rightarrow \pi^*$), which obscure ligand-metal charge-transfer bands. Under conditions where the trigonal structure is maintained, bond lengths in solution appear to be similar to those in the solid state. Using large angle X-ray scattering (LAXS), Persson and Zintl (152) report average solution bond lengths at 2.454(11) and 2.457(7) Å for mononuclear, trigonal [Hg(S-*n*-Bu)₃]⁻ and [Hg(SC₆H₅)₃]⁻, respectively. This is consistent with the solid-state data (202).

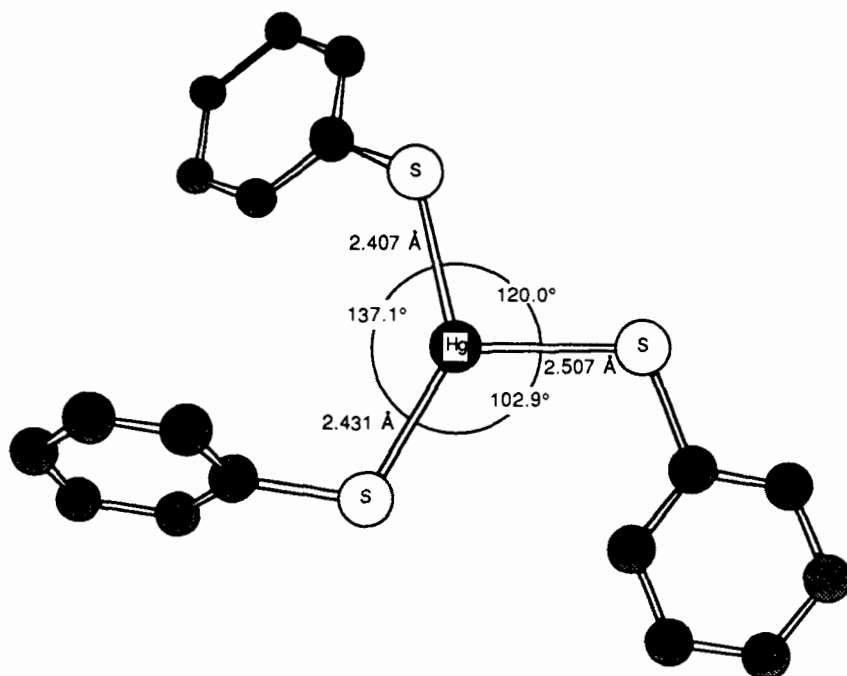


Figure 3. Molecular structure with Hg-S bond lengths and angles of [Hg(SC₆H₅)₃]⁻ anion, based on Ref. 45.

Other Hg-thiolate complexes with a stoichiometry of Hg(SR)₃⁻, are dimeric [Hg₂(SR)₆]²⁻ clusters with bridging thiolates. Figure 5 shows the structure of [(MeS)₂Hg(μ-SMe)₂Hg(SMe)₂]²⁻ (23). The central sulfurs are shown to bridge asymmetrically (2.629 vs. 2.706 Å), with each "half" of the dimer strongly distorted towards trigonal geometry. Indeed, these dimers are believed to dissociate upon solvation to form the mononuclear, trigonal species (22).

Only three monomeric four-coordinate complexes, [Me₄N][Hg(SC₆H₄Cl)₄] (43), [Et₄N][Hg(S₆)₂] (138), and [Ph₄P]₂[Hg(S₄)₂] (139) (Table IV) have been structurally characterized. All these complexes have a distorted tetrahedral geometry with the largest S-Hg-S angle at 119.8°, 117°, and 124.4°, respectively. Bond lengths range between 2.505 and 2.606 Å, and although some exceed the 2.52 Å sum of the covalent radii given in Table II, the lack of any obvious short or long Hg-S bonds and the relatively undistorted S-Hg-S angles (~109°) make it clear that these bonds are all

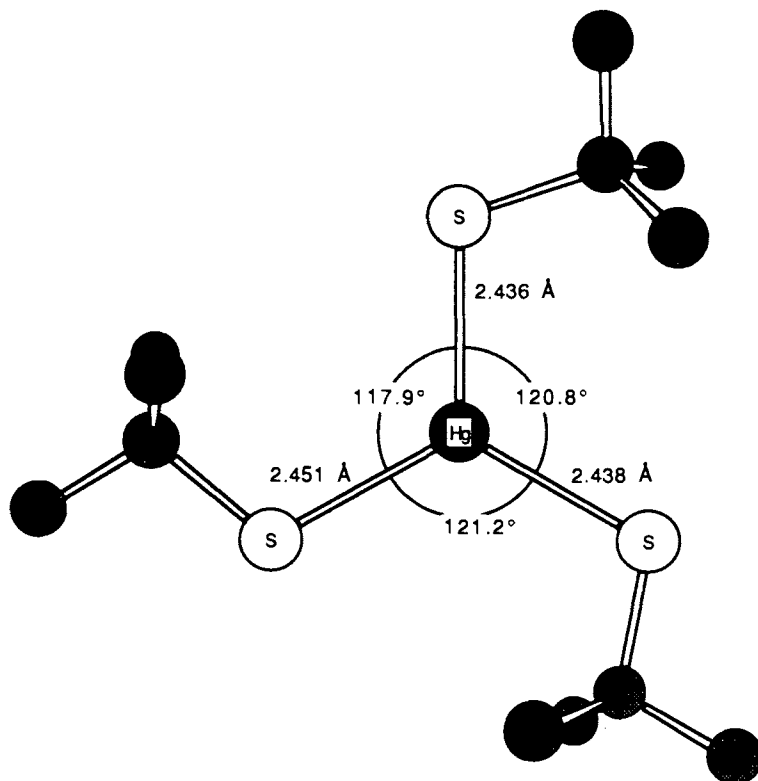


Figure 4. Molecular structure with Hg-S bond lengths and angles of $[\text{Hg}(\text{S}-t\text{-Bu})_3]^{2-}$ anion, based on Ref. 202.

covalent. Figure 6 shows the $[\text{Hg}(\text{SC}_6\text{H}_4\text{Cl})_4]^{2-}$ anion, the only structurally characterized mononuclear, tetrahedral Hg-thiolate complex in the literature to date. These distances are all longer than those in two- and three-coordinate Hg-thiolate complexes, continuing the trend toward longer bonds upon increasing coordination number.

2. Polynuclear Complexes

The Hg(II) center easily forms four-coordinate multimeric complexes with bridging thiolate ligands. This binding motif was proposed for Hg(II)-metallothionein after titration with four equivalents of Hg(II) (101). Table IV lists several four-coordinate model cluster compounds. All the compounds are anionic except for the neutral $\{\text{Hg}(\text{S}-t\text{-Bu})_2\}_n$ (114) (Fig. 7) and

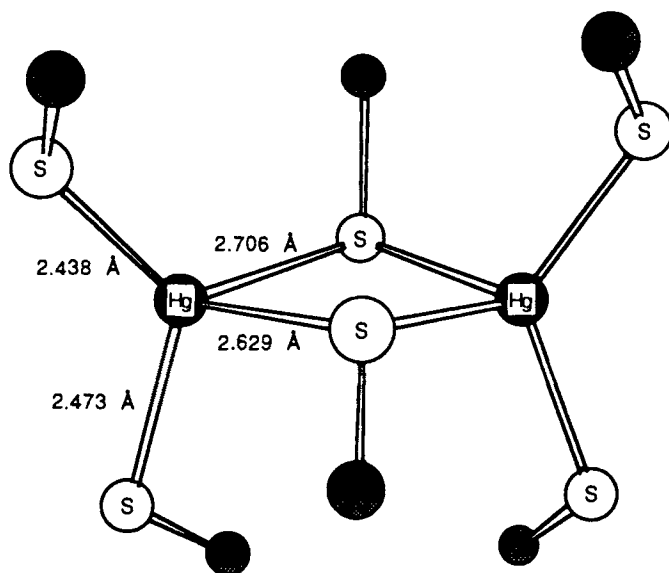


Figure 5. Molecular structure and Hg-S bond lengths of $[(\text{MeS})_2\text{Hg}(\mu_2\text{-SMe})_2\text{Hg}(\text{SMe})_2]^{2-}$ anion, based on Ref. 23.

$\{\text{Hg}(\text{S}-n\text{-Bu})_2\}_n$ (178). Structural trends are difficult to rationalize for this series since the sterically smaller ligands EtS^- and MeS^- form neutral, linear, mononuclear two-coordinate compounds (24, 25).

The trinuclear anion, $[\text{Hg}_3(\text{SC}_2\text{H}_4\text{S})_4]^{2-}$ (85), was originally described with one central four-coordinate Hg atom with bridging thiolate ligands with two symmetrically related four-coordinate Hg' atoms. A better description, indicated in Fig. 8, is one central four-coordinate Hg atom with a pair of *two-coordinated Hg' atoms*: the coordination environment of Hg' is thus $[2 + 2]$. Bond lengths are consistent with four- and two-coordinate terminal thiolate coordination about Hg and Hg' , respectively (Table IV). The "bridging" thiolates are viewed instead as intramolecular secondary bonding interactions. Spectroscopic data for this complex should be particularly useful in substantiating the bonding definition proposed in this chapter.

E. Thioether Complexes

Methionine weakly coordinates Cu(II) in the native and Hg(II) in the metal substituted poplar plastocyanin (46, 48). Although secondary bond-

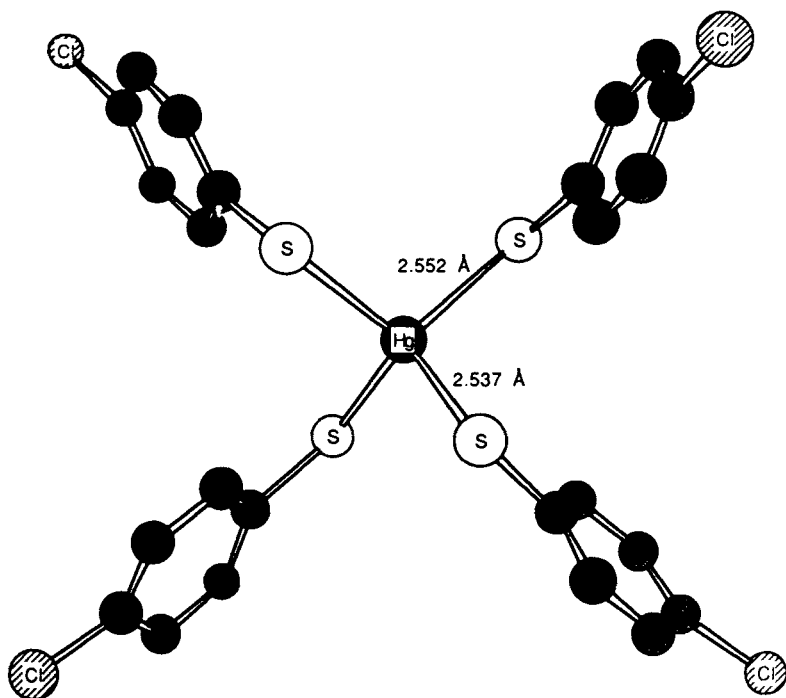


Figure 6. Molecular structure and Hg-S bond lengths of $[\text{Hg}(\text{p-SC}_6\text{H}_4\text{Cl})_4]^{2-}$ anion, based on Ref. 43.

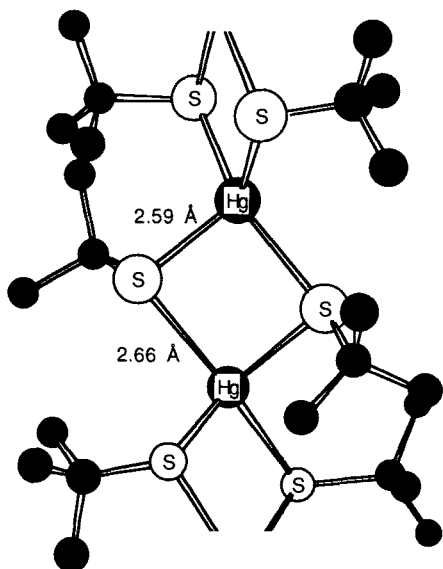


Figure 7. Molecular structure and Hg-S bond lengths of the polymeric $\{\text{Hg}(\text{S-}t\text{-Bu})_2\}_n$, based on Ref. 114.

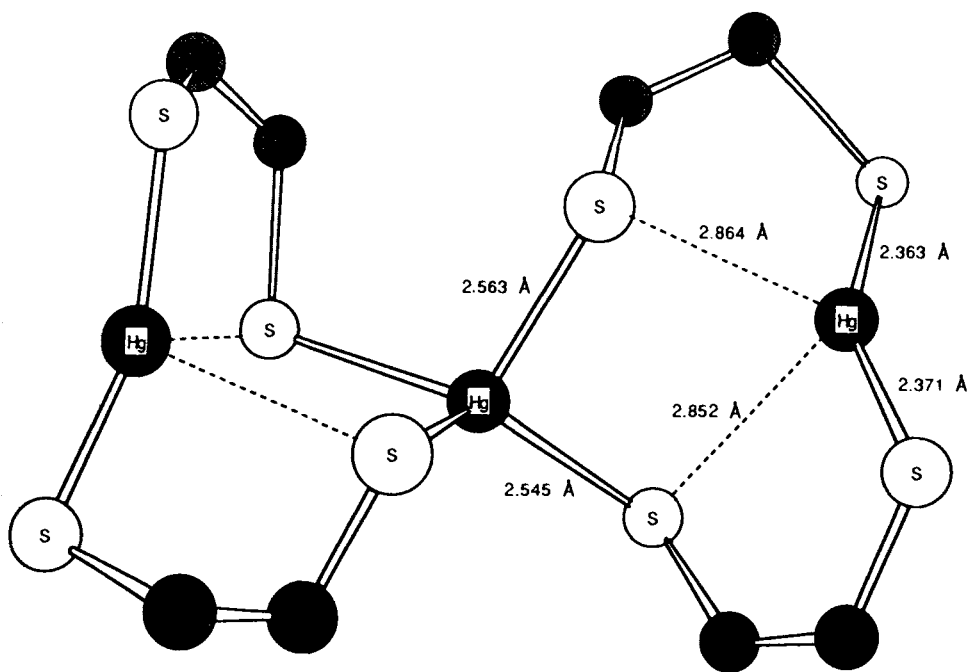


Figure 8. Molecular structure and Hg-S bond lengths of the trimetallic cluster $[\text{Hg}_3(\text{SC}_2\text{H}_4\text{S})_4]^{2-}$, based on (85). Intramolecular secondary bonding interactions are indicated by the dashed line.

ing interactions can be important for overall stability, this mode is not the only type of coordination observed for thioether ligands. The neutral sulfur donor, although a poor ligand relative to thiolate, can bond covalently to Hg(II) preferentially over anionic ligands such as chloride (see Table V). Two-coordinate complexes are much less numerous and have shorter primary bonds than higher coordinate complexes [average Hg-(SR₂) 2.451 and 2.580 Å, respectively]. Halides and other common counterions play an important role in primary and secondary bonding.

Coordination numbers are not as readily apparent for thioether complexes because many secondary bonding interactions for sulfur, chloride, and oxygen lie within 0.1 Å of the listed covalent bond lengths (Table II). A list of some of the structurally characterized Hg-thioether complexes is given in Table V. Thioether containing complexes have been assigned primary coordination numbers and secondary bonding interactions as with the thiolate complexes; however, some assignments may have little chemical or physical significance.

TABLE V
Selected Bond Distances and Angles in Mercuric-Thioether Compounds

Compound	Primary Coordination Number ^a	Secondary Bonding Interactions ^b	Ligand ^c	Hg-L(Å)	L-HC-L(°) ^d	Reference
[Hg(6-mercaptopurine) ₂ Cl ₂]	2	2	2 S 2 Cl'	2.460(3) 2.622(3)	139.8(1)* 95.7(1) 116.8(1) 105.1(1)	116
{[Hg(Mc(EtCHPhCH ₂)S)Cl ₂] _n } (polymeric chain)	2	3	1 S 1 Cl 1 μ ₃ -Cl' 1 μ ₃ -Cl' 1 μ ₃ -Cl'	2.433(4) 2.315(5) 2.677(5) 2.838(10) 2.995(10)	149.8(2) 103.5(2) 91.4(2) 79.0(2) 103.2(2)	17
[Hg(TODTCOD)Cl ₂] [HgCl ₂] (e)	4	0	Hg1 1 S 1 S 1 μ ₂ -Cl 1 Cl	2.552(6) 2.672(7) 2.427(6) 2.460(6)	85.2(2)* 134.19(19) 101.3(2) 110.6(2)	53
	2	1	Hg2 1 Cl 1 Cl 1 μ ₂ -Cl	2.315(7) 2.313(7) 2.900(6)	166.8(2) 95.2(2)	
[Hg(1,4-thioxan) ₂ Cl ₂]	4	0	1 S 1 S 1 Cl 1 Cl	2.54(2) 2.59(2) 2.43(2) 2.52(2)	115.0(8)* 112.0(6) 114.0(6) 103.0(3)	131
[Hg(TTCTD)Cl ₂] (f) (two equivalent Hg sites)	4	0	1 S 1 S 1 Cl 1 Cl	2.580(2) 2.699(2) 2.407(3) 2.419(3)	83.15(6)* 109.11(8) 112.19(8) 117.54(9)	3
[Hg(TTCTD)OH ₂][ClO ₄] ₂ (f)	4	1	1 S 1 S 1 S 1 S 1 O'	2.58(4) 2.51(5) 2.60(5) 2.71(4) 2.35(4)	76(1) 157(1) 97(2) 152(1) 93(1)	3
[Hg(TTCHD)][ClO ₄] ₂ (g)	4	1	1 S 1 S 1 S 1 S 1 O'	2.663(5) 2.587(6) 2.650(6) 2.563(5) 2.76(2)	91.5 159.6 163.5	106
[Hg(ethH) ₂ (ClO ₄) ₂] (h)	4	2	1 S 1 S 1 O 1 O 1 O' 1 O'	2.436(5) 2.537(4) 2.28(1) 2.259(9) 3.00(1) 3.03(1)	123.2(1)* 120.2(2) 94.5(3) 130.2(3) 46.3(3)	20

TABLE V (Continued)
Selected Bond Distances and Angles in Mercuric-Thioether Compounds

Compound	Primary Coordination Number ^a	Secondary Bonding Interactions ^b	Ligand ^c	Hg-L(Å)	L-HC-L(°) ^d	Reference
[Hg(metH)] ₂ [(ClO ₄) ₂ ·2H ₂ O(<i>t</i>) (intermolecular cross-linking thru carboxylates)	4	2	1 S	2.500(4)	122.7(1) ^e	37
			1 S	2.475(4)		
			1 O	2.27(1)		
			1 O	2.32(1)		
			1 O'	2.82(1)		
			1 O'	2.86(1)		

^aPrimary coordination number indicating the number of ligands that fall within a reasonable range of the normal sum of the appropriate covalent radii.

^bSecondary bonding interactions indicate the total number of ligands around the mercuric ion that are bound at a distance greater the sum of the covalent radii but less than or equal to the sum of the appropriate van der Waals radii.

^c(') indicates secondary bonding interaction.

^d(°) indicates S-Hg-S bond angles for primary Hg-S bonds from independent ligands.

^eTODTCOD = 1,4,7,10-tetraoxa-13,16-dithiacyclooctadecane.

^fTTCTD = 1,4,8,11-tetrathiacyclotetradecane.

^gTTCHD = 1,5,9,13-tetrathiacyclohexadecane.

^hethH = cthionine zwitterion.

ⁱmetH = methionine zwitterion.

F. Statistical Survey of Thiolate-Containing Complexes of Hg(II)

Table VI is a statistical analysis of the primary bond length data presented in Tables III-V. A cautionary note is in order when considering such small data sets, highlighting the need for more model complexes. With this current definition of coordination number, however, a simple correlation between the Hg-S bond length and the primary coordination number can be drawn. The mean Hg-S bond lengths increase ~0.1 Å with primary coordination number for both mononuclear and polynuclear complexes and distinct ranges of bond lengths are apparent for each type of coordination. These data are useful in interpreting EXAFS results and permit judicious deduction of the binding site geometry. Coupled with modern spectroscopic and molecular biological tools, it should be possible to critically examine and refine the molecular structural interpretation of Hg-binding sites in proteins.

Only one crystal structure of a Hg(II)-substituted metalloprotein has been solved where the Hg binding site is known to high resolution (1.9 Å). The structure of Hg(II)-substituted poplar plastocyanin provides a particularly interesting example, with Hg(II) coordinated to two histidines (His), one cysteine (Cys) and one methionine (Met) (46). The effect of Hg sub-

TABLE VI
Statistical Survey of Coordination Number and Hg-S Bond Length

Coordination Number ^a	Range (Å)	Mean (Å)	σ^b	Number of Complexes
<i>Mononuclear, Thiolate</i>				
Two ^c	2.316–2.361	2.34	0.02	7
Three ^d	2.407–2.507	2.44	0.03	2
Four ^e	2.505–2.606	2.54	0.02	3
<i>Cluster, Thiolate</i>				
Two, bridging ^f	2.378–2.490	2.42	0.04	13
Three, bridging ^g	2.488–2.509	2.50	0.01	2
Four, bridging ^h	2.482–2.772	2.62	0.07	6
Four, terminal ⁱ	2.420–2.442	2.43	0.01	3
<i>Mononuclear, Thioether</i>				
Two ^j	2.433–2.460	2.451	0.013	2
Four ^k	2.470–2.710	2.580	0.074	7

^aOnly primary bonding interactions.

^bStandard deviation of measurements.

^cReferences 5, 10, 21, 25, 37, 189, 207.

^dReferences 45, 202.

^eReferences 43, 138, 139.

^fReferences 16, 32, 33, 39, 155, 179, 189.

^gReferences 32, 33.

^hReferences 16, 23, 86, 114, 178.

ⁱReferences 23, 85, 86.

^jReferences 17, 116.

^kReferences 3, 20, 37, 53, 106, 131.

stitution for Cu had little effect on the geometry of the metal binding site, indicating that the polypeptide structure defines the metal binding site. Our analysis of the structural data does include complexes with one thiolate ligand, and the basic correlations and coordination requirements are expected to be analogous. Church et al. (46) report the one His–Hg–His and two His–Hg–Cys bond angles at 100° and 133°, 119° respectively, forming a distorted trigonal geometry, and the Hg atom lies only 0.036 Å out of the N(His), N(His), S(Cys) plane. The weak Hg–Met interaction (3.02 Å) is considered a secondary bond. They point out that the unusually short Hg–Cys bond (2.38 Å) for the three- or four-coordinate Hg(II) ion is more typical of two-coordinate Hg(II) and report normal Hg–N bond distances (Hg–His at 2.34 and 2.36 Å) with respect to pyridine adducts of the polymeric (–Hg–(SR)–)_n complexes (as seen in Table III, compounds No.

12, 13, 15, 16) (46). Compared to the data in Table VI, the Hg–Cys bond length is consistent with three coordination, allowing for a slight additional shortening due to a net positive charge on Hg(II). The Hg–His bonds are longer than the sum of the Hg(II) and N covalent radii (2.23 Å) however, and by the definition in Section II.C are secondary bonding interactions. Short Hg–N(pyridine) bonds ranging from 2.11 to 2.27 Å are reported in several two coordinate $[\text{Hg}(\text{py})_2]\text{L}_2$ complexes (where $\text{L} \neq$ thiolate) (31, 76, 90), which are more consistent with primary bonding. The statistical data suggest the reported Hg–N bond lengths are too long. This postulate is supported by recent EXAFS results on Hg poplar plastocyanin that indicate shorter Hg–His bonds at 2.25 (3) Å and Hg–Cys at 2.32 (3) Å, which, within experimental error, are primary Hg–N bonds (112). The discrepancy between EXAFS and the crystallographic results is not large, however, considering the relative experimental errors, and points out the limits of interpretation for data obtained by these methods.

G. The Zinc Family Paradox

The low coordination numbers for Hg(II) are scarcely seen in Zn(II) and Cd(II), which favor four and six coordination. Theoretical rationalizations must explain such complex behavior within the framework of the filled d^{10} orbitals. Four coordination for Cd and Zn is described simply using sp^3 hybridization of the empty s and p orbitals and expansion of the coordination sphere. Nyholm used ionization potential data to compare Hg coordination to that in Cd and Zn complexes and attributed the unusual two-coordinate chemistry of Hg(II) to a large $6s$ – $6p$ orbital separation scheme favoring s – p linear hybrids over tetrahedral sp^3 hybrids (142). Orgel pointed out that the actual difference in $6s$ – $6p$ orbital separation was too small to account for the observed prevalence of linear coordination (146). Instead, Orgel suggested that the rather small difference in the Hg(II) $5d^{10} \rightarrow 5d^9 6s$ promotion energy, approximately one-half that of Zn(II) and Cd(II), allows significant $5d_{z^2}$ – $6s$ orbital hybridization for certain HgL_2 complexes, stabilizing the linear conformation. This electronic rearrangement permits formation of an empty orbital with d_{z^2} character that is available for linear bonding interactions.

Relativistic arguments lend support to both proposed hybrid schemes. The relativistic effect on the heavy sixth row elements lowers the energy of the s and p orbitals and, as a result of more effective nuclear screening, effectively raises the d and f orbital energies. Nonrelativistic $6s$ – $6p$ energy differences are one-half the relativistic separations, while the lowered $6s$ and raised $5d$ orbitals explain the low $5d^{10}$ – $5d^9 6s$ promotion energy (156). Fisher and Drago have extended Orgel's hybridization scheme to include

some $6p_z$ participation (61). The extent of the orbital mixing is dependent on the electron-donating strength of the ligand. Methide is an exceptionally strong electron donor and causes extensive $d-s-p$ hybridization in $\text{Hg}(\text{CH}_3)_2$, which is linear and shows little tendency to expand its coordination sphere (61). Chloride, on the other hand, is much less electron donating and effects only minor $d-s-p$ hybridization; thus, strong secondary bonding interactions characterize these Hg-Cl complexes (61). Compared to halides, thiolates are stronger, more polarizable donor ligands and so behave in their coordination chemistry with Hg(II). Secondary bonding interactions are observed in both the solid state and in solution, but they are neither as strong nor as prevalent as with the mercuric halides.

Tossel and Vaughan argue that the $d-s$ hybridization alone does not specifically favor low coordination numbers, but rather the overriding factor in determining the bonding geometry for Hg(II) is minimization of the metal d (Md) orbital interactions with ligand p (Lp) nonbonding orbitals (190). Upon increasing coordination number, the energy of the Md orbitals is raised, whereas those of the Lp orbitals are unchanged. If the Md orbitals have slightly lower energy than the Lp orbitals, low coordination number is favored so as to minimize the resulting interaction. Conversely, high coordination number is favored if the reverse is true. The Md orbitals for Zn(II) and Cd(II) lie well below the nonbonding p orbitals for sulfur and apparently do not significantly interact even for higher coordination numbers. The Md for Hg(II) lie only slightly below the sulfur Lp , because of the relativistic effects on the $5d$ atomic orbitals, however, and much stronger destabilization is felt with increasing coordination number (190).

Complete theoretical explanations of bonding in three- and four-coordinate Hg(II) complexes are, at present, lacking. Fisher and Drago explain Zn(II) and Cd(II) bonding as essentially $n-s$ and $n-p$ in character as the larger $nd-ns$ separation prevents $d-s$ mixing (61). A simplistic description for Hg(II) would then assume higher coordination numbers suppress $d-s$ hybridization and bonding is chiefly $6s$ and $6p$ in character. The $Md-Lp$ orbital interaction scheme proposed above by Tossel and Vaughan (190) does not adequately explain the dearth of higher coordination number compounds for Hg(II).

H. EXAFS Characterization of a Hg(Cys)₃ Binding Site in MerR

The Hg(II) substituted proteins can be studied using extended X-ray absorption fine structure (EXAFS) (112, 170). Although EXAFS affords information only for an average structural environment, and furnishes no indication of sample homogeneity, the technique can yield accurate information on average metal-ligand distances.

To investigate the coordination Hg(II) environment in MerR, Hg X-ray absorption spectra have been obtained utilizing the Hg-L_{III} absorption edge (191, 209). EXAFS data were collected on structurally characterized model Hg(II) compounds having two, three, and four thiolate ligands (209). Protein EXAFS data were collected on lyophilized and ammonium sulfate-precipitated Hg-MerR. The EXAFS spectra and corresponding Fourier transforms showed only a single resolved shell of scatterers. The best fits for a single shell of S scatterers are shown in Table VII (191). Only modest improvements in the quality of fit were obtained by including either a second shell of 1 S atom or 2 N atoms. For fits including N atoms, it was not possible to refine Hg-N distances consistently from sample to sample. Furthermore, possible histidine coordination was ruled out by the absence of a second shell of C atoms. A survey of the available structurally characterized Hg(II)-thiolate coordination complexes suggested that the most reasonable interpretation of the EXAFS results is for Hg(II) bound by three thiolate ligands at an average bond distance of 2.43 Å. As seen in Table VI, the average bond distance of three-coordinate Hg(II)-thiolate complexes is 2.44(3) Å. The EXAFS results for the Hg(II) protein are consistent with an Hg(SR)₃ environment. Chloride or exogenous buffer thiol ligation was ruled out by spectrophotometric titrations and gel filtration studies using radiolabeled thiols (210). Since addition of a third thiolate ligand to Hg(II) can be thermodynamically favored in some environments, as discussed in Section III.A, a three-coordinate thiolate Hg(II)-binding site in MerR can provide an additional driving force favoring Hg(II) binding to the MerR receptor site over the cellular thiol pool.

TABLE VII
EXAFS Curve-Fitting Results for a Single Lyophilized Sample of Hg-MerR^a

Type	Hg-SR (Å)	<i>n</i> (Hg-S) (Bonds)	$\Delta\sigma^2$ (<i>b</i>) (Å ² × 10 ³)	Hg-X' (Å)	<i>n</i> (Hg-X) (Bonds)	$\Delta\sigma^2$ (<i>b</i>) (Å ² × 10 ³)	"F" ^b
1 Shell S	2.43	2.8	-1.2				4.3
1 Shell S <i>n</i> fixed	2.43	3	-0.8				4.4
2 Shell S	2.41	2	-3.2	2.51	1	0.3	4.0
1 Shell S	2.43	2	-1.0	2.27	2	8.6	4.0
1 Shell N							

^aData are for a lyophilized sample with the optimum signal to noise. An average of three data sets does not statistically distinguish a model composed of a single shell of 3 S atoms from a model with a single shell composed of 1 N and 2 S atoms (209).

^b $\Delta\sigma^2$ is the variation in the Debye-Waller factor relative to the appropriate model compound.

^cThe goodness of fit, $F = [(\chi_{\text{calc}} k^3 - \chi_{\text{exp}} k^3)^2 / (N - 1)]^{1/2} [(\chi k^3)_{\text{max}} - (\chi k^3)_{\text{min}}]^{-1} \cdot 100\%$.

III. AQUEOUS Hg(II) CHEMISTRY

Apart from the ionic Hg(II) complexes derived from strong oxy acids, (e.g., sulfate, nitrate, and perchlorate), acetate, and fluoride, the overwhelming majority of Hg(II) compounds are covalent. Unfortunately, simple thiolate complexes of Hg(II) tend to be quite insoluble in aqueous solution. As a result, thermodynamic data for aqueous Hg(II) thiolate or halide complexes are scarce. Thiolate ligands are often considered to be pseudohalides. Consequently, an understanding of mercuric halide chemistry can be utilized in studying thiolate chemistry. This comparative approach will be used in several of the following sections as thermodynamic and spectroscopic data are used to predict trends for the chemical behavior of thiolate ligands. The following sections on the solution chemistry of Hg(II) serve to introduce us to the general trends observed for the formation of thiolate complexes with Hg(II). Although not intended to be a complete survey of all the reported thermodynamic values for complexes involving the Hg(II)-thiolates, the lack of thermodynamic information available, particularly for the formation reactions involving the three- and four-coordinate complexes, highlights the need for further study of Hg-thiolate chemistry.

A. Thermodynamics

As reviewed by Ahrland, Hg(II) compounds follow the expected thermodynamic trends for the formation of soft metal ion complexes: reactions between soft acceptors and soft donors are strongly exothermic, with very little change in entropy (2). Since soft metal ions are generally much more weakly hydrated than are hard metal ions, the energy released upon formation of a covalent bond between the metal and soft ligand is not offset by a large energy requirement for dehydration of the metal ion. Thus, no large entropy increases are likely to occur upon complexation and the formation free energies are dominated by the exothermicity of the covalent bond formation. These trends are nicely illustrated by the halides of Hg(II), as seen in Table VIII. The first and second stepwise formation enthalpies for mercuric halides, ΔH_1 and ΔH_2 , are similar, as are the third and fourth stepwise formation enthalpies, ΔH_3 and ΔH_4 . Throughout the series of halides, the first two formation enthalpies are much larger than those for the addition of the third and fourth ligands. The change in the magnitude of the stepwise formation enthalpy upon addition of the third undoubtedly reflects the change in coordination geometry from linear to trigonal or tetrahedral. As the halides become softer on going from chloride to iodide, the ΔH_n (and consequentially ΔG_n) for all steps become dramatically larger.

TABLE VIII
Thermodynamic Functions for Stepwise Formation of Selected Hg(II) Complexes in Aqueous Solution or Pyridine Solution^a

Ligand	ΔG_1°	ΔG_2°	ΔG_3°	ΔG_4°	ΔH_1	ΔH_2	ΔH_3	ΔH_4	References
<i>Aqueous Solution</i>									
Cl ⁻	-40.3	-39.4	-4.3	-7.9	-24.2	-27.2	-4.3	-6.2	2, 175
Br ⁻	-53.65	-49.0	-15.8	-8.5	-40.0	-40.2	-10.8	-18.6	2, 175
I ⁻	-73.45	-62.5			-75.3	-67.8		$\Delta H_3 + \Delta H_4 = 42.0$	2, 175
EDTA	-126								175
L-Cysteine		$\Delta G_1 + \Delta G_2 = -247$				-209			180
L-Cysteine			-5.0						42
Glutathione		$\Delta G_1 + \Delta G_2 = -239$				-202			180
Glutathione			-18.7						42
Penicillamine	-219	-34.8							40
Penicillamine			-20.48						42
<i>Pyridine Solution</i>									
PhS ⁻	-61.2	-51.1	-50.5		-60.8	-54.4	-48.5		213
PhSH	-59.5	-44.9	-43.4		-65.4	-59.3	-53.5		213
BuS ⁻	-55.8	-39.6	-37.7		-73.1	-39.2	-65.6		213
BuSH	-55.3	-38.7	-38.7		-65.2	-32.3	-52.3		213

^aValues in kJ·mol⁻¹. Where necessary, free energies of formation were calculated for 25°C from the relevant formation constants. All values are for stepwise formation reactions, except where noted as the sum of two values.

For example, ΔH_1 is $-24.7 \text{ kJ}\cdot\text{mol}^{-1}$ for chloride, $-42.2 \text{ kJ}\cdot\text{mol}^{-1}$ for bromide, and $-75.3 \text{ kJ}\cdot\text{mol}^{-1}$ for iodide. Thus, the increasingly covalent character of the Hg–X bonds is reflected in the larger ΔH_n values measured as the ligands to Hg(II) become softer. The formation reactions and thermodynamics for inorganic ligands with Hg(II) have been thoroughly reviewed (89).

In aqueous solution the stepwise formation constants for thiolate complexes follow the same general trend as those of the halides, but the difference between the first two formation enthalpies and the third and fourth formation enthalpies are much larger than in the halide series. Until recently, aqueous studies of cysteine and glutathione formation constants have been unable to provide evidence for three- and four-coordinate Hg–thiolate species. These studies have typically indicated large formation constants for the two-coordinate complexes with thiolate ligands. For example, cysteinatate has been found to have $\log \beta_2$ values ranging from 39.4 to 43.6, where β_2 is the cumulative formation constant for addition of two ligands (180, 197). Similarly, the formation constant for addition of the first ligand, K_1 , was reported to be $\sim 10^{14.2}$ (117). Despite the large ranges of experimentally determined formation constants for several thiolate containing ligands, reflecting limitations of the mercury electrode systems commonly used for these measurements, systematic studies have been made of the chelating ability of various sulfhydryl containing ligands (40). Formation constants and thermodynamic functions for some principal Hg–thiolate complexes are tabulated in Tables VIII and IX.

Mercury(II)–thiolate complexes have been successfully studied in pyridine solution (152, 213). Unlike the bis complexes described above, several trigonal mononuclear thiolate–Hg(II) complexes have been postulated for butane thiolate and benzene thiolate ligands in pyridine solution. In these studies the sharp differences between the formation energies for the addition of the first, second, and third ligands is lost. Although ΔH_1 is slightly larger than the ΔH_2 and ΔH_3 values, the latter two formation enthalpies are similar in magnitude. These trends are depicted in Table VIII. In pyridine it is quite evident that three very strong bonds are made to Hg(II); there was no evidence for the addition of a fourth thiolate ligand (213). Pyridine solutions of the trigonal *n*-butylthiolato- and phenylthiolato-mercury(II) complexes were studied by large angle X-ray scattering and found to be trigonal planar with average bond distances of 2.454(11) and 2.475(7) Å, respectively (152). These results are consistent with the crystalline structures for homologous trigonal compounds, for which the few examples available have been shown to have average bond distances of 2.44(3) Å, as discussed in Section II. D.

TABLE IX
Stepwise Equilibrium Constants with Hg(II) for Some S Containing Ligands

Ligand(s)	Solvent ^a	log K_1	log K_2	log K_3	log K_4	log β_2^b	References
SCN				2.88	1.99	17.26	2, 175
L-Cysteine				0.87		43.57, 39.4	42, 175, 180, 197
D,L-Penicillamine		38.3	6.1	3.59			40, 42
Glutathione				3.29		41.58	42, 180
Glutathione				3.18			174
PhS	Pyridine	10.72	8.96	8.86			213
PhSH	Pyridine	10.42	7.87	7.60			213
BuS	Pyridine	9.77	6.94	6.60			213
BuSH	Pyridine	9.69	6.78	6.77			213
2,3-Dimercaptopropanol			7.11				40
Phthalyltetraethio-				44.8			104
acetic acid (PTTA)		18.8 (Hg ₂ PTTA)					
S(CH ₂ CH ₂ OH) ₂		45 [HgPTTA(OH ₂)]	4.33				2
		5.57					

^aUnless otherwise stated, all systems were aqueous with constant ionic strength maintained by neutral salts.

^bLog β_2 represents the cumulative formation constant for the addition of two ligands.

Recent ^{13}C NMR investigations of Hg(II)–thiol ligand exchange kinetics have demonstrated the existence of three-coordinate aqueous Hg(II) complexes with L-cysteine, glutathione, and D,L-penicillamine (42). These complexes have been further studied by polarimetry; the complex formation constants for glutathione are in good agreement with those obtained from ^{13}C NMR data (174). Calculations based upon the formation constants obtained for addition of the third thiolate ligand from NMR data indicate that significant amounts of the three-coordinate complex are formed with Hg(II) when thiolate ligand is present in large excess. For example, the formation constants obtained for glutathione predict that nearly 10% of the Hg(II) from a $1 \times 10^{-4} \text{ M}$ Hg(II) solution will be found as the $[\text{Hg}(\text{SR})_3]^-$ species at physiological glutathione concentrations and pH (42).

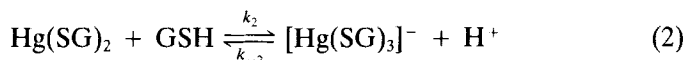
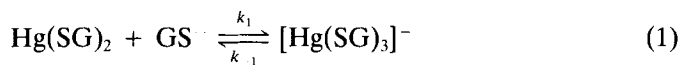
Thioethers have also been shown to form strong complexes with Hg(II) in aqueous solution (47, 104, 105, 127, 137). The chelate effect has been utilized in several of these thioether compounds in efforts to improve chelation therapy in Hg(II) poisoning (13). Several of the formation constants of ligand systems based on thioethers are in Table IX. In contrast to thiolates, only weak Hg(II)–thioether complexes are formed in highly donating solvents such as dimethyl sulfoxide and pyridine (213).

B. Lability of Hg(II)–Thiolate Ligand Complexes

As discussed in previous sections, sulfhydryl ligands have an extremely high affinity for mercuric ion. Despite the strength of these complexes, a considerable body of evidence is consistent with the lability of Hg(II)–thiolate complexes toward exchange with sulfhydryl ligands. Evidence for the role of thiol ligands as being the predominant ligand to mercury in biological systems comes from ^1H NMR studies of intact erythrocytes, which indicate that the sulfhydryl-containing tripeptide glutathione complexes Hg(II) (95). In aqueous solution, ^{13}C NMR spectra of $\text{Hg}(\text{SR})_2$ complexes fail to detect ^{13}C – ^{199}Hg coupling; this result has also been interpreted as a result of the lability of Hg(II)–thiol bonds (66). For glutathione (GSH) complexes of Hg(II), ^{13}C resonances are exchange-averaged between the free and complexed forms of glutathione, suggesting exchange rates that are fast on the NMR time scale.

In an effort to determine the reactions involved in Hg(II)–thiol exchange, Cheesman et al. (42), have studied complexes of Hg(II) formed in the presence of excess glutathione, cysteine, and penicillamine. Measurements of ^{13}C NMR spectra as a function of pH provide data suggesting that $[\text{Hg}(\text{SR})_3]^-$ complexes are formed in significant concentrations at

thiol:Hg ratios >2:1. These results were particularly surprising given the absence of detectable aqueous $[\text{Hg}(\text{SR})_3]^-$ species in earlier investigations of Hg(II) reactions with glutathione and cysteine ligands (40, 180, 197). The presence of significant quantities of $[\text{Hg}(\text{SR})_3]^-$ in aqueous solution in the physiological pH range provides a convenient mechanism for rapid thiol exchange. The only $[\text{Hg}(\text{SR})_3]^-$ complexes characterized structurally to date have trigonal planar geometry, although vibrational spectroscopic studies of alkyl thiolate complexes suggest other geometries are possible (119). The addition of the third glutathione ligand to Hg(II) may result in the formation of a symmetric planar complex. All of the ligands in such a complex have the same probability of dissociating; an $[\text{Hg}(\text{SR})_3]^-$ complex would then provide a convenient mechanism for the rapid exchange of thiol between the bound and free forms. Since an associative exchange mechanism via a three-coordinate intermediate is expected, the existence of the three-coordinate complex provides a kinetic explanation for the observation that Hg(II)-thiolate complexes are more labile in cell extracts (42). These studies also provided rate constants for the exchange of glutathione, as outlined in Eqs. 1 and 2.



The rates for loss of the third thiolate or thiol ligand (k_{-1} and k_{-2}) are $6.3(3.0) \times 10^3 \text{ s}^{-1}$ and $6.3(1.0) \times 10^9 \text{ L} \cdot \text{mol}^{-1} \text{ s}^{-1}$, respectively. At pH 7, the average lifetime of the $[\text{Hg}(\text{SG})_3]^-$ species was calculated to be $1.4 \times 10^{-4} \text{ s}$. Using ligand-to-metal ratios (RSH:Hg) as high as 6:1, these workers did not find it necessary to include $[\text{Hg}(\text{SG})_4]^{2-}$ to fit the chemical shift data expressed either as functions of GSH:Hg ratio or pH. The absence of four-coordinate species in this system may reflect a smaller formation constant for addition of the fourth ligand, implying that large excesses of thiol are necessary for formation of a four-coordinate species. For example, in an investigation of the electronic spectra of tetrahalide complexes of Hg(II), Day and Seal reported that qualitatively a minimum of 10-fold molar excess of halide over complex was necessary to position the equilibrium towards full formation of the four-coordinate bromo- and chloro-species (55).

The extent to which one thiol displaces another in bis complexes has also been demonstrated by using ^{13}C NMR and polarimetry for the ligands

glutathione, penicillamine, and mercaptoethylamine (174). The stability of these complexes at physiological pH was found to decrease in the order $\text{Hg}(\text{mercaptoethylamine})_2 > \text{Hg}(\text{penicillamine})_2 > \text{Hg}(\text{glutathione})_2$. Equilibrium constants for the displacement reactions were found to be 1.12 for the displacement of glutathione by penicillamine and 1.19 for the displacement of penicillamine by mercaptoethylamine. These studies also examined the formation of $[\text{Hg}(\text{SR})_3]^-$ species for glutathione; the formation constant obtained by polarimetry was consistent with that obtained from NMR data (42, 174).

A dramatic demonstration of the facile exchange between Hg(II) and thiolate ligands has been observed in metal exchange reactions of the all-Cd(II) form of metallothionein (MT) with the all-Hg(II) metallothionein monitored by the changes in absorbance of a ligand-to-metal charge transfer (LMCT) band at 300 nm (101). A consequence of the strong complexes that Hg(II) makes with thiolate ligands is that the expected formation constants for the Hg(II) and Cd(II) forms of metallothionein are noticeably large (e.g., Table IX). While the reactions of the divalent heavy metals with thiolate ligands is expected to be nearly diffusion controlled, the expected off-rates for Cd(II) and Hg(II) from metallothionein are expected to be quite low. Consequently, the free metal ion concentrations in these protein solutions is expected to be much lower, and the ability of Hg(II) and Cd(II) to exchange in a facile manner led Johnson and Armitage to suggest that a direct interaction between the Cd-MT and Hg-MT metal sites accounted for the rapid exchange (101). Displacement reactions of Cd(II) from Cd-metallothionein by Hg(II) were also observed to occur rapidly, again suggesting that exchange occurs via a metal-thiolate intermediate. The ready displacement of Cd(II) from Cd-metallothionein by Hg(II) is not unexpected given the large formation constants for Hg-thiolate complexes. The 2D NMR solution and crystal structures of metallothionein indicate that the metal sites are not deeply buried in the small protein (26, 67, 199), presumably insuring that thiolate ligands are readily available either to coordinate or exchange metals. The exchange kinetics were best fit to a bimolecular reaction expression with a calculated rate constant of $182 \text{ M}^{-1} \text{ s}^{-1}$. The bimolecular kinetics support the contention that metal exchange occurs via a direct exchange mechanism involving the metal clusters.

The ready availability of thiolate ligands in biological systems implies that thiolate complexes dominate Hg(II) coordination in biological systems. Despite some controversy regarding the accuracy of formation constants for Hg-thiolate complexes, extremely large formation constants are consistently reported in the literature. Recent results suggest that Hg(II) ap-

pears to display some flexibility for its coordination geometry in thiolate complexes. The formation constants for addition of a third thiolate ligand, although not nearly so large as those for the first two thiolates, are not inconsequential, particularly at pH values near and above the physiological pH. There has been no definitive observation to date of mononuclear $[\text{Hg}(\text{SR})_4]^{2-}$ complexes with biologically relevant ligands, although tetra-coordinate species may be quite readily formed in bridging thiolate environments.

IV. ELECTRONIC SPECTROSCOPY OF Hg(II) COMPLEXES

Since Hg(II) has a closed-shell d^{10} electronic structure, it is often considered "spectroscopically silent" in optical and EPR spectroscopy. Recent advances in a variety of spectroscopic techniques have made this description of Hg(II) complexes obsolete. Relativistic effects tend to lower energy of the Hg 6s orbital (156), and consequently the LMCT spectra of Hg(II) tetrahalides and three- or four-coordinate alkyl thiolate complexes are distinctly different than those obtained for two-coordinate complexes. As described below, ultraviolet spectroscopy has provided details about the Hg(II) coordination in the MerR protein (202, 210).

The earliest reports correlating UV spectra with the coordination environment of Hg(II)-thiolate complexes have come from the biochemical literature, whereas similar correlations with model complexes have only recently been reported (202). Mercury(II) substitution has been used to examine coordination sites in a variety of proteins. A systematic electronic spectroscopy study of mammalian metallothionein derivatives prepared from the Group IIB metals has led Vasák et al. (198) to propose that Hg(II), Cd(II), and Zn(II) atoms are coordinated in sites with tetrahedrally related geometry. These interpretations were based on the location of the lowest energy band, assigned as the S \rightarrow Hg ligand-to-metal CT transition. Gaussian analysis of the Hg(II)-metallothionein vs. metallothionein difference spectrum resolved a lowest energy LMCT band at 303 nm, which was assigned using Jørgensen's semiempirical theory of charge-transfer spectra (107). In this approach, the electronegativity of the ligands bound to a central atom can be empirically correlated to the optical spectra of these complexes. Using the correlation between the optical electronegativities of the halide and the pseudo-halide thiolate, and the lowest LMCT energies of the corresponding tetrahedral complexes of Hg(II), these authors tentatively assigned the transition as arising from a tetrahedral geometry at the Hg(II) site, despite a lack of three- or four-coordinate thiolate

model data. Similar difference spectra were observed by Johnson and Armitage for metallothionein in titrations of Cd(II)₇-metallothionein with 1–14 equivalents of Hg(II) (101). Initially, Hg(II) quantitatively replaces Cd(II), in a site that is assigned tetrahedral geometry by analogy to the work of Vasák et al. (198). Analysis of the spectral data by the method of singular value decomposition indicated that at ratios above 4 Hg(II) per metallothionein, some Hg(II) centers adopt a linear geometry. The X-ray crystal structure and the NMR solution structure of Cd(II), Zn(II)-metallothionein confirm that the predictions made by Vasák et al. (198) are correct for Zn(II) and Cd(II) (26, 67, 199). Given the absence of optical spectra for mononuclear four-coordinate alkyl thiolate complexes of Hg(II) in the literature, and the presence of similar transitions in Hg(SR)₃⁻ model complexes (see below), acceptance of a four S-coordination site for Hg(II) in metallothionein requires some caution, although the Hg(II) site might well involve bridging thiolates as found for the Cd(II) and Zn(II) sites.

An investigation of Zn(II), Cd(II), Co(II), and Ni(II) binding to *Neurospora crassa* Cu(I)-metallothionein led to the assignment of a distorted tetrahedral coordination for Hg(II) by the presence of a LMCT band at 283 nm (14). The *Neurospora* metallothionein differs structurally from mammalian metallothionein, consisting only of 25 amino acids, and as isolated, binding six Cu(I) ions to seven cysteinyl residues. Conversely, mammalian metallothioneins are typically composed of 61 amino acids of which 20 residues are cysteines. Substitution of the Ni(II), Co(II), Zn(II), Cd(II), and Hg(II) into *Neurospora* metallothionein resulted in a metal-to-protein stoichiometry of 3:1. Spectroscopic titrations with these various metals suggested that the first two of the metal ions to bind are in nearly indistinguishable geometries (distorted tetrahedron), with the third metal bound in a different, undetermined fashion. The significant blue shift observed in *Neurospora* metallothionein over the mammalian metallothionein may reflect contributions to the spectrum from thiolate bridging among metals in the mammalian form. Alternatively, the blue shift may reflect higher symmetry in the *Neurospora* Hg(II) site. Although these results were interpreted in terms of Hg(II) binding in a distorted tetrahedron, Hg(II) might bind in the *Neurospora* site in a Hg(Cys)₃-type environment.

Electronic difference spectra of the Hg(II)-substituted blue copper protein plastocyanin have been interpreted in terms of an unusually low energy charge transfer from a cysteine S atom to the central Hg(II) atom (188). The Hg(II)-plastocyanin affords a unique opportunity for investigating the coordination geometry via the UV spectrum since the three-dimensional structure of the Hg(II)-protein complex is known to high resolution (46), as is the structure of the native copper protein (48, 74). In plastocyanin,

Hg(II) is coordinated in a distorted tetrahedral or trigonal environment through bonds to a thiolate S atom of cysteine at a distance of 2.34(5) Å and to two imidazole N atoms of histidines with bond lengths of 2.34(5) and 2.36(5) Å. The thioether S atom of methionine at 3.02(5) Å is best considered a secondary bonding interaction. Substitution of Hg(II) for Cd(II) resulted in only minor changes in the geometry of the metal site. The trace of the peptide backbone and conformations of side chains did not dramatically change. Recent EXAFS data for Hg(II)-plastocyanin are reasonably consistent with the X-ray structure, with best fits obtained to data using a 2N shell with average Hg-N distance of 2.25(3) Å and a single S shell with a bond distance of 2.32(3) Å. The distal methionine S atom could not be distinguished from the EXAFS data (112). Difference UV spectra of Hg(II) derivatives of this protein have a λ_{\max} of 247 nm ($\Delta\epsilon = 9800 M^{-1} \text{ cm}^{-1}$) with a distinct shoulder at 280 nm ($\Delta\epsilon = 2100 M^{-1} \text{ cm}^{-1}$) (188).

Electronic spectra of the tetrahedral halide complexes $[\text{Et}_4\text{N}]_2[\text{HgX}_4]$ have been analyzed in terms of symmetry-related linear combinations of ligand orbitals utilizing the conventions of Ballhausen and Gray (9). The spectra obtained by Day and Seal (55) are consistent with the lowest energy absorption bands being one-electron transitions of the type $t_2 \rightarrow a_1$. Based on their MO scheme, this observation corresponds to molecular orbitals that are composed almost entirely of ligand localized πp ($3t_2$) and metal localized $6s$ ($3a_1$). Alternatively, an MO scheme has been proposed by Gunter et al. (73) that interprets the absorption spectra of the tetrahedral halides in terms of transfer from ligand-localized p molecular orbitals to either Hg-localized $6s$ - or $6p$ -like orbitals. Magnetic circular dichroism (MCD) spectra were used to interpret this model in favor of charge transfer into the empty $6p$ -like Hg-centered MO from the ligand localized p MO (type $t_2 \rightarrow t_1^*$). The energy of the lowest energy charge-transfer band of a complex has been described in the context of the optical electronegativities of the central atom and ligands in the complex by Jørgensen (107). This type of analysis has been performed for the Cd(II) and Hg(II) derivatives of mammalian metallothionein (198). Utilizing the tetrahedral halide complexes as model electronic environments, and the optical electronegativity value for the thiolate ligand reported by McMillin (132), Hg(II) was assigned a distorted tetrahedral coordination geometry in metallothionein. An example of an optical electronegativity analysis is shown in Fig. 9.

Low-energy LMCT bands in the wavelength range from 280 to 310 nm are hallmarks of distorted tetrahedral complexes containing a Hg-SR bond. To investigate whether Hg(II) recognition by the MerR protein involves Hg(II) binding to the protein in a nonlinear coordination geometry, spec-

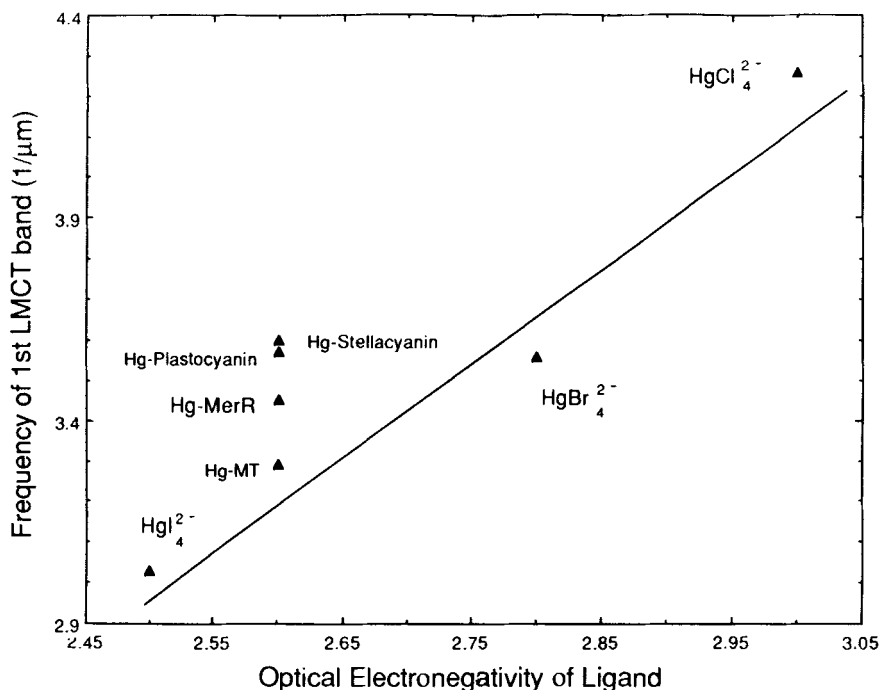


Figure 9. Lowest energy LMCT bands of several proteins plotted as a function of ligand optical electronegativity. For comparison, the lowest energy bands of tetrahedral halide Hg(II) complexes are shown, along with a line obtained from the halide data. As bis Hg(II)-thiolate complexes have significantly higher LMCT energies, these data suggest that Hg(II) in the MerR protein is in a higher number coordination environment.

troscopic titrations of MerR have been performed with Hg(II) in the presence of competing thiol ligands, as shown in Fig. 10 (202, 210). These titrations confirm the earlier reports of one Hg(II) per protein dimer, and a typical data set is plotted in Fig. 10 as the change in absorbance vs. Hg(II) added (82, 145, 171, 172). The difference spectra delineate a characteristic peak at 245 nm ($\Delta\epsilon = 12,500 M^{-1} \text{ cm}^{-1}$) and a distinct shoulder at 290 nm ($\Delta\epsilon = 3550 M^{-1} \text{ cm}^{-1}$), with both titration curves displaying an endpoint of one Hg(II) atom bound per dimer of protein. The Hg-MerR difference spectrum is quite similar to that reported for Hg-metallothionein (198). Table X summarizes the observed optical spectra for several Hg(II) substituted proteins, as well as two-, three-, and four-coordinate model complexes.

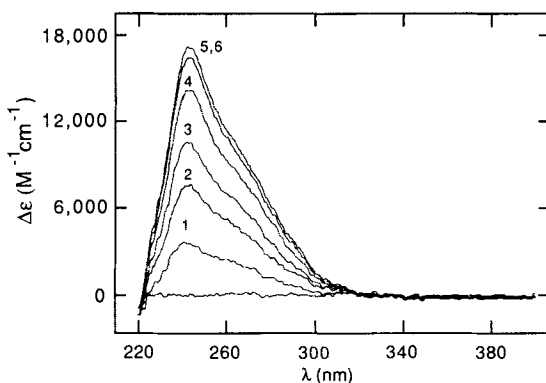


Figure 10. Difference electronic spectra obtained by anaerobic Hg(II) titration of $1.25 \times 10^{-5} M$ MerR solution in the presence of $0.001 M$ 2-mercaptoethanol, $1 M$ NaCl, $0.01 M$ sodium phosphate at pH 7.00. Similar spectra were obtained over a wide range of competitor thiol and chloride concentrations, as well as in buffered $0.5 M$ NaBr or $0.5 M$ KF.

Despite the obvious similarities between the difference spectra obtained for Hg–MerR and the other Hg-substituted proteins discussed above and as shown in Fig. 11, some caution is advised in assigning a distorted tetrahedral or tetrahedral geometry to Hg(II) in this protein. A vital point to consider in evaluating Hg(II) environments in these metalloproteins is that no study analogous to those of Day and Seal, which relates LMCT spectra and ligand optical electronegativity for Hg(II) tetrahalides, exists for trigonal Hg(II) complexes. Absorption spectra obtained from the recently characterized trigonal planar complex $[\text{Et}_4\text{N}][\text{Hg}(\text{S}-t\text{-Bu})]$ strongly suggest that, while electronic spectra may indicate that Hg(II) is indeed in a site with higher than two coordination, it may not readily distinguish between three and four coordination (202). This complex exhibits a λ_{max} of 245 nm ($\epsilon = 17,000 M^{-1} \text{ cm}^{-1}$) in ethanol. The lowest energy transition in the aliphatic $[\text{Hg}(\text{SR})_3]^-$ complex varies in energy with changes in the solvent dielectric and is found at 300 nm in benzene. Thus, in terms of the position of the lowest energy LMCT band, the spectrum of this model complex is not significantly different from those of *Neurospora* Hg-substituted metallothionein, Hg–MerR, and the Hg-substituted blue copper proteins. These recent results indicate that three-coordinate Hg–SR centers could be responsible for Hg–protein transitions and underscore the need for other aliphatic thiolate complexes of Hg(II) with primary coordination numbers of three and four. The lower energy of the analogous LMCT band in Hg-substituted mammalian metallothioneins may reflect either a higher co-

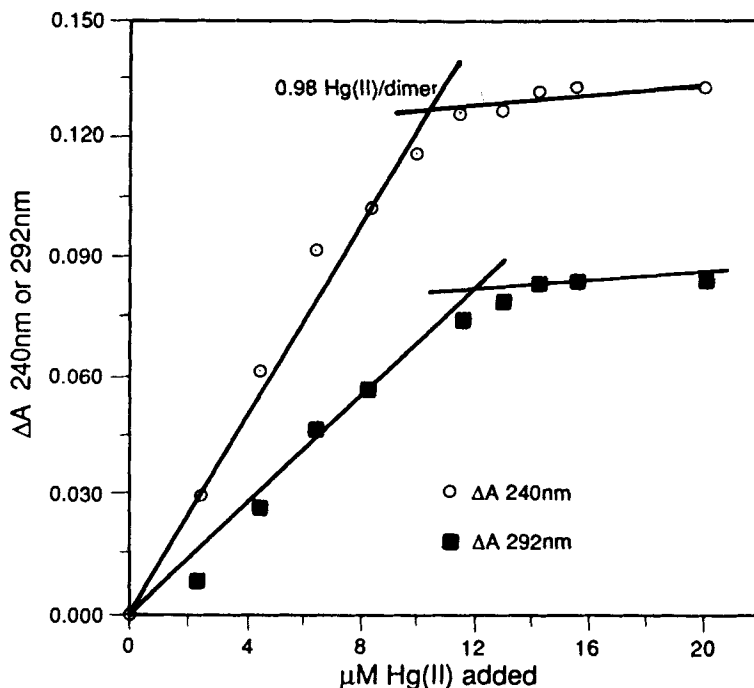


Figure 11. Titration curves obtained from difference electronic spectra for titration of MerR with Hg(II). Titrations were performed in anaerobically sealed 1-cm path cuvettes with 0.001M 2-mercaptoethanol competitor. Protein was buffered at pH 7.00 with 0.01M sodium phosphate, 1M NaCl, 0.1% w/v octyl- β -glucopyranoside.

ordination number for Hg(II), a pronounced difference in site geometry, or simply a change in the electronic environment arising from bridging thiolate ligands.

V. VIBRATIONAL SPECTROSCOPY OF Hg(SR)_n

Vibrational spectroscopy is useful in elucidating aspects of the structure and geometry of Hg(II) compounds. The Hg-S stretching and bending modes are of low energy, due to the large atomic weight of mercury. Consequently, vibrations are observed in the far IR and in the low-energy Raman shift regions, 50–500 cm^{-1} . The fundamental parameters of interest with respect to Hg(II)-thiolate compounds are the number and energies

TABLE X
Lowest Energy Electronic Transitions in Hg(II)-Substituted Proteins and Model Compounds

Hg-Substituted Proteins	$\lambda_{\text{shoulder}}$ (difference)(nm)	$\Delta\epsilon$ (/cm mol protein)	Reference
<i>Neurospora</i> Hg ₃ -MT	283	8,800	14
Hg ₇ -MT	245	Not reported	198
	304	Not reported	198
Hg-plastocyanin	245		188
	280	2,100	188
Hg-stellacyanin	240	13,000	210
	278	2,180 ^a	210
Hg-MerR ^b	245 (λ_{max})	12,500	202
	290	3,350	202
Model Compounds	λ_{max} (nm)	ϵ	
Four coordinate			
Hg(Cys ₄) peptide ^c	280	Not reported	38
Three coordinate			
Hg(S- <i>t</i> -Bu) ₃	245(EtOH)	17,000	202
	260(CH ₃ CN)	17,700	
Two coordinate			
Hg(S- <i>i</i> -Pr) ₂	228CH ₃ CN)	3,400	
	262(CH ₃ CN)	650	

^aValue based on a single measurement. Stellacyanin was the gift of K. Burns, F. Klemens, D. R. McMillin, Purdue University.

^bBased on a dimer formulation for MerR.

^cAmino acid sequence: N-Ac-Pro-Cys-Orn-Cys-Pro-Gln-Cys-Gln-Cys-Arg-Arg-Val; Orn is ornithine.

of Hg-S vibrations in both the Raman and the IR. In principle, for a given local symmetry around Hg(II), and for a given coordination number, simple symmetry considerations predict a certain number of IR-active and Raman-active normal vibrational modes (51). Furthermore, there is a reasonable correlation between the coordination number and the energy of the vibrational modes. Thus, from the IR and Raman spectra of Hg(SR)_n, it may be possible to deduce the coordination number and geometry.

In practice, two factors complicate analyses of vibrational spectra. First, the assignment of low-energy bands to specific Hg-S vibrations is sometimes difficult, because of ligand modes in the same spectral region. In such cases either metal or ligand variation can be used to unravel complex spectra. Fortunately, there is extensive literature on the vibrational spectroscopy of the Hg-Cl bond (22); since the atomic weights of S and Cl are

nearly identical, vibrational modes of isostructural $\text{Hg}(\text{Cl})_n$ and $\text{Hg}(\text{SR})_n$ compounds are isoenergetic, and in some cases Hg–S vibrational modes have been assigned on the basis of comparison to previously assigned Hg–Cl modes (23). Alternatively, the analogous Cd(II) or Zn(II) compounds can be prepared. The M–S stretches appear in different low-energy regions ($\text{Zn} > \text{Cd} > \text{Hg}$), but the ligand modes are invariant. The second complexity in extracting information from vibrational spectra is that there is no simple correlation between Hg(II)–thiolate stoichiometry and Hg(II) coordination number, particularly when thiolates bridge metal centers or the R groups contain potential ligands. In the absence of other structural information such as crystallography, EXAFS, or NMR, prediction of the identity, number, and geometric disposition of ligands in the coordination sphere of Hg(II) solely on the basis of vibrational spectra, however well resolved, is very difficult.

Despite the aforementioned difficulties, Raman and IR spectroscopies are valuable because they can be used to rule out certain geometries, both from the energies of vibrations and from symmetry-based arguments. For example, the symmetric mode of two-coordinate Hg–S compounds is typically found above 300 cm^{-1} , and often above 350 cm^{-1} , and hence is easily distinguished from complexes with $\text{CN} = 3$ or $\text{CN} = 4$, where Hg–S modes are found below 250 cm^{-1} . Predictions based on group theory can provide incontrovertible evidence about local symmetry around Hg(II). For instance, linear $\text{Hg}(\text{SR})_2$ compounds possess the symmetry of the point group $D_{\infty h}$, which is centrosymmetric. Coincidental vibrational bands in Raman and IR spectra would rule out centrosymmetric structures, thereby indicating a lowering of symmetry through solvent coordination to Hg(II).

A. Vibrational Spectroscopy of Hg(II) Halides

Thiolate has been described as a pseudo-halide (92), and a close structural correspondence exists between halide and thiolate complexes of Hg(II). It is therefore worthwhile to review several features of the vibrational spectroscopy of the Hg–X ($\text{X} = \text{Cl}^-$, Br^- , and I^-) bond, which has been extensively studied (22). We focus in particular on Hg–Cl bonds in HgCl_2 , HgCl_3^- , and HgCl_4^{2-} , the three species of most relevance to mercury–thiolate chemistry.

Since the chemistry of mercuric ion is replete with bridging ligands and with secondary bonding interactions in both condensed media and in the solid state (see above), gas-phase studies are useful for obtaining information about isolated species. In Raman studies of vapor phase HgCl_2 , the symmetric Hg–Cl stretch (ν_s) has been assigned at 358 cm^{-1} (22), and

IR studies give the asymmetric stretch (ν_{as}) at 413 cm^{-1} . Data from solution studies, when compared to gas-phase measurements, provide a measure of solvent interaction with HgCl_2 . Even noncoordinating solvents such as benzene interact with complexes, as evidenced by a lowering of ν_s and ν_{as} by 19 and 21 cm^{-1} , respectively, to 339 and 392 cm^{-1} (151). Presumably these interactions are van der Waals in nature. The effects of solvent interaction are to lengthen the Hg-Cl bond (and thus lower the energy of vibrations). Solvents containing O, N, S, and P exhibit increasing interaction with HgCl_2 . In the extreme case, a strongly coordinating solvent like triethylphosphine causes a lowering of ν_s and ν_{as} to 209 and 195 cm^{-1} , respectively (151). These shifts must be considered coordination complexes of the form HgCl_2L_2 ; for L = pyridine, the solid state Raman spectrum of $\text{HgCl}_2(\text{py})_2$ and the solution Raman spectrum of HgCl_2 in pyridine have nearly identical $\nu(\text{Hg-Cl})$.

By using a variety of techniques, the species MX^+ , MX_2 , MX_3^- , and MX_4^{2-} have been observed in titrations of Hg(II) with varying quantities of Cl^- . Importantly, increasing the coordination number results in a lower frequency vibration in the Raman spectrum (22). For Zn and Cd, MX_3^- is not trigonal planar in tri-*n*-butyl phosphate solutions, as evidenced by observation of an IR band for the totally symmetric stretching mode ν_s , forbidden in D_{3h} symmetry; for Hg(II), the D_{3h} geometry is observed.

B. "Linear" Hg(II)-Thiolates

By far the most studied of Hg(II)-thiolate compounds are those with the stoichiometry $\text{Hg}(\text{SR})_2$. While no vibrational studies have been carried out in the vapor phase or in matrix isolation, a number of solution studies exist, and many solid-state vibrational spectra have been reported. In some cases, significant differences in solution and solid-state spectra are found. The vibrational data are consistent with linear coordination in the vast majority of compounds. Where important secondary interactions exist or when the geometry changes from linear to tetrahedral (as in the structurally characterized $\text{Hg}(\text{S}-t\text{-Bu})_2$, Fig. 7), the Raman and IR data reflect deviation from simple linear coordination, although in some cases, the proper assignment of Hg-S vibrational modes is unclear, for the reasons described above.

Table XI lists solid-state and solution Raman and IR data for compounds with the stoichiometry $\text{Hg}(\text{SR})_2$. Of the five compounds structurally characterized, $\text{Hg}(\text{SMe})_2$ (25), $\text{Hg}(\text{SEt})_2$ (23), and $[\text{Hg}(4\text{-MP})_2]^{2+}$ (10) are essentially linear, while $\text{Hg}(\text{S}-t\text{-Bu})_2$ (Fig. 7) and $\text{Hg}(\text{S}-n\text{-Bu})_2$ have polymeric structures, with all thiolates bridging the Hg centers to provide a distorted

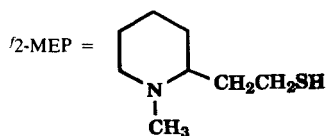
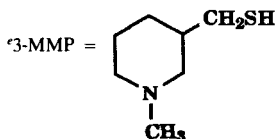
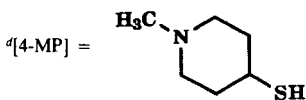
TABLE XI
 Vibrational Spectroscopy of Hg(SR)_n

Compound	Structure	Solid State			Solution			
		IR (cm ⁻¹)	Raman (cm ⁻¹)	Reference	Solvent	IR (cm ⁻¹)	Raman (cm ⁻¹)	Reference
Hg(SMe) ₂	Linear	337 338 338	297 295 298	34 97 18	Pyridine	335		18
Hg(SEt) ₂	Linear	268 405 268	246 394 245	18 34	Pyridine	330	304	18
Hg(S- <i>n</i> -Pr) ₂		256		18	CCl ₄ Pyridine	330 359	329	18 18
Hg(S- <i>n</i> -Bu) ₂	Tetrahedral	252	218	18	Pyridine CCl ₄	361 358	325	18 18
Hg(S- <i>t</i> -Bu) ₂	Tetrahedral	337 172	185 188	18 34	Pyridine CCl ₄	246 274	223	18 18
Hg(BALH) ^a		~348	~298	28				
Hg(BME) ₂ ^b		371	352	30, 35				
Hg(SPh) ₂		365	344	30, 35				
Hg(DMPH) ^c		353	325	30, 35				
[Hg(4-MP) ₂][(ClO ₄) ₂] ^d	Linear	395	372	10				
[Hg(3-MMP) ₂][(ClO ₄) ₂] ^e		350	326	10				
[Hg(2-MEP) ₂][(ClO ₄) ₂] ^f		350	302	10				
Hg(SCH ₂ C(O)NH(CH ₃) ₂) ₂		311	305	148, 214				
Hg(SCys) ₂			327	195				
[Et ₄ N] ₂ [Hg ₂ (SMe) ₆]	Bridging tetrahedral	260-280	259	23	EtOH		282	23
[Et ₄ N][Hg(S- <i>t</i> -Bu) ₃]	Trigonal	206	208	23	EtOH		206	23
[Bu ₄ N][Hg(S- <i>t</i> -Bu) ₃]		201	203	23				
[N(PPh ₃) ₂][Hg(S- <i>t</i> -Bu) ₃]		212	211	23				
[PPh ₄][Hg(SPh) ₃]		178	180	119				
[PPh ₄] ₂ [Hg(SPh) ₄]		158						
		165	179	119				

^aBALH = 2,3-dimercaptopropanol.

^bBME = 2-mercaptoethanol.

^cDMPH = 1,3-dimercapto-2-propanol.



tetrahedral environment in the solid state. In the remaining compounds, the geometry has been tentatively assigned as linear, based on the symmetric stretch (Raman-active) and the asymmetric stretch (IR-active).

Three groups have reported vibrational data for Hg(SMe)₂ in the solid state, all of which are in agreement: $\nu_{as} = 337 \text{ cm}^{-1}$ in the IR, and $\nu_s = 297 \text{ cm}^{-1}$ in the Raman (18, 34, 97). In all cases where the geometry is

linear, the symmetric stretch is at lower energy, as expected. Furthermore, none of the linear compounds have the coincidence of Raman and IR bands expected for noncentrosymmetric species. As seen in Table III, $\text{Hg}(\text{SMe})_2$ exhibits significant secondary interactions in the solid state not found in $\text{Hg}(\text{SEt})_2$. It is not surprising, then, that the vibrational spectra for the ethyl and methyl derivatives differ; however, two groups have proposed radically different assignments for $\nu(\text{Hg-S})$. In a study of several aliphatic $\text{Hg}(\text{SR})_2$ derivatives, Biscarini et al. (18) assigned ν_s and ν_{as} at 268 and 246 cm^{-1} , respectively, for $\text{Hg}(\text{SEt})_2$. Canty et al. (34), on the basis of comparison with Zn and Cd derivatives and of the physical properties of $\text{Hg}(\text{SMe})_2$ (mp = 175°C) and $\text{Hg}(\text{SEt})_2$ (mp = 76°C), favored the assignment of ν_s at 405 cm^{-1} and ν_{as} at 394 cm^{-1} .

Two lines of reasoning favor Canty's assignment follow. First, the vibrations of most of the other linear compounds fall between 300 and 400 cm^{-1} . Indeed, the only other spectroscopic data on a crystallographically determined example of linear coordination is for $[\text{Hg}(\text{4-MP})_2]^{2+}$ (the complex is positively charged because the ligand is zwitterionic), where $\nu_{as} = 395 \text{ cm}^{-1}$ and $\nu_s = 372 \text{ cm}^{-1}$ (10). The second point is that in the absence of secondary interactions in the solid state, one would expect the Hg-S modes in the solid to occur at higher energy than in solution, where even noncoordinating solvents exhibit some interaction. Biscarini et al. (17) measured the solution spectrum of $\text{Hg}(\text{SEt})_2$ in CCl_4 and in pyridine, and, in both solvents, ν_{as} was 330 cm^{-1} . This value suggests the higher set of values for the Hg-S modes are correct.

A number of $\text{Hg}(\text{SR})_2$ complexes with potentially chelating ligands have been studied: $\text{Hg}(\text{BALH})$, $\text{Hg}(\text{BME})_2$, and $\text{Hg}(\text{DMPH})$ (Table XI). In all cases, a linear geometry is reported, on the basis of the vibrational data. The only aromatic R group studied is phenyl (35), and the reported data point to linear coordination as well ($\nu_{as} = 365 \text{ cm}^{-1}$, $\nu_s = 344 \text{ cm}^{-1}$).

The only $\text{Hg}(\text{SR})_2$ compounds with nonlinear coordination in the solid state are $\text{Hg}(\text{S-}t\text{-Bu})_2$ and $\text{Hg}(\text{S-}n\text{-Bu})_2$, which have bridging thiolates to give a distorted tetrahedral coordination. The crystal structure of the *t*-Bu derivative (Fig. 7) reveals the presence of two long and two short pairs of Hg-S bonds differing by 0.07 Å. The Raman band in this compound has been assigned between 185 and 188 cm^{-1} (18, 34), but of the two assignments for the asymmetric stretch (Table XI), the lower energy band (172 cm^{-1}) is almost certainly correct: Raman data on the tetrahedral analogues $\text{Cd}(\text{S-}t\text{-Bu})_2$ and $\text{Zn}(\text{S-}t\text{-Bu})_2$ identify the 338 cm^{-1} vibration as a ligand mode (34). Solution studies on $\text{Hg}(\text{S-}t\text{-Bu})_2$ indicate the tetrahedral interaction is diminished, if not completely removed. Both in CCl_4 and in pyridine, energies for ν_s and ν_{as} are increased relative to the solid state, but are lower than those reported for the Et, Me, and *n*-Pr derivatives (18). For $\text{Hg}(\text{S-}n\text{-Bu})_2$, the low values for the symmetric and asymmetric

stretches (218 and 252 cm^{-1} , respectively) also reflect higher coordination. Thus, $\text{Hg}(\text{S}-t\text{-Bu})_2$ and $\text{Hg}(\text{S}-n\text{-Bu})_2$ reveal anomalous vibrational properties relative to other $\text{Hg}(\text{SR})_2$ compounds due to the polymeric, distorted-tetrahedral coordination.

Vibrational data on the other compounds in Table XI of the stoichiometry $\text{Hg}(\text{SR})_2$, which have not been structurally characterized, is consistent. For linear coordination, symmetric and asymmetric vibrations may be expected in the Raman and IR, respectively, between 250 and 400 cm^{-1} . If the *S-n-Pr* species is removed from consideration, the window is narrowed from 330 to 400 cm^{-1} for the IR and 300 to 370 cm^{-1} for the Raman. From the correspondence of the remaining data, one must conclude that either the *S-n-Pr* derivative exhibits important secondary interactions or has been misassigned, more likely the former. In any case, as we will see below, the "two-coordinate window" clearly distinguishes linear coordination, even in cases with strong secondary bonding interactions, from trigonal or tetrahedral coordination. There exists a need for more solution-phase and gas-phase (or matrix isolation) vibrational studies on $\text{Hg}(\text{SR})_2$ to obtain vibrational data when tetrahedral coordination or secondary interactions are clearly absent, and thus definitively establish the vibrational profiles for two-coordinate complexes.

C. Three- or Four-Coordinate Hg(II) Thiolates

Under certain conditions, the preference of Hg(II) for a CN = 2 with thiolate as a ligand can be overcome, and a few simple mononuclear complexes of the formulas $[\text{Hg}(\text{SR})_3]^-$ and $[\text{Hg}(\text{SR})_4]^{2-}$ have been structurally characterized. Unfortunately, only Bowmaker et al. (23) and Liesk et al. (119) have reported vibrational data. As was found with chloride compounds, the structure, and hence the vibrational spectra, of anionic Hg(II) thiolates are very cation dependent. Moreover, these studies considered only phenyl, methyl, and *t*-Bu derivatives, which are more dissimilar than similar. Nonetheless, the data are consistent and effectively distinguish bonding interactions (primary CN = 3,4) from secondary interactions (primary CN = 2). Based on correlation of the structurally characterized complexes and vibrational data it is not possible at this time to distinguish between three- and four-coordinate complexes on vibrational data alone.

Vibrational analysis of crystalline $[\text{Et}_4\text{N}]_2[\text{Hg}_2(\text{SMe})_6]$ has been carried out. This compound is a dimer of $[\text{Hg}(\text{SMe})_3]^-$ subunits, containing both bridging and terminal thiolates, as shown in Fig. 5. The geometry about Hg(II) is distorted tetrahedral. The vibrations were assigned by comparison to the isostructural $[\text{Hg}_2\text{Cl}_6]^{2-}$ anion (23). In the Raman, bands at 271 and 259 cm^{-1} are assigned to terminal Hg-S modes, while bands between 250

and 180 cm^{-1} correspond to modes involving bridging thiolates (Table XI). In EtOH solution, the Raman spectrum exhibits noticeable changes, including loss of bridging modes. The increase in the terminal stretch from $(260\text{--}270)$ to 282 cm^{-1} is consistent with a decrease in coordination number; hence, Bowmaker et al. suggested that dissociation to $[\text{Hg}(\text{SMe})_3]^-$ monomers occurred. Further evidence for dissociation comes from the coalescence of the two sharp $\nu(\text{CS})$ bands (bridging and terminal) split by 7 cm^{-1} in the solid state. The Raman spectrum has one fewer band (two) than expected (three) for a trigonal planar molecule with local D_{3h} symmetry, but this difference could result from accidental degeneracy or large differences in intensity.

Bowmaker et al. also studied [cation][$\text{Hg}(\text{S}-t\text{-Bu})_3$] vibrational spectra (cation = $[\text{Et}_4\text{N}]$, $[\text{Bu}_4\text{N}]$, and $[(\text{Ph}_3\text{P})_2\text{N}]$). In the solid state, with all three cations, asymmetric and symmetric stretches between 200 and 212 cm^{-1} were observed. The Raman spectrum of a concentrated EtOH solution of $[\text{Et}_4\text{N}][\text{Hg}(\text{S}-t\text{-Bu})_3]$ gave excellent agreement with the solid-state spectrum, indicating a lack of structural change upon dissolution. The ratio of the totally symmetric modes for the $t\text{-Bu}$ and Me in solution ($282:206 = 1.4$) is equal to the ratio of the square root of the masses of the ligands. The recently determined crystal structure of $[\text{Et}_4\text{N}][\text{Hg}(\text{S}-t\text{-Bu})_3]$ showed a trigonal planar geometry about Hg(II) (202), which is likely adopted in solution, and corroborates the vibrational assignment.

The solid-state vibrational study of $[\text{Ph}_4\text{P}][\text{Hg}(\text{SPh})_3]$ is interesting because Liesk and Klar consider the possibility of trigonal nonplanar coordination (119). Group theory predicts that for trigonal planar geometry, ν_s and ν_{as} are Raman-active, while only ν_{as} is IR active. In contrast, in a trigonal pyramid, both bands are active in both the Raman and IR. They observed two strong bands in the IR and consequently assigned a trigonal pyramid structure to the anion. X-ray crystallography of the analogous complex $[\text{Bu}_4\text{N}][\text{Hg}(\text{SPh})_3]$ showed a trigonal planar coordination; however, this result in no way precludes the trigonal pyramid structure for the $[\text{Ph}_4\text{P}]^-$ complex since the structures of $[\text{HgX}_3]^-$ and $[\text{Hg}(\text{SR})_3]^-$ anions exhibit cation-dependent vibrational spectra. The corresponding $[\text{Me}_4\text{N}]^+$ salt is reported to contain binuclear anions of the type observed for $\text{R} = \text{Me}$. The chemistry of $[\text{HgI}_3]^-$ provides an even clearer example of the influence of the cation on crystal structure: with $[\text{Bu}_4\text{N}]^+$, discrete monomers are found; with the smaller $[\text{Pr}_4\text{N}]^+$, dimeric $[\text{Hg}_2\text{I}_6]^{2-}$ units are formed; with smaller yet $[\text{SMe}_3]^+$, an infinite chain of trigonal bipyramids is crystallized (22). Thus, what could be construed as negligible changes in cation size dramatically alter the structures of these Hg(II) compounds. The interactions responsible for these structural alterations is necessarily weak, as the vibrational modes of the $[\text{Bu}_4\text{N}]^+$ and $[\text{SMe}_3]^+$ salts are almost

the same (22). Clearly, the subtle differences between trigonal planar and trigonal pyramidal geometry cannot be resolved on the basis of vibrational spectra alone, because of the difficulties associated in assigning all possible modes in both the Raman and IR.

A single tetracoordinate mononuclear anion, $[\text{Ph}_4\text{P}]_2[\text{Hg}(\text{SPh})_4]$, has been characterized by vibrational spectroscopy (119) and X-ray crystallography. Infrared and Raman bands are observed at 165 and 179 cm^{-1} , respectively. A second Raman band, expected for tetrahedral coordination, was not located. As for $[\text{Hg}(\text{SPh})_3]^-$, the low wavenumber vibrations in part reflect the increased ligand mass relative to *t*-Bu or Me. Vibrational data on examples of aliphatic compounds of the form $[\text{Hg}(\text{SR})_4]^{2-}$ must be obtained before coherent predictions for the vibrational window of these compounds can be made. The data in Table XI illustrate a clear delineation between linear, $\text{CN} = 2$ and trigonal-tetrahedral, $\text{CN} = 3,4$. It is safe to say that positive identification of Hg-S stretches below 260 cm^{-1} rules out linear coordination in favor of trigonal or tetrahedral geometry. No example of trigonal bipyramidal coordination has been elucidated, but such complexes would likely also fall in this range.

Many compounds of the form MX_2L_2 are known, and generally a pseudotetrahedral geometry is adopted (57). When the local symmetry is C_{2v} , there should be two M-X modes, both IR and Raman active, with the M-X modes falling roughly in the region of 175–300 cm^{-1} . Thus, it may be difficult to distinguish $\text{Hg}(\text{SR})_4$ compounds from $\text{Hg}(\text{SR})_3\text{L}$ or $\text{Hg}(\text{SR})_2\text{L}_2$ analogues on the basis of vibrational energy alone; in the absence of other physical data, only the number and coincidences of vibrational modes can be used for structural characterization.

VI. ^{199}Hg NMR SPECTROSCOPY OF $\text{Hg}(\text{II})$ -THIOLATE COMPLEXES

The use of NMR spectroscopy to characterize diamagnetic transition metal and posttransition metal complexes has increased tremendously in the past decade (111, 129). Mercury has two NMR-active isotopes, ^{201}Hg (natural abundance = 13.22%) and ^{199}Hg (natural abundance = 16.84%). The former is quadrupolar (nuclear spin, $I = \frac{3}{2}$), and consequently, much more difficult to observe, due to line broadening. The latter, on the other hand, is one of approximately 20 nuclides in the periodic table with the preferred spin $I = \frac{1}{2}$. Its receptivity, a measure of relative signal strength, is five times that of ^{13}C ; for comparison, ^{113}Cd , the most widely studied of the posttransition nuclei, has a receptivity of only 8 relative to ^{13}C . Magnetic resonance frequencies are intimately connected with the quantity and dis-

tribution of charge around the nucleus of interest; thus, NMR studies of Hg(II)-thiolate complexes can be expected to shed light on the nature of the Hg(II) coordination environment.

Because of the important link between coordination environment and chemical shift, a brief review of the components of shielding are presented here (99). To a certain extent, circulation of electrons screens a nucleus from an external magnetic field, B_0 , so that the effective field felt by the nucleus, B_{eff} , is defined in Eq. 3, where σ (the shielding) is a measure of the nuclear screening. The resonant frequency is proportional to the ef-

$$B_{\text{eff}} = B_0 (1 - \sigma) \quad (3)$$

fective magnetic field, so at a fixed magnetic field strength, shielded nuclei resonate at low frequency, and deshielded nuclei resonate at high frequency. Resonant frequencies are converted to chemical shifts, δ (in ppm), and compared with a standard, typically $\text{Hg}(\text{CH}_3)_2$, which is assigned a chemical shift of 0 ppm. On a relative scale, $\text{Hg}(\text{CH}_3)_2$ is highly deshielded, and so most ^{199}Hg chemical shifts are upfield (negative ppm). The shielding, a reflection of the electronic surroundings of the nucleus, is a tensor quantity but only the diagonal elements, σ_{11} , σ_{22} , and σ_{33} are of relevance. In solution, free rotation renders the shielding isotropic, and what is measured is σ_{ave} (Eq. 4). In a solid-state NMR experiment, the individual tensor elements can be determined. Of the posttransition metal NMR-active nuclides, only ^{199}Hg and ^{113}Cd have received significant attention. The other

$$\sigma_{\text{ave}} = (\sigma_{11} + \sigma_{22} + \sigma_{33})/3 \quad (4)$$

nuclei are limited by either very low receptivity, excessively long spin lattice relaxation times, or in the case of Cu(I), large quadrupole moments (129). In contrast, ^{113}Cd has been the subject of extensive study in solution and in the solid state, both for Cd(II)-thiolate compounds (75) and for Cd(II) metalloproteins with coordinated cysteines (69, 109, 177, 186). Where possible, comparisons of ^{113}Cd and ^{199}Hg data will be used to learn about the periodic properties of shielding.

A. Solution ^{199}Hg NMR

Although solution spectra of Hg(II) compounds are relatively easy to obtain (124), they have proven hard to interpret. Aside from minor difficulties that arise from solvent-dependent and concentration-dependent chemical shifts, the solution structure of dissolved Hg(II)-thiolate com-

plexes is not always clear. As noted in Section IIB.D, the tendency for Hg(II) to increase its coordination number through secondary interactions is great, and in some cases vibrational spectra in the solid and solution states correspond to completely different species. Furthermore, thiolate exchange is very rapid in aqueous solutions (36, 42). Thus, the aqueous Hg(II)-thiolate interaction is dynamic, and care is required in assigning solution chemical shifts to particular species. Fortunately, the shielding range for Hg(II) is about 4500 ppm, larger than for any other metal in Groups IB and IIB, and often big enough to allow meaningful conclusions to be drawn about the electronic environment at the nucleus, even in the fast-exchange limit.

Table XII lists representative chemical shifts for a large number of $CN = 2$ Hg(II) thiolates. The chemical shifts fall into a range from -1200 to -800 ppm. The data encompass thiols containing straight-chain alkyls, branched alkyls, aromatic rings, saturated rings, and heteroatom-functionalized alkyls (glutathione). Notice that $Hg(SCN)_2$ and $Hg(Et_2dte)_2$ fall in this 400-ppm range, even though they are not simple thiolates. The chemical shift is dependent on solvent; for example, $Hg(SEt)_2$ has a δ at -805 ppm in chloroform, and -758 in 1:1 DMSO-pyridine. In fact, the shift in $CDCl_3$ is reported at $\delta = -983$ ppm, although this difference could be due to different concentrations of Hg(II). Among two-coordinate Hg(II) compounds, thiolates exhibit a moderate amount of shielding. At the two extremes of ^{199}Hg chemical shifts are $Hg[Si(C_2H_5)_3]_2$, with an extremely deshielded chemical shift of 815 ppm, and HgI_2 , highly shielded at -3435 ppm (71). The thiolate compounds as a class have the most narrow window of chemical shifts. As can be discerned from Table XII, thiolates span a window of ~ 850 ppm. The compounds $HgCl_2$, $HgBr_2$, and HgI_2 have shifts of -1550 , -2212 , and -3435 ppm, respectively, a span of almost 2000 ppm, while the chemical shifts of dialkyl mercury compounds vary by over 1000 ppm (71, 111).

Variation of the R group in $Hg(SR)_2$ reveals trends in shielding, shown by the chemical shifts for $Hg(SR)_2$ in $CHCl_3$ (56). In the homologous series $Hg(SCH_2R)_2$ ($R = H, Me, Et, n-Bu, \text{ and } C_6H_5$), the hydrogen and phenyl derivatives are more shielded by ~ 70 ppm. Branching on the alkyl substituents has no effect. The most shielded of the linear compounds is the $Hg(SPh)_2$; replacement of S by Se in this compound further increases the shielding.

Carson and Dean have also studied tetracoordinate anions formed by solubilizing Hg(II) salts with excess RSH and NaOH (36). Both with monodentate and chelating thiolates, the observed chemical shifts for the resulting species in solution are far removed from those for the linear compounds. The potentially chelating dithiols are deshielded with respect to

TABLE XII
Solution ^{199}Hg Chemical Shifts of Mercuric-Thiolate Compounds

Compound	Solvent	$\delta(^{199}\text{Hg})^a$	Reference
Hg(glutathione) ₂	H ₂ O	-993	182
Hg(SCN) ₂	DMSO ^b	-1101	150
Hg(SC ₆ H ₅) ₂	DMSO ^b	-976	150
Hg(SC ₆ H ₅) ₂	DMSO/pyridine 1:1 ^c	-893	150
Hg(SET) ₂	DMSO/pyridine 1:1 ^c	-758	150
Hg(SC ₆ H ₄ Cl) ₂ (<i>d</i>)	DMSO	-1136	136
Hg(S- <i>n</i> -Pr) ₂	CDCl ₃	-814	113
Hg(S- <i>i</i> -Pr) ₂	DMSO	-889	136
Hg(SET) ₂	CDCl ₃	-983	113
Hg(SeC ₆ H ₅) ₂	0.5M pyridine	-1270	149
Hg(Et ₂ dtc) ₂ (<i>e</i>)	0.5M pyridine	-1181	149
Hg(SMe) ₂	CHCl ₃ (sat.)	-871	56
Hg(SET) ₂	CHCl ₃ (0.1M)	-805	56
Hg(S- <i>n</i> -Pr) ₂	CHCl ₃ (0.1M)	-807	56
Hg(S- <i>i</i> -Pr) ₂	CHCl ₃ (0.1M)	-795	56
Hg(S- <i>n</i> -Bu) ₂	CHCl ₃ (0.1M)	-801	56
Hg(S- <i>t</i> -Bu) ₂	CHCl ₃ (sat.)	-793	56
Hg(SC ₃ H ₇) ₂	CHCl ₃ (0.1M)	-801	56
Hg(Scyclohexyl) ₂	CHCl ₃ (0.1M)	-772	56
Hg(SCH ₂ Ph) ₂	CHCl ₃ (0.1M)	-889	56
Hg(SPh) ₂	CHCl ₃ (sat.)	-1065	56
Hg(SePh) ₂	CHCl ₃ (sat.)	-1512	56
[Hg(SC ₆ H ₄ Cl) ₄] ²⁻	DMSO	-569	135
[Hg(SC ₆ H ₅) ₃]	DMSO	-354	135
[Hg(S- <i>t</i> -Bu) ₃]	DMSO	-157	135
[Hg(SMe) ₄] ²⁻	1:1 H ₂ O/D ₂ O ^f	-374	36
[Hg(SET) ₄] ²⁻	1:1H ₂ O/D ₂ O ^f	-302	36
[Hg(S- <i>i</i> -Pr) ₄] ²⁻	1:1H ₂ O/D ₂ O ^f	-275	36
[Hg(S- <i>i</i> -Pr) ₄] ²⁻	CH ₃ OH	-152	136
[Hg(SPh) ₄] ²⁻	1:1H ₂ O/D ₂ O ^f	-585	36
[Hg(SCH ₂ CH ₂ S) ₂] ²⁻	1:1H ₂ O/D ₂ O ^g	-60	36
[Hg(SCH(Et)CH ₂ S) ₂] ²⁻	1:1H ₂ O/D ₂ O ^g	-51	36
[Hg(tdt) ₂] ²⁻ (<i>h</i>)	1:1H ₂ O/D ₂ O ^g	-19	36
[Hg(SePh) ₄] ²⁻	1:1H ₂ O/D ₂ O ⁱ	-978	36

^aIn ppm relative to Hg(CH₃)₂.

^bEquilibrated mixtures of 0.5M Hg(C₂Cl₃)₂ and 0.5M Hg(SR)₂.

^cEquilibrated mixtures of 0.25 M Hg(C₂Cl₃)₂ and 0.25M Hg(SR)₂.

^dSC₆H₄Cl = 4-Cl-thiophenolate.

^eEt₂dtc = *N,N*-diethyldithiocarbamate.

^fIn solution containing thiol: Hg(NO₃)₂:NaOH = 12:1:24; [Hg(II)] ≈ 0.1 M.

^gIn solution containing dithiol: Hg(NO₃)₂:NaOH = 6:1:18; [Hg(II)] ≈ 0.1 M.

^htdt²⁻ = toluene-3,4-dithiolate.

ⁱPhSeH: Hg(NO₃)₂:NaOH = 10:1:20 [Hg(II)] ≈ 0.1 M.

the monothioils. The aromatic chelate, toluene-3,-4-dithiolate (tdt), is least shielded among Hg complexes of the bidentate ligands. This result is quite perplexing in that, for CN = 2, 3, and 4 Hg(II) complexes of monothioils, the phenyl derivatives are more shielded than the alkyl derivatives. It is therefore quite possible that the observed deshielded chemical shift arises from a species other than $[\text{Hg}(\text{tdt})_2]^{2-}$, perhaps a cluster similar to $[\text{Hg}_3(\text{SCH}_2\text{CH}_2\text{S})_4]^{2-}$, which contains the bidentate $^-\text{SCH}_2\text{CH}_2\text{S}^-$. As can be seen from the structure of a complex isolated from the reaction of excess $^-\text{SCH}_2\text{CH}_2\text{S}^-$ (Fig. 8), none of the ethanedithiolate ligands chelate a single Hg(II); rather, each of the four bridges two Hg centers in this trinuclear cluster. This cluster is isolated under conditions similar to those used for the ^{199}Hg NMR study, so it is possible that the observed shift corresponds to the cluster, as opposed to the assigned $[\text{Hg}(\text{tdt})_2]^{2-}$ center. However, based on solid-state studies of other aromatic thiolates (see below), a cluster is unlikely, and the chemical shift reported for this species remains enigmatic. Solution chemical shifts for a variety of four-coordinate Hg complexes with O, N, and P ligands have been reported (71).

Both of the structurally characterized three-coordinate Hg(II)-thiolates, $[\text{Hg}(\text{S}-t\text{-Bu})_3]^-$ and $[\text{Hg}(\text{SPh})_3]^-$, have been studied in solution using ^{199}Hg NMR (135, 136), and the ^{199}Hg chemical shifts seem to fall in the same broad range as the four-coordinate complexes. Figure 12 shows a plot of

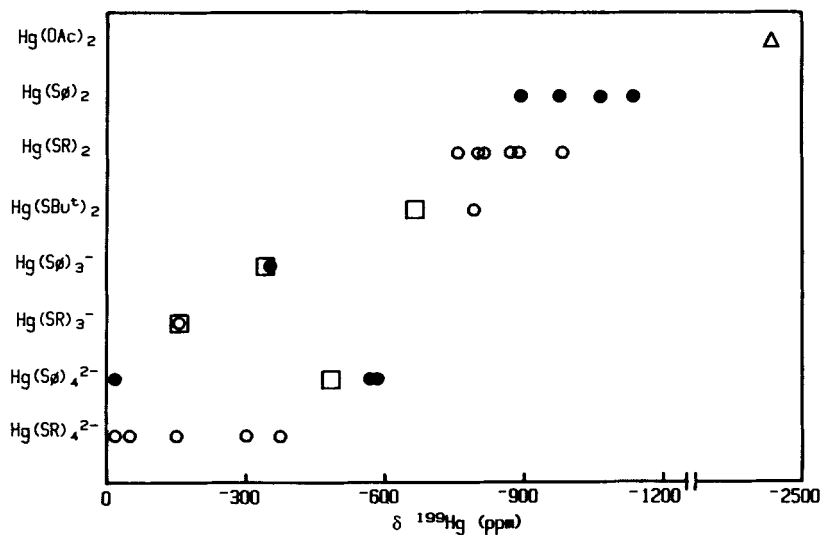


Figure 12. Solution and solid-state ^{199}Hg chemical shifts of Hg(II)-thiolate complexes. \bullet = aromatic thiols; \circ = aliphatic thiols; \square = solid-state chemical shifts; Δ = $\text{Hg}(\text{O}_2\text{CCH}_3)_2$.

chemical shifts vs. decreasing coordination number, and illustrates the general trend that in solution, the isotropic shift is deshielded as the coordination number increases. The chemical shift of $\text{Hg}(\text{OOCCH}_3)_2$ is very highly shielded compared to the thiolate compounds, and illustrates the potential utility of the isotropic chemical shift in distinguishing Hg-S from Hg-O environments.

The fundamental problem with the data in Table XII, and a danger in overinterpreting any trends in the solution data of Fig. 12, is that in most cases the coordination number, the solution structure, and the degree of polymerization are not well established. In addition to the problem of determining Hg nuclearity described above, solution NMR data on Group IIB thiolates indicate ligand exchange is commonplace and rapid on the NMR time scale (36). In fact, Carson and Dean were unable to obtain slow exchange ^1H or ^{13}C NMR of any Hg(II)-thiolates, and they report that the lability of tetrathiometallates increases in the order $\text{Zn(II)} < \text{Cd(II)} < \text{Hg(II)}$. This finding implies that the observed chemical shifts in solution are averages of at least two species in rapid exchange. The high lability of Hg(II)-thiolates poses a significant barrier to quantitative arguments about shielding vs. coordination number, particularly under conditions where different types of mercury coordination environments can exist. For example, the strongly basic conditions used for the four-coordinate studies suggest the possibility that hydroxide could compete as a ligand. In ^{113}Cd NMR, the influence of dynamic solution processes on observed chemical shifts was the primary impetus for the development of solid-state ^{113}Cd NMR (186). Despite problems in sensitivity inherent to solid-state NMR, one key advantage to this technique is that the coordination environment is static and, when combined with X-ray crystallography, provides a definitive structure-chemical shift correlation against which solution data can be compared.

B. Solid-State ^{199}Hg NMR

Solid-state ^{199}Hg NMR can clearly resolve several issues raised by solution NMR studies. If the solid-state isotropic shift is equal to the solution shift, then the solution chemical shift does not represent an average of several species in rapid exchange. As has been shown with ^{113}Cd NMR (186), correspondence between solution and solid-state chemical shifts greatly increases the ability of the inorganic chemist to use solution spectra to classify molecular structure and bonding. Equally important, analysis of the solid-state chemical shift and the shielding tensor components can provide information about coordination number and asymmetry at the metal center in solids, even when other structural information is lacking.

In solid-state NMR, the individual diagonal elements of the shielding tensor, σ_{11} , σ_{22} , and σ_{33} can be determined, provided the molecule possesses appropriate symmetry (see below). The shielding anisotropy, $\Delta\sigma$, is a measure of the distortion from spherical symmetry (Eq. 5). Another parameter of interest is the asymmetry factor, η , defined in eq. 6. Eta is a measure

$$\Delta\sigma = \sigma_{33} - (\sigma_{22} + \sigma_{11})/2 \quad (5)$$

of deviation from axial symmetry; by definition, in axially symmetric systems, $\sigma_{11} = \sigma_{22}$, and thus $\eta = 0$. Ideally, the chemical shift (δ), shift

$$\eta = (\sigma_{22} - \sigma_{11})/(\sigma_{33} - \sigma_{\text{ave}}) \quad (6)$$

anisotropy ($\Delta\sigma$), and asymmetry represent powerful probes of stereochemistry and bonding in spin = $\frac{1}{2}$, diamagnetic metal compounds such as Hg(II), Cd(II), and Ag(I).

Given the differences between solution and solid-state structures for Hg(II)-thiolates, one would like to measure NMR spectra of defined complexes in the solid state routinely, and utilize the additional information contained in the shielding tensor elements. Unfortunately, the major obstacle to solid-state NMR spectroscopy is excessive line broadening, which results from spin-spin relaxation (through dipolar interaction), and is inherent to oriented materials. One way to overcome this obstacle is to spin the solid sample very rapidly (1–15 kHz) at an angle of 54.9° with respect to B_0 . This technique, magic angle spinning (MAS), effectively decouples the nuclei responsible for dipolar broadening, yielding an envelope of narrow lines separated by the spinning speed. The isotropic chemical shift is invariant, and is determined by spinning the sample at different speeds (Fig. 13), and identifying the sideband that does not move (126).

For magnetically dilute species, such as ^{13}C and ^{199}Hg , cross-polarization (CP) can be used to further enhance solid-state signals. In this technique, spin is transferred from abundant, highly receptive nuclei like ^1H to the dilute spin by simultaneous application of two magnetic fields. The net effect is to create a reservoir of spin for the weak signal, through dipolar interaction. Note that the goal of MAS was to decouple dipolar interactions; thus, CP requires a reduction, but not elimination, of MAS in order to restore dipolar interactions. Coupling of the two techniques (CP MAS) is currently the best method available for measuring NMR spectra of solids (212).

The chemical shift anisotropy of $\text{Hg}(\text{CH}_3)_2$ and of a number of other linear dialkyl Hg(II) compounds has been measured either in liquid

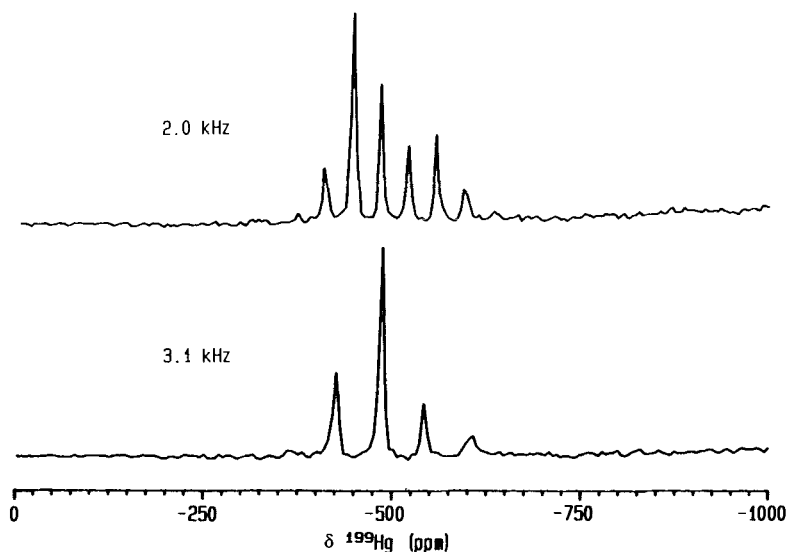


Figure 13. The ^{199}Hg CP MAS NMR spectra of $[\text{Me}_4\text{N}]_2[\text{Hg}(4\text{-chlorothiophenolate})_4]$ at spinning speeds of 2.0 and 3.1 kHz. The chemical shifts are referenced to $\text{Hg}(\text{CH}_3)_2$.

crystals or by the magnetic field dependence of the relaxation time, T_1 (70, 102, 110, 115, 201). The data indicate a huge chemical shift anisotropy for linear $\text{Hg}(\text{II})$ ($\Delta\sigma = 5000\text{--}7000$ ppm), twice that of $\text{Cd}(\text{II})$ (71). The ramification of such high anisotropy is that, for purely linear $\text{Hg}(\text{II})$ compounds, the solid-state spectra will be too broad to be interpretable.

The first report of solid-state CP MAS ^{199}Hg NMR came in 1987 from Harris and Sebold in their survey of NMR of several heavy metal spin $\frac{1}{2}$ nuclei (78). Failure to obtain spectra of $\text{Hg}(\text{Ph})_2$, $\text{CH}_3\text{HgO}_2\text{CCH}_3$, or $\text{PhHgO}_2\text{CCH}_3$, was attributed to excessive sideband patterns ($\gg 125$ kHz), a result of the large shift anisotropy expected for linear compounds. They were able to obtain a high-resolution spectrum of $\text{Hg}(\text{O}_2\text{CCH}_3)_2$, which they classified as a distorted four-coordinate Hg center. The crystal structure of $\text{Hg}(\text{O}_2\text{CCH}_3)_2$ (4) shows two oxygen atoms at 2.05–2.07 Å with an O–Hg–O bond of 175°, and three more oxygen atoms at a distance of 2.75 Å (Table III). The latter oxygen atoms are inside the sum of the van der Waals radii for Hg and O, but well outside the typical bond distances. Coupled with the nearly linear geometry of the bonding oxygen atoms, $\text{Hg}(\text{O}_2\text{CCH}_3)_2$ is in fact a two-coordinate linear molecule with three significant secondary interactions; the $\Delta\sigma$ and η parameters are consistent with this assignment. While this result is not unusual for Hg coordination

chemistry, it is surprising that the secondary interactions contribute so significantly to lowering of the anisotropy.

We have recently obtained solid-state CP MAS ^{199}Hg NMR spectra for a number of Hg(II) thiolate complexes of $\text{CN} > 2$ (Table XIII and Figs. 12 and 13) (135, 136). The data are significant in several respects. Most importantly, they show that solid-state ^{199}Hg NMR, like solid-state ^{113}Cd NMR, is an extremely useful tool for characterizing posttransition metal thiolate complexes. Unlike vibrational spectroscopy and electronic spectroscopy, the chemical shift is sensitive only to the coordination environment of the metal. Comparison of isotropic shifts to the corresponding solution data unambiguously confirms or denies the presence of multiple species in solution. Finally, when shift tensor analysis can be performed, information on anisotropy and axial symmetry may be extracted, which are by themselves good indicators of coordination number, as discussed below.

The isotropic shifts of the three-coordinate $[\text{Hg}(\text{SR})_3]^-$ anions agree quite well with the solution chemical shifts, indicating the lack of multiple species in solution (Table XIII). The isotropic chemical shifts of the three-coordinate species are deshielded from the two-coordinate compounds by

TABLE XIII
Solid-State ^{199}Hg NMR Spectroscopic Data

Compound	Coordination Number	Tensor Elements (ppm) ^a	Solution Shift (ppm) ^a	Anisotropy ppm ^a ($\Delta\sigma$)	Asymmetry (η)	References
$\text{Hg}(\text{O}_2\text{CCH}_3)_2$	[2 + 3]	$\sigma_{11} = -1770$ $\sigma_{22} = -2106$ $\sigma_{33} = -3594$ $\sigma_{\text{iso}} = -2490$	-2389 ^b	-1656	0.30	78, 135
$[(\text{CH}_3)_4\text{N}][\text{Hg}(\text{SC}_6\text{H}_4\text{Cl})_4]$	4	$\sigma_{11} = -424$ $\sigma_{22} = -428$ $\sigma_{33} = -602$ $\sigma_{\text{iso}} = -485$	-569 ^c	-176	0.03	135, 136
$\text{Hg}(\text{S}-t\text{-Bu})_2$	4	$\sigma_{11} = -454$ $\sigma_{22} = -557$ $\sigma_{33} = -984$ $\sigma_{\text{iso}} = -665$	-793 ^d	-478	0.32	56, 135
$[(\text{C}_4\text{H}_9)_4\text{N}][\text{Hg}(\text{SPh})_3]$	3	$\sigma_{11} = 180$ $\sigma_{22} = -216$ $\sigma_{33} = -996$ $\sigma_{\text{iso}} = -344$	-354 ^c	> -978	~0.61	135
$[(\text{C}_2\text{H}_5)_4\text{N}][\text{Hg}(\text{S}-t\text{-Bu})_3]$	3	$\sigma_{\text{iso}} = -158$	-157 ^c	~ -1050	0.2-0.6	135

^aPositive chemical shift is deshielded relative to $\text{Hg}(\text{Me})_2$.

^bIn 1M $\text{CH}_3\text{CO}_2\text{H}$.

^cIn DMSO solution.

^dIn CHCl_3 solution.

at least 500 ppm, which is useful in distinguishing between them, but also are slightly deshielded from the four-coordinate species. This trend runs counter to that observed for Cd and Sn toward increased shielding with increasing coordination number (128, 186), but is in agreement with data for non-thiolate Hg(II) complexes (see below).

For the two four-coordinate complexes we have measured by ^{199}Hg CP MAS NMR, $\text{Hg}(\text{S}-t\text{-Bu})_2$ and $[\text{Hg}(\text{SC}_6\text{H}_4\text{Cl})_4]^{2-}$, the solid-state isotropic chemical shifts (Table XIII) do not agree with those obtained in solution (Table XII). The discrepancy arises because $\text{Hg}(\text{S}-t\text{-Bu})_2$ is a polymer in the solid state but is two coordinate in solution. The chemical shift of $\text{Hg}(\text{S}-t\text{-Bu})_2$ in solution more closely corresponds to those measured for other two-coordinate complexes (202). In the case of $[\text{Hg}(\text{SC}_6\text{H}_4\text{Cl})_4]^{2-}$, the complex dissolved in DMSO has a chemical shift of -569 ppm and titration with RS^- leads to a deshielding that approaches the solid-state value (-485 ppm) (136). This finding illustrates the importance of dynamic processes and ligand-dissociated states in solution and is a graphic demonstration of the value of solid state ^{199}Hg NMR (136).

C. Contributions to the ^{199}Hg NMR Chemical Shift

The shielding parameter, σ , is the sum of two terms, σ_d , the diamagnetic shielding, and σ_p , the paramagnetic shielding (Eq. 7). The diamagnetic

$$\sigma = \sigma_d + \sigma_p \quad (7)$$

shielding is that provided by free rotation of electrons about the nucleus while paramagnetic shielding represents the hindrance of free rotation by other electrons and nuclei. The paramagnetic shielding arises from a magnetic field-induced mixing of the ground state with excited states of magnetic dipole-allowed electronic transitions (such as LM CT and $d-d$ transitions). Ramsey developed exact equations, which are beyond the scope of this chapter, to describe σ_d and σ_p . Simplified versions of these equations are given in Eqs. 8 and 9, where $\langle r^{-3} \rangle$ refers to the inverse cube of the

$$\sigma_d \propto \langle r^{-3} \rangle \quad (8)$$

$$\sigma_p \propto -(\Delta E)^{-1} \langle r^{-3} \rangle \langle 0|L^2|0 \rangle \quad (9)$$

radius of the valence orbitals (in this case the d and s manifolds), ΔE is the energy gap between magnetically active optical excitations, and $\langle 0|L^2|0 \rangle$ is the integral of the product of angular momentum operator L squared and the ground-state wave functions (111, 128, 129).

For Hg (and other heavy metals), relativistic contraction of the s and p shells (156), and accompanying expansion of the d orbitals, has a large effect on σ_d , leading to increased screening of the nucleus. It is generally accepted that for d^{10} ions, the *total* shielding is dominated by the diamagnetic term. This phenomenon may be less the case for Hg than for Zn and Cd, because of an increased tendency for d - s orbital mixing, but since σ_d is relatively independent of the chemical environment, it does not come into play in understanding *changes* in screening. Rather, the chemical shifts are dominated by the paramagnetic shielding term. From Eq. 9, it is seen that shielding decreases (σ_p goes down) as r is reduced, as ΔE is reduced, or as angular imbalance of charge increases (through the L term). These factors are all influenced by the identity and geometrical disposition of the ligands around the metal.

Since LMCT bands are magnetic dipole-allowed, the near-UV bands present in three- and four-coordinate complexes, as described in Section IV. B, would serve to deshield ^{199}Hg resonances relative to linear coordination. This shielding pattern has been observed for Hg(II)-thiolates both in solution and the solid state, as well as for $[\text{Hg}\{\text{PO}(\text{OEt})_2\}_n]^{2-n}$, for which the two-coordinate species is about 800 ppm upfield from the three- and four-coordinate complexes (206). If d orbitals are ignored, the angular momentum component of σ_p for three- and four-coordinate species are quite similar; thus, chemical shifts for three- and four-coordinate Hg(II) complexes having similar values for ΔE should be the same, as is found for Hg-S and Hg-P environments (71, 206). The effects of LMCT may not be restricted to changes in ΔE ; *ab initio* calculations have shown that increasing population of metal orbitals possessing nonzero angular momentum leads to increasing paramagnetic contributions (deshielding) (49, 108, 140). The nephelauxetic, or cloud expanding, properties of some ligands may also affect σ_p , through reduction of $\langle r^{-3} \rangle$.

D. Shielding Parameters from Solid-State Spectra

The beauty of CP MAS solid-state NMR spectra comes from the useful chemical information can be extracted from the envelope of narrow lines. Using methods developed by Maricq and Waugh (126) or by Herzfeld and Berger (91), the diagonal tensor elements σ_{11} , σ_{22} , and σ_{33} can be extracted when the isotropic shift is known. Using the tensor elements, the shielding anisotropy and asymmetry are calculated, as shown in Eqs. 5 and 6.

For $[\text{Hg}(\text{SC}_6\text{H}_4\text{Cl})_4]^{2-}$, the very low $\Delta\sigma$ and near-zero asymmetry reveal a high degree of charge symmetry around Hg(II), in accord with the crystallographic data for this compound (Fig. 6). The tetrahedral $\text{Hg}(\text{S}-t\text{-Bu})_2$ shows a pronounced D_{2d} distortion (Fig. 7) and $\Delta\sigma$ increases by ~ 300 ppm. The tetrahedral compounds exhibit the lowest anisotropy, because even

distorted tetrahedral coordination is closer to spherical symmetry than other geometries available to Hg(II). For example, the trigonal planar $[\text{Hg}(\text{SPh})_3]^-$ and $[\text{Hg}(\text{S}-t\text{-Bu})_3]^-$, have substantially larger anisotropies, in the range 800–1000 ppm. Importantly, the anisotropy alone is enough to distinguish three- and four-coordinate Hg(II)-thiolates; the combination of isotropic chemical shift with shift anisotropy and asymmetry data constitutes the most powerful discriminant available of the stereochemistry of CN = 3, 4 Hg(II) thiolates.

Analysis of the $\text{Hg}(\text{O}_2\text{CCH}_3)_2$ spectrum gives $\Delta\sigma = -1656$ ppm, even larger than for the trigonal compounds. This result accords well with the structure, which as described above is more linear than tetrahedral. Clearly, the chemical shift anisotropy is sensitive enough to distinguish strong secondary interactions from primary bonding interactions, and more importantly, from mere van der Waals interactions. In the limit of no secondary interaction, the anisotropy would be expected to be 5000–7000 ppm and could not be measured in a typical CP MAS experiment. While the observed chemical shift anisotropy in $\text{Hg}(\text{O}_2\text{CCH}_3)_2$ is large compared to the other Hg(II) species in Table XIII, the secondary interactions with the nonbonding oxygen atoms at 2.75 Å obviously affect the magnetic field felt by the Hg(II) nucleus.

The information on shielding, coupled with the isotropic chemical shift, provides a detailed view of bonding in these compounds. Using solution and solid-state ^{199}Hg NMR, differences between two-, three- and four-coordinate Hg(II) thiolates are clear, and further classification within a given coordination number is certainly possible. Correlation of solid-state chemical shifts with solution values provides a means of characterizing the dynamic properties of solution species and, with information from vibrational and electronic spectroscopy, should provide a reasonably detailed picture of Hg(II) thiolate chemistry. In principle, ^{199}Hg NMR spectra can provide a detailed picture of the chemical environment of Hg metalloproteins. As with ^{113}Cd metalloprotein NMR, practical limitations include long-term stability of the metalloprotein in the probe, and problems associated with sample spinning even at speeds < 5 kHz (109). These difficulties notwithstanding, ^{199}Hg NMR in the solid state has tremendous potential as a physical-inorganic and bioinorganic tool.

VII. BIOCHEMISTRY AND SITE SPECIFIC MUTAGENESIS OF MerR

Resistance mechanisms specific for mercuric compounds are commonly encountered in both Gram-positive and Gram-negative bacteria; several

detailed reviews are available (176, 182, 183). Genetic studies have defined two classes of plasmid-derived mercury resistance (169). Narrow-spectrum systems provide protection against inorganic mercuric complexes while broad-spectrum resistance provides for detoxification of inorganic Hg(II), as well as a large variety of organomercurials. The central component of the detoxification mechanism in both cases involves the flavoenzyme mercuric ion reductase, which reduces Hg(II) to the less toxic and more volatile Hg(0) by using NADPH as a source of reducing equivalents. The broad-spectrum systems also produce the enzyme organomercurial lyase, which hydrolyzes organomercurials to hydrocarbon and Hg(II) (176, 200). A wide range of organomercurials, such as dimethyl mercury and phenylmercuric acetate, are readily detoxified by this system. The mechanisms of both enzymes have been examined in detail, and kinetic data for mercuric ion reductase and several mutant forms lacking key cysteine residues suggest that mercuric ion may bind to more than two cysteine residues forming a three- or four-coordinate catalytic site for mercuric reductase; however, there is no physical or spectroscopic data supporting this hypothesis at this time (134).

A number of highly homologous MerR proteins native to Gram-negative and Gram-positive bacteria have been defined by mapping of the plasmid-born resistance operons. At least five sequences for MerR proteins are available from various sources, providing broad- and narrow-spectrum resistances. Of these, three proteins have been overexpressed and purified, including the Tn21 and Tn501 MerR proteins, which regulate narrow-spectrum resistance, and *Bacillus* RC607 MerR, which regulates broad-spectrum resistance (81, 82). As can be seen in Fig. 14, the amino acid sequences of these five proteins are generally homologous. The 144 amino acid Tn21 and Tn501 proteins are identical in nearly 94% of their residues; the differences between the three are quite conservative. The remaining proteins display greater differences from one another, but the most dramatic conservation of the proteins is in the spacing and number of cysteine residues throughout the family. Three cysteine residues are preserved in all the proteins and the relative positions of these residues, defined by C-X₃₄-C-X₇-C, remains conserved throughout the family (208). Presumably the differences observed between the broad spectrum (RC607, pDU1358, and pI258) and the narrow spectrum resistance MerR protein sequences reflect the ability of the former to respond to organomercurials, although this difference remains to be demonstrated. Random and site-directed mutagenesis studies have defined putative regions involved in Hg(II) binding and DNA binding suggested from protein sequence homologies (143, 144, 164, 171, 173), as diagrammed in Fig. 15.

Tn21 1 MENNLENLTI GVF**AKAAGVN** VETIRFY**Q**RK GLLRE**P**DKPY GSIRRYGEAD VVRV**K**FKV**KSA** QRLG**F**SLDEI
Tn501 1 MENNLENLTI GVF**AKAAGVN** VETIRFY**Q**RK GLLLE**P**DKPY GSIRRYGEAD VTRV**R**FKV**KSA** QRLG**F**SLDEI
pDU1358 1 MEKNLENLTI GVF**AKAAGVN** VETIRFY**Q**RK GLLPE**P**DKPY GSIRRYGEAD VTRV**R**FKV**KSA** QRLG**F**SLDEI
RC607 1 MKFRI GEL**ADKCGVN** KETIRY**Y**ERL GLIPE**P**ERTE KGYRMY**S**OQY VDR**LHF**IKRM QELG**F**TLNEI
pI258 1 MGMI SEL**AKACDVN** KETVRY**Y**ERK GLIAG**P**PRNE SGYRIY**S**EET ADRV**R**FIKRM KEL**D**FS**L**KEI

Tn21 71 --AELLRLDDGT H**C**EEASSLAE H**K**LKDVRE**KM** ADLARMETVL SELV**C**A**C**CHAR KGNV**S****C**PLIA SLQGEAGLAR SAMP
Tn501 71 --AELLRLEDGT H**C**EEASSLAE H**K**LKDVRE**KM** ADLARMEAVL SELV**C**A**C**CHAR RGNV**S****C**PLIA SLOGGASLAG SAMP
pDU1358 71 --AELLRLDDGT H**C**EEASSLAE H**K**LQDVRE**KM** TDLARMETVL SELV**F**A**C**CHAR QGNV**S****C**PLIA SLQGEKEPRG ADAV
RC607 66 DKLLGWVDRD EAK**C**RD**M**YDF TILKIEDIQR KIEDL**K**RIER MLMD**L**KER**C**P ENKDIY**E****C**PI IETLMKK
pI258 66 HLLFGVWDQD GER**C**KD**M**YAF TVQ**K**TEIER KVQ**G**LLRIQR LLE**L**LKE**C**P DEKAM**Y**T**C**PI IETLMGGPDK

Figure 14. Sequences of the five reported MerR proteins. The Tn21 and Tn501 MerR proteins are from narrow-spectrum resistance systems to mercuric ion, while the pDU1358, RC607, and pI258 MerR proteins come from broad-spectrum mercuric ion and organomercurial resistance systems (82, 176, 208). Bold residues indicate the residues that are strictly conserved among the five proteins. Bold, double underlined residues highlight the three cysteinyl residues believed to be involved in Hg(II) recognition and transcriptional activation.

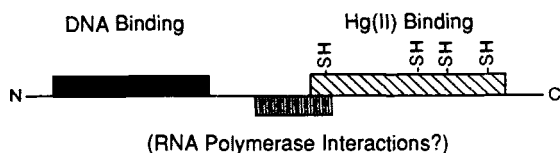


Figure 15. Localization of protein functions as suggested by both the mutagenesis studies of Ross, Shewchuk, and their co-workers (164, 171–173) and protein sequence homology analyses (143, 144, 210).

A. Chemical Modification Studies of MerR

The overexpression and purification of the dimeric, 144 amino acid Tn501 MerR protein in large quantities has made detailed chemical studies possible (143, 145, 171). A variety of studies including gel filtration, equilibrium dialysis, nonequilibrium dialysis, and spectrophotometric titration have indicated that the MerR proteins isolated to date bind a single mercuric ion per protein dimer (82, 145, 171, 202). All of these studies have been performed in the presence of 10–10,000-fold excess buffer thiol competitors, indicating that Hg(II) binds tightly to the protein.

Biochemical and genetic experiments have been reported that attempted to address which protein residues contribute ligands to the Hg(II) atom (82, 164, 171–173). The Tn501 protein sequence, available from the DNA gene sequence, contains a number of residues capable of binding Hg(II) in each monomer, most notably four cysteine residues, three histidines, and four methionines. Three of the four cysteine residues from each monomer react under nondenaturing conditions with the thiol specific reagents 5,5'-dithiobis-(2-nitrobenzoic acid) (DTNB) and iodoacetamide (172, 209). Colorimetric DTNB titrations of the Tn501 Hg–MerR complex yielded different results in different labs. The DTNB titrations of the Hg–MerR complex performed in a slight excess of DTNB (2×10^{-5} M protein and 0.001M DTNB) at pH 7.0 suggest that Hg(II)-binding leads to the protection of 3.2 (0.4) thiols from DTNB reaction in the Tn501 MerR dimer, with no loss of bound Hg(II) (209). These results indicate that the Hg(II) either binds to at least three cysteinyl residues in the Hg–protein complex or exerts a conformational change that prevents cysteines from reacting with the bulky DTNB reagent. Previous reports, under unspecified reaction conditions that apparently used a large excess of DTNB, found that Hg(II) protected two thiols from DTNB reaction in the Tn501 protein (172). Similar studies on the *Bacillus* RC607 protein have shown that bound Hg(II) protects four cysteine residues from reaction with DTNB (82). The reasons for the discrepancies among these different reports are not clear.

If more DTNB is used, the excess aromatic thiol or disulfide could compete with the protein for Hg(II) and thus expose additional protein thiols for reaction with the DTNB reagent. Protein thiol titrations with DTNB are often subject to inaccuracies resulting from oxidation of the thiol residues, background DTNB hydrolysis, and the inherent uncertainty in measuring protein concentrations (161). Any or all of these factors may play a role in the discrepancies in results described above. In efforts to eliminate these contributions, we performed DTNB measurements with relatively low DTNB concentrations of 0.001M and at relatively low pH to eliminate hydrolysis interference. Protein concentration determinations were based on the experimentally determined extinction coefficient of $5800 M^{-1} cm^{-1}$ found for MerR (145).

Alkylation of Tn501 MerR for short duration with [^{14}C]-iodoacetamide suggested that a single cysteine residue in each monomer was protected by Hg(II) ligation, with tryptic mapping of the alkylated protein identifying either Cys-115 or Cys-117 as the protected cysteine (172). Because Cys-115 is the only cysteine residue not evolutionarily conserved among the MerR proteins, Shewchuk et al. have suggested that this residue is not involved in Hg(II) ligation (81, 208). The alkylation reagent can, in the presence of buffer components that compete for Hg(II), readily react with thiolates involved in Hg(II) ligation (27) or a coordinated protein thiolate in rapid exchange with buffer thiols, thus complicating the alkylation results. Paradoxically, in the highly homologous Tn21 MerR protein, non-conservative single site mutagenesis of Cys-82, Cys-117, and Cys-126 to tyrosyl residues does not implicate Cys-117 in Hg(II) binding, but rather suggest a major role for Hg(II) binding by Cys-126, with Cys-82 playing an undefined role in the protein dimerization interface (164, 171).

B. Mutagenesis Studies of MerR

Random mutagenesis studies of MerR, in which activity was monitored *in vivo*, are consistent with three of the four cysteine residues providing the ligation to Hg(II), since mutations in residues Cys-82, Cys-117, and Cys-126 result in complete loss of transcriptional activation *in vivo* (164). These interesting results implicate three cysteine residues per monomer as having some role in Hg(II) binding, and Ross et al. (164) propose a four-coordinate Hg(II)-binding site. These studies also indicated that mutations of protein residues very near these cysteines also had marked effects on the level of transcriptional activation, suggesting that maintenance of the local protein conformation about the Hg(II)-binding site is essential for molecular recognition. The mutagenesis studies of Ross et al. (164), and Helmann et

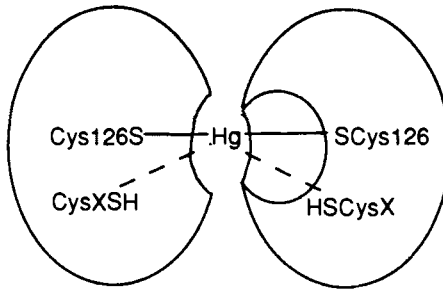
al. (81), have also been helpful in defining protein residues important for DNA binding (Fig. 15). DNA binding specificity is beyond the scope of this chapter, but has recently been reviewed elsewhere (81).

Conservative mutation studies on Tn501 MerR, substituting alanine or serine residues (Cys-82 → Ala, Cys-115 → Ala, Cys-117 → Ala, Cys-126 → Ser), suggest: (a) the presence of Cys-126 is essential for both Hg(II) binding and transcriptional activation, (b) Cys-82 plays a lesser, nonessential role in Hg(II) binding, while remaining essential to activation by Hg(II), and (c) Cys-117 is not necessarily for full Hg(II) binding, but is necessary for attaining full levels of transcriptional activity (173).

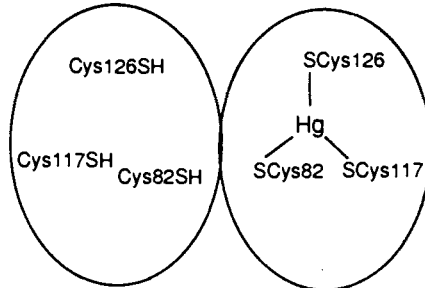
Clearly, the biochemical and genetic data do not adequately resolve the roles of the various cysteinyl residues in the coordination of Hg(II). The potential for three separate residues from each protein monomer to play a role in binding Hg(II) when a single Hg(II) is bound to each protein dimer suggests that a complicated series of reactions may be involved in the initial metal binding event. These may include cysteinyl residues for recognition of Hg(II), discrimination between Hg(II) and other soft metal ions, and separate cysteinyl residues that determine transcriptional activation by Hg(II). For example, despite the role of Cys-126 in initially binding Hg(II), as defined by the site directed mutagenesis studies, alkylation protection studies by the same group demonstrated that, while either Cys-115 or Cys-117 were protected from alkylation by the presence of Hg(II), Cys-126 was alkylated. Based on the mutagenesis results, Shewchuk and co-workers (173) have proposed a model for linear, bis Hg(II) coordination involving primary Hg-S bonds provided by Cys-126 residues from each of two monomers, thus forming a Hg(II) cross-linked dimer (Fig. 16). Although binding constants are not available, the slightly weaker binding of Hg(II) to Cys-82 mutants has led these workers to propose that "ancillary" ligation, presumably secondary Hg-S bonding interactions, is involved in Cys-82-Hg(II) interactions. In this study it was not possible to assign specific roles for Cys-82 or Cys-117, although mutations in both these residues result in dramatically decreased levels of transcriptional activation.

C. Impact of Metal Coordination on Mechanism

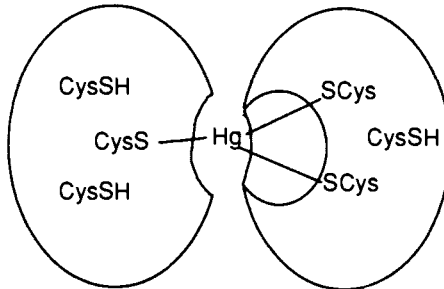
As previously discussed, the stepwise formation constant for the addition of a third thiol or thiolate ligand to Hg(SR)₂ compounds range from ~10 to 10⁸ (Tables VIII and IX). In thiol buffered solutions of micromolar protein concentrations, MerR has been shown to bind Hg(II) at least 10⁷ times better than the competing buffer thiols (82, 171, 210). A combination



Model 1. "Linear bis Hg(II) coordination"



Model 2. Asymmetric binding to single monomer.



Model 3. Hg(II) crosslinking MerR monomers by three primary Hg-S bonds

Figure 16. General models for Hg(II) binding to the MerR protein. Mutagenesis studies led to the proposal of model 1 having linear bis coordination with "ancillary" ligation (173). Studies by electronic spectroscopy and Hg-EXAFS, indicate that Hg(II) is bound by three primary thiolate ligands, consistent with models 2 and 3, above (202, 209). Mutant complementation studies with *Bacillus* MerR support the model for Hg(II) bound by three primary bonds (83).

of the chelate effect and the additional thermodynamic stability of a $[\text{Hg}(\text{SR})_3]^-$ complex vs. $\text{Hg}(\text{SR})_2$ are both responsible for the extraordinary affinity of MerR for Hg(II), even in thiol-rich media (209, 210).

As described earlier, mutational analysis has provided some insight into potential roles for the specific cysteinyl residues in MerR; however, the chemical protection results lead to different conclusions. Based on mutagenesis results of Tn501 MerR, Hg(II) was proposed to bridge protein monomers in a linear bis-coordinate mode (via Cys-126), along with possible ancillary bonding interactions with another cysteine residue (Cys-182) [Fig. 16, model 1, adapted from (173)]. Chemical protection studies, as well as electronic and X-ray absorption spectral data, on the other hand, are consistent with three primary thiolate ligands binding Hg(II) (202, 209, 210). As discussed in Sections II.B–D, Hg(II) complexes often demonstrate a range of secondary bonding interactions in restricted environments such as a crystal lattice and may exhibit similar tendencies in a chelating protein environment. The EXAFS data show no hint of longer distance secondary interactions; if any such interactions are present, they are insufficiently strong to perturb the three-coordinate Hg center (209).

It is unusual to find a dimeric protein, which recognizes a palindromic DNA sequence as a DNA binding site, yet binds its effector, Hg(II), in a three-coordinate manner to bridge two monomers. Models with an Hg(II) atom bridging two monomers through two or four cysteine ligands are not consistent with the EXAFS and UV spectroscopy (Sections II. H and IV. A). In light of the latter data, it is likely that the two protein monomers are asymmetrically arranged with Hg(II) bound so as to cross-link the two protein monomers, as depicted in Fig. 16, models 2 and 3. Hg(II) either could be interacting with one monomer in a manner that prevents Hg(II) binding to the complimentary site in the other monomer (model 2) or could be bridging two monomers (model 3). These two possibilities are being addressed by physical studies of Hg(II)-induced MerR cross-linking (210) and by heterodimer complementation studies of mutant proteins (83). The cysteine residues might be arranged at the surface of each symmetrically opposed monomer in a manner such that four (or more) potential thiolate ligands are always available for Hg(II) coordination; Hg(II) then binds in a stable complex to three of the four ligands.

In another mechanism, Cys-126 would play a transitory role in the initial recognition or recruitment of Hg(II) into a final binding site consisting of other cysteine residues. In this new model, some of the cysteines are involved in initial metal ion sequestration and discrimination and may play a kinetic role in recognizing Hg(II). Given the rapid rate of ligand exchange observed in model complexes, the metal could be transferred to a site containing other cysteines. Occupation of the latter site would induce the

conformational changes in MerR that are required for the transcription switching event described in the next section. The current site-directed mutagenesis, chemical protection, and spectroscopic studies do not distinguish between mechanisms in which one or both Cys-126 side chains are among the ultimate Hg(II) binding residues, or are simply required for initial recognition and binding of Hg(II). The latter case may explain the essential roles of Cys-82 and Cys-117 in the transcriptional switching event. This mechanism is largely conjectural; however, it is consistent with the mutagenesis results and points out difficulties in assigning specific roles to side chains in the structure and function of the biopolymer. It is important to recognize that mutations in cysteine residues that result in the loss of the MerR Hg(II) binding function may not be the ultimate Hg binding residues. Clarification of the roles for protein cysteinyl residues in Hg(II) recognition and transcriptional switching awaits further experimentation.

VIII. MOLECULAR BIOLOGY AND MECHANISM OF THE Hg(II)-RESPONSIVE SWITCH

A. Background

A variety of *in vivo* and *in vitro* studies have been performed to establish the effect of mercuric ion–MerR interaction on RNA polymerase and DNA during the switching event. Genetic studies first demonstrated that the *merR* gene was involved in both repression and activation of genes encoding the detoxification proteins, as well as the negative regulation of its own expression (11, 62, 63, 141, 182). Initial analysis of contacts between DNA and the overproduced and partially purified protein indicated that, in the presence and absence of mercuric ion, MerR was bound to a single site located between the divergently oriented *merR* gene and the *merTPAD* detoxification genes (143). MerR/DNA footprints generated with the low-resolution DNAase I method did not change upon addition of Hg(II) to the complex, raising the possibility that other cellular factors might participate in the metal-responsive switching event. The latter possibility was eliminated by demonstrating that the MerR-dependent, metal-responsive activity of transcriptional switching could be reconstituted *in vitro* using samples of *Escherichia coli* RNA polymerase and MerR protein that had been purified to homogeneity (145). Similarly, the *Bacillus* RC607 MerR can mediate *in vitro* transcription by the *Bacillus* RNA polymerase (82). These experiments demonstrated that *in vitro* switching occurred at mercuric ion concentrations corresponding to those required for expression of

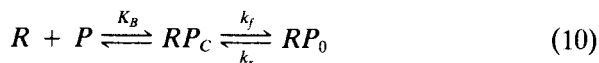
the resistance phenotype *in vivo*. This observation, in conjunction with the fact that MerR is not a membrane-spanning or periplasmic protein, led us to postulate that MerR is an intracellular sensor for an extracellular signal.

In order to understand why an intracellular sensor is unusual for the mercuric ion detoxification system and why an extracellular sensor might be anticipated, it is necessary to consider the role of each of the induced proteins in protecting the cell from Hg(II) poisoning. Mercuric ion detoxification genes encode a periplasmic scavenging protein and a membrane-bound transport protein that import the toxic ion into the cell for processing by the enzyme mercuric ion reductase. The transport proteins are essential and have apparently evolved to protect Hg(II)-sensitive functions in the periplasmic membrane. Thus, a sensor at the membrane would provide the cell with a means of detecting the metal at a site where it apparently does significant damage. Many signal transduction systems in bacteria employ an extracellular sensor for small inorganic and organic molecules that communicates with the genetic apparatus through multiprotein relay systems (162). In light of the mechanism of mercuric ion resistance and the precedents for extracellular sensor systems, it is interesting to ask why MerR acts as an intracellular receptor and to consider the mechanistic advantages of a single component system. The kinetic analysis presented below suggests that MerR gains the ability to function in an ultrasensitive manner (see Section I. D) by virtue of its direct interaction, in either the "off" [without Hg(II)] or "on" [with Hg(II)] position with the enzyme it regulates. Thus as an intracellular, DNA-bound receptor with high specificity and sensitivity, MerR can mediate a more efficient and expedient response than an extracellular receptor. Other advantages undoubtedly exist for the intracellular sensor in this case, such as absence of cross-talk with other regulatory cascades. MerR apparently circumvents the disadvantages of being located remotely from the initial signal by having a high affinity for Hg(II). It thus senses intracellular Hg(II) concentrations (10^{-8} M) that are well below the toxic threshold (1×10^{-6} M) for the cell. Interestingly, most other characterized metalloregulatory proteins are single-component signal transduction systems that, like MerR, act as both the signal molecule receptor and signal-transducing protein (160). An intracellular receptor is expected in some cases, such as with iron, where an accurate gauge of the intracellular concentration is essential.

B. Kinetics of Hg(II)-Induced Transcriptional Activation

The abortive initiation assay (130) was used to pinpoint the Hg(II)-responsive step in transcriptional initiation of the genes responsible for detoxifying Hg(II). This analysis provides information on the specific site

of Hg(II) stimulation in the pathway of transcriptional initiation. The abortive initiation assay is based on the following general reaction scheme for formation of the open, transcriptionally competent complex, RP_0 (41), where R and P stand for free RNA polymerase and promoter-bearing DNA, respectively. K_B is the equilibrium constant for the



binding of free polymerase to the promoter to form the closed transcription complex, RP_C , and k_f and k_r are the forward and reverse rates, respectively, of isomerization to the activated state, or open complex (RP_0). The complex Hg–MerR exerts its stimulatory effect at one or more of these steps, and analysis of these parameters in the presence and absence of Hg(II) has led to a model for the role of the metal ion and the protein in the switching event. The constants K_B and k_f in Eq. 10 can be calculated from the dependence of the rate of open complex formation on the concentration of RNA polymerase, provided pseudo-first-order conditions are maintained (80) (excess RNA polymerase and $k_f \gg k_r$). Open complex formation is measured by the incorporation of a radioactive rNTP into oligonucleotides generated by nucleotide-limited abortive cycling of RNA polymerase.

A reaction scheme, elaborated from Eq. 10, for initiation of transcription in the presence and absence of mercuric ion is presented in Fig. 17. Comparison of the kinetic constants for each state has shown that Hg(II) binding to the MerR protein results in an increase in the isomerization rate constant (k_f) of RNA polymerase of almost two orders of magnitude, whereas the binding (K_B) of RNAP to the promoter is not greatly affected (158).

C. Topology of the Transcription Complex

Chemical nucleases provide detailed information concerning the interactions of regulatory proteins with DNA (12) and have recently been applied to intact transcription complexes. High-resolution probes such as hydroxyl radical–FeEDTA (192), as well as dimethyl sulfate (DMS) and DNaseI, were used to deconvolute the interactions of MerR, Hg–MerR, and RNA polymerase with P_T , the DNA sequences in the regulatory region (the promoter) of the mercuric ion responsive genes (145). These studies provide a structural map, also known as a “footprint”, of the interactions of both proteins with the DNA in complexes isolated at different stages in the activation process and provide structural information on the physical role Hg–MerR in the activation mechanism. Several of the kinetic inter-

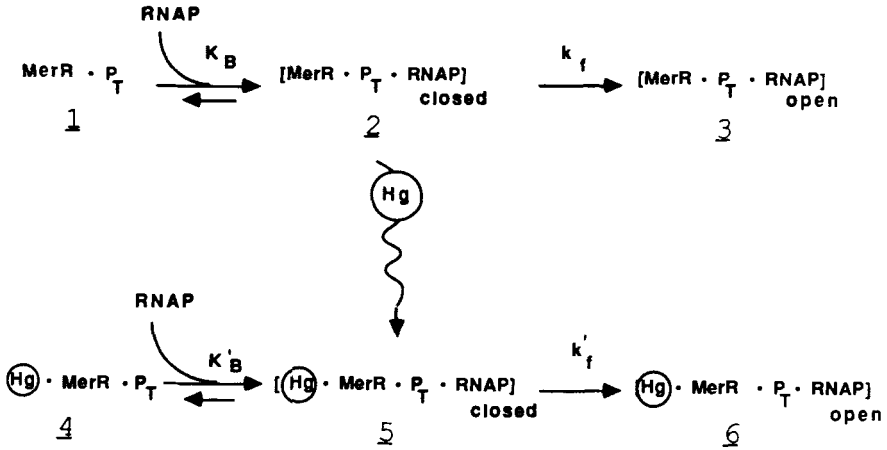


Figure 17. Schematic representation of the pathway of transcriptional activation at the Hg(II)-responsive promoter in the absence (top) and presence of Hg(II) (bottom). K_B , K'_B represent the equilibrium binding constants for RNA polymerase (RNAP) for the repressed [$-$ Hg(II)] and activated [$+$ Hg(II)] transcription complexes, respectively. k_f and k'_f represent the RNAP isomerization rate constants for the conversion from closed to open transcription complexes for repressed and activated conditions, respectively (158). Each complex is numbered for reference in the text.

mediates shown in Fig. 17 have been trapped by substrate limitation and footprinted directly (complexes 1, 2, 4, 6) or first isolated by non-denaturing gel electrophoresis techniques and subsequently analyzed by footprinting (complexes 1, 4, 6). The latter method is preferable since the solution footprint can represent a composite of the various complexes in solution. The *on* position of the switching apparatus is represented by the transcriptionally competent, mercuric ion-induced conformation, complex 6. This species directly correlates with a stable intermediate formed between *E. coli* RNA polymerase and DNA sequences known as an *open complex*. The open complex of most promoters is stable under non-denaturing gel electrophoresis, DNA-polyanion competition experiments, and in the absence of nucleotide substrates. It can be kinetically differentiated from other intermediates, such as the precursor closed complex (see above) and is characterized by the presence of 10–15 base pair area of double-strand DNA that has been locally unpaired (melted-out) at the start site for transcription. The presence of a melted out region from +2 to –12 relative to the start site (+1) was detected in complex 6 using KMnO_4 as a probe (145). KMnO_4 rapidly oxidizes unpaired thymidine residues in the DNA but reacts slowly with duplex regions of protein–DNA complexes as detected in Maxim–Gilbert sequencing reactions (64). Thus, it is an ex-

cellent reagent for detecting the melted out transcription "bubble" in nucleoprotein complexes in general (168).

Other remarkable features of the *on* conformation of this switch (Fig. 17, complex 6) are the relative positions of the activator protein (Hg-MerR) and RNA polymerase on the DNA template and the alteration of MerR-DNA contacts. Unlike other prokaryotic transcriptional activators that bind upstream of the -35 region, which is a conserved promoter sequence for RNA polymerase binding, Hg-MerR is nestled within the RNA polymerase binding site, between the -35 region and the melted-out transcription bubble. There are gross changes in DMS protection pattern at the center of the Hg-MerR/DNA binding site in comparison to footprints in the absence of RNA polymerase. These changes implicate a Hg-MerR induced change in local DNA structure, and are discussed below. The fundamental structural aspects of complexes 1 and 6 can be seen in a projection of the footprinting and KMnO_4 results on to regular B-form DNA helix shown in Fig. 18. Note that this schematic representation is constructed from footprinting results for gel-separated complexes and nothing is known about the actual shapes of the proteins. Contacts at the center of the DNA binding site may arise from peptide arms that extend around the DNA; however, other biochemical and structural evidence is required.

The repressed state, or the *off* conformation, of the switch is best represented as complex 2, an intermediate in the kinetic scheme of Fig. 17, and is less well understood than its open counterpart. While a corresponding complex cannot be physically isolated using gel electrophoresis techniques, DNase I and KMnO_4 solution footprints suggest complex 2 exists as a rapidly formed closed complex with a small DNAase I footprint that slowly isomerizes to the open conformation in the absence of Hg(II) (65). A summary of these results is seen in Fig. 20 where complexes 2 and 6 from the kinetic scheme are shown in panel (b) and (d), respectively. As discussed above, the rate of isomerization is increased by approximately two orders of magnitude when Hg(II) is bound to MerR. The presence of complex 2 in the cell is indicated by DMS footprints *in vivo* (84). Complex 2 can be thought of as a poised complex, which very slowly proceeds to a transcriptionally active form. The binding of Hg(II) to MerR induces the conversion of complex 2 into the closed complex 5, which like most other closed complexes cannot be physically isolated by gel techniques. Complex 5 rapidly isomerizes to the active open form complex 6 and cannot be footprinted. The structural and kinetic data both clearly indicate that RNA polymerase can readily form a long-lived closed complex with MerR/ P_T that is rapidly converted to the activated open form by Hg(II). Insights into this process have been obtained from chemical nucleases that use metal ions in the cleavage mechanism.

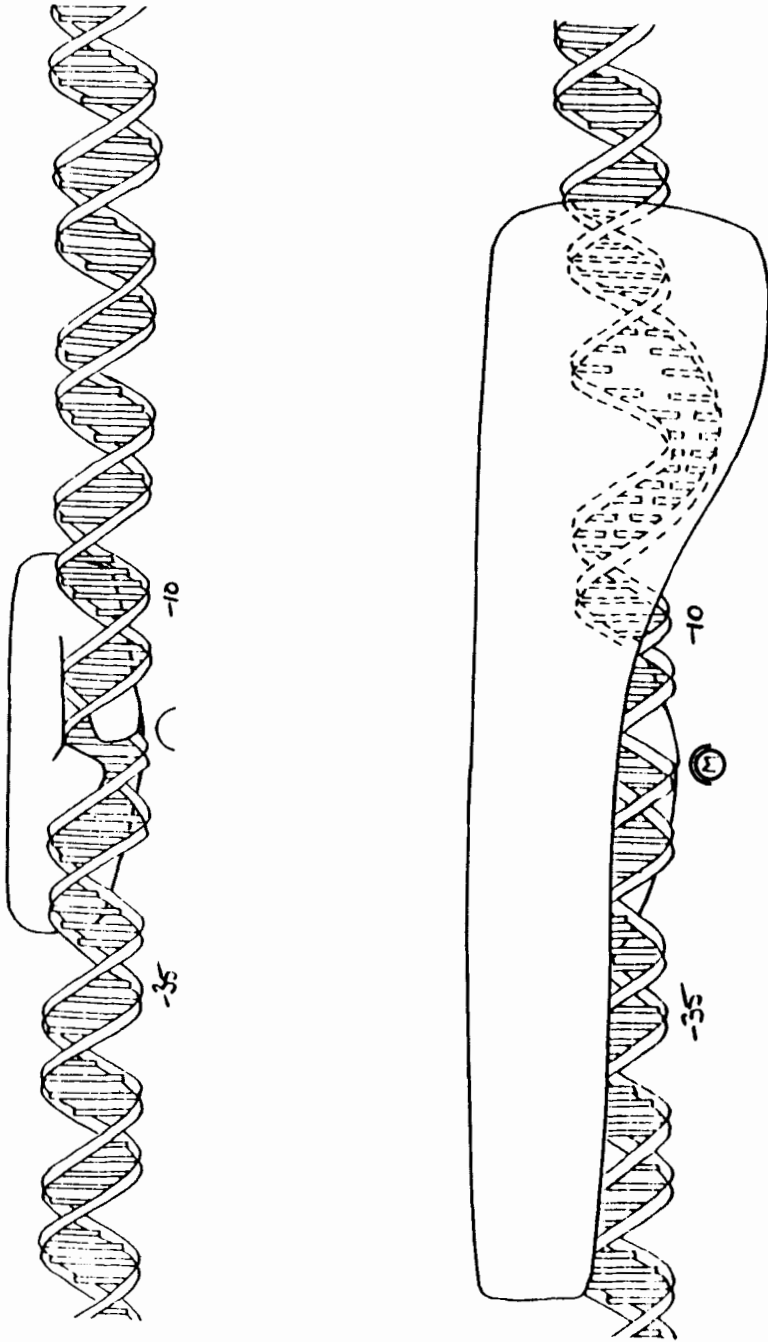


Figure 18. Representation of surface protection of *mer* DNA sequences by MerR (top) and by Hg-MerR and RNA polymerase (bottom) based on footprinting results (145).

D. Hg-MerR-Induced Distortions in DNA Structure

Mercuric ion switches *on* transcription by first binding to MerR. The binding of Hg(II) induces a conformational change in the protein and this change is evident in the threefold decrease in the MerR/DNA binding constant (145). Then Hg-MerR stimulates the conversion of the closed transcription complex to an open complex as described above. There are two commonly proposed mechanisms for this type of activation event, as represented in Scheme I. Activator proteins such as lambda repressor and the catabolite activating protein (CAP) apparently stimulate RNA polymerase transcription through energetically favorable *protein-protein contacts* (154). Alternatively, an activator protein can induce a conformational change in the local structure of the DNA template. This *altered DNA conformation* could accelerate RNA polymerase open complex formation and thereby stimulate transcription. RNA polymerase must melt out ca. 15 base pairs and a number of DNA distortions could facilitate this process, but there are no well-documented examples for this model. The two chemical nucleases, methidium propyl EDTA·Fe(II) (MPE) and copper-5-phenyl-*o*-phenanthroline (phenyl-CuOP), depicted in Fig. 19, use different binding and cleavage mechanisms, yet both detect an alteration in the local DNA structure of the Hg-MerR/DNA but not the MerR/DNA complex. The mercury-induced hypersensitivity to phenyl-CuOP found at the center of the Hg-MerR/DNA complex is also observed in the Hg-MerR/P_T/RNAP complex discussed above (Fig. 17, complex 6) (65). Thus this nuclease hypersensitivity correlates directly with the activation of transcription. While the exact binding mode is not clear for phenyl-CuOP, MPE

Step 1

Hg(II) binding induces a conformational change in the MerR protein, as demonstrated by a three fold decrease in the affinity of MerR for DNA in the presence of Hg(II).

Step 2

Model A: Hg-MerR induces a conformational change in RNA polymerase through *protein-protein interactions*.

or

Model B: Hg-MerR induces a conformational change in the local structure of the DNA. The *altered DNA conformation* accelerates RNA polymerase open complex formation.

Scheme 1. Steps in the activation of transcription by Hg-MerR.

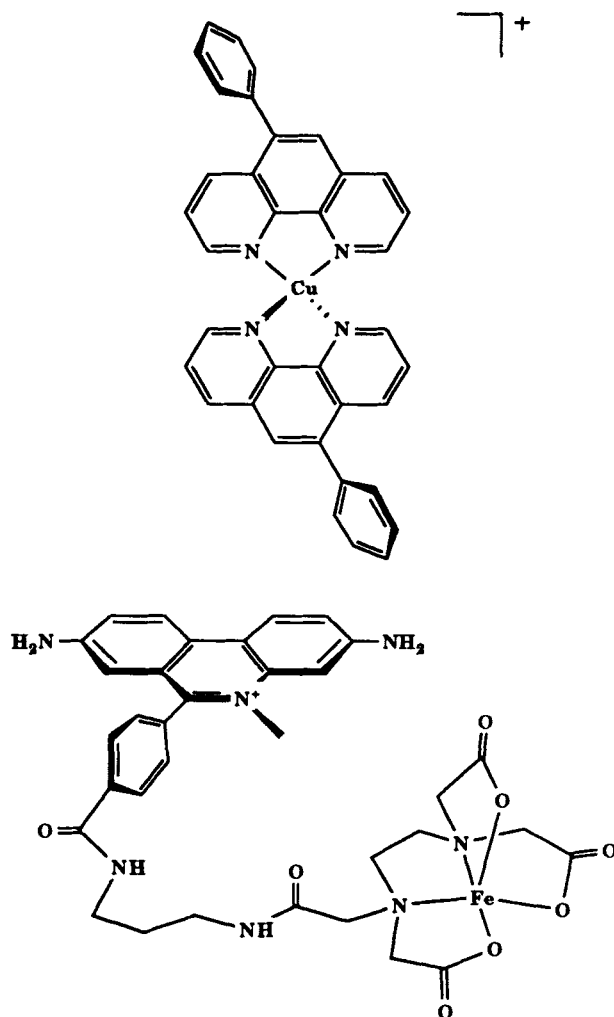


Figure 19. Structures of the chemical nucleases methidium propyl EDTA-Fe(II) (MPE) (bottom) and copper-5-phenyl-*o*-phenanthroline (phenyl-CuOP) (top).

clearly intercalates from the minor groove of DNA. A protein-induced underwound region of DNA could exhibit enhanced sensitivity to MPE since, in general, the intercalator must underwind B-form DNA in order to bind.

The proposed structural change in the promoter, such as a Hg-MerR induced kinking or unwinding of the B-form complex by 30°-70°, could

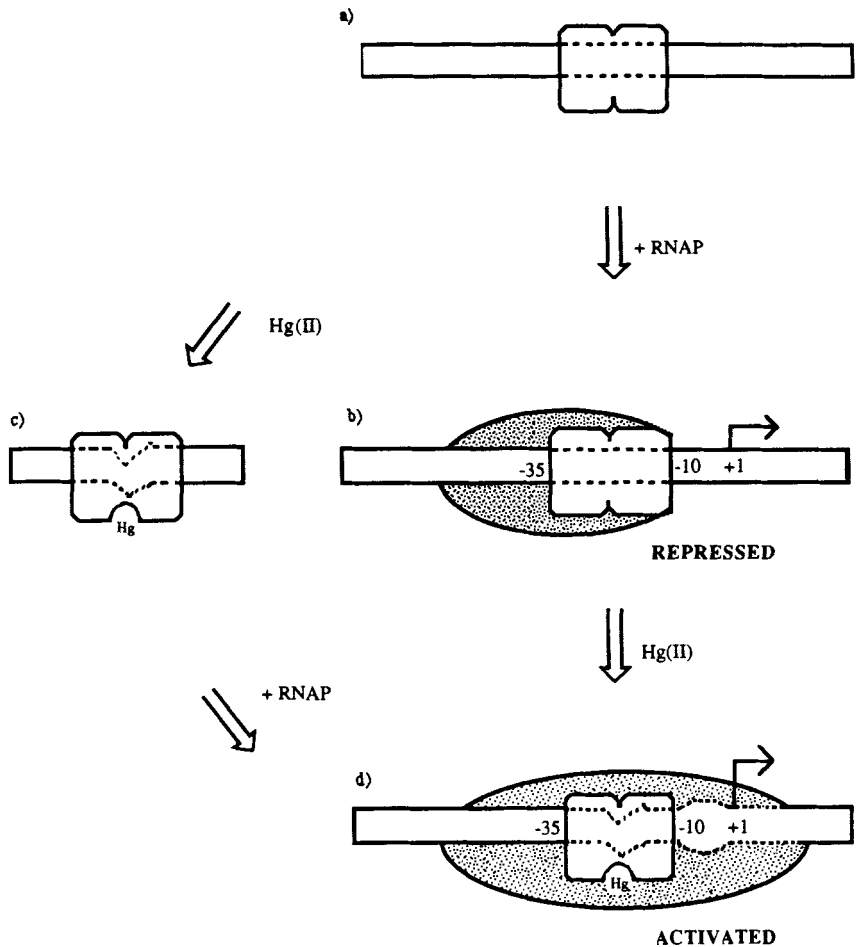


Figure 20. Schematic mechanism of mercuric ion-responsive activation of transcription. A distortion of the DNA at the center of the Hg–MerR binding site, deduced by hyperreactivity of chemical nucleases, is represented by V-shaped dashed lines. This distortion is present when MerR is associated with Hg(II) in both the presence and absence of RNA polymerase, as shown. Nucleases that demonstrate hyperreactivity are MPE and phenyl-CuOP (65). Bars represent DNA sequences of *mer* genes; joined rectangles represent the dimeric protein MerR, shown associated with Hg(II) in complexes *c* and *d*. Shaded ellipsoids represent the protein RNA polymerase.

circumvent a physical barrier to rapid transcription at the P_T promoter, namely, the unusually long 19 bp spacing between the -10 and -35 RNA polymerase binding regions (65). The extra two base pairs in this region extend the spacer length from the consensus 17 bp and dramatically weaken what would otherwise be a fairly strong promoter (121). These two extra bases between the -10 and -35 regions also change the dihedral angle relating the center of each conserved of these promoter sequences. Unwinding and/or kinking induced by Hg–MerR could convert the local structure to one which more closely resembles the consensus promoter and local underwinding may lower the barrier to formation of the melted out transcription bubble at the start site for transcription initiation. Deletion and point mutations in P_T support a MerR-mediated change in DNA structure in response to Hg(II) (121, 122). In addition, the chemical nuclease results support a role for MerR involving DNA distortion; however, analysis of footprints for the open complex (Fig. 17, complex 6), suggest that there must be a variety of contacts between RNA polymerase and Hg–MerR. Whether these contacts play an important role in the activation process remains to be seen. The model shown in Fig. 20 summarizes the current understanding of the kinetic and topological results.

E. Overview of the Switching Mechanism

We conclude that Hg(II) binding to MerR/DNA complexes results in a protein imposed distortion in DNA structure (Fig. 20 complex *c*) and that this distortion plays an important role in stimulating the activity of RNA polymerase at the promoter for the mercuric ion resistance genes, depicted here as the conversion of complex *c* to complex *d* in Fig. 20. Mercury-induced protein–protein interactions between RNA polymerase and MerR may also play some role, however, there is no such evidence from the present studies. The free energy required for the distortion of DNA structure most likely is derived from the free-energy change for Hg(II) binding to a receptor site in MerR, although a more detailed thermodynamic analysis is warranted.

IX. SUMMARY

Although the structural literature on mononuclear Hg–SR complexes is dominated by linear bis-coordinate species that exhibit weak secondary bonding interactions, a few complexes with higher primary coordination number have recently been characterized. Thermodynamic studies of Hg–thiolate solution chemistry suggest that these species may be more tractable and abundant than an inspection of the structural literature might suggest.

In light of recent advances in solid state ^{199}Hg NMR, Raman, IR, EXAFS, and electronic spectroscopies summarized here, Hg(II) complexes can no longer be considered as "spectroscopically silent." A formidable barrier to establishing reliable spectroscopic correlations with the coordination environment still exists because of the small number of well characterized small molecule complexes. Solution ^{199}Hg NMR, vibrational, and electronic spectroscopies can distinguish complexes with a coordination number of 2 from those with $\text{CN} = 3$ or 4. None of these techniques can readily distinguish between three and four coordination however. Recent advances in solid-state ^{199}Hg NMR spectroscopy unequivocally demonstrate that Hg-SR complexes with a primary coordination number of three or four can be readily distinguished.

Comparison of results from EXAFS and electronic spectroscopy for the Hg-MerR protein with mononuclear two-, three-, and four-coordinate complexes leads to a trigonal $\text{Hg}(\text{SCys})_3$ model for the coordination environment in the Hg-MerR protein. This model provides a structural and chemical explanation for the high sensitivity and selectivity of this protein-binding site for Hg(II) in comparison to other soft metals such as Zn(II) and Cd(II). In the latter cases the metal thiolate chemistry is dominated by tetrahedral $[\text{M}(\text{SR})_4]^{2-}$ complexes. Apparently, the thermodynamic barrier to dissociating a thiol from $[\text{Zn}(\text{SR})_4]^{2-}$ or from $[\text{Cd}(\text{SR})_4]^{2-}$ to form a trigonal species in a thiol-rich media is higher than the barrier of adding an additional thiol to a linear $\text{Hg}(\text{SR})_2$ compound. These aspects of the recognition process await characterization of the Cd(II) and Zn(II) forms of the protein, as well as additional studies of Hg-MerR, which test the trigonal model and distinguish planar and pyramidal variants.

ACKNOWLEDGMENTS

Some of the research described here was supported by grants from the National Institutes of Health (GM38784) to T. V. O. and a National Research Service Award Predoctoral Training Program Fellowship (GM08061) to D. M. R. T. V. O. is a recipient of a Searle Scholars Award from the Chicago Community Trust and a National Science Foundation Presidential Young Investigator. We thank C. Walsh and J. Helmann for providing results prior to publication. We thank S. Watton for art work and scientific discussion and S. Johnson for useful discussions and proofing of this manuscript. EXAFS results were obtained in collaboration with H.-T. Tsang and J. Penner-Hahn (University of Michigan). We thank F. Klemens, K. Burns, and D. R. McMillin (Purdue University) for their gift of stellacyanin.

REFERENCES

1. S. Ahrland, *Structure and Bonding*, Vol. 5, Springer-Verlag, New York, 1968, p. 118.
2. S. Ahrland, *Structure and Bonding*, Vol. 15, Springer-Verlag, New York, 1973, p. 167.
3. N. W. Alcock, N. Herron, and P. Moore, *J. Chem. Soc. Dalton Trans.*, 394 (1978).
4. V. R. Allmann, *Z. Kristal.*, 138, 366 (1973).
5. B. M. Alsaadi and M. Sandström, *Acta Chim. Scand. A.*, 36, 509 (1982).
6. B. J. Aylett, *Comprehensive Inorganic Chemistry*, Vol. 3, J. C. Bailar, Jr., H. J. Eméleus, R. S. Nyholm, and A. F. Trotman-Dickerson, Eds., Pergamon Press, Oxford, 1973, Chapter 3.
7. A. Bagg and J. B. Neilands, *Biochemistry*, 26, 5471 (1987).
8. A. Bagg and J. B. Neilands, *Microbiol. Rev.*, 51, 509 (1987).
9. C. J. Ballhausen and H. B. Gray, *Molecular Orbital Theory*, Benjamin Press, New York, 1964.
10. H. Barrera, J. C. Bayon, P. González-Duarte, J. Sola, and J. M. Viñas, *Polyhedron*, 1, 647 (1982).
11. P. J. Barrineau and A. O. Summers, *Gene*, 25, 209 (1983).
12. L. A. Basile and J. K. Barton, *Metal Ions in Biological Systems*, Vol. 25, H. Sigel and A. Sigel, Eds., Marcel Dekker, New York, 1989.
13. M. A. Basinger, J. S. Casas, M. M. Jones, A. D. Weaver, and N. H. Weinstein, *J. Inorg. Nucl. Chem.*, 43(6), 1419 (1981).
14. M. Beltramini, K. Lerch, and M. Vasák, *Biochemistry*, 23, 3422 (1984).
15. C. L. Bender and D. A. Cooksey, *J. Bacteriol.*, 169, 470 (1987).
16. P. Biscarini, E. Foresti, and G. Pradella, *J. Chem. Soc. Dalton Trans.*, 953 (1984).
17. P. Biscarini and G. Pelizzi, *J. Chem. Soc. Dalton Trans.*, 2915 (1988).
18. P. Biscarini, L. Fusina, and G. Nivellini, *J. Chem. Soc. Dalton Trans.*, 2140 (1974).
19. P. J. Blower and J. R. Dilworth, *Coor. Chem. Rev.*, 76, 121 (189).
20. L. Book, A. J. Carty, and C. Chieh, *Can. J. Chem.*, 59, 144 (1981).
21. L. Book and T. C. W. Mak, *Inorg. Chim. Acta*, 92, 265 (1984).
22. G. A. Bowmaker, *Spectroscopy of Inorganic-Based Materials*, R. J. H. Clark and R. E. Hester, Eds., Wiley, New York, 1987, and references cited therein.
23. G. A. Bowmaker, I. G. Dance, B. C. Dobson, and D. A. Rogers, *Aust. J. Chem.*, 37, 1607 (1984).
24. D. C. Bradley and N. R. Kunchur, *Can. J. Chem.*, 43, 2786 (1965).
25. D. C. Bradley and N. R. Kunchur, *J. Chem. Phys.*, 40, 2258 (1964).

26. W. Braun, G. Wagner, E. Wörgörten, M. Vasák, J. H. R. Kägi, and K. Wüthrich, *J. Mol. Biol.*, **187**, 125 (1986).
27. Y. Burstein and R. Sperling, *Biochim. Biophys. Acta*, **221**, 410 (1970).
28. A. J. Canty, R. Kishimoto, G. B. Deacon, and G. J. Farquharson, *Inorg. Chim. Acta*, **20**, 161 (1976).
29. A. J. Canty and G. B. Deacon, *Inorg. Chim. Acta*, **45**, L225 (1980).
30. A. J. Canty and R. Kishimoto, *Nature (London)* **253**, 123 (1975).
31. A. J. Canty, C. L. Raston, B. W. Skelton, and A. H. White, *J. Chem. Soc. Dalton Trans.*, 15 (1982).
32. A. J. Canty, C. L. Raston, and A. H. White, *Aust. J. Chem.*, **31**, 677 (1978).
33. A. J. Canty, C. L. Raston, and A. H. White, *Aust. J. Chem.*, **32**, 311 (1979).
34. A. J. Canty, R. Kishimoto, G. B. Deacon, and G. J. Farquharson, *Inorg. Chim. Acta*, **20**, 161 (1976).
35. A. J. Canty and R. Kishimoto, *Inorg. Chim. Acta.*, **24**, 109 (1977).
36. G. K. Carson and P. A. W. Dean, *Inorg. Chim. Acta*, **66**, 157 (1982).
37. A. J. Carty and N. J. Taylor, *J. Chem. Soc. Chem. Commun.*, 214 (1976).
38. A. Schäffer, K. Williman, and H. Willner, *J. Inorg. Biochem.* **36(3-4)**, 186 (1989).
39. I. Casals, P. González-Duarte, J. Sola, C. Miravittles, and E. Molins, *Polyhedron*, **7**, 2509 (1988).
40. J. S. Casas and M. M. Jones, *J. Inorg. Nucl. Chem.*, **42**, 99 (180).
41. M. Chamberlin, *Ann. Rev. Biochem.*, **43**, 721 (1974).
42. B. V. Cheesman, A. P. Arnold, and D. L. Rabenstein, *J. Am. Chem. Soc.*, **110**, 6359 (1988).
43. S. Choudhury, I. G. Dance, P. J. Guernsey, and A. D. Rae, *Inorg. Chim. Acta*, **70**, 227 (1983).
44. M. F. Christman, R. N. Morgan, F. S. Jacobson, and B. N. Ames, *Cell*, **41**, 753 (1985).
45. G. Christou, K. Folting, and J. C. Huffman, *Polyhedron*, **3**, 1247 (1984).
46. W. B. Church, J. M. Guss, J. J. Potter, and H. C. Freeman, *J. Biol. Chem.*, **261**, 234 (1986).
47. R. L. Coates and M. M. Jones, *J. Inorg. Nucl. Chem.*, **38**, 1549 (1976).
48. P. M. Colman, H. C. Freeman, J. M. Guss, M. Murata, V. A. Norris, J. A. M. Ramshaw, and M. P. Venkatappa, *Nature (London)*, **272**, 319 (1978).
49. J. E. Combariza, J. H. Enemark, M. Barfield, and J. C. Facelli, *J. Am. Chem. Soc.*, **111**, 7619 (1989).
50. P. A. Cotter and R. P. Gunsalas, *J. Bacteriol.*, **171**, 3817 (1989).
51. F. A. Cotton, *Chemical Applications of Group Theory*, Wiley, New York, 1973.
52. D. Coucouvanis, *Prog. Inorg. Chem.*, **26**, 301 (1979).

53. N. K. Dalley and S. B. Larson, *Acta Cryst.*, B37, 2225 (1981).
54. I. G. Dance, *Polyhedron*, 5, 1037 (1986).
55. P. Day and R. H. Seal, *J. Chem. Soc. Dalton Trans.*, 2054 (1972).
56. P. A. W. Dean, J. J. Vittal, and M. H. Trattner, *Inorg. Chem.*, 26, 4245 (1987).
57. P. A. W. Dean, *Prog. Inorg. Chem.*, 24, 109 (1978).
58. D. M. Durnam and R. D. Palmiter, *J. Biol. Chem.*, 256, 5712 (1981).
59. K. H. Falchuk, L. J. Goldwater, and B. L. Vallee, *The Chemistry of Mercury*, C. A. McAuliffe, Ed., MacMillan, Toronto, Canada, 1977.
60. W. V. Farrar and A. R. Williams, *The Chemistry of Mercury*, C. A. McAuliffe, Ed., MacMillan, Toronto, Canada, 1977.
61. K. J. Fisher and R. S. Drago, *Inorg. Chem.*, 14, 2804 (1975).
62. T. J. Foster, N. Nakahara, A. A. Weiss, and S. Silver, *J. Bacteriol.*, 140, 167 (1979).
63. T. J. Foster and N. L. Brown, *J. Bacteriol.*, 163, 1153 (1985).
64. B. Frantz and T. V. O'Halloran, ACS Symposium Series: *Metal-DNA Chemistry*, Vol. 402, T. D. Tullius, Ed., American Chemical Society, Washington, DC, 1989.
65. B. Frantz and T. V. O'Halloran, *Biochemistry*, 29, 4747, (1990).
66. B. J. Fuhr and D. L. Rabenstein, *J. Am. Chem. Soc.*, 95, 6944 (1973).
67. W. F. Furey, A. H. Robbins, L. L. Clancy, D. R. Winge, B. C. Wang, and C. D. Stout, *Science*, 231, 704 (1986).
68. P. Fürst, S. Hu, R. Hackett, and D. Hamer, *Cell*, 55, 705 (1988).
69. D. P. Giedroc, B. A. Johnson, I. M. Armitage, and J. E. Coleman, *Biochemistry*, 28, 2410 (1989).
70. D. G. Gillies, L. P. Blaauw, G. R. Hays, R. Huis, and A. D. H. Claguc, *J. Magn. Reson.*, 42, 420 (1981).
71. R. J. Goodfellow, *Multinuclear NMR*, J. Mason, Ed., Plenum Press, New York, 1987.
72. D. Grdenić, *Q. Rev.*, 19, 303 (1955). (a) E. S. Gruff and S. A. Koch, *J. Chem. Soc.*, 112, 1245 (1990).
73. J. D. Gunter, A. F. Schreiner, and R. S. Evans, *Inorg. Chem.*, 14, 1589 (1975).
74. J. M. Guss and H. C. Freeman, *J. Mol. Biol.*, 169, 521 (1983).
75. R. A. Haberkorn, L. Que, Jr., W. O. Gillum, R. H. Holm, C. S. Lin, and R. C. Lord, *Inorg. Chem.* 15, 2408 (1976).
76. J. Halfpenny, R. W. H. Small, and F. G. Thorpe, *Acta Cryst. Sect. B.*, 34, 3075 (1978).
77. D. H. Hamer, *Ann. Rev. Biochem.*, 55, 913 (1986).
78. R. K. Harris and A. Sebald, *Magn. Reson. Chem.*, 25, 1058 (1987).
79. H. M. Hassan and C. S. Moody, *J. Biol. Chem.*, 262, 173 (1987).

80. D. K. Hawley and W. R. McClure, *Proc. Natl. Acad. Sci. USA* 77, 6381 (1980).
81. J. D. Helmann, L. M. Shewchuk, and C. T. Walsh, *Advanced Inorganic Biochemistry*, Vol. 8. Metal-Ion Induced Regulation of Gene Expression. G. L. Eichorn and L. Marzilli, Eds., 1 1990.
82. J. D. Helmann, Y. Wang, I. Mahler, and C. T. Walsh, *J. Bacteriol.*, 171, 222 (1989).
83. J. D. Helmann and C. T. Walsh, personal communication. (a) J. D. Helmann, D. T. Ballard, and C. T. Walsh, *Science*, 247, 946 (1990).
84. A. Heltzel, P. Totis, and A. O. Summers, *Metal Ion Homeostasis: Molecular Biology and Chemistry*, Vol. 98, D. H. Hamer and D. R. Winge, Eds.; Liss, New York, 1989, p. 427.
85. G. Henkel, P. Betz, and B. Krebs, *J. Chem. Soc. Chem. Commun.*, 1498 (1985).
86. G. Henkel, P. Betz, and B. Krebs, *Inorg. Chim. Acta*, 134, 195 (1987).
87. M. W. Hentze, T. A. Roualt, J. B. Harford, and R. D. Klausner, *Science*, 244, 357 (1989).
88. A. Hergold-Brundić, B. Kamenar, and G. Jovanovski, *Acta Cryst.*, C45, 556 (1989).
89. L. G. Hepler and G. Olofsson, *Chem. Rev.*, 75, 585, (1975).
90. A. Hergold-Brundić and B. Kamenar, *Acta Cryst.* C45, 556 (1989).
91. J. Herzfeld and A. E. Berger, *J. Chem. Phys.*, 73, 6021 (1979).
92. R. R. Hollebone and R. S. Nyholm, *J. Chem. Soc. (A)*, 332 (1971).
93. J. M. Huibregtse, D. R. Engelke, and D. J. Thiele, *Proc. Natl. Acad. Sci. USA*, 86, 65 (1989).
94. J. E. Huheey, *Inorganic Chemistry*, 3rd. ed., Harper & Row, New York, 1983, 258.
95. A. A. Isab and D. L. Rabenstein, *Biochim. Biophys. Acta*, 721, 374 (1982).
96. S. Iuchi and E. E. C. Lin, *Proc. Natl. Acad. Sci., USA*, 84, 3901 (1987).
97. N. Iwasaki, J. Tomooka, and K. Toyoda, *Bull. Chem. Soc. Jpn.*, 47, 1323 (1974).
98. M. R. Jacobsen, R. Premakumar, and P. E. Bishop, *J. Bacteriol.*, 167, 480 (1986).
99. C. K. Jameson and J. Mason, *Multinuclear NMR*, J. Mason, Ed., Plenum Press, New York, 1987.
100. M. G. Jobling and D. A. Ritchie, *Mol. Gen. Genet.*, 208, 228 (1987).
101. B. A. Johnson and I. M. Armitage, *Inorg. Chem.*, 26, 3139 (1987).
102. J. Jokisaari and P. Diehl, *Org. Magn. Reson.*, 13, 359 (1980).
103. M. M. Jones, M. J. Meredith, M. L. Dodson, R. J. Topping, and E. Baralt, *Inorg. Chim. Acta*, 153, 87 (1988).
104. M. M. Jones, A. J. Banks, and C. H. Brown, *J. Inorg. Nucl. Chem.*, 36, 1833 (1974).

105. M. M. Jones, A. J. Banks, and C. H. Brown, *J. Inorg. Nucl. Chem.*, **37**, 761 (1975).
106. T. E. Jones, L. S. W. L. Sokol, D. B. Rorabacher, and M. D. Glick, *J. Chem. Soc. Chem. Comm.*, 140 (1979).
107. C. K. Jørgensen, *Prog. Inorg. Chem.*, **12**, 101 (1970).
108. K. Kanada, H. Nakatsuji, and T. Yonezawa, *J. Am. Chem. Soc.*, **106**, 5888 (1984).
109. M. A. Kennedy and P. D. Ellis, *J. Am. Chem. Soc.*, **111**, 3195 (1989).
110. J. D. Kennedy and W. McFarlane, *J. Chem. Soc. Faraday 2*, **72**, 1653 (1976).
111. R. G. Kidd and R. J. Goodfellow, *NMR and The Periodic Table*, R. K. Harris and B. E. Mann, Eds., Academic Press, 1978.
112. A. S. Klemens, D. R. McMillin, H. T. Tsang, and J. E. Penner-Hahn, *J. Am. Chem. Soc.*, **111**, 6398 (1989).
113. M. M. Kubicki, R. Kergoat, J. E. Guerchais, I. Bkouche-Waksman, C. Bois, and P. L'Haridon, *J. Organomet. Chem.*, **219**, 329 (1981).
114. N. R. Kunchur, *Nature (London)*, **204**, 468 (1964).
115. C. R. Lassigne and E. J. Wells, *Can. J. Chem.*, **55**, 1301 (1977).
116. P. Lavertue, J. Hubert, and A. Beauchamp, *Inorg. Chem.*, **15**, 322 (1976).
117. G. R. Lenz and A. E. Martell, *Biochemistry*, **3**, 745 (1964).
118. E. A. Leibold and H. N. Munro, *Proc. Natl. Acad. Sci. USA*, **85**, 2171 (1988).
119. J. Liesk and G. Klar, *Z. Inorg. Allg. Chem.*, **435**, 103 (1977).
120. W. Levason and C. A. McAuliffe, *The Chemistry of Mercury*, C. A. McAuliffe, Ed., MacMillan, Toronto, Canada, 1977.
121. P. A. Lund and N. Brown, *Nucl. Acids. Res.*, **17**, 5517 (1989).
122. P. A. Lund and N. L. Brown, *J. Mol. Biol.*, **205**, 343 (1989).
123. F. M. MacDonnell and T. V. O'Halloran, unpublished results.
124. G. E. Maciel and M. Borzo, *J. Magn. Reson.*, **10**, 388 (1973).
125. T. Maitini and K. T. Suzuki, *Chem. Pharm. Bull.*, **30**, 4164 (1981).
126. M. M. Maricq and J. S. Waugh, *J. Chem. Phys.*, **70**, 3300 (1979).
127. F. Marsicano and R. D. Hancock, *J. Coord. Chem.*, **6**, 21 (1976).
128. J. Mason, *Chem. Rev.*, **87**, 1299 (1987).
129. J. Mason, Ed., *Multinuclear NMR*, Plenum Press, New York, 1987.
130. W. R. McClure, C. L. Cech, and D. E. Johnston, *J. Biol. Chem.*, **253**, 8941 (1978).
131. R. S. McEwen and G. A. Sim, *J. Chem. Soc. (A)*, 271 (1967).
132. D. R. McMillin, *Bioinorg. Chem.*, **8**, 179 (1978).
133. S. Merchant and L. Bogorad, *EMBO J.*, **6**, 2531 (1984).
134. S. M. Miller, M. Moore, V. Massey, C. H. Williams, Jr., M. Distefano, D. Ballou, C. T. Walsh, *Biochemistry*, **28**, 1194, 1989.

135. M. J. Natan, C. Millikan, J. G. Wright, and T. V. O'Halloran, *J. Am. Chem. Soc.*, 112, 3255 (1990).
136. C. Millikan and T. V. O'Halloran, unpublished results.
137. W. G. Mitchell and M. M. Jones, *J. Inorg. Nucl. Chem.*, 40, 1957 (1978).
138. A. Müller, J. Schimanski, and U. Schimanski, *Angew. Chem. Int. Ed. Engl.*, 23, 159 (1984).
139. A. Müller, J. Schimanski, U. Schimanski, and H. Bögge, *Z. Naturforsch.*, 40b, 1277 (1985).
140. H. Nakatsuji, K. Kanada, K. Endo, and T. Yonezawa, *J. Am. Chem. Soc.*, 106, 4653 (1984).
141. N. N. Ni'Bhriain, S. Silver, and T. J. Foster, *J. Bacteriol.*, 155, 690 (1983).
142. R. S. Nyholm, *Proc. Chem. Soc. London*, 273 (1961).
143. T. V. O'Halloran and C. T. Walsh, *Science*, 235, 211 (1987).
144. T. V. O'Halloran, *Metal Ions in Biological Systems*, Vol. 25, H. Sigel, Ed., Marcel Dekker, New York, 1989.
145. T. V. O'Halloran, B. Frantz, M. K. Shin, D. M. Ralston, and J. G. Wright, *Cell*, 56, 119 (1989).
146. L. E. Orgel, *J. Chem. Soc.*, 4186 (1958).
147. L. Pauling, *The Nature of the Chemical Bond*, 3rd ed., Cornell University Press, Ithaca, New York, 1960, pp. 246-260.
148. C. Perchard, G. Zuppioli, F. Gouzerh, Y. Jeannin, and F. Robert, *J. Mol. Struct.*, 72, 119 (1981).
149. P. Peringer, *Monatsh. Chem.*, 111, 1245 (1980).
150. P. Peringer and P.-P. Winkler, *Inorg. Chim. Acta*, 52, 257 (1981).
151. I. Persson, M. Sandström, and P. L. Goggin, *Inorg. Chim. Acta*, 129, 183 (1987).
152. I. Persson and F. Zintl, *Inorg. Chim. Acta*, 129, 47 (1987).
153. K. Pfeiffer, B. Arcangioli, and L. Guarente, *Cell*, 49, 9 (1987).
154. M. Ptashne, *Nature (London)*, 335, 683 (1988).
155. V. H. Puff, R. Sievers, and G. Elsner, *Z. Anorg. Allg. Chem.*, 413, 37 (1975).
156. P. Pyykkö and J.-P. Desclaux, *Acc. Chem. Res.*, 12, 276 (1979).
157. D. M. Ralston and T. V. O'Halloran, *Proc. Natl. Acad. Sci. USA*, 87, 3846, 1990.
158. D. M. Ralston, M. T. Szatkowski, M. S. Shin, and T. V. O'Halloran, unpublished data.
159. D. M. Ralston, B. Frantz, M. S. Shin, J. G. Wright, and T. V. O'Halloran, *Metal Ion Homeostasis: Molecular Biology and Chemistry*, Vol. 98, UCLA Symposium on Molecular and Cellular Biology, New Series, D. Winge and D. Hamer, Eds., Liss, New York, 1989.

160. D. M. Ralston and T. V. O'Halloran, *Advances in Inorganic Biochemistry*, Vol. 8. Metal-Ion Induced Regulation of Gene Expression. G. L. Eichorn and L. Marzilli, Eds., 1 1990.
161. P. W. Riddles, R. L. Blakeley, and B. Zerner, *Methods Enzymol.*, *91*, 49 (1983).
162. C. W. Ronson, B. T. Nixon, and F. M. Ausubel, *Cell*, *49*, 579 (1987).
163. B. P. Rosen, V. Weigel, C. Karkaria, and P. Gangola, *J. Biol. Chem.*, *263*, 3067 (1988).
164. W. Ross, S. J. Park, and A. O. Summers, *J. Bacteriol.*, *171*(7), 4009 (1989).
165. D. Rouch, J. Camakaris, B. T. O. Lee, and R. K. J. Luke, *J. Gen. Microbiol.*, *31*, 939 (1985).
166. P. C. Salinas, M. E. Tolmasky, and J. H. Croso, *Proc. Natl. Acad. Sci., USA* *86*, 3529 (1989).
167. M. Sandström and D. H. Liem, *Acta Chim. Scand.*, *A32*, 509 (1978).
168. S. Sasse-Dwight and J. Gralla, *J. Biol. Chem.*, *264*, 8074 (1989).
169. J. L. Schottel, A. Mandal, D. Clark, S. Silver, and W. Hedges, *Nature (London)*, *251*, 335 (1974).
170. R. A. Scott, *Methods Enzymol.*, *117*, 414 (1985).
171. L. M. Shewchuk, J. D. Helmann, W. Ross, S. J. Park, A. O. Summers, and C. T. Walsh, *Biochemistry*, *28*, 2340 (1989).
172. L. M. Shewchuk, G. L. Verdine, and C. T. Walsh, *Biochemistry*, *28*, 2331 (1989).
173. L. M. Shewchuk, G. L. Verdine, H. Nash, and C. T. Walsh, *Biochemistry*, *28*, 6140 (1989).
174. M. H. Shoukry, B. V. Cheesman, and D. L. Rabenstein, *Can. J. Chem.*, *66*, 3184 (1988).
175. L. G. Sillén and A. E. Martell, *Stability Constants of Metal-Ion Complexes*, The Chemical Society, London, Special Publication No. 17, 1964.
176. S. Silver, *Environmental Inorganic Chemistry*, K. J. Irgolic and A. E. Martel, Eds., VCH, Florida, 1985, p. 513.
177. T. L. South, B. Kim, and M. F. Summers, *J. Am. Chem. Soc.*, *111*, 395 (1989).
178. C. Stålhandske and F. Zintl, *Acta Cryst.*, *C43*, 863 (1987).
179. C. Stålhandske and F. Zintl, *Acta Cryst.*, *C42*, 1731 (1986).
180. W. Stricks and I. M. Kolthoff, *J. Am. Chem. Soc.*, *75*, 5673 (1953).
181. J. L. Sudmeier, R. R. Birge, and T. G. Perkins, *J. Magn. Reson.*, *30*, 491 (1978).
182. A. O. Summers, *Ann. Rev. Microbiol.*, *40*, 607 (1986).
183. A. O. Summers, J. Schottel, D. Clark, and S. Silver, *Microbiology—1974*, D. Schlessinger (Ed.), American Society of Microbiology, Washington, DC, 1975, p. 219.

184. A. O. Summers and S. Silver, *J. Bacteriol.*, *112*, 1228 (1972).
185. A. O. Summers and L. I. Sugarman, *J. Bacteriol.*, *119*, 292 (1974).
186. M. Summers, *Coord. Chem. Rev.*, *86*, 43 (1988).
187. D. Swenson, N. C. Baenziger, and D. Coucouvanis, *J. Am. Chem. Soc.*, *100*, 1932 (1978).
188. R. Tamilarasan and D. R. McMillin, *Inorg. Chem.*, *25*, 2037 (1986).
189. N. J. Taylor and A. J. Carty, *J. Am. Chem. Soc.*, *99*, 6143 (1977).
190. J. A. Tossell and D. J. Vaughan, *Inorg. Chem.*, *20*, 3333 (1981).
191. H.-T. Tsang, J. G. Wright, J. E. Penner-Hahn, and T. V. O'Halloran, unpublished results.
192. T. D. Tullius, ACS Symposium Series: *Metal-DNA Chemistry*, Vol. 402, T. D. Tullius, Ed., American Chemical Society, Washington, DC, 1989.
193. J. E. Turner, E. H. Lee, K. B. Jacobson, N. T. Christie, M. W. Williams, and J. D. Hoeschele, *Sci. Total Environ.*, *28*, 343 (1983).
194. N. Ueyama, T. Sugawara, K. Sasaki, A. Nakamura, S. Yamashita, Y. Wakatsuki, H. Yamazaki, and N. Yasuoka, *Inorg. Chem.*, *27*, 741 (1988).
195. N. Ueyama, M. Nakata, and A. Nakamura, *Bull. Chem. Soc. Jpn.*, *58*, 464 (1985).
196. N. Ueyama, T. Sugawara, K. Sasaki, A. Nakamura, S. Yamashita, Y. Wakatsuki, H. Yamazaki, and N. Yasoka, *Inorg. Chem.*, *27*, 741 (1988).
197. W. E. Van der Linden and C. Beers, *Anal. Chim. Acta*, *68*, 143 (1973).
198. M. Vasák, J. H. R. Kägi, and H. A. O. Hill, *Biochemistry*, *20*, 2852 (1981).
199. G. Wagner, D. Neuhaus, E. Wörgötter, M. Vasák, J. H. R. Kägi, and K. Wüthrich, *J. Mol. Biol.*, *187*, 131 (1986).
200. C. T. Walsh, M. D. Distefano, M. J. Moore, L. M. Shewchuk, and G. Verdine, *FASEB J.*, *2*, 124 (1988).
201. R. E. Wasylshen, R. E. Lenkinski, and C. Roger, *Can. J. Chem.*, *60*, 2113 (1982).
202. S. P. Watton, J. G. Wright, F. M. MacDonnell, J. W. Bryson, and T. V. O'Halloran, *J. Am. Chem. Soc.*, *112*, 2824, (1990).
203. J. Welch, S. Fogel, C. Buchman, and M. Karin, *EMBO J.*, *8*, 255 (1989).
204. A. F. Wells, *Structural Inorganic Chemistry*, 4th ed., Clarendon Press, Oxford, 1975, p. 1161.
205. G. Westin and W. Schaffner, *EMBO J.*, *7*, 3763 (1988).
206. P.-P. Winkler and P. Peringer, *Inorg. Chim. Acta*, *76*, L59 (1983).
207. W. Wojnowski, M. Wojnowski, and H. G. von Schnering, *Z. Anorg. Allg. Chem.*, *531*, 153 (1985).
208. S. Silver and T. K. Misra, *Ann. Rev. Microbiol.*, *42*, 717 (1988).
209. J. G. Wright, H.-T. Tsang, J. E. Penner-Hahn, T. V. O'Halloran, *J. Am. Chem. Soc.*, *112*, 2434 (1990).
210. J. G. Wright and T. V. O'Halloran, unpublished results.

211. B. J. Wu, R. E. Kingston, and R. I. Morimoto, *Proc. Natl. Acad. Sci, USA*, 83, 629 (1986).
212. C. S. Yanoni, *Acc. Chem. Res.*, 15, 201 (1982).
213. F. Zintl and I. Persson, *Inorg. Chim. Acta*, 131, 21 (1987).
214. C. Zuppioli, C. Perchard, M. H. Baron, and C. deLoze, *J. Mol. Struct.*, 72, 131 (1981).

NOTES ADDED IN PROOF:

The second structure of a mononuclear three-coordinate Hg(II) complex with aromatic thiolate ligands has recently been reported (72a). Although the S–Hg–S bond angles of the planar complex are distorted significantly from 120°, the average Hg–S–bond distance is 2.44(3) Å, in good agreement with the averages from the other three-coordinate Hg(II)–thiolate complexes summarized in Table VI. In the same paper, Gruff and Koch report the first structurally characterized example of a three-coordinate Cd(II)–thiolate complex. Comparison of the properties of this complex with the Cd(II)-MerR protein will facilitate characterization of the coordination in the latter.

Dimer complementation studies of site-directed cysteinyl mutants for the *Bacillus* RC607 MerR protein, as discussed in Sections VIIB and C, have recently been reported (83a).

Probing Nucleic Acids with Transition Metal Complexes

ANNA MARIE PYLE and **JACQUELINE K. BARTON***

*Department of Chemistry,
Columbia University
New York, New York*

CONTENTS

I. INTRODUCTION	414
II. FEATURES OF TRANSITION METAL COMPLEXES USEFUL IN PROBING NUCLEIC ACIDS	417
A. Binding Modes of Metal Complexes	418
B. Metal Complexes as Spectroscopic Tags	420
C. Redox Reactions of Metal Complexes	423
D. Metal Complexes as Structural Probes	426
III. APPLYING TRANSITION METAL COMPLEXES AS GENERAL NUCLEIC ACID PROBES	429
A. Metal Complexes as Probes of DNA-Protein Contacts	429
1. Chemical Footprinting by Metal Complexes	432
2. Photofootprinting by Metal Complexes	435
B. Heavy Metal Complexes as Covalent Labels	437
C. Spectroscopic Probes for DNA Structure	439
1. Techniques for Reporting on the Probe	440
2. Probing Recognition Parameters on B-DNA	442
3. A Spectroscopic Probe for Z-DNA	444
D. General Redox Cleaving Agents	447
1. Simple Coordination Complexes	447
2. Coordination Complexes Linked to DNA Binding Proteins	450

*Present Address: Division of Chemistry and Chemical Engineering, California Institute of Technology, Pasadena, CA 91125.

Progress in Inorganic Chemistry: Bioinorganic Chemistry, Vol. 38, Edited by Stephen J. Lippard.

ISBN 0-471-50397-5 © 1990 John Wiley & Sons, Inc.

IV. NUCLEIC ACID PROBES THAT COMBINE STRUCTURAL RECOGNITION AND REDOX CHEMISTRY	452
A. A Shape-Selective Probe for the A-Conformation	453
B. A Photocleaving Probe for Z-form DNA	456
C. Probing Variations within the B Conformation	458
D. Probing Biologically Interesting Sites	460
V. PROBING MORE COMPLEX STRUCTURES AND MORE COMPLEX PROBES	462
A. Metal Complexes as Probes of DNA Tertiary Structures	462
B. Probing RNA Structure	466
C. Hydrolytic Cleavage of Nucleic Acids	468
PROSPECTS FOR THE FUTURE	470
ACKNOWLEDGMENTS	471
REFERENCES	471

I. INTRODUCTION

For many years bioinorganic chemistry has been synonymous with the study of metal ions in biology. Metal centers that are critical in mediating cellular redox processes have been described and characterized. Metalloenzymes essential in catalyzing metabolic reactions have been discovered and the role of the metal in these reactions has been elucidated. The structure and coordination environment of metals in proteins with diverse functions have been explored. In all these studies what has been clear is the essentiality of the metal to the processes themselves and indeed even to probing these processes. The metal is essential because of its reactivity, its coordination geometry, which defines the molecular architecture about it, and importantly because of its electronic properties, which permit our spectroscopic investigation. In addition, bioinorganic chemists are now beginning to take advantage of the many characteristics of transition metal complexes in order to explore biological molecules which themselves do not contain a metal center. The same center of reactivity, structural complexity, and spectroscopic accessibility that has proved to be valuable in the examination of metalloproteins can be applied to probe biopolymers lacking a metal. In making such applications of transition metal chemistry, new exciting challenges and opportunities are becoming available to the inorganic chemist.

In this chapter we explore the utility and applications of transition metal

complexes in probing nucleic acids and the recognition of specific sites on the nucleic acid polymer. Nucleic acids under physiological conditions are polyanions composed of heterocyclic bases linked to a sugar-phosphate backbone. As such they are quite amenable to probing with positively charged transition metal ions and complexes that are stable in aqueous solution. A central question in biological research today involves the determination of how specific sites on the nucleic acid polymer are recognized and distinguished. Along the DNA double helical polymer, for example, how is a specific sequence of nucleic acid bases targeted? Proteins that regulate the expression of genetic information, for example, are able to bind to and discriminate among DNA sites with high affinity and fidelity. In developing new chemotherapeutic agents targeted to DNA and new tools for biotechnology, an understanding of the principles governing such site-specific recognition would be valuable. Indeed, understanding how molecules find unique positions on a seemingly uniform piece of DNA ranks among the most fascinating and important current chemical or biochemical questions.

One element of this problem involves the determination of the structural variations in a nucleic acid. Although represented commonly as a one-dimensional sequence of bases, nucleic acids adopt a variety of conformations. Double helical DNA is polymorphic in structure and along the polymer strand there exists a rich heterogeneity of conformation. Fig. 1 (see also color plate) shows the structures of three different, structurally characterized conformations of double helical DNA: the A (1), B (2), and Z (3) forms. These structures are all double helical in form and rely upon Watson-Crick hydrogen-bonding interactions between the two antiparallel strands of nucleic acid. The resulting shapes associated with these conformations are remarkably different, however. The B form, considered to be most common, is a right-handed helix, with base pairs stacked in the center of the helix and average base planes aligned normal to the helical axis. There are two well-defined right-handed grooves, termed the major and minor grooves, and each has a characteristic width and depth, which together result in the distinctive shape associated with this helical form. The A conformation (Fig. 1), is also a right-handed helix, but in other respects it is distinctly different from the B-form structure. Compared to the B-form structure, here, owing to a change in sugar pucker, the bases are pushed outward toward the minor groove direction and are tilted substantially with respect to the helix axis. The resulting helix has a very shallow and wide minor groove and a major groove pulled deeply into the interior of the structure; the major groove becomes largely inaccessible to molecules in solution. Double-stranded RNAs and DNA-RNA hybrids are thought in general to adopt predominantly the A conformation, but local

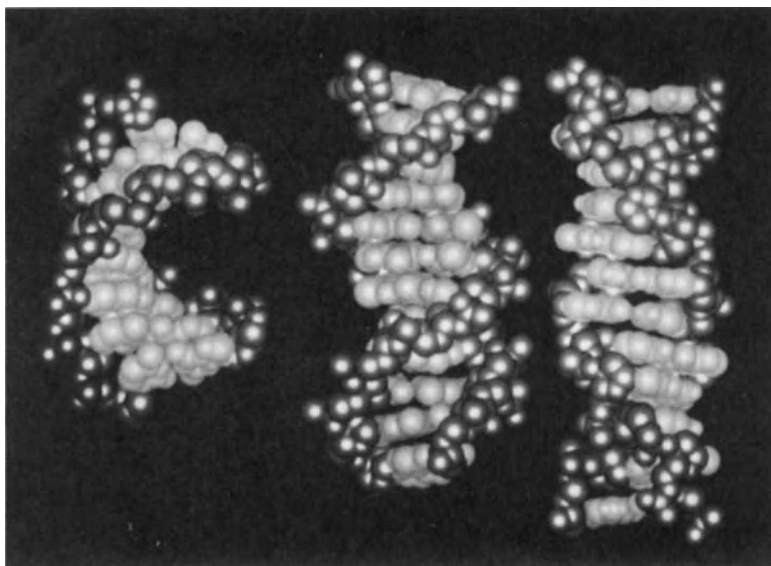


Figure 1. A- (left), B- (center), and Z- (right) DNA. Shown are space-filling models for the different double-stranded DNA helical conformations based upon crystallographic data for each form (1-3). The sugar-phosphate backbone is shown in red and the base pairs, in green. This and subsequent graphical representations were obtained using the program, Macromodel, for which we gratefully acknowledge W. C. Still.

regions of duplex DNA of a particular sequence (mainly homopurine-homopyrimidine segments) or under particular conditions (dehydrating solvents or environments) can also adopt A-like conformations. The remaining structurally characterized double helical conformation is that of Z-DNA (3). Although also composed of Watson-Crick hydrogen-bonded base pairing between antiparallel strands, this helical structure is strikingly different because it spirals with a left-handed sense. The structure is distinctive in other respects as well. The repeating unit is a dinucleotide, resulting in a *zigzag* helix, because of the alternation in sugar pucker and disposition of the bases about the glycosidic bond. Alternating purine-pyrimidine sequences have the greatest propensity to adopt this conformation. The helix is long (largest helical pitch) and slender. The major "groove" is in fact a shallow, almost convex surface, and the minor groove is a narrow crevice, zigzagging in a left-handed fashion along the side of the major "groove." These different structures illustrate a range of variation within the double helical framework, but even within these families a host of structural variations are evident. Within the B form, for example,

variations are seen in base pair tilt and twist, and even within a base pair, as a function of local sequence, the bases may be propeller twisted one to another, breaking the planarity of the base pair. There are a host of other local variations in conformation that have not been structurally characterized in detail. Examples include H-DNA (4), cruciforms (5), and bent DNA sites (6).

This chapter describes the impressive battery of probes for nucleic acid structure based upon transition metal chemistry and how these metal-based probes are being applied to elucidate elements of site-specific recognition. For the most part we focus our attention on probes for DNA. In Section II we illustrate the different features of transition metal chemistry in terms of its utility in probing nucleic acids and in the remaining sections we describe a variety of specific applications using metal-based probes. This chapter is not intended to be an exhaustive review of the field. Many other articles have been written, describing the variety of interactions of metal ions with nucleic acids (7). An abundance of articles is also available, which report on the mechanism of action of metal-based chemotherapeutic agents that target DNA, notably describing research on cisplatin and Fe-bleomycin (8). Most recently, also, review articles have appeared that describe the current state of knowledge of the interactions of metal-containing proteins with DNA (9). Although the field of metal-nucleic acids has become one of great excitement and ever-expanding topics, articles do not appear to have been written which, using what we know about the interactions of metal ions and complexes with nucleic acids as a foundation, describe how transition metal complexes are now being used as chemical probes. We therefore intend this chapter to illustrate the problem at hand and show how inorganic chemistry is currently being used and may become still more useful in developing probes to tackle these important questions in biology.

II. FEATURES OF TRANSITION METAL COMPLEXES USEFUL IN PROBING NUCLEIC ACIDS

Here we consider the advantages of transition metal chemistry in probing nucleic acids. Metal complexes bind to DNA through a variety of modes and each may be exploited in probe development. The redox and spectroscopic characteristics of the metal complexes, furthermore, offer a range of methods to assay sensitively these probe interactions. The spectroscopic perturbations in the metal complex on binding to its target serve as a reporter, or tag for binding, and a means to examine characteristics of that binding interaction. Redox reactions of the metal complexes bound to the nucleic acid also provide sensitive chemical reporters that mark specifically

the sites of binding on the polymer. Finally, and perhaps most subtly, the structures of the metal complexes themselves and how those structures influence binding yield powerful probes for nucleic acid structure and site recognition. The matching in shape and symmetry of a coordination complex to its nucleic acid binding site permits a structural view of the complementary nucleic acid binding site itself and how variations in structure may occur along the polymer strands. By keeping in mind these different characteristics of inorganic complexes, one may imagine a multitude of possibilities for how to exploit transition metal chemistry in probing nucleic acids.

A. Binding Modes of Metal Complexes

A great diversity exists in the design of nucleic acid probes upon transition metal chemistry in part because of the abundance of different binding interactions to nucleic acids that may be exploited. Metal complexes bind to DNA through both covalent and noncovalent modes as illustrated in Fig. 2.

Perhaps the most frequently considered binding interaction of heavy metals with DNA is that of DNA base binding (7), illustrated in Fig. 2 through the coordination of *cis*[diammineplatinum(II)]²⁺ to the guanine N7 nitrogen atom. The DNA lesion introduced by *cis*-platin, an important inorganic antitumor drug, is an intrastrand cross-link between neighboring guanine residues created by covalent binding of the metal center to the two soft purine nitrogen atoms (8, 10); binding to the adenine N7 position is also observed although to a lesser extent. Heavy metal ions in general appear to bind covalently to DNA through this mode of coordination and therefore, to first order, covalent tagging of guanine sites may be obtained by using such heavy metal reagents. Other coordination sites are present on the nucleic acid (the N1 positions on purines and N3 nitrogen atoms on pyrimidines) but these are not easily accessible in the double-stranded helix (7).

The metal ions may bind also to the sugar-phosphate backbone, either electrostatically or, less commonly, through association with the sugar. Hard metal ions like magnesium associate with the anionic phosphates (7). The pentose ring of the nucleotide is perhaps the poorest ligand for metal coordination but osmate esters of ribose can form and this kind of interaction has been suggested as a basis for heavy metal staining of RNA (11).

Non-covalent interactions between the ligands surrounding a coordinatively saturated metal center and the nucleic acid may also be used advantageously in probe design. The most common of such interactions is

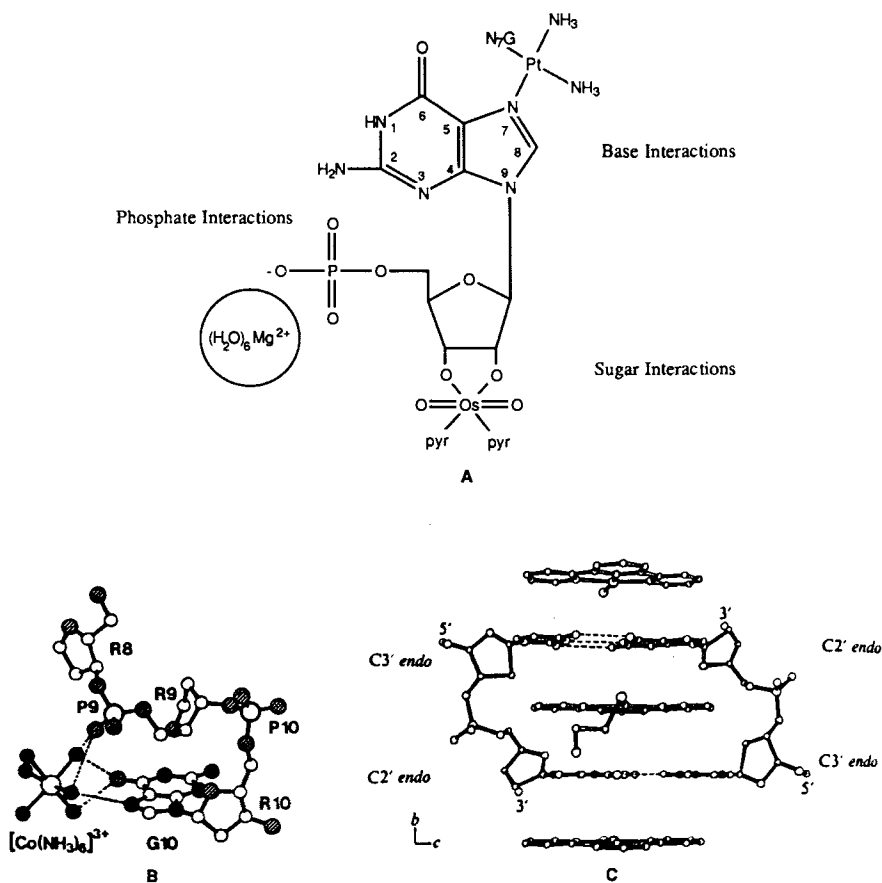


Figure 2. A diversity of covalent and noncovalent binding modes of metal complexes with DNA. (a) Representative covalent interactions. Shown schematically are examples of coordination to the DNA base, sugar, and phosphate moieties given, respectively, by the covalent association of *cis*diammineplatinum(II)²⁺ to the N7 nitrogen atom of neighboring guanine residues, the formation of an osmate ester with ribose hydroxyl groups, and the primarily electrostatic association between $[\text{Mg}(\text{H}_2\text{O})_6]^{2+}$ and guanosine phosphate. (b) An illustration of hydrogen bonding of coordinated ligands. Shown is a partial view of the crystal structure (12) of Z-form d(CG)₃ with $[\text{Co}(\text{NH}_3)_6]^{3+}$ hydrogen bonded both to the guanine base (G10) and phosphate backbone (P9). (c) Intercalative stacking of a metal complex. Shown is the crystal structure of (terpyridyl)(2-hydroxyethanethiolate)platinum(II) intercalated and stacked above and below the base paired dinucleotide d(CpG) (15).

likely that of hydrogen bonding of coordinated ligands to the nucleic acid. Figure 2*b* shows the several hydrogen-bonding interactions between amine hydrogen atoms and both phosphate oxygen and base acceptor positions evident in the crystal structure of cobalt hexammine bound to Z-form d(CG)₃ (12).

Many recent studies have focused on applications of metallointercalation, which is also an important noncovalent interaction of metal complexes with nucleic acids. Intercalation is a common mode of association of small molecules with DNA, where a flat aromatic heterocyclic moiety inserts and stacks in between the DNA base pairs (13). Lippard and co-workers (14) determined in 1974 that platinum(II) complexes containing an aromatic heterocyclic ligand such as terpyridine could intercalate in DNA. Figure 2*c* shows such a stacking interaction of such a complex in a dinucleotide (15). Recently, we have found that intercalation is not restricted to completely flat, square planar complexes, but partial intercalation of ligands coordinated to octahedral metal centers is feasible as well (16). We have found that tris(phenanthroline)metal complexes bind to DNA by two noncovalent modes, one described as a surface- or groove-bound interaction in the minor groove of the helix and the other appearing to be an intercalative interaction in the major groove of the helix (17). As can be seen even in the crystal structure of [Pt(trpy)(SCH₂CH₂OH)]⁺ bound to d(CG)₂, it seems that, in general, metallointercalators tend to bind from the major groove direction of the duplex. From the point of view of probe design, this specific targeting can be advantageous since the number of DNA recognition elements available as donor-acceptor interactions in the major groove exceeds those in the minor groove. Furthermore, protein-DNA interactions occur predominantly in the major groove of the helix. In addition, this intercalative binding mode permits the anchoring of the small molecule (and of its chemistry) with a well-defined orientation with respect to the helix.

B. Metal Complexes as Spectroscopic Tags

It was clearly demonstrated in the many beautiful studies conducted on spectroscopically active metal centers in proteins, that the electronic structure of a metal center can provide a sensitive spectroscopic handle to examine the region to which the metal complex is bound. This same spectroscopic sensitivity can be utilized in studies of nucleic acids.

The variety of studies conducted with tris(phenanthroline)metal complexes and DNA perhaps most easily illustrate this point (16). Tris(phenanthroline) complexes of ruthenium(II) and its derivatives possess an intense luminescent metal-to-ligand charge-transfer state that is

perturbed on binding to DNA (17, 18). Absorption hypochromism and luminescence enhancements accompany binding to the helix and may be used to monitor such binding (19). Figure 3a, for example displays the luminescence spectra of $[\text{Ru}(\text{phen})_3]^{2+}$ in the absence of DNA and of each enantiomer in the presence of DNA. The luminescence is enhanced and indeed is enhanced to an even greater extent for the Δ -isomer. These data are consistent with the increase in excited-state lifetime of the ruthenium complex found for the intercalative mode of binding and simply illustrate the enantioselectivity associated with this binding mode (16–19). As is evident, then, the spectroscopic as well as structural characteristics of the metal complex report on features of the binding interactions. Since binding varies with the environment about the metal complex, these perturbations allow us to monitor binding to different DNA sites and to learn about the nature of those sites.

Figure 3b illustrates how paramagnetic metal complexes may be used to assay binding to oligonucleotides in NMR experiments (20). The complex $[\text{Ni}(\text{phen})_3]^{2+}$, of comparable structure to $[\text{Ru}(\text{phen})_3]^{2+}$, is paramagnetic and therefore influences the magnetic properties of sites to which it is bound. The NMR signals of protons in proximity to the metal complex are preferentially broadened, allowing precise delineation of metal binding sites along the short polymer. Figure 3b shows the ^1H NMR spectrum of the duplex hexamer $d(\text{GTGCAC})_2$ in the presence of increasing concentration of $[\Lambda\text{-Ni}(\text{phen})_3]^{2+}$. While all resonances broaden with increasing nickel concentration, the adenine AH2 broadens preferentially. From this result we concluded that the surface bound mode, the other noncovalent mode of association of tris(phenanthroline)metal complexes with DNA (which favors the Λ -isomer), occurs in the minor groove of the helix (where the AH2 proton is found). This surface- or groove-bound interaction could not be explored in detail using other spectroscopic techniques.

In early studies of metal–nucleic acid interactions, it was the electron dense metal center that was exploited (7). Metal complexes were used as heavy metal tags in forming metal-containing isomorphous derivatives of nucleic acid complexes for crystallographic studies and as stains for nucleic acids in electron microscopy studies. It was hoped that specific heavy metal tagging might be applied for DNA sequencing by electron microscopy (21). Recently, it became clear that the full range of techniques available to the inorganic chemist may be applied to probing metal complex interactions with nucleic acids, thus indirectly allowing the use of these methods to probe the nucleic acids themselves. Bard and co-workers (22) have recently demonstrated the application of cyclic voltammetry to examine the binding to polynucleotides of the tris(phenanthroline) metal complexes. In these experiments, the cobaltic complex was employed to permit maximal elec-

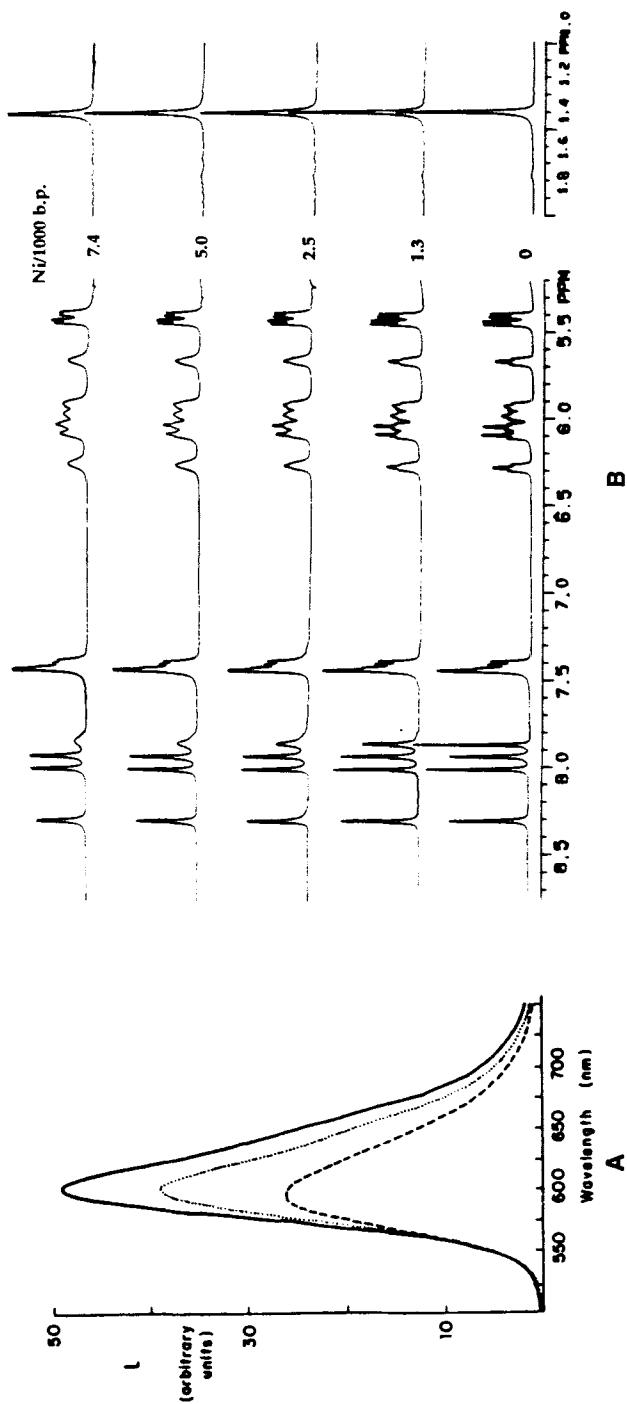


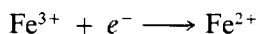
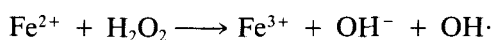
Figure 3. Spectroscopic methods to probe nucleic acids. (a) An illustration of the variation in luminescence characteristics of a metal complex with DNA binding. Shown is the emission spectrum of free $[\text{Ru}(\text{phen})_3]^{2+}$ (-----), $[\Delta\text{-Ru}(\text{phen})_3]^{2+}$ in the presence of DNA (.....), and $\Delta\text{-}[\text{Ru}(\text{phen})_3]^{2+}$ in the presence of DNA (—) illustrating the enantioselective binding of the complexes to the helix (16–19). (b) An application of paramagnetic broadening by metal complexes to obtain structural information as to their association with nucleic acids. Shown is the ^1H NMR spectrum of $d(\text{GTGCAC})_2$ with increasing amounts of $[\Delta\text{-Ni}(\text{phen})_3]^{2+}$ (20). Noteworthy is the preferential broadening of the adenine AH2 resonance (7.8 ppm) indicating the association of the enantiomer in the minor groove of the helix.

trochemical detection. As the many varied applications with phenanthroline complexes now demonstrate, by the judicious choice of a metal center, the use of transition metal complexes allows us to tune and select the spectroscopic properties of a given molecular probe. Such flexibility is simply not available for organic molecules without significantly altering their molecular geometry.

C. Redox Reactions of Metal Complexes

One way for a probe or drug to act on a biological molecule is to perform a chemical reaction at its binding site. This reaction imparts new characteristics to the biomolecule specifically at the binding site, which can be detected using biochemical techniques. For example, a currently used sensitive technique to probe DNA structure is the application of site-specific DNA cleavage chemistry. Spectroscopic methods to examine binding of a complex to the polynucleotide permit the determination of the quantity of complex bound to the polymer. But, if the bound complex promotes the scission of the DNA sugar-phosphate backbone, for example, through oxidative degradation of the sugar moiety, then biochemical methods can be used to determine *where* the polymer scission occurred and, therefore, where along the polymer the complex was bound (23). This strategy is schematically illustrated in Fig. 4a. The strand break, induced by the redox reaction of the metal complex, sensitively marks the binding site.

Figure 4b shows the structure of the first synthetic DNA cleaving molecule based upon transition metal chemistry. The structure of the complex MPE-Fe(II) illustrates how a DNA binding moiety may be converted to a DNA cleaving molecule by the coupling of metal based redox reactions (24). Ethidium is a prototypical DNA intercalator. MPE-Fe(II) was constructed by Dervan and co-workers (25) by tethering onto methidium the classical iron chelating agent, EDTA. Upon addition of stoichiometric ferrous sulfate, hydrogen peroxide and a reductant, such as dithiothreitol, MPE-Fe(II) efficiently cleaves DNA. It is considered that the methidium intercalates into the helix and delivers the iron-centered redox chemistry at short proximity to the sugar-phosphate backbone. In the presence of reductant to regenerate the ferrous species, the metal complex may then catalytically promote the Fenton reaction, generating hydroxyl radicals at high local concentration in the vicinity of the helix.



These diffusing radicals are thought to degrade the sugar oxidatively primarily through hydrogen abstraction at the C4' position on the sugar. Some debate concerning the mechanism still remains, however.

Chemical or photochemical oxidation of a nucleic acid is accomplished very efficiently by a variety of metal complexes. In the presence of hydrogen peroxide and thiol, bis(phenanthroline) cuprous ion very efficiently cleaves DNA (26). Tris(phenanthroline) complexes of cobalt(III) or rhodium(III) promote redox reactions in their excited states (27, 28). These photoactivated probes bind to the DNA helix in a fashion comparable to the spectroscopic probes described above and then, upon photoactivation, promote DNA strand cleavage.

The different kinds of photoreactions carried out by tris(phenanthroline)metal complexes may illustrate how such cleavage chemistry is applied in probe design. The rhodium and cobalt complexes, upon irradiation, target the DNA sugar (28, 29). The cleavage products of an oligonucleotide are a 5'-phosphate, 3'-phosphate, free base, and presumably a sugar fragment (the sugar fragment has not been identified). In the case of photocleavage with $[\text{Co}(\text{phen})_3]^{3+}$, cobaltous ion and free phenanthroline are also formed. These photoreactions do not require oxygen and no intermediate diffusible species appears to be involved, based upon experiments conducted with analogues. These results have suggested to us that irradiation leads to photoreduction of the metal complex (either ligand centered or involving ligand-to-metal charge transfer, LMCT), with formation of a ligand radical and thereupon direct hydrogen atom abstraction from the sugar. This mechanism contrasts the photocleavage reactions found with $[\text{Ru}(\text{phen})_3]^{2+}$. Here photolysis in the LMCT band sensitizes formation of singlet oxygen (30). This reactive intermediate then oxidatively adds to the different DNA bases. The bases, once modified, can be liberated from the polymer upon treatment with piperidine, resulting thereafter in strand scission. Here the reaction depends on the oxygen concentration and a diffusible species, $^1\text{O}_2$, is involved which targets the DNA base.

Binding of all tris(phenanthroline)metal complexes to DNA is comparable, the structures being essentially identical and the charge differences only affect the relative proportions of surface vs. intercalative binding. Different patterns of cleavage are evident along the DNA strand for the tris(phenanthroline)metal complexes, however, as revealed by using gel electrophoresis and autoradiography for analysis. For the rhodium and cobalt complexes, the binding is quite uniform along the strand, and since it is the sugar that is targeted, to a first approximation the sugars at each position should be equally reactive. Hence, a uniform pattern of cleavage is obtained. If this photoactivated, nondiffusible chemistry is instead cou-

pled to a site-specific binding molecule, then single site cleavage is observed (see below). For the ruthenium complexes, although binding is equally uniform, here the target is the DNA base, and $^1\text{O}_2$ reacts with different efficiencies with the different DNA bases ($\text{G} \gg \text{T} > \text{A,C}$). Hence, for uniform binding, preferential reactivity at all guanine sites is obtained (30). With site-selective ruthenium analogues (Fig. 4), superimposed over the guanine-specific reaction, some preferential sites of cleavage are apparent where the ruthenium complex is bound and the singlet oxygen concentration is locally much higher. Since singlet oxygen diffuses outward from the binding site, cleavage at several sites emanating outward from the center is observed. This kind of cleavage pattern, over several base pairs, typifies a reaction involving a diffusing species. Figure 4c schematically illustrates the different kinds of cleavage patterns one expects for different reagents. Each scheme may be usefully exploited, depending on the question being addressed.

D. Metal Complexes as Structural Probes

Rigid, coordinatively saturated metal complexes can also act as structural probes for nucleic acids simply as a result of the recognition of a complementarity in the shape of binding sites. The same notions that apply in constructing ligands of different well-defined geometries to model receptor site structures may be applied in probing local variations in nucleic acid structures. The well-defined and varied architectures of transition metal complexes have been extremely valuable for probe design. In this instance one considers primarily an ensemble of weak, noncovalent interactions between a rigid coordinatively saturated probe and its matching binding site. Indeed nature has already incorporated transition metal chemistry in the design of rigid, coordinatively saturated structures that recognize specific sites on DNA through the synthesis of "zinc finger" proteins. This family of eukaryotic DNA transcriptional factors shares a common structural motif defined by the scaffolding of a peptide domain about a zinc center coordinated in a tetrahedral fashion to two cysteine and two histidine side chains (31). This example of site-specific DNA binding by a natural metal complex, with the metal defining the structure of the complex, underscores the potential utility of these species for the study of site recognition along a DNA strand.

Transition metal chemistry provides a rich variety of structural elements, (a) geometric variability, (b) rigidity, and (c) dissymmetry necessary for construction of nucleic acid probes. First, consider in contrast the structural constraints imposed by the carbon atom. It has a maximum coordination geometry of four and a relatively limited set of possible structural forms

that it can assume. Biological systems such as the active site of an enzyme or ribozyme are often intricate assemblies that would best fit a probe molecule of alternate geometry, such as trigonal bipyramid or an octahedron. Functional groups designed to interact with the site may be best arranged about a transition metal in one of these alternate shapes. Transition metal and rare earth complexes, with their variety of coordination geometries, provide templates for construction of novel shapes that may be tailor-made for interaction with biological targets. Second is the question of the rigidity of a given structure. When a molecule possesses many degrees of freedom in its motion, we can never say with certainty what shape it is assuming. Thus, if we want to study how it interacts with a biological macromolecule, we cannot understand precisely how the probe molecule and the biomolecule contact each other, which makes it difficult to draw structural conclusions. For example, the structural complexity of polysaccharides is immense and commonly used by nature to define recognition elements for proteins binding to the surface of cells and other surfaces. It would be difficult, however, to use sugars as probes of structure because their floppy rings may assume many different geometries. One could never say with certainty what shape the probe adopted. By using rigid metal complexes with a strict definition of the shape of the complex, and therefore of the complementary site being probed, some certainty in structural information is achieved. Last we consider the feature of structural dissymmetry in a probe. There is perhaps nothing more specific and well or poorly "matched" than is a diastereomeric interaction between two dissymmetric structures. Since nucleic acids are themselves chiral, chirality in the design of a probe for nucleic acids may be logically and specifically exploited (16). Transition metal structures, here as well, offer a diversity in structural asymmetry to be used advantageously.

The enantioselective binding of tris(phenanthroline)metal complexes to B-DNA illustrates this notion of applying rigid molecular shape and symmetry to probe nucleic acid structure. Figure 5 (see also color plate) displays a model for the intercalation of Λ - and Δ -tris(phenanthroline)metal complexes into right-handed B-form DNA. Intercalation favors the Δ -isomer for this binding mode. The tris(phenanthroline)metal complex is rigid in structure and the intercalative interaction, the stacking of one phenanthroline ligand between the base pairs of the helix, orients and anchors the complex with respect to the helix. In so doing, for the Δ -isomer, the ancillary, nonintercalated ligands are necessarily oriented along the helical groove, with the same chirality as the right-handed helix. For the Λ -isomer, with one phenanthroline ligand intercalated and therefore held in a similar fashion, the ancillary ligands are oriented with a disposition contrary to that of the right-handed helix; steric interactions then result between the

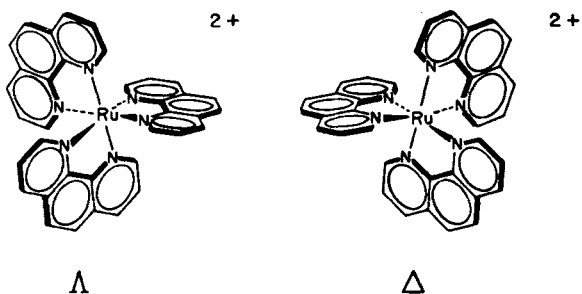


Figure 5(a). Λ - (left) and Δ - (right) $[\text{Ru}(\text{phen})_3]^{2+}$.

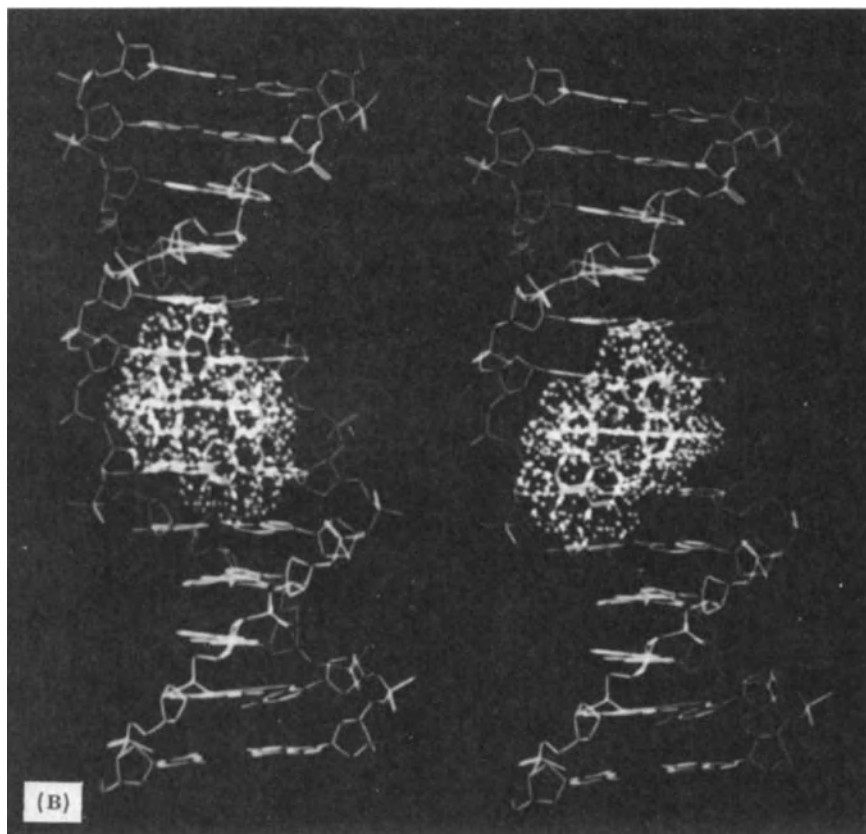


Figure 5(b). Illustration of $[\text{Ru}(\text{phen})_3]^{2+}$ enantiomers bound by intercalation to B-DNA and the basis for the enantioselectivity (16). The Δ -enantiomer (right) fits easily into the right-handed helix, since the ancillary ligands are oriented along the right-handed groove. For the Λ -isomer (left), in contrast, steric interference is evident between the ancillary phenanthroline ligands and the phosphate backbone, since for this left-handed isomer the ancillary ligands are disposed contrary to the right-handed groove.

phenanthroline hydrogen atoms and the sugar-phosphate backbone both above and below the intercalation site. The enantioselectivity in binding by intercalation, which favors the Δ -isomer, could therefore be rationalized by the matching, or not matching, of the symmetry of the metal complex to that of the DNA helix. This chiral discrimination provides the basis for probes to distinguish DNA helical chirality (see below). The rigid, dissymmetric structure or shape of the tris(phenanthroline)metal complex therefore itself serves as the basis for probing the nucleic acid.

III. APPLYING TRANSITION METAL COMPLEXES AS GENERAL NUCLEIC ACID PROBES

Keeping in mind the fundamental advantages available when using transition metal complexes in designing nucleic acid probes (Section II), we consider here a variety of general applications of simple coordination complexes. Transition metal complexes have been particularly useful in developing chemical footprinting agents to examine protein-DNA contacts. These reagents (many are now available), are replacing exonucleases in molecular biology laboratories to explore protein-DNA interactions. Simple metal complexes have also become useful in exploring subtle variations in structure of DNA in the absence of protein, by exploiting the differential reactivity of sites along the polymer to the metal complexes, or by examining differential spectroscopic properties of metal complexes depending on the DNA conformations where the metal complexes are bound. Metal complexes have also been useful as tags either for the nucleic acids themselves in electron microscopic studies or as tags linked to DNA binding proteins to report their site of binding along the helix. In considering these different applications, what has become quite remarkable is the impressive array of techniques and important biological questions that can now be addressed, and addressed uniquely, with these transition metal reagents.

A. Metal Complexes as Probes of DNA-Protein Contacts

Footprinting is one of the most powerful techniques in molecular biology for visualizing the site-specific binding of proteins to DNA (32). Since most nonenzymatic footprinting reagents are in fact metal complexes, inorganic chemistry has played a key role in our understanding of protein-DNA interactions.

In order to function as an effective footprinting reagent, a metal complex must be a relatively nonspecific DNA cleaving agent. The presence of a

protein or peptide bound to DNA blocks the normal cleavage by the reagent, and therefore, the greater the sequence neutrality of the cleaving agent, the easier it becomes to detect the sites blocked. When radioactively end-labeled cleavage products of the reaction between the footprinting reagent and DNA–protein complex are denatured and electrophoresed on a polyacrylamide gel, one sees a blank spot, or “footprint”, in the position of DNA protected by bound protein. Figure 6 illustrates this methodology and Fig. 7 shows the variety of transition metal complexes that have been applied in footprinting experiments.

Chemical footprinting reagents that have been most successful in mapping DNA–protein contacts and determining the binding site sizes of the proteins are methidium–propyl–EDTA Fe(II), $[\text{Fe}(\text{EDTA})]^{2-}$, $[\text{Cu}(\text{phen})_2]^+$, and metalloporphyrins (Fig. 7a). Each reagent has specific advantages that render it useful for probing particular systems. Another class of footprinting reagents are those that are activated by light (Fig. 7b). There are some distinct experimental advantages to photofootprinting re-

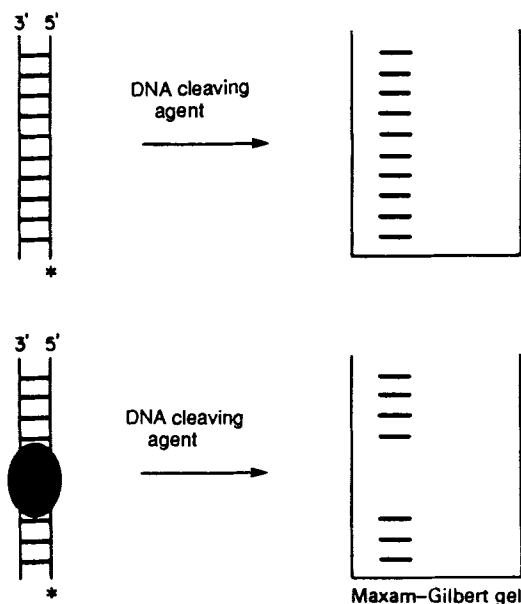
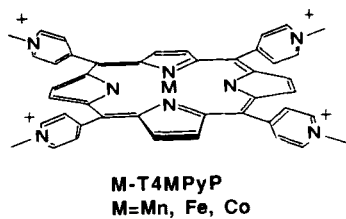
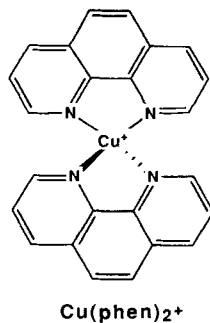
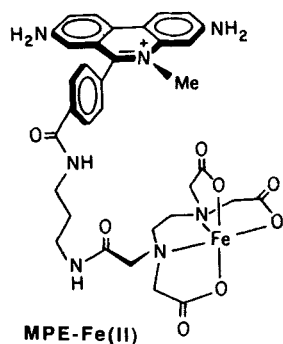
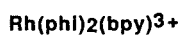
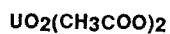
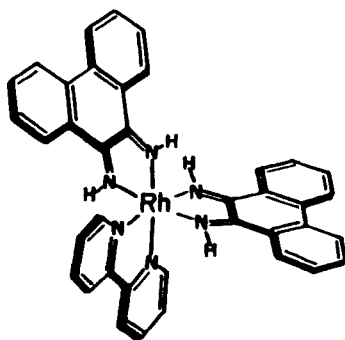


Figure 6. Schematic illustrating DNA footprinting methodology. DNA cleaved by a sequence-neutral cleaving agent yields an even distribution of cuts on end labeled and then denatured fragments (top). When protein is bound to a specific site on the DNA, cleavage at that site is inhibited, and the cleavage pattern on end-labeled DNA shows a blank spot, or footprint (bottom).



A



B

Figure 7. Chemical (a) and photochemical (b) footprinting reagents.

agents, because they can be added to a protein–DNA complex and remain inert until photoactivation. One therefore has control over the timing of these reactions and hence the potential to examine protein–DNA interactions directly with some time resolution. Furthermore, light activation in principle may permit footprinting experiments inside a living cell. Photofootprinting reagents thus far include uranium nitrate and acetate salts, light-activated metalloporphyrins, and phenanthrenequinone diimine complexes of rhodium(III).

1. Chemical Footprinting by Metal Complexes

MPE–Fe(II). One of the most successful and commonly used footprinting reagents is the unique hybrid of inorganic and organic molecules described in Section II.C, MPE–Fe(II) (33, 34). One part of the molecule, a reactive $[\text{Fe}(\text{EDTA})]^{2-}$ complex, undergoes Fenton chemistry, releasing hydroxyl radicals. These reactive species are brought into proximity of the DNA backbone by tethering the metal center to methidium, an organic dye that intercalates into DNA in a relatively sequence-neutral fashion. One advantage of MPE–Fe(II) not shared even by enzymatic footprinting agents is that its cleavage pattern is almost entirely nonspecific. Since each nonprotected nucleotide is cleaved by the reagent, single-base resolution of protein binding site sizes is possible. With this complex, it is also possible to map the binding to DNA both of small molecules (33), such as netropsin, distamycin, actinomycin and CC-1065, and of large proteins (34).

One disadvantage of using MPE–Fe(II) is that the hydroxyl radicals it releases are highly diffusible. DNA cleavage is observed as much as four nucleotides away from the likely position of the iron. Consequently, the borders to the footprint can be fuzzy, which diminishes the resolution of the exact protein binding site. Resolution is further hampered by the flexibility of the tether between the methidium binding moiety and the reactive metal center.

Additionally, since chelation of a metal ion is required for reactivity, it becomes impractical to footprint certain metalloproteins using this or similar reagents. Many of the most interesting subjects for footprinting studies are metalloprotein transcription factors, containing endogenous metal ions that are in fast or slow exchange with the solvent. When footprinting with MPE–Fe(II), as with many other footprinting reagents such as $[\text{Fe}(\text{EDTA})]^{2+}$ or $[\text{Cu}(\text{phen})_2]^+$, ligand and an excess of metal ion are added to the reaction mixture separately. Difficulty in footprinting metalloproteins and metalloenzymes may occur because endogenous Zn(II) or Cu(II) ions can be pulled out of the protein by EDTA ligands on MPE before it reacts with

iron. Conversely, the excess metal ion may interfere with weak, but structurally important metal binding sites on the protein.

[Fe(EDTA)]²⁻. This reagent is used to generate a chemical snapshot of solvent-accessible regions on DNA (35). The reactivity is based upon that developed with MPE-Fe(II), but the principle of binding is opposite. Since it is negatively charged, [Fe(EDTA)]²⁻ does not actually interact directly with the helix. Instead, it remains in solution and releases a massive blast of free hydroxyl radicals upon combination with hydrogen peroxide. A uniform concentration of hydroxyl radicals is therefore generated along the DNA helix and hydroxyl radicals that reach the DNA cut the backbone where it is exposed. In addition to its utility as a footprinting reagent, [Fe(EDTA)]²⁻ has been successfully used to visualize deviations in B-form geometry and to probe DNA tertiary structures (see below).

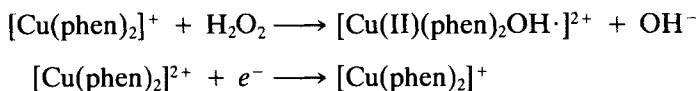
The lack of any direct contact between the metal complex and DNA is a unique advantage for [Fe(EDTA)]²⁻ footprinting. Any molecule that binds to DNA will have some effect on its structure. For example, footprinting reagents that bind by intercalation unwind the DNA helix and this may change the observed binding site or orientation of a protein. Since [Fe(EDTA)]²⁻ does not bind, we can be fairly sure that the footprint observed is not influenced by structural distortions introduced by the probe molecule.

Like MPE-Fe(II), [Fe(EDTA)]²⁻ gives a clear, sequence neutral DNA cleavage pattern (36). However, the lack of a DNA binding functionality requires that [Fe(EDTA)]²⁻ be used in very large excess to generate enough hydroxyl radicals near the helix, so problems caused by free Fe(II), EDTA, and H₂O₂ are conceivably more serious than with MPE-Fe(II). In particular, an excess of free EDTA will pull most of the endogenous metals out of a DNA binding protein, possibly affecting its DNA binding domain. Potentially worse, the demetallated protein may bind to alternate sites thus giving an inaccurate representation of the preferred protein binding. Despite these potential problems, [Fe(EDTA)]²⁻, a common reagent on the laboratory shelf, is now routinely used for footprinting studies for a wide variety of DNA binding proteins.

[Cu(phen)₂]⁺. This complex is thought to bind with a low level of sequence specificity in the minor groove of DNA (26). The lack of sequence neutrality in the cleavage pattern of this reagent makes [Cu(phen)₂]⁺ a useful probe of structural microheterogeneity within the minor groove of DNA, but it limits the utility of this complex as a high-resolution footprinting reagent. Despite the gaps in the cleavage pattern of [Cu(phen)₂]⁺

because of its nonuniformity in site cleavage, it has been used to footprint the binding sites of several proteins to DNA (37). For example, protein binding to the immunoglobulin heavy chain genes has been studied using $[\text{Cu}(\text{phen})_2]^+$ (38). In these cases, DNA-protein complexes were suspected of being unstable to conditions of isolation from a preparative gel. In order to footprint the DNA-protein complex without removing it from the stabilizing gel, $[\text{Cu}(\text{phen})_2]^+$ was diffused into the gel and the cleavage reaction was performed *in situ*. The high solubility and diffusibility of the complex in the gel allowed it to perform well in this interesting adaptation of the footprinting protocol.

The radical generated by $[\text{Cu}(\text{phen})_2]^+$ may be less diffusible than that released by $[\text{Fe}(\text{EDTA})]^{2-}$ derivatives. Cleavage by $[\text{Cu}(\text{phen})_2]^+$ appears to be more precise and sharper on a polyacrylamide gel. The reasons for this difference may lie in the nature of the reactive species (39). DNA strand scission by this reagent requires the addition of Cu^{2+} , phenanthroline, hydrogen peroxide, and a thiol or other reducing agent (e^-). The proposed mechanism for this reaction is as follows (26):



When footprinting with $[\text{Cu}(\text{phen})_2]^+$ is performed, one adds solutions of free Cu^{2+} , excess phenanthroline, and H_2O_2 to a DNA-protein complex. Phenanthroline is a particularly powerful chelating agent and transition metal ions are commonly found in certain types of enzymes. Furthermore, it has been found that $[\text{Cu}(\text{phen})_2]^+$ can oxidize free cysteine thiols in proteins to disulfide bridges (40). Thus, it is apparent that either $[\text{Cu}(\text{phen})_2]^+$ or its components could be potentially damaging to the native structure of a DNA binding protein. This, coupled with a high level of sequence selectivity, somewhat limits the use of $[\text{Cu}(\text{phen})_2]^+$ as a footprinting reagent.

Metalloporphyrins. When combined with ascorbate, potassium superoxide, or iodobenzene, certain metalloporphyrins, in particular those containing manganese, promote DNA cleavage in a reaction thought to be similar to that of $[\text{Cu}(\text{phen})_2]^+$. The reactive species proposed is a high-valent manganese-oxo complex (41). Again, like $[\text{Cu}(\text{phen})_2]^+$, metalloporphyrins tend to have a fairly high level of sequence selectivity and therefore are relatively poor reagents for high-resolution footprinting. The type of metalloporphyrins most commonly used for footprinting and DNA cleavage have been the Type III or groove binding porphyrins (42). Al-

though some planar metalloporphyrins are capable of intercalating into DNA (43), the groove binding Type III derivatives contain axial ligands or bulky axial substituents on the porphyrin ring itself that disrupt potential intercalative interactions. An example of a complex of this type would be *meso*-tetrakis(*N*-methyl-4-pyridiniumyl)porphine (TMpyP4) Co(III), which interacts differently with biological molecules than its ostensibly planar cousins.

Group III metalloporphyrins prefer to bind to the surfaces of DNA, which are rich in AT sequences (42). High resolution mapping of DNA cleavage mediated by Fe(III) or Mn(III) complexes of TMpyP4 in the presence of reducing agent shows that cleavage occurs preferentially at regions containing a minimum binding requirement of (A·T)₃. Intense DNA cleavage is observed at sites ATAAA, AATTTAA, and other long AT-rich tracts (44). Because these sequences may have a larger negative potential along the surface of the minor groove, the Group III metalloporphyrins may be recognizing these sites as a result of electrostatic considerations. These sequences also have a propensity to melt easily. Alternatively, it has been proposed that a general preference of small molecules for AT-rich regions in the minor groove of DNA may be due to the extreme narrowness of the groove at these sequences (45). Part of the porphyrin ring might "intercalate" sideways into the narrow cavity and thus become involved in favorable stacking interactions on the outside of the bases. In any case, the strong preference of Type III metalloporphyrins for AT-rich regions is precisely the characteristic that limits their widespread use as routine footprinting reagents.

2. Photofootprinting by Metal Complexes

Uranium Nitrate and Acetate Salts. Visible light (420 nm) activates these metal complexes to cleave DNA in a completely sequence-neutral fashion. In order to demonstrate this effect, UO₂(CH₃COO)₂ and UO₂(NO₃)₂ were used to footprint λ-repressor binding to OR1-operator sequences on a 225 base pair DNA fragment (46), and uranyl salts have also been used to examine contacts between *Escherichia coli* RNA polymerase and DNA (47). These complexes are particularly promising for several reasons. First of all, light of this wavelength is low enough in energy to preclude completely any direct photodamage to DNA. Second, the sequence neutrality of cleavage makes it possible to identify any type of small protein binding site.

It is apparent from studies on footprinting by uranyl salts, however, that very high concentrations of reagent (millimolar) are required in order to

obtain a reasonable level of cleavage. This becomes a problem in considering applications to *in vivo* footprinting, as a cell would probably not tolerate high levels of uranium salts. A more serious difficulty lies with the quality of the footprints themselves. The observable footprint of repressor covers only two-to-four nucleotides. It is known that the binding site size of this protein is much larger than that. Thus, it appears that the small size of the uranium reagents and the diffusible nature of their reactive species conspire to give an underestimation of the overall protein binding site size. Nonetheless, as conditions are worked out for the use of this reagent, uranium salts could become highly successful photofootprinting reagents.

[Rh(phi)₂(bpy)]³⁺. Coordinatively saturated phenanthrenequinonediimine (phi) complexes of Rh(III) are highly efficient DNA photocleaving agents (48). In particular, [Rh(phi)₂(bpy)]³⁺ has been shown to be an almost sequence-neutral photocleavage reagent upon activation with long-wavelength UV light. The complex [Rh(phi)₂(bpy)]³⁺ has therefore been developed for high-resolution footprinting (49). With this complex, we can map the precise binding locations and site sizes of small molecules such as distamycin-A or large DNA binding proteins, such as the restriction endonuclease, EcoR1. Site sizes of distamycin and EcoR1 on oligonucleotides have been determined crystallographically and these correspond exactly to those found with [Rh(phi)₂(bpy)]³⁺ footprinting. Furthermore, since distamycin binds in the minor groove and EcoR1 binds in the major groove, it is apparent that [Rh(phi)₂(bpy)]³⁺ is able to footprint DNA-bound molecules without regard to their groove location.

The major reasons for the success of [Rh(phi)₂(bpy)]³⁺ as a footprinting reagent, aside from the convenience of photoactivation, are the high resolution of its cleavage patterns, its sequence neutrality, and the fact that one need not add chemically reactive reagents to the DNA-protein complex. The reactive species produced by [Rh(phi)₂(bpy)]³⁺ is not diffusible, so the footprints are precise to single nucleotide resolution. Free metal ions, chelators, and reducing agents need not be added to the system because the [Rh(phi)₂(bpy)]³⁺ complex is fully assembled and activated only with light. Also, photofootprinting reagents, which are taken up inside cells, show particular promise for *in vivo* footprinting. Finally, as an avidly binding metallointercalation reagent, [Rh(phi)₂(bpy)]³⁺ is easily able to footprint proteins bound in the major groove of DNA. Many sequence-specific transcription factors bind from the major groove, so it is valuable to have available footprinting reagents that are sensitive to proteins bound in this region.

B. Heavy Metal Complexes as Covalent Labels

Perhaps the earliest applications of heavy metals to nucleic acid chemistry have been with regard to the design of sequence- or structure-specific electron dense tags for electron microscopy. Such applications still remain, although now such applications may also include electroactive tags for scanning tunneling microscopy. The chemistry to develop such specific, covalent tags on DNA is also of interest from the viewpoint of new (and old) pharmaceutical design. Indeed, if not for its utility as an antitumor agent, one could imagine a function of *cis*-[Pt(NH₃)₂Cl₂] quite simply as a covalent tag for guanine sites on DNA.

Osmium Tetroxide–Pyridine. Osmium(VI) tetroxide is one of the most extensively used probes for DNA structure. It is an example of a high-valent transition metal complex which, due to its uniquely reactive center, is able to functionalize specific bonds on DNA. This powerful oxidant is known to form cisoid osmate esters upon attack of an electron-rich double bond. By tuning the reactivity of OsO₄ and its esters with the addition of other ligands, it has been possible to generate a family of reactive probes for exposed pyrimidine bases.

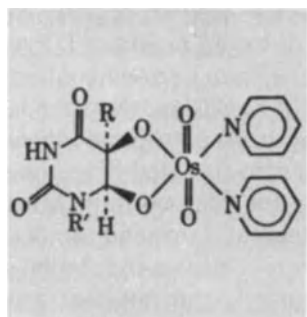
DNA that is ostensibly double stranded can adopt local conformational variations such as short stretches of single-stranded character. These exposed regions possess a uniquely high chemical reactivity that distinguishes them from the double-stranded helix. In double-stranded DNA, most of the reactive functional groups on nucleic acid bases are involved in hydrogen bonding to the complementary strand. But once two strands separate, the bases become more exposed to solvent and to electrophilic species in solution. Many unusual DNA conformations locally lead to regions of single-stranded character. The B–Z junction is a distorted region of DNA where hydrogen bonding is partly disrupted. Cruciform regions contain single-stranded loops at their termini. Within H-DNA structures, two strands are partly separated, allowing one strand to wind back onto the double-stranded DNA, while the other strand forms a single-stranded hinge between flanking double-stranded regions. Regions that contain long poly(dA·dT) regions are known to melt at low temperatures and are believed to be in equilibrium with single-stranded forms. Given the similarities in the chemical reactivity of the single-stranded segments that are common to these structures. OsO₄ is able to recognize and tag them by covalent binding.

Single-stranded or distorted DNA results in solvent accessibility to the double bonds of pyrimidine bases. In the presence of tertiary nitrogen

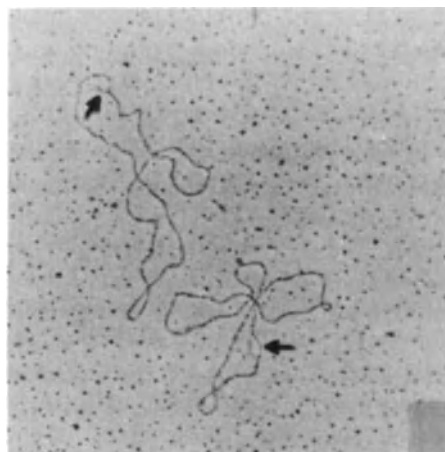
donor ligands such as pyridine, OsO_4 adds across the 5,6 double bond of pyrimidines, forming an osmate ester (Fig. 8a) (7a). Reactivity is highest for thymine but the complex will also react with cytosine and uracil. The addition of pyridine or bipyridine to this reaction stabilizes the osmate ester and keeps it from disproportionating.

Nucleic acids were first modified with OsO_4 in an attempt to label thymines along a DNA strand with heavy atoms and thus permit their visualization by electron microscopy (21). This form of nucleotide-specific heavy atom labeling was an early attempt to provide a method for sequencing DNA. A study of OsO_4 reactions on polynucleotides revealed that the reagent reacted with single-stranded poly(C), poly(T), and poly(U) (50). In order to use OsO_4 as a structural probe, Palacek and co-workers (51) treated plasmid DNA with OsO_4 , generating a covalent modification at single positions on the DNA, which can be visualized as bubbles by electron microscopy. This staining pattern is apparent in Fig. 8b. These binding sites were also mapped in an electrophoresis experiment by treating modified plasmid with S1 nuclease, which cleaves the strand opposite the OsO_4 lesion.

High-resolution sequencing methods can be used to determine the exact site of osmium attack because the modified sites are susceptible to cleavage with piperidine treatment. In this way, OsO_4 has successfully been used



(a)



(b)

Figure 8. Heavy metal labeling of nucleic acids. (A) OsO_4 modification of a thymine residue. (B) An electron micrograph of DNA showing the OsO_4 modification and resultant local denaturation of the helix. Arrows indicate bubbles where OsO_4 has attacked a thymine, unwinding the helix (51).

to probe cruciform structures, B-Z junctions, and H-DNA in homopurine-homopyrimidine stretches (52). The success of OsO_4 as a DNA probe illustrates how differential reactivity along a strand may be used advantageously.

$\text{Ru}(\text{phen})_2\text{Cl}_2$ and $\text{Rh}(\text{phen})_2\text{Cl}_3$. Coordinatively unsaturated octahedral metal complexes (or those with highly labile leaving ligands) may also bind covalently to heteroatoms on the DNA bases. The N7 nitrogen atom on guanine is an excellent ligating center for heavy metals. Through coordination of the heteroatom, one can easily tag a DNA strand with a covalently bound metal for use in heavy atom labeling or studies on the binding of coordinating drugs.

$[\text{Rh}(\text{phen})_2\text{Cl}_2]\text{Cl}$ has been observed to bind covalently to DNA in a reaction that requires light (53). The complex is itself substitutionally inert but chloride exchange may be facilitated by photolysis. Upon loss of coordinated chloride, with likely substitution of an aquo ligand, the complex becomes activated to ready displacement of the aquo species by direct coordination to a DNA base. Analogously, $\text{Ru}(\text{phen})_2\text{Cl}_2$ binds covalently to DNA (54). Here, however, although photolysis in the metal-to-ligand charge-transfer band furthermore promotes substitution, the reaction proceeds readily in the dark; bis(phenanthroline) ruthenium(II) complexes more easily undergo exchange for nitrogen donor ligands than do their rhodium analogues. An intriguing aspect of this reaction is that one observes a dramatic enantioselectivity in the covalent binding of racemic $\text{Ru}(\text{phen})_2\text{Cl}_2$ to DNA. The Λ enantiomer preferentially binds to the helix while the Δ isomer is excluded. In fact, the extent of chiral discrimination observed for covalent binding is greater than that observed with intercalative binding by $[\text{Ru}(\text{phen})_3]^{2+}$. If $\text{Ru}(\text{phen})_2\text{Cl}_2$ binds to the N7 atom of guanines in a manner similar to that of the antitumor drug cisplatin, the metal might chelate adjacent bases on the same strand. This model, with the complex coordinating *against* the helix, is consistent with the observation of Λ selectivity upon coordination: The complementary screw axis of the Λ isomer will permit the phenanthroline ligands to fit within the groove of the DNA while steric interactions between phenanthrolines and the phosphate backbone will limit similar covalent binding by the Δ isomer (16). This work helped to demonstrate that covalent binding by metal complexes, and perhaps by DNA binding drugs in general, may take place with substantial chiral discrimination.

C. Spectroscopic Probes for DNA Structure

Metal complexes often have intense optical transitions in the visible spectrum and many are capable of fluorescing under ambient conditions.

These optical transitions of metal complexes are commonly affected by their microenvironment, thereby outfitting metal complexes with sensitive spectroscopic handles on their molecular surroundings. In particular, complexes of Ru(II) and other d^6 metal complexes have optical properties that are strongly affected by the extent and type of binding to DNA. One means for a metal complex to impart information about DNA structure is to elicit a spectroscopic change upon binding. This method is noninvasive and provides an excellent means to obtain solution-state data about DNA conformation and structure.

There is an impressive battery of spectroscopic techniques available for probing interactions between metal complexes and DNA. The oldest of these, UV/vis spectroscopy, is still one of the most sensitive ways to analyze dye–DNA interactions. For chiral metal complexes, circular dichroism is an invaluable tool. Fluorescence spectroscopy has in particular made great strides in recent years with respect to these applications, and aside from the measurement of simple emission from an excited metal complex, one can utilize emission polarization, luminescence lifetimes, and differential fluorescence quenching to obtain still more information about the environment about a metal complex. The application of ruthenium complexes, in particular, to developing probes for DNA, has been initiated in our laboratory and we focus here on some of its applications.

1. *Techniques for Reporting on the Probe*

With simple tris(dipyridyl) complexes of ruthenium(II) and their derivatives, a battery of luminescence techniques have been developed for studying the interactions and dynamics of metal complexes on DNA. Most of these methods depend on and exploit the rich photophysics and photochemistry of dipyridyl(bpy) complexes of ruthenium(II) characterized by inorganic chemists.

A range of photophysical parameters can be measured and found to vary with DNA binding (17–19). The first two spectral perturbations found with $[\text{Ru}(\text{phen})_3]^{2+}$ upon binding to DNA, absorption hypochromism and luminescence enhancements, were described in Section II and shown in Fig. 3. The extent of luminescence enhancement, the absorption hypochromism, and the red shift associated with spectra of the bound forms seem to reflect the extent of overlap of the ligand with the base pairs of the helix. If the complex does not bind, or binds by a weak, nonintercalative mode, neither the luminescence nor absorption intensity are appreciably changed. When $[\text{Ru}(\text{phen})_3]^{2+}$ binds to DNA in a physiological buffer solution, a twofold increase in $[\text{Ru}(\text{phen})_3]^{2+}$ emission is observed. In the presence of $[\text{Ru}(\text{bpy})_3]^{2+}$, in contrast, under the same conditions, no spec-

tral changes are detected. Indeed the variety of photophysical experiments performed indicate that $[\text{Ru}(\text{bpy})_3]^{2+}$ binds only electrostatically to the helix, with neither an intercalative nor surface bound component and no associated enantioselectivity.

The increased luminescence intensity reflects the increase in excited-state lifetime of the ruthenium complexes bound to DNA. For $[\text{Ru}(\text{phen})_3]^{2+}$ in the presence of DNA, single photon counting experiments show a biexponential decay in emission from the bound complex (18). There is a long lived component [$2 \mu\text{s}$ for $[\text{Ru}(\text{phen})_3]^{2+}$], which we have assigned to the intercalative binding mode, and a component indistinguishable from the free form ($0.6 \mu\text{s}$ in aerated solutions), which we ascribe to a mixture of free and surface-bound forms. The enantiomeric selectivity differs for the two components, consistent with the notion that intercalation favors the Δ isomer and surface binding favors the Λ isomer. The increase in excited-state lifetime likely is a function both of the fact that the complex is more rigidly held when bound to the helix compared to free in solution, limiting vibrational modes for relaxation from the excited state, and because the intercalative mode likely limits collision and energy dissipation with water.

These binding modes may also be probed through mode-selective quenching experiments (19). The complex $[\text{Fe}(\text{CN})_6]^{4-}$ is an efficient quencher of the excited state of ruthenium(II). Since ferrocyanide is anionic, however, its association with the DNA polyanion is unfavorable. Hence, in the presence of DNA, ferrocyanide preferentially quenches ruthenium species that are bound to DNA to a lesser extent or less intimately. For the series of complexes $[\text{Ru}(\text{bpy})_3]^{2+}$, $[\text{Ru}(\text{phen})_3]^{2+}$, and $[\text{Ru}(\text{DIP})_3]^{2+}$ (where DIP = 4,7-diphenylphenanthroline), the quenching efficiency, k , by ferrocyanide in the presence of DNA is inversely correlated with the hydrophobicity of the complex: $k(\text{bpy}) > k(\text{phen}) > k(\text{DIP})$. The DIP complex, more tightly or closely held along the helix, is the least efficiently quenched. Similarly in time resolved experiments, only the shorter lived surface bound component could be quenched appreciably, and the intercalative component, presumably deeply held in the helix, was inaccessible to the anionic quencher (18). The converse was also found if a cationic quencher, such as $[\text{Co}(\text{phen})_3]^{3+}$, which binds to DNA comparably to the ruthenium analogue, was employed. Indeed the DNA remarkably increases the extent of electron-transfer quenching of $[\text{Ru}(\text{phen})_3]^{2+}$ by $[\text{Co}(\text{phen})_3]^{3+}$, leading us to examine whether DNA can mediate, both by facilitated diffusion and at long-range, electron-transfer reactions between bound donors and acceptors (55).

Another photophysical technique used to probe the dynamics of these interactions is steady state luminescence polarization (18, 19). The ruthenium complex bound to the DNA is excited with polarized light. If, on

the time scale of the emission (microsecond for the ruthenium complexes), the complex is rigidly held on the helix, then polarization is retained in the emitted light. Complexes of $[\text{Ru}(\text{DIP})_3]^{2+}$ show the greatest extent of luminescence polarization, followed by $[\text{Ru}(\text{phen})_3]^{2+}$, with no polarized emission found with $[\text{Ru}(\text{bpy})_3]^{2+}$. This result is consistent with the extent of intercalation for the series of complexes. In other words, the steady state polarization experiments indicate how rigidly the complex resides on the helix. These experiments were also coupled with measurements of enantiomeric selectivity and the addition of differential quenchers to quench either the intercalative or surface bound form, and these were used to characterize in detail the intercalative and surface-bound modes of binding to the helix. Such experiments, taken together, provided a powerful picture of binding of the metal complexes to DNA. Ruthenium complexes are now being tethered or incorporated into other DNA binding moieties (56), and coupled to these techniques, will likely provide a sensitive means to report on how these binding agents interact with the helix.

2. *Probing Recognition Parameters on B-DNA*

Mixed-Ligand Complexes. The photophysical properties of the ruthenium complexes have been exploited to examine systematically those features necessary for intercalative and surface binding on the helix. The photophysical properties of a wide variety of mixed-ligand derivatives can be exploited to compare and contrast their recognition characteristics in a systematic fashion (57, 58). A family of 12 octahedral metal complexes, which varied in the arrangement and composition of their ligands, was synthesized (57). The ligands used in this mixed-ligand study were all bidentate and differed primarily in the extent and planarity of their aromatic surface area. Some of the ligands were functionalized with hydrogen-bonding groups as well. Examples are shown in Fig. 9.

A comparison of emission enhancements for luminescent molecules in the mixed-ligand study showed that, as one replaces dipyriddy ligands with phenanthrolines, emission enhancement increases dramatically for bound metal complexes. The degree of enhancement parallels the relative DNA binding affinity of the molecules as determined by equilibrium dialysis. Substitution of bpy with DIP ligands also appreciably increases both emission enhancement and DNA binding. Taken together, these results showed that the extent of intercalation (as measured roughly by emission enhancement) increases as the planar surface area of intercalating ligands becomes more expansive. Furthermore, the relative magnitude of intercalative interaction for these metal complexes is linked to their ability to bind strongly to DNA.

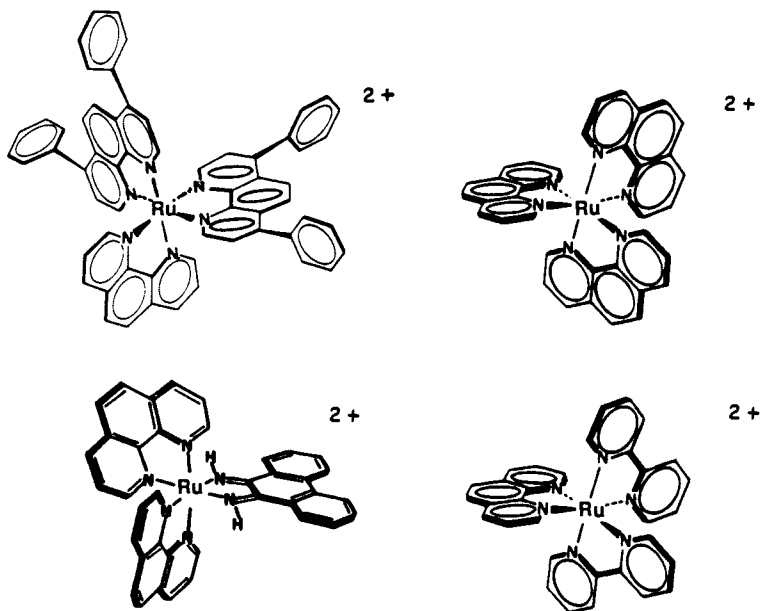


Figure 9. Mixed-ligand complexes of ruthenium(II) (57). Clockwise from top left: $[\text{Ru}(\text{DIP})_2(\text{phen})]^{2+}$, $[\text{Ru}(\text{phen})_3]^{2+}$, $[\text{Ru}(\text{bpy})_2(\text{phen})]^{2+}$, and $[\text{Ru}(\text{phen})_2(\text{phi})]^{2+}$.

Luminescence lifetime measurements on the mixed-ligand complexes showed that those containing either phen or DIP possessed both short- and long-lived components to their luminescence decay. These findings indicate that all the complexes bind to DNA by a combination of intercalation and surface binding modes. It also suggested that the DIP ligand is more perturbed upon binding than phen and perhaps has greater overlap with the DNA bases.

Similar results were seen through examination of the perturbations in the visible absorption spectra of the complexes. Substantive absorption hypochromism and a shift in the absorption maximum to longer wavelengths indicate good intercalative overlap between DNA base pairs and the DNA binding chromophore. Within the mixed-ligand study, ruthenium complexes containing the phi ligand (phi = phenanthrenequinone diimine) showed the greatest degree of hypochromism, followed by DIP, phen, and then bpy complexes. The phi ligand is perhaps best matched of the variety of ligands studied in its shape for stacking to that of the DNA base pairs. Binding constants were also determined based upon absorption titration data. Collectively, this information indicated that strength of binding was linked strongly to intercalation and the extent of ligand-base pair over-

lap. The extent of this overlap and of binding followed the order $\text{phi} \gg \text{DIP} > \text{phen} \gg \text{bpy}$. Complexes containing the phi ligand appear to bind avidly to DNA by intercalation, although the absence of luminescence for this complex limited the spectroscopic studies that could be performed.

Interestingly, when dipyridyl ligands were substituted with functional groups capable of hydrogen bonding to the base pairs, such as ketones and nitro groups, overall binding and spectroscopic changes were not enhanced over unfunctionalized analogues. In fact, binding was even slightly inhibited. This result indicated that, for this set of molecules, binding to DNA is driven primarily by the strength of stacking interactions between base pairs and ligands. Hydrophobicity of the metal complexes seems to play a large role, and hydrogen bonding at least in these instances seems less of a factor.

The synthetic variation of molecular shape and functionality, coupled to spectroscopic studies, can be useful in probing the parameters that drive binding to B-form DNA. In the transition metal complexes examined, the most important factor driving overall binding of these molecules to DNA appeared to be the match of shape and overlap between metal complex and the B-DNA helix.

3. *A Spectroscopic Probe for Z-DNA*

$\Lambda\text{-Ru}(\text{DIP})_3]^{2+}$. Octahedral metal complexes of the 4,7-diphenylphenanthroline (DIP) family are versatile probes for Z-form structure. Using both spectroscopic studies of $[\Lambda\text{-Ru}(\text{DIP})_3]^{2+}$ binding (59, 60) and photochemical cleavage studies with $[\Lambda\text{-Co}(\text{DIP})_3]^{3+}$ (see below), one observes that the complexes can scan large pieces of primarily B-form DNA and bind exclusively to Z-form sites or sites of other unusual geometries. The battery of spectroscopic techniques described in the first part of this section was used to determine the relative affinity for $[\text{Ru}(\text{DIP})_3]^{2+}$ enantiomers to different forms of DNA and to derive spectroscopic probes for Z-like DNA structures.

The application of $[\Lambda\text{-Ru}(\text{DIP})_3]^{2+}$ as a probe for Z-DNA was based upon the finding of chiral discrimination associated with binding to DNA of the tris(phenanthroline)metal complexes and the fact that the chiral discrimination appeared to be governed by matching the symmetry of the metal complex to that of the DNA helix (see above). Tris(phenanthroline)metal complexes show enantioselectivity, depending on ionic strength and temperature, but the extent of discrimination could be enhanced by enhancing the steric bulk of the complex as with the DIP complexes. Given an enantiospecific interaction, then, one might use a metal complex to discriminate between DNAs of differing chirality, instead

of using the B-form DNA to discriminate between isomers of the metal complex. The premise in developing a probe for the Z form therefore resided in developing a complex that was unable to bind to the right-handed helix but, owing to its left-handed symmetry, could bind instead to a left-handed helix. Models based upon the crystal structure of $[\text{Ru}(\text{DIP})_3]^{2+}$ (61) show that $[\Delta\text{-Ru}(\text{DIP})_3]^{2+}$ may intercalate into right-handed B-DNA without significant steric interference between the ancillary ligands and the curve of the phosphate backbone. Absorption titrations indicated binding of the DIP complexes to B-DNA to be enantiospecific (59). Other luminescence methods were consistent with intercalative binding of the Δ isomer and furthermore supported a high enantioselectivity with B-DNA; spectroscopic results with $[\Lambda\text{-Ru}(\text{DIP})_3]^{2+}$ do not indicate its similar intercalation into B-DNA (18, 19, 59, 60). Table I summarizes these results.

$[\Lambda\text{-Ru}(\text{DIP})_3]^{2+}$, nonetheless, binds avidly to the Z-form helix, hence providing the basis for the probe. Interestingly, both Λ and Δ isomers bind preferentially to the Z-form helix over the B form, perhaps because of the shallowness of the groove. Irrespective of the properties of the Δ isomer, for the purpose of a Z-form probe, however, the necessary criteria were met. $[\Lambda\text{-Ru}(\text{DIP})_3]^{2+}$ binds well to the Z-form helix and poorly to the B-form helix. Spectroscopic assays for $[\Lambda\text{-Ru}(\text{DIP})_3]^{2+}$ binding to an unknown nucleic acid sample therefore provides a measure of Z-form (non-B form) content.

How do the metal complexes actually bind to the Z-form helix? Considering the flat shape of the major groove of left-handed Z-DNA, one would expect it to be a poor template for chiral discrimination. Furthermore, intercalation into Z-DNA is thought to be unfavorable due to its extremely rigid structure and limited base pair stacking. It was surprising to discover (60), therefore, that a very large enantiomeric discrimination is observed upon binding of $[\text{Ru}(\text{DIP})_3]^{2+}$ to Z-DNA and this binding based

TABLE I
Luminescence Measurements of $[\text{Ru}(\text{DIP})_3]^{2+}$ Enantiomers Bound to B- and Z-DNAs

Enantiomer and DNA	Relative Emission Enhancement ^a	Luminescence Polarization ^b	Relative Stern-Volmer Quenching Rates ^c
Δ and B-DNA	1.8	0.19	1.0
Λ and B-DNA	1.0	0.03	2.2
Δ and Z-DNA	1.0	0.05	2.4
Λ and Z-DNA	2.0	0.21	1.0

^aFor a single type of DNA, enhancements are expressed as normalized values.

^bSteady state polarization values are given.

^cNormalized rates are given with respect to quenching by $[\text{Fe}(\text{CN})_6]^{4-}$, which preferentially quenches complexes bound in a mode more accessible to solvent.

upon spectroscopic parameters appears consistent with intercalation. In fact, the trends observed upon binding of enantiomers to B-DNA are cleanly reversed when using Z-DNA of opposite handedness. The complex $[\Lambda\text{-Ru}(\text{DIP})_3]^{2+}$ shows a twofold greater emission enhancement than does the Δ isomer upon binding to Z-DNA. Luminescence polarization results indicate substantial retention of polarization in emitted light for the Λ isomer with Z-DNA, but no significant retention of polarization with the Δ isomer. Table I shows the comparison in spectroscopic results with the two forms.

These experiments reveal that $[\text{Ru}(\text{DIP})_3]^{2+}$ enantiomers differentiate B and Z forms of DNA by detecting differences in the chirality and geometries of the two polymers. Work with $[\text{Ru}(\text{DIP})_3]^{2+}$ enantiomers demonstrates that chiral metal complexes are able to selectively recognize subtle differences in the symmetry of large biological molecules. Perhaps just as important, it now appears that Z-DNA may also bind molecules in an intercalative fashion and that, despite its flat major groove, it can discriminate between enantiomers of a bound complex. With these metal complexes, we have therefore learned much about recognition by two different helical forms and have gained structural information about the flexibility of Z-form DNA.

TABLE II
DNA Cleavage Chemistry of Metal Complexes

Complex	Target ^a	Chemistry ^b	Diffusibility ^c	DNA Binding ^d	Site Selectivity ^e
Fe(EDTA) ²⁻	Sugars	OH·, Fenton	Diffusible	None	None
MPE-Fe(II)	Sugars	OH·, Fenton	Diffusible	Sequence neutral	None
[Co(NH ₃) ₆] ³⁺	Base	e ⁻ transfer	Diffusible	Hydrogen bonding	G
[Cu(phen) ₂] ⁺	Sugars	Cu ²⁺ -OH·	Slight	AT-rich	AT-rich
M-Porphyrin	Sugars	M=O	None	AT-rich	AT-rich
U(O ₂)(NO ₃) ₂	<i>f</i>	<i>f</i>	Diffusible	<i>f</i>	None
[Ru(TMP) ₃] ²⁺	Base	¹ O ₂	Diffusible	A-form	A-form, G
[Ru(phen) ₃] ²⁺	Base	¹ O ₂	Diffusible	Sequence neutral	G
[Co(DIP) ₃] ³⁺	Sugar	Radical	None	Z-form	Z-form
[Rh(DIP) ₃] ³⁺	Sugar	Radical	None	Z, cruciforms	Z, cruciform
[Rh(phen) ₂ (phi)] ³⁺	Sugar	Radical	None	Open major groove	5'CCAG3'
[Rh(phi) ₂ (bpy)] ³⁺	Sugar	Radical	None	Sequence neutral	None

^aDNA may be modified by attack either at the sugar or at the nucleotide base position.

^bThe reactive species involved in DNA cleavage, if known.

^cSome reactive species are diffusible, producing broad patterns of DNA damage on the strand. Others are nondiffusible, resulting in single cuts.

^dThe site of metal complex binding to DNA, if known.

^eThe sites cleaved by the metal complex.

^fNot known.

D. General Redox Cleaving Agents

As described above, redox reactions of metal complexes can be used to promote DNA strand scission, and such strand scission events may be sensitively detected to report on the location of the metal (or its reaction) on the polymer. Here we describe how the redox reactions of quite simple coordination complexes have been used to examine structural variations in DNA and how such metal complexes may be coupled to DNA binding proteins to report on their recognition characteristics.

1. Simple Coordination Complexes

The simple coordination complexes we describe may be useful in probing subtle variations in DNA structure despite containing few specific structural elements upon which to base differential binding at sites on the helix. The complex $[\text{Cu}(\text{phen})_2]^+$ may display some level of selectivity in its binding if not reactivity, but the anionic $[\text{Fe}(\text{EDTA})]^{2-}$ clearly detects variations in DNA structure depending only on the differential accessibility of DNA surfaces to hydroxyl radical, which mediates the reaction by the metal complex. Cobalt hexammine, also a very simple coordination complex, promotes DNA strand scission upon photoactivation. Here reactivity along the strand depends on electron-transfer oxidation chemistry on DNA rather than reflecting structural variations being recognized on the helix.

$[\text{Fe}(\text{EDTA})]^{2-}$ The complex $[\text{Fe}(\text{EDTA})]^{2-}$ has been used as a probe for several different types of variations in B-form geometry (35). Since this metal complex generates free $\text{OH}\cdot$ radicals that abstract hydrogen atoms from DNA sugars in a sequence-neutral fashion, structural anomalies that shield the sugars at specific sites or render sugar hydrogen atoms less accessible to attack result in dramatic decreases in cleavage intensity. Reactions with this complex therefore can be used with high sensitivity to detect local variations in sugar atom accessibilities as a function of DNA sequence.

Electrophoretic mobility experiments have shown that DNA containing long poly(A) tracts become "bent" if these tracts are phased every 10 base pairs along the strand (6). It was of interest to determine the molecular structure of bent regions, and $[\text{Fe}(\text{EDTA})]^{2-}$ has provided some of the best available information about the chemical nature of a bent site in the context of a long strand (62). Consider a DNA segment containing repeated bending elements phased at each turn of the helix. Conceivably, if bent enough, it would form a circle. The sugar-phosphate backbone within the interior of the circle would then be protected, or relatively inaccessible to

$\text{OH}\cdot$ compared to sugar-phosphate backbone segments lying on the exterior of the circle. As can be seen in Fig. 10, unlike the uniform cleavage pattern displayed by normal B-DNA, cleavage by $\text{OH}\cdot$ on a bent, phased poly(A) tract yields a pattern that is sinusoidal. This pattern helps confirm that the helix is protected from cleavage on the inside (the circle center) and that on the molecular level the helix must be bent. Additionally, a gradual diminution in cleavage from 5' \rightarrow 3' along the poly(A) tract is observed. This observation, together with a two nucleotide shift to the 3' side in this cleavage pattern, was consistent with $\text{OH}\cdot$ abstracting hydrogen atoms from the minor groove, and with the minor groove being gradually narrowed in width as the bend progresses. The bend in DNA, which other studies (63) indicated to be toward the minor groove, may then be pinched together with a smooth variation across the poly(A) tracts, rendering the segment gradually more protected from DNA cleavage agents.

In addition to large B-form structural variations, $[\text{Fe}(\text{EDTA})]^{2-}$ has been used to probe for subtle changes in the sequence-dependent helical twist of DNA (64). As can be seen in Fig. 10, by depositing the rodlike DNA on an inert surface (in this case calcium phosphate crystals), one can protect an entire face of the helical polymer. Exposed backbone on the other side is then cleaved with a periodicity that reflects the number of base pairs per turn of the helix. Experiments with $[\text{Fe}(\text{EDTA})]^{2-}$ have therefore helped to illustrate that there are sequence-dependent deviations in the number of bases that can pack into a helical turn.

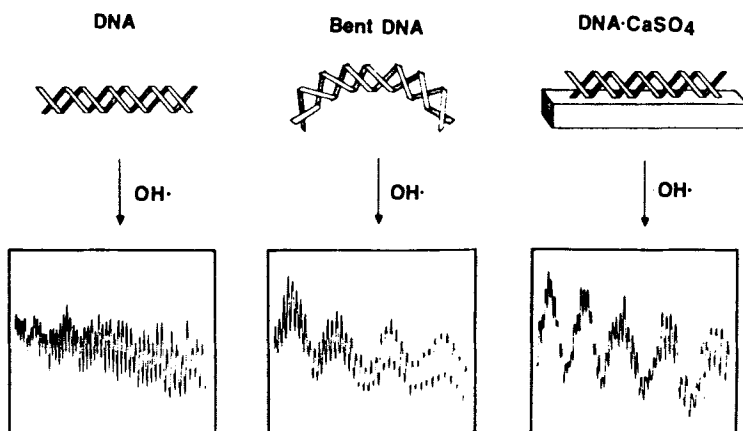


Figure 10. Schematic and densitometric traces illustrating the effects of $[\text{Fe}(\text{EDTA})]^{2-}$ mediated $\text{OH}\cdot$ attack on different types of DNA. Densitometric traces obtained after cleaving with $[\text{Fe}(\text{EDTA})]^{2-}$ (left) B-DNA; (center) bent DNA; and (right) DNA bound on one face of CaSO_4 crystals (35).

[Cu(phen)₂]⁺. [Cu(phen)₂]⁺ is a tetrahedral metal complex which, as discussed previously, cleaves DNA in the presence of H₂O₂. This molecule also recognizes structural dishomogeneities in the minor groove of B-form DNA. In chromosome mapping studies it was shown that [Cu(phen)₂]⁺ does not cleave indiscriminantly, but shows a definite preference for certain regions along the chromosome (65). When used to map the locus 67B1 from *Drosophila*, [Cu(phen)₂]⁺ cleaved preferentially at spacer regions between genes and the frequency of cleavage was much lower in transcribed regions. It is known that the regions between genes bind a host of regulatory proteins and may therefore display a higher frequency of structural dishomogeneity that aids in DNA-protein recognition. Thus, [Cu(phen)₂]⁺ was able to identify sites of local structural dishomogeneity. Cleaving DNA between genes or at protein binding sites is a characteristic shared by other metal complexes (see below) and may indicate a link between the structures and biological functions of nucleic acids.

Another line of evidence suggesting that [Cu(phen)₂]⁺ is sensitive to structural variations on DNA was that it shared many cleavage sites with known endonucleases (66). Upon cleaving a long stretch of linear DNA (150–400 base pairs) with [Cu(phen)₂]⁺ or with the enzyme micrococcal nuclease and coelectrophoresing the respective products on a denaturing polyacrylamide gel, strikingly similar cleavage patterns are obtained. In fact, these cleavage sites are a subset of those of another nuclease that is sensitive to minor groove dimensions, DNase I.

An analysis of the sequences preferred by these nucleases, both natural and artificial, reveals that, in general, there is a preference for "AT-rich" regions. Alternating d(AT) is preferred over poly(dAdT) (67). In addition, Cartwright observed that many "A-T-rich" regions are not cut unless preceded by a cytosine on the 5'-side (65). These findings suggest that some alternating dAT sequences may have a minor groove well matched to the nucleases. Since TAT is a triplet site very susceptible to attack by [Cu(phen)₂]⁺, Veal and Rill studied the effect of point mutations in this triplet (68). They found that replacement of A with G completely eliminated cleavage while substitution of A with inosine (I), which has no bulky functional groups in the minor groove, restored activity at these regions. Thus, they propose that direct steric interactions in the minor groove may play a role in recognition of [Cu(phen)₂]⁺ sites. Taken together, this work indicates that [Cu(phen)₂]⁺ can be a probe for narrowing and steric perturbations in the minor groove of DNA.

[Co(NH₃)₆]³⁺. This complex binds DNA through a mixture of electrostatic interactions and hydrogen-bonding interactions to both base and

phosphate acceptors. Such interactions are available throughout the DNA strand but may be particularly well-matched in Z-DNA segments, as depicted in Fig. 2 (12). The complex $[\text{Co}(\text{NH}_3)_6]^{3+}$ and structurally similar transition metal di- and trications all promote B \rightarrow Z transitions (69). Cobalt hexaammine, furthermore, upon photoactivation, also promotes DNA strand cleavage, but this cleavage appears not to be sensitive to DNA structural variations (28). Cleavage is found at all guanine residues that contain an additional purine to the 3'-side. One explanation for this cleavage pattern lies in the possibility of a specific hydrogen-bonding framework that becomes available at such sites. No cleavage is found at corresponding positions on the opposite strand, however, suggesting that the sequence selectivity in cleavage may not mark a differential binding event. The other explanation, suggested also by the photochemical characteristics of the complex, lies in the ready oxidation of guanine bases by the potent photooxidant and, in particular, of guanines (having the lowest oxidation potential of the four bases) with a purine stacked at a neighboring site so as to further lower the oxidation potential at that residue. This electron-transfer-based cleavage chemistry has also been observed with other potent photooxidants (30b) and might be helpful in probing subtle redox variations associated with unusual nucleic acid structures.

2. *Coordination Complexes Linked to DNA Binding Proteins*

The metal complexes described above have at most a low level of specificity for different DNA sequences or structures. One can transform them into probes for single sites on genomic DNA, however, by tethering them to sequence-selective DNA binding moieties (70, 71). Redox-active metal ions may be tethered onto oligonucleotides that target specific complementary DNA sites, either so as to form double-stranded units (70) or, remarkably, specific triple-stranded segments (71). Here we concentrate on the conversion of DNA binding proteins to site-specific endonucleases. Just like many natural endonucleases, the resultant protein is composed of two domains, one responsible for DNA binding, the other responsible for DNA cleavage. Metal complexes such as $[\text{Cu}(\text{phen})_2]^+$, $[\text{Fe}(\text{EDTA})]^{2-}$, and most recently, a Cu(II) polypeptide complex have been used successfully to functionalize sequence-specific DNA binding molecules.

There are distinct advantages that this approach has over other methods of detecting DNA-protein interactions. First of all, DNA cleavage at a single site on many kilobases of DNA yields a positive autoradiographic signal, easy to detect in an electrophoresis experiment. The opposite method,

footprinting, is instead based upon an inhibitory response and is therefore hard to detect on large pieces of DNA unless one knows roughly where to look for the region protected by protein. Although it is very useful in other respects, footprinting is not suitable for detection of single protein binding sites within an entire genome.

The first examples of tethering redox-active metal complexes to DNA binding proteins involved the attachment of $[\text{Cu}(\text{phen})_2]^+$ to the tryptophan gene (*trp*) repressor (72) and $[\text{Fe}(\text{EDTA})]^{2-}$ to *Hin* Recombinase (73). Each of these semisynthetic nucleases was able to recognize and cleave DNA at the specific target sequences of the binding moiety. This work represented a big step in engineering new proteins for analysis of gene structure and function.

For effective protein engineering, however, it is desirable for the entire artificial nuclease to be composed of amino acids. In the previous example either the protein was nonspecifically tagged with metal at several lysine positions or elaborate synthetic methods were employed for attachment of an unnatural chelating group (phenanthroline or EDTA) to the terminus of the protein. These approaches are not amenable to large-scale synthesis of artificial nucleases through overexpression of the proteins using molecular biological techniques. More appealing would be the incorporation of a natural metal chelating polypeptide into a DNA binding protein. The natural tripeptide glycine-glycine-histidine from albumin is known to bind metals tightly, and it was chosen for synthetic attachment to the amino terminus of *Hin* Recombinase, as illustrated in Fig. 11 (74). Once combined with Cu(II) and other metal ions, the tripeptide can form a square planar complex that extends from the DNA binding domain of the protein. Like the tethered $[\text{Fe}(\text{EDTA})]^{2-}$, this nuclease cleaves DNA specifically at the end of the *Hin* binding site, and since Cu(II) complexes generate a less diffusible species than $\text{Fe}(\text{EDTA})^{2-}$, the observed cleavage pattern is found to be sharper and less diffuse.

It is intriguing that the inspiration for a new type of metal complex for highly selective DNA cleavage came from nature itself. An understanding of metal binding to proteins such as albumin has led to versatile new ligands for the inorganic chemist. Functional metal complexes of polypeptides are an exciting new area of research, especially in the generation of site-selective probes for DNA structure. Proteins containing peptide chelating groups can be produced in large amounts from bacteria, obviating the need for extensive synthetic preparations. By combining the techniques of molecular biology and inorganic chemistry, it may be possible to generate an unlimited set of functionalized proteins that can carry out operations on other proteins and on DNA.

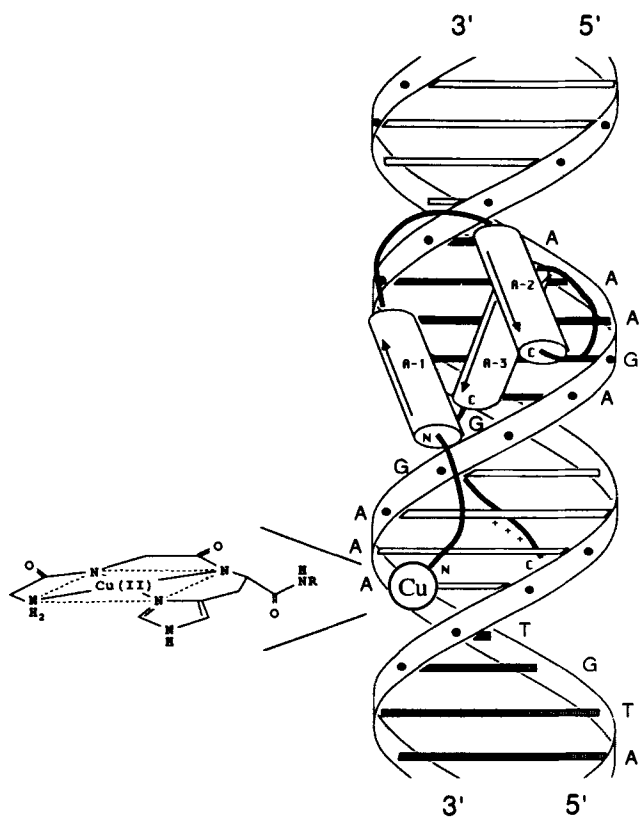


Figure 11. A schematic illustration of a synthetic DNA-cleaving peptide bound to DNA that was constructed by synthesis of the DNA binding domain of *Hin* Recombinase with gly-gly-his at the N-terminus to coordinate copper (74).

IV. NUCLEIC ACID PROBES THAT COMBINE STRUCTURAL RECOGNITION AND REDOX CHEMISTRY

As described above, simple redox-active metal complexes can promote DNA strand scission through a variety of routes, and such reagents may be tethered onto DNA binding moieties, for example, proteins or oligonucleotides, so as to convert them into DNA-cleaving molecules. In this fashion the metal functionality is exploited to explore the recognition characteristics of the DNA binding agent. Also, as described above, a transition metal complex of defined structure and symmetry may be designed that possesses its own intrinsic recognition characteristics. DNA cleavage ac-

tivity with such complexes may be achieved by substitution of a redox-active metal directly into its structural framework, forming the isomorphous, reactive coordination complex. Using this strategy, transition metal complexes that bind selectively to DNA sites may therefore be converted into site-selective DNA cleaving molecules.

In this section we will describe some examples and applications of this idea. Table II summarizes the various binding and cleavage characteristics of molecules described either in this or in earlier sections. Molecules may be constructed that are matched in terms both of their shape and symmetry to conformations of DNA. The DNA cleaving analogues of these complexes serve as conformationally selective cleaving agents. Such complexes, therefore, become useful probes with which to explore variations in conformation along the helical strands. Furthermore, DNA recognition and reaction based upon such structural matching, or *shape selection*, leads to a remarkably high level of site specificity.

A. Shape-Selective Probe for the A Conformation

[Ru(TMP)₃]²⁺. A distinctive characteristic of the A conformation is its shallow and wide minor-groove surface. Tris(phenanthroline)metal complexes bind to DNA both through intercalation in the major groove and through a surface-bound interaction in the minor groove (18–20) (see above). It is this surface-bound interaction that has been exploited in the construction of a complex, a derivative of tris(phenanthroline)ruthenium(II) that selectively targets A-form helical structures (30, 75).

The notion behind the design of the A-form probe, tris(3, 4, 7, 8-tetramethylphenanthroline)ruthenium(II), [Ru(TMP)₃]²⁺, is illustrated in Fig. 12. (see also color plate) The surface bound interaction is apparently stabilized by hydrophobic as well as electrostatic interactions. The addition of methyl groups about the periphery of the molecule ought, therefore, only to enhance the association of the phenanthroline complex with nucleic acid through the surface-bound mode. Furthermore, addition of the bulky methyl substituents eliminates any intercalative stacking by the complex. Despite, then, the clear favoring of binding to a polynucleotide via a surface-bound association, binding to the B form is limited. The complex is simply too large to associate closely with the minor groove of a B-form helix. The complex is nonetheless able to bind easily against the shallow surface of the A-form helix. The [Ru(TMP)₃]²⁺ complex is therefore poorly matched in terms of its shape with the shape of a B-form polymer but well matched with that shape which is characteristic of an A-form helix.

As shown in Fig. 13, experiments conducted with both A- and B-form synthetic polynucleotides support the model. The [Ru(TMP)₃]²⁺ complex

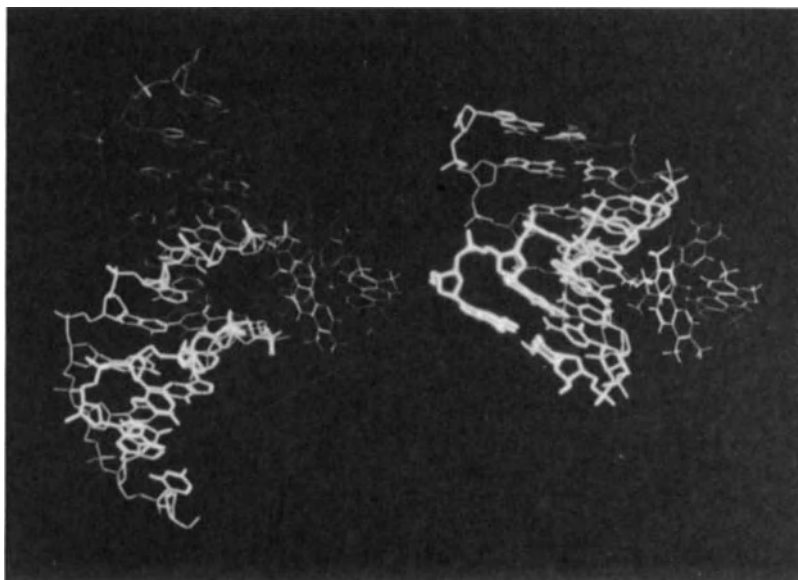


Figure 12. An illustration of the notion behind the design of $[\text{Ru}(\text{TMP})_3]^{2+}$, a probe for the A conformation, based upon shape selection. As is evident, the shape of the complex is well matched to bind against the shallow minor groove surface of the A conformation (right) but is simply too large to fit snugly into the minor groove of B-DNA (left).

binds avidly and cooperatively to poly(rC)·poly(dG), an A-like helix, under conditions where little binding to poly(dGC), an ostensibly B-form polymer, is detected (30a). Also consistent with the surface-bound model, preferential binding of the Λ isomer to the right-handed helix is observed. Furthermore, upon photoactivation, the complex preferentially cleaves A-form helices. As for $[\text{Ru}(\text{phen})_3]^{2+}$, excitation of the metal-to-ligand charge-transfer state of $[\text{Ru}(\text{TMP})_3]^{2+}$ sensitizes the formation of singlet oxygen and this reactive species may be exploited to mediate DNA damage. Figure 13 shows cleavage experiments with A- and B-form synthetic polynucleotides (75). Again, cleavage is apparent with the A-form polymer while little cleavage is found with the B-form helix, despite the fact that the same sensitization of singlet oxygen must occur in both solutions upon irradiation. Just as the complex binds preferentially to the A form, the complex also preferentially promotes cleavage of the A form. In addition, a higher extent of cleavage is obtained with the Λ isomer, which binds preferentially. The characteristic recognition features are therefore preserved in these cleavage reactions.

The rigid ruthenium complex can also be employed to probe sequences

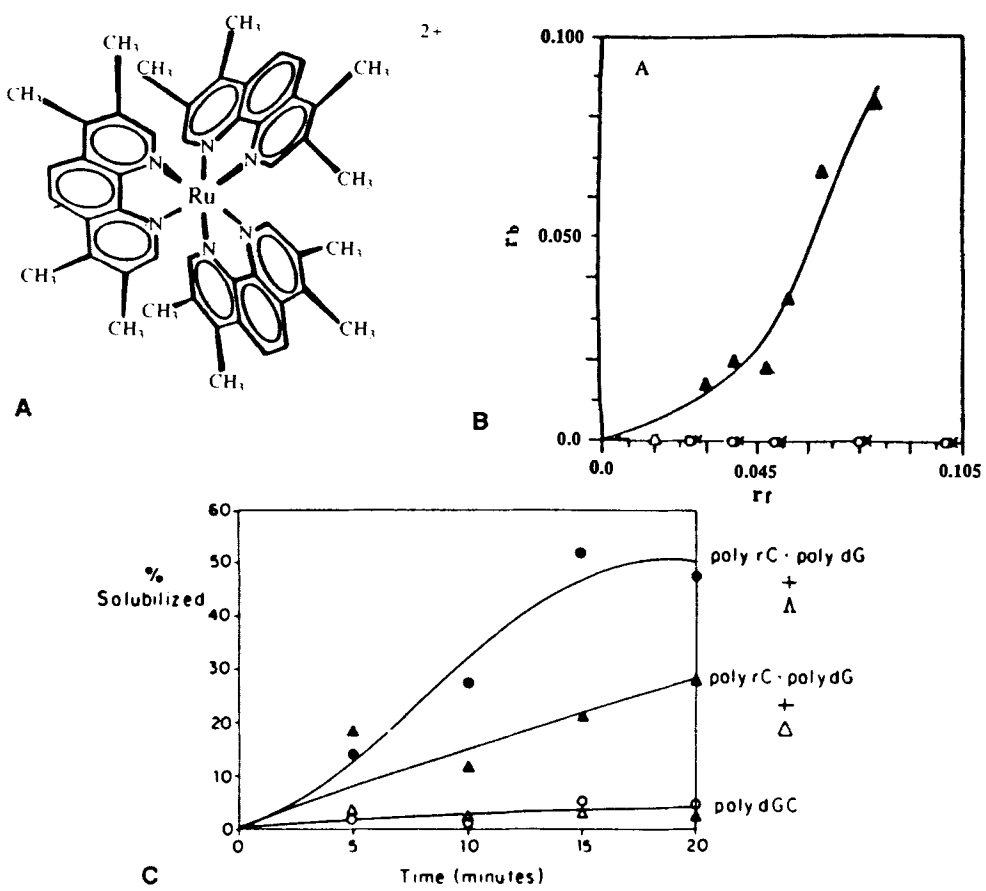


Figure 13. Shape-selective binding and cleavage by the A-form probe, $[\text{Ru}(\text{TMP})_3]^{2+}$ (30a, 75). (A) Tris(tetramethylphenanthroline)ruthenium(II), $[\text{Ru}(\text{TMP})_3]^{2+}$. (B) Preferential binding to A-form polymers. The plot of the ratio of bound metal-nucleotide (r_b) vs. formal added metal-nucleotide (r_f) shows the avid and cooperative binding of $[\text{Ru}(\text{TMP})_3]^{2+}$ to A-form poly(rG)·poly(rC) (\blacktriangle) with no detectable binding to B- (o) or Z- (x) form poly[d(G-C)]. (C) Photocleavage of A-form (closed symbols) poly(rC)·poly(d ^3H)-G) and B-form (open symbols) poly[d ^3H]-GC) with A-(O) and Δ -(Δ) $[\text{Ru}(\text{TMP})_3]^{2+}$. Cleavage was monitored by the retention on filters of acid-precipitable radioactivity and is plotted as the percentage counts solubilized as a function of irradiation time. With photoactivation, enantioselective cleavage of the A-form helix is apparent, while little cleavage is detected on the B-form polymer.

along a DNA helix which locally are A-like in structure, or in other words, which are characterized by containing a shallow, accessible minor-groove surface. Photoactivated cleavage by $[\text{Ru}(\text{TMP})_3]^{2+}$ on ^{32}P end-labeled polynucleotides revealed selective cleavage at homopyrimidine–homopurine stretches such as 5'-CCCTTTCGTCTTC-3' and 5'-TATTTTATCC-3' (30a). Whether these sequences in particular are strictly A-like or not in solution is unknown, but it is interesting that a variety of studies showed that homopyrimidine–homopurine regions may adopt unusual conformations, many of which are A-like in character. The site-selective probe for this structural feature may therefore be extremely valuable in connecting one-dimensional DNA sequence information with three-dimensional structural information to characterize locally the sequence-dependent variations in structure on the polymer.

B. A Photocleaving Probe for Z-Form DNA

$[\text{Co}(\text{DIP})_3]^{3+}$. The success of $[\Lambda\text{-Ru}(\text{DIP})_3]^{2+}$ as a spectroscopic probe for Z-DNA prompted the design of an analogous complex that could target Z-DNA in a similar fashion but which would report upon such targeting through specific redox-activated strand cleavage. By application of a spectroscopic probe, such as the ruthenium complex, one may determine the quantity of Z- (actually non-B-form) DNA in a sample, but the introduction of the redox cleaving functionality permits the identification of where Z-form regions may be embedded in a long helical, ostensibly B-form polymer. Shape- and symmetry-selective recognition here may be converted into shape- or symmetry-selective reaction to determine conformationally distinct sites along the strand.

A logical strategy to accomplish such conformationally selective cleavage takes advantage of the quite common approach of inorganic chemists, the application of simple metal substitution. DNA cleavage activity may be incorporated into the recognition functionality by utilizing the same molecular shape and symmetry as $[\Lambda\text{-Ru}(\text{DIP})_3]^{2+}$, the spectroscopic Z-form probe, but changing the central metal ion to one that is redox active. Diimine complexes of cobaltic ion are known to undergo photoreduction reactions (76). Such photoreduction might therefore be coupled to Z-form site recognition to effect oxidative cleavage at the bound Z-form site. The $[\Lambda\text{-Co}(\text{DIP})_3]^{3+}$ complex, shown in Fig. 14, was therefore synthesized as a conformationally selective photocleavage agent (27, 77).

Whether such substitution would be effective on Z-DNA sites was determined in comparative photocleavage experiments on plasmid DNAs containing or lacking Z-form insert sequences (77). Plasmid DNAs containing small regions in the Z form had earlier been constructed by insertion

of the DIP complexes for non-B rather than B-form sites based upon shape as well as symmetry. Subsequent studies have indicated that the various sites targeted represent several different conformations. Perhaps most intriguing were the locations of these various conformationally distinct sites on pBR322. The alternate conformations appear to border coding regions on the plasmid, representing in some respects conformational punctuation marks along the helix. The intriguing correspondence of conformationally distinct sites targeted by the metal complexes to “biologically interesting” places has been seen in other contexts as well (see below). Site-specific cleavage by $[\text{Co}(\text{DIP})_3]^{3+}$ therefore represented not only a demonstration of how both elements of recognition and reaction might be combined into one species to effect site-specific reactions but how such probes might be applied to begin to explore DNA polymorphism along the strand and its relationship to biological function.

C. Probing Variations within the B Conformation

Thus far we described the application of shape selection to target distinctive non-B conformations of DNA. Can shape selection also be applied in probing more subtle variations in structure within even an ostensibly B-form family? B-DNA, as we define it, really represents only the average of a family of structures. X-ray crystallography of oligonucleotides and more recently high-resolution NMR experiments showed that B-DNA displays a range of sequence-dependent local polymorphism (79). Different stacked base pairs are twisted and tilted one with respect to another and even within a single base pair, the bases may be propeller twisted one to another to a substantial extent (80). Experiments conducted with $[\text{Fe}(\text{EDTA})]^{2-}$, described earlier (Section III.D), illustrated how hydroxyl radical reactivity might be used to probe the differential accessibility of sugar protons along an ostensibly B-form polymer. Shape-selective targeting is useful here as well, since the matching of the structure of the transition metal complex to even a right-handed B-form DNA site can be used to sense not only gross but also more subtle variations in structure along the helix.

$[\text{Rh}(\text{phen})_2\text{phi}]^{3+}$. Perhaps the best illustration of shape-selective recognition within B-form polymers is provided by the sequence-selective cleavage by $[\text{Rh}(\text{phen})_2\text{phi}]^{3+}$. Complexes containing the phenanthrene-quinone diimine (phi) ligand bind avidly to DNA by intercalation and, for the rhodium(III) derivatives, cleave DNA efficiently upon photoactivation. By mapping sites recognized and cleaved by the complex, it was found that $[\text{Rh}(\text{phen})_2\text{phi}]^{3+}$ appears to recognize subtle openings in the major

groove of the helix (48). Until this complex was synthesized, there were no known natural or artificial probes of major-groove geometry.

$[\text{Rh}(\text{phen})_2\text{phi}]^{3+}$, shown in Fig. 15, contains an expansive intercalating ligand (the phi), which overlaps strongly with aromatic portions of the DNA base pairs. The phi ligand is well matched with the base pairs for intercalative stacking and, as with other metallointercalating agents, binding appears to occur from the major groove of the helix. Earlier studies with mixed-ligand complexes of ruthenium(II) containing the phi ligand indicated an avid intercalative association (57). Besides the intimate stacking of the phi ligand, for $[\text{Rh}(\text{phen})_2\text{phi}]^{3+}$, however, the ancillary phenanthroline ligands serve to provide steric bulk above and below the plane of the phi ligands close to the intercalating moiety (the intercalating side of the axial coordination plane). Thus, as illustrated schematically in Fig. 15, the stacking of the phi ligand intimately between the base pairs is only facile at those sites that are open in the major groove so as to accommodate similarly the bulk of the ancillary phenanthroline ligands.

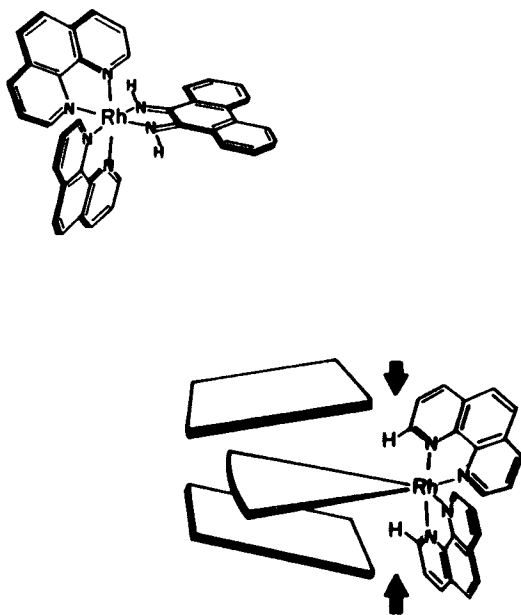


Figure 15. The complex $[\text{Rh}(\text{phen})_2(\text{phi})]^{3+}$ and illustration of its recognition characteristics (48). The steric interactions with the ancillary phenanthroline ligands (indicated by the arrows) permit an intimate intercalation of the phi ligand only at sites where the major groove is open.

The basis for this model came from the finding that cleavage by $[\text{Rh}(\text{phen})_2\text{phi}]^{3+}$ occurs at the sequence 5'-CCAG-3' (48). Information from crystal structures of 5'-pyrimidine-pyrimidine-purine-3' steps and rules for predicting the sequence-dependent microconformational geometry of B-form grooves suggest that this sequence should possess an unusually wide and open major groove (81). This type of sequence appears to be more unwound (more ladderlike due to a small twist angle) and the bases have slid sideways to alleviate the steric clash between propeller-twisted purines in the minor groove of DNA. In essence, there is more room for the non-planar intercalator to bind from the major groove at this sequence-encoded step.

If intercalation by the phi ligand occurs more easily at sites that are open in the major groove, those DNA sites having the propensity to bend toward the minor groove should also be recognition sites for the complex. Studies of oligonucleotide sequences containing oligo dT stretches have shown that these sequences appear to be bent away from the major groove and NMR NOE studies indicate a progressive narrowing of the minor groove at oligo dT stretches (6, 62). In order for the minor groove to narrow, the major groove must widen, and a bend would naturally occur at the center of the poly(dT) stretch. Strong cleavage by $[\text{Rh}(\text{phen})_2\text{phi}]^{3+}$ at the center of oligo dT sequences is observed and provides evidence in support of the recognition model and also in support of a locally bent structure at oligo dT sites along the strand. Also of interest are comparative experiments being conducted with enantiomerically pure complexes of $[\text{Rh}(\text{phen})_2\text{phi}]^{3+}$. Differences in cleavage between enantiomers are observed at the 5'-CCAG-3' sites but not at the bent sites, and these differences indicate the differential propeller twisting associated with these different sequences (82). The rhodium complex, through shape and symmetry selection, is therefore likely to be applicable in probing subtle sequence-dependent features of propeller twisting and unwinding on long helical polymers.

D. Probing Biologically Interesting Sites

Probes have now been described that are tailored in their shapes to corresponding sequence-dependent shapes along the DNA helix. These probes can therefore be used to examine the topology of the DNA helix, or, in other words, the local variations in structure that occur along the strand as a function of sequence and as a function of biological location. After all, the DNA sequence encodes both the amino acids needed for the construction of protein and also the recognition sites for the binding of

regulatory proteins that determine which genes are next to be transcribed or repressed. By probing variations in DNA topology along sequences for which some biological information exists, some clues about the relationship of DNA structural polymorphism to biological expression can be obtained by using these metal complexes. X-ray crystallography and NMR spectroscopy, the most powerful techniques available for obtaining structural information, cannot be applied in this context because the regions of interest on the polymer are either too large or embedded in sequences that are too large. In addition, NMR and x-ray crystallographic studies often require the examination of DNA under nonphysiological conditions. A new technique is therefore emerging that uses shape-selective chemical probes to explore local structure on long pieces of DNA and correlate them with function. Perhaps still of more interest, shape-selective mapping experiments are already providing exciting hints that local structural variations may be important elements in protein–DNA recognition.

One example of this notion is apparent quite graphically in Fig. 14, which shows the low-resolution map of cleavage sites for $[\text{Co}(\text{DIP})_3]^{3+}$ on the SV40 genome (83). The 5 kilobase pairs of circular DNA of this simian virus contain several overlapping genes (demarcated by the arrows in the figure) and an extensive regulatory region, which binds a variety of different transcription factors. Specific cleavage by the cobalt complex (Section IV.B) delineates sites of altered non-B conformations. Remarkably, sites of cleavage by $[\text{Co}(\text{DIP})_3]^{3+}$ correspond to the borders of gene segments. Indeed one site marks an intron border, a structural demarcation perhaps more applicable on the RNA level. Extensive cleavage is also evident in the regulatory region. This intriguing map, obtained with a simple coordination complex, and the fascinating correlation between structurally distinct sites and sites of biological function underscores the importance of shape selection to protein–DNA recognition as well as to the simple recognition of DNA sites by metal complexes.

Structurally distinct conformations are evident as well when specific protein binding sites are examined. The binding sites for two zinc finger eukaryotic transcription factors was mapped using the metal complex probes and these show interesting variations in topology that may reflect structural features necessary for protein recognition (84). At the borders of the putative zinc finger binding sites, for example, specific cleavage by $[\text{Ru}(\text{TMP})_3]^{2+}$, the complex that senses a shallow minor groove, is observed; at the center of the finger sites, it appears that the major groove is more open, based upon the specific cleavage in these regions by $[\text{Rh}(\text{phen})_2\text{phi}]^{3+}$. It appears, then, that just as the coordination complexes can target DNA sites based upon a complementarity in shape (as defined

by the coordination complex) that also DNA-binding proteins, in particular those that themselves contain a coordinatively saturated metal ion, may also recognize their binding sites based at least in part upon shape selection.

V. PROBING MORE COMPLEX STRUCTURES AND MORE COMPLEX PROBES

Here we examine systems that appear to involve still greater complexity than found in the interactions of small metal complexes with double-stranded DNA. RNA and even DNA can adopt a rich variety of shapes, varying not only in primary and secondary structure but indeed in tertiary structure, in how the polymer is folded. Such distinctive if complicated forms are perhaps more difficult to probe and define because of their complexity, but metal complexes are now being applied here as well in dissecting the latticework folding patterns of nucleic acids. In addition, metal complexes themselves are being constructed with still greater complexity so that they may efficiently perform functions of recognition and reactivity that may approach those of DNA binding enzymes. The complexity in metal complex design may offer new tools for molecular biology which mimic those designed by nature.

A. Metal Complexes as Probes of DNA Tertiary Structures

We are accustomed to thinking about DNA as a one-dimensional polymer. Like the strands of amino acids that fold into proteins, however, DNA strands form "tertiary structures." Nucleic acid strands are capable of forming folded or alternately paired structures that differ greatly from the one-dimensional polymer we think of as DNA. Many of these structures may be transiently involved in gene expression and protein binding. The Holliday junction, for example, is a structural element in genetic recombination (85). Below we examine two related DNA tertiary structures, the Holliday junction and the DNA cruciform, and how metal complexes may be applied in targeting and sorting out their intricate structural distortions.

$[\text{Fe}(\text{EDTA})]^{2-}$. During genetic recombination, two DNA double helices fuse together into a structure known as a Holliday junction. While one can draw in two dimensions how such a recombination event might take place, we have little structural insight into the three-dimensional structure for this recombination intermediate. Cleavage experiments conducted with $[\text{Fe}(\text{EDTA})]^{2-}$ have been helpful in this regard and in particular in distinguishing between several models for the Holliday junction (86). These

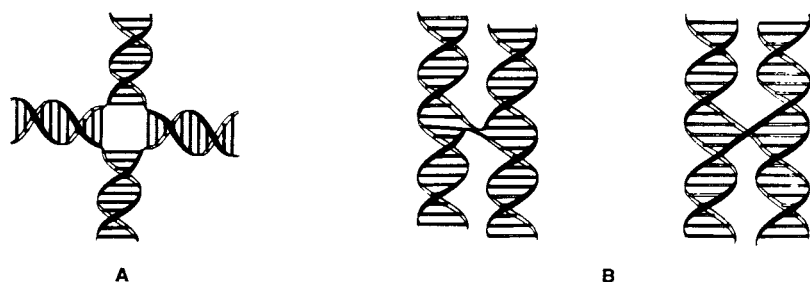


Figure 16. Models for the Holliday junction showing in (A) a fourfold symmetric model and in (B) two possible twofold symmetric models (86).

possibilities are schematically illustrated in Fig. 16. When formulating models for the structure of the junction, one would imagine that the helical arms could arrange themselves in a cross or remain stacked with a perturbed bridge between the strands. In order to discriminate between these two possibilities, a four-armed oligonucleotide model of the Holliday recombination site was synthesized and treated with $[\text{Fe}(\text{EDTA})]^{2-}$ under reducing conditions. If the cross-model were operative, one would expect very little protection from $\text{OH}\cdot$. The stacked model, in contrast, requires that the two bridged strands lie very close to one another and the sugar-phosphate backbone of the helices which face one another would be protected from cleavage by $\text{OH}\cdot$, yielding a periodic cleavage pattern with gaps at protected regions. In the junction DNA would, much like a bound protein, cause a footprint in $[\text{Fe}(\text{EDTA})]^{2-}$ cleavage. Upon treatment of the Holliday junctions with $[\text{Fe}(\text{EDTA})]^{2-}$, a periodic cleavage pattern indicative of interstrand protection is indeed observed, consistent with a twofold rather than fourfold symmetry at the Holliday recombination site. As this experiment illustrates, hydroxyl radical cleavage experiments obtained with $[\text{Fe}(\text{EDTA})]^{2-}$ can therefore be utilized in probing not only how proteins interact with DNA, but how the helical nucleic acid structures themselves interact and fold into another.

$[\text{Rh}(\text{DIP})_3]^{3+}$. A nucleic acid structure which is likely to resemble that of the Holliday junction but is formed within a single double helical region of DNA is the DNA cruciform (5). Cruciforms occur in supercoiled DNA as a result of an extrusion of an inverted repeat sequence into two intra-strand hydrogen-bonded segments so as to relieve the torsional strain associated with the supercoiling. A two-dimensional representation of this cross-like structure is shown in Fig. 17. Although chemical probes such as OsO_4 have shown that the cruciform loops are single stranded and that the

stems are double stranded, a definitive model for the three-dimensional disposition of the cruciform has not yet been established. It could be as flat and opened as shown in Fig. 17; it could be folded up like tRNA; or it could have one helical arm folded over another as in the models for the Holliday junction. Clearly, a DNA cruciform is grossly distinctive in structure and therefore a clear target for shape-selective recognition.

Racemic $[\text{Rh}(\text{DIP})_3]^{3+}$, an analogue of the Z-form probe discussed above (Section IV.B), which cleaves Z-DNA as well as other altered structures with high efficiency upon photoactivation (87), was shown to target DNA cruciforms through double-stranded cleavage (88). Cruciforms that differ in their sequence but share the topology of a cruciform all appear to be targets for double-stranded cleavage by the metal complex. High-resolution experiments reveal a remarkably specific cleavage by the rhodium complex. As shown in Fig. 17, intense cleavage is found at a single interbase-pair site directly adjacent to the cruciform stem. Again consistent with a targeting based upon shape rather than sequence, if the same DNA plasmid is first linearized with a restriction enzyme before treatment with the metal complex so as to relieve the supercoil stress in the plasmid and therefore relax the cruciform, no specific cleavage is observed. If the sequence is not extruded into a cruciform structure, no site-specific recognition is achieved. The high specificity associated with reaction of this simple coordination complex at cruciform sites is possibly our most graphic example of the specificity to be derived from shape-selective targeting.

The cleavage pattern obtained with $[\text{Rh}(\text{DIP})_3]^{3+}$ has much to tell us also about the cruciform structure itself. Enantiomers of $[\text{Rh}(\text{DIP})_3]^{3+}$ both cleave adjacent to cruciforms, suggesting that the site they are recognizing is low in symmetry and not a good template for chiral recognition. It is important to note that the targeting occurs asymmetrically to only one side, the AT-rich side, of a cruciform, and not on the stem or loop of the structure. This asymmetry indicates that the structure of the complexed cruciform in solution is not, in fact, symmetrical. It also indicates that although $[\text{Rh}(\text{DIP})_3]^{3+}$ cleavage occurs in an AT-rich region, which is adjacent to the cruciform, similar AT sequences elsewhere on the plasmid remain uncut; AT-rich sequences are known to be more easily melted and deformed than bulk DNA. It is therefore likely that the flexible AT-rich sequences are important elements in stabilizing the complex into a folded, possibly hydrophobic pocket between neighboring strands. The structure of the cruciform may resemble the models shown above for the Holliday junction with the metal complex wedged electrostatically and hydrophobically between adjacent arms of the complex structure. Cleavage experiments conducted with arms of different lengths and sequence may provide

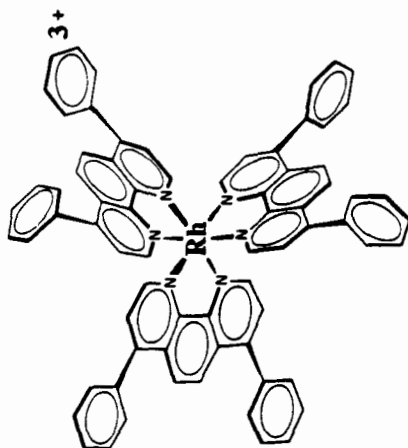
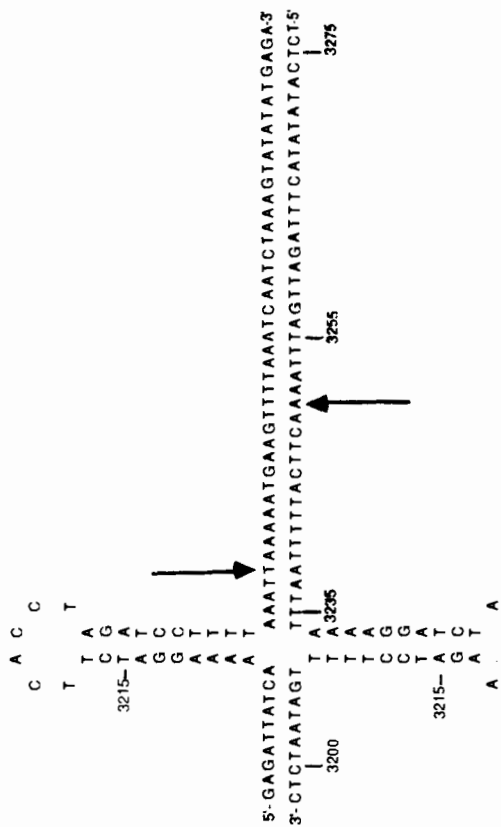


Figure 17. Probing DNA cruciforms (88). Shown on the left is tris(diphenylphenanthroline)-rhodium(III), $[\text{Rh}(\text{DIP})_3]^{3+}$, which cleaves DNA cruciforms in a double-stranded fashion with photoactivation. On the right are shown the major cleavage sites for $[\text{Rh}(\text{DIP})_3]^{3+}$ (delineated by the arrows) on a pBR322 cruciform.

still more information regarding the distinctive bundled shape associated with this tertiary structure.

B. Probing RNA Structure

The highest degree of nucleic acid structural diversity is found in RNA. Functional pieces of RNA contain single- and double-stranded regions, connected by knots and loops of byzantine complexity. Alternative forms of hydrogen bonding and interstrand association are often observed. Indeed, some pieces of RNA seem to have folded, almost like a protein, into compact structures. The many biological functions of RNA, including storage of genetic information, its transfer into protein, and even catalysis of biochemical reactions depend sensitively on the distinctive shapes that the RNA molecule is able to assume. Given the diversity of structural elements available for recognition, metal complexes are particularly promising reagents for the study of RNA.

A variety of metal complexes have been used to probe RNA and it has already become clear that these metal complexes each appear to recognize unique elements of the RNA structure. One class of reagents can differentiate between single- and double-stranded regions of an RNA molecule. Others can detect protected or infolded regions of RNA, while still another class is able to detect sites of strictly tertiary interactions. The sites of tRNA cleavage by different metal complexes are shown in Fig. 18. Understandably, in most cases studied thus far, work has focused on tRNA, since it is the only structurally well-characterized RNA polymer to date (89). As is perhaps best illustrated in Fig. 18 by the diversity of cleavage sites found on tRNA, transition metal complexes are a distinctively useful family of compounds which, used in concert, may aid in the construction of a detailed picture of RNA topology.

MPE-Fe(II) and [Cu(phen)₂]⁺. Almost all positions of tRNA^{Phe} are cleaved by MPE-Fe(II) (90, 91); however, this probe seems to have particularly high affinity for certain double-stranded or helically stacked regions of the tRNA molecule. Larger RNA molecules such as a 16S ribosomal RNA from *E. Coli* and the catalytically active intervening sequence (IVS) from *Tetrahymena* have been probed more successfully with MPE-Fe(II), yielding distinctive regions of cleavage (90, 91). These regions correspond to RNA sequences involved in base pairing with other sequences and are in some sense helical, rather than single stranded. Perhaps as a result of intercalation, MPE-Fe(II) is able to recognize certain double-stranded regions within a large RNA structure. Conversely, [Cu(phen)₂]⁺ has been observed to cleave tRNA^{Phe} at single-stranded regions and loops

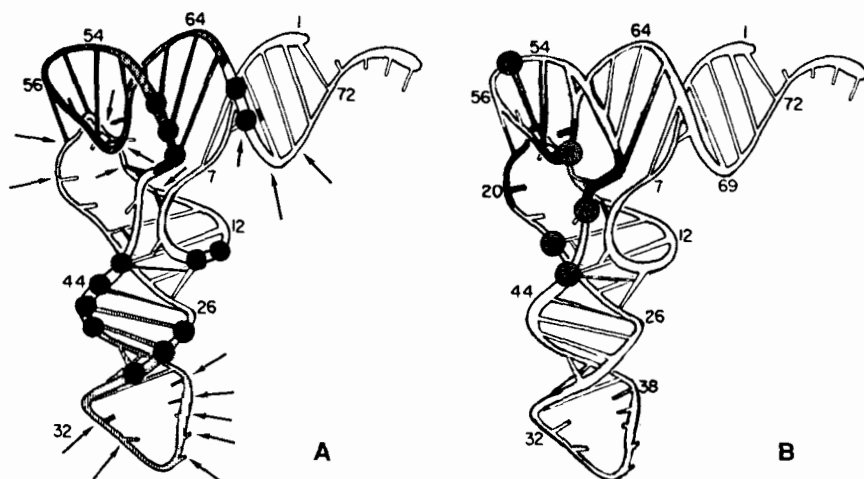


Figure 18. The diversity of cleavage sites for metal complexes on tRNA^{Phe}. (a) Cleavage by probes that primarily detect features of RNA secondary structure: [Cu(phen)₂]⁺ (arrows) (92) and MPE-Fe(II) (black dots) (90). (b) Probes that detect protected or complex structures on tRNA: Sites of OH[•] protection after treatment with [Fe(EDTA)]²⁻ (93) are shown as shaded portions of the molecule and specific cleavage by [Rh(phen)₂(phi)]³⁺ (95) is indicated by the circles.

(92). As shown in Fig. 18, this probe predominantly recognizes RNA which is not involved in base pairing.

[Fe(EDTA)]²⁻. Hydroxyl radical cleavage reactions with [Fe(EDTA)]²⁻ reveal an interesting shadowing of protected RNA structures. [Fe(EDTA)]²⁻ has been successfully used to determine which regions of an RNA molecule are less solvent accessible than others (93). Native RNA contains regions that are in-folded, and less susceptible to cleavage by [Fe(EDTA)]²⁻. It is apparent from experiments on tRNA^{Phe}, that very little of this particular RNA molecule is folded up, as a mere 7% of the residues are protected from cleavage. Conversely, when the catalytic intervening sequence from *Tetrahymena* rRNA is subjected to [Fe(EDTA)]²⁻ treatment, 40% of the RNA molecule is protected and remains uncleaved. This comparison suggests that catalytic rRNAs, in contrast to tRNAs, may have a more "folded" structure with a solvent accessible exterior and a protected interior. In fact, the sequences that were found to lie in the protected pocket are the same regions that are believed to compose the catalytic core of the *Tetrahymena* ribozyme. [Fe(EDTA)]²⁻ may therefore be considered a valuable tool for defining the interior and exterior of RNA molecules.

Uranyl Acetate. The complex $\text{UO}_2(\text{OAc})_2$ cleaves HIV mRNA upon photoactivation in a uniform fashion unless the nucleic acid is associated with protein (94). Recently, it has been shown that intense, specific cleavage occurs on RNA which is bound to HeLa cell nuclear protein. Rather an imprint than a footprint, this strong cleavage indicates that the structure of the RNA and its accessibility to metal complexes in solution is changed in the presence of protein.

$[\text{Rh}(\text{phen})_2\text{phi}]^{3+}$. Earlier (Section IV.C) $[\text{Rh}(\text{phen})_2\text{phi}]^{3+}$ was described as a probe for open, accessible sequences within the major groove of DNA. Interestingly, this probe appears to recognize similar regions on tRNA, leading to a potentially powerful probe for RNA tertiary structure. As on DNA, $[\text{Rh}(\text{phen})_2\text{phi}]^{3+}$ cleaves with high specificity on tRNA at sites where the major groove of RNA is distorted and more open than in an A-like conformation characteristic of an RNA duplex (95). Photolysis of $[\text{Rh}(\text{phen})_2\text{phi}]^{3+}$ bound to tRNA^{Phe} results in five major sites of cleavage: G45, U47, G22, yU55, and U59. All of these sites are located in the core region of the L-shaped molecule where the various loops of RNA fold in together. Inspection of where the rhodium cleavage sites occur on the folded tRNA graphically specifies the orientations of the rigid complex bound to the polymer. The complex appears to target the only available regions on the molecule through which access from the major groove is permissible. Three of the $[\text{Rh}(\text{phen})_2\text{phi}]^{3+}$ cleavage sites (G45, U47, and G22) correspond to sites of triple base interactions. Triple interactions are places where three nucleotides are joined together in a plane through a network of hydrogen bonds, and of interest with regard to the recognition characteristics of the rhodium complex, the addition of a third base into the network appears to increase the accessibility of the major groove. The only triple interactions not cleaved by the rhodium complex are those that have poor solvent accessibility. It therefore appears that the characteristic recognition features of $[\text{Rh}(\text{phen})_2\text{phi}]^{3+}$, based upon shape selection, are preserved in targeting RNA as well as DNA. Certainly the high specificity of cleavage and the interesting areas cleaved makes the rhodium complex of utility in probing mutant tRNAs to see if the parent tRNA structure is preserved. Moreover, if the complex is indeed a general probe for tertiary interactions in RNAs, then it will be extremely useful in characterizing the folding of larger, more complex RNAs with ill-defined structures.

C. Hydrolytic Cleavage of Nucleic Acids

All metal complexes that cleave polynucleotides discussed thus far in this chapter utilize redox chemistry to attack the nucleic acid strand. These

cleavage mechanisms are distinctly different from cleavage reactions performed by nucleolytic enzymes in the cell. Restriction endonucleases, for example, are enzymes that bind to specific DNA sequences and cleave each of the two strands hydrolytically to produce 5'-phosphate and 3'-hydroxyl termini (96). These enzymes, used in concert with DNA ligases, which join together such termini and form a new phosphodiester linkage, have served as the base for recombinant DNA technology, since such molecular tools have permitted the cutting and splicing of DNAs apart and back together. The metal-containing synthetic cleaving agents we have described, although extremely useful in probing nucleic acid structure and protein–nucleic acid interactions, cannot be applied directly as “synthetic restriction enzymes” and therefore as new synthetic tools for recombinant DNA technology, since the redox cleavage chemistry yields termini that cannot be religated. Redox-mediated cleavage is exquisitely sensitive in determining where a molecule is bound along the strand. But the redox reaction is strikingly unsubtle in marking its target site, irreversibly damaging either the sugar or base moiety. Hydrolytic cleavage mechanisms instead involve nucleophilic attack on the phosphodiester and preserve both sugar and base functionalities. Intensive work is underway to develop synthetic metal complexes that cleave DNA by a mechanism involving hydrolysis of the phosphodiester backbone. These metal complexes, as true artificial nucleases, would be extremely important tools for molecular biology.

Toward this end, tris(diphenylphenanthroline)ruthenium(II) has been functionalized with arms that are able to chelate additional non-redox-active metal ions to promote hydrolysis of proximal phosphates (97, 98). $[\text{Ru}(\text{DIP})_2(\text{Macro})]^{2+}$, as this molecule is called, is shown in Fig. 19. The complex has been constructed to contain a recognition domain, $[\text{Ru}(\text{DIP})_3]^{2+}$, in its core, as well as two metal-binding cleaving arms, formed by condensation of tren through sulfonamide linkages. The complex binds to similar regions of DNA as other tris(diphenylphenanthroline) complexes (99). In the presence of copper(II), hydrogen peroxide and a reducing agent, the complex, much like $[\text{Cu}(\text{phen})_2]^+$, efficiently cleaves DNA through a redox pathway (97). In the presence of Zn^{2+} , however, $[\text{Ru}(\text{DIP})_2\text{Macro}]^{2+}$ cleaves the DNA strands hydrolytically, producing products which to some extent may be religated enzymatically (98). These cleavage reactions are quite inefficient and much needs to be done before a practically useful artificial nuclease is available. Nonetheless, non-redox cleavage of DNA with $\text{Ru}(\text{DIP})_2\text{Macro}$ represents the first example of hydrolytic cleavage of DNA by a synthetic complex.

As can be seen in Fig. 19, $[\text{Ru}(\text{DIP})_2\text{Macro}]^{2+}$ is perhaps also an apt illustration of the complexity in design that can be accomplished with

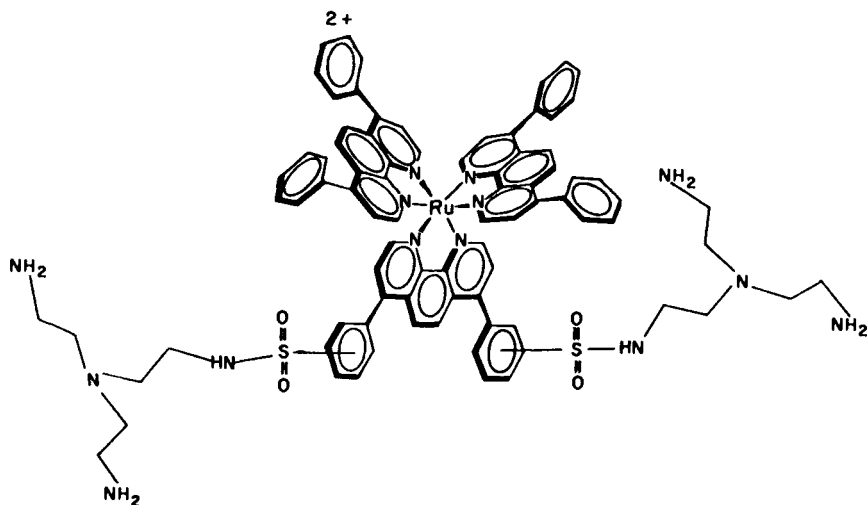


Figure 19. Ru(DIP)₂Macro (97, 98).

transition metal chemistry. The ruthenium sits at the center of the complex, defining the scaffolding of ligands about it, maintaining the center of structure and spectroscopic activity for the complex and the core for DNA recognition. Tethered onto each side are additional metal binding domains, the cleaving functionalities, derived also from metal-based chemistry, and here, upon chelation of Zn(II), chemistry that could promote hydrolytic reaction on the DNA polyanion. Using, then, the simple principles of coordination chemistry, a trinuclear metal complex may be assembled to perform a biologically important reaction. New derivatives, better designed to effect hydrolytic cleavage, are being synthesized currently, but this transition metal complex represents, nonetheless, an exciting start in the development of true synthetic restriction enzymes.

PROSPECTS FOR THE FUTURE

The applications of transition metal complexes to probe nucleic acids have grown in astounding quantity and sophistication since the first early studies of heavy metal labeling of DNA. It is clear that the tools, ranging in complexity from [Fe(EDTA)]²⁻ to [Ru(DIP)₂Macro]²⁺ and beyond, will increasingly be designed as practically useful reagents and applied in laboratories of diverse disciplines to explore biological problems. The techniques employed will not be restricted to those borrowed from biochemistry, and they already include NMR spectroscopy, photophysical methods,

and quite likely soon will include methods of surface science. As we explore the structures and biological functions of nucleic acids from an increasingly chemical point of view, the inorganic chemist will have an essential role to play in developing these tools and unraveling the clues that their applications permit. The design and application of new transition metal complexes to probe nucleic acids in as yet unimagined ways and the discovery of new structures and functions for nucleic acids using these transition metal probes provide an exciting challenge for the future.

ACKNOWLEDGMENTS

We are grateful to the National Institute of Health, the National Science Foundation, and the National Foundation for Cancer Research for their financial support. In addition we thank all our co-workers and collaborators, mentioned in the individual references, for their valuable contributions.

REFERENCES

1. M. McCall, T. Brown, and O. Kennard, *J. Mol. Biol.*, **183**, 385 (1985).
2. R. Wing, H. Drew, T. Takano, C. Broka, S. Tanaka, K. Itakura, and R. E. Dickerson, *Nature (London)*, **287**, 755 (1980).
3. A. H.-J. Wang, G. J. Quigley, F. J. Kolpak, J. L. Crawford, J. H. van Boom, G. van der Marel, and A. Rich, *Nature (London)*, **282**, 680 (1979).
4. J. S. Lee, M. L. Woodsworth, L. P. Latimer, and A. R. Morgan, *Nucl. Acids Res.*, **12**, 6603 (1984). V. I. Lyamichev, *J. Biomol. Struct. Dyn.*, **3**, 667 (1986). H. Htun and J. E. Dahlberg, *Science*, **241**, 1791 (1988).
5. M. Gellert, K. Mizuuchi, M. H. O'Dea, H. Ohmori, and J. Tomizawa, *Cold Spring Harbor Symp. Quant. Biol.*, **43**, 35 (1979). D. M. J. Lilley, *Proc. Natl. Acad. Sci. USA*, **77**, 6468 (1980).
6. E. N. Trifonov and J. L. Sussman, *Proc. Natl. Acad. Sci. USA*, **77**, 3816 (1980). J. C. Marini, S. D. Levenc, D. M. Crothers, and P. T. Englund, *Proc. Natl. Acad. Sci. USA*, **79**, 7664 (1982). H.-S. Koo, H.-M. Wu, and D. M. Crothers, *Nature (London)*, **320**, 501 (1986).
7. (a) L. G. Marzilli, *Prog. Inorg. Chem.*, **23**, 255 (1977). (b) S. J. Lippard, *Accs. Chem. Res.*, **11**, 211 (1978). (c) J. K. Barton and S. J. Lippard, *Metal Ions in Biology*, **1**, 31 (1980). (d) J. K. Barton, *Comments Inorg. Chem.*, **3**, 321 (1985).
8. S. J. Lippard, Ed., *Platinum, Gold and Other Metal Chemotherapeutic Agents*, ACS Symposium Series, 209 (1983). S. E. Sherman and S. J. Lippard, *Chem. Rev.*, **87**, 1153 (1987). J. C. Dabrowiak, *Adv. Inorg. Biochem.*, **4**, 69 (1982). J. Stubbe and J. W. Kozarich, *Chem. Rev.*, **87**, 1107 (1987).

9. (a) L. A. Basile and J. K. Barton, *Metal Ions Biol. Systems*, 25, 31 (1989).
(b) T. V. O'Halloran, *Metal Ions Biol. Systems*, 25, 105 (1989). (c) J. M. Berg, *Metal Ions Biol. Systems*, 25, 235 (1989).
10. S. E. Sherman, D. Gibson, A. H.-J. Wang, and S. J. Lippard, *J. Am. Chem. Soc.*, 110, 7368 (1988).
11. F. B. Daniel and E. J. Behrman, *J. Am. Chem. Soc.*, 97, 7352 (1975).
12. R. V. Gessner, G. J. Quigley, A. H.-J. Wang, G. A. van der Marel, J. H. van Boom, and A. Rich, *Biochemistry*, 24, 237 (1985).
13. L. S. Lerman, *J. Mol. Biol.*, 3, 18 (1961).
14. Y.-S. Wong and S. J. Lippard, *J. Chem. Soc. Chem. Commun.*, 824, (1977).
K. W. Jennette, S. J. Lippard, G. A. Vassiliades, and W. R. Bauer, *Proc. Natl. Acad. Sci. USA*, 71, 3839 (1974).
15. A. H.-J. Wang, J. Nathans, G. van der Marel, J. H. van Boom, and A. Rich, *Nature (London)*, 276, 471 (1978).
16. J. K. Barton, *Science*, 233, 727 (1986).
17. J. K. Barton, J. J. Dannenberg, and A. L. Raphael, *J. Am. Chem. Soc.*, 104, 4967 (1982). J. K. Barton, A. T. Danishefsky, and J. M. Goldberg, *J. Am. Chem. Soc.*, 106, 2172 (1984).
18. J. K. Barton, J. M. Goldberg, C. V. Kumar, and N. J. Turro, *J. Am. Chem. Soc.*, 108, 2081 (1986).
19. C. V. Kumar, J. K. Barton, and N. J. Turro, *J. Am. Chem. Soc.*, 107, 5518 (1985).
20. J. P. Rehmann and J. K. Barton, *Biochemistry*, 29, 1701 (1990); 1710 (1990).
21. M. Beer, S. Stern, D. Carmalt, and K. H. Mohlenrich, *Biochemistry*, 5, 2283 (1966).
22. M. T. Carter and A. J. Bard, *J. Am. Chem. Soc.*, 109, 7528 (1987).
23. P. B. Dervan, *Science*, 232, 464 (1986).
24. R. P. Hertzberg and P. B. Dervan, *J. Am. Chem. Soc.*, 104, 313 (1982).
25. R. P. Hertzberg and P. B. Dervan, *Biochemistry*, 23, 3934 (1984).
26. D. S. Sigman, *Acc. Chem. Res.*, 19, 180 (1986).
27. J. K. Barton and A. L. Raphael, *J. Am. Chem. Soc.*, 106, 2466 (1984).
28. M. B. Fleisher, K. C. Waterman, N. J. Turro and J. K. Barton, *Inorganic Chemistry*, 25, 3549 (1986). M. B. Fleisher, H.-Y. Mei and J. K. Barton, *Nucl. Acids Mol. Biol.*, 2, 65 (1988).
29. E. C. Long, M. J. Absalon, J. Stubbe, and J. K. Barton, submitted for publication. A. M. Pyle, "Phenanthrenequinone Diimine Complexes of Ru(II) and Rh(III)," Columbia University (1989).
30. H.-Y. Mei and J. K. Barton, *Proc. Natl. Acad. Sci. USA*, 85, 1339 (1988). H.-Y. Mei, "The Design and Applications of a Chiral Probe for A-form Nucleic Acids," Ph.D. Thesis, Columbia University (1989). J. M. Kelly, A. B. Tossi, D. J. McConnel, and C. OhUigin, *Nucleic Acids Res.*, 13, 6017 (1985).

31. D. Rhodes and A. Klug, *Cell*, **46**, 123 (1986). A. Klug and D. Rhodes, *Trends Biochem. Sci.*, **12**, 464 (1987). R. M. Evans and S. M. Hollenberg, *Cell*, **52**, 1, (1988).
32. D. J. Galas and A. Schmitz, *Nucleic Acids Res.*, **5**, 3157 (1978).
33. M. W. van Dyke, R. P. Hertzberg, and P. B. Dervan, *Proc. Natl. Acad. Sci. USA*, **79**, 5470 (1982). M. W. van Dyke, and P. B. Dervan, *Nucleic Acids Res.*, **11**, 5555 (1983).
34. I. L. Cartwright and S. C. R. Elgin, *Mol. Cell. Biol.*, **6**, 779 (1986). S. I. Gunderson, K. A. Chapman, and R. R. Burgess, *Biochemistry*, **26**, 1539 (1987). G. J. M. Pruijn, R. T. van Miltenberg, J. A. J. Claessens, and P. C. van der Vliet, *J. Virol.*, **62**, 3092 (1988).
35. T. D. Tullius, *Trends Biochem. Sci.*, **12**, 297 (1987).
36. T. D. Tullius, B. A. Dombroski, M. E. A. Churchill, and L. Kam, *Methods Enzymol.*, **155**, 537 (1987).
37. A. Spassky and D. S. Sigman, *Biochemistry*, **24**, 8050 (1985).
38. R. Law, M. D. Kuwabara, M. Briskin, N. Fasel, G. Hermanson, D. S. Sigman, and R. Wall, *Proc. Natl. Acad. Sci. USA*, **84**, 9160 (1987). C. L. Peterson and K. L. Calame, *Mol. Cell. Biol.*, **7**, 4194 (1987).
39. S. Goldstein and G. Czapski, *J. Am. Chem. Soc.*, **108**, 2244 (1986).
40. K. Kobashi, *Biochim. Biophys. Acta*, **158**, 239 (1968).
41. J. C. Dabrowiak, B. Ward, and J. Goodisman, *Biochemistry*, **28**, 3314 (1989).
42. M. J. Carvlin, E. Mark, R. J. Fiel, and J. C. Howard, *Nucleic Acids Res.*, **11**, 6141 (1983). R. F. Pasternack, E. J. Gibbs, and J. J. Villafranca, *Biochemistry*, **22**, 2406 (1983). R. F. Pasternack, E. J. Gibbs, and J. J. Villafranca, *Biochemistry*, **22**, 5409 (1983).
43. M. J. Carvlin and R. J. Fiel, *Nucl. Acids Res.*, **11**, 6121 (1983). R. J. Fiel, J. C. Howard, E. H. Mark, and N. Datta Gupta, *Nucleic Acids Res.*, **6**, 3093 (1979).
44. B. Ward, A. Skorobogaty, and J. C. Dabrowiak, *Biochemistry*, **25**, 6875 (1986).
45. H. R. Drew and A. A. Travers, *Cell*, **37**, 491 (1984).
46. P. E. Nielsen, C. Jeppesen, and O. Buchardt, *FEBS Lett.*, **235**, 122 (1988).
47. C. Jeppeson, P. E. Nielsen, *Nucleic Acids Res.*, **17**, 4947 (1989).
48. A. M. Pyle, E. C. Long and J. K. Barton, *J. Am. Chem. Soc.*, **111**, 4520 (1989).
49. K. Uchida, A. M. Pyle, T. Morii, and J. K. Barton, *Nucleic Acids Res.*, **17**, 10259 (1989).
50. C. H. Chang, M. Beer, and L. G. Marzilli, *Biochemistry*, **16**, 33 (1977).
51. G. C. Glikin, M. Vojtiskova, L. Rena-Descalzi, and E. Palacek, *Nucleic Acids Res.*, **12**, 1725 (1984).
52. (a) B. H. Johnston and A. Rich, *Cell*, **42**, 713 (1985). (b) K. Nejedly, M. Kwinkowski, J. K. Galazka, J. Klysik, and E. Palacek, *J. Biomol. Struct. Dyn.*,

- 3, 467 (1985). (c) E. Palacek, E. Rasovska, and P. Boublikova, *Biochem. Biophys. Res. Commun.*, *150*, 731 (1988).
53. R. E. Mahnken, M. Bina, R. M. Deibel, K. Luebke, and H. Morrison, *Photochem. Photobiol.*, *49*, 519 (1989).
54. J. K. Barton and E. Lolis, *J. Am. Chem. Soc.*, *107*, 708 (1985). A. Danishefsky, Ph.D. Thesis, Columbia University (1987).
55. J. K. Barton, C. V. Kumar, and N. J. Turro, *J. Am. Chem. Soc.*, *108*, 6391 (1986). M. D. Purugganan, C. V. Kumar, N. J. Turro, and J. K. Barton, *Science*, *241*, 1645 (1988).
56. W. Bannworth and D. Schmidt, *Tetrahedron Lett.*, *30*, 1513 (1989).
57. A. M. Pyle, J. P. Rehmann, R. Meshoyrer, C. V. Kumar, N. J. Turro, and J. K. Barton, *J. Am. Chem. Soc.*, *111*, 3051 (1989).
58. A. B. Tossi and J. M. Kelly, *Photochem. Photobiol.*, *49*, 545 (1989).
59. J. K. Barton, L. A. Basile, A. Danishefsky, and A. Alexandrescu, *Proc. Natl. Acad. Sci. USA*, *81*, 1961 (1984).
60. A. E. Friedman, C. V. Kumar, N. J. Turro, and J. K. Barton, manuscript in preparation.
61. B. M. Goldstein, J. K. Barton, and H. M. Berman, *Inorg. Chem.*, *25*, 842 (1986).
62. A. M. Burkhoff and T. D. Tullius, *Cell*, *48*, 935 (1987). A. M. Burkhoff and T. D. Tullius, *Nature (London)*, *331*, 455 (1988).
63. H.-M. Wu and D. M. Crothers, *Nature (London)*, *308*, 509 (1984).
64. T. D. Tullius, B. A. Dombroski, *Science*, *230*, 679 (1985).
65. I. L. Cartwright and S. C. R. Elgin, *Nucleic Acids Res.*, *10*, 5835 (1982).
66. B. Jessee, G. Gargiulo, F. Razvi, and A. Worcel, *Nucleic Acids Res.*, *10*, 5823 (1982).
67. J. W. Suggs and R. W. Wagner, *Nucleic Acids Res.*, *14*, 3703 (1986).
68. J. M. Veal and R. L. Rill, *Biochemistry*, *28*, 3243 (1989).
69. M. Behe and G. Felsenfeld, *Proc. Natl. Acad. Sci. USA*, *78*, 1619 (1981).
70. G. B. Dreyer and P. B. Dervan, *Proc. Natl. Acad. Sci. USA*, *82*, 968 (1985). C. B. Chen and D. S. Sigman, *Proc. Natl. Acad. Sci. USA*, *83*, 7147 (1986). C. F. Chu and L. E. Orgel, *Proc. Natl. Acad. Sci. USA*, *82*, 963 (1985). B. L. Iverson and P. B. Dervan, *J. Am. Chem. Soc.*, *109*, 1241 (1987).
71. H. E. Moser and P. B. Dervan, *Science*, *238*, 645 (1987).
72. C.-B. Chen and D. S. Sigman, *Science*, *237*, 1197 (1987).
73. J. P. Sluka, S. J. Horvath, M. F. Bruist, M. Simon, and P. B. Dervan, *Science*, *238*, 1129 (1987).
74. D. P. Mack, B. L. Iverson, and P. B. Dervan, *J. Am. Chem. Soc.*, *110*, 7572 (1988).
75. H.-Y. Mei and J. K. Barton, *J. Am. Chem. Soc.*, *108*, 7414 (1986).
76. L. Moggi, N. Sabbatini, and O. Traverso, *Mol. Photochem.*, *5*, 11 (1973). V.

- Balzani, L. Moggi, M. F. Manfrin, F. Boletta, and G. S. Laurence, *Coord. Chem. Rev.*, *15*, 321 (1975).
77. J. K. Barton and A. L. Raphael, *Proc. Natl. Acad. Sci. USA*, *82*, 6460 (1985).
78. L. J. Peck, A. Nordheim, A. Rich, and J. C. Wang, *Proc. Natl. Acad. Sci. USA*, *79*, 4560 (1982).
79. C. Yoon, G. G. Prive, D. S. Goodsell, and R. E. Dickerson, *Proc. Natl. Acad. Sci. USA*, *85*, 6332 (1988). R. Wing, H. Drew, T. Takano, C. Broka, S. Tanaka, K. Itakura, and R. E. Dickerson, *Nature (London)*, *287*, 755 (1980). J. G. Nadeau and D. M. Crothers, *Proc. Natl. Acad. Sci. USA*, *86*, 2622 (1989).
80. R. E. Dickerson, *J. Biomol. Struct. Dyn.*, *6*, 627 (1989).
81. W. N. Hunter, B. L. D'Estaintot, and O. Kennard, *Biochemistry*, *28*, 2444 (1989). U. Heinemann, H. Lauble, R. Frank, and H. Blöcker, *Nucleic Acids Res.*, *15*, 9531 (1987). R. Dickerson and H. R. Drew, *J. Mol. Biol.*, *149*, 761 (1981).
82. A. M. Pyle, T. Morii and J. K. Barton, submitted for publication.
83. B. C. Müller, A. L. Raphael, and J. K. Barton, *Proc. Natl. Acad. Sci. USA*, *84*, 1764 (1987).
84. P. W. Huber, H.-Y. Mei, T. Morii, and J. K. Barton, submitted for publication.
85. R. Holliday, *Genet. Res.*, *5*, 282 (1964).
86. M. E. A. Churchill, T. D. Tullius, N. R. Kallenbach, and N. R. Seeman, *Proc. Natl. Acad. Sci. USA*, *85*, 4653 (1988).
87. M. R. Kirshenbaum, "Shape-Selective Targeting of Unusual DNA Structures by Tris(4,7-Diphenyl-Phenanthroline) Rhodium(III)," Ph.D. Thesis, Columbia University (1989).
88. M. R. Kirshenbaum, R. Tribolet, and J. K. Barton, *Nucleic Acids Res.*, *16*, 7943 (1988).
89. G. J. Quigley and A. Rich, *Science*, *194*, 796 (1976).
90. J. M. Kean, S. A. White, and D. E. Draper, *Biochemistry*, *24*, 5062 (1985).
91. N. K. Tanner and T. R. Cech, *Nucleic Acids Res.*, *13*, 7759 (1985).
92. G. J. Murakawa, C. B. Chen, M. D. Kuwabara, D. P. Nierlich, and D. S. Sigman, *Nucleic Acids Res.*, *17*, 5361 (1989).
93. J. A. Latham and T. R. Cech, *Science*, *245*, 276 (1989).
94. R. Gaynor, E. Soultanakis, M. Kuwabara, J. Garcia, and D. S. Sigman, *Proc. Natl. Acad. Sci. USA*, *86*, 4858 (1989).
95. C. S. Chow and J. K. Barton, *J. Am. Chem. Soc.*, *112*, 2839 (1990).
96. J. K. Barton, *Frontiers in Chemistry: Biotechnology*, Chemical Abstracts Service, Columbus, Ohio, p. 5 (1989).
97. L. A. Basile and J. K. Barton, *J. Am. Chem. Soc.*, *109*, 7548 (1987).
98. L. A. Basile, A. L. Raphael, and J. K. Barton, *J. Am. Chem. Soc.*, *109*, 7550 (1987).
99. L. A. Basile, "The Design of an Artificial Nuclease," Ph.D. Thesis, Columbia University (1989).

Biological Processing of DNA Modified by Platinum Compounds

**SUZANNE L. BRUHN, JEFFREY H. TONEY, and
STEPHEN J. LIPPARD**

*Department of Chemistry
Massachusetts Institute of Technology
Cambridge, MA*

CONTENTS

I. HISTORICAL BACKGROUND AND SCOPE OF THE REVIEW	478
II. RECENT ADVANCES IN UNDERSTANDING Pt-DNA INTERACTIONS	480
A. Binding Modes of <i>cis</i> - and <i>trans</i> -DDP to DNA	480
B. Role of Interstrand Cross-Links	484
C. Kinetics of <i>cis</i> - and <i>trans</i> -DDP Binding to DNA	485
D. Structural Distortions in DNA Induced by Covalent Binding of Platinum Complexes	489
III. EFFECTS OF Pt(II) COMPLEXES ON DNA REPLICATION	491
A. Prokaryotic Systems	491
B. Eucaryotic Systems	492
C. Studies Employing Site-Specifically Modified DNA	493
IV. MUTAGENESIS AND REPAIR OF Pt-DNA ADDUCTS	495
A. Repair Studies in Prokaryotic Systems	495
B. Repair Studies in Mammalian Systems	498
C. Mutagenesis	500
D. Use of Modified DNA Fragments as Probes for DNA Repair Factors	501

Progress in Inorganic Chemistry: Bioinorganic Chemistry, Vol. 38, Edited by Stephen J. Lippard.
ISBN 0-471-50397-5 © 1990 John Wiley & Sons, Inc.

V. POSSIBLE MECHANISMS OF ACQUIRED RESISTANCE TO <i>cis</i> -DDP	505
A. The Resistance Phenomenon	505
B. Differential Uptake of Platinum Compounds	506
C. Inactivation by Sulfur-Containing Agents	506
D. Differential Repair of Platinum Compounds	507
VI. EFFECT OF Pt(II) COMPLEXES ON OTHER CELLULAR PROCESSES	508
VII. GENERAL CONCLUSIONS AND CHALLENGES FOR THE FUTURE	510
ACKNOWLEDGMENTS	511
REFERENCES	511

I. HISTORICAL BACKGROUND AND SCOPE OF THE REVIEW

Platinum anticancer compounds are currently in widespread use for the treatment of genitourinary and other tumors. In order to understand the mechanism of action of this interesting class of chemotherapeutic agents, attention has focused on DNA as the generally accepted target. Through intensive research efforts over the past several years, there is now a fairly detailed understanding of how these complexes bind to DNA and how the DNA is structurally modified as a result of this interaction. Attention now must turn to the key questions of how platinum complexes selectively kill tumor cells while being of only limited toxicity to normal tissues, why certain classes of tumors are refractory or resistant to platinum chemotherapy, and what structural features of platinated DNA underlie these differences. These issues require knowledge of how platinum–DNA adducts are processed in the cell, a subject that is the principal focus of this chapter. Before exploring this topic in depth, however, we first present some historical background and update structural information about Pt–DNA adducts.

In experiments initially designed to study the effects of electric fields upon the growth of the bacterium *Escherichia coli* (*E. coli*), Rosenberg et al. (109) observed the unusual phenomenon of filamentous growth. The bacterial cells, which normally divide rapidly, grew to 300 times their usual size and did not divide. This observation was eventually found to derive from the presence of Pt(II) and Pt(IV) ammine chloride complexes formed *in situ* by electrolysis at the platinum electrodes. Further studies showed one cause of the filamentation to be *cis*-diamminedichloroplatinum(II) (*cis*-

DDP or cisplatin), a classic coordination complex, the synthesis and structure of which were known for more than a century (80, 133). Subsequent investigations of the effects of *cis*-DDP on rapidly dividing mammalian tumor cells indicated significant antitumor activity against sarcoma 180 and leukemia L1210 in mice (110). Clinical trials commenced soon thereafter and in 1979 cisplatin was approved by the FDA for the treatment of several human cancers.

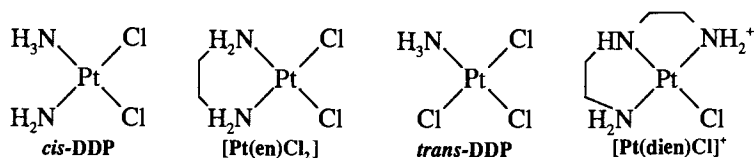
With the use of cells from mice bearing the Ehrlich ascites tumor (61), and human amnion AV₃ cells (55), the effect of *cis*-DDP on the synthesis of DNA, RNA, and proteins was measured by monitoring the incorporation of radiolabeled precursors into these macromolecules. Although at high concentrations or long incubation times RNA and protein synthesis were inhibited, this effect was judged to be of secondary significance. In both cases, DNA synthesis was preferentially and persistently suppressed at all concentrations. Other convincing evidence suggesting that *cis*-DDP was a DNA damaging agent came from a study involving the indirect induction of prophage lysis (104), a phenomenon known for other DNA damaging agents such as UV irradiation. When donor F' gal⁺ nonlysogenic cells were exposed to subtoxic doses of cisplatin and then conjugated to F⁻ gal⁻ lysogenic cells, prophage induction occurred. Since only DNA is transferred during conjugation, platinated DNA must have caused the derepression of the lytic prophage function. It is now generally accepted that the effectiveness of *cis*-DDP results from its ability to bind DNA and block replication.

Interestingly, while *cis*-[Pt(NH₃)₂Cl₄] was active as an antitumor agent and in the inhibition of DNA synthesis in human AV₃ cells (55), its geometric isomer was not. The compound *trans*-[Pt(NH₃)₂Cl₄] had no influence on tumor growth or DNA and RNA synthesis, and only a slight effect on protein synthesis. These early findings strongly suggested important differences in the chemistry of *cis* versus *trans* platinum ammine halide complexes with macromolecules such as DNA. Comparative studies of the two isomers, an active area of research, recently began to shed light on their differential toxicity in biological systems. In particular, the lack of biological activity of the *trans* isomer affords a powerful way to calibrate the consequences and relative importance of various *cis*-DDP-DNA interactions.

The impact on a living cell of a toxic (109), mutagenic (18) agent such as *cis*-DDP is complex and dependent on several factors, including the inherent sensitivity of a particular cell type to the drug. While cisplatin is not active against cancers of all cell types, it is remarkably effective in treating testicular carcinomas, which are now considered nearly curable even in progressive stages of the disease. The drug is also active in ovarian, lung, head and neck, bladder, and cervical cancers (81). The differential activity of *cis*-DDP for cancers of various cell types as well as the differential

toxicity of the *cis* and *trans* isomers may be the result of the different biological processing of Pt–DNA adducts. These phenomena could be a manifestation of the tolerance of cells for particular Pt–DNA adducts once they are formed or of the directed removal or repair of Pt–DNA adducts. The importance of cisplatin in current clinical protocols emphasizes the need to understand its biological chemistry with the ultimate goal of using this information to design even more effective drugs.

In this chapter we draw upon studies from our laboratory and others that address the question of how cells differentially process the Pt(II) complexes shown below, and their DNA adducts. Structural and chemical aspects of Pt–DNA interactions have been largely elucidated and exten-



sively reviewed (35, 102, 103, 116). This information is updated in Section II, which discusses recent progress made in unraveling the kinetics of DNA binding reactions, and new results relating to the binding modes and structural distortions to DNA. A much more detailed analysis of this topic may be found elsewhere (Ref. 76). Section III discusses the effects of Pt complexes on DNA replication in prokaryotic and eukaryotic systems, including work using site-specifically modified genomes. Section IV reviews studies of the mutagenesis and repair of Pt–DNA adducts in prokaryotic and eukaryotic systems. Recent work describing the search for cellular factors that may be involved in recognition or repair of Pt-induced structural perturbations of DNA is also discussed. Section V describes studies aimed at understanding acquired resistance to *cis*-DDP, a phenomenon that is the major cause of treatment failure for this drug. Section VI details the effects of *cis*-DDP on cellular processes other than DNA replication. Finally, in Section VII, we draw some general conclusions and outline challenges for the future.

II. RECENT ADVANCES IN UNDERSTANDING Pt–DNA INTERACTIONS

A. Binding Modes of *cis*- and *trans*-DDP to DNA

Both *cis*- and *trans*-DDP are small, neutral molecules that retain their coordination environment in circulating plasma, where the chloride ion concentration is ~ 100 mM. Once passing through the cell membrane into

the cytoplasm of the cell, where the chloride ion concentration drops to 4 mM, the compounds undergo hydrolysis. It has been estimated that the relative ratios of hydrolyzed products of cisplatin in cells is 0.46 $[\text{Pt}(\text{NH}_3)_2(\text{H}_2\text{O})_2]^{2+}$: 3.63 $[\text{Pt}(\text{NH}_3)_2(\text{OH})_2]$: 2.90 $[\text{Pt}(\text{NH}_3)_2(\text{H}_2\text{O})(\text{OH})]^+$: 1.0 $[\text{Pt}(\text{NH}_3)_2(\text{H}_2\text{O})(\text{Cl})]^+$: 1.0 $[\text{Pt}(\text{NH}_3)_2(\text{OH})(\text{Cl})]$: 0.915 $[\text{Pt}(\text{NH}_3)_2\text{Cl}_2]$ (60,79).

Molecules containing sulfur or nitrogen donor atoms can serve as ligands to form stable complexes with the relatively kinetically inert Pt(II) center (for a review see Ref. 60). It is likely that cisplatin binds to many cellular components, the result of which is general toxicity, but coordination to the heterocyclic nitrogen atoms of DNA nucleobases is most likely responsible for its antitumor activity.

Each strand of DNA has a backbone comprised of repeating deoxyribose phosphodiester units, attached through the sugar moiety to the N9 atoms of the purine bases adenine (A) and guanine (G) or the N1 atoms of the pyrimidines cytosine (C) and thymine (T). The ordering of bases from 5' to 3' on the DNA strand defines the sequence of that strand. Complementary strands of DNA are stabilized by hydrogen bonds between guanine and cytosine (G-C) and between adenine and thymine (A-T), called "Watson-Crick" base pairs for their discoverers. The numbering scheme of the bases and the hydrogen-bonding interactions are shown in Fig. 1. The

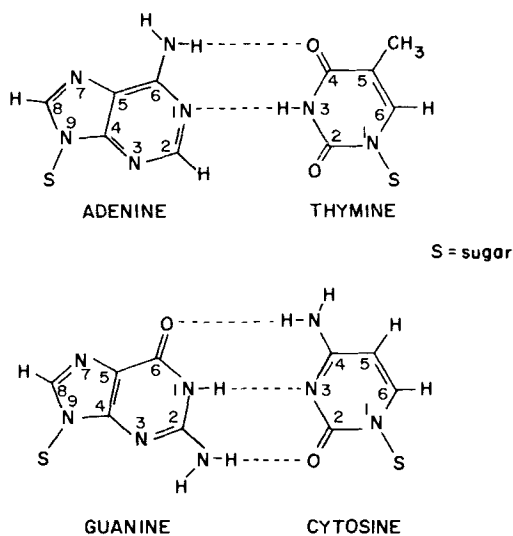


Figure 1. Numbering scheme of nucleotide bases of DNA, showing hydrogen-bonding interactions between G-C and A-T base pairs. As depicted in the diagrams, the top of each base pair points to the major groove, and the bottom, to the minor groove. Reproduced with permission from Ref. 116 (copyright © 1987, American Chemical Society).

complementary strands are aligned in antiparallel fashion to form a double helix, which is also stabilized by stacking interactions between the parallel bases, as shown in Fig. 2. This polyanionic macromolecule offers an electrostatic potential that attracts the positively charged platinum hydrolysis products.

Coordination of these platinum species to DNA occurs in two steps, with considerable sequence specificity. The first step involves formation of monofunctional adducts, primarily at the N7 position of guanine or adenine. These monofunctional Pt-DNA adducts react further to form bifunctional adducts, mainly at the N7 position of nearby guanines, and to a lesser extent, adenine. If the coordinated nucleotide bases are on the same strand of DNA, an intrastrand cross-link is formed. If platinum links two bases on opposite DNA strands, the result is an interstrand adduct.

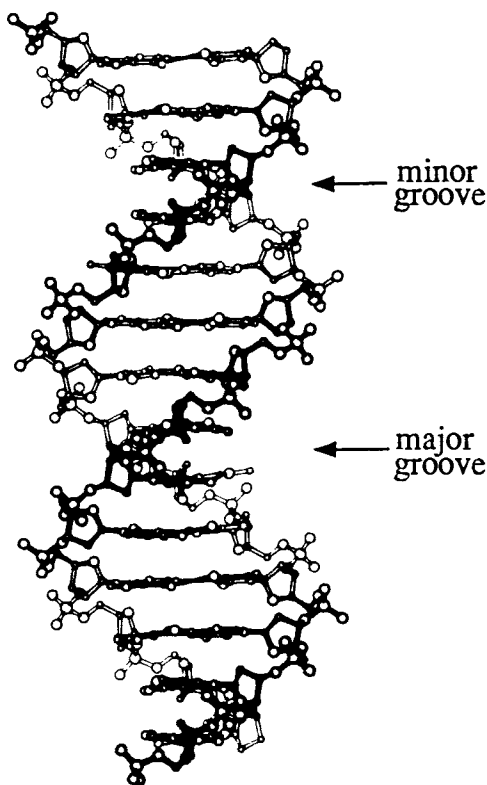


Figure 2. Ball-and-stick representation of B-DNA showing the sugar-phosphate backbone, stacking interactions of parallel bases, and major and minor grooves.

Platinum was also shown to link DNA and proteins (for reviews see Refs. 35, 95, 102, 103, and 116).

The relative amount of each adduct was determined by first treating DNA with cisplatin *in vitro* and then enzymatically degrading the DNA to nucleotides with DNase I and nuclease P1. The products were chromatographically separated and identified by their ^1H NMR spectra (40). The relative proportions of adducts were *cis*-[Pt(NH₃)₂{d(GpG)}], 47–50%, *cis*-[Pt(NH₃)₂{d(ApG)}], 23–28% (intrastrand cross-links to adjacent bases), *cis*-[Pt(NH₃)₂{d(GMP)₂}] 8–10% (the sum of intrastrand adducts between nonadjacent guanines and interstrand adducts), and [Pt(NH₃)₃{d(GMP)}] 2–3% (monofunctional adducts). These results were obtained by using DNA with a bound drug–nucleotide ratio, (D/N)_b, of 0.055, meaning that 55 Pt atoms are bound per 1000 bases of DNA. Another study using similar methodology revealed an adduct spectrum of 65% *cis*-[Pt(NH₃)₂{d(GpG)}], 25% *cis*-[Pt(NH₃)₂{d(ApG)}], and 6% *cis*-[Pt(NH₃)₂{d(GpNpG)}] for the compound [^3H]*cis*-[Pt(en)Cl₂] (34), which reportedly gives the same adduct spectrum as *cis*-DDP (32).

Although the (D/N)_b ratios used in these experiments were 2–3 orders of magnitude greater than commonly observed for experiments carried out *in vivo*, when studies were performed using leukocytes collected from seven cancer patients treated with cisplatin for the first time, similar adduct profiles were observed (42). As before, the DNA was isolated, enzymatically digested, and the products separated chromatographically. Because of the extremely low number of adducts present, the more sensitive enzyme-linked immunosorbant assay (ELISA) was required for their detection. With the use of antibodies raised against *cis*-DDP–DNA adducts, an adduct profile of *cis*-[Pt(NH₃)₂{d(GpG)}] (65%), *cis*-[Pt(NH₃)₂{d(ApG)}] (22%), *cis*-[Pt(NH₃)₂{d(GMP)₂}] (13%), and [Pt(NH₃)₃{d(GMP)}] (0.7%) was obtained for one patient. Although there were strong interindividual differences in total adduct levels, the relative amount of each adduct did not vary among patients. In another study, ELISA was again used to detect *in vivo* Pt–DNA adduct levels, employing an antibody that recognized *cis*-[Pt(NH₃)₂{d(GpG)}] cross-links (101). Analysis of DNA from the buffy coat cells of patients treated with cisplatin for testicular and ovarian cancers revealed an increase in the number of measurable platinum–DNA adducts with cumulative dose during 21- or 28-day cycles. In addition, there was a positive correlation between disease response and the formation of this DNA intrastrand cross-link for both testicular (correlation coefficient, 0.81) and ovarian (correlation coefficient, 0.90) cancers. These data, taken together, create a very strong case for the importance of Pt–DNA adducts in general and the d(ApG) and d(GpG) intrastrand adducts, in particular, as determinants of the antitumor properties of cisplatin.

Unfortunately, less information is available about the clinically ineffective *trans* isomer. Recently, several chemically defined adducts formed by *trans*-DDP with short oligonucleotides have confirmed that the platinum binds through the N7 position of guanine and adenine forming 1,3-intrastrand adducts (49, 77, 78, 129); the N3 position of cytosine was also found to coordinate to platinum in a 1,4-intrastrand adduct (25). Unlike the *cis* isomer, *trans*-DDP is stereochemically incapable of forming intrastrand adducts between adjacent nucleotide bases (78). In a replication mapping experiment, considerably lower sequence specificity was observed for *trans*- versus *cis*-DDP, although there appeared to be a preference for d(GpNpG) sequences, where N is any intervening nucleotide (96). Platination of double-stranded DNA with *trans*-DDP followed by enzymatic degradation, high-performance liquid chromatography (HPLC) separation, and ¹H NMR analysis revealed an adduct spectrum of dG-Pt-dC (50%), dG-Pt-dG (40%), and dG-Pt-dA (10%) (38).

Although most bifunctional adducts formed by *trans*-DDP with DNA appear to be kinetically stable (49, 77, 78, 129), the *trans*-[Pt(NH₃)₂{d(G*CG*)}] 1,3-intrastrand cross-link in d(TpCpTpApCpG*pCpG*-pTpTpCpT), where the asterisk denotes positions of platinum coordination, isomerizes under approximately physiological conditions to a thermodynamically more stable *trans*-[Pt(NH₃)₂{d(C*GCG*)}] 1,4-intrastrand cross-link (25). The equilibrium constant for this linkage isomerization reaction is ~3, in favor of the 1,4 adduct. The half-life for this isomerization ranges from 129 h at 30°C to 3.6 h at 62°C, leading to activation parameters consistent with associative hydrolysis as the rate-determining step. Such a linkage isomerization does not occur with the *cis*-DDP 1,3-intrastrand d(G*CG*) adduct in the identical oligonucleotide (19).

These data thus reveal that both *cis*- and *trans*-DDP can bind to DNA through the N7 positions of adenine and guanine. Significant differences exist, however. Stereochemical limitations preclude *trans*-DDP from forming 1,2-intrastrand cross-links, which comprise 60–80% of the adducts formed by *cis*-DDP *in vitro* and *in vivo*. *trans*-DDP also seems to form a large percentage of cross-links between guanine and cytosine residues, making the adduct spectrum quite different for these two isomers. It is possible that the biological processing of these adducts also differs.

B. Role of Interstrand Cross-Links

Although the majority of adducts formed by platinum on DNA are intrastrand cross-links, interstrand cross-linking also occurs both *in vitro* (33, 40) and *in vivo* (122, 134, 135). Estimates of the frequency of formation of interstrand cross-links range from 1–7% (33, 54, 108). Although

some laboratories have found a correlation between interstrand cross-linking and cytotoxicity (134), others have not (122). Such studies are complicated because only interstrand cross-links were monitored, without regard to the effects of the more prevalent intrastrand adduct.

It was hypothesized that the minor interstrand adduct is the "critical" lesion responsible for the cytotoxic effects of *cis*-DDP. Both *cis* and *trans* isomers can form interstrand cross-links (94, 134, 135). At the reported frequency for interstrand cross-linking, 100 platinum atoms would have to bind to DNA for 1–7 interstrand adducts to form. Studies of SV40 (for simian virus 40) DNA replication *in vivo* have shown that as few as 4 bound platinum atoms per genome can inhibit DNA synthesis by 50% (23). Bacteriophage T7 can be inactivated by an average of 1.5 platinum atoms per genome (117). When the activity of the bacterial enzyme chloramphenicol acetyltransferase (CAT) was measured in Chinese hamster ovary (CHO) cells 8 platinum atoms coordinated to the CAT gene eliminated its expression (113). The enzyme xanthine guanine phosphoribosyltransferase (XGPRT) was inactivated when fewer than 100 platinum atoms were bound to the gene (69). Taken together, these studies indicate that *cis*-DDP inhibits DNA synthesis and inactivates DNA templates at bound platinum levels for which the formation of interstrand cross-links is highly unlikely.

C. Kinetics of *cis*- and *trans*-DDP Binding to DNA

The kinetics of binding of *cis*- and *trans*-DDP to DNA, often cited as the cause of their differential activity, have been greatly studied and disputed. Several groups hypothesized that the differential activity of the *cis* and *trans* isomers results from differing half-lives for their monofunctional adducts (20, 37, 38). If, for example, conversion of monofunctional to bifunctional adducts was much slower for the *trans* isomer, the monochloro or mono-aqua species might be relatively long lived or bind to sulfur or nitrogen containing nucleophiles in the cell. DNA synthesis could proceed, unaffected, past these monofunctional lesions or they could be removed or repaired more readily than bifunctional adducts. One group (20) measured monofunctional adduct lifetimes of 15 h for the *cis* isomer and 30 h for the *trans* isomer by trapping the adducts with ^{14}C -labeled guanosine. Other workers have added sulfur donors such as thiourea or glutathione to prevent closure to bifunctional adducts, and measured a half-reaction time of 24 h for closure of *trans*-DDP–DNA monofunctional adducts (37).

Variations in monofunctional adduct lifetimes were also invoked to explain the relative ratios of different platinum adducts formed by *cis*-DDP on DNA. When the reaction of $[^3\text{H}][\text{Pt}(\text{en})\text{Cl}_2]$ with DNA was allowed to occur in the presence of thiourea, subsequent enzymatic digestion of the

DNA followed by HPLC separation of the products revealed the presence of some sulfur-bound intermediates. It was hypothesized that monofunctional binding to a random base was followed by the platinum atom traversing the DNA helix until bifunctional adducts formed (34). This hypothesis could explain a preponderance of bifunctional adducts without the involvement of direct bifunctional attack, but does not account for the preference for d(GpG) over d(ApG) sequences. Others have suggested that monofunctional platinum-guanine adducts react rapidly with neighboring guanine bases but more slowly with neighboring adenine bases (38, 66). This explanation is reasonable since the 6-amino group of adenine would repel the ammine ligand on the nearby platinum atom, whereas the 6-oxo residue of guanine would form a stabilizing hydrogen bond with such an ammine ligand. As shown in Fig. 3, however, the spectrum of adducts remains the same over 24 h, when expressed either as adducts per nucleotide base or as a percentage of total platinum. In other words, the relative rates of formation of different Pt-DNA adducts are invariant with time.

Unfortunately, the indirect measurement of monofunctional adduct lifetimes by using chemical trapping agents is problematical. In some cases (20, 38, 41) the rate of reaction with the trapping agent may be slower than the rate-determining step of the DNA binding reaction being investigated. Moreover, sulfur-containing nucleophiles such as thiourea or glutathione can remove platinum from DNA (37, 77), and it is not clear that the rates of reaction with *cis*- and *trans*-DDP monofunctional adducts are comparable (6).

One early study (64), employing ^{195m}Pt -radiolabeled analogues to monitor directly the binding reactions, concluded that the rates of reaction of *cis*- and *trans*-DDP with DNA were governed mainly by their rates of hydrolysis. The reaction rates of both isomers were also found to be the same on double- and single-stranded DNA, implying that local DNA conformation was not a major factor in binding. A very recent study (6) employed ^{195}Pt NMR spectroscopy to follow the formation of monofunctional adducts of *cis*- and *trans*-DDP to ~40 bp random sequence DNA and their closure to bifunctional adducts. Similar half-lives were measured for the initial binding to DNA, $t_{1/2} = 1.9$ h for *cis*-DDP and $t_{1/2} = 2.0$ h for *trans*-DDP, values identical to the half-lives for hydrolysis for these compounds. Interestingly, the half-lives of closure of the monofunctional adducts were relatively fast and quite similar, being $t_{1/2} = 2.1$ h for the *cis* isomer and $t_{1/2} = 3.1$ h for the *trans* isomer with either double- or single-stranded DNA. These values, all measured at 37°C, are also comparable to those for hydrolysis of the second chloride ligand, suggesting this step to be rate determining. A stepwise mechanism, together with rate constants for both *cis*- and *trans*-DDP, is shown in Fig. 4. In these ^{195}Pt NMR investigations, the trapping of monofunctional adducts with glutathione

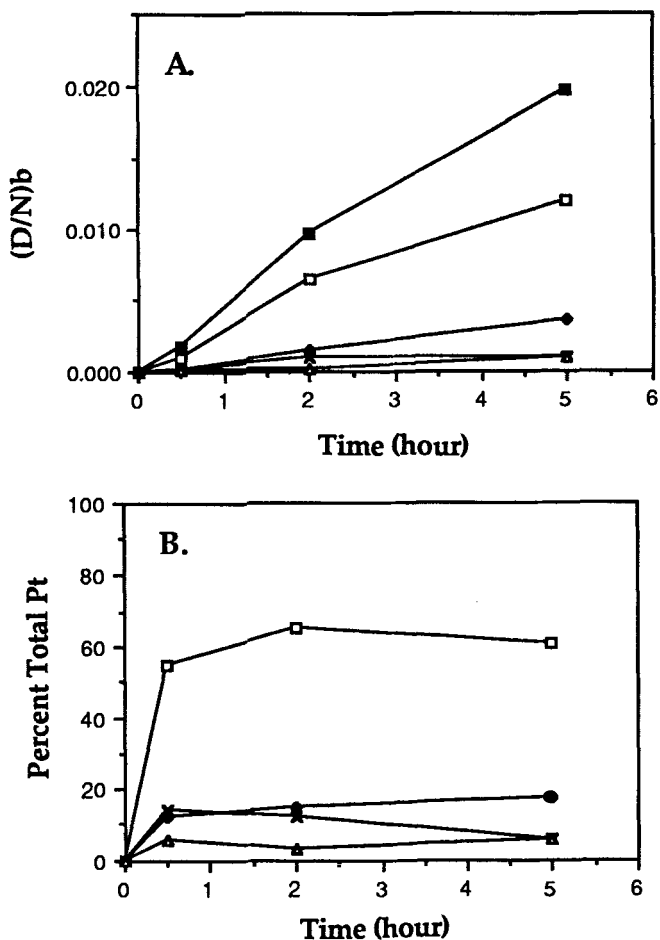


Figure 3. Formation at various *cis*-DDP-DNA adducts with time. DNA was platinated at 37°C for various periods, enzymatically digested, and the products separated chromatographically. In (a) the cross-links are expressed as a function of their (D/N)_b values; in (b) cross-links are expressed as a percentage of total platinum (from Ref. 40). Symbols: —■—, total platinum; —□—, *cis*-[Pt(NH₃)₂{d(GpG)}]; —◆—, *cis*-[Pt(NH₃)₂{d(ApG)}]; —×—, [Pt(NH₃)₃dGMP]; —△—, *cis*-[Pt(NH₃)₂{d(GMP)₂}]

was also monitored. Monofunctional DNA adducts of *trans*-DDP reacted more rapidly with this agent, while bifunctional adducts of both isomers were unreactive towards glutathione, in agreement with earlier work (36).

From these studies, which directly measured the rates of *cis*- and *trans*-DDP binding to DNA, it seems clear that their reaction kinetics are quite similar, at least *in vitro*. The rates of formation of monofunctional adducts

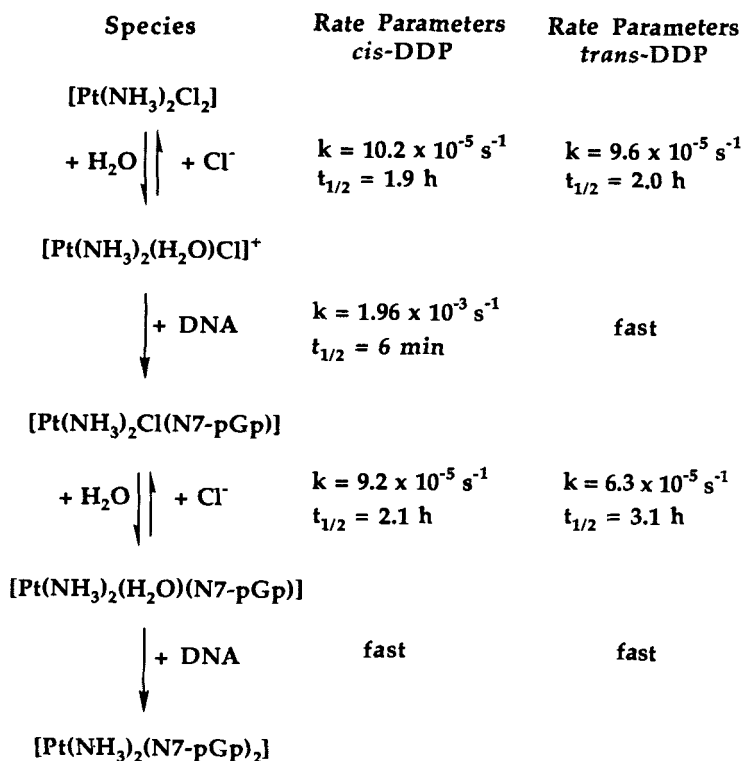


Figure 4. Mechanism, with rate constants, for the binding of *cis*- and *trans*-DDP to DNA (Ref. 6).

and their closure to bifunctional adducts are comparable. Monofunctional adducts of DNA formed by *trans*-DDP react more rapidly with sulfur containing nucleophiles, which could both prevent their closure to bifunctional adducts or labilize the Pt–DNA linkage. The inability of trapping agents such as ammonium ion or thiourea to reflect accurately the lifetimes of monofunctional adducts remains to be explained.

Variations in monofunctional adduct lifetimes do not appear to be directly responsible for the differential activity of the *cis* and *trans* isomers. In fact, it is also unnecessary to invoke differential monofunctional adduct lifetimes to explain the sequence specificity of these compounds. Theoretical calculations of the electrostatic potential of B-DNA reveal sequence-specific variations along the surface of this macromolecule (75). The most negative potentials are concentrated in the grooves of DNA, rather than along the sugar–phosphate backbone. The largest negative potentials were found in the major groove for poly(dG)·poly(dC), and in the minor groove

for poly(dA)·poly(dT). The N7 position of guanine was much more negative than that of adenine, and would therefore provide a stronger attraction for positively charged platinum hydrolysis products. Thus, the majority of platinum binds to the most negatively charged regions on the surface of the polyanion DNA.

D. Structural Distortions in DNA Induced by Covalent Binding of Platinum Complexes

Early studies (24, 82, 112) revealed that both *cis*- and *trans*-DDP unwind DNA and shorten the double helix by as much as 50% at saturation binding levels. By using gradient denaturing gel electrophoresis, a single *cis*-[Pt(NH₃)₂{d(GpG)}] intrastrand cross-link was found to lower the melting temperature (i.e., decrease the helix stability) of DNA (90). Nuclear magnetic resonance and X-ray crystallographic studies of small DNA fragments containing a *cis*-[Pt(NH₃)₂{d(GpG)}] (N7,N7) intrastrand cross-link revealed a structure characterized by complete base destacking (1, 114, 115). Weak hydrogen-bonding interactions occur between the platinum ammine nitrogen atoms and keto (O6) oxygen atoms of the bases, and a stronger intramolecular hydrogen bond forms between a coordinated ammine and an oxygen atom of the 5' phosphate group. In addition to unwinding and base destacking, platinum coordination may also cause bending or kinking of the DNA helix axis. Molecular mechanics calculations (70–72) predict the existence of energetically accessible structural states characterized by base destacking, an ammine hydrogen bond to the 5' phosphate, and a kink angle of 40–60° for DNA platinated with *cis*-DDP (Fig. 5). Models for the binding of *trans*-DDP to DNA look quite different (Fig. 5) and predict a bend angle of only 18° (77).

Nuclear magnetic resonance spectral studies of oligonucleotides containing the *cis*-[Pt(NH₃)₂{d(GpG)}] cross-link (28, 130) are consistent with a bend in the double helix of 40–70°. The most convincing evidence for platinum induced DNA bending, however, derives from gel electrophoretic mobility studies of oligonucleotides containing this adduct. A bend angle of 35–45° toward the major groove of DNA was measured (105). The altered gel mobility of oligomers containing *cis*-[Pt(NH₃)₂{d(ApG)}] and *cis*-[Pt(NH₃)₂{d(G*pTpG*)}] adducts were also attributed to DNA bending (83). In competitive ELISA experiments, anti-*cis*-DDP antibodies recognized only *cis*-DDP platinated poly(dG)·poly(dC) and poly[d(AG)]·poly[d(TC)] but not adducts of *trans*-DDP or Pt[(dien)Cl]Cl (125). This result suggested that platinated d(GpG) and d(ApG) residues are structurally similar, yet quite different from the adducts of *trans*-DDP or those formed by monofunctional DNA-binding compounds.

Recently, the method of altered gel electrophoretic mobility was used

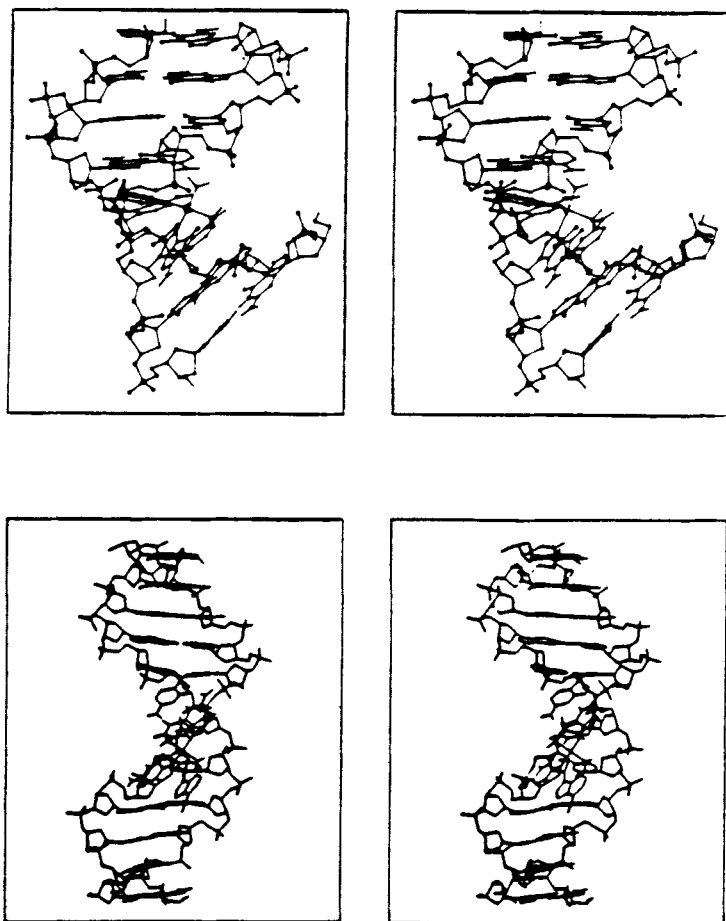


Figure 5. Stereo views of molecular mechanics models for structural perturbations to DNA caused by *cis*-DDP (top) and *trans*-DDP (bottom). Reproduced with permission from Ref. 124 (copyright © 1990, Elsevier Science Publishers).

to study DNA bending for a number of platinum adducts in parallel (12). Duplex oligonucleotides containing site-specific *cis*-[Pt(NH₃)₂{d(GpG)}], *cis*-[Pt(NH₃)₂{d(ApG)}], and *cis*-[Pt(NH₃)₂{dG*pTpG*}] cross-links were found to contain directed bends in DNA of 32°, 34°, and 35°, respectively. In contrast, a duplex oligonucleotide containing *trans*-[Pt(NH₃)₂{d(G*pTpG*)}] adducts bent the DNA in a nondirected fashion, attributed to a flexible hinge joint at the site of platination. A monofunctional platinum–DNA adduct did not bend the DNA at all. These different

conformational distortions induced in DNA by platinum coordination may serve as important recognition signals for their cellular processing.

III. EFFECTS OF Pt(II) COMPLEXES ON DNA REPLICATION

A. Prokaryotic Systems

During replication, the complementary strands of double-stranded DNA separate at the Watson-Crick hydrogen bonds, and a new strand is synthesized using one of the original strands as a template. This reaction requires nucleoside triphosphates and is mediated by DNA polymerase. DNA polymerases have been isolated from bacterial, viral, and eucaryotic sources. All have in common the ability to synthesize DNA in the 5' → 3' direction, the newly synthesized strand being oriented antiparallel to the template strand. The new sequence extends from a preexisting primer, adding nucleotides according to the sequence of the complementary, template strand.

DNA replication is an essential part of the cell cycle, and interference with this process has dire consequences for the cell. Indeed, it was the demonstration of the inhibition of DNA synthesis in *E. coli* by cisplatin (109) that spurred its development as an anticancer agent. One early study (63) examined the inhibition of replication of bacteriophage T7 DNA in cell extracts by ^{195m}Pt-labeled *cis*- and *trans*-DDP. Both isomers inhibited DNA replication, although, at $(D/N)_b = 3 \times 10^{-4}$, *cis*-DDP was found to be approximately five times more efficient than *trans*-DDP in this system.

One enzyme widely used in studies of replication inhibition by platinum complexes is DNA polymerase I (pol I) from *E. coli*. The large, or Klenow, fragment of the enzyme has capabilities both for DNA synthesis and for 3' → 5' exonuclease (proofreading) activities. Both functions are inhibited by *cis*- and *trans*-DDP (13). This system was used to investigate *cis*- or *trans*-DDP platinated primed, single-stranded bacteriophage M13mp8 DNA (96). DNA synthesis occurred in the presence of DNA polymerase I until the enzyme was blocked by coordinated platinum. Separation of the various fragments on a sequencing gel allowed mapping of the positions of platinum binding, a technique termed "replication mapping" and shown in Fig. 6. For *cis*-DDP, inhibition of DNA synthesis occurred principally at $(dG)_n$, $n \geq 2$, sequences, now known to be the major platinum binding sites on DNA. Inhibition of DNA synthesis occurred with less sequence specificity for *trans*-DDP, although there was a preference for $d(GpNpG)$ sequences. The monofunctional compound $[Pt(dien)Cl]Cl$ was unable to block DNA

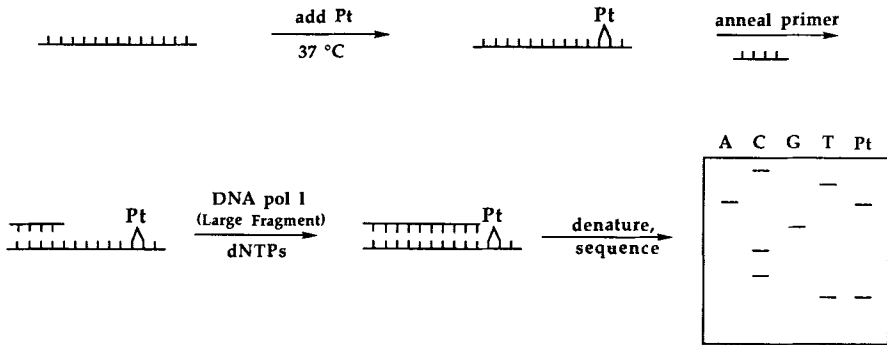


Figure 6. Schematic diagram showing the replication mapping methodology. A platinum complex is added to DNA to form a cross-link and the site of platination is revealed by primer annealing, DNA polymerase chain extension, and gel electrophoresis analytical steps (see Ref. 96 for details).

synthesis in these experiments. More recently, workers who were looking at the effects of *cis*-DDP on DNA replication of the SV40 virus by using pol I also saw blockage at runs of two or more guanines (50). A G-rich regulatory region called a GC box, important for replication of viral DNA and for expression of a viral transformation gene, was a particularly strong target for cisplatin binding as inferred from replication blockage results. Platinum binding in this region is fully consistent with its high affinity for oligo(dG) sequences. It is possible that targeting of G-rich-regulatory regions plays some part in the biological activity of cisplatin.

While adjacent guanines lead to the formation of the major platinum-DNA adduct, which effectively blocks DNA synthesis as revealed in replication mapping experiments, other platinum-DNA adducts also inhibit replication. Replication inhibition studies of primed, platinated M13mp10 DNA using the enzyme pol I (131) revealed stops at sequences that could represent d(GpG), d(ApG), and d(G*pNpG*) adducts. Other possible sites of replication inhibition included d(GpC) and d(GpA). Some of the stops scored by the authors as d(GpA) could actually be d(A*pNpG*) cross-links based on their sequence context. Studies employing the same system but treating the DNA with high concentrations of cisplatin for very short (<5 min) time intervals, followed by addition of 0.5M NaCl to prevent hydrolysis of the second chloride ion, led to trapped monofunctional adducts that did not appear to block DNA synthesis (58).

B. Eucaryotic Systems

The fact that *cis*-DDP inhibits replication in mammalian cells was established by early investigations (55, 61). In general, however, less is known

about the effects of *cis*- and *trans*-DDP on higher organisms, which are inherently more complex and difficult to study. In replication mapping experiments on primed, platinated M13mp10 DNA using the eucaryotic enzyme DNA polymerase α , blockage was observed at sites virtually identical to those seen with the procaryotic enzyme DNA pol I, namely, at potential d(GpG), d(ApG), and d(G*pNpG*) cross-links. Other minor sites of replication inhibition scored were d(GpC) and d(GpA) cross-links, some of the latter possibly being d(A*pNpG*) cross-links (131). Also, as found for pol I, monofunctional adducts formed by *cis*-DDP do not block replication by polymerase α to nearly the extent as bifunctional adducts do (58). Thus, platinum-DNA adducts block *in vitro* replication of both procaryotic and eucaryotic polymerases.

The DNA tumor virus SV40, used extensively to model *in vivo* chromatin function, was employed to study the effects of *cis*- and *trans*-DDP on replication in mammalian cells. This virus infects permissive cells, such as African green monkey kidney CV-1 cells, replicates autonomously, and can be recovered. When the effects of *cis*- and *trans*-DDP on these phenomena were examined (23), it was discovered that 14 times more *trans*- than *cis*-DDP had to be present in the culture medium to inhibit *in vivo* SV40 replication to the same extent. Analysis of the DNA revealed that, for equal numbers of platinum atoms bound per SV40 genome, the two isomers were equally effective at blocking replication (see Fig. 7a). Differential uptake into CV-1 cells could not account for this disparity. Rather, when the DNA of CV-1 cells was studied, an interesting difference in the kinetics of binding was seen. As depicted in Fig. 7b, whereas *cis*-DDP binds continuously to DNA with time, the *trans* isomer binds rapidly at first but, after 6 h, total binding decreases. This difference was attributed to differential repair of *trans*-DDP-DNA adducts. It appears that, although both *cis*- and *trans*-DDP can bind to DNA and inhibit replication in procaryotic and eucaryotic systems, their DNA adducts may be processed differently by biological systems such as repair.

C. Studies Employing Site-Specifically Modified DNA

Since a number of different platinum-DNA adducts formed both *in vitro* and *in vivo* block replication, it is not possible to assess the biological role of an individual adduct in DNA that is randomly (globally) platinated. In order to address this problem, the methodology shown in Fig. 8 was developed for the construction of bacteriophage M13 genomes containing a platinum-DNA adduct at a single, chemically defined site (89, 97). Studies of a viral M13 genome constructed with a single *cis*-[Pt(NH₃)₂{d(GpG)}] (N7,N7) intrastrand cross-link revealed reduction in survival of the single-stranded genome to 10–12% that of a control, unplatinated genome (90).

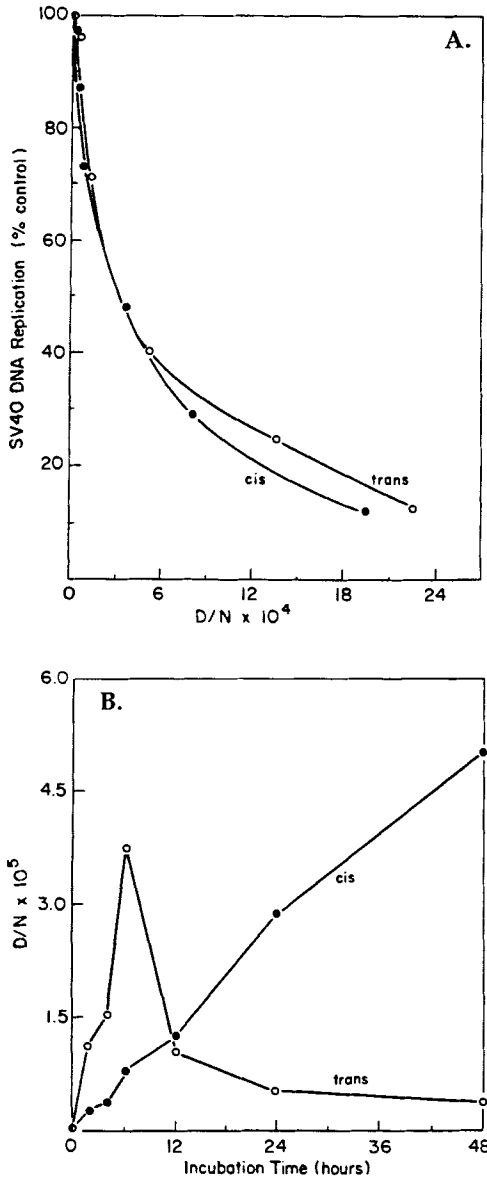


Figure 7. (a) Replication of SV40 DNA in CV-1 cells in the presence of *cis*-DDP (●) or *trans*-DDP (○) as a function of $(D/N)_0$. (b) Kinetics of binding of *cis*- and *trans*-DDP to the DNA of CV-1 with time. Reproduced with permission from Ref. 23 (copyright © 1985, American Chemical Society).

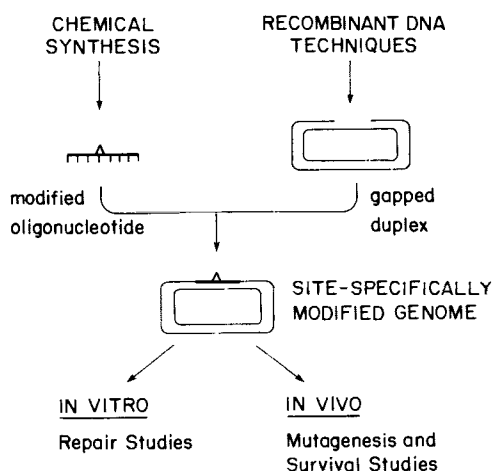


Figure 8. Scheme for construction of an M13 genome containing an individual, chemically defined adduct. Reproduced with permission from Ref. 89 (copyright © 1988, Marcel Dekker).

This experiment provided compelling evidence that a solitary intrastrand d(GpG) adduct can be a lethal event in a single-stranded bacteriophage. The extent to which the other adducts, formed by *cis*- and *trans*-DDP on DNA, affect replication and survival is currently being addressed by studies of other site-specifically platinated genomes.

IV. MUTAGENESIS AND REPAIR OF Pt-DNA ADDUCTS

A. Repair Studies in Prokaryotic Systems

DNA is subjected to numerous chemical damaging agents on a regular basis, from both metabolic pathways in the cell and exogenous damaging agents such as UV light. The cell must have mechanisms for repairing modified nucleotide bases in order to maintain genetic integrity and survive. One of these regulatory networks in *E. coli* is called the SOS response. The SOS network regulates several repair pathways by using the repressor LexA, which binds DNA and inhibits the production of the SOS genes. When DNA is damaged, however, the LexA protein is autocatalytically cleaved, and the cascade of SOS genes involved in various repair pathways is turned on. Two such pathways induced by the SOS response are excision repair and recombination repair.

In nucleotide excision repair, a complex called ABC excinuclease is involved in binding to the region of damaged DNA and hydrolyzing the eighth phosphodiester bond 5' and the fourth or fifth phosphodiester bond 3' to the site of damage. Removal of the resultant 12 or 13 base oligomer leaves a gap that is filled in by DNA polymerase I and sealed by DNA ligase using the redundant information of the complementary strand. The complex recognizes structural distortions in DNA, not the damaging agent itself, as evidenced by its ability to repair modifications made by a wide variety of such agents. The three subunits of ABC excinuclease system are encoded by the genes *uvrA*, *uvrB*, and *uvrC*.

The recombination repair mechanism is required if the action of polymerase is blocked by DNA damage such that DNA synthesis must be reinitiated beyond the adduct. The result is a region of single-stranded DNA containing a damaged nucleotide. This "post-replication gap" is filled in by transfer of the complementary strand from the sister duplex. Recognition of the single-strand gap, as well as pairing with the sister duplex and strand exchange, are facilitated by the protein RecA. Once the region containing the damage is double stranded, the adduct can be removed by ABC excinuclease. It is the activation of the RecA protein that accelerates the cleavage of LexA and induces the SOS response. A more detailed discussion of DNA repair is beyond the scope of this chapter. For more information, Refs. 47 and 111 should be consulted.

Studies using mutant cell lines defective in various steps of repair have revealed that more than one repair mechanism may be involved in the biological processing of platinum-induced damage to DNA. *Escherichia coli* cell lines mutant in both recombinational repair (*lex1*, *recA*, *recB*, *recC*) and excision repair (*uvrA*, *uvrB*, *uvrC*), as well as a mutant lacking DNA polymerase I (*polA*), were highly sensitive to *cis*-DDP (2, 8, 10). The effect was cumulative for a double mutant (*lex1*, *uvrA6*) deficient in both excision and recombination repair (8). These cell lines were not sensitive to *trans*-DDP at intermediate concentrations (18 μ M) (10), but at very high doses (up to 120 μ M) (2) *trans*-DDP had the same relative effect. The complex [Pt(dien)Cl]Cl had an effect only on the *recA* mutant, and only at very high concentrations (2). In another study it was shown that a functional *uvrB* gene, and to a lesser extent, the *recA* gene are essential for survival of *cis*- but not *trans*-DDP treated plasmid DNA (100).

Cisplatin is highly toxic to *dam*⁻ mutants, suggesting a role for mismatch repair (44). Mismatch repair involves repair of mismatched bases at the replication fork. The *dam*⁻ mutants are not sensitive to *trans*-DDP, however (44). In contrast, another repair system called the adaptive response, used to repair bases damaged by alkylating agents, does not appear to be involved in mediating cisplatin toxicity (48). The adaptive response removes

alkyl groups at a reactive cysteine sulfhydryl residue. It is interesting that platinum damage is not repaired by this system in view of the high affinity of Pt for sulfur donor ligands.

These studies using repair deficient mutants reveal that several biological repair systems are responsive to Pt-DNA adducts. The response may differ, however, according to the adducts formed by different compounds. This conclusion is supported by the fact that induction of the SOS response increases survival of wild-type *E. coli* treated with *cis*- but not *trans*-DDP (100). In another study, repair synthesis in wild-type *E. coli* cells was examined by density-gradient sedimentation. In this technique, repair is allowed to proceed in the presence of [³H]bromodeoxyuridine. The repaired, high density DNA can be separated from unrepaired, normal density DNA on CsCl gradients. This methodology revealed that more repair synthesis occurs in cells treated with *cis*-DDP than *trans*-DDP. No repair was detected for the monofunctional DNA binding compound [Pt(dien)Cl]Cl (2).

With use of an *in vitro* repair assay, it was found that both *cis*- and *trans*-DDP, when bound to supercoiled plasmid DNA, create substrates for ABC excinuclease (10, 100). This enzyme system is more active on adducts formed by the *cis* isomer (100). Moreover, only DNA adducts of cisplatin afford incision products from linear DNA fragments. When analyzed on sequencing gels, these products were attributed to incision at the eighth phosphodiester bond 5' and the fourth phosphodiester bond 3' to platinated d(GpG) sites (10). Recently, this assay was extended to compare the relative effectiveness of individual platinum-DNA adducts as substrates for ABC excinuclease (93). Oligonucleotides 43 base pairs in length were constructed, each containing a specific platinum adduct of the compound [³H][Pt(en)Cl₂]. Incubation of these site-specifically modified oligonucleotides with ABC excinuclease revealed differences in both the extent and rate of excision for different adducts in the order [Pt(en){d(GpNpG)}] ≥ [Pt(en){d(G)}] > [Pt(en){d(ApG)}] > [Pt(en){d(GpG)}]. It is not yet known whether platinum adducts possessing the highest affinity for recognition by ABC excinuclease are the least cytotoxic.

These studies point out important differences in the biological processing of the *cis* and *trans* isomers. Both isomers inhibit DNA replication in wild-type *E. coli* and, as expected, the effect is greatly enhanced in repair deficient mutants (*recA* > *uvrA*). In both mutant and wild-type cell lines, *cis*-DDP is sixfold more effective at replication blockage (2). Since binding of both isomers to cellular DNA (2) and plasmid DNA (10) is similar over time, and since the adducts of *cis*-DDP are more readily repaired (2, 10, 100), some authors suggested that the efficiency of replication blockage by the *cis* versus *trans* isomer might explain its greater toxicity in bacteria (2). It

is possible that *trans*-DDP-DNA adducts can be more effectively bypassed by the replication machinery, which is better blocked by *cis*-DDP-DNA adducts, at least in bacterial systems. The generality of such a conclusion remains to be established, however.

B. Repair Studies in Mammalian Systems

Little is known about the process of DNA repair in mammalian systems, but deficiencies in various repair systems are associated with several human diseases (for a review, see Ref. 16). For example, individuals with the autosomal recessive disease xeroderma pigmentosum (XP) are extremely sensitive to UV radiation and are at high risk for developing skin cancers. Studies using cells from these patients showed that they are deficient in excision repair and thus unable to repair damage to their DNA caused by UV light or other modifying agents. Individuals with the disease Fanconi's anemia (FA) are believed to have a deficiency in the repair of damage by cross-linking agents. Cells from patients with repair related disorders have been helpful in understanding more about the process of DNA repair but also reveal its complexity. In XP, for example, there are believed to be nine complementation groups, denoted A-I, with varying sensitivities to UV light, implying at least nine steps in the biochemical pathway for mammalian excision repair.

As found for excision repair deficient *E. coli* mutants, cells from xeroderma pigmentosum complementation groups A (29, 46, 98) and F (98) are very sensitive to cisplatin relative to wild-type cells. *cis*-DDP is also very toxic to cells from FA patients (29, 98). When the activity of proteins encoded by marker genes on cisplatin damaged plasmid shuttle vectors was investigated as a measure of repair, differences were seen in normal versus repair deficient cell lines. Modification by cisplatin decreased the activity of chloramphenicol transferase in cells from XP complementation groups A, C, and F (21) and in repair deficient CHO cells (113). There was, moreover, very little activity for *cis*-DDP platinated XGPRT in XP(A) cells (21). The sensitivity of repair deficient mutants to *cis*-DDP-induced damage suggests a role for this biological process in mediating the effects of the drug *in vivo*.

The issue of the repair of damage caused by *cis*- versus *trans*-DDP has been studied in mammalian systems. As discussed in Section IIIB and shown in Fig. 3B, differences in the kinetics of binding of *cis*- and *trans*-DDP to the DNA of monkey CV-1 cells suggested that adducts of the *trans* isomer may be repaired more readily (23). Subsequent studies (107) have reproduced these relative binding trends but attributed the difference to

DNA synthesis that occurred during the experiment. These latter authors claimed that, when a correction factor was applied, the overall binding to DNA increased in a similar fashion for both isomers. These experiments were complicated because the platinum compounds were dissolved in the coordinating solvent Me_2SO , which is known to react with *trans*-DDP with a half-life of 8 min (123). The compound *trans*- $[\text{Pt}(\text{NH}_3)_2(\text{Me}_2\text{SO})\text{Cl}]\text{Cl}$ alters both the kinetics of binding to DNA as well as the adduct spectrum (123). Curiously, attempts to control for this effect in phosphate-buffered saline were performed under different conditions than those described in Ref. 23. The later of the only two time points tested does not appear to fit the trend of continuously increasing *trans*-DDP-DNA adducts, even after correction for DNA synthesis (107).

In an *in vitro* assay, repair of plasmid DNA damaged by *cis*- or *trans*-DDP was studied in the presence of extracts from mammalian cells (54). Both compounds formed adducts that were repaired in this system, although *trans*-DDP treated plasmids stimulated about twice as much repair synthesis. Extracts prepared from XP(A) cells could not repair adducts formed by either isomer (54). The observation of more efficient repair of *trans*-DDP-DNA adducts was recently independently confirmed using the same system (57). In addition, by using an *in vitro* SV40 replication system it was shown that *cis*- and *trans*-DDP were equally effective at blocking replication (57), in agreement with earlier work (23). When *trans*-DDP treated plasmid DNA was preincubated in cell extracts to allow repair processes to occur, the template was partially reactivated for replication. This effect was not seen for *cis*-DDP treated plasmid DNA, indicating once again that cross-links formed by *trans*-DDP are more readily repaired (57). The difference in the activation of procaryotic and eucaryotic repair processes by *cis*- versus *trans*-DDP platinated DNA remains to be explained.

The repair of particular Pt-DNA adducts has been an active area of research. In a study of the repair of interstrand cross-links, it was found that a CHO cell line hypersensitive to UV was also very sensitive to *cis*-platin; this cell line was less able to repair interstrand cross-links (87). Other investigators did not find such a correlation, however, and reported that interstrand cross-links were repaired more slowly in an FA cell line than in an XP cell line even though the XP cells were more sensitive to *cis*-DDP (98). Interstrand cross-links formed by *trans*-DDP were repaired more rapidly than those of *cis*-DDP in CHO cells, implying that the persistence of the *cis*-DDP interstrand cross-links may be responsible for its cytotoxicity (99). Once again, however, the findings of these studies are equivocal since only one type of adduct was monitored without regard to other, more prevalent adducts. An *in vitro* repair assay using *cis*- and *trans*-

DDP treated plasmid DNA suggested that the repair observed in this system was due to removal of abundant adducts rather than excision of rare lesions (54).

Recently, antibodies raised against specific platinum–DNA adducts have been utilized to investigate relative repair rates. In one study (29), the distribution of adducts formed by cisplatin was found to be the same in XP(A), FA, and normal cell lines, as previously reported (34, 40). All adducts, including d(GpG), d(ApG), dG-Pt-dG (corresponding to inter-strand and long-range intrastrand cross-links), and monofunctional dG adducts were repaired in all three cell lines, although the kinetics of repair differed among them. In the normal and FA cell line, a rapid 4 h decrease followed by a slow decline was seen for all adducts, while in an XP cell line, adducts were repaired very slowly with time without a rapid initial period of repair. Although the Fanconi's anemia cells are very sensitive to cisplatin, it appears that this sensitivity is related to the high initial numbers of adducts formed, and not to a deficiency in their repair. The kinetics of repair of all adducts in the repair-deficient XP cell line differed from that found for the other cell lines, with the inherent sensitivity to cisplatin agreeing well with the number of unrepaired platinum–DNA adducts. Other work (11) has confirmed this observation. Survival of a bladder and two testicular cell lines 1 h after cisplatin treatment did not correlate with the $(D/N)_t$ values which, in turn, did not reflect intracellular platinum concentrations. The sensitivity of these three cell lines to *cis*-DDP did, however, correlate directly with the number of unrepaired platinum–DNA adducts remaining 18 h after treatment.

C. Mutagenesis

Mutations can occur when cellular replication and/or repair mechanisms insert an incorrect base at or near a damaged nucleotide. Secondary malignancies reported for patients treated with cisplatin (85) might conceivably arise from such mutagenesis. Cisplatin is mutagenic in both procaryotic (3, 18) and mammalian (65, 99) systems, inducing mainly single base pair substitutions as well as a small proportion (measured at <10%, Ref. 18) of frame-shift mutations (3, 18). Auxotrophic mutations are induced by *cis*- but not *trans*-DDP (9). Other investigators have shown that the *trans* isomer is not mutagenic in mammalian systems (65, 99).

Recent work has suggested that mutagenesis by *cis*-DDP is dependent on induction of the SOS response (18). A functional UvrA and UvrB, but not UvrC, protein was necessary for cisplatin induced mutagenesis (17). The *umuDC* locus, which mediates mutagenesis as part of the SOS re-

sponse, was shown by some (44), but not others (18), to be involved in mutagenesis by *cis*-DDP.

The platinum-DNA adduct that is the major source of mutation induction by *cis*-DDP is a matter of controversy. One study (17) found platinated d(GpNpG) sequences to be the most mutagenic loci for base pair substitution. Another (18) reported that d(ApG) and d(GpG) cross-links accounted for 90% of single base pair mutations, and that d(ApG) cross-links were five times more mutagenic. This conflict may be due to the different systems used for these studies, and the range of mutations they detect. Site-specifically modified M13 genomes were constructed in part to answer the question of the mutability of individual platinum-DNA adducts (90).

D. Use of Modified DNA Fragments as Probes for DNA Repair Factors

Taken together, the studies discussed thus far indicate that mammalian cells have the potential to repair a variety of DNA adducts formed by *cis*- and *trans*-DDP. The isolation and cloning of such factors will shed light on the complex process of mammalian DNA repair, since proteins involved in the recognition of damage are likely to respond to more than one mode of damage. Motivated by the observation that bacterial ABC excision nuclease recognizes and binds to both UV-irradiated and *cis*-DDP-modified DNA, investigators (22, 30) recently employed gel electrophoretic mobility shift assays to seek the mammalian analogue of this protein complex. Specific DNA-binding factors present in a complex mixture of proteins can be studied by this technique, in which a damage recognition protein (DRP) binds strongly to radiolabeled modified DNA fragments in the presence of a large molar excess ($\sim 10^4$ – 10^5 -fold) of nonspecific competitor DNA. This technique, shown in Fig. 9, was used previously to identify mammalian transcription factors (119).

By employing DNA fragments containing on average 1.8 UV-induced thymine dimers, or fragments modified with *cis*-DDP at a $(D/N)_6$ of 0.06, as probes, factors were identified in mammalian cell extracts that bound to and altered the electrophoretic mobility of both probes (22). Competition studies aimed at determining the specificity of these factors revealed that both UV-irradiated and *cis*-DDP-modified, unlabeled DNA fragments competed effectively for the UV-damage recognition protein. Interestingly, UV-irradiated DNA could not compete for binding of the *cis*-DDP-DNA protein. The *cis*-DDP-modified DNA binding protein identified in this work was present in both the cytosol and nucleus as well as in the eight

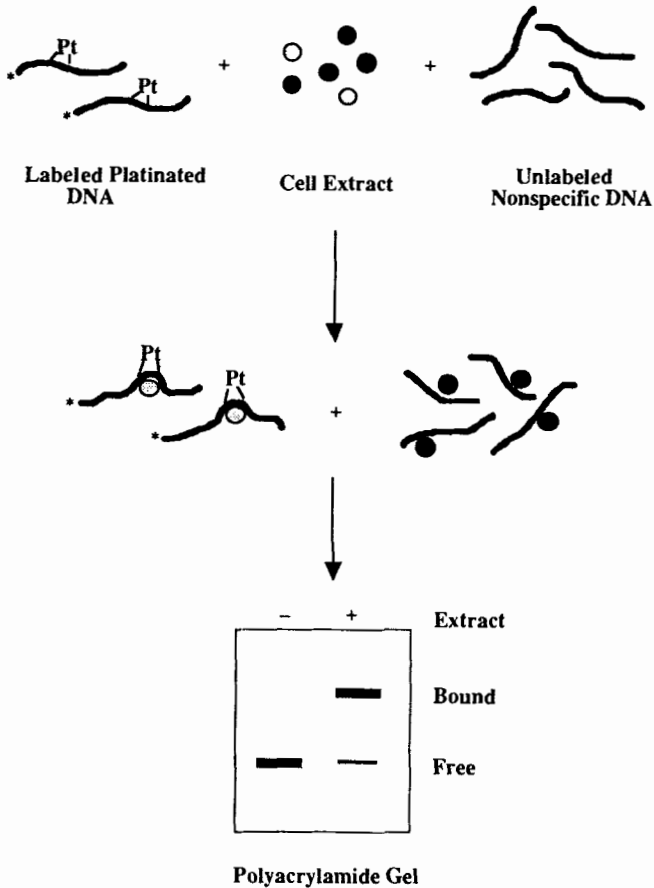


Figure 9. Schematic representation of electrophoretic mobility shift assay used to identify protein-DNA binding interactions.

complementation groups of XP (A-H) that were tested. In contrast, the UV DNA binding protein was present predominantly in the nucleus and was completely missing in XP complementation group E cells, providing an important link to function.

A similar approach was used to identify a mammalian cellular factor that selectively recognized adducts of active antitumor platinum compounds as well as individual adducts formed by *cis*-DDP on DNA (30). This factor was found in human HeLa and hamster V79 cells. The damage-recognition protein binds to *cis*-DDP platinated DNA at $(D/N)_b \geq 0.007$

with a K_d in the range $1-20 \times 10^{-10}$ M. Interestingly, the DRP did not bind to UV-treated DNA.

When DNA was modified with a variety of platinum compounds, it was found that the DRP is selective for antitumor-active compounds such as *cis*-DDP or [Pt(en)Cl₂]. No recognition was seen for DNA modified by the inactive compounds *trans*-DDP or [Pt(dien)Cl]Cl. In order to probe the recognition specificity further, site-specific oligomers containing individual platinum adducts were used as substrates for binding. The protein recognized both *cis*-DDP platinated d(GpG) and d(ApG) sequences, but neither *cis*-DDP platinated d(G* pTpG*) nor *trans*-DDP modified d(G* pTpG*) adducts. Since all three *cis*-DDP adducts tested bend DNA to similar extents (12), the structural motif that induces recognition is likely to be more complex, possibly a combination of duplex bending and unwinding. Purification of this protein is in progress (31).

In order to understand further the mechanisms underlying selective recognition and processing of DNA damaged by cisplatin or other agents, *cis*-DDP-modified DNA was used as a probe for cloning the gene that encodes this protein or related factors (128). This approach was used successfully to isolate clones encoding sequence-specific DNA binding proteins (118). A human B cell cDNA library constructed in the vector λ gt11 was screened with DNA modified by *cis*-DDP at a (D/N)_b ~ 0.043. The protocol is shown in Fig. 10. Two positive clones, designated λ Pt1 and λ Pt2, were isolated and purified that bound preferentially to *cis*-DDP platinated DNA.

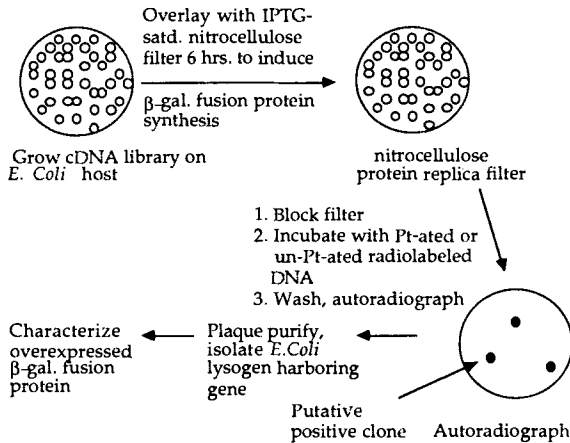


Figure 10. Protocol for isolating cDNA clones encoding proteins that bind selectively to DNA modified by *cis*-DDP.

Figure 11 shows the result of Southwestern blotting experiments designed to study the DNA binding ability of proteins encoded by these two clones. In this method, cellular proteins are separated by gel electrophoresis, transferred to nitrocellulose, and probed with radiolabeled platinated DNA fragments to reveal specific binding interactions. The DRP clones are fused to the protein β -galactosidase (MW = 116 kDa), which allows their expression in the vector. Lanes 3 and 4 reveal that the fusion proteins recognize *cis*-DDP platinated (*b*) but not unmodified (*a*) DNA. The β -gal protein produced in a vector lacking an insert does not possess specific binding capacity, as indicated in lane 2.

The encoded proteins bind selectively to double-stranded DNA fragments modified by either *cis*-DDP or [Pt(en)Cl₂], while little or no binding occurs to DNA modified with the clinically ineffective *trans*-DDP or [Pt(dien)Cl]Cl compounds. Low levels of binding to single-stranded DNA modified with *cis*-DDP were seen, while unmodified single-stranded DNA was not recognized. The extent of binding of the expressed protein to DNA depended on the level of modification by *cis*-DDP. Similar substrate specificity was observed for a protein present in HeLa cells of apparent molecular weight 100 kDa, shown in lane 1 of Fig. 11.

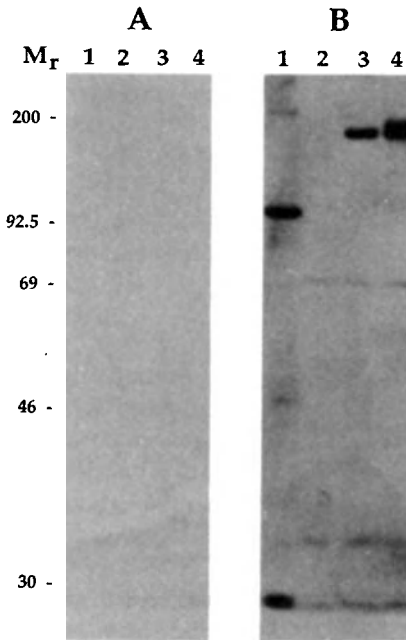


Figure 11. Southwestern blotting experiment showing the size and specificity of platinum-DNA binding factor. In (*a*), unmodified DNA was used as a probe; In (*b*), DNA platinated with *cis*-DDP at a (D/N)₀ of 0.043 was used as a probe. Lane 1, HeLa whole cell extract; lane 2, extract from *E. coli* lysogen from λ gt11 with no insert; lane 3, extract from *E. coli* lysogen from λ Pt2; lane 4, extract from *E. coli* lysogen from λ Pt1. Reproduced with permission from Ref. 128.

Northern blot analysis of cytoplasmic RNA prepared from HeLa, murine leukemia L1210, and Chinese hamster V79 cells revealed that the full length message encoded by λ Pt2 cDNA is ~ 2.8 kb, and is conserved in these species. Thus, the cloned cDNA inserts represent about one half of the full length gene. Based on the size of the mRNA, the full length protein is predicted to have a molecular weight of approximately 100 kDa, within experimental error of the measured size of the factor present in HeLa cellular extracts seen in Fig. 11, lane 1. The specificity of this factor is the same as that of the DRP seen in gel mobility shift assays (30). This fact, coupled with a size estimate of 91 kDa from sucrose gradients of partially purified DRP (30), indicate that these proteins may be the same. The biological role of these proteins remains to be determined.

V. POSSIBLE MECHANISMS OF ACQUIRED RESISTANCE TO *cis*-DDP

A. The Resistance Phenomenon

After remission or regression of tumor growth, a previously successful treatment regimen can become ineffective owing to acquired resistance of malignant cells to chemotherapy. This phenomenon occurs for patients treated with cisplatin and, despite its clinical utility, acquired resistance remains the major cause of treatment failure. In fact, resistance to one chemotherapeutic agent can confer resistance to a variety of other structurally and functionally different drugs, a phenotype called multidrug resistance (mdr). Drugs in the mdr class are pumped out of resistant cells in an energy-dependent process by a membrane protein present at elevated levels (26). Cisplatin, however, was found not to be cross-resistant to human sarcoma cells that are resistant to a number of drugs in the mdr class (56). In a multidrug resistant CHO cell line, cisplatin exhibited collateral sensitivity (51), meaning that these cells were more sensitive to cisplatin than the parental cell line.

A number of different mechanisms could account for the phenomenon of acquired resistance to *cis*-DDP based on information known about its mechanism of action and biological processing. Most studies have focused on the possibilities of altered uptake or efflux, inactivation of the drug by sulfur containing agents, or differential repair of Pt-DNA adducts.

Resistance is measured relative to a parental cell line of the same origin that is sensitive to the drug. The ratio of survival (typically 50% survival, or IC_{50}) at a particular concentration of drug for resistant versus parental cell line defines the resistance level of that cell line. For example, if the

cell line is 40-fold resistant to *cis*-DDP it would take 40 times more drug to kill 50% of the resistant cells than the parental cells.

B. Differential Uptake of Platinum Compounds

One hypothesis that could explain acquired resistance is that these cells somehow reduce their uptake of the drug. In fact, decreased uptake was found in a number of cisplatin resistant L1210 cell lines. One study reported uptake of [^{14}C][Pt(en)Cl $_2$] to decrease threefold *in vitro* and *in vivo* with no change in efflux. These cells were 18-fold resistant to cisplatin, however (132). A series of L1210 cell lines 20-, 50-, and 100-fold resistant to cisplatin exhibited a 40% reduction in accumulation of [^3H][Pt(en)Cl $_2$] (39). In an L1210 cell line 30-fold resistant to *cis*-DDP, uptake was reduced by a factor of 2–5, yet the number of platinum atoms bound to DNA was the same for parental and resistant cells (43). Similarly, a 3.3-fold resistant human ovarian cell line accumulated 50% the amount of drug as its parental cell line (5), and a 30-fold resistant human head and neck squamous cell carcinoma cell line showed a fourfold reduction in uptake, with no change in drug efflux in resistant cells (127). No difference in uptake was seen in a human small cell lung carcinoma cell line 6.4-fold resistant to *cis*-DDP relative to its parental cell line, however (59). For most of these cell lines, reduced uptake was a factor in cisplatin resistance, but did not correlate with or account quantitatively for the level of resistance measured.

C. Inactivation by Sulfur-Containing Agents

Another mechanism by which resistant cells might tolerate higher doses of *cis*-DDP is through inactivation of the drug by sulfur-containing compounds in the cell. Platinum has a high affinity for sulfhydryl groups, elevated intracellular levels of which could block coordination of the drug to DNA. The total sulfhydryl concentration in cells is composed of protein and nonprotein components. Nonprotein sulfhydryl residues consist mainly of the tripeptide L- γ -glutamyl-L-cysteinylglycine known as glutathione (GSH). Glutathione is the most abundant intracellular thiol. Its concentration in mammalian cells is 0.5–10 mM (86). An L1210 cell line 15-fold resistant to *cis*-DDP had 74% more GSH than its parental cell line, and treatment of these cell lines with buthionine sulfoximine (BSO), an inhibitor of GSH (86), resulted in equal cisplatin sensitivity for parental and resistant cell lines (62). Another cisplatin resistant L1210 cell line, however, was reported to have the same total and nonprotein sulfhydryl content as its parental cell line (132). Various cisplatin resistant human cell lines have shown two- to threefold higher amounts of glutathione, including a fivefold

resistant colon carcinoma (45), 6.4-fold resistant small cell lung carcinoma (59), and a 14-fold resistant ovarian carcinoma (53). In the human colon cancer cell line, loss of resistance was accompanied by lower GSH levels (45). It was shown, however, that severalfold changes in GSH and in enzymes required for GSH synthesis occurred in both parental and cisplatin resistant human ovarian cell lines with cell passage time (7).

A major component of the intracellular protein thiol pool is the class of inducible, cysteine-rich metallothionein (MT) proteins, important in heavy metal detoxification in eucaryotes (52). Studies of a human head and neck carcinoma cell line revealed no difference in nonprotein sulfhydryl content between parental cells and cells 30-fold resistant to cisplatin, but the latter had twofold greater levels of total protein sulfhydryl content (127). Several human and murine tumor cell lines resistant to cisplatin showed increased expression of one metallothionein, MT II_a, and increased levels of the protein (68). In addition, mouse cells transfected with the gene encoding metallothionein II_a showed a 10-fold increase in the level of MT accompanied by a 4.4-fold level of resistance to *cis*-DDP (68). By contrast, treatment of rats with cisplatin followed by chromatographic resolution of kidney metallothioneins showed that platinum did not elute with the MT fractions (84). Moreover, pretreatment of rats with Cd²⁺ to induce MT production had no effect on the metabolism of platinum in kidney or liver (84). *In vitro* studies of the relative affinity of Cu-metallothionein for a variety of metal ions revealed very weak binding of divalent platinum (91). This result is consistent with the tetrahedral coordination exhibited by MT for most other divalent metal ions (67), a geometry that is not favored by *d*⁸ transition metals such as Pt(II). It is not yet clear that the increased levels of sulfhydryl-containing compounds in resistant cells is the cause of their acquired resistance or merely part of a more general response to stress.

D. Differential Repair of Platinum Compounds

One leading hypothesis to explain acquired resistance is that the resistant cells have lower levels and/or more efficient repair of Pt-DNA adducts. A 1 h treatment of 18-fold resistant L1210 cells or 6.4-fold resistant human small cell lung carcinoma cells with a range of *cis*-DDP concentrations resulted in two- to threefold lower levels of bound platinum per nucleotide in the resistant cell lines (59, 132). Comparison of Pt-DNA levels of sensitive and 100-fold resistant L1210 cells at equitoxic IC₅₀ values, however, revealed that the resistant cells could tolerate a (D/N)_b that was 50-fold greater (39). Analysis of the adduct spectrum for these resistant L1210 cells indicated no differences from that previously reported for wild-type

cell lines (34). While studies using L1210 cells revealed no correlation between interstrand cross-links and resistance (88, 122), studies in cisplatin resistant human colon carcinoma cells (45) and head and neck carcinoma cells (127) indicated slightly lower levels of these cross-links in resistant lines.

Indirect evidence for DNA repair as a determinant in acquired resistance was obtained with the discovery that a mouse leukemia cell line 50-fold resistant to *cis*-DDP had a fourfold increase in the level of DNA polymerase β , an enzyme involved in DNA repair (73). This hypothesis was supported by a study in which a human ovarian carcinoma cell line 20-fold resistant to *cis*-DDP showed two to three times more repair synthesis than the parental cell line after a 1-h exposure to the drug (74). Also, studies in L1210 cells found that, although d(GpG), d(ApG), and d(ApNpG) cross-links formed by [^3H][Pt(en)Cl₂] were all repaired, resistant cells repaired fourfold more adducts during an initial 6-h phase of repair (39).

Although the origin of cisplatin resistance is still unknown, one study suggested that a genetic component is involved. Intraspecies hybrids between sensitive and resistant L1210 cell lines exhibited an intermediate resistance level (106). The decreased drug uptake and increased intracellular GSH levels measured in the original resistant cell lines were not transferred to the hybrid cells in this experiment, indicating that these factors were not responsible for resistance in those cell lines (106). In another investigation, however, evidence was found that pointed to hormonal interactions between tumor and normal tissues as mediators of acquired resistance, suggesting that the phenomenon of resistance may be very different *in vitro* and *in vivo*. A mouse mammary carcinoma tumor, made resistant *in vivo* by repeatedly treating mice with intraperitoneal injections of cisplatin, did not exhibit resistance *in vitro*. When these cells were reimplanted after 4–6 weeks in culture they showed the same resistance levels relative to the parental cell line (126).

Clearly, acquired resistance to cisplatin is a complex phenomenon that warrants further study. Understanding drug resistance will aid in the development of more effective chemotherapeutic regimens, as well as in the design of new anticancer drugs.

VI. EFFECT OF Pt(II) COMPLEXES ON OTHER CELLULAR PROCESSES

Although DNA is generally accepted to be the critical cellular target for cisplatin, the drug undoubtedly interacts with other cellular components, especially those containing sulfhydryl groups. Glutathione inhibits

the reaction between DNA and $[\text{Pt}(\text{en})\text{Cl}_2]$ (36) and binds to platinum–DNA monofunctional adducts, preventing closure to more toxic bifunctional adducts (6, 36). Recent studies employing ^{14}N NMR have detected release of an ammine ligand from cisplatin in human blood plasma (92), believed to be a result of interactions with L-methionine and diethyldithiocarbamate (DDTC). *cis*-DDP reacts with 1 mM DDTC with a half-life of 150 min (14), comparable to its rate of hydrolysis. Administration of DDTC following cisplatin treatment reduced kidney and bone marrow toxicity, with no effect on antitumor activity in mice, rats, and dogs. In dogs it also showed an antiemetic effect (15). While these interactions are of clinical relevance in overcoming the dose limiting toxicity of cisplatin, they are not likely to be important determinants of the mechanism of action of the compound.

Comparisons of reactions of *cis*- versus *trans*-DDP with sulfur donors and other cellular components may afford some insight into their relative biological effects, however. *trans*-DDP is much more reactive than the *cis* isomer with GSH (6, 27). Depletion of GSH with use of the inhibitor BSO had no effect on the cisplatin sensitivity of two human ovarian carcinoma cell lines, but made them 2.7 times more sensitive to *trans*-DDP (4). In a related finding, it was necessary to add 14 times more *trans*- than *cis*-DDP to cells in culture to achieve the same percent inhibition of *in vivo* SV40 DNA replication (23). These results suggest that part of the differential activity of these isomers in biological systems may arise from the differential reactivity of *trans*-DDP toward cellular components other than DNA. Thus *trans*-DDP could be more effectively inactivated prior to encountering DNA, or be better blocked as monofunctional platinum–DNA cross-links.

Recently, the effects of cisplatin on cell cycle progression were investigated. This cycle consists of a sequence of events through which cells must pass to grow and divide. There are several stages: in G_1 , cytoplasmic organelles are replicated; in S phase, DNA synthesis occurs; in G_2 , structures necessary for mitosis are assembled; in mitosis, the nucleus of the cell divides; and finally, in cytokinesis, the cytoplasm of the cell divides. Arrest of the cell cycle at a particular point by an exogenous agent can reveal the target of that agent. Progression through the cell cycle can be monitored by flow cytometry. This technique measures the DNA content of cells, which is at a maximum at the end of S phase, by fluorescence.

cis-DDP is cytotoxic at $(D/N)_b$ values of 10^{-5} – 10^{-6} *in vivo*, levels that would allow the vast majority of DNA to undergo replication. Therefore, arrest in late S phase seems likely. When L1210 and CHO cells were treated with *cis*-DDP and analyzed by flow cytometry, however, it appeared that they were blocked at G_2 . It was hypothesized that transcription, rather than replication, was responsible for the anticancer activity of the drug

(120, 121). Such a conclusion is equivocal, however, since the detection of blockage late in S phase versus blockage in G₂, a small difference between large numbers in terms of DNA content, is not feasible using the technique of flow cytometry. In addition, most transcription occurs throughout the cell cycle. Further study of this interesting phenomenon, perhaps following the expression of cell-cycle specific transcripts, is clearly warranted.

VII. GENERAL CONCLUSIONS AND CHALLENGES FOR THE FUTURE

The past several years have brought great progress in understanding both the chemistry of platinum(II) complexes with nucleic acids and the biochemistry and molecular biology of DNA systems that recognize platinum adducts on DNA. The differential toxicity of *cis*- versus *trans*-DDP remains a challenging problem that promises to shed light on the mechanism of action of cisplatin. Both isomers bind to the same sites on DNA, with similar *in vitro* kinetics and mechanism, and both can block replication in procaryotic and eucaryotic systems. The spectrum of adducts differs, however, as does their recognition by DRPs and cellular processes such as repair. The construction of site-specifically modified genomes for the study of replication, repair, and mutagenesis has begun to reveal the relative biological roles of individual adducts formed on DNA by *cis*- and *trans*-DDP.

The structural changes in DNA that occur as a result of platination are becoming more fully understood as a result of studies of DNA bending. Obtaining crystal structure data on platinum bound to duplex oligomers remains a challenging goal that will impart considerable missing information about the way platinum interacts with DNA. The cellular apparatus must utilize these structural perturbations to identify and differentiate various platinum-DNA adducts. Proteins present in cell extracts were identified that bind selectively to particular adducts formed by active antitumor platinum compounds, and cloning of a portion of this factor or a related factor from mammalian cells was accomplished. Further characterization of these proteins is eagerly awaited. A greater understanding of repair systems in mammalian cells will aid in the study of platinum-induced damage to DNA. Reconstitution of a DNA repair system in cell-free mammalian extracts, analogous to ABC excision nuclease in *E. coli*, would be an important first step toward this goal. Meeting these challenges promises to lead to an understanding of the mechanism of action of *cis*-DDP, and ultimately, to the development of more effective and less toxic platinum(II) antitumor complexes.

ACKNOWLEDGMENTS

This work was supported by grants from the National Cancer Institute and Bristol-Myers Company. J. H. T. was supported by National Research Service Award CA07951.

REFERENCES

1. G. Admiraal, J. L. van der Veer, R. A. G. de Graaff, J. H. J. den Hartog, and J. Reedijk, *J. Am. Chem. Soc.*, **109**, 592 (1987).
2. R. Alazard, M. Germanier, and N. P. Johnson, *Mutat. Res.*, **93**, 327 (1982).
3. K. S. Anderson, *Mutat. Res.*, **67**, 209 (1979).
4. P. A. Andrews, M. P. Murphy, and S. B. Howell, *Cancer Res.*, **45**, 6250 (1985).
5. P. A. Andrews, S. Velury, S. C. Mann, and S. B. Howell, *Cancer Res.*, **48**, 68 (1988).
6. D. P. Bancroft, C. A. Lepre, and S. J. Lippard, *J. Am. Chem. Soc.*, in press.
7. G. Batist, B. C. Behrens, R. Makuch, T. C. Hamilton, A. G. Katki, K. G. Louie, C. E. Myers, and R. F. Ozols, *Biochem. Pharmacol.*, **35**, 2257 (1986).
8. D. J. Beck and R. R. Brubaker, *J. Bacteriol.*, **116**, 1247 (1973).
9. D. J. Beck and R. R. Brubaker, *Mutat. Res.*, **27**, 181 (1975).
10. D. J. Beck, S. Popoff, A. Sancar, and W. D. Rupp, *Nucleic Acids Res.*, **13**, 7395 (1985).
11. P. Bedford, A. M. J. Fichtinger-Schepman, S. A. Shellard, M. C. Walker, J. R. W. Masters, and B. T. Hill, *Cancer Res.*, **48**, 3019 (1988).
12. S. F. Bellon and S. J. Lippard, *Biophys. Chem.*, **35**, 179 (1990).
13. F. Bernges and E. Holler, *Biochemistry*, **27**, 6398 (1988).
14. D. L. Bodenner, P. C. Dedon, P. C. Keng, and R. F. Borch, *Cancer Res.*, **46**, 2745 (1986).
15. D. L. Bodenner, P. C. Dedon, P. C. Keng, J. C. Katz, and R. F. Borch, *Cancer Res.*, **46**, 2751 (1986).
16. V. A. Bohr, M. K. Evans, and A. J. Fornace, Jr., *Lab. Invest.*, **61**, 143 (1989).
17. J. Brouwer, L. Vollebregt, and P. van de Putte, *Nucleic Acids Res.*, **16**, 7703 (1988).
18. D. Burnouf, M. Daune, and R. P. P. Fuchs, *Proc. Natl. Acad. Sci. USA*, **84**, 3758 (1987).
19. J. N. Burstyn and S. J. Lippard, unpublished results.
20. J.-L. Butour and N. P. Johnson, *Biochemistry*, **25**, 4534 (1986).
21. G. Chu and P. Berg, *Mol. Biol. Med.*, **4**, 277 (1987).
22. G. Chu and E. Chang, *Science*, **242**, 564 (1988).

23. R. B. Ciccarelli, M. J. Solomon, A. Varshavsky, and S. J. Lippard, *Biochemistry*, **24**, 7533 (1985).
24. G. L. Cohen, W. R. Bauer, J. K. Barton, and S. J. Lippard, *Science*, **203**, 1014 (1979).
25. K. M. Comess, C. E. Costello, and S. J. Lippard, *Biochemistry*, **29**, 2102 (1990).
26. J. M. Croop, P. Gros, and D. E. Housman, *J. Clin. Invest.*, **81**, 1303 (1988).
27. P. C. Dedon and R. F. Borch, *Biochem. Pharmacol.*, **36**, 1955 (1987).
28. J. H. J. den Hartog, C. Altona, J. H. van Boom, G. A. van der Marel, C. A. G. Haasnoot, and J. Reedijk, *J. Biomol. Struct. Dynam.*, **2**, 1137 (1985).
29. F. J. Dijt, A. M. J. Fichtinger-Schepman, F. Berends, and J. Reedijk, *Cancer Res.*, **48**, 6058 (1988).
30. B. A. Donahue, M. Augot, S. F. Bellon, D. K. Treiber, J. H. Toney, S. J. Lippard, and J. M. Essigmann, *Biochemistry*, **29**, 5872 (1990).
31. B. A. Donahue, S. J. Lippard, and J. M. Essigmann, unpublished results.
32. A. Eastman, *Biochemistry*, **22**, 3927 (1983).
33. A. Eastman, *Biochemistry*, **24**, 5027 (1985).
34. A. Eastman, *Biochemistry*, **25**, 3912 (1986).
35. A. Eastman, *Pharmacol. Ther.*, **34**, 155 (1987).
36. A. Eastman, *Chem.-Biol. Interact.*, **61**, 241 (1987).
37. A. Eastman and M. A. Barry, *Biochemistry*, **26**, 3303 (1987).
38. A. Eastman, M. M. Jennerwein, and D. L. Nagel, *Chem.-Biol. Interact.*, **67**, 71 (1988).
39. A. Eastman and N. Schulte, *Biochemistry*, **27**, 4730 (1988).
40. A. M. J. Fichtinger-Schepman, J. L. van der Veer, J. H. J. den Hartog, P. H. M. Lohman and J. Reedijk, *Biochemistry*, **24**, 707 (1985).
41. A. M. J. Fichtinger-Schepman, J. L. van der Veer, P. H. M. Lohman, and J. Reedijk, *J. Inorg. Biochem.*, **21**, 103 (1984).
42. A. M. J. Fichtinger-Schepman, A. T. van Oosterom, P. H. M. Lohman, and F. Berends, *Cancer Res.*, **47**, 3000 (1987).
43. M. Foka, J. Belehradek, Jr., and J. Paoletti, *Biochem. Pharmacol.*, **37**, 3467 (1988).
44. R. J. Fram, P. S. Cusick, J. M. Wilson, and M. G. Marinus, *Mol. Pharmacol.*, **28**, 51 (1985).
45. R. J. Fram, B. A. Woda, J. M. Wilson, and N. Robichaud, *Cancer Res.*, **50**, 72 (1990).
46. H. N. A. Fraval, C. J. Rawlings, and J. J. Roberts, *Mutat. Res.*, **51**, 121 (1978).
47. E. C. Friedberg, *DNA Repair*, Freeman, New York, 1985.

48. M. Germanier, M. Defais, N. P. Johnson, and G. Villani, *Mutat. Res.*, **145**, 35 (1984).
49. D. Gibson and S. J. Lippard, *Inorg. Chem.*, **26**, 2275 (1987).
50. J. D. Gralla, S. Sasse-Dwight, and L. G. Poljak, *Cancer Res.*, **47**, 5092 (1987).
51. R. S. Gupta, *Cancer Treat. Rep.*, **69**, 515 (1985).
52. D. H. Hamer, *Annu. Rev. Biochem.*, **55**, 913 (1986).
53. T. C. Hamilton, M. A. Winker, K. G. Louie, G. Batist, B. C. Behrens, T. Tsuruo, K. G. Grotzinger, W. M. McKoy, R. C. Young, and R. F. Ozols, *Biochem. Pharmacol.*, **34**, 2583 (1985).
54. J. Hansson and R. D. Wood, *Nucleic Acids Res.*, **22**, 8073 (1989).
55. H. C. Harder and B. Rosenberg, *Int. J. Cancer*, **6**, 207 (1970).
56. W. G. Harker and B. I. Sikic, *Cancer Res.*, **45**, 4091 (1985).
57. W. J. Heiger-Bernays, J. M. Essigmann, and S. J. Lippard, *Biochemistry*, in press.
58. J.-S. Hoffman, N. P. Johnson, and G. Villani, *J. Biol. Chem.*, **264**, 15130 (1989).
59. G. A. P. Hospers, N. H. Mulder, B. de Jong, L. de Ley, D. R. A. Uges, A. M. J. Fichtinger-Schepman, R. J. Scheper, and E. G. E. de Vries, *Cancer Res.*, **48**, 6803 (1988).
60. M. E. Howe-Grant and S. J. Lippard, *Metal Ions in Biological Systems*, H. Sigel, Ed., Vol. 20, Marcel Dekker, New York, 1980, pp. 63-125.
61. J. A. Howle and G. R. Gale, *Biochem. Pharmacol.*, **19**, 2757 (1970).
62. R. A. Hromas, P. A. Andrews, M. P. Murphy, and C. P. Burns, *Cancer Lett.*, **34**, 9 (1987).
63. N. P. Johnson, J. D. Hoeschele, N. B. Kuemmerle, W. E. Masker, and R. O. Rahn, *Chem.-Biol. Interact.*, **23**, 267 (1978).
64. N. P. Johnson, J. D. Hoeschele, and R. O. Rahn, *Chem.-Biol. Interact.*, **30**, 151 (1980).
65. N. P. Johnson, J. D. Hoeschele, R. O. Rahn, J. P. O'Neill, and A. W. Hsie, *Cancer Res.*, **40**, 1463 (1980).
66. N. P. Johnson, A. M. Mazard, J. Escalier, and J. P. Macquet, *J. Am. Chem. Soc.*, **107**, 6376 (1985).
67. J. H. R. Kagi and A. Schaffer, *Biochemistry*, **27**, 8509 (1988).
68. S. L. Kelley, A. Basu, B. A. Teicher, M. P. Hacker, D. H. Hamer, and J. S. Lazo, *Science*, **241**, 1813 (1988).
69. R. J. Knox, D. A. Lydall, F. Friedlos, C. Basham, and J. J. Roberts, *Biochim. Biophys. Acta*, **908**, 214 (1987).
70. J. Kozelka, S. Archer, G. A. Petsko, S. J. Lippard, and G. J. Quigley, *Biopolymers*, **26**, 1245 (1987).
71. J. Kozelka, G. A. Petsko, S. J. Lippard, and G. J. Quigley, *J. Am. Chem. Soc.*, **107**, 4079 (1985).

72. J. Kozelka, G. A. Petsko, G. J. Quigley, and S. J. Lippard, *Inorg. Chem.*, **25**, 1075 (1986).
73. A. J. Kraker and C. W. Moore, *Cancer Lett.*, **38**, 307 (1988).
74. G.-M. Lai, R. F. Ozols, J. F. Smyth, R. C. Young, and T. C. Hamilton, *Biochem. Pharmacol.*, **37**, 4597 (1988).
75. (a) R. Lavery and B. Pullman, *J. Biomol. Struct. Dyn.*, **2**, 1021 (1985);
(b) R. Lavery, A. Pullman, and B. Pullman, *Theoret. Chim. Acta*, **62**, 93, (1982).
76. C. A. Lepre and S. J. Lippard, *Nucleic Acids in Molecular Biology*, F. Eckstein and B. M. J. Lilley, Eds., Vol. 4, in press.
77. C. A. Lepre, L. Chassot, C. E. Costello, and S. J. Lippard, *Biochemistry*, **29**, 811 (1990).
78. C. A. Lepre, K. G. Strothkamp, and S. J. Lippard, *Biochemistry*, **26**, 5651 (1987).
79. M. C. Lim and R. B. Martin, *J. Inorg. Nucl. Chem.*, **38**, 1911 (1976).
80. S. J. Lippard, *Science*, **218**, 1075 (1982).
81. P. J. Loehrer and L. H. Einhorn, *Ann. Intern. Med.*, **100**, 704 (1984).
82. J.-P. Macquet and J.-L. Butour, *Biochim.*, **60**, 901 (1978).
83. L. Marrot and M. Leng, *Biochemistry*, **28**, 1454 (1989).
84. R. Mason, I. R. Edwards, and S. J. McLaren, *Chem.-Biol. Interact.*, **49**, 165 (1984).
85. G. M. Mead, J. A. Green, F. R. Macbeth, C. J. Williams, and J. M. A. Whitehouse, *Cancer Treat. Rep.*, **67**, 410 (1983).
86. A. Meister and M. E. Anderson, *Annu. Rev. Biochem.*, **52**, 711 (1983).
87. R. E. Meyn, S. F. Jenkins, and L. H. Thompson, *Cancer Res.*, **42**, 3106 (1982).
88. K. Micetich, L. A. Zwelling, and K. W. Kohn, *Cancer Res.*, **43**, 3609 (1983).
89. L. J. Naser, A. L. Pinto, S. J. Lippard, and J. M. Essigmann, *DNA Repair*, Vol. 3, E. C. Friedberg and P. C. Hanawalt, Eds., Marcel Dekker, New York, 1988.
90. L. J. Naser, A. L. Pinto, S. J. Lippard, and J. M. Essigmann, *Biochemistry*, **27**, 4357 (1988).
91. K. B. Nielson, C. L. Atkin, and D. R. Winge, *J. Biol. Chem.*, **260**, 5342 (1985).
92. R. E. Norman and P. J. Sadler, *Inorg. Chem.*, **27**, 3583 (1988).
93. J. D. Page, I. Husain, A. Sancar, and S. G. Chaney, *Biochemistry*, **29**, 1016 (1990).
94. J. M. Pascoe and J. J. Roberts, *Biochem. Pharmacol.*, **23**, 1345 (1974).
95. A. L. Pinto and S. J. Lippard, *Biochem. Biophys. Acta*, **780**, 167 (1985).
96. A. L. Pinto and S. J. Lippard, *Proc. Natl. Acad. Sci. USA*, **82**, 4616 (1985).
97. A. L. Pinto, L. J. Naser, J. M. Essigmann, and S. J. Lippard, *J. Am. Chem. Soc.*, **108**, 7405 (1986).

98. A. C. M. Plooy, M. van Dijk, F. Berends, and P. H. M. Lohman, *Cancer Res.*, **45**, 4178 (1985).
99. A. C. M. Plooy, M. van Dijk, and P. H. M. Lohman, *Cancer Res.*, **44**, 2043 (1984).
100. S. C. Popoff, D. J. Beck, and W. D. Rupp, *Mutat. Res.*, **183**, 129 (1987).
101. E. Reed, S. H. Yuspa, L. A. Zwelling, R. F. Ozols, and M. C. Poirier, *J. Clin. Invest.*, **77**, 545 (1986).
102. J. Reedijk, *Pure Appl. Chem.*, **59**, 181 (1987).
103. J. Reedijk and P. H. M. Lohman, *Pharm. Weekbl. Sci. Ed.*, **11**, 173 (1985).
104. S. Reslova-Vasilukova, *Recent Results in Cancer Research*, Vol. 48, T. A. Connors and J. J. Roberts, Eds. Springer-Verlag, 1974, pp. 105–106.
105. J. A. Rice, D. M. Crothers, A. L. Pinto, and S. J. Lippard, *Proc. Natl. Acad. Sci. USA*, **85**, 4158 (1988).
106. V. M. Richon, N. Schulte, and A. Eastman, *Cancer Res.*, **47**, 2056 (1987).
107. J. J. Roberts and F. Friedlos, *Cancer Res.*, **47**, 31 (1987).
108. J. J. Roberts and F. Friedlos, *Pharmac. Ther.*, **34**, 215 (1987).
109. B. Rosenberg, L. Van Camp, and T. Krigas, *Nature (London)*, **205**, 698 (1965).
110. B. Rosenberg, L. Van Camp, J. E. Trosko, and V. H. Mansour, *Nature (London)*, **222**, 385 (1969).
111. A. Sancar and G. B. Sancar, *Annu. Rev. Biochem.*, **57**, 29 (1988).
112. W. M. Scovell and L. R. Kroos, *Biochem. Biophys. Res. Commun.*, **104**, 1597 (1982).
113. N. Shebani, M. M. Jennerwein, and A. Eastman, *Biochemistry*, **28**, 3120 (1989).
114. S. E. Sherman, D. Gibson, A. H.-J. Wang, and S. J. Lippard, *Science*, **230**, 412 (1985).
115. S. E. Sherman, D. Gibson, A. H.-J. Wang, and S. J. Lippard, *J. Am. Chem. Soc.*, **110**, 7368 (1988).
116. S. E. Sherman and S. J. Lippard, *Chem. Rev.*, **87**, 1153 (1987).
117. K. V. Shooter, R. Howse, R. K. Merrifield, and A. B. Robins, *Chem.-Biol. Interact.*, **5**, 289 (1972).
118. H. Singh, J. H. LeBowitz, A. S. Baldwin, Jr., and P. A. Sharp, *Cell*, **52**, 415 (1988).
119. H. Singh, R. Sen, D. Baltimore, and P. A. Sharp, *Nature (London)*, **319**, 154 (1986).
120. C. M. Sorenson and A. Eastman, *Cancer Res.*, **48**, 4484 (1988).
121. C. M. Sorenson and A. Eastman, *Cancer Res.*, **48**, 6703 (1988).
122. M. C. Strandberg, E. Bresnick, and A. Eastman, *Chem.-Biol. Interact.*, **39**, 169 (1982).
123. W. I. Sundquist, K. J. Ahmed, L. S. Hollis, and S. J. Lippard, *Inorg. Chem.*, **26**, 1524 (1987).

124. W. I. Sundquist and S. J. Lippard, *Coord. Chem. Rev.*, **100**, 293 (1990).
125. W. I. Sundquist, S. J. Lippard, and B. D. Stollar, *Biochemistry*, **25**, 1520 (1986).
126. B. A. Teicher, T. S. Herman, S. A. Holden, Y. Wang, M. R. Pfeffer, J. W. Crawford, and E. Frei III, *Science*, **247**, 1457 (1990).
127. B. A. Teicher, S. A. Holden, M. J. Kelley, T. C. Shea, C. A. Cucchi, A. Rosowsky, W. D. Henner, and E. Frei III, *Cancer Res.*, **47**, 388 (1987).
128. J. H. Toney, B. A. Donahue, P. J. Kellett, S. L. Bruhn, J. M. Essigmann, and S. J. Lippard, *Proc. Natl. Acad. Sci. USA*, **86**, 8328 (1989).
129. J. L. van der Veer, G. J. Ligtvoet, H. van den Elst, and J. Reedijk, *J. Am. Chem. Soc.*, **108**, 3860 (1986).
130. B. van Hemelryck, E. Guittet, G. Chottard, J.-P. Girault, F. Herman, T. Huynh-Dinh, J.-Y. Lallemand, J. Igolen, and J. C. Chottard, *Biochem. Biophys. Res. Commun.*, **138**, 758 (1986).
131. G. Villani, U. Hubscher, and J.-L. Butour, *Nucleic Acids Res.*, **21**, 4407 (1988).
132. W. R. Waud, *Cancer Res.*, **47**, 6549 (1987).
133. A. Werner, *Z. Anorg. Chem.*, **3**, 267 (1893).
134. L. A. Zwelling, T. Anderson, and K. W. Kohn, *Cancer Res.*, **39**, 365 (1979).
135. L. A. Zwelling, K. W. Kohn, W. E. Ross, R. A. G. Ewig, and T. Anderson, *Cancer Res.*, **38**, 1762 (1978).

Subject Index

- ABC excinuclease, 496
 platinum–DNA adducts, repair of, 497
 site-specific, 497
 uvrA, *uvrB*, *uvrC*, 496
- Aconitase, 2, 17, 18, 19–22, 26
 cluster interconversion, 21, 22
 ENDOR, 25, 28
 EPR, 27
 mechanism of action, 27–30
 Mössbauer spectra, 19, 29
 structures, active and inactive forms, 24
- A-DNA, 453
- ADP, 205, 249, 251
 norenzymic hydrolysis of, 249–251
- Alkaline phosphatase, 237, 252
- Alkane hydroxylation, 149
- Amino acid analysis, 293
- Anticancer compounds, 478
- Antiferromagnetic coupling, 112, 117, 118,
 119, 127, 138, 140, 161, 179, 180
- Aquoferriheme, 309
- Aromatic amino acids, 299
- Atomic absorption analysis, 293
- Atomic emission analysis, 293
- ATP, 202, 210, 248, 249, 250
 nonenzymic hydrolysis of, 249–251
- Axial ligation, 309
- Azotobacter vinelandii* (*Av*) Fd I, 2, 17
 structure, 23, 25–26
- Azurin, 287, 293, 295, 306
- Bacterial resistance, 385
 broad-, narrow-spectrum, 386
- Beef heart succinate-ubiquinone
 oxidoreductase, 18
- Binding modes of metal complexes,
 418–420
- Binding modes to nucleic acids, 418
- Binuclear metal complexes, 279
- Bis(phenanthroline) cuprous ion, DNA
 cleavage, 425
- Blue copper proteins, 284, 304–306
 inner-sphere reorganization energy, 305
 outer-sphere reorganization energy, 305
- Cell cycle, stages monitored by flow
 cytometry, 509–510
- Chromatium* high-potential (HP) protein, 2
- Chromatium* HP_{red}, 7
- Cisplatin, *see cis*-
 Diamminedichloroplatinum(II)
- [Co(DIP)₃]³⁺, 456–458
- [Co(NH₃)₆]³⁺, 449–450
- Coordination complexes linked to DNA
 binding proteins, 450–451
- Coordination number, two, 335
- [Co(phen)₃]³⁺:
 DNA cleavage, 425
 electron-transfer reactions, 441
- Covalent labels, heavy metal complexes as,
 437
- Cruciform, 463
- [Cu(phen)₂]⁺, 430, 433–434, 449, 466–467
- Cyclic-AMP, hydrolysis of, 219, 220
- Cytochrome *b*-2, 311
- Cytochrome *b*-5, 310, 311
- Cytochrome *c*, 280, 284, 289, 290, 293, 295,
 299, 300, 302, 310, 311
 binding sites with inorganic complexes,
 282
 directional ET, 304
 glutamate and aspartate modification,
 291
 kinetic accessibility, 283
 lysine modification, 291
- Cytochrome *c*₅₅₁, 300
- Cytochrome *c* myoglobin, reorganization
 enthalpy, 297
- Cytochrome *c* peroxidase, 311
- Cytochrome *cd*-1, 281
- Cytochrome *f*, 285
- Damage-recognition protein (DRP), 501,
 502–503, 504
 mobility shift assays, 505
- cis*-DDP, *see cis*-
 Diamminedichloroplatinum(II)
- trans*-DDP, *see trans*-
 Diamminedichloroplatinum(II)

- Density-gradient sedimentation, 497
- Deoxyhemerythrin, 105, 141
- EPR, 128
 - magnetic circular dichroism, 127
 - Mössbauer spectra, 128
 - near IR CD spectroscopy, 130
 - NMR, 127
- Deoxyhemoglobin, 308
- 3-Deoxy-D-*arabino*-Heptulosonate 7-phosphate synthase, 165–166
- Deoxyribonucleic acid, *see* DNA
- Desulfovibrio gigas* (*Dg*) Fd II, 2, 17, 19, 22–23
- cluster interconversion, 22
 - Mössbauer spectrum, 22
 - structure $[3\text{Fe}-4\text{S}]^{1+}$ core, 23, 24
- cis*-Diamminedichloroplatinum(II)
- acquired resistance, 505–508
 - ^1H NMR adduct spectrum, 483
 - background, 478–480
 - binding modes to DNA, 480–484
 - DNA replication:
 - eucaryotic systems, 492–493
 - site-specifically modified DNA, 493–495
 - effect on other cellular processes, 508–510
 - effects on cell cycle, 509
 - reactions with sulfur donors, 509
 - effects on DNA replication, procaryotic systems, 491–492
 - interstrand cross-links, 484–485
 - kinetics of binding to DNA, 485–489
 - mutagenesis, 500–501
 - repair of adducts:
 - mammalian systems, 498–500
 - procaryotic systems, 495–498
 - structural distortions in DNA induced by binding, 489–491
- trans*-Diamminedichloroplatinum(II)
- ^1H NMR adduct spectrum, 484
 - background, 478–480
 - binding modes to DNA, 480–484
 - DNA replication:
 - eucaryotic systems, 492–493
 - site-specifically modified DNA, 493–495
 - effect on other cellular processes, 508–510
 - effects on cell cycle, 509
 - reactions with sulfur donors, 509
 - effects on DNA replication, procaryotic systems, 491–492
 - interstrand crosslinks, 484–485
 - kinetics of binding to DNA, 485–489
 - mutagenesis, 500–501
 - repair of adducts:
 - mammalian systems, 498–500
 - procaryotic systems, 495–498
 - structural distortions in DNA induced by binding, 489–491
- Differential pulse polarography, on modified proteins, 293
- Dimanganese model complexes:
 - electronic spectra, 177
 - EPR properties, 178
 - magnetic properties, 179–180
 - redox properties, 180–182

DNA, *see also* Double helical DNA

 - A-, B-, Z-DNA, 415
 - backbone, 481
 - bases, numbering scheme, 481
 - binding proteins, 503, 504
 - cleavage chemistry of metal complexes, 446
 - cleavage reagent probe of cruciform, 464
 - cleavage reagents, 456, 458
 - coordination, 482
 - damaging agent, 479
 - hydrogen-bonding interactions, 481
 - DNA polymerase I, 239
 - DNA polymerase I (pol I), 491–492, 493
 - DNA polymerase α , 493
 - DNA polymerase β , 508
 - DNA repair:
 - adaptive response, 496–497
 - Fanconi's anemia, 498
 - in vitro* repair assay, 497, 499–500
 - mismatch repair, 496
 - SOS response:
 - excision repair, 495
 - recombination repair, 495
 - xeroderma pigmentosum*, 498
 - DNA repair factors, use of modified DNA fragments as probes for, 501–505

Donor-acceptor compounds, 262, 281

 - aliphatic bridges, 276
 - amide bridges, 275
 - bicyclobutane bridges, 269
 - bicyclooctane bridges, 275
 - cyclobutane bridges, 269
 - decalin bridges, 278
 - dithiaspiro bridges, 276

- flexible linker, 268
- methylene linker, 268
- norbornyl bridges, 269, 271
- peptide bridges, 275
- polyene bridges, 273
- polyphenyl bridges, 273
- polyproline units, 272
- porphyrin donor, 263
- porphyrin-porphyrin-quinone trimer, 280
- quinone acceptors, 263
- steroid bridges, 269
- steroid spacer, 263
- thiaspirobutane bridges, 275
- Double helical DNA, 415
- Electronic coupling, 266, 271, 274, 275, 276, 277, 278, 279, 280, 306
 - charge recombination:
 - contact radical pairs, 279
 - geminate radical pairs, 279
 - solvent-separated radical pairs, 279
 - cytochrome *c*, 303
 - donor-acceptor coupling, orientation, 280
 - hydrogen-bond interactions, 278
 - myoglobin, 301, 303
 - superexchange, 267, 277, 278, 281
 - through-bond interaction, 277
 - through-space interactions, 278
- Electronic spectroscopy, as related to Hg complexes, 382, 403
 - LM CT, 361-362, 363, 364, 365, 366
 - optical electronegativity, 361-366
- Electron transfer:
 - activation parameters, 268
 - charge recombination, 262, 263, 302
 - geminate radical pairs, 265, 278
 - charge separation, 262, 263, 266, 302
 - charge-shift reactions, 266
 - distance dependence, 267-281
 - donor-acceptor separation, 268
 - driving force, 262, 301, 302
 - driving-force dependence, 265
 - free-energy dependence, 261-267
 - orientation effects in proteins, 28
- Electron transfer reaction, conformational control, 304
- ELISA, *see* Enzyme-linked immunosorbant assay
- Enantioselectivity, binding to DNA and, 445
 - tris(phenanthroline) metal complexes, 427
- Enzyme-linked immunosorbant assay (ELISA), 483
 - Escherichia coli* fumarate reductase, 18
 - Escherichia coli* nitrate reductase, 18
- EXAFS, 339, 349, 351, 352-353, 363, 368, 391, 392
- Fast atom bombardment mass spectrometry, 293
- [Fe(EDTA)]²⁻, 430, 433, 447-448, 462-463, 467
- Ferriheme acceptor, 308, 309
- Ferredoxin, spinach, 22
- Footprinting, photofootprinting by metal complexes, 435-436
- Footprinting reagents, 430
- Formation constants, 355, 360, 390
 - equilibrium constants, 357
 - halides, 356
 - thiolate, 356
- (-*O*,*O*-Formato)bis(μ -*O*,*O'*-formato)diiron, BIPhMe, 131
- Gel electrophoretic mobility, ABC excision nuclease, 501
- Gradient denaturing gel electrophoresis, 489
- Heme crevice, 283
- Heme ligation, 309
- Hemerythrin:
 - diferrous forms, 127
 - EPR, 131, 132
 - magnetic circular dichroism, 127
 - mechanism for dioxygen binding, 140
 - mixed-valence forms, 131-135
 - redox chemistry, 142-143
 - redox potential, 143, 144
- Hemoglobin, 299, 302, 309
- (Fe, Zn)-Hemoglobin, 311
- Hemoglobin hybrids, 308
- Hemoprotein, 83
- ¹⁹⁹Hg NMR, 340, 368, 403
 - asymmetry factor, 380, 382
 - chemical shift, anisotropy, 380-381, 382, 384, 385
 - chemical shifts, 375, 376, 377, 378, 379, 383-384
 - diamagnetic shielding, 383

- ¹⁹⁹Hg NMR (*Continued*)
isotropic shifts, 380
paramagnetic shielding, 383, 384
rapid exchange, 379
shielding, 375, 376, 383, 384–385
solid-state, 375, 378, 379, 380, 382, 385
solution, 375–379, 403
- Hg-MerR, 353
- Hin Recombinase, 451, 452
- His-33-modified horse heart cytochrome *c*, 301
- His-48-modified sperm whale myoglobin, 301
- Hydrolytic cleavage of nucleic acids, 468–470
- (μ -Hydroxo)bis(μ -carboxylato)diiron(II), Me₃TACN, 131
- Indoleamine 2,3-dioxygenase, 78, 80–85
interferon, 85
lipopolysaccharide, 85
self-defense, 89
transplantation, 89
tryptophan deprivation, 87
- Integer spin EPR, 128, 129, 131
- Interstrand cross-links:
correlation with cytotoxicity, 485
as “critical” lesion, 485
frequency of, 484–485
- Intervalence spectra, 260, 273, 275
- Iron-sulfur clusters, 2, 308
electron-transfer series, 6
hydrogen bonding, 7
ligand substitution, 4
- Iron-sulfur proteins:
conformational change, 289
high-potential (HiPIP), 288
- Iso-1-cytochrome *c*, 291, 299
- Iso-1-cytochrome *c* mutants, 312
- Kinases, 247–249
- Kinetic methods, in ET, 294–295
flash photolysis, 294, 310
pulse radiolysis, 294, 304, 306, 307, 310
- Kinetics:
double- and single-stranded DNA, 486
monofunctional DNA adducts, 487–488
rates of formation, 487–488
reaction rates, 486
- Kinetics, binding to DNA, 493, 494, 498, 499
- cis*-DDP to DNA, monofunctional adduct lifetimes, 485
- cis*-Diamminedichloroplatinum(II), stepwise mechanism, 486, 488
- trans*-Diamminedichloroplatinum(II), stepwise mechanism, 486, 488
- trans*-DDP to DNA, monofunctional adduct lifetimes, 485
- Klenow fragment, 239
- Ligand substitution, in Fe-S clusters and:
aqueous micellar solutions, 12–14
cyclodextrin thiolate ligands, 12
cysteinyl peptide environments, 7–10
immobilization on solid supports, 14–15
inclusion into non-Fe-S proteins, 14
macrocyclic thiolate environments, 10–12
mechanism, 4–7
statistical, 15–16
- Magnesium mesoporphyrin IX, 297
- Manganese catalase, 166
crystal structure, 167
EPR, 167
ESEEM study, 183
- Marcus theory, 261
charge recombination, geminate radical pair, 266
electronic factor, 301
inverted region, 262, 264, 266, 267
normal region, 264, 279
nuclear factor, distance dependence, 273
nuclear frequency factor, 301
- Mercuric halides, 332, 354
- Mercuric-thiolate complexes, 332
effective coordination number, 332
primary coordination number, 332–334, 336–338, 341–342, 348–349
thermodynamics, 354, 356, 390, 402–403
vibrational spectroscopy, 359, 366–367, 376, 382
asymmetric stretch, 369, 371–372, 373
bridging thiolates, 373
Hg(II) halides, 368–369
IR, 340, 367, 368, 369, 370, 372, 373, 374, 403
ligand mode, 371
M-S stretches, 368
normal vibrational modes, 367
Raman, 340, 361, 367, 368, 369, 370, 371, 372, 373, 374, 403

- symmetric mode, 368, 369
- symmetric stretch, 371–372, 373
- MerR, 328, 340, 352–353, 363, 367, 403
 - abortive transcriptional initiation, 329
 - broad-spectrum, 388
 - broad-spectrum resistance, 386
 - chemical modification, 387–389, 392, 393
 - DTNB, 387, 389
 - iodoacetamide, 387, 389
 - conformational changes, 392
 - cooperativity, 329
 - DNA distortion, 399–401
 - footprinting, 393, 397
 - gratuitous inducers, 330
 - metal ion selectivity, 329–331
 - mutagenesis, 389–390, 391, 393
 - narrow-spectrum resistance, 386, 388
 - three- and four-coordinate complexes as models, 340
 - titrations, 364
 - transcriptional activation, 329, 331, 388, 390, 393, 394–395
 - kinetics, 397, 402
 - transcription complex topology, 395–397
 - ultrasensitivity, 329, 394
- Metallointercalation, 420
- Metalloporphyrins, 303, 430, 434–435
- Metalloregulatory proteins, 326, 394
 - gratuitous inducers, 328
 - metal ion selectivity, 328
 - metal ion sensitivity, 328
 - metal-responsive gene expression, 327–328
 - metal-responsive gene regulation, 325
- Metallothionein, 325, 327, 328, 330, 360, 361, 362, 365, 366, 367
- Metaphosphate, 203, 204, 205, 210
- Methane monooxygenase, 102, 104, 105
 - diferrous forms, 127
 - electronic spectrum, 125
 - EPR, 128, 131, 132, 133, 135
 - EXAFS, 127, 135
 - integer spin EPR, 183
 - mixed-valence forms, 131
 - Mössbauer spectra, 125, 128
 - oxygen activation, 144
- Methemerythrin, 104
 - crystal structure, 99, 101, 103
 - electronic spectra, 113
 - EXAFS, 124
 - magnetic susceptibility, 112
 - Mössbauer spectra, 112
 - resonance Raman, 114, 117
- Methidium-propyl-EDTA Fe(II), 430
- Molecular oxygen, 76
- MPE-Fe(II), 423, 432–433, 466–467
- Mutations:
 - auxotrophic mutations, 500
 - frame-shift mutations, 500
 - single base pair substitutions, 500
 - substitutions, 500
- Myoglobin, 293, 295, 302, 304
- Nitrogenase, P-clusters, 30–32
- Osmium tetroxide-pyridine, 437–438
- (μ -Oxo)bis(μ -carboxylato)diiron(III)
 - complexes:
 - CpCo[OP(OEt)₂]₃, 106
 - cyclic voltammetry, 136
 - electronic spectra, 113
 - electronic transitions, 115
 - HBpz₃, 106, 109, 115, 117, 136, 144, 149
 - Me₃TACN, 109, 115, 116, 117, 136, 144
 - {[OP(OEt)₂]₃Co(C₃H₅)₂}, 109, 144
 - {[OP(OEt)₂]₃CoCp)₂}, 117
 - resonance Raman, 114, 117
 - TACN, 106, 109, 115, 117
- (μ -Oxo)bis(μ -phosphato)diiron(III)
 - complexes:
 - HBpz₃, 163
 - Me₃TACN, 163
- (μ -Oxo)(μ -carboxylato)diiron(III)
 - complexes:
 - cyclic voltammetry, 136
 - HDP, 109, 117, 118
 - resonance Raman, 117, 119, 120
 - TPA, 109, 115, 117, 118, 119, 136, 144
- (μ -Oxo)(μ -phosphato)-diiron(III)
 - complexes:
 - HDP, 163
 - TPA, 163
- Oxygenases, 76
 - tryptophan 2,3-dioxygenase, 78
- Oxygen evolving center from Photosystem II:
 - EPR, 169
 - EXAFS, 169
- Oxyhemerythrin, 104
 - EXAFS, 139, 140
 - models, 147
 - Mössbauer spectra, 139

- Oxyhemerythrin (*Continued*)
 resonance Raman, 117, 139
 Oxyhemoglobin, 308
- P-clusters:
 controlled potential coulometry, 31
 EPR, 31
 MCD, 31
 Mössbauer spectroscopy, 31
- Peptide mapping, 293
- Peptococcus aerogenes* Fd, 2
Peptococcus aerogenes Fd_{ox}, 7
- (μ -Phenoxy)bis(μ -carboxylato)diiron:
 BBMP, 137, 144
 BIMP, 137
 BPMP, 131, 137, 144
 5-MeHXTA, 137
 Mössbauer spectra, 137
 NMR, 137
- (μ -Phenoxy)bis(μ -carboxylato)diiron,
 (Me₄N)[Fe₂(5-MeHXTA)(OAc)₂], 117
- Phosphate:
 bis(4-nitrophenyl)phosphate (BNPP),
 211, 213, 220, 221, 222, 223, 230
 chelation of, 233–236
 cyclic, 207, 209
 diesters, 206, 209
 2,4-dinitrophenylphosphate, 204, 205, 227
 diphenyl-4-nitrophenylphosphate,
 210
 DNPP, 219
 ENPP, 221, 227
 ethylene, 207, 228
 ethyl-4-nitrophenylphosphate, 211, 229
 ethylphosphate, 229
 fluorophosphate, 226
 methyl, 234
 methylethylenephosphate, 207
 monoesters, 206
 4-nitrophenylphosphate, 216, 218, 225
 NPP, 222, 231, 232
 nucleophilic attack:
 alkoxide ion, 218
 amido ion, 225, 229
 coordinated hydroxide, 216
 intramolecular, 216, 221
 nucleophilic attack, 214
 2-(1,10-phenanthrolyl)phosphate, 212
 phenylphosphate, 205
 polyphosphates, 210, 218
 pyrophosphate, 240, 242–244
 triesters, 206, 209, 212
 trimethylphosphate (TMP), 214
 triphosphate, 244–247
 (μ -Phosphato)diiron(III) complexes, 109,
 110
 Phospholipase C, 238
 Phosphonate, 212
 ethyl-4-nitrophenyl-methylphosphonate,
 218
 GD, nerve agent, 213
 nitrophenyl-methylphosphonate, 218
 Phosphoramidate, 224, 225, 227, 228
 ethylphosphoramidate, 228, 229, 230
 Phosphorane, 206, 208, 214
 aminophosphorane, 226, 227
 Phosphorene, aminophosphorane, 225
 Photofootprinting by metal complexes,
 435–436
 Photoinduced ET, driving force study, 303
 Photoinduced ET reaction, energy level
 diagram for, 264
 Photosynthesis, 260, 266, 267
 Photosystem I, 285
 Plant plastocyanins, 287
 Plastocyanin, 284, 306, 345, 349, 362–363,
 367. *See also* Plant plastocyanins
 acidic residues, 286
 reactions with inorganic complexes, 287
- Platinum(II) complexes:
cis-DDP, 480
 [Pt(en)Cl₂], 480
 [Pt(dien)Cl]⁺, 480
trans-DDP, 480
- Platinum-DNA adducts, 478, 492, 495, 497,
 505
 bound drug–nucleotide ratio, (D/N)_b,
 483
 Fanconi's anemia, 498, 500
 intrastrand, 482, 483
 bifunctional, 482
 interstrand, 482
 monofunctional, 482
 linkage isomerization, 484
 monofunctional adduct lifetimes, 488
 relative proportions, 483
 relative rates of formation,
 monofunctional adduct lifetimes, 486,
 487
 single base pair mutations, 501
 SOS response, 497, 500–501
xeroderma pigmentosum, 499, 500, 502

- Poplar Cu^{II}-plastocyanin, 285
 Probes of DNA tertiary structures, 462–466
 Probes of RNA structure, 466–468
 Protein–protein complexes, ET in, 308
 cytochrome b₅(Fe, Zn) hemoglobin, 311
 cytochrome *c*-cytochrome *c* peroxidase, 311
 cytochrome *c*-cytochrome b₂, 311
 cytochrome *c*-cytochrome b_s, 310–311
 reorganization energy, 312
 Purine bases:
 adenine, 481
 guanine, 481
 Purple acid phosphatases, 149. *See also*
 Uteroferrin
 amino acid sequences, 150
 anion complexes, 155
 biological role, 150
 ENDOR, 154
 EPR, 11, 155, 156, 157, 164
 ESEEM, 154
 EXAFS, 151, 159, 161, 162
 ¹H NMR, 151, 152, 153
 magnetic susceptibility, 157, 161
 mechanism, 157
 Mössbauer spectra, 161
 phosphate complex, 161
 resonance Raman, 152, 153, 155, 161
 Pyrimidine bases
 cytosine, 481
 thymine, 481
 Recombination repair, 495, 496
 post-replication gap, 496
 Redox reactions of metal complexes with
 nucleic acids, 423–426
 photocleavage reactions with
 [Ru(phen)₃]²⁺, 425
 Reorganization energy, 279, 283, 310, 313
 Reorganization enthalpy, 306
 Replication mapping, 491, 492
 Resistance to *cis*-DDP:
 adduct spectrum, 507
 differential repair, to DNA, 507–508
 hormonal interactions, 508
 inactivation by sulfur-containing
 compounds, 506–507
 Glutathione, 506
 metallothionein (MT), 507
 interstrand cross-links, 508
 intraspecies hybrids, 508
 measurement, 505
 multidrug resistance (mdr), 505
 reducing uptake of drug, 506, 508
 sulfhydryl-containing compounds, 507
 [Rh(DIP)₃]³⁺, 463–466
 Rh(phen)₂Cl₃, 439
 [Rh(phen)₂phi]³⁺, 458–459, 468
 [Rh(phi)₂(bpy)]³⁺, 436
 Ribonucleotide reductase, 99–103, 104, 105
 crystal structure, 102, 125
 diferrous forms, 127
 EPR, 123, 128
 EXAFS, 120, 121, 123, 124
 iron content, 101
 manganese-containing, 167
 Mössbauer spectra, 120, 121, 128
 NMR, 124, 125, 128
 oxygen activation, 144–147
 resonance Raman, 117, 123
 tyrosine radical, 125
 tyrosyl radical, 123, 145
 Rubrerythrin, 105, 164–165
 EPR, 165
 Mössbauer spectra, 165
 UV/vis spectrum, 165
 [Ru(DIP)₂Macro]²⁺, 469
 [Ru(DIP)₃]²⁺, 444–446
 Ru(phen)₂Cl₂, 439
 [Ru(phen)₃]²⁺:
 electron-transfer reactions, 441
 mixed-ligand complexes of
 Ruthenium(II), 442–444
 photophysics with DNA, 440
 Ruthenated histidine, 290
 Ruthenated proteins, ET rates in, 305
 Ruthenated sperm whale myoglobin, 297
 Ruthenium-modified plastocyanin, 305
 [Ru(TMP)₃]²⁺, 453–456
 Secondary bonding interactions, 333, 334,
 335, 336–338, 341–342, 347, 348–349,
 372, 392
 Secondary interactions, 369, 376, 382, 385
 Semimethemerythrin, 132
 CD, 182
 EPR, 133, 135
 EXAFS, 134, 135
 MCD, 182
 NMR, 133
 Shape-selective probe for the A
 conformation, 453

- Site-directed mutagenesis, 291, 299
- Solvent polarizability, 278
- Spectroelectrochemistry, 293
- Spectroscopic probes for DNA structure, 439–446
- Spectroscopic probe for Z-DNA, 444–446
- Spectroscopic tags, 420
- cyclic voltammetry, 421
 - heavy metal tags, 421
 - in NMR experiments, 421
 - paramagnetic metal complexes, 421
- Stellacyanin, 306
- reactions with inorganic complexes, 287
- Structural distortions of DNA:
- base destacking, 489
 - bending or kinking, 490, 503, 510
 - altered gel electrophoretic mobility, 489–490
 - gel electrophoretic mobility studies, 489
 - molecular mechanics calculations, 489
 - NMR studies, 489
 - shortening of the double helix, 489
 - unwinding, 489, 503
- Subsite-differentiated synthetic clusters, 36
- bridged double-cubane clusters, 48–53
 - cluster linkage to iron complexes, 53–55
 - modulation of electron distribution and coupling, 59–63
 - relative stabilities of oxidation states, 55–59
 - solution structure, 41–44
 - structure, solid state, 38–40
 - substitution reactions, 44–48
 - symbols and nomenclature, 40
 - synthesis, 37–38
 - tridentate trithiolate ligand, 37
- Subsite-specific properties, 16–35
- cluster conversion reactions, 19
 - formation of heterometal clusters, 26–27
 - interconversion of [4Fe–4S] and [3Fe–4S] clusters, 17–23
 - P-clusters of nitrogenase, 30–32
 - sulfite reductase, 33–35
- Succinate dehydrogenase, 18
- Sulfite reductase, 33–35
- ENDOR, 34
 - EPR, 34
 - structure, 34
- Superoxide utilizing enzyme, 75–92
- SV40 virus, 499
- in vivo* chromatin model, 493
- Synthetic diiron(III) peroxide complexes, 147
- Thioethers, 358
- TMP, 214, 215
- Tris(phenanthroline) complexes of cobalt(III), DNA cleavage, 425
- Tris(phenanthroline) complexes of rhodium(III), DNA cleavage, 425
- Tris(phenanthroline)ruthenium(II), 420
- Tuna ferricytochrome, 283
- Uranium nitrate and acetate salts, 435–436
- Uranyl acetate, 468
- Uteroferrin, 104, 105, 149. *See also* Purple acid phosphatases
- amino acid sequences, 150
 - biological role, 150
 - EPR, 156, 157, 159
 - ESEEM, 159
 - EXAFS, 159, 161, 162
 - magnetic susceptibility, 157, 161
 - Mössbauer spectra, 156, 159, 161
 - phosphate complex, 156, 157
 - resonance Raman, 161
- Yeast inorganic pyrophosphatase (YIP), 240
- Z-DNA, 456
- Zinc family paradox, relativistic effects, 351
- Zinc mesoporphyrin IX diacid, 297
- Zn-substituted cytochrome *c*, 284

Cumulative Index, Volumes 1–38

	VOL.	PAGE
Abel, Edward W., Orrell, Keith, G., and Bhargava, Suresh K., <i>The Stereodynamics of Metal Complexes of Sulfur-, Selenium-, and Tellurium-Containing Ligands</i>	32	1
Adams, Richard D. and Istvan T. Horvath, <i>Novel Reactions of Metal Carbonyl Cluster Compounds</i>	33	127
Adamson, A. W., <i>see</i> Fleischauer, P. D.		
Addison, C. C. and Sutton, D., <i>Complexes Containing the Nitrate Ion</i>	8	195
Albin, Michael, <i>see</i> Horrocks, William DeW., Jr.		
Allen, G. C. and Hush, N. S., <i>Intervallence-Transfer Absorption. Part I Qualitative Evidence for Intervallence Transfer Absorption in Inorganic Systems in Solution and in the Solid State</i>	8	357
Allison, John, <i>The Gas-Phase Chemistry of Transition-Metal Ions with Organic Molecules</i>	34	627
Asprey, L. B. and Cunningham, B. B., <i>Unusual Oxidation States of Some Actinide and Lanthanide Elements</i>	2	267
Baird, Michael C., <i>Metal-Metal Bonds in Transition Metal Compounds</i>	9	1
Balhausen, C. J., <i>Intensities of Spectral Bands in Transition Metal Complexes</i>	2	251
Barton, Jacqueline K., <i>see</i> Pyle, Anna Marie		
Basolo, Fred and Pearson, Ralph G., <i>The Trans Effect in Metal Complexes</i>	4	381
Beattie, I. R., <i>Dinitrogen Trioxide</i>	5	1
Beattie, J. K. and Haight, G. P., Jr., <i>Chromium (VI) Oxidation of Inorganic Substrates</i>	17	93
Becke-Goehring, <i>Von Margot, Uber Schwefel Stickstoff Verbindungen</i>	1	207
Becker, K. A., Plieth, K. and Stranski, I. N., <i>The Polymorphic Modifications of Arsenic Trioxide</i>	4	1
Bennett, L. F., <i>Metalloprotein Redox Reactions</i>	18	1
Beno, Mark A., <i>see</i> Williams, Jack M.		
Berg, Jeremy M., <i>Metal-Binding Domains in Nucleic Acid-Binding and Gene-Regulatory Proteins</i>	37	143
Bertrand, J. A., and Eller, P. G., <i>Polynuclear Complexes with Aminoalcohols and Iminoalcohols as Ligands: Oxygen-Bridged and Hydrogen-Bonded Species</i>	21	29
Bhargava, Suresh K., <i>see</i> Abel, Edward W.		
Bickley, D. G., <i>see</i> Serpone, N.		
Bowler, Bruce E., Raphael, Adrienne L., and Gray, Harry B., <i>Long-Range Electron Transfer in Donor (Spacer) Acceptor Molecules and Proteins</i>	38	259
Bradley, D. C., <i>Metal Alkoxides</i>	2	303
Brookhart, Maurice, Green, Malcom L. H. and Wong, Luet-Lok, <i>Carbon-Hydrogen-Transition Metal Bonds</i>	36	1
Brothers, Penelope, J., <i>Heterolytic Activation of Hydrogen by Transition Metal Complexes</i>	28	1

Brown, Dennis G., <i>The Chemistry of Vitamin B12 and Related Inorganic Model Systems</i>	18	177
Brown, Frederick J., <i>Stoichiometric Reactions of Transition Metal Carbene Complexes</i>	27	1
• Brown, S. B., Jones, Peter and Suggett, A., <i>Recent Developments in the Redox Chemistry of Peroxides</i>	13	159
Brudvig, Gary W. and Crabtree, Robert H., <i>Bioinorganic Chemistry of Manganese Related to Photosynthetic Oxygen Evolution</i>	37	99
Bruhn, Suzanne L., Toney, Jeffrey H., and Lippard, Stephen J., <i>Biological Processing of DNA Modified by Platinum Compounds</i>	38	477
Brusten, Bruce E. and Green, Michael R., <i>Ligand Additivity in the Vibrational Spectroscopy, Electrochemistry, and Photoelectron Spectroscopy of Metal Carbonyl Derivatives</i>	36	393
Busch, Daryle H., <i>see</i> Meade, Thomas J.		
Cannon, Roderick D., White, Ross P., <i>Chemical and Physical Properties of Triangular Bridged Metal Complexes</i>	36	195
Carty, A., <i>see</i> Tuck, D. G.		
Carty, Arthur J., <i>see</i> Sappa, Enrico		
Carlson, K. Douglas, <i>see</i> Williams, Jack M.		
Catlow, C. R. A., <i>see</i> Thomas, J. M.		
Cattalini, L., <i>The Intimate Mechanism of Replacement in d⁵ Square-Planar Complexes</i>	13	263
Chaffee, Eleanor and Edwards, John O., <i>Replacement as a Prerequisite to Redox Processes</i>	13	205
Chakravorty, A., <i>see</i> Holm, R. H.		
Chaudhuri, Phalguni and Wieghardt, Karl, <i>The Chemistry of 1,4,7-Triazacyclononane and Related Tridentate Macrocyclic Compounds</i>	35	329
Chisholm, M. H. and Godleski, S., <i>Applications of Carbon-13 NMR in Inorganic Chemistry</i>	20	299
Chisholm, Malcolm H. and Rothwell, Ian P., <i>Chemical Reactions of Metal-Metal Bonded Compounds of Transition Elements</i>	29	1
Chock, P. B. and Titus, E. O., <i>Alkali Metal Ions Transport and Biochemical Activity</i>	18	287
Chow, S. T. and McAuliffe, C. A., <i>Transition Metal Complexes Containing Tridentate Amino Acids</i>	19	51
Churchill, Melvyn R., <i>Transition Metal Complexes of Azulene and Related Ligands</i>	11	53
Ciurli, A., <i>see</i> Holm, Richard M.		
Corbett, John D., <i>Homopolyatomic Ions of the Post-Transition Elements - Synthesis, Structure, and Bonding</i>	21	129
Cotton, F. A., <i>Metal Carbonyls: Some New Observations in an Old Field</i>	21	1
Cotton, F. A., <i>see</i> Wilkinson, G.		
Cotton, F. A., and Lukehart, C. M., <i>Transition Metal Complexes Containing Carbonoid Ligands</i>	16	487
Coucovanis, Dimitri, <i>The Chemistry of the Dithioacid and 1,1-Dithiolate Complexes</i>	11	233
Coucovanis, Dimitri, <i>The Chemistry of the Dithioacid and 1,1-Dithiolate Complexes, 1968-1977</i>	26	301

	VOL.	PAGE
Cowley, Alan, H., <i>UV Photoelectron Spectroscopy in Transition Metal Chemistry</i>	26	45
Cowley, Alan H., and Norman, Nicholas C., <i>The Synthesis, Properties, and Reactivities of Stable Compounds Featuring Double Bonding Between Heavier Group 14 and 15 Elements</i>	34	1
Crabtree, Robert H., <i>see</i> Brudvig, Gary W.		
Cramcr, Stephen P. and Hodgson, Keith O., <i>X-Ray Absorption Spectroscopy: A New Structural Method and Its Applications to Bioinorganic Chemistry</i>	25	1
Creutz, Carol, <i>Mixed Valence Complexes of d^5-d^6 Metal Centers</i>	30	1
Cunningham, B. B., <i>see</i> Asprey, L. B.		
Darensbourg, Marcetta York, <i>Ion Pairing Effects on Metal Carbonyl Anions</i>	33	221
Daub, G. William, <i>Oxidatively Induced Cleavage of Transition Metal-Carbon Bonds</i>	22	375
Dean, P. A. W., <i>The Coordination Chemistry of the Mercuric Halides</i>	24	109
Dechter, James J., <i>NMR of Metal Nuclides. Part I. The Main Group Metals</i>	29	285
Dechter, James J., <i>NMR of Metal Nuclides. Part II: The Transition Metals</i>	33	393
Deutsch, Edward, Libson, Karen, Jurisson, Silvia and Lindoy, Leonard F., <i>Technetium Chemistry and Technetium Radiopharmaceuticals</i>	30	75
Diamond, R. M. and Tuck, D. G., <i>Extraction of Inorganic Compounds into Organic Solvents</i>	2	109
DiBenedetto, John, <i>see</i> Ford, Peter C.		
Doedens, Robert J., <i>Structure and Metal-Metal Interactions in Copper (II) Carboxylate Complexes</i>	21	209
Donaldson, J. D., <i>The Chemistry of Bivalent Tin</i>	8	287
Donini, J. C., Hollebone, B. R. and Lever, A. B. P., <i>The Derivation and Application of Normalized Spherical Harmonic Hamiltonians</i>	22	225
Dori, Zvi, <i>The Coordination Chemistry of Tungsten</i>	28	239
Drago, R. S. and Purcell, D. F., <i>The Coordination Model for Non-Aqueous Solvent Behavior</i>	6	271
Drew, Michael G. B., <i>Seven-Coordination Chemistry</i>	23	67
Dye, James L., <i>Electrides, Negatively Charged Metal Ions, and Related Phenomena</i>	32	327
Earley, Joseph, E., <i>Nonbridging Ligands in Electron-Transfer Reactions</i>	13	243
Edwards, John O., <i>see</i> Chaffee, Eleanor		
Eisenberg, Richard, <i>Structural Systematics of 1,1- and 1,2-Dithiolate Chelates</i>	12	295
Eller, P. G., <i>see</i> Bertrand, J. A.		
Emge, Thomas J., <i>see</i> Williams, Jack M.		
Endicott, John F., Kumar, Krishan, Ramasami, T. and Rotzinger, Francois P., <i>Structural and Photochemical Probes of Electron Transfer Reactivity</i>	30	141
Epstein, Arthur J., <i>see</i> Miller, Joel S.		

	VOL.	PAGE
Espenson, James H., <i>Homolytic and Free Radical Pathways in the Reactions of Organochromium Complexes</i>	30	189
Everett, G. W., <i>see</i> Holm, R. H.		
Fackler, John P., Jr., <i>Metal B-Ketoenolate Complexes</i>	7	361
Fackler, John P., Jr., <i>Multinuclear d⁵-d¹⁰ Metal Ion Complexes with Sulfur-Containing Ligands</i>	21	55
Favas, M. C. and Kepert, D. L., <i>Aspects of the Stereochemistry of Four-Coordination and Five-Coordination</i>	27	325
Favas, M. C. and Kepert, D. L., <i>Aspects of the Stereochemistry of Nine-Coordination, Ten-Coordination, and Twelve-Coordination</i>	28	309
Felthouse, Timothy R., <i>The Chemistry, Structure, and Metal-Metal Bonding in Compounds of Rhodium (II)</i>	29	73
Fenske, Richard F., <i>Molecular Orbital Theory, Chemical Bonding, and Photoelectron Spectroscopy for Transition Metal Complexes</i>	21	179
Ferguson, J., <i>Spectroscopy of 3d Complexes</i>	12	159
Ferguson, James, <i>see</i> Krausz, Elmars		
Figgis, B. N. and Lewis, J., <i>The Magnetic Properties of Transition Metal Complexes</i>	6	37
Fleischauer, P. D., Adamson, A. W. and Sartori, G., <i>Excited States of Metal Complexes and Their Reactions</i>	17	1
Ford, Peter C., Wink, David, and DiBenedetto, John, <i>Mechanistic Aspects of the Photosubstitution and Photoisomerization Reactions of d⁶ Metal Complexes</i>	30	213
Fowles, G. W. A., <i>Reaction by Metal Halides with Ammonia and Aliphatic Amines</i>	6	1
Fratiello, A., <i>Nuclear Magnetic Resonance Cation Solvation Studies</i> ...	17	57
Friedman, H. L., <i>see</i> Hunt, J. P.		
Geiger, William E., <i>Structural Changes Accompanying Metal Complex Electrode Reactions</i>	33	275
Geiser, Urs, <i>see</i> Williams, Jack M.		
Geoffroy, Gregory L., <i>Photochemistry of Transition Metal Hydride Complexes</i>	27	123
George, J. W., <i>Halides and Oxyhalides of the Elements of Groups Vb and Vlb</i>	2	33
George, Philip and McClure, Donald S., <i>The Effect of Inner Orbital Splitting on the Thermodynamic Properties of Transition Metal Compounds and Coordination Complexes</i>	1	381
Gerloch, M., <i>A Local View in Magnetochemistry</i>	26	1
Gerloch, M. and Miller, J. R., <i>Covalence and the Orbital Reduction</i> ...	10	1
Gerloch, Malcolm and Woolley, R. Guy, <i>The Functional Group in Ligand Field Studies: The Empirical and Theoretical Status of the Angular Overlap Model</i>	31	371
Gibb, Thomas, R. P., Jr., <i>Primary Solid Hydrides</i>	3	315
Gillard, R. C., <i>The Cotton Effect in Coordination Compounds</i>	7	215
Gillespie, Ronald J., <i>see</i> Sawyer, Jeffery F.		
Glasel, Jay A., <i>Lanthanide Ions as Nuclear Magnetic Resonance Chemical Shift Probes in Biological Systems</i>	18	383

	VOL.	PAGE
Glick, Milton D. and Lintvedt, Richard L., <i>Structural and Magnetic Studies of Polynuclear Transition Metal β-Polyketonates</i>	21	233
Godleski, S., <i>see</i> Chisholm, M. H.		
Gordon, Gilbert, <i>The Chemistry of Chlorine Dioxide</i>	15	201
Gray, Harry B., <i>see</i> Bowler, Bruce E.		
Green, Malcom L. H., <i>see</i> Brookhart, Maurice		
Green, Michael R., <i>see</i> Bursten, Bruce E.		
Grubbs, Robert H., <i>The Olefin Metathesis Reaction</i>	24	1
Gruen, D. M., <i>Electronic Spectroscopy of High Temperature Open-Shell Polyatomic Molecules</i>	14	119
Gultneh, Yilma, <i>see</i> Karlin, Kenneth D.		
Hahn, James E., <i>Transition Metal Complexes Containing Bridging Alkylidene Ligands</i>	31	205
Haight, G. P., Jr., <i>see</i> Beattie, J. K.		
Haim, Albert, <i>Mechanisms of Electron Transfer Reactions: The Bridged Activated Complex</i>	30	273
Hall, Kevin P. and Mingos, D. Michael P., <i>Homo- and Heteronuclear Cluster Compounds of Gold</i>	32	237
Hall, Tracy H., <i>High Pressure Inorganic Chemistry</i>		
Hancock, Robert D., <i>Molecular Mechanics Calculations as a Tool in Coordination Chemistry</i>	37	187
Hendry, Philip, and Sargeson, Alan M., <i>Metal Ion Promoted Reactions of Phosphate Derivatives</i>	38	201
Hennig, Gerhart R., <i>Interstitial Compounds of Graphite</i>	1	125
Henrick, Kim, Tasker, Peter A. and Lindoy, Leonard F., <i>The Specification of Bonding Cavities in Macrocyclic Ligands</i>	33	1
Herbert, Rolfe H., <i>Chemical Applications of Mössbauer Spectroscopy</i>	8	1
Hobbs, R. J. M., <i>see</i> Hush, N. S.		
Hodgson, D. J., <i>The Structural and Magnetic Properties of First-Row Transition Metal Dimers Containing Hydroxo, Substituted Hydroxo, and Halogen Bridges</i>	19	173
Hodgson, Derek J., <i>The Stereochemistry of Metal Complexes of Nucleic Acid Constituents</i>	23	211
Hodgson, Keith O., <i>see</i> Cramer, Stephen P.		
Hollebone, B. R., <i>see</i> Donini, J. C.		
Holloway, John H., <i>Reactions of the Noble Gases</i>	6	241
Holm, R. H., Everett, G. W. and Chakravorty, A., <i>Metal Complexes of Schiff Bases and B-Ketoamines</i>	7	83
Holm, R. H. and O'Connor, M. J., <i>The Stereochemistry of Bis-Chelate Metal (II) Complexes</i>	14	241
Holm Richard M., Ciurli, A., and Weigel, A., <i>Subsite-Specific Structures and Reactions in Native and Synthetic (4Fe-4S) Cubane-Type Clusters</i>	38	1
Holmes, Robert R., <i>Five-Coordinated Structures</i>	32	119
Horrocks, William DeW., Jr. and Albin, Michael, <i>Lanthanide Ion Luminescence in Coordination Chemistry and Biochemistry</i>	31	1
Horváth, István T., <i>see</i> Adams, Richard D.		

	VOL.	PAGE
Humphries, A. P. and Kaesz, H. D., <i>The Hydrido-Transition Metal Cluster Complexes</i>	25	145
Hunt, J. P., and Friedman, H. L., <i>Aquo Complexes of Metal Ions</i>	30	359
Hush, N. S., <i>Intervallence Transfer Absorption Part 2. Theoretical Considerations and Spectroscopic Data</i>	8	391
Hush, N. S., <i>see</i> Allen, G. C.		
Hush, N. S. and Hobbs, R. J. M., <i>Absorption Spectra of Crystals Containing Transition Metal Ions</i>	10	259
Isied, Stephan S., <i>Long-Range Electron Transfer in Peptides and Proteins</i>	32	443
Isied, Stephan S., <i>see</i> Kuehn, Christa		
James, B. D. and Wallbridge, M. G. H., <i>Metal Tetrahydroborates</i>	11	99
James, David W., <i>Spectroscopic Studies of Ion-Ion Solvent Interaction in Solutions Containing Oxyanions</i>	33	353
James, David W. and Nolan, M. J., <i>Vibrational Spectra of Transition Metal Complexes and the Nature of the Metal-Ligand Bond</i>	9	195
Jardine, F. H., <i>The Chemical and Catalytic Reactions of Dichlorotris(triphenylphosphine)ruthenium(II) and Its Major Derivatives</i>	31	265
Jardine, F. H., <i>Chlorotris (triphenylphosphine) rhodium (I): Its Chemical and Catalytic Reactions</i>	28	63
Jeffrey, G. A. and McMullan, R. K., <i>The Clathrate Hydrates</i>	8	43
Johnson, B. F. G. and McCleverty, J. A., <i>Nitric Oxide Compounds of Transition Metals</i>	7	277
Jolly, William L., <i>Metal-Ammonia Solutions</i>	1	235
Jones, Peter, <i>see</i> Brown, S. B.		
Jorgensen, Chr., Klíxbull, <i>Electron Transfer Spectra</i>	12	101
Jorgensen, Chr., Klíxbull, <i>The Nephelauxetic Series</i>	4	73
Jurisson, Silvia, <i>see</i> Deutsch, Edward		
Kadish, Karl M., <i>The Electrochemistry of Metalloporphyrins in Non-aqueous Media</i>	34	435
Kaesz, H. D., <i>see</i> Humphries, A. P.		
Karlin, Kenneth D. and Gultneh, Yilma, <i>Binding and Activation of Molecular Oxygen by Copper Complexes</i>	35	219
Kennedy, John D., <i>The Polyhedral Metallaboranes Part I. Metallaborane Clusters with Seven Vertices and Fewer</i>	32	519
Kennedy, John D., <i>The Polyhedral Metallaboranes. Part II. Metallaborane Clusters with Eight Vertices and More</i>	34	211
Keperť, D. L., <i>Aspects of the Stereochemistry of Eight-Coordination</i> ...	24	179
Keperť, D. L., <i>Aspects of the Stereochemistry of Seven-Coordination</i> ..	25	41
Keperť, D. L., <i>Aspects of the Stereochemistry of Six-Coordination</i>	23	1
Keperť, D. L., <i>Isopolytungstates</i>	4	199
Keperť, D. L., <i>see</i> Favas, M. C.		
Kice, J. L., <i>Nucleophilic Substitution at Different Oxidation States of Sulfur</i>	17	147
King, R. B., <i>Transition Metal Cluster Compounds</i>	15	287

	VOL.	PAGE
König, Edgar, <i>Structural Changes Accompanying Continuous and Discontinuous Spin-State Transitions</i>	35	527
Krausz, Elmars and Ferguson, James, <i>The Spectroscopy of the [Ru(bpy)₃]²⁺ System</i>	37	293
Kubas, Gregory J., <i>see</i> Vergamini, Philip J.		
Kuehn, Christa and Isied, Stephan S., <i>Some Aspects of the Reactivity of Metal Ion-Sulfur Bonds</i>	27	153
Kumar, Krishan, <i>see</i> Endicott, John F.		
Kustin, Kenneth and Swinehart, James, <i>Fast Metal Complex Reactions</i>	13	107
Laane, Jaan and Ohlsen, James R., <i>Characterization of Nitrogen Oxides by Vibrational Spectroscopy</i>	27	465
Lagow, Richard J. and Margrave, John L., <i>Direct Fluorination: A "New" Approach to Fluorine Chemistry</i>	26	161
Laudise, R. A., <i>Hydrothermal Synthesis of Single Crystals</i>	3	1
Laure, B. L. and Schmulbach, C. D., <i>Inorganic Electrosynthesis in Non-aqueous Solvents</i>	14	65
Lentz, Dieter, <i>see</i> Seppelt, Konrad		
Leung, Peter C. W., <i>see</i> Williams, Jack M.		
Lever, A. B. P., <i>see</i> Donini, J. C.		
Lewis, J., <i>see</i> Figgis, B. N.		
Libson, Karen, <i>see</i> Deutsch, Edward		
Liehr, Andrew D., <i>The Coupling of Vibrational and Electronic Motions in Degenerate Electronic States of Inorganic Complexes. Part I. States of Double Degeneracy</i>	3	281
Liehr, Andrew D., <i>The Coupling of Vibrational and Electronic Motions in Degenerate Electronic States of Inorganic Complexes. Part II. States of Triple Degeneracy and Systems of Lower Symmetry</i>	4	455
Liehr, Andrew D., <i>The Coupling of Vibrational and Electronic Motions in Degenerate and Nondegenerate Electronic States of Inorganic and Organic Molecules. Part III. Nondegenerate Electronic States</i>	5	385
Lindoy, Leonard F., <i>see</i> Deutsch, Edward		
Lindoy, Leonard F. <i>see</i> Henrick, Kim		
Lintvedt, Richard L., <i>see</i> Glick, Milton D.		
Lippard, Stephen J., <i>see</i> Bruhn, Suzanne L.		
Lippard, Stephen J., <i>Eight-Coordination Chemistry</i>	8	109
Lippard, Stephen J., <i>Seven and Eight Coordinate Molybdenum Complexes, and Related Molybdenum (IV) Oxo Complexes, with Cyanide and Isocyanide Ligands</i>	21	91
Lippert, Bernhard, <i>Platinum Nucleobase Chemistry</i>	37	1
Lobana, Tarlok S., <i>Structure and Bonding of Metal Complexes of Tertiaryphosphine-Arsine Chalcogenides Including Analytical, Catalytic, and Other Applications of the Complexes</i>	37	495
Lockyer, Trevor N. and Martin, Raymond L., <i>Dithiolium Salts and Dithio-β-diketone Complexes of the Transition Metals</i>	27	223
Long, L. H., <i>Recent Studies of Diborane</i>	15	1
Lorand, J. P., <i>The Cage Effect</i>	17	207
Lukehart, C. M., <i>see</i> Cotton, F. A.		

	VOL.	PAGE
McAuliffe, C. A., <i>see</i> Chow, S. T.		
McCleverty, J. A., <i>Metal 1,2-Dithiolene and Related Complexes</i>	10	49
McCleverty, J. A., <i>see</i> Johnson, B. F. G.		
McClure, Donald S., <i>see</i> George, Philip		
MacDonnell, Frederick M., <i>see</i> Wright, Jeffrey G.		
McMullan, R. K., <i>see</i> Jeffrey, G. A.		
Maier, L., <i>Preparation and Properties of Primary, Secondary and Tertiary Phosphines</i>	5	27
Malatesta, Lamberto, <i>Isocyanide Complexes of Metals</i>	1	283
Margrave, John L., <i>see</i> Lagow, Richard J.		
Marks, Tobin J., <i>Chemistry and Spectroscopy of f-Element Organometallics Part I: The Lanthanides</i>	24	51
Marks, Tobin J., <i>Chemistry and Spectroscopy of f-Element Organometallics Part II: The Actinides</i>	25	223
Martin, Raymond L., <i>see</i> Lockyer, Trevor N.		
Marzilli, Luigi G., <i>Metal-ion Interactions with Nucleic Acids and Nucleic Acid Derivatives</i>	23	225
Marzilli, Luigi G., <i>see</i> Toscano, Paul J.		
Meade, Thomas J. and Busch, Daryle H., <i>Inclusion Complexes of Molecular Transition Metal Hosts</i>	33	59
Meyer, Thomas J., <i>Excited-State Electron Transfer</i>	30	389
Meyer, T. J., <i>Oxidation-Reduction and Related Reactions of Metal-Metal Bonds</i>	19	1
Miller, J. R., <i>see</i> Gerloch, M.		
Miller, Joel S. and Epstein, Arthur J., <i>One-Dimensional Inorganic Complexes</i>	20	1
Mingos, D. Michael P., <i>see</i> Hall, Kevin P.		
Mitra, S., <i>Chemical Applications of Magnetic Anisotropy Studies on Transition Metal Complexes</i>	22	309
Muetterties, E. L., <i>see</i> Tachikawa, Mamoru		
Natan, Michael J., <i>see</i> Wright, Jeffrey G.		
Nathan, Michael J. and Wrighton, Mark S., <i>Chemically Modified Microelectrode Arrays</i>	37	391
Nolan, M. J., <i>see</i> James, David W.		
Norman, Nicholas, C., <i>see</i> Cowley, Alan H.		
Oakley, Richard T., <i>Cyclic and Heterocyclic Thiazines</i>	36	299
O'Connor, Charles J., <i>Magnetochemistry—Advances in Theory and Experimentation</i>	29	203
O'Connor, M. J., <i>see</i> Holm, R. H.		
O'Halloran, Thomas V., <i>see</i> Wright, Jeffrey G.		
Ohlsen, James R., <i>see</i> Laane, Jaan		
Oldham, C., <i>Complexes of Simple Carboxylic Acids</i>	10	223
Orrell, Keith G., <i>see</i> Abel, Edward W.		
Osamu Hayaishi, Takikawa Osamu, and Ryotaro Yoshida, <i>Indoleamine 2,3-Dioxygenase: Properties and Functions of a Superoxide Utilizing Enzyme</i>	38	75

	VOL.	PAGE
Ozin, G. A., <i>Single Crystal and Gas Phase Raman Spectroscopy in Inorganic Chemistry</i>	14	173
Ozin, G. A. and Vander Voet, A., <i>Cryogenic Inorganic Chemistry</i>	19	105
Parish, R. V., <i>The Interpretation of 119 Sn-Mössbauer Spectra</i>	15	101
Peacock, R. D., <i>Some Fluorine Compounds of the Transition Metals</i> ..	2	193
Pearson, Ralph G., <i>see</i> Basolo, Fred		
Perlmutter-Hayman, Berta, <i>The Temperature-Dependence of the Apparent Energy of Activation</i>	20	229
Pethybridge, A. D. and Prue, J. E., <i>Kinetic Salt Effects and the Specific Influence of Ions on Rate Constants</i>	17	327
Plieth, K., <i>see</i> Becker, K. A.		
Prue, J. E., <i>see</i> Pethybridge, A. D.		
Purcell, D. F., <i>see</i> Drago, R. S.		
Pyle, Anna Marie and Barton, Jacqueline K. Barton, <i>Probing Nucleic Acids with Transition Metal Complexes</i>	38	413
Que, Lawrence, Jr., True, Anne E., <i>Dinuclear Iron- and Manganese-Oxo Sites in Biology</i>	38	97
Ralston, Diana M., <i>see</i> Wright, Jeffrey G.		
Ramasami, T., <i>see</i> Endicott, John F.		
Raphael, Adrienne L., <i>see</i> Bowler, Bruce E.		
Reynolds, Warren L., <i>Dimethyl Sulfoxide in Inorganic Chemistry</i>	12	1
Rothwell, Ian P., <i>see</i> Chisholm, Malcolm H.		
Rotzinger, Francois P., <i>see</i> Endicott, John F.		
Sappa, Enrico, Tiripicchio, Antonio, Carty, Arthur J., and Toogood, Gerald E., <i>Butterfly Cluster Complexes of the Group VIII Transition Metals</i>	35	437
Sargeson, Alan M., <i>see</i> Hendry, Philip		
Sartori, G., <i>see</i> Fleischauer, P. D.		
Sawyer, Jeffery F., and Gillespie, Ronald J., <i>The Stereochemistry of SB (III) Halides and Some Related Compounds</i>	34	65
Schatz, P. N., <i>see</i> Wong, K. Y.		
Schmulbach, C. D., <i>Phosphonitrile Polymers</i>	4	275
Schmulbach, C. D., <i>see</i> Laure, B. L.		
Schultz, Arthur J., <i>see</i> Williams, Jack M.		
Searcy, Alan W., <i>High-Temperature Inorganic Chemistry</i>	3	49
Seppelt, Konrad and Lentz, Dieter, <i>Novel Developments in Noble Gas Chemistry</i>	29	167
Serpone, N. and Bickley, D. G., <i>Kinetics and Mechanisms of Isomerization and Racemization Processes of Six-Coordinate Chelate Complexes</i>	17	391
Seyferth, Dietmar, <i>Vinyl Compounds of Metals</i>	3	129
Spiro, Thomas G., <i>Vibrational Spectra and Metal-Metal Bonds</i>	11	1
Stiefel, Edward I., <i>The Coordination and Bioinorganic Chemistry of Molybdenum</i>	22	1
Stranski, I. N., <i>see</i> Becker, K. A.		

	VOL.	PAGE
Strouse, Charles E., <i>Structural Studies Related to Photosynthesis: A Model for Chlorophyll Aggregates in Photosynthetic Organisms</i>	21	159
Suggett, A., <i>see</i> Brown, S. B.		
Sutin, Norman, <i>Theory of Electron Transfer Reactions: Insights and Hintsights</i>	30	441
Sutton, D., <i>see</i> Addison, C. C.		
Swinehart, James, <i>see</i> Kustin, Kenneth		
Sykes, A. G. and Weil, J. A., <i>The Formation, Structure, and Reactions of Binuclear Complexes of Cobalt</i>	13	1
Tachikawa, Mamoru and Muetterties, E. L., <i>Metal Carbide Clusters</i>	28	203
Takikawa, Osamu, <i>see</i> Hayaishi, Osamu		
Tasker, Peter A., <i>see</i> Henrick, Kim		
Taube, Henry, <i>Interaction of Dioxygen Species and Metal Ions—Equilibrium Aspects</i>	34	607
Templeton, Joseph L., <i>Metal-Metal Bonds of Order Four</i>	26	211
Thomas J. M., and Catlow, C. R. A., <i>New Light on the Structures of Aluminosilicate Catalysts</i>	35	1
Thorn, Robert J., <i>see</i> Williams, Jack M.		
Tiripicchio, Antonio, <i>see</i> Sappa, Enrico		
Titus, E. O., <i>see</i> Chock, P. B.		
Tofield, B. C., <i>The Study of Electron Distributions in Inorganic Solids: A Survey of Techniques and Results</i>	20	153
Toney, Jeffrey, H., <i>see</i> Bruhn, Suzanne L.		
Toogood, Gerald E., <i>see</i> Sappa, Enrico		
Toscano, Paul J., and Marzilli, Luigi G., <i>B₁₂ and Related Organocobalt Chemistry: Formation and Cleavage of Cobalt Carbon Bonds</i>	31	105
Trofimenko, S., <i>The Coordination Chemistry of Pyrazole-Derived Ligands</i>	34	115
True, Anne E., <i>see</i> Que, Lawrence Jr.		
Tuck, D. G., <i>Structures and Properties of Hx₂ and HXY Anions</i>	9	161
Tuck, D. G., <i>see</i> Diamond, R. M.		
Tuck, D. G., and Carty, A., <i>Coordination Chemistry of Indium</i>	19	243
Tyler, David R., <i>Mechanistic Aspects of Organometallic Radical Reactions</i>	36	125
Vander Voet, A., <i>see</i> Ozin, G. A.		
van Leeuwen, P. W. N. M., <i>see</i> Vrieze, K.		
Vannerberg, Nils-Gosta, <i>Peroxides, Superoxides, and Ozonides of the Metals of Groups Ia, IIa, and IIb</i>	4	125
Vergamini, Phillip J. and Kubas, Gregory J., <i>Synthesis, Structure, and Properties of Some Organometallic Sulfur Cluster Compounds</i>	21	261
Vlek, Antonin A., <i>Polarographic Behavior of Coordination Compounds</i>	5	211
Vrieze, K. and van Leeuwen, P. W. N. M., <i>Studies of Dynamic Organometallic Compounds of the Transition Metals by Means of Nuclear Magnetic Resonance</i>	14	1
Wallbridge, M. G. H., <i>see</i> James, B. D.		
Walton, R., <i>Halides and Oxyhalides of the Early Transition Series and Their Stability and Reactivity in Nonaqueous Media</i>	16	1

	VOL.	PAGE
Walton, R. A., <i>Ligand-Induced Redox Reactions of Low Oxidation State Rhenium Halides and Related System in Nonaqueous Solvents</i>	21	105
Wang, Hua H., <i>see</i> Williams, Jack M.		
Ward, Roland, <i>The Structure and Properties of Mixed Metal Oxides</i> . . .	1	465
Weigel, A., <i>see</i> Holm, Richard M.		
Weil, J. A., <i>see</i> Sykes, A. G.		
Whangbo, Myung-Hwan, <i>see</i> Williams, Jack M.		
White, Ross P., <i>see</i> Cannon, Roderick D.		
Wieghardt, Karl, <i>see</i> Chaudhuri, Phalguni		
Wilkinson, G. and Cotton, F. A., <i>Cyclopentadienyl and Arene Metal Compounds</i>	1	1
Williams, Jack M., <i>Organic Superconductors</i>	33	183
Williams, Jack M., Wang, Hau H., Emge, Thomas J., Geiser, Urs, Beno, Mark A., Leung, Peter C. W., Carlson, K. Douglas, Thorn, Robert J., Schultz, Arthur J. and Whangbo, Myung-Hwan, <i>Rational Design of Synthetic Metal Superconductors</i>	35	51
Williamson, Stanley M., <i>Recent Progress in Sulfur-Fluorine Chemistry</i>	7	39
Winchester, John W., <i>Radioactivation Analysis in Inorganic Geochemistry</i>	2	1
Wink, David, <i>see</i> Ford, Peter C.		
Wong, Luet-Lok, <i>see</i> Brookhart, Maurice		
Wong, K. Y. and Schatz, P. N., <i>A Dynamic Model for Mixed-Valence Compounds</i>	28	369
Wood, John S., <i>Stereochemical Electronic Structural Aspects of Five-Coordination</i>	16	227
Woolley, R. Guy, <i>see</i> Gerloch, Malcolm		
Wright, Jeffrey G., Natan, Michael J., MacDonnell, Frederick M., Ralston, Diana, M., and O'Halloran, Thomas V. <i>Mercury(II)-Thiolate Chemistry and the Mechanism of the Heavy Metal Biosensor MerR</i> . .	38	323
Wrighton, Mark S., <i>see</i> Natan, Michael J.		
Yoshida, Ryotaro, <i>see</i> Hayaishi, Osamu		
Zubieta, J. A. and Zuckerman, J. J., <i>Structural Tin Chemistry r-Coordination</i>	24	251
Zuckerman, J. J., <i>see</i> Zubieta, J. A.		